

VOLUME 75

JULY 8, 1971

NUMBER 14

JPCA X

THE JOURNAL OF

PHYSICAL
CHEMISTRY

ห้องสมุด กรมวิทยาศาสตร์

PUBLISHED BIWEEKLY BY THE AMERICAN CHEMICAL SOCIETY

American Chemical Society

"Primary Publications on Microfilm"

Your Key to—

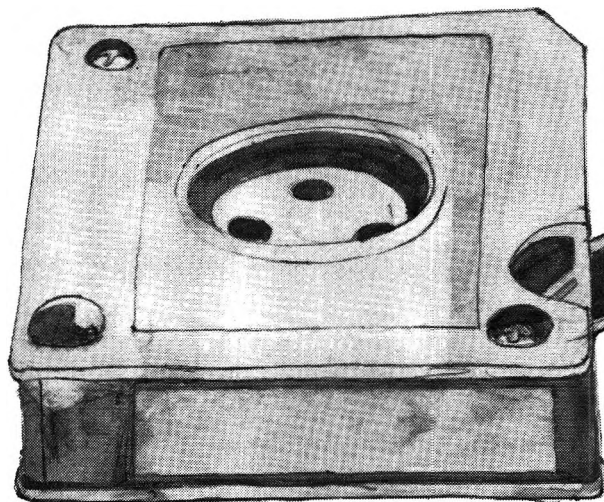
■ Dramatic savings in archival space and dollars . . . over **1,000,000** pages of chemical literature contained in a carousel measuring only 17" x 17" x 39".

■ Faster access to needed data. Slash costly search and retrieval time required of your scientists and librarians.

■ Unlimited distribution of copyrighted scientific data. "ACS Primary Publications on Microfilm" are available under a unique licensing agreement permitting you to make as many enlarged photocopies per page as desired . . . for distribution throughout your company.

American Chemical Society Primary Publications included in this microfilm program:

JOURNAL OF THE AMERICAN CHEMICAL SOCIETY
INDUSTRIAL & ENGINEERING CHEMISTRY
CHEMICAL TECHNOLOGY
CHEMICAL & ENGINEERING NEWS
CHEMICAL & ENGINEERING NEWS ANNUAL INDEXES
ANALYTICAL CHEMISTRY
JOURNAL OF PHYSICAL CHEMISTRY
JOURNAL OF AGRICULTURAL AND FOOD CHEMISTRY
JOURNAL OF ORGANIC CHEMISTRY
JOURNAL OF CHEMICAL AND ENGINEERING DATA
CHEMICAL REVIEWS
JOURNAL OF CHEMICAL DOCUMENTATION
I&EC FUNDAMENTALS
I&EC PROCESS DESIGN AND DEVELOPMENT
I&EC PRODUCT RESEARCH AND DEVELOPMENT
BIOCHEMISTRY
INORGANIC CHEMISTRY
JOURNAL OF MEDICINAL CHEMISTRY
CHEMISTRY
ENVIRONMENTAL SCIENCE & TECHNOLOGY
ACCOUNTS OF CHEMICAL RESEARCH
MACROMOLECULES



For information on "ACS Primary Publications on Microfilm", write or call:

Mr. George Virvan
Special Issues Sales
American Chemical Society
1155 16th Street, N.W.
Washington, D.C. 20036
(202-737-3337)

THE JOURNAL OF PHYSICAL CHEMISTRY

BRYCE CRAWFORD, Jr., *Editor*

STEPHEN PRAGER, *Associate Editor*

ROBERT W. CARR, Jr., FREDERIC A. VAN CATLEDGE, *Assistant Editors*

EDITORIAL BOARD: A. O. ALLEN (1970-1974), R. BERSOHN (1967-1971), J. R. BOLTON (1971-1975), S. BRUNAUER (1967-1971), M. FIXMAN (1970-1974), H. S. FRANK (1970-1974), J. R. HUIZENGA (1969-1973), M. KASHA (1967-1971), W. J. KAUZMANN (1969-1973), W. R. KRIGBAUM (1969-1973), R. A. MARCUS (1968-1972), W. J. MOORE (1969-1973), J. A. POPLE (1971-1975), B. S. RABINOVITCH (1971-1975), H. REISS (1970-1974), S. A. RICE (1969-1975), R. E. RICHARDS (1967-1971), F. S. ROWLAND (1968-1972), R. L. SCOTT (1968-1972), R. SEIFERT (1968-1972)

CHARLES R. BERTSCH, *Manager, Editorial Production*

AMERICAN CHEMICAL SOCIETY, 1155 Sixteenth St., N.W., Washington, D. C. 20036

FREDERICK T. WALL, *Executive Director*

Books and Journals Division

JOHN K. CRUM, *Director (Acting)*

JOSEPH H. KUNEY, *Head, Business Operations Department*

RUTH PEYNARD, *Assistant to the Director*

©Copyright, 1971, by the American Chemical Society. Published biweekly by the American Chemical Society at 20th and Northampton Sts., Easton, Pa. 18042. Second-class postage paid at Easton, Pa.

All manuscripts should be sent to *The Journal of Physical Chemistry*, Department of Chemistry, University of Minnesota, Minneapolis, Minn. 55455.

Additions and Corrections are published once yearly in the final issue. See Volume 74, Number 26 for the proper form.

Extensive or unusual alterations in an article after it has been set in type are made at the author's expense, and it is understood that by requesting such alterations the author agrees to defray the cost thereof.

The American Chemical Society and the Editor of *The Journal of Physical Chemistry* assume no responsibility for the statements and opinions advanced by contributors.

Correspondence regarding accepted copy, proofs, and reprints should be directed to Editorial Production Office, American Chemical Society, 20th and Northampton Sts., Easton, Pa. 18042. Manager: CHARLES R. BERTSCH. Assistant Editor: EDWARD A. BORGER. Editorial Assistant: EVELYN J. UHLER.

Advertising Office: Century Communications Corporation, 142 East Avenue, Norwalk, Conn. 06851.

Business and Subscription Information

Remittances and orders for subscriptions and for single copies,

notices of changes of address and new professional connections, and claims for missing numbers should be sent to the Subscription Service Department, American Chemical Society, 1155 Sixteenth St., N.W., Washington, D. C. 20036. Allow 4 weeks for changes of address. Please include an old address label with the notification.

Claims for missing numbers will not be allowed (1) if received more than sixty days from date of issue, (2) if loss was due to failure of notice of change of address to be received before the date specified in the preceding paragraph, or (3) if the reason for the claim is "missing from files."

Subscription rates (1971): members of the American Chemical Society, \$20.00 for 1 year; to nonmembers, \$40.00 for 1 year. Those interested in becoming members should write to the Admissions Department, American Chemical Society, 1155 Sixteenth St., N.W., Washington, D. C. 20036. Postage to Canada and countries in the Pan-American Union, \$4.00; all other countries, \$5.00. Single copies for current year: \$2.00. Rates for back issues from Volume 56 to date are available from the Special Issues Sales Department, 1155 Sixteenth St., N.W., Washington, D. C. 20036.

This publication and the other ACS periodical publications are now available on microfilm. For information write to: MICROFILM, Special Issues Sales Department, 1155 Sixteenth St., N.W., Washington, D. C. 20036.

FUEL CELL SYSTEMS—II

ADVANCES IN CHEMISTRY SERIES NO. 90

Thirty-one papers from the fifth of the biennial Fuel Cell Symposia sponsored by the Division of Fuel Chemistry, chaired by Bernard S. Baker. Topics include:

- fuel cell power systems
- electrode structure
- use of hydrocarbons
- electrode catalysis and mechanisms
- high temperature fuel cells
- fuel cell systems

Fuel cells are still doing their job well in the space program. Total energy, stationary fuel cell power plants seem worth a commercial push, and some hybrid devices look promising.

456 pages with index Cloth bound (1969) \$17.50

Free set of L. C. cards with library orders upon request

Other books in the ADVANCES IN CHEMISTRY SERIES in fuel chemistry include:

No. 80 Chemical Reactions in Electrical Discharges. A wide range of topics is covered in 37 papers by chemists, physicists, and engineers—treatments of decomposition and dissociation reactions, ion-molecule reactions, chemical syntheses, and chemical engineering aspects and physics of reactions in electrical discharges. 514 pages
Cloth (1969) \$15.00

No. 78 Literature of Chemical Technology. Forty articles discuss the literature of many aspects of chemical technology; seven of these are related to fuel cells, including electrochemistry of non-metals, noble metals, ceramics, enamels and glass, refractories, resources for petroleum chemicals, rocket propulsion, and rocket construction materials. 732 pages
Cloth (1968) \$17.50

No. 69 Fuel Gasification. Waning natural gas supplies and the threat of nuclear fuels are renewing interest in converting solid fuels to high B.t.u. gas. Sixteen studies survey current research in the U.S. and elsewhere from which commercial processes seem imminent. 276 pages
Cloth (1967) \$10.50

No. 64 Regenerative EMF Cells. Seventeen papers survey current progress and research on regenerative systems for converting and storing electrical energy. Principal emphasis is on thermally regenerative systems, but chemical and photochemical systems are considered. 309 pages
Cloth (1967) \$11.00

No. 55 Coal Science. Forty-seven papers include coal origins, coal metamorphosis, coal as an organic rock, physical and chemical structure of coals, reactivity and reactions of coal in relation to structure and rank. 743 pages
Cloth (1966) \$17.50

No. 54 Advanced Propellant Chemistry. Primarily directed toward the search for new oxidizers. Topics include theoretical approaches to advanced oxidizers, surveys of oxygen- and fluorine-containing oxidizers, fuels and binders, liquid systems. 290 pages
Cloth (1966) \$10.50

No. 47 Fuel Cell Systems. New systems for the energy converter proving itself in military and space uses. Topics include fuel cells for submarines and satellites, hydrogen-bromine fuel cells, molten carbonate fuel cells, and a coal burning fuel-cell power plant. 360 pages
Cloth (1965) \$10.50

No. 20 Literature of the Combustion of Petroleum. Twenty-one papers about the chemistry and kinetics of combustion, petroleum products as the fuel for engines, and combustion studies in engines. 295 pages
Paper (1958) \$8.00

No. 5 Progress in Petroleum Technology. Survey of 25 years of progress at the ACS Diamond Jubilee. Thirty-two papers on all aspects of petroleum processing and products. 392 pages
Paper (1951) \$8.00

Postpaid in U.S. and Canada; plus 30 cents elsewhere.

Order from:

SPECIAL ISSUES SALES
AMERICAN CHEMICAL SOCIETY
1155 SIXTEENTH ST., N.W.
WASHINGTON, D.C. 20036

THE JOURNAL OF
PHYSICAL CHEMISTRY

Volume 75, Number 14 July 8, 1971

Radical Reactions of Highly Polar Molecules. Reactivities in Atom Abstractions from Chloroalkanes by Fluoroalkyl Radicals	Leonard O. Moore	2075
Photolytic Reactions of 1,3-Diphenylpropene	E. W. Valyocsik and Paul Sigal	2079
Direct Determination of Singlet \rightarrow Triplet Intersystem Crossing Quantum Yield. II. Quinoline, Isoquinoline, and Quinoxaline.	Steven G. Hadley	2083
Pulse Radiolysis of Ammonia Gas. II. Rate of Disappearance of the $\text{NH}_2(\text{X}^2\text{B}_1)$ Radical	Sheffield Gordon, W. Mulac, and P. Nangia	2087
On the Theory of the Stabilization of Dispersions by Adsorbed Macromolecules. II. Interactions between Two Flat Particles.	F. Th. Hesselink, A. Vrij, and J. Th. G. Overbeek	2094
The Adsorption of Fibrinogen. An Electron Microscope Study	R. R. Gorman, G. E. Stoner, and A. Catlin	2103
Adsorption Inhibition as a Mechanism for the Antithrombogenic Activity of Some Drugs. I. Competitive Adsorption of Fibrinogen and Heparin on Mica	G. E. Stoner, S. Srinivasan, and E. Gileadi	2107
Spontaneous Dissolution of Metals in Aqueous Electrolytes. I. Kinetic Isotope Effects in the Reaction of Iron with Hydrochloric Acid Solutions in Protium and in Deuterium Oxide.	I. R. Bellobono and F. Mazza	2112
The Kinetics of the Reaction between Uranium(III) and $\text{Co}(\text{NH}_3)_4(\text{H}_2\text{O})_2^{3+}$ in Aqueous Perchlorate Solutions	James D. White and T. W. Newton	2117
Proton Exchange in Aqueous Urea Solutions.	Donald L. Hunston and Irving M. Klotz	2123
Complex Formation between Some Acetylenic Compounds and Benzene	David M. Coleman, Y. Aviva Sataty, and J. Tyrrell	2128
A Dielectric Constant Study of Molecular Association in Polar-Polar Mixtures. <i>o</i> -Dichlorobenzene-Butyl Alcohol	L. L. Combs, William H. McMahan, Jr., and Stephen H. Farish	2133
Biionic Potentials of a Liquid-Membrane Electrode Sensitive toward Calcium	J. Bagg, O. Nicholson, and R. Vinen	2138
The Mean Molal Activity Coefficient of Polymethacrylic Acid at Various Degrees of Neutralization	G. Torrence, S. Amdur, and J. A. Marinsky	2144
Free Energy Changes on Mixing Solutions of Alkali Halides and Symmetrical Tetraalkylammonium Halides	Wen-Yang Wen, Koichiro Miyajima, and Akinobu Otsuka	2148
Formation of Diamond. IV. The Behavior of the Diamond-Forming Reaction with Respect to Catalyst Composition	P. Cannon and E. T. Conlin, II	2158
Intramolecular Energy Relaxation. Nonrandom Decomposition of Hexafluorobicyclopropyl	J. D. Rynbrandt and B. S. Rabinovitch	2164
Energy Transfer in Thermal Isocyanide Isomerization. <i>n</i> -Alkenes and <i>n</i> -Alkenes in the Ethyl Isocyanide System	S. P. Pavlou and B. S. Rabinovitch	2171
Flash Photolysis of Chlorate Ion in Aqueous Solution	F. Barat, L. Gilles, B. Hickel, and B. Lesigne	2177
Reaction of Hexamethyldisilazane with Silica	W. Hertl and M. L. Hair	2181
The Rate and Mechanism of Interaction of Oxygen Atoms and Hydrogen Atoms with Silver and Gold	Bernard J. Wood	2186
Temperature-Dependent Splitting Constants in the Electron Spin Resonance Spectra of Cation Radicals. III. The Hydroxyl Group.	Paul D. Sullivan	2195
The Spectrum of Matrix-Isolated Carbon Disulfide.	L. Bajema, M. Gouterman, and B. Meyer	2204

- On the Interpretation of Electrode Admittance in the Case of Specific Reactant Adsorption. Application to the Bis(ethylenediamine)cobalt(III-II) System **M. Sluyters-Rehbach and J. H. Sluyters** 2209

NOTES

- An Investigation of Aqueous Mixtures of Nonionic Surfactants by Membrane Osmometry **D. Attwood, P. H. Elworthy, and S. B. Kayne** 2212
- On the Use of "Concentration-Time" Integrals in the Solutions of Complex Kinetic Equations. **B. Saville** 2215
- The Radiolysis of Liquid 1,1,2-Trichlorotrifluoroethane. **A. R. Kazanjian and D. R. Horrell** 2217
- Solvent and Temperature Effects on the Hydrogen Bond **E. A. Robinson, H. D. Schreiber, and J. N. Spencer** 2219
- An Infrared Spectral Study of Hydrogen Bonding in Solutions Containing Hydrogen Fluoride **Hidekazu Touhara, Haruyuki Shimoda, Koichiro Nakanishi, and Nobuatsu Watanabe** 2222
- Pressure Dependence of the Cross-Combination Ratio for CF_3 and CH_3 Radicals **P. C. Kobrinsky, G. O. Pritchard, and S. Toby** 2225
- The Gas-Phase Acidities of Alcohols **Mary Jane McAdams and Larry I. Bone** 2226
- Electron Spin Resonance Spectra of Copper Acetate in Acetic Acid Solutions **Graeme Nyberg** 2228
- Enthalpy of Transfer of Sodium Chloride from Water to Aqueous Hydrogen Peroxide at 25° **J. H. Stern and W. R. Bottenberg, Jr.** 2229

AUTHOR INDEX

- | | | | | |
|------------------------------|------------------------|---------------------------|--------------------------------|---------------------------|
| Amdur, S., 2144 | Farish, S. H., 2133 | Kobrinsky, P. C., 2225 | Otsuka, A., 2148 | Srinivasan, S., 2107 |
| Attwood, D., 2212 | Gileadi, E., 2107 | Lesigne, B., 2177 | Overbeek, J. T. G., 2094 | Stern, J. H., 2229 |
| Bagg, J., 2138 | Gilles, L., 2177 | Marinsky, J. A., 2144 | Pavlou, S. P., 2171 | Stoner, G. E., 2103, 2107 |
| Bajema, L., 2204 | Gordon, S., 2087 | Mazza, F., 2112 | Pritchard, G. O., 2225 | Sullivan, P. D., 2195 |
| Barat, F., 2177 | Gorman, R. R., 2103 | McAdams, M. J., 2226 | Rabinovitch, B. S., 2164, 2171 | Toby, S., 2225 |
| Bellobono, I. R., 2112 | Gouterman, M., 2204 | McMahan, W. H., Jr., 2133 | Robinson, E. A., 2219 | Torrence, G., 2144 |
| Bone, L. I., 2226 | Hadley, S. G., 2083 | Meyer, B., 2204 | Rynbrandt, J. D., 2164 | Touhara, H., 2222 |
| Bottenberg, W. R., Jr., 2229 | Hair, M. L., 2181 | Miyajima, K., 2148 | Sataty, Y. A., 2128 | Tyrell, J., 2128 |
| Cannon, P., 2158 | Hertl, W., 2181 | Moore, L. O., 2075 | Saville, B., 2215 | Valyocsik, E. W., 2079 |
| Catlin, A., 2103 | Hesselink, F. T., 2094 | Mulac, W., 2087 | Schreiber, H. D., 2219 | Vinen, R., 2138 |
| Coleman, D. M., 2128 | Hickel, B., 2177 | Nakanishi, K., 2222 | Shimoda, H., 2222 | Vrij, A., 2094 |
| Combs, L. L., 2133 | Horrell, D. R., 2217 | Nangia, P., 2087 | Sigal, P., 2079 | Watanabe, N., 2222 |
| Conlin, E. T., II, 2158 | Hunston, D. L., 2123 | Newton, T. W., 2117 | Sluyters, J. H., 2209 | Wen, W.-Y., 2148 |
| Elworthy, P. H., 2212 | Kayne, S. B., 2212 | Nicholson, O., 2138 | Sluyters-Rehbach, M., 2209 | White, J. D., 2117 |
| | Kazanjian, A. R., 2217 | Nyberg, G., 2228 | Spencer, J. N., 2219 | Wood, B. J., 2186 |
| | Klotz, I. M., 2123 | | | |

THE JOURNAL OF PHYSICAL CHEMISTRY

Registered in U. S. Patent Office © Copyright, 1971, by the American Chemical Society

VOLUME 75, NUMBER 14 JULY 8, 1971

Radical Reactions of Highly Polar Molecules. Reactivities in Atom

Abstractions from Chloroalkanes by Fluoroalkyl Radicals

by Leonard O. Moore

Research and Development Department, Chemicals and Plastics, Union Carbide Corporation,
South Charleston, West Virginia 25303 (Received March 1, 1971)

Publication costs assisted by the Union Carbide Corporation

Telomerization of the chloromethanes with tetrafluoroethylene provides a measure of relative reactivities of both chlorine and hydrogen to abstraction by fluoroalkyl radicals in solution. The reactivities are correlated to the bond dissociation energies of the atoms. The method appears to be general for studying the reactivities of more complex haloalkanes.

There has been a continuing interest in the effects of substituents on radical abstraction reactions.¹ Most of the work has involved abstraction of hydrogen by halogen atoms since the replacement of the hydrogen by halogen provides an easy means of determining the points of attack and thus of measuring the relative reactivities. Such reactivities have been measured for a variety of compounds.

The abstraction of atoms by organic radicals rather than halogen has not been studied to the same extent. In general, organic radicals abstract atoms to form molecules which can be measured, but the new radicals formed in the process undergo coupling and disproportionation reactions and the analysis of the position of attack is difficult. The reactivities of the atoms in simple molecules containing only two types of abstractable atoms have been studied where the products formed from the attacking radicals can be measured and used to indicate reactivities.

Alcock and Whittle,² for example, have studied the abstraction of hydrogen and chlorine from the chloromethanes with trifluoromethyl radicals in the vapor phase. Fluoroform and chlorotrifluoromethane were the products, and the yields provided reactivities of the hydrogen and chlorine. Similarly, reactions of phenyl radicals³⁻⁵ and methyl radicals⁶ with chlorinated methanes have been studied.

A procedure is reported here for analyzing the radicals formed when atoms are abstracted from haloalkanes by fluoroalkyl radicals. In this procedure the radicals generated from the haloalkanes are trapped in a telomerization reaction utilizing tetrafluoroethylene and in so doing new abstracting radicals are formed in the reaction mixture.

The chloromethanes were chosen as a starting point for these studies because of the data already available on their reactivities with trifluoromethyl radicals² and the relatively direct analytical solution.

Results

Telomerizations of the chloromethanes with tetrafluoroethylene were carried out under conditions in which less than 2% of the chloromethane and 34-60%

(1) For example see W. A. Pryor, "Free Radicals," McGraw-Hill, New York, N. Y., 1966, pp 149-199.

(2) W. G. Alcock and E. Whittle, *Trans. Faraday Soc.*, **62**, 664 (1966).

(3) D. H. Hey and J. Peters, *J. Chem. Soc.*, 79 (1960).

(4) G. A. Razuvaev, Yu. A. Ol'dekop, and I. F. Bagaev, *Dokl. Akad. Nauk SSSR*, **74**, 73 (1950).

(5) G. A. Razuvaev and Yu. A. Ol'dekop, *Zh. Obshch. Khim.*, **19**, 736 (1949).

(6) F. A. Raal and E. W. R. Steacie, *J. Chem. Phys.*, **20**, 578 (1952); R. J. Cvetanovic, F. A. Raa, and E. W. R. Steacie, *Can. J. Chem.*, **31**, 171 (1953).

of the tetrafluoroethylene were incorporated into the telomeric product.

The reaction was initiated by the thermal decomposition of benzoyl peroxide for which the rate of decomposition is known⁷ and for which the mode of reaction of the intermediate phenyl radicals with chloroalkanes is known.³⁻⁵ The product consisted of compounds having a wide range of molecular weights so they were separated into two fractions by acetone extraction.

Elemental analyses of both fractions were used to determine an overall chain-transfer constant for the reaction, which is a measure of reactivity. However, the total sample could not be used for nmr end group analysis because of lack of solubility. Nmr spectra were made of only the fractions which had been extracted by acetone. Samples for analyses were dissolved in deuteriobenzene, 50% solutions, and analyzed at 80° with both Varian A-60 and HA-100 nmr spectrometers. The signals were not strong since the telomer molecules had a molecular weight averaging 1000 and contained only one to three protons. The assignments of bands were made by comparison with known spectra.⁸⁻¹¹

Since the areas of the nmr peaks are equal to the molar amounts of the hydrogens, evaluation of reactivities of both hydrogen and chlorine was straightforward.

The chain-transfer constants for each bond broken, representing also the relative reactivities, are given in Table I.¹²

Table I: Reactivities of Atoms to Abstraction

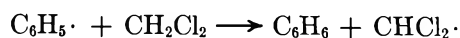
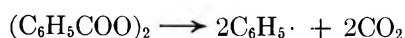
Atom	Chain-transfer liquid phase ^a	CF ₃ · gas phase ^b	Chlorination ^c
CCl ₃ -H	4.0	41.0	1.00
CHCl ₂ -H	2.3	17.0	6.05
CH ₂ Cl-H	1.4	3.4	5.27
CCl ₃ -Cl	1.9	12.0	
CHCl ₂ -Cl	1.0	1.0	
CH ₂ Cl-Cl	0.72	0.16	
CH ₃ -Cl	0.35	0.00005	

^a This work, 125°. Results reported as relative reactivities, with that of chlorine abstraction from chloroform given the value of 1.0. ^b Results of Alcock and Whittle² extrapolated to 125°. ^c Chlorination rates of Knox¹² extrapolated to 125°.

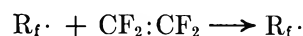
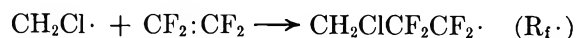
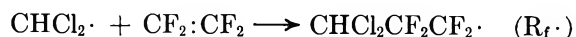
Discussion

Telomerization reactions with tetrafluoroethylene provide a unique method for determining the reactivities of atoms to abstraction by fluoroalkyl radicals. The series of reactions involves essentially four steps, illustrated below with methylene chloride as an example.

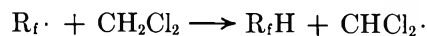
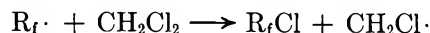
I. Initiation



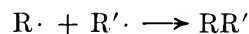
II. Propagation



III. Chain Transfer



IV. Termination



Two of these steps involve the abstraction of an atom from a chloroalkane, the initiation and the chain transfer.

Initiation involves the reaction of phenyl radicals with the chloroalkane. This has been studied and shown to result only in hydrogen abstraction, except for perchlorocarbons.³⁻⁵

Chain transfer provides the measure of reactivity of hydrogen and chlorine to abstraction by a fluoroalkyl radical. For this measure to be valid, the extent of chain transfer must be large by comparison to the initiation by benzoyl peroxide. That this is so is evidenced by first the extensive chlorine abstraction which would not have occurred with phenyl-radical abstraction, and second the relatively low, 52%, yield of benzene from the decomposition of benzoyl peroxide in the presence of chloroalkane under the conditions used in this study.¹³ That phenyl radicals did not initiate many telomer chains was indicated by the small signal for phenyl hydrogens in the nmr spectra of the products. Chain termination has little effect on the results also because of the apparently large number of chain-transfer reactions compared with the number of initiation and, consequently, termination steps. Further, the results of reactivity are similar in sequence but not magnitude to those reported by Alcock and Whittle² using trifluoromethyl radicals in the vapor phase. The differences that are observed can be due to either the dif-

(7) C. Walling, "Free Radicals in Solution," Wiley, New York, N. Y., 1957, p 474 ff.

(8) H. F. White, *Anal. Chem.*, **36**, 1291 (1964).

(9) H. F. White, *ibid.*, **37**, 403 (1965).

(10) Y. Yukawa, Ed., "Handbook of Organic Structural Analysis," W. A. Benjamin, New York, N. Y., 1965, pp 469-489.

(11) J. W. Emsley, J. Feeney, and L. H. Sutcliffe, "High Resolution Nuclear Magnetic Resonance Spectroscopy," Vol. 2, Pergamon Press, New York, N. Y., 1966, pp 1115-1129.

(12) J. H. Knox, *Trans. Faraday Soc.*, **58**, 275 (1962).

(13) The 52% yield was observed in an experiment at the conditions used in the remainder of this study. No chlorobenzene was found and the remainder of the products were not identified. Any biphenyl formed in the telomerization experiments would have remained with the acetone-soluble telomer. The relatively small nmr signal for aromatic hydrogens indicates that this is not a significant product.

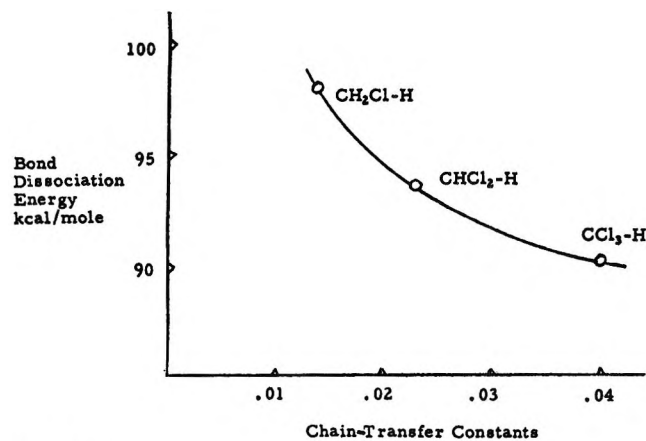


Figure 1.

ferences of the radicals involved^{14,15} or the differences of phase¹⁶ or both.¹⁷ Because the differences of the reactivities of chlorine abstraction are significantly different from those of hydrogen abstraction, it is felt that the transition state is significantly polar and that solvent effects are probably the major difference.

Hydrogen Abstraction. The ease of hydrogen abstraction increases with increasing chlorine content, inversely to the bond energies. Indeed, the chain-transfer constants for the hydrogens in the chloromethanes correlate well with the measured bond energies,¹⁸ as seen in Figure 1.

Two factors of opposite influence are expected to have an effect on the reactivity of the hydrogens. The inductive effect of the chlorine would reduce the ease of hydrogen abstraction, whereas resonance stabilization of the transition state would increase the reactivity. In the present study, additional chlorine increases the reactivity, so that resonance stabilization of the transition state is more important than the incremental inductive increase.

In regard to the properties of fluoroalkyl radicals, it is of interest to compare them with chlorine atoms. In chlorination of the chloromethanes there is a slight increase in reactivity with increasing amounts of chlorine on the carbon, but with a sharp decrease for chloroform. It is proposed, therefore, that in the transition state of hydrogen abstraction by fluoroalkyl radicals, that there is more bond breaking than in the same abstraction by chlorine atoms. This leads to a larger influence of resonance in the transition state.

The difference of reactivity between chlorine atoms and fluoroalkyl radicals cannot be due to the electronegativity since the groups are about equal on the Pauling scale.¹⁹ One possible explanation is their difference of polarizability.²⁰

Chlorine Abstraction. The reactivity of chlorine to abstraction by fluoroalkyl radicals increases with chlorine content in the molecule in a pattern similar to that of hydrogen abstraction. It also can be correlated to bond energies,¹⁸ and the arguments of the effects of substituents would be similar.

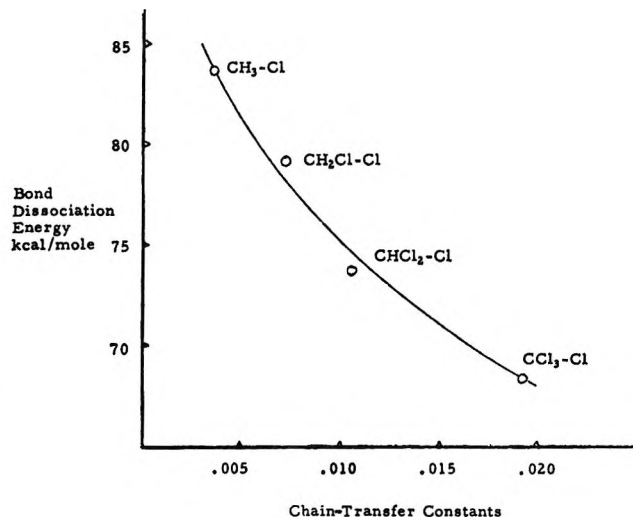


Figure 2.

Experimental Section

In order to obtain results which could be compared as directly as possible, a standard set of conditions was chosen for the telomerization runs of the various chlorinated methanes. A typical run is described here, and the results of the series are given in Table II.

To a 300-cc autoclave²¹ were charged 80 g of chloroalkane and 1.6 g of benzoyl peroxide. The autoclave was closed, cooled to about -70° in a Dry Ice-acetone bath, evacuated to below 50 mm pressure, and charged with tetrafluoroethylene²² from a cylinder. The line from the cylinder to the autoclave was evacuated before the tetrafluoroethylene was fed to reduce the quantity of oxygen in the reaction system. Usually more than the desired 20 g of tetrafluoroethylene was charged to the autoclave. The slight excess was bled off after the autoclave had warmed slightly.

The autoclave was stirred and heated. It required

(14) S. J. W. Price and K. O. Kutschke, *Can. J. Chem.*, **38**, 2128 (1960).

(15) P. P. Infelta and R. H. Schuler, *J. Phys. Chem.*, **73**, 2083 (1969).

(16) For a discussion of the differences of reactions of radicals in the liquid phase and the vapor phase see: F. R. Mayo, *J. Amer. Chem. Soc.*, **89**, 2654 (1967).

(17) A reviewer has pointed out the possibility that since part of the telomer is insoluble under some conditions that some of the reactive radicals might be buried, thus resulting in the relatively small difference of reactivity observed. It seems though, in comparing the rates of chlorination, that the vapor phase abstraction by $CF_3\cdot$ radicals are the anomalous results. See also the chlorination of the chloroethanes, C. Cillien, P. Goldfinger, G. Huybrechts, and G. Martens, *Trans. Faraday Soc.*, **63**, 1631 (1967).

(18) Yu. Papulov, *Zh. Obshch. Khim.*, **34**, 1252 (1964).

(19) J. J. Lagowski, *Quart. Rev. Chem. Soc.*, **13**, 233 (1959).

(20) J. W. Le Fevre, *Rev. Pure Appl. Chem.*, **20**, 67 (1970).

(21) The reaction vessel was a Parr Magnedash autoclave of 316 stainless steel.

(22) The tetrafluoroethylene used in this study was purchased from Peninsular ChemResearch of Gainesville, Fla. It is sold as 99.9% purity containing 1% α -pinene as an inhibitor.

Table II: Telomerization of Halomethanes with Tetrafluoroethylene^a

Experi- ment no.	Telogen	wt, g	Moles	C ₂ F ₄ , mol	Pressure, psig	\bar{n}^b	Chain-transfer constant ^{c, d}		
							Telogen	H	Cl
1	Chloromethane	80	1.5845	0.200	650.0	13.24	0.0115	0.014	0.0035
2	Dichloromethane	80	0.9420	0.200	250.0	10.89	0.0151	0.023	0.0072
3	Trichloromethane	80	0.6701	0.200	225.0	11.15	0.0176	0.040	0.010
4	Tetrachloromethane	80	0.5201	0.200	190.0	12.90	0.0192		0.019

^a These runs were made using the standard procedure described in the Experimental Section. ^b The average chain length, \bar{n} , was determined by elemental analysis indicating the degree of incorporation of fluorine in the final product. ^c The chain-transfer constant was determined by the method of Walling, see ref 23. ^d The uncertainty of these values is estimated to be about 5%.

2–4 hr to reach 125° where it was held for 1 hr. After cooling, the excess tetrafluoroethylene was bled off into a trap cooled in a Dry Ice–acetone bath, the bomb was opened, and the contents transferred to a still. Methylene chloride or ether was used to rinse the last material out. Distillation separated the wash liquid and the excess telogen from the telomer product which was left as a residue. The residue was extracted with acetone to give two portions. The two portions were then analyzed for chlorine and fluorine to determine the average molecular weight. The chlorine analysis is the most significant, and results from these analyses were used in calculating the molecular weight and the degree of telomerization " \bar{n} ."

$$\text{mol wt telomer} = \frac{3545.3 \times (\text{no. Cl in telogen})}{\% \text{ Cl (from analysis)}}$$

$$\bar{n} = \frac{3545.3 \times (\text{no. Cl in telogen}) - \% \text{ Cl} \times (\text{mol wt telogen})}{\% \text{ Cl} \times (\text{mol wt C}_2\text{F}_4)}$$

The fluorine analysis was used as a check of these results.

$$\bar{n} = \frac{\% \text{ F} \times (\text{mol wt telogen})}{4 \times 18.998 \times 100 - \% \text{ F} \times (\text{mol wt C}_2\text{F}_4)}$$

mol wt telomer =

$$\text{mol wt telogen} + \bar{n} \times \text{mol wt C}_2\text{F}_4$$

For determining the chain-transfer constant and subsequently the relative reactivities the following steps were used. The total pressure was observed, the partial pressure of telogen was estimated from a vapor pressure curve, and the difference of pressure was assumed to be due to tetrafluoroethylene. The amount of tetrafluoroethylene in the vapor state

$$P_{\text{C}_2\text{F}_4} = P_{\text{total}} - P_{\text{telogen}}$$

was then estimated by the gas equation, where the volume was that volume above the liquid phase. Then

$$PV = nRT$$

the concentration of tetrafluoroethylene in the liquid phase could be calculated.

$$\text{C}_2\text{F}_{4\text{soln}} = \text{C}_2\text{F}_{4\text{total}} - \text{C}_2\text{F}_{4\text{vapor}}$$

The chain-transfer constant was calculated by the method of Walling.²³

$$C = \frac{1}{\bar{n}} \frac{[\text{C}_2\text{F}_4]}{[\text{telogen}]}$$

Nmr spectra of the acetone-soluble portion were obtained using Varian A-60 and HA-100 spectrometers. The sample was dissolved in deuteriobenzene at 80° to make a 50% solution, and the spectra were obtained at 80°. The signal from the A-60 was weak so was amplified by utilizing a computer average of 30 scans. A single scan was satisfactory when using the HA-100. The relative areas of the signals representing the various hydrogens, see Table III, were measured and used with

Table III: Nmr Results^a

Telogen	Group	Chem shift, ^b ppm of δ
CH ₃ Cl	CH ₃ CF ₂ -	2.4
	CH ₂ ClCF ₂ -	3.3–3.6
	HCF ₂ CF ₂ -	6.1
CH ₂ Cl ₂	CH ₂ ClCF ₂ -	3.4–3.7
	CHCl ₂ CF ₂ -	5.4
	HCF ₂ CF ₂ -	6.1
CHCl ₃	CHCl ₂ CF ₂ -	5.3
	HCF ₂ CF ₂ -	6.0

^a These results were obtained on Varian HA-100 and A-60 nmr spectrometers using C₆D₆ as solvent and operating with the probe at 80° to increase solubility. ^b TMS was used as an internal standard.

the overall chain-transfer constant to calculate a chain-transfer constant for the individual atoms

$$\frac{x\text{C}_{\text{Cl}} + y\text{C}_{\text{H}}}{x + y} = C$$

(23) C. Walling, "Free Radicals in Solution," Wiley, New York, N. Y., 1957, p 150.

where x = no. Cl atoms, y = no. H atoms and

$$\frac{C_{\text{Cl}}}{C_{\text{H}}} = \frac{\text{nmr area for } -\text{CCl}_{x-1}\text{H}_y}{\text{nmr area for } -\text{CF}_2\text{H}}$$

The results of these calculations are presented in Table I.

Acknowledgment. Appreciation is expressed to C. B. Strow, Jr., who assisted in obtaining the nmr spectra.

Photolytic Reactions of 1,3-Diphenylpropene¹

by E. W. Valyocsik and Paul Sigal*

Department of Chemistry, University of Detroit, Detroit, Michigan 48221 (Received September 8, 1970)

Publication costs borne completely by The Journal of Physical Chemistry

The kinetics of photoisomerization of the *cis* and *trans* isomers of 1,3-diphenylpropene has been studied in cyclohexane at 2537 Å at 25°. No photostationary state is attained between the geometrical isomers of 1,3-diphenylpropene because of the depletion which results from the high rate of polymer formation during photolysis. The primary quantum yields of all products except polymer have been measured. It has been observed that 1,3-diphenylpropene cyclizes to 1,2-diphenylcyclopropane with a quantum yield of 5×10^{-3} . A reaction scheme postulating two diradical intermediates has been proposed to account for the observed distribution of photoproducts.

Introduction

In the course of an investigation of the kinetics of the photoisomerization of 1,2-diphenylcyclopropane,² a study of the photolytic reactions of the geometrical isomers of 1,3-diphenylpropene at 2537 Å was undertaken. These geometrical isomers had been produced by ring opening during the photolysis of 1,2-diphenylcyclopropane. The results of the work on the photolytic reactions of 1,3-diphenylpropene are reported here.

Experimental Section

Materials. A base-catalyzed condensation³ was employed in the preparation of *trans*-1,3-diphenylpropene. The *trans*-1,3-diphenylpropene was purified by elution from an alumina column with *n*-hexane followed by recrystallization several times from *n*-hexane. After solvent removal, the *trans*-1,3-diphenylpropene was further purified by gas chromatography, using a 3/8 in. o.d. \times 10 ft 15% SE-30 column operating at 170°. The collected sample was 98.3% *trans*-1,3-diphenylpropene with the remainder being the *cis* isomer. The presence of the 966 cm^{-1} absorption in the infrared spectrum verified the *trans* geometry.^{4,5}

cis-1,3-Diphenylpropene may be obtained by the hydrogen reduction, in the presence of Lindlar's catalyst,⁶ of 1,3-diphenylpropyne,⁷ which is prepared by the action of phenylethynylmagnesium bromide on benzyl *p*-toluenesulfonate,⁸ but it was found that a photochemical procedure similar to that of Raunio and Bonner⁹

was the most convenient route for preparing adequate quantities of *cis*-1,3-diphenylpropene for this work. In this procedure 0.53 g of pure *trans*-1,3-diphenylpropene was dissolved in 5 ml of cyclohexane. This solution was photolyzed with cooling at 2537 Å in a degassed quartz tube in the center of a 1600-W Hanovia SC-2537 helical coil low-pressure mercury lamp. After photolysis, the polymer was crystallized out of solution by placing the reaction tube into liquid nitrogen. The soluble reaction mixture was then decanted from the crystallized polymer. After removal of the cyclohexane, the *cis*-1,3-diphenylpropene was separated from the reaction mixture by gas chromatography. The collected sample of oily liquid was colorless and had an isomeric purity of 97.3% *cis*-1,3-diphenylpropene.

The preparation and purification of *cis*- and *trans*-1,2-diphenylcyclopropane, 1-phenylindene, 1-phenyl-

(1) Abstracted from the Ph.D. dissertation of E. W. Valyocsik, University of Detroit, 1969.

(2) E. W. Valyocsik and P. Sigal, *J. Org. Chem.*, **36**, 66 (1971).

(3) R. Stoermer, C. Thier, and E. Laage, *Chem. Ber.*, **B58**, 2607 (1925).

(4) J. E. Kilpatrick and K. S. Pitzer, *J. Res. Nat. Bur. Stand.*, **38**, 191 (1947).

(5) R. S. Rasmussen and R. R. Brattain, *J. Chem. Phys.*, **15**, 131 (1947).

(6) H. Lindlar, *Helv. Chim. Acta*, **35**, 450 (1952).

(7) J. R. Johnson, T. L. Jacobs, and A. M. Schwartz, *J. Amer. Chem. Soc.*, **60**, 1887 (1938).

(8) R. S. Tipson, *J. Org. Chem.*, **9**, 239 (1944).

(9) E. K. Raunio and W. A. Bonner, *ibid.*, **31**, 396 (1966).

indane, 1,3-diphenylpropane, and bibenzyl has previously been described.² The cyclohexane used as the solvent in all photolyses was spectrophotometric grade¹⁰ and was transparent to 2537-Å radiation. This solvent was used as received without further purification.

Apparatus. The optical bench, light source, and chemical actinometry employed in our kinetic studies have been described in detail elsewhere.²

Procedure. A 22 mm o.d. cylindrical cell of "suprasil" quartz with a 1 mm path length was used for the photolytic reactions. The procedure was to begin with either geometrical isomer of 1,3-diphenylpropene and observe the growth of products with irradiation time. Solutions near $2.8 \times 10^{-4} M$ were made up with the purified isomers of 1,3-diphenylpropene in cyclohexane. These concentrations were chosen so that the incident radiation would not be totally absorbed during photolysis. The transmitted radiation was continuously monitored during a run on the optical bench by detection with an RCA 935 phototube and by passing the d.c. signal into a strip chart recorder. These charts were retained for quantum yield calculations. For each run an aliquot of starting solution was transferred to the cell, and at the same time an aliquot of starting solution was frozen down for later analysis to determine the initial concentrations of solution components. The cell was then degassed on a grease-free vacuum line five times by the freeze-pump-thaw procedure at a pressure of 5×10^{-6} Torr before sealing off under vacuum. The solutions were irradiated for varying times at 2537 Å on the optical bench with periodic mixing during photolysis.

Analysis. The irradiated solutions were analyzed by gas chromatography with a 1/4 in. o.d. \times 10 ft 15% SE-30 column on 60-80 mesh NAW Chromasorb P, using flame ionization detection. Bibenzyl was employed as an internal standard. After irradiation, the cell was opened and a measured quantity of bibenzyl solution was added to the cell and thoroughly mixed. All products were identified by comparing the retention times and infrared spectra with those of authentic samples. The concentrations of photolytic products were determined from area ratios by employing calibrated conversion factors. The final component concentrations were corrected for the values determined from the aliquot of initial solution.

The primary quantum yields of photoproducts were calculated from the corrected product concentrations and the total quanta absorbed by the substrate for runs with less than 4% conversion of the initial substrate. The light absorbed by the initial substrate alone was calculated by a method described by Ishakawa and Noyes.¹¹ Corrections were also made for any decrease in incident light intensity during a run.

Results and Discussion

Photolysis of cis-1,3-Diphenylpropene. Figure 1

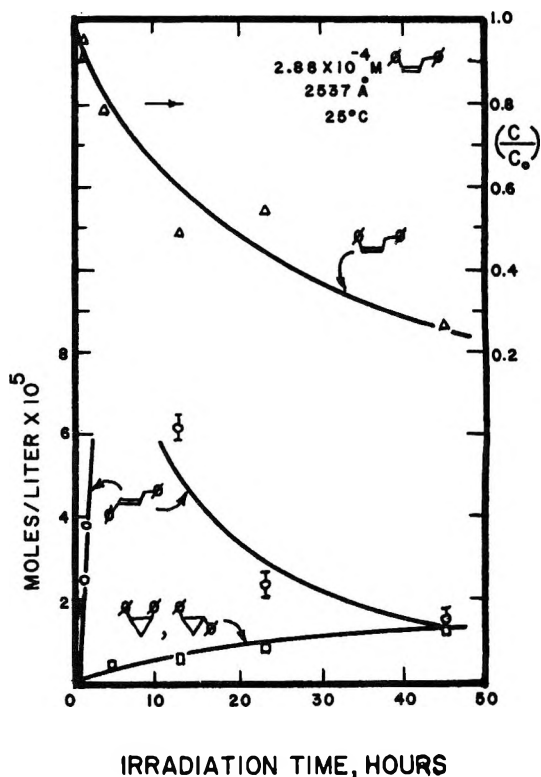


Figure 1. Photolysis of $2.88 \times 10^{-4} M$ *cis*-1,3-diphenylpropene in cyclohexane at 25° with 2537-Å radiation.

shows the results for the photolytic reaction of *cis*-1,3-diphenylpropene at room temperature. The growth of products during photolysis was followed from short exposure times. The product yields shown in the figures represent a separate irradiation with a fresh sample. The disappearance of *cis*-1,3-diphenylpropene is indicated in terms of the ratio of the concentration at the end of an exposure interval to the initial concentration (c/c_0). One significant observation to be made about the photolytic reaction of *cis*-1,3-diphenylpropene is the very large mass deficiency that results with prolonged irradiation of the solution. The *trans*-1,3-diphenylpropene yield increases initially, but with continued photolysis its concentration decreases. This drastic deviation from mass balance as the photoreaction continues may be explained by a high yield of polymer. The polymer is not observed by gas chromatographic analysis, but preparatory-scale photolyses of the 1,3-diphenylpropenes, mentioned earlier, do produce visible quantities of polymer in the reaction vessel. This polymer was not characterized.

In agreement with Griffin and coworkers¹² it was observed that *cis*-1,3-diphenylpropene does cyclize to 1,2-

(10) James Hinton, 268 Ewing Court, N. W. Ft. Walton Beach, Fla.

(11) H. Ishakawa and W. A. Noyes, Jr., *J. Chem. Phys.*, **37**, 583 (1962).

(12) G. W. Griffin, J. Covell, R. C. Petterson, R. M. Dodson, and G. Klöse, *J. Amer. Chem. Soc.*, **87**, 1410 (1965).

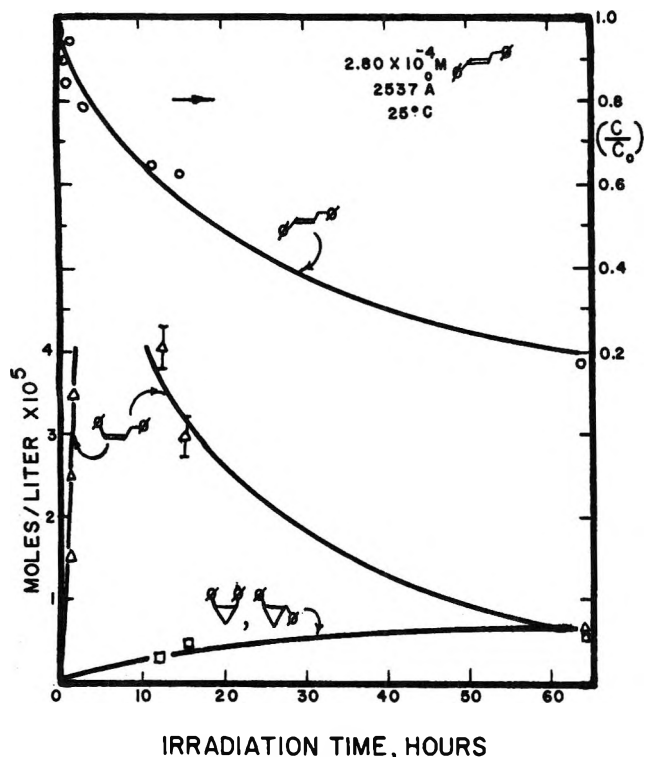


Figure 2. Photolysis of $2.80 \times 10^{-4} M$ *trans*-1,3-diphenylpropene in cyclohexane at 25° with $2537\text{-}\text{\AA}$ radiation.

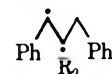
diphenylcyclopropane. Under the experimental conditions used the cyclization yields are small. Equal yields of both *cis*- and *trans*-1,2-diphenylcyclopropane were produced. Other products looked for but not observed were 1-phenylindane, 1-phenylindene, 1,2-diphenylpropene, 1,2-diphenylpropane, and 1,3-diphenylpropene. The lower limit of detectability of the analytical method is $1 \times 10^{-6} M$ concentration, which corresponds to a lower limit of 10^{-4} for the product quantum yields.

Photolysis of *trans*-1,3-Diphenylpropene. The photolytic reactions of *trans*-1,3-diphenylpropene were examined in the same manner as those of the *cis* isomer. The results are shown in Figure 2. In this case the *cis*-1,3-diphenylpropene yield is observed to increase at short irradiation times and then to drop off. Again, very pronounced deviations from mass balance were observed with continued photolysis. The question arose as to whether or not this mass loss was resulting from loss of sample through cyclization and subsequent polymerization of the initial substrate. A sample of $1.39 \times 10^{-3} M$ *trans*-1,3-diphenylpropene was photolyzed for 12 hr. After this irradiation period, a 15% mass deficiency was observed. A comparable exposure time produced no mass deficiency during photolysis of 1,2-diphenylcyclopropane.² The mass deficiency is attributed to the high rate of polymer formation from *trans*- and *cis*-1,3-diphenylpropene during photolysis. The back reaction from polymer is probably insignificant,

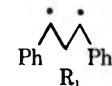
since the mass deficiency becomes quite pronounced with continued irradiation. It appears that no photo-stationary state between the geometrical isomers of 1,3-diphenylpropene can be reached because of mass depletion that results from polymer formation.

Equal yields of *cis*- and *trans*-1,2-diphenylcyclopropane were again observed. The independence of the *cis/trans* 1,2-diphenylcyclopropane mole ratio on 1,3-diphenylpropene isomer implies a common intermediate for these structural isomers. It appears that once the intermediate is formed it can go *cis* or *trans* without preference. The products listed above that were not observed in the photolytic reaction of *cis*-1,3-diphenylpropene were also not observed in the case of the *trans*-1,3-diphenylpropene photolysis at room temperature.

The photoisomerization of 1,3-diphenylpropene can be most easily visualized as proceeding through a dirad-



ical intermediate R_2 . The unsymmetrical diradical of the type R_2 has a previous history and has been proposed as an intermediate in polymerization reactions.¹³ The cyclized products, *cis*- and *trans*-1,2-diphenylcyclopropane, can be accounted for by postulating a trimethylene diradical, R_1 , which could be formed from R_2 by hydrogen or phenyl migration^{2,14} or by hydrogen abstraction from solvent molecules. The extent of sol-



vent participation in this rearrangement is unknown at the present time. The diradical R_2 would provide an easy path to polymer formation if the rate constant for the conversion of R_2 into R_1 was much less than the rate constant for polymer formation from R_2 .

If the rearrangement of diphenylpropene to diphenylcyclopropane were to proceed by a concerted mechanism, it might be expected that the rates of production of the cyclized geometrical isomers would be dependent upon the geometry of the initial diphenylpropene isomer. The paths taken along the potential *cis*-1,3-diphenylpropene should differ from the paths taken along the surface from *trans*-1,3-diphenylpropene;¹⁵ hence, one would expect different activation energies for the processes. However, the yields and rates of production of both geometrical isomers of 1,2-diphenylcyclopropane are found to be equal and independent of the geometry of the initial 1,3-diphenylpropene isomer.

Primary Quantum Yields for 1,3-Diphenylpropene Reactions. Runs of less than an hour total irradiation time were used for determining the primary quantum



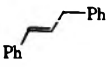
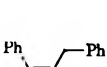
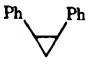
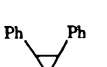
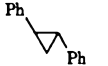

(13) P. J. Flory, *J. Amer. Chem. Soc.*, **59**, 24 (1937).

(14) G. W. Griffin, A. F. Marcantonio, and H. Kristinsson, *Tetrahedron Lett.*, 2951 (1965).

(15) W. Th. A. M. van der Lugt and L. J. Oosterhoff, *J. Amer. Chem. Soc.*, **91**, 6042 (1969).

yields of products. The quantum yields were determined at less than 4% conversion of the initial substrates. The results shown in Table I are the average of three runs and reflect the initial slopes of the product yield curves.

Table I: Primary Quantum Yields for 1,3-Diphenylpropene Reactions

1,3-Diphenylpropene isomer	Photolysis Φ	1,2-Diphenylcyclopropane isomer	Photolysis Φ
			
	0.139 ± 0.005		0.121 ± 0.003
	5×10^{-3}		4×10^{-3}
	5×10^{-3}		4×10^{-3}

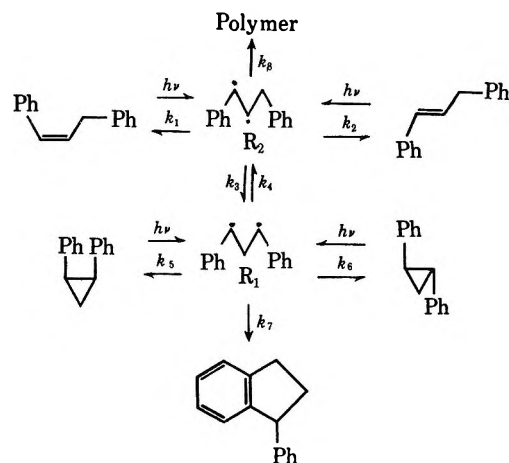
The measured quantum yields for geometrical isomerization of 1,3-diphenylpropene are nearly equal. This result is consistent with the observation that neither 1,3-diphenylpropene isomer dominates when these products are produced by branching during photolysis of 1,2-diphenylcyclopropane.² An equilibrium is probably rapidly established between the 1,3-diphenylpropene isomers during photolysis of 1,2-diphenylcyclopropane. From the results recorded in Table I it is apparent that less than 14% of the absorbed energy is being utilized for geometrical isomerization. The quantity of energy consumed in producing polymer is not known, since the yield of polymer was not determined. At present no data are available on the radiative and radiationless processes operative in this system.

The cyclization yields of 1,2-diphenylcyclopropane from either isomer of 1,3-diphenylpropene are small. The equal yields of 1,2-diphenylcyclopropane implies equal rates of formation of these products from a common intermediate.

The other possible products, 1-phenylindane, 1-phenylindene, 1,2-diphenylpropene, 1,2-diphenylpropane, and 1,3-diphenylpropane, must be formed with $\Phi < 10^{-4}$, if they are formed at all.

Mechanism. The results obtained can be accounted for in a reasonably consistent manner by postulating at least two diradical intermediates of the type R_1 and R_2 . The reaction scheme below is consistent with the distribution of photoproducts observed during photolysis of 1,3-diphenylpropene and 1,2-diphenylcyclopropane.²

The results of the photoisomerization of 1,2-diphenyl-



cyclopropane showed that the equal yields of *cis*- and *trans*-1,3-diphenylpropene implied that $k_1 = k_2$. The formation of 1-phenylindane during 1,2-diphenylcyclopropane photolysis was found to be an irreversible reaction.² In the present study of 1,3-diphenylpropene equal yields of the geometrical isomers of 1,2-diphenylcyclopropane were found, implying that $k_5 = k_6$. Since 1-phenylindane was not observed as a product during photolysis of 1,3-diphenylpropene, this suggests that $k_7 < k_5$.

During photolysis of 1,2-diphenylcyclopropane, geometrical isomerization is favored over branching into olefins by a ratio of 4:1. The rate of formation of polymer from 1,2-diphenylcyclopropane is also lower than the rate of polymer formation from 1,3-diphenylpropene, as the mass deficiency indicates. The symmetric diradical R_1 may be more resonance stabilized, and the slow step in the process may be the formation of R_2 from R_1 . Hence $k_5 > k_4$.

Since geometrical isomerization and polymer production dominates over cyclization during 1,3-diphenylpropene photolysis, it would appear that $k_3 < k_1$, k_8 . Again the slow step in the process is probably the formation of R_1 from R_2 .

Attempts were made to intercept the postulated radical intermediates by photolyzing 1,2-diphenylcyclopropane with iodine.² These experiments did not prove successful. Other workers have also been unsuccessful in scavenging radical intermediates in these and similar systems.^{12,16,17}

Acknowledgment. E. W. V. wishes to thank the National Science Foundation for financial support under a traineeship held during the period 1966-1969.

(16) G. S. Hammond and R. S. Cole, *J. Amer. Chem. Soc.*, **87**, 3256 (1965).

(17) R. C. Cookson, M. J. Nye, and G. Subrahmanyam, *Proc. Chem. Soc.*, 144 (1964).

Direct Determination of Singlet \rightarrow Triplet Intersystem Crossing Quantum Yield. II. Quinoline, Isoquinoline, and Quinoxaline

by Steven G. Hadley

Department of Chemistry, University of Utah, Salt Lake City, Utah 84112 (Received November 10, 1970)

Publication costs assisted by the National Science Foundation

The quantum yields for radiationless singlet \rightarrow triplet intersystem crossing of several aza-substituted molecules have been determined under well-characterized experimental conditions. In a rigid alcoholic glass at 77°K the quantum yields and their uncertainties were found to be: quinoline, 0.50 ± 0.1 ; isoquinoline, 0.24 ± 0.05 ; quinoxaline, 0.18 ± 0.04 . In a hydrocarbon glass at 77°K these values were determined to be: quinoline, 0.43 ± 0.08 ; isoquinoline, 0.19 ± 0.04 ; quinoxaline, 0.27 ± 0.05 . Within the stated error no significant enhancement of the intersystem crossing quantum yield is observed in changing the rigid glass from a hydrocarbon to hydroxylic medium. The data imply significant internal conversion from the first excited singlet for quinoline in a hydrocarbon matrix and quinoxaline in hydrocarbon and hydroxylic matrices.

Introduction

The radiative and radiationless processes in aromatic molecules have been the subject of considerable theoretical and experimental effort during the last 20 years.¹ The aza-substituted aromatic systems have been of particular interest. Cohen and Goodman have discussed these processes in three azabenzene.² We wish to report direct measurement of the intersystem crossing quantum yield of three aza-substituted naphthalenes: quinoline (1-azanaphthalene); isoquinoline (2-azanaphthalene); and quinoxaline (1,4-diazanaphthalene). These systems were chosen for study as there are already considerable data available in the literature regarding their radiative properties. Also, there have been some theoretical investigations directed at these particular systems. However, quantitative knowledge of a process as fundamental as intersystem crossing is not available. The work reported in this paper is directed toward obtaining some of this information.

The experimental reports on the emission properties of these molecules are in general agreement. The parent hydrocarbon, naphthalene, when dissolved in either a hydrocarbon or hydroxylic rigid glass at 77°K, emits both fluorescence and phosphorescence when excited by ultraviolet radiation absorbed by its singlet \leftarrow singlet bands.³ Under similar experimental conditions quinoline emits both fluorescence and phosphorescence in a hydroxylic glass. Early investigators have reported no fluorescence from quinoline in a hydrocarbon glass, only phosphorescence.⁴ Recently, very weak fluorescence from quinoline in a hydrocarbon glass has been reported.⁵ Isoquinoline dissolved in a hydrocarbon solvent under similar experimental conditions emits phosphorescence and weak fluorescence. Isoquinoline's fluorescence to phosphorescence ratio is

greatly enhanced in a hydroxylic medium over that observed in a hydrocarbon medium.⁶ Quinoxaline emits only phosphorescence under these experimental conditions in either a hydrocarbon or a hydroxylic solvent.⁴

The electronic states of these molecules have been studied by several investigators. This knowledge is summarized in Figure 1. The lowest excited electronic states of singlet and triplet multiplicity of quinoline and isoquinoline in rigid glasses at 77°K appear to be (π , π^*).⁶ It has been suggested⁴ that the lowest excited singlet state of quinoline in a hydrocarbon rigid glass is (n , π^*); however, this is not apparent from the absorption spectrum. It is believed that in these molecules the lowest $^1(n, \pi^*)$ state has slightly greater energy than the lowest $^1(\pi, \pi^*)$ state.⁷ The vibronic interactions that would occur between nearly degenerate $^1(n, \pi^*)$ and $^1(\pi, \pi^*)$ states are expected to be strong enough to thoroughly mix these levels. This might reduce the importance of the knowledge of the exact location of the lowest $^1(n, \pi^*)$ and $^1(\pi, \pi^*)$ states.⁶ The energy levels of quinoxaline are better known. The $^1(n, \pi^*)$ and $^3(\pi, \pi^*)$ states are the lowest in energy of their respective multiplicity. A $^3(n, \pi^*)$ state is be-

(1) Much of the information is contained in (a) R. S. Becker, "Theory and Interpretation of Fluorescence and Phosphorescence," Wiley, New York, N. Y., 1969; (b) S. P. McGlynn, T. Azumi, and M. Kinoshita, "Molecular Spectroscopy of the Triplet State," Prentice-Hall, Englewood Cliffs, N. J., 1969.

(2) B. J. Cohen and L. Goodman, *J. Chem. Phys.*, **46**, 713 (1967).

(3) Reference 1a, p 118.

(4) M. A. El-Sayed and M. Kasha, *Spectrochim. Acta*, **15**, 758 (1959).

(5) $\Phi_F < 0.01$, E. C. Lim, private communication.

(6) E. C. Lim and J. M. H. Yu, *J. Chem. Phys.*, **47**, 3270 (1967).

(7) G. Coppens, C. Gillet, J. Nasielski, and E. V. Donck, *Spectrochim. Acta*, **18**, 1441 (1962).

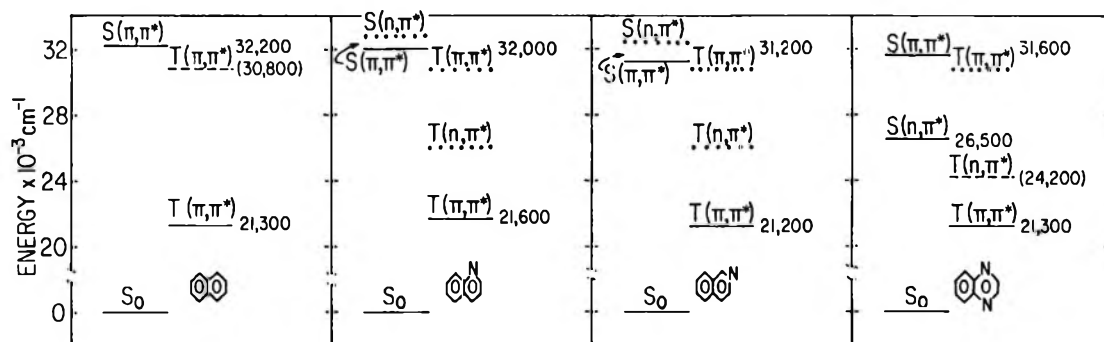


Figure 1. Energy of the lower singlet and triplet states of naphthalene, quinoline, isoquinoline, and quinoxaline. Those levels shown as — have been experimentally observed in the present work. The energy of these states is shown in centimeters⁻¹. Those states that have been observed in pure materials are shown as - - - - - . Their energy in pure materials are shown in parentheses, in centimeters⁻¹. Those states that are anticipated from either studies on the parent hydrocarbon, naphthalene, or from theory are shown as Their energy is not well known.

tween the $^3(\pi, \pi^*)$ and $^1(n, \pi^*)$ states.⁸ A higher $^1(\pi, \pi^*)$ state has been observed. By analogy to naphthalene a $^3(\pi, \pi^*)$ state is believed to have similar energy in all these molecules.

Radiationless processes have been examined in several theoretical frameworks. Henry and Kasha have reviewed this work.⁹ El-Sayed has developed some theoretical predictions based upon assuming the validity of the Born-Oppenheimer approximation.¹⁰ Within this framework he has shown that $S_1(n, \pi^*) \rightsquigarrow T_k(\pi, \pi^*)$ and $S_1(\pi, \pi^*) \rightsquigarrow T_k(n, \pi^*)$ ought to be at least 1000 times as fast as either $S_1(n, \pi^*) \rightsquigarrow T_k(n, \pi^*)$ or $S_1(\pi, \pi^*) \rightsquigarrow T_k(\pi, \pi^*)$. El-Sayed has offered the explanation of the radiative properties of quinoline in terms of an interchange of the $^1(n, \pi^*)$ and $^1(\pi, \pi^*)$ states upon changing the solvent from a hydrocarbon to a hydroxylic medium, the $^1(n, \pi^*)$ state being lowest in the hydrocarbon solvent.⁴ This behavior of the $^1(n, \pi^*)$ and $^1(\pi, \pi^*)$ states is consistent with their known solvent shifts, but the spectroscopic evidence is lacking. He has also compared the emission properties of quinoline and naphthalene in a hydroxylic glass. A comparison of the total emission spectra of these two molecules lead to the conclusions that the rate of intersystem crossing in quinoline is enhanced over that in naphthalene, and that in quinoline radiationless losses from S_1 (other than intersystem crossing) are occurring.¹⁰

Lim and Yu have discussed the mechanism of intersystem crossing in terms of a second-order spin-orbit coupling involving $(n, \pi^*)-(\pi, \pi^*)$ vibronic interactions. They believe that this mechanism plus the "orbital interchange" mechanism can explain the solvent effects upon fluorescence.⁶ Lim and Li have emphasized that nonplanar vibrations may be important in deactivation, *via* internal conversion, of the lowest excited singlet state of nitrogen heterocycles.¹¹

Experimental Section

The previously used experimental technique¹² was modified to permit its extension to molecules whose

triplet state lifetime is as short as 0.2 sec. A flash lamp that dissipated over 16,000 J in less than 100 μsec was used to pump the molecules into the triplet state. For studies on quinoxaline a Corning 7-54 filter was used to isolate the emission region of the lamp that was incident upon the sample. For the studies on quinoline and isoquinoline a filter solution of 200 g of $\text{NiSO}_4 \cdot 6\text{H}_2\text{O}$ and 10 mg of cn^{13} in 1 l. of water was used in a quartz cell to isolate the appropriate radiation. When the absorption spectrum of the filter was compared with that of the corresponding molecule, it was estimated that over 90% of the radiation from the flash lamp incident upon the sample was absorbed by the sample.

Isoquinoline and quinoxaline were obtained from Distillation Products Industries; quinoline was obtained from Matheson Coleman and Bell. The quinoline and isoquinoline were purified by vacuum distillation. The quinoxaline was purified by repeated vacuum sublimation. No impurities with concentrations greater than 1% were observed in any of these materials after purification. Solutions of these solutes were prepared using a mixture of 30% 1-butanol and 70% isopentane by volume as an alcoholic solvent and a mixture of 20% methylcyclohexane and 80% isopentane was used as a hydrocarbon solvent. All solvents were spectrograde supplied by Matheson Coleman and Bell. The methylcyclohexane was distilled from P_2O_5 to remove any residual water that may have been present. The other solvents were used as received. When cooled to the temperature of boiling nitrogen, these two solvent systems formed clear rigid glasses. The solute con-

(8) R. M. Hochstrasser and C. Marzocco, *J. Chem. Phys.*, **49**, 971 (1968).

(9) B. R. Henry and M. Kasha, *Annu. Rev. Phys. Chem.*, **19**, 161 (1968).

(10) M. A. El-Sayed, *J. Chem. Phys.*, **38**, 2834 (1963).

(11) E. C. Lim and Y. H. Li, *Chem. Phys. Lett.*, **4**, 25 (1969).

(12) S. G. Hadley and R. A. Keller, *J. Phys. Chem.*, **73**, 4356 (1969).

(13) *cn* is 2,7-dimethyl-3,6-diazacyclohepta-1,6-diene iodide.

Table I: Intersystem Crossing Quantum Yields

Molecule	Solvent	$\frac{OD(0)}{i_0} \times 10^{-4}$, einstein cm^{-2}	$\epsilon_T \times 10^{-4}$, $\text{l. mol}^{-1} \text{cm}^{-1}$ ^b	Φ_{ISC} ^c	Φ_{IC} ^d
Quinoline	Alcoholic	3.56 ± 0.23	7.1 ± 0.7	0.50 ± 0.1	
Quinoline	Hydrocarbon	2.85 ± 0.30	6.7 ± 0.7	0.43 ± 0.08	0.57 ± 0.08
Isoquinoline	Alcoholic	3.61 ± 0.29	14.9 ± 1	0.24 ± 0.05	
Isoquinoline	Hydrocarbon	2.71 ± 0.25	14.0 ± 1	0.19 ± 0.04	
Quinoxaline ^e	Alcoholic	1.40 ± 0.30	8.1 ± 0.8	0.18 ± 0.04	0.82 ± 0.04
Quinoxaline	Hydrocarbon	2.33 ± 0.30	8.7 ± 0.7	0.27 ± 0.05	0.73 ± 0.05
Naphthalene ^e	Alcoholic	1.15 ± 0.2	40.0 ± 6	0.29 ± 0.06	

^a The alcoholic solvent was a mixture of 30% 1-butanol and 70% isopentane by volume. The hydrocarbon solvent was 20% methylcyclohexane and 80% isopentane. ^b Values from Hadley (see ref 14) or determined in a similar fashion. ^c Uncertainty estimated at $\pm 20\%$. ^d Determined from $\Phi_F + \Phi_{IC} + \Phi_{ISC} = 1$ for those cases where it is known that $\Phi_F = 0$. ^e Values from S. Hadley, *Chem. Phys. Lett.*, **6**, 549 (1970).

centration was adjusted so that most of the light from the flash lamp was absorbed in the first centimeter of the sample.

The sample dewar has been previously described.¹⁴ The optical density of the triplet \leftarrow triplet absorption following the discharge of the flash lamp was measured using a Jarrell-Ash 0.25-m monochromator equipped with a 1P28A photomultiplier. The small optical densities necessitated the use of a Type W preamplifier on a Tektronix 544 oscilloscope to record the time dependence of the change in light transmission of the sample. The analytic beam radiation was supplied by a PEK X-151 high-pressure xenon lamp. The change in the optical density was measured as a function of time. By extrapolating these first-order decay curves to $t = 0$, the initial optical density of the triplet \leftarrow triplet absorption was determined. Typical initial optical densities were of the order of 0.05. We have previously shown that permanent photoinduced changes are unimportant in these systems.¹⁴

After the optical density of the triplet \leftarrow triplet absorption was measured, the sample dewar was removed and a quartz cuvette containing the ferrioxalate actinometer solution was inserted in its place. The previously used actinometry procedure was followed,¹² except bathophenanthroline¹⁵ was used in determining the ferrous ion. Up to 15 flashes were necessary to produce sufficient ferrous ion to permit accurate determination of its concentration on a Cary 14 spectrophotometer. The extinction coefficient of the ferrous ion-bathophenanthroline complex was determined to be $\epsilon_{\text{max}} = 2.21 \times 10^4 \text{ l. mol}^{-1} \text{ cm}^{-1}$. In this fashion values of i_0 were determined. Typical values of i_0 for quinoline and isoquinoline were 5×10^{-9} einstein cm^{-2} flash⁻¹ while for quinoxaline typical values were 2×10^{-8} einstein cm^{-2} flash⁻¹.

Results

The values of the intersystem crossing quantum yield for quinoline, isoquinoline, and quinoxaline in a

hydrocarbon solvent (80% isopentane, 20% methylcyclohexane) and in an alcoholic solvent (70% isopentane, 30% 1-butanol by volume) are shown in Table I. They were calculated from

$$\Phi_{ISC} = \frac{OD(0)}{\epsilon_T i_0} \quad (1)$$

OD(0) is the initial optical density of the triplet \leftarrow triplet absorption at a wavelength where the extinction coefficient is ϵ_T . i_0 is the absolute intensity of the light absorbed by the molecules. The errors shown in Table I for OD(0)/ i_0 are the standard deviations of between three and five separate determinations. The values of ϵ_T have been reported.¹⁴ The values of the $S_1 \rightarrow S_0$ internal conversion quantum yield were calculated in those cases where the fluorescence quantum yield is known to be zero or insignificant relative to Φ_{ISC} .

Our results indicate that within our error there is *no significant change in the intersystem crossing quantum yield in changing the solvent from an alcoholic mixture to a hydrocarbon for each heterocycle*. The values of the intersystem crossing quantum yield for isoquinoline and quinoxaline show no enhancement relative to that previously measured for naphthalene.¹² (See footnote e, Table I.) The value for quinoline is about a factor of 2 greater than that observed for naphthalene.

Discussion

The intersystem crossing quantum yields of aromatic heterocycles have not been extensively studied by previous investigators. Lamola and Hammond¹⁶ have reported values of $\Phi_{ISC} = 0.31$ for quinoline in dry benzene and $\Phi_{ISC} = 0.16$ in moist benzene, both measured at room temperature. Their values were determined using a photosensitized reaction of piperylene. More

(14) S. G. Hadley, *J. Phys. Chem.*, **74**, 3551 (1970).

(15) Bathophenanthroline is 4,7-diphenyl-1,10-phenanthroline.

(16) A. A. Lamola and G. S. Hammond, *J. Chem. Phys.*, **43**, 2129 (1965).

recent work has shown that these values may be low due to complicating side reactions.^{17,18}

El-Sayed has compared the total emission spectra of naphthalene and quinoline in hydroxylic glasses at 77°K.¹⁰ He concluded that there are significant radiationless losses from the first excited singlet state and that the rate of intersystem crossing in quinoline is enhanced relative to that in naphthalene. This is in accord with our findings. However, this agreement may be fortuitous as relative intensities of the phosphorescence emission spectra depend upon both the quantum yields for intersystem crossing and phosphorescence. Reliable phosphorescence quantum yield data are not available.

Lim and Yu have examined the total emission spectra of isoquinoline in EPA (a hydroxylic glass) and 3-methylpentane (a hydrocarbon glass) under experimental conditions similar to ours. They found that the fluorescence intensity was greater in EPA than in 3-methylpentane, while the phosphorescent emission intensity was greater in 3-methylpentane than in EPA. They have interpreted these observations in terms of more efficient intersystem crossing in hydrocarbon solvents than in hydroxylic solvents. This is not in agreement with our results. This discrepancy may be due to a change in the phosphorescence quantum yield with solvent. Until reliable phosphorescence quantum yield data are available, one can only speculate on the effect of solvent on relative phosphorescence intensities. The solvent may change the rate constants of both the radiative and nonradiative decay of the triplet state. The sum of these effects has been observed in the solvent dependency of the triplet state lifetimes of quinoline and isoquinoline.⁶

Conclusions

We have extended our previous measurements on

singlet \rightarrow triplet intersystem crossing quantum yields of aromatic hydrocarbons to aza-substituted aromatics. In principle this technique can be extended to molecules whose triplet state lifetime is as short as 1 msec when the extinction coefficient of triplet \leftarrow triplet absorption bands have been determined.

The intersystem crossing quantum yields of isoquinoline and quinoxaline have been found to be similar to that measured for naphthalene. The value for quinoline was determined to be about a factor of 2 greater. The intersystem crossing quantum yield was found to be insensitive to changing the solvent from a hydrocarbon to a hydroxylic medium. The data imply significant internal conversion from S_1 for these cases where fluorescent emission has not been observed, or is observed to be very weak.

Unfortunately these quantum yield data do not readily permit direct comparison with the presently developed theories of radiationless processes. These theories are in terms of the rate constants. Once the lifetime of S_1 is determined under these experimental conditions, these quantum yields will permit calculation of the rate constants. These measurements are planned for the near future. Our data do indicate that the intersystem crossing quantum yield is not particularly sensitive to the order or energy separation of the $^1(n,\pi^*)$, $^1(\pi,\pi^*)$, $^3(n,\pi^*)$, and $^3(\pi,\pi^*)$ states.

Acknowledgments. The financial support of the Research Corporation, the Petroleum Research Fund (Grant No. 1432-G2), and the National Science Foundation (Grant No. 19750) is gratefully acknowledged.

(17) J. B. Birks, "Photophysics of Aromatic Molecules," Wiley-Interscience, London, 1970, p 200.

(18) L. M. Stephenson, D. G. Whitten, G. F. Vesley, and G. S. Hammond, *J. Amer. Chem. Soc.*, **88**, 3665 (1966).

Pulse Radiolysis of Ammonia Gas. II. Rate of Disappearance of

the $\text{NH}_2(\text{X}^2\text{B}_1)$ Radical¹

by Sheffield Gordon,* W. Mulac, and P. Nangia

Department of Chemistry, Argonne National Laboratory, Argonne, Illinois 60439 (Received January 15, 1971)

Publication costs assisted by the Argonne National Laboratory

The free-radical species NH_2 and NH have been produced by irradiating NH_3 vapor at pressures ranging from 250 to 1520 Torr with pulses of 2-MV electrons. The rate of disappearance of these radicals was followed by measuring the decrease in absorption at 597.6 (NH_2) and 336.0 nm (NH). Rate constants for the following reactions have been determined. In the pressure range 250 to 1520 Torr NH_3 , $k_{\text{NH}_2+\text{NH}_2} = 6.2 \times 10^{10} \text{ M}^{-1} \text{ sec}^{-1}$. Between 250 and 1000 Torr NH_3 , $k_{\text{NH}_2+\text{H}+\text{M}} = 2.2 \times 10^{12} \text{ M}^{-2} \text{ sec}^{-1}$, and appears to approach a second-order limit beyond this pressure. $k_{\text{NH}_2+\text{NO}} = 1.6 \times 10^{10} \text{ M}^{-1} \text{ sec}^{-1}$, and $k_{\text{NH}+\text{NO}} = 2.3 \times 10^{10} \text{ M}^{-1} \text{ sec}^{-1}$.

Introduction

The production of the NH radical in its ground state ($\text{X}^3\Sigma$) by the radiolysis of ammonia gas with 130-nsec pulses of 300-kV electrons was recently reported.² The absorption spectrum of this radical due to the $\text{A}^3\pi \leftarrow \text{X}^3\Sigma$ transition was photographed, and the kinetics of its decay was studied under various experimental conditions.

We have extended these studies by looking at the decay of the NH_2 radical produced by the radiolysis of NH_3 gas at pressures ranging from 250 to 1520 Torr with 30-nsec pulses of 2-MV electrons. Under these conditions we were able to observe photographically many absorption bands assigned to the NH_2 radical.³ By following the decay of the partially resolved vibronic band at 597.6 nm ($^2\text{A}_1 \leftarrow ^2\text{B}_1$) photometrically we were able to study the decay of this radical in pure ammonia gas and in ammonia gas containing electron and hydrogen atom scavengers.

Experimental Section

The source of pulsed electrons used in this work was a Model 705 Febetron manufactured by the Field Emission Corp. This accelerator provides a 30–50-nsec pulse (half-width) of electrons with a maximum current per pulse of approximately 5000 A. Figure 1 shows the Cerenkov radiation from a pulse and is indicative of the pulse shape.

A schematic drawing of the stainless steel irradiation cell used in this investigation is shown in Figure 2. The electrons enter the cell in the direction shown, through a 1-mil stainless steel window (A). The analyzing light travels the cell at right angles to the electron beam axis, entering through suprasil window B, and exiting through C. The cell is used with an internal multiple pass mirror system (D, E, and F) based on the White design.⁴ The adjustable mirrors (D and E) are manipulated by external controls (G and H). These controls made it possible to vary the optical

path length through the cell from 40 to 240 cm by changing the number of traversals of the analyzing light beam. The distance between the spherical reflecting mirrors was 10 cm. The volume of the cell was 950 cc. For experiments above 400.0 nm, the quartz mirror blanks were front-surfaced with silver and for experiments below 400.0 nm, aluminum-surfaced mirrors were used. The cell was equipped with a pump-out lead, a metal trap, and cutoff valves. The top of the cell has a suprasil window which was used for observing the number of light passes. Viton O-rings were used on the metal flanges of the cell and on the adjustment controls.

The spectra were photographed on a 0.75-m Jarrell-Ash Model 75-000 spectrograph. The spectrophotometric data for kinetic analysis were obtained with a 1-m Hilger-Engis Model 600/1000 grating spectrometer-spectrograph combination used with a 1200 lines/mm grating blazed at 500.0 nm. The detector was a RCA 1P28 photomultiplier. The photomultiplier signal was fed to a preamplifier and the amplified signal was fed to a Tektronix Model 454 oscilloscope and photographed on Polaroid (Type 47, ASA 3000) film. For the Cerenkov measurement and the NH_2 growth measurement no preamplifier was used, the signal from the photomultiplier being fed directly to the oscilloscope with a rise time of approximately 3 nsec.

The analyzing spectral lamp was a 450-W high-pressure xenon lamp. When used with the photomultiplier detector, the lamp was pulsed over a period of several milliseconds using a circuit developed by Michaels.⁵ This pulse increased the lamp intensity at

(1) Based on work performed under the auspices of the U. S. Atomic Energy Commission.

(2) G. M. Meaburn and S. Gordon, *J. Phys. Chem.*, **72**, 1592 (1968).

(3) G. Herzberg and D. A. Ramsay, *Discuss. Faraday Soc.*, **14**, 11 (1953).

(4) J. White, *J. Opt. Soc. Amer.*, **32**, 285 (1942).

(5) B. Michaels, unpublished work.

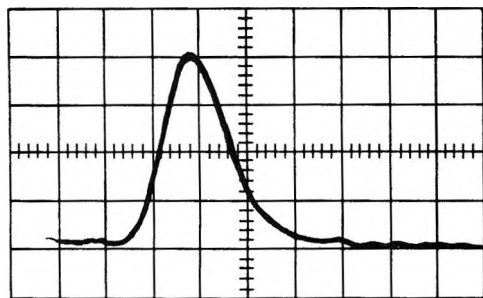


Figure 1. Oscilloscope trace of Cerenkov radiation resulting from 1.7-MV electron pulse into empty cell. Abscissa 10 nsec/div.

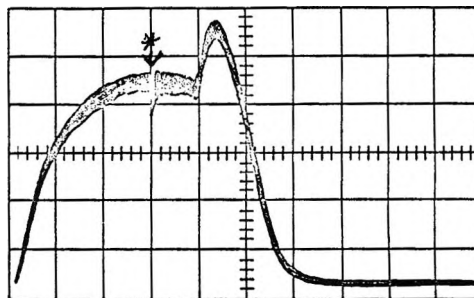


Figure 3. Oscilloscope trace of analyzing light pulse showing transient pip (*) abscissa, 0.5 msec/div; ordinate, 0.2 V/div.

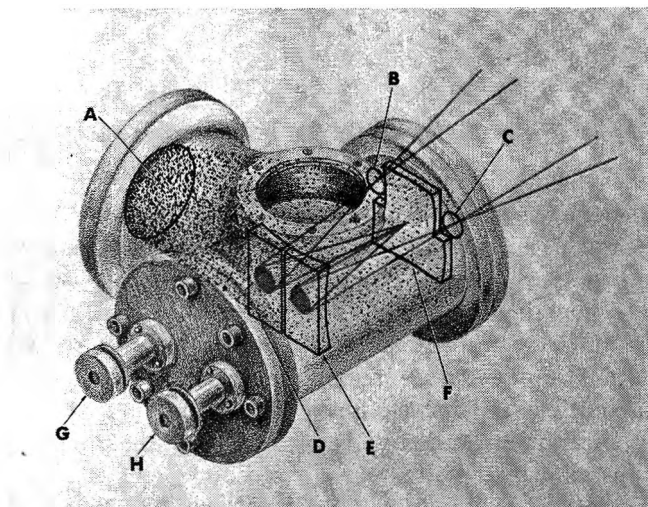


Figure 2. Variable path multiple pass irradiation cell.

600.0 nm by a factor of 40. The lamp intensity was constant to within a few per cent over a period of 1 msec or more. The detected species decay over a period of tens of microseconds and the lamp intensity are constant within our limits of detection during this period. Figure 3 shows an oscilloscope trace of the light pulse with a spike representing the pulse and decay of the transient at the center of the flat portion. An oscilloscope trace of the transient decay was photographed simultaneously with the light pulse on a second scope with a much faster sweep rate.

Photographs of the spectra were taken with Eastman Kodak 103-0 plates. The same xenon lamp was used. However, the lamp was fired by charging a low inductance 0.5- μ F coaxial condenser to 19 kV and discharging the energy (100 J) through the lamp by means of a spark gap trigger operated with a variable time delay trigger amplifier. The analyzing spectrographic light source operated in this manner had a half-width of approximately 8 μ sec. One flash gave a good continuum from 250.0 to 700.0 nm with sufficient optical density for adequate measurement with a Joyce Loebel microdensitometer.

Ammonia was dried by condensing it over metallic sodium. The ammonia was then pumped from this

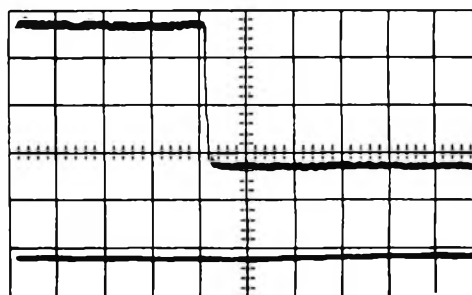


Figure 4. Oscilloscope trace showing absorption at 268.0 nm in ozone produced by a 1.7-MeV pulse in 403 Torr of oxygen. Optical path 40 cm, abscissa 0.5 msec/div. Upper line 100% transmission. Lower line 0% transmission.

solution and subsequently distilled from trap to trap several times in a mercury-free vacuum system. Only the middle fraction of this distillation was used. The cell was pumped to better than 10^{-5} Torr and filled to the desired pressure which was measured with a Texas Instrument Co., Model 145 quartz spiral pressure gauge. A similar technique was used to purify and introduce the additive gases.

Dosimetry was performed by using both the N_2 production from N_2O and the O_3 production from O_2 . The ozone was measured *in situ* after the pulse by measuring the O_3 absorption at 268.0 and 285.0 nm. Figure 4 is a typical oscilloscope trace of the O_3 production. The G value for N_2 from N_2O obtained by Willis, *et al.*,^{6a} and the G value for O_3 production from O_2 obtained by Ghormley, *et al.*,^{6b} were used. Corrections were made for the stopping power of NH_3 (S_{NH_3}) relative to N_2O (S_{N_2O}). A value of $S_{NH_3}/S_{N_2O} = 0.5$ was used.⁷ Figure 5 gives the measured dose per pulse absorbed in the multiple reflection cell filled with N_2O at a number of different pressures and at ambient temperature (25°).

The variation of the dose absorbed in the volume occupied by the multiple reflection cell was determined

(6) (a) C. Willis, O. A. Miller, A. E. Rothwell, and A. W. Boyd, *Advan. Chem. Ser.*, **81**, 539 (1968); (b) J. A. Ghormley, C. J. Hochenadel, and J. W. Boyle, *J. Chem. Phys.*, **50**, 419 (1969).

(7) N. A. Baily and G. C. Brown, *Radiat. Res.*, **11**, 745 (1959).

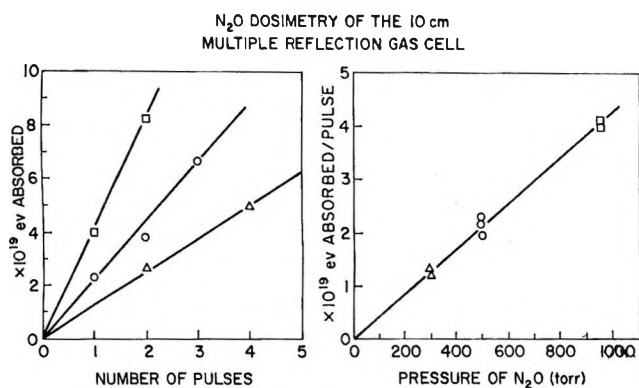


Figure 5. Nitrous oxide dosimetry (1.7-MV incident electron pulses): Δ = 250 Torr; \circ = 500 Torr; \square = 960 Torr.

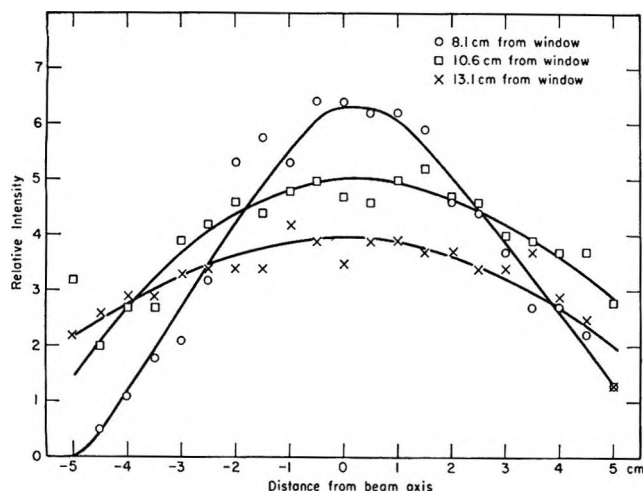


Figure 6. Dose contours in variable path, multiple pass cell resulting from a single pulse by 1.7-MV incident electrons.

by measuring the bleaching of blue cellophane.⁸ Figure 6 shows the relative dose as measured by this technique. Each curve represents the variation in dose across the cell parallel to the analyzing light beam at different positions in the cell (front, center, and back). From this plot, it can be seen that the variation in dose parallel to the analyzing light is about 2.5 and that the variation across the light path is about 2. The homogeneity of the dose inside the light path volume was well within the limits examined by both Sauer⁹ and Boag¹⁰ for the determination of second-order rate constants.

One feature of the high-current accelerator used is the electrical noise introduced by the voltage discharge during the pulse. This effectively blocks any measurement prior to 2 μ sec after triggering the pulse. During the course of this work it was found that placing the entire detection system in a Faraday Cage (double copper screened room) some 32 ft from the accelerator eliminated this electrical interference and enabled measurements to be made over a short time scale limited only by the pulse width (50 nsec).

An important consideration in using this technique for studying reaction kinetics of transient species is the

applicability of the Lambert-Beer relation. This becomes important when the band used consists of sharp lines which are only partially resolved. If one plots the optical density of $\text{NH}_2(^2A_1 \leftarrow ^2B_1)$ and $\text{NH}(A^3\Pi \leftarrow X^3\Sigma)$ vs. optical path length or pressure (related to concentration in this case), one obtains plots which do not pass through the origin. However, if the log of the optical density is plotted against the log of path length or vs. the log of the concentration, a straight line is obtained. The plot is described by the equation

$$D = (\epsilon cl)^n$$

where D is the optical density, ϵ is an "extinction coefficient" of the species being observed, l is the optical path length, and n is a constant.

This relationship has been discussed in earlier publications.^{11,12} When $n = 1$, the Lambert-Beer relationship holds. When $n = 0.5$, there is 100% absorption at the line center. Figure 7 shows our determination of n for $\text{NH}_2(^2A_1 \leftarrow ^2B_1)$ at 597.6 nm and for $\text{NH}(A^3\Pi \leftarrow X^3\Sigma)$ at 336.0 nm, at a pressure of 760 Torr of ammonia using 100- μ slits with a spectrometer whose dispersion is 0.8 nm/mm. Also shown is our determination of n for $\text{OH}(A^2\Sigma^+ \leftarrow X^2\Pi)$ produced by irradiating 8 Torr of H_2O vapor in 760 Torr of argon. Over the NH_3 pressure range studied, n for NH_2 does not vary significantly (within experimental error) and was assumed at all pressures used to be equal to the n determined at 760 Torr. This modified Lambert-Beer equation was applied to the data obtained in this investigation.

Results

Figure 8 shows an oscilloscope trace of the growth of the absorption at 597.6 nm of the NH_2 radical. This trace indicates that the NH_2 concentration has reached a maximum in 150 nsec after the start of the pulse. Figure 9 shows a typical oscilloscope trace of the NH_2 transient decay. The data reported here were calculated from traces of this type by an automatic reading and analysis system¹³ which plotted both the log of the optical density and the reciprocal of the optical density vs. time.

The data represented by the points in Figure 10 show the change in $D^{-1.3}$ (relative concentrations of NH_2) with time at different pressures of NH_3 . From these curves it is seen that second-order kinetics are apparently followed in the initial portion of the decay of the NH_2 at 250 Torr of NH_3 and 505 Torr of NH_3 . With

- (8) E. J. Henley and D. Richman, *Anal. Chem.*, **28**, 1580 (1956).
- (9) M. C. Sauer, Argonne National Laboratory Report, 1966, No. 7327.
- (10) J. W. Boag, *Trans. Faraday Soc.*, **64**, 677 (1968).
- (11) A. B. Callear and W. J. Tyerman, *ibid.*, **62**, 371 (1966).
- (12) P. Fowles, M. deSorgo, A. J. Yarwood, O. P. Stowersy, and H. E. Gunning, *J. Amer. Chem. Soc.*, **89**, 1352 (1967).
- (13) M. C. Sauer, Argonne National Laboratory Report, 1966, No. 7113.

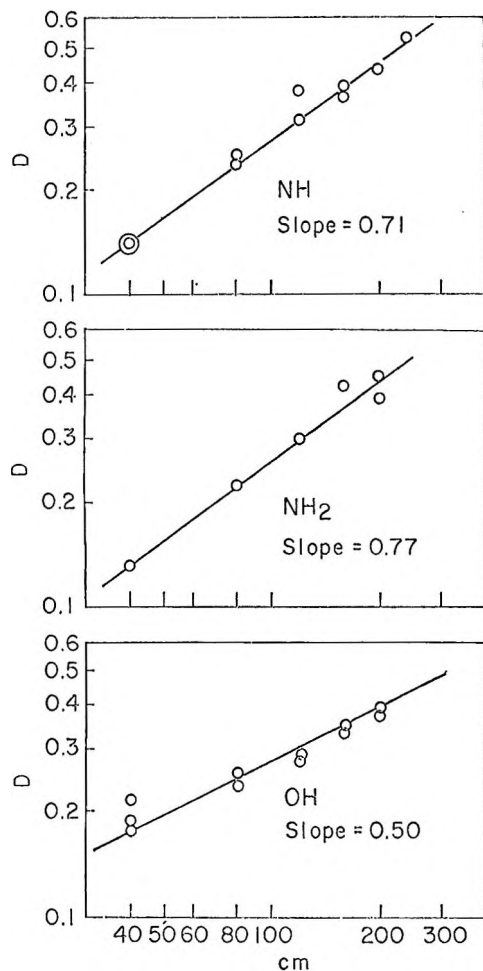


Figure 7. Lambert-Beer law plots: NH_2 in 500 Torr of NH_3 ; NH in 500 Torr of NH_3 ; OH in 8.0 Torr of H_2O + 760 Torr of argon.

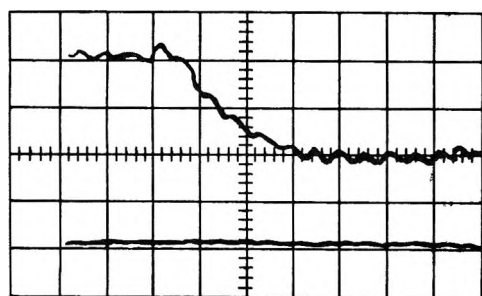


Figure 8. Oscilloscope trace of NH_2 growth. Abscissa, 50 nsec/div; ordinate, 0.2 V/div NH_3 pressure 762 Torr.

increasing ammonia pressure the plots show a curvature which increases with ammonia pressure. The solid curves in Figure 10 represent computer calculated decay curves which were fitted to the experimental points using a program written by Schmidt¹⁴ (see Discussion).

The data in Figure 11 show the difference in decay of $D^{-1.3}$ of NH_2 produced in 505 Torr of NH_3 and in a mixture containing 505 Torr of NH_3 and 50 Torr of SF_6 . Here again the solid lines represent computer calculated

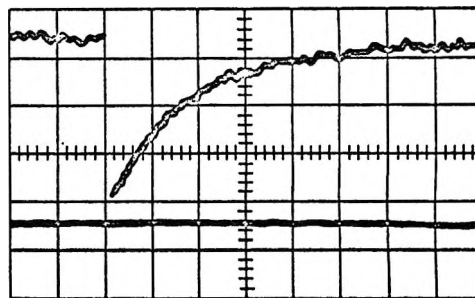


Figure 9. Oscilloscope trace of NH_2 absorption at 597.6 nm produced in 1520 Torr of NH_3 . Abscissa 2 $\mu\text{sec}/\text{div}$; ordinate 0.2 V/div.

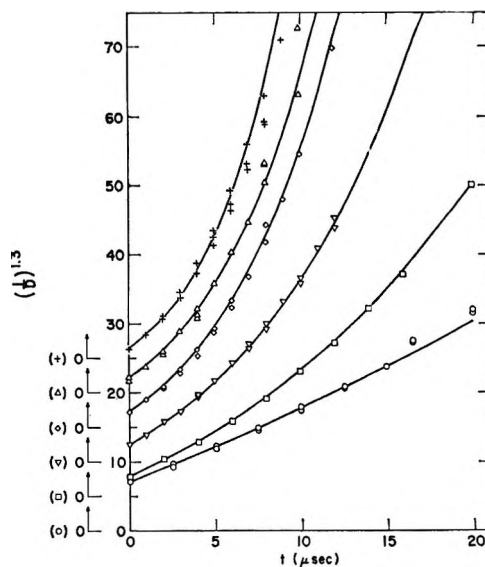


Figure 10. Decay of NH_2 absorption at 597.6 nm at different pressures of NH_3 : \circ , 250 Torr; \square , 505 Torr; ∇ , 760 Torr; \diamond , 1000 Torr; \triangle , 1250 Torr; $+$, 1520 Torr.

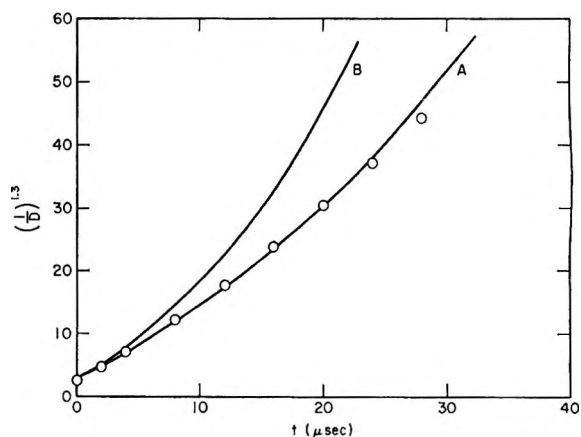


Figure 11. Effect of SF_6 on NH_2 absorption at 597.6 nm; A, 505 Torr of NH_3 + 50 Torr of SF_6 ; B, 505 Torr of NH_3 .

curves and the points represent the experimental data (see Discussion).

(14) K. H. Schmidt, Argonne National Laboratory Report, 1966, No. 7693.

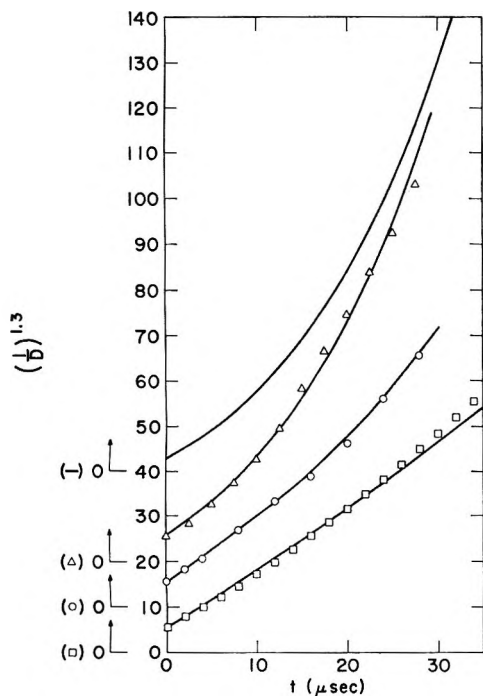
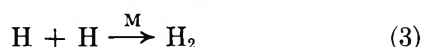
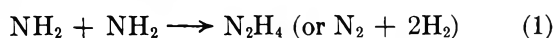


Figure 12. Effect of C_3H_6 on NH_2 absorption at 597.6 nm in 500 Torr of NH_3 ; (\square) 10 Torr of C_3H_6 ; (\circ) 25 Torr of C_3H_6 ; (Δ) 48 Torr of C_3H_6 ; (—) pure NH_3 .

Figure 12 represents the decay of the NH_2 in a mixture of 505 Torr of NH_3 with three different pressures of propylene. The solid curves again represent the computer calculated curves and the points represent the experimental data (see Discussion).

Discussion

The kinetics of the decay of the NH_2 radical illustrated in Figure 10 can be understood in terms of the following three reactions.



The rate of disappearance of the NH_2 will be governed by the two following rate expressions

$$-\frac{d(NH_2)}{dt} = 2k_1(NH_2)^2 + k_2(H)(NH_2) \quad (4)$$

$$-\frac{d(H)}{dt} = k_2(H)(NH_2) + 2k_3(H)^2 \quad (5)$$

It is useful to consider qualitatively how the integrated rate expression for the disappearance of the NH_2 should depend on the relative values of the rate constants in eq 4 and 5. This can be done by looking at the limiting cases as well by looking at the effect of changing the relative values of these rate constants and comparing these results with what we obtain from the computer calculated values and the experimental points.

Initially $[NH_2]_0 = [H]_0$ and $k_3 \ll k_1$ or k_2 . If k_2 is sufficiently smaller than $2k_1$, the second term of eq 4 can be neglected. In this case a plot of $1/[NH_2]$ vs. time will be a straight line (second order). However, if the ratio k_2/k_1 is sufficiently large and since initially three NH_2 radicals disappear for every H atom, the ratio $[H]/[NH_2]$ will increase with time, and a contribution, pseudo-first-order in $[H]$ (second term in eq 4), will become significant. This will result in a departure from linearity in the second-order plot of $[NH_2]$. The greater the ratio k_2/k_1 , the sooner will this departure from linearity be observed and the greater will be the curvature.

The data in Figure 10 show this effect. At 250 Torr of NH_3 , second-order kinetics are obeyed except for a very slight curvature. At 505 Torr of NH_3 , the second-order plot is slightly more curved. As the initial NH_3 pressure is increased, the curvature observed is more pronounced.

The solid lines in Figure 10 represent computer calculated curves for the change in $D^{-1.5}$ of NH_2 with time according to eq 1-3. A value for k_3 of $3 \times 10^8 M^{-2} \text{ sec}^{-1}$ was used,¹⁵ and values of $k/\epsilon l$ for reactions 1 and 2, which gave the best fit with the experimental points, were selected. The agreement between the calculated curves and the experimental points was not very sensitive to the value of k_3 .

The values of $k_1/\epsilon l$ and $k_2/\epsilon l$ determined in this fashion for the various pressures of NH_3 used are tabulated in Table I. The probable error in these values is less than $\pm 5\%$. In both cases ϵ is the "extinction coefficient" of NH_2 and l is the absorbing path length. From these rate constants, it is seen that k_1 is independent of pressure between 250 and 1520 Torr, whereas k_2 depends on pressure and appears to become pressure independent between 1000 and 1520 Torr. This is illustrated in Figure 13. These values are not inconsistent with the lower value of k_1 reported by Hanes and Bair¹⁶ and Saltzman and Bair¹⁷ who studied this reaction at a much lower NH_3 pressure.

Table I

P_{NH_3} , Torr	$\frac{k_1}{\epsilon l} \times 10^{-6}$	$\frac{k_2}{\epsilon l} \times 10^{-6}$	$\frac{k_1 \times 10^{-10}}{\text{sec}^{-1} \text{ } \epsilon l} M^{-1}$	$\frac{k_2 \times 10^{-10}}{\text{sec}^{-1} \text{ } \epsilon l} M^{-1}$
250	3.75	1.9	5.8	2.9
500	4.0	2.7	6.2	4.2
760	4.0	5.0	6.2	7.7
1000	4.0	7.9	6.2	12.2
1250	4.0	8.2	6.2	12.7
1520	4.0	7.5	6.2	11.6

^a $G_{NH_2} = 8.4$ (see text), $l = 200$ cm, $\epsilon = 775 M^{-1} \text{ cm}^{-1}$.

(15) C. B. Knetschmen and H. C. Peterson, *J. Chem. Phys.*, **39**, 1772 (1963).

(16) M. H. Hanes and E. J. Bair, *ibid.*, **38**, 672 (1963).

(17) J. D. Saltzman and E. J. Bair, *ibid.*, **41**, 3654 (1964).

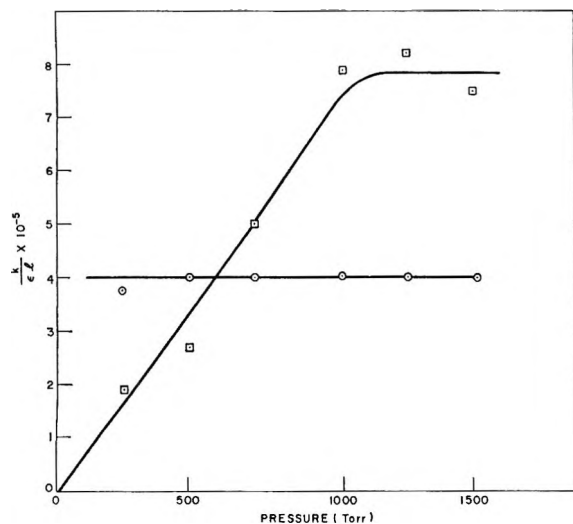
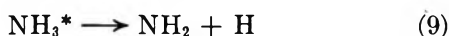
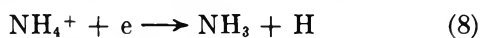
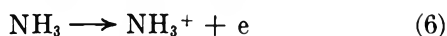
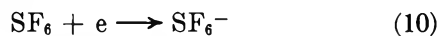


Figure 13. Dependence of k_1 (O) and k_2 (□) on NH_2 pressure.

The effect of SF_6 on the decay of NH_2 leads to some interesting conclusions. The addition of SF_6 results in no change in the initial optical density of NH_2 but reduces the curvature of the $D^{-1.3}$ vs. time curve considerably. NH_2 is assumed to be formed *via* an ion-molecule reaction as well as from excited NH_3 (excited by direct electron impact) in the following way



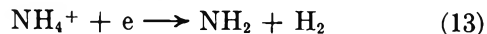
Since SF_6 is an efficient electron scavenger, the addition of SF_6 will prevent H-atom formation resulting from reaction 8 in the following manner



Thus SF_6 eliminates H-atom formation from reaction 8 and instead NH_4F is formed. This is actually observed as a white cloud after a single pulse.

Using the rate constants $k_1/\epsilon l$ and $k_2/\epsilon l$ determined as described for pure ammonia, we were not able to get a computer calculated fit with the experimental points using equal initial concentrations of H and NH_2 when SF_6 was added. When one uses a ratio of $[\text{H}]_0/[\text{NH}_2]_0$ equal to 0.55, good agreement with the experimental points is obtained as illustrated in Figure 11. This means that 55% of the hydrogen atoms are formed *via* excited ammonia (reaction 9). Melton,¹⁸ using mass spectrometric detection at lower pressures of NH_3 , found that 44% of the primary species formed were neutral species and 56% were ions, whereas Nishikawa and Shinahara¹⁹ concluded from product analyses that 58% of the primary species results from reaction 9.

From the fact that the initial optical density of NH_2 did not change upon the addition of SF_6 , we can conclude that reaction 8 takes place rather than



One can calculate a G value for NH_3^+ from the W value for NH_3 .²⁰ $G_{\text{NH}_3^+}$ calculated in this way is 3.8. Therefore, the total G_{NH_2} must be $3.8/0.45 = 8.4$.

From the relationship

$$C = \frac{\text{Dose} \times G_{\text{NH}_2}}{6.03 \times 10^{26}}$$

and the relationship between optical density, concentration, and path length given previously, one can calculate an "extinction coefficient" for NH_2 in terms of the G value for NH_2 . At 760 Torr of ammonia, D_{NH_2} equals 0.45 using a path length of 200 cm. For this pressure the dose absorbed is 1.62×10^{19} eV. Therefore, with the above relationship, the following expression can be derived

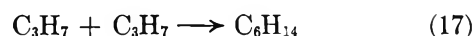
$$\epsilon_{\text{NH}_2} = \frac{6510}{G_{\text{NH}_2}}$$

Using this expression one can convert the values of $k/\epsilon l$ into absolute value of k by means of the equation

$$k = \frac{(k/\epsilon l) \times 1.30 \times 10^6}{G_{\text{NH}_2}}$$

This has been done in Table I using a value for $G_{\text{NH}_2} = 8.4$.

The effect of adding a hydrogen scavenger, C_3H_6 (shown in Figure 12) is to reduce the curvature of the second-order NH_2 plots compared with those of the pure ammonia runs, while affecting the initial slopes to a minor extent. The following reactions in addition to reactions 1-6 were used for the computer calculated curves which agree with the experimental points in Figure 12.



Again using values of k_1 and k_2 listed in Table I and the value of k_3 referred to, one can get an acceptable agreement of the computer calculated curve (solid line of Figure 12) with the experimental points by assuming the following rate constants: $k_{14} = 4.5 \times 10^8$,²¹ $k_{15} =$

(18) C. E. Melton, *J. Chem. Phys.*, **45**, 4414 (1966).

(19) M. Nishikawa and N. Shinahara, *Radiat. Res.*, **33**, 194 (1968).

(20) G. G. Meisel, *J. Chem. Phys.*, **41**, 51 (1964).

(21) J. Eyre, private communication.

1.65×10^7 , $k_{17} = 1.95 \times 10^{11}$,²² $k_{18} = 4.95 \times 10^{10} M^{-1} \text{sec}^{-1}$.

The only unknown rate constants in this mechanism are k_{15} and k_{18} (k_{16} does not enter into the computation). We find that a variation in k_{15} or k_{18} of 10% causes a deviation of the calculated curve from the experimental curve of from 3–5%, the probable error in our experimental points.

From the computer calculated products, using the above rate constants, one can calculate the efficiency of scavenging at the three pressures of C_3H_6 used (Table II).

Table II: Scavenging Efficiencies of C_3H_6 in 505 Torr of NH_3

Pressure C_3H_6 , Torr	% of H scavenged
48	96.7
25	94.9
10	89.7

The computer calculation based on these rate constants and a yield of $G(NH_2) = 8.4$ deduced from the SF_6 results, yield the following G values (Table III) for the products of reaction 1, [$G(N_2H_4) + G(N_2)$] and the yield for the product of reaction 18, [$G(C_3H_7NH_2)$]. Included in Table III are yields for these reactions as reported by Willis, *et al.*²³

Table III: Product Yields from Pulse Radiolysis of 505 Torr of NH_3 with C_3H_6

C_3H_6 press, Torr	—Computed yields this work—		From ref 23 $G(N_2H_4) +$ $G(N_2)$
	$G(C_3H_7NH_2)$	$G(N_2H_4) +$ $G(N_2)$	
10	1.16	2.50	2.28
25	1.16	2.16	1.84
48	1.08	1.80	1.70

Addition of NO had a pronounced effect on the decay of both $NH_2(^2A_1 \rightarrow ^2B_1)$ and $NH(A^3\Pi \leftarrow X^3\Sigma)$. The NH was followed spectrophotometrically as described at 336.0 nm. Both radicals react with NO according to pseudo-first-order kinetics. Figure 14 shows the pseudo-first-order disappearance of these radicals as a function of NO pressure. From these curves, one can calculate the following rate constants

$$k_{NH_2+NO} = 1.6 \times 10^{10} M^{-1} \text{sec}^{-1} \quad (19)$$

$$k_{NH+NO} = 2.3 \times 10^{10} M^{-1} \text{sec}^{-1} \quad (20)$$

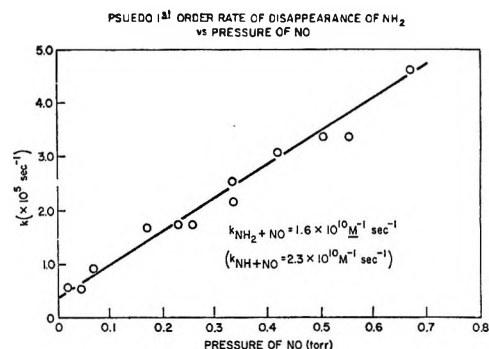
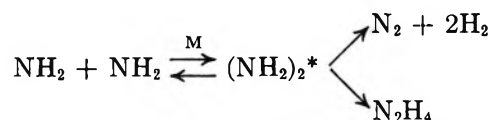


Figure 14. Pseudo-first-order disappearance of NH_2 vs. pressure of NO.

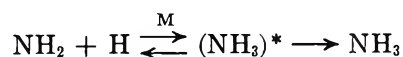
It should be pointed out that these rate constants do not require a knowledge of the extinction coefficients of either NH_2 or NH.

Conclusion

Using direct spectrophotometric observation of the decay of the NH_2 radical, the rate constant for the reaction between two NH_2 radicals has been shown to be pressure independent between 250 and 1520 Torr of ammonia in accordance with eq 1. This, together with the results of previous investigators^{16,17} who found that this reaction is pressure dependent at much lower pressures than used in the present study, indicates that the reaction proceeds through an activated complex in equilibrium with the reactants



The rate constant for the reaction between an NH_2 radical and an H atom is shown to be pressure dependent between 250 and 1000 Torr of NH_3 and seems to tend toward a second-order limit beyond 1000 Torr of NH_3 . This also indicates that this reaction proceeds according to the scheme



In addition it has been possible by this method to determine the rate constants for a number of NH_2 radical reactions. These are of great interest in interpreting the results of the radiolysis and photolysis of ammonia vapor.

(22) E. L. Metcalfe and H. F. Trotman-Dickenson, *J. Chem. Soc.*, 4620 (1962).

(23) C. Willis, A. W. Boyd, and O. A. Miller, *Can. J. Chem.*, **47**, 3007 (1969).

On the Theory of the Stabilization of Dispersions by Adsorbed Macromolecules. II. Interaction between Two Flat Particles

by F. Th. Hesselink,*¹ A. Vrij, and J. Th. G. Overbeek

van't Hoff Laboratorium der Rijksuniversiteit, Sterrenbos 19, Utrecht, The Netherlands (Received December 14, 1970)

Publication costs borne completely by The Journal of Physical Chemistry

A theory for the stabilization of dispersions by adsorbed macromolecules ("protective action") is given in terms of a volume restriction repulsion, due to the decrease of configurational entropy of adsorbed loops and tails on the approach of a second particle, an osmotic repulsion due to the mixing of the adsorbed polymeric clouds when two particles approach each other (in a very poor solvent this can be an attraction effect), and the van der Waals attraction between the particles. The adsorbed macromolecules are described by a random walk model. No molecules are adsorbed on more than one particle (no "bridging"). The interaction between two flat particles covered by adsorbed macromolecules is described using the Flory-Huggins approximation for four different modes of attachment of the macromolecules: equal loops, equal tails, and the loop size distributions found before for an adsorbed homopolymer and for an adsorbed copolymer. Interaction curves are found which predict reversible flocculation and the occurrence of thixotropic systems as intermediates of flocculated and deflocculated systems. The main parameters determining the interaction are the average loop (tail) size and the size distribution of these loops (tails), the amount of polymer adsorbed, the quality of the solvent, the Hamaker attraction constant, and the particle size. For flat particles the stability is inversely proportional with the square of the linear dimension of the particles, whereas for spherical particles in Derjaguin's approximation the stability is shown to be inversely proportional with the radius of the spheres. In general, stabilization is enhanced by long adsorbed chains and an extreme size distribution, a high amount of polymer adsorbed, a good solvent, a low Hamaker constant, and a small particle size. These predictions appear to be in reasonable agreement with the only scarcely available experimental evidence on this subject.

Introduction

Adsorbed nonionic macromolecules are known to stabilize emulsions and suspensions in aqueous and non-aqueous media. Examples² are alkyd resins, cellulose derivatives, uncharged proteins, and block copolymers which are used for the stabilization of pigment dispersions, latices, emulsions, etc. The mechanism by which adsorbed polymers can keep the particles dispersed in solution by counteracting the ever-existing attraction, due to van der Waals forces³ and occasionally to magnetic forces,⁴ is of two kinds.⁵

(I) A macromolecule adsorbed on a colloidal particle loses configurational entropy on the approach of a second particle. This is called the *volume restriction effect*.

(II) When the layers of adsorbed macromolecules on the two particles interpenetrate, the higher polymer segment concentration between the particles will lead to a local "*osmotic pressure*" in most cases counteracting the approach.

The volume restriction effect has a certain resemblance to the concept of rubber elasticity, as if the dispersion is stabilized because of an elastic wrapping⁶ around the particles. Mackor and van der Waals^{7,8} have shown for rather short, rodlike molecules that when the loss of configurational entropy leads to desorption the interfacial free energy rises in agreement with Gibbs' adsorption isotherm. Using a Monte Carlo

simulation technique permitting only self-avoiding walks on a cubic lattice, Clayfield and Lumb⁹ have calculated the rise in free energy due to volume restriction for macromolecules adsorbed on an impermeable interface. Their calculations apply to irreversibly adsorbed "tails" (chains terminally adsorbed with one end group) and to copolymers attached to the particles by anchor segments in a solvent having no net interaction with the unadsorbed part of the molecule. Fischer¹⁰ was probably the first to point out that the increase of the free energy due to the overlapping of segment clouds should be taken into account. For irreversibly adsorbed tails Meier⁵ considered both effects I and II using random flight statistics to calculate the volume

(1) Address correspondence to this author at the Department of Chemistry, Cornell University, Ithaca, N. Y. 14850.

(2) J. Lyklema, *Advan. Colloid Interface Sci.*, **2**, 65 (1968).

(3) (a) B. Derjaguin and L. D. Landau, *Acta Physicochim. URSS*, **14**, 633 (1941); (b) E. J. W. Verwey and J. Th. G. Overbeek, "Theory of the Stability of Lyophobic Colloids," Elsevier, Amsterdam, 1948.

(4) J. P. McTague, *J. Chem. Phys.*, **51**, 133 (1969); J. R. Thomas, *J. Appl. Phys.*, **37**, 2914 (1966).

(5) D. J. Meier, *J. Phys. Chem.*, **71**, 1861 (1967).

(6) K. Jäckel, *Kolloid-Z. Z. Polym.*, **197**, 143 (1964).

(7) E. L. Mackor, *J. Colloid Sci.*, **6**, 492 (1951).

(8) E. L. Mackor and J. H. van der Waals, *ibid.*, **7**, 535 (1952).

(9) E. J. Clayfield and E. C. Lumb, *J. Colloid Interface Sci.*, **22**, 285 (1966); *Macromolecules*, **1**, 133 (1968).

(10) E. W. Fischer, *Kolloid Z.*, **160**, 120 (1958).

restriction effect and the Flory-Huggins approach for the osmotic effect. He showed that the osmotic effect contributes substantially to the stabilization, especially at high surface coverage of polymer. This originates from the fact that the volume restriction effect increases linearly with the amount of polymer adsorbed, whereas the osmotic effect increases quadratically, being due to the interaction between the two polymeric clouds. Due to an incorrect derivation of the density distribution¹¹ for the segments of the adsorbed chains, Meier's values for the osmotic effect are somewhat too low.

In this paper we have corrected this error and extended the theory to systems in which the polymer molecules are adsorbed with many segments, connected by loops dangling in solution. With the results of our previous paper¹² on the configurational statistics of adsorbed macromolecules on the approach of a second interface, the repulsion due to volume restriction and osmotic effects is calculated for four different modes of attachment of the macromolecules: equal tails, equal loops, a loop size distribution derived by Hoeve, *et al.*,¹³ for a homopolymer where all the segments have *a priori* an equal chance to become adsorbed, and a loop size distribution¹² for a copolymer attached to the surface with anchor segments randomly distributed along the chain.

The repulsion thus calculated is then compared with the van der Waals attraction between the particles. The independent parameters determining the stability are listed and the effect of these parameters on the stability is discussed.

Model

Our previous results¹² on the configurational behavior of adsorbed macromolecules on the approach of a second interface are based on random flight statistics on a six-choice cubic lattice and the spatial dimensions are expressed in units $(il^2)^{1/2}$ where i is the number of segments each with length l . In this paper we need the real dimensions of polymer chains and therefore we will equalize $(il^2)^{1/2}$ with the experimental root mean square end-to-end distance $\langle r^2 \rangle^{1/2}$ of a chain; thus $il^2 = \langle r^2 \rangle$. The expansion α of the chains due to long-range intramolecular interactions is taken into account by using $\langle r^2 \rangle^{1/2} = \alpha \langle r^2 \rangle_0^{1/2}$ where $\langle r^2 \rangle_0^{1/2}$ is the unperturbed root mean square end-to-end distance to be measured in a θ solvent.

As previously¹² we will treat the case of the interaction between two flat interfaces. Extension to the case of the interaction between two spheres highly complicates the mathematics. Ottewill and Walker¹⁴ have calculated the osmotic effect for two spheres covered by rather short polyethylene oxide chains approximating the density distribution by a step function. This, however, is too crude an approximation for a quantitative analysis.¹⁵ As before¹² our argument is limited to

cases where each macromolecule is adsorbed only on one particle. Extension to cases of macromolecules adsorbed on more than one particle would lead to a quantitative treatment of sensitized flocculation.¹⁶ This, however, is beyond the scope of this paper because of the several simultaneous kinetic processes involved. As usual¹⁷ we assume the polymeric clouds around the particles to be interpenetrable whereas the particles are thought of as impenetrable interfaces.

In general, macromolecules adsorbed on colloidal particles will form loops with a certain size distribution. The loop size distribution for an adsorbed homopolymer is given by¹²

$$n_i = na\pi^{-1/2}(\bar{i})^{-1}i^{-3/2} \exp[-ia^2/(\bar{i})^2] \quad (1)$$

where n_i is the number of loops of i segments per unit area, \bar{i} the average number of segments per loop, n the total number of segments in the loops per unit area, and $a \cong 0.7$ (numerical constant). This loop size distribution has originally been formulated^{13,18} in a slightly different form for an infinitely long isolated macromolecule on an infinite surface, neglecting interactions between loops and solvent. Taking into account end effects (each molecule may have one or two loose tails), Roe¹⁹ and recently Motomura and Matuura²⁰ have found that these tails may contain a considerable fraction of the adsorbed macromolecule. This seems to be confirmed by experiments on the thickness of the adsorbed layer,^{21,22} which suggest that in practically all cases investigated, the adsorbed macromolecules are attached to the interface by only a few segments with long chains protruding in solution. However, when the end effects are small eq 1 seems to be valid. Another complication arises because of the fact that for a homopolymer the quality of the solvent, the average size of the adsorbed chains and the amount adsorbed cannot be considered as independent parameters.^{13,19-25}

(11) F. Th. Hesselink, *J. Phys. Chem.*, **73**, 3488 (1969).

(12) F. Th. Hesselink, *ibid.*, **75**, 65 (1971).

(13) C. A. J. Hoeve, E. A. DiMarzio, and P. Peyser, *J. Chem. Phys.*, **42**, 2558 (1965).

(14) R. H. Ottewill and T. Walker, *Kolloid-Z. Z. Polym.*, **227**, 108 (1968).

(15) For example, applying this approximation to the interaction between two flat interfaces gives that the "osmotic" force between the particles does not depend on the extent of the overlap.

(16) V. K. La Mer, *Discussions Faraday Soc.* **42**, 248 (1966); W. E. Wallis, *J. Colloid Interface Sci.*, **27**, 797 (1968).

(17) P. J. Flory, "Principles of Polymer Chemistry," Cornell University Press, Ithaca, N. Y., 1953.

(18) R.-J. Roe, *Proc. Nat. Acad. Sci. U. S.*, **53**, 50 (1965).

(19) R.-J. Roe, *J. Chem. Phys.*, **43**, 1591 (1965); **44**, 4264 (1966).

(20) K. Motomura and R. Matuura, *ibid.*, **50**, 1281 (1969).

(21) R. R. Stromberg in "Treatise on Adhesion and Adhesives," Vol. I, R. L. Patrick, Ed., Marcel Dekker, New York, N. Y., 1967.

(22) E. Killmann and H. C. Wiegand, *Makromol. Chem.*, **132**, 239 (1970).

(23) A. Silberberg, *J. Chem. Phys.*, **48**, 2835 (1968).

(24) M. J. Schick and E. N. Harvey, Jr., *Advan. Chem. Ser.*, **87**, 63 (1968).

The problem of the size distribution being unsolved, no theory can correlate these parameters correctly. Because of these uncertainties we will use eq 1 only to obtain a qualitative picture of the stabilizing action of adsorbed homopolymers. In our more quantitative discussion we shall not investigate this case. It can be said beforehand that the error involved using eq 1 will become more serious the shorter the adsorbed homopolymer and the higher the surface coverage.

For a copolymer attached to the particle by some anchor segments randomly distributed along the chain, we have found, neglecting end effects, an exponential loop size distribution¹²

$$n_i = n(\bar{i})^{-2} \exp(-i/\bar{i}) \quad (2)$$

The repulsion due to volume restriction and osmotic effects can now be calculated for particles covered by adsorbed homopolymers and adsorbed copolymers using eq 1 and 2 and also for particles covered by equal tails and equal loops.

Volume Restriction Effect

On the approach of a second interface adsorbed loops and tails lose configurational entropy. Previously¹² we have derived for this relative loss of configurations for a single tail, $R_1(i,d)$ and for a single loop $R_2(i,d)$

$$R_1(i,d) = \sum_{v=-\infty}^{\infty} [\exp\{-6v^2d^2/il^2\} - \exp\{-3(2v+1)^2d^2/2il^2\}] \quad (3)$$

and

$$R_2(i,d) = \sum_{v=-\infty}^{\infty} (1 - 12v^2d^2/il^2) \exp(-6v^2d^2/il^2) \quad (4)$$

where i is the number of segments per tail (loop) and d the distance between the interfaces. When two interfaces both covered by $\nu (= n/i)$ tails (loops) per unit area approach each other, the resulting rise in free energy, ΔF_{VR} , per unit area due to volume restriction is given by

$$\Delta F_{VR} = -2kT \sum_i n_i \ln R(i,d) \quad (5)$$

where k is the Boltzmann constant and T the absolute temperature, whereas for $R(i,d)$ either eq 3 or 4 is to be substituted. For the case of equal tails (loops) $n_i = \nu$ whereas for a homopolymer and a copolymer n_i is given by eq 1 and 2, respectively. Substitution of eq 4 into eq 5 and replacement of the summation over i by an integration gives

$$\Delta F_{VR} = 2\nu kT V(\bar{i},d) \quad (6)$$

with

$$V(\bar{i},d) = -\bar{i}n^{-1} \int_0^{\infty} n_i \ln \sum_{v=-\infty}^{\infty} (1 - 12v^2d^2/il^2) \times \exp(-6v^2d^2/il^2) di \quad (7)$$

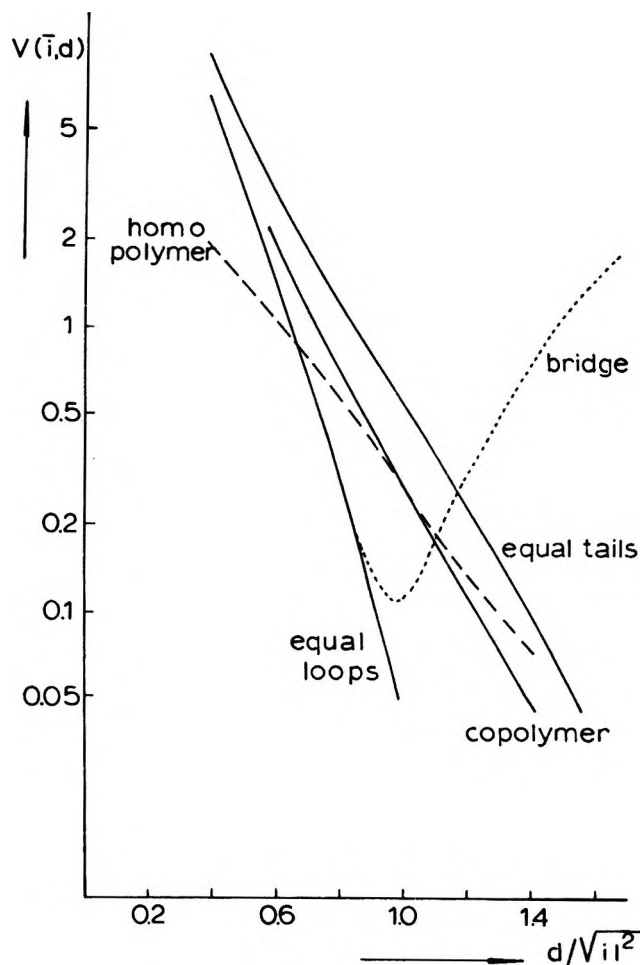


Figure 1. The rise in free energy per average chain $V(\bar{i},d)$ (see eq 7) due to the volume restriction imposed by a second interface at distance $d/\sqrt{il^2}$ for several modes of attachment of the macromolecules. Only the homopolymer curve (---) depends on \bar{i} ; it is calculated for $\bar{i} = 10$. The curve for equal tails has been found before by Meier.⁵ The curve for a bridge (see ref 12) gives the free energy for a chain connecting two particles.

$V(\bar{i},d)$ gives the rise in free energy per average loop in units kT . It is evaluated as a function of $d/\sqrt{il^2}$ by numerical integration of eq 7 using an Electrologica X8 computer. For equal loops and $d/\sqrt{il^2} \geq 1$ a good approximation²⁶ for $V(\bar{i},d)$ is given by

$$V(\bar{i},d) = -2(1 - 12d^2/il^2) \exp(-6d^2/il^2) \quad (7a)$$

In Figure 1 and more precisely in Table I the results are given for particles covered by equal tails, equal loops, and copolymers. Figure 1 also shows $V(\bar{i},d)$

(25) The relevance of this point is easily demonstrated; e.g., raising the quality of the solvent for the adsorbed polymer generally increases the stability of the system (see Discussion) but it decreases the amount adsorbed^{23,24} which effect tends to destabilization of the system.

(26) For equal loops the integration in eq 7 over i vanishes whereas for $d/\sqrt{il^2} \geq 1$ the summation over v converges rapidly. Equation 7a is found by taking only the first terms of this sum ($v = 0, \pm 1$), developing the logarithm in a power series, and neglecting the higher terms of this series.

Table I: Values for the Dimensionless Volume Restriction Function, $V(\bar{i}, d)$ (eq 7), and Osmotic Function, $M(\bar{i}, d)$ (eq 11), Independent of $d/\sqrt{\bar{i}l^2}$

$d/\sqrt{\bar{i}l^2}$	$V(\bar{i}, d)$			$M(\bar{i}, d)$		
	Equal tails	Equal loops	Copolymer	Equal tails	Equal loops	Copolymer
0.6	2.996	1.476	2.030	3.723	2.974	3.428
0.8	1.284	0.339	0.760	2.397	1.716	2.078
1.0	0.582	0.0561	0.307	1.585	0.837	1.280
1.2	0.262	0.00578	0.1282	1.043	0.314	0.801
1.4	0.1118	0.00035	0.0542	0.667	0.0940	0.480
1.6	0.0439		0.0231	0.406	0.0204	0.281
1.8	0.01582		0.0109	0.232	0.0034	0.150
2.0	0.00497		0.0041	0.127		0.081
2.5	0.00018			0.018		

for adsorbed homopolymers. The curves of $V(\bar{i}, d)$ against $d/\sqrt{\bar{i}l^2}$ for equal tails, equal loops, and copolymers are independent of the particular choice of \bar{i} , whereas the curve for a homopolymer depends on \bar{i} . This is directly related to the fact that for the first three cases¹² the root mean square extension of the segments from the interface, $\langle x^2 \rangle^{1/2}$, is proportional to $(\bar{i})^{1/2}$ whereas for a homopolymer^{12,23} $\langle x^2 \rangle^{1/2}$ is proportional to \bar{i} . Figure 1 will be discussed further in connection with the results for the osmotic effect.

Osmotic Effect

The increase in free energy, ΔF_M , per unit area caused by the increased mixing of polymer segments at the approach of two interfaces covered with polymeric material gives rise to a local osmotic repulsion between the particles. In spite of its shortcomings,^{27,28} mostly due to ignored changes in volume on mixing, we will use the classical Flory-Huggins approximation¹⁷ to evaluate this repulsion.²⁹

Meier⁵ has derived for ΔF_M in this approximation

$$\Delta F_M = kTV_s^2V_1^{-1}(1/2 - \chi) \times \left[\int_0^d (\rho_a + \rho_b)_d^2 dx - \int_0^\infty (\rho_a + \rho_b)_\infty^2 dx \right] \quad (8)$$

Here V_s and V_1 are the volumes of a polymeric segment and a solvent molecule, χ is the Flory-Huggins interaction parameter, ρ_a and ρ_b are the number densities of the segments of the macromolecules adsorbed on interface A and B per unit volume, while suffix d and ∞ , respectively, indicate the distance between A and B; the integration of $(\rho_a + \rho_b)^2$ is to be performed over the interval between A and B. The quality of the solvent is characterized both by $(1/2 - \chi)$ and by the expansion parameter α . Therefore we will express $(1/2 - \chi)$ in terms of α using Flory's¹⁷ relation³⁰

$$\alpha^5 - \alpha^3 = \frac{27i^2V_s^2(1/2 - \chi)}{(2\pi)^{3/2}V_1(i\bar{l}^2)^{3/2}} \quad (9)$$

With eq 9 we find from eq 8 taking into account that

$$\int \rho_a^2 dx = \int \rho_b^2 dx; \quad \int (\rho_a\rho_b)_\infty dx = 0$$

$$\Delta F_M = 2(2\pi/9)^{3/2}(\alpha^2 - 1)kTV_s^2\langle r^2 \rangle M(\bar{i}, d) \quad (10)$$

where $\langle r^2 \rangle = \alpha^2\bar{i}l^2$ and

$$M(\bar{i}, d) = \langle r^2 \rangle^{1/2} \left[\int_0^d (\hat{\rho}_a)_d^2 dx + \int_0^d (\hat{\rho}_a\hat{\rho}_b)_d dx - \int_0^\infty (\hat{\rho}_a)_\infty^2 dx \right] \quad (11)$$

The caret at the top of ρ indicates that this $\hat{\rho}$ is normalized so that $\int \hat{\rho} dx = 1$. Equation 10 has been given before by Meier⁵ using slightly different symbols.

Now we will derive $\hat{\rho}_a$ for several modes of attachment of the macromolecules. For the normalized density distribution of the segments of a single tail, $\hat{\rho}_1(x, i, d)$, and of a single loop, $\hat{\rho}_2(x, i, d)$, both of i segments in the direction x normal to the interface in a slab of thickness d we have derived previously¹²

$$\hat{\rho}_1(x, i, d) = 3(i\bar{l}^2)^{-1}R_1^{-1}(i, d) \times \sum_{v=-\infty}^{+\infty} \left[v \int_0^d \{ \exp[-q(vd - d + x - b/2)^2] - 2 \exp[-q(vd - b/2)^2] + \exp[-q(vd + d - x - b/2)^2] \} db + \int_x^d \{ \exp[-q(vd + b/2)^2] - \exp[-q(vd + x - b/2)^2] \} db \right] \quad (12)$$

(27) D. Patterson, *Macromolecules*, **2**, 672 (1969).

(28) P. J. Flory, J. L. Ellenson, and B. E. Eichinger, *ibid.*, **1**, 279 (1968); B. E. Eichinger and P. J. Flory, *Trans. Faraday Soc.*, **64**, 2035 (1968).

(29) The Flory-Huggins interaction parameter χ is then to be regarded as an empirical parameter to be determined from, e.g., osmotic and light-scattering experiments and not to be associated with a heat of solution of the polymer. The concentration dependence of χ will be neglected.

(30) Strictly speaking we should not use Flory's relation between α and χ because it is derived from the swelling equilibrium of a free coil in solution and not of an adsorbed chain. The swelling equilibrium of adsorbed chains however, has not been described yet and Flory's relation is expected to be a reasonable approximation.

where $q = 6/(i\bar{l}^2)$ and $R_1(i,d)$ is given by eq 3. Further¹²

$$\hat{\rho}_2(x,i,d) = 12(i\bar{l}^2)^{-1}R_2^{-1}(i,d) \times \sum_{v=-\infty}^{\infty} \{ (v+1)(vd+x) \exp[-q(vd+x)^2] - v^2d \exp(-qv^2d^2) \} \quad (13)$$

where $R_2(i,d)$ is given by eq 4. For particles covered by equal tails the number density ρ_a is given by

$$\rho_a = n\hat{\rho}_1(x,i,d) \quad (14)$$

ρ_b is then found by substitution of $(d-x)$ instead of x . For particles covered by loops³¹ we have

$$\rho_a = \sum_i in_i\hat{\rho}_2(x,i,d) \quad (15)$$

In the case of equal loops eq 15 reduces to

$$\rho_a = n\hat{\rho}_2(x,i,d) \quad (16)$$

For a homopolymer and for a copolymer we substitute eq 1 and 2 in eq 15. Replacing the summation over i by an integration and substituting eq 13 we obtain

$$\rho_a = ns \int_0^{\infty} i^{-t} \exp(-iu) \times \left\{ \sum_{v=-\infty}^{\infty} [(v+1)(vd+x) \exp\{-q(vd+x)^2\} - dv^2 \exp(-qv^2d^2)] \int_{v=-\infty}^{\infty} (1 - 2qv^2d^2) \times \exp(-qv^2d^2) \right\} di \quad (17)$$

with $q = 6/i\bar{l}^2$, while for a copolymer $s = 12(i\bar{l})^{-2}$, $t = 0$, and $u = (\bar{i})^{-1}$ and for a homopolymer $s = 12a\pi^{-1/2}(i\bar{l}^2)^{-1}$, $t = 3/2$, and $u = a^2(\bar{i})^{-2}$. For neither of these two cases does the integration over i have an analytic solution. For a copolymer numerical evaluation of the integrand shows that the integration over i is satisfactorily performed with $0.1\bar{i} < i < 10\bar{i}$. This is due to the factor $\exp(-iu)$ with $u = (\bar{i})^{-1}$. For a homopolymer, however, u is proportional with $(\bar{i})^{-2}$ and this causes the integral to be very slowly convergent until $i \cong (\bar{i})^2$. Now, numerical integration is very unattractive but fortunately an analytic approximation is close at hand.

The fact is that we reasonably can neglect for the moment the sum in the denominator for eq 17, for we are mainly interested in cases when $d/\sqrt{i\bar{l}^2} > 1$ and then this sum has values between 0.95 and 1. Putting the denominator equal to 1 we can solve the integration over i and the summation in the numerator over v and we get

$$\hat{\rho}_a = bP \{ \exp(-xb/2) - \exp(-bd + bx/2) \}^2 \{ 1 - \exp(-bd) \}^{-2} \quad (18)$$

where $b = 2a\sqrt{6/\bar{i}l}$ and P is introduced to account

for the normalization necessary due to the neglect of the sum in the denominator. P is easily found from $\int_0^d \hat{\rho}_a dx = 1$ to be

$$P = \{ 1 - \exp(-bd) \}^2 / \{ 1 - 2bd \exp(-bd) - \exp(-2bd) \} \quad (19)$$

For $d \rightarrow \infty$, $P \rightarrow 1$ and eq 18 gives the exponential decrease of ρ with x as found before (eq 5 in ref 12).

Now we have expressions for $\hat{\rho}_a$ for the case of equal tails (eq 14), equal loops (eq 16), and for the loop size distribution for an adsorbed copolymer (eq 17) and homopolymer (eq 18). Substitution of the results in eq 11 and subsequent numerical integration gives the osmotic repulsion between particles covered by these specific combinations of polymer chains. Only for a homopolymer an analytic function is found after substitution of eq 18 in eq 11 and subsequent integration

$$M(\bar{i},d) = 2a(6/\bar{i})^{1/2} p [1 - 2bdp - p^2]^{-2} \times [3bd - 7 + p(1 + 10bd - 2b^2d^2) + p^2(7 - bd) - p^3] \quad (20)$$

where $p = \exp(-bd)$ and $b = 2a\sqrt{6/\bar{i}l}$.

For the case of equal loops and for $d/\sqrt{i\bar{l}^2} \geq 1$ a good approximation (deviations $< 2\%$) for $M(i,d)$ is given by³²

$$M(i,d) = (3\pi)^{1/2} \{ 6d^2/(i\bar{l}^2) - 1 \} \exp(-3d^2/i\bar{l}^2) \quad (21)$$

In Figure 2 and with more precision in Table I the results are given for the dimensionless osmotic repulsion function $M(\bar{i},d)$ as a function of $d/\sqrt{i\bar{l}^2}$ for particles covered by equal tails, equal loops, and copolymers. Figure 2 shows also $M(\bar{i},d)$ for adsorbed homopolymers. As in Figure 1 the curves for the first three cases are independent of \bar{i} whereas the curves for homopolymers depend on the particular choice of \bar{i} . Qualitatively, however, it can be used as representative for the osmotic effect with adsorbed homopolymers.

Both Figure 1 and 2 show that under comparable conditions, *i.e.*, an equal amount of polymer adsorbed and an equal average size (\bar{i}) per adsorbed chain, a cover of equal loops is less effective in preventing flocculation of the particles than a cover of loops adsorbed in an exponential size distribution as in the case of a copolymer. A cover of equal tails, however, gives even more repulsion and it is an obvious extrapolation to expect that an exponential tail size distribution would again be more effective. This order of effectivity is a completely in line with the density distribution curves shown be-

(31) For particles covered by loops and tails a combination of eq 14 and 15 is to be used. We shall not investigate this case.

(32) Putting $M(i,d) = \langle r^2 \rangle^{1/2} \int_0^d (\hat{\rho}_a)_\infty (\hat{\rho}_b)_\infty dx$ with $(\hat{\rho}_a)_\infty = 12x(i\bar{l}^2)^{-1} \exp(-6x^2/i\bar{l}^2)$ as derived previously¹¹ (and as can be seen from eq 13) and leaving out some minor terms, eq 21 is found.

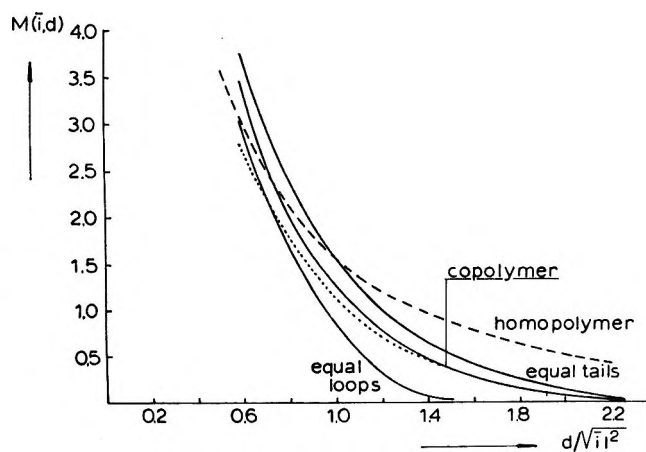


Figure 2. The dimensionless osmotic repulsion function $M(\bar{i}, d)$ (see eq 11) for several modes of attachment of the macromolecules. Only the homopolymer curve depends on \bar{i} ; it is calculated for $\bar{i} = 10$. The dotted curve gives Meier's results⁶ for equal tails.

fore,^{11,12} since the curve for tails extends farthest from the adsorbing interface whereas the curve for equal loops is the most compressed one and the curve for a copolymer takes a middle position. This is also directly demonstrated by the root mean square extension, $\langle x^2 \rangle^{1/2}$, of the segments from the interface, for in the case of equal loops we have¹² $\langle x^2 \rangle_e = il^2/6$, for a copolymer $\langle x^2 \rangle_c = il^2/3$, and for equal tails¹¹ $\langle x^2 \rangle_t = 7il^2/18$. Also the curve for the homopolymer fits into this picture, for the density distribution for an adsorbed homopolymer falls off much less sharply than for the other cases (see Figure 1 in ref 12), and now we find also that the repulsion works over a larger range. This suggests that homopolymers might be very effective as stabilizers for colloidal dispersions. This conclusion, however, is liable to the same serious doubt as its "mother" equation 1. Another drawback of the use of homopolymers is that ν , \bar{i} , and α cannot be controlled independently.

For the case of equal tails Meier⁶ has also calculated $M(\bar{i}, d)$ (or actually $M(\bar{i}, d)/9$ is tabulated in his Table IV), but he used a density distribution which we showed before¹¹ to be too compressed to the adsorbing interface. Table II shows his values for $M(\bar{i}, d)$ to be about 20–30% too low.

Table II: Osmotic Repulsion Function, $M(\bar{i}, d)$, for Equal Tails According to Meier,⁶ M (Meier), and to the Present Paper, M (HVO)

$d/\sqrt{\bar{i}^2}$	M (Meier)	M (HVO)	$\frac{M \text{ (Meier)}}{M \text{ (HVO)}}$
0.4	4.995	6.313	0.79
0.6	2.780	3.723	0.75
0.8	1.809	2.397	0.75
1.0	1.161	1.585	0.73
1.2	0.738	1.043	0.71
1.4	0.459	0.667	0.69

Interaction

According to the classical picture of colloid stability^{2,3} particles in a medium attract each other due to van der Waals–London forces. The free energy of attraction per unit area between two flat particles is given by

$$\Delta F_A = -A/12\pi d^2 \quad (22)$$

where A is the Hamaker constant. This equation neglects effects of electromagnetic retardation, of adsorbed polymer layers,³³ and of the finiteness of the particle thickness. In this paper we are mainly involved in deriving a correct theory for the repulsion between two particles due to adsorbed macromolecules, and therefore we will use eq 22 anyhow for the attraction between the particles.

The change in free energy, ΔF , per unit area when two particles approach each other is now found by adding the repulsion terms ΔF_{VR} and ΔF_M and the attraction term ΔF_A or

$$\Delta F = \Delta F_{VR} + \Delta F_M + \Delta F_A \quad (23)$$

Substitution of eq 6, 10, and 22 in eq 23 gives

$$\Delta F = 2\nu kTV(\bar{i}, d) + 2(2\pi/9)^{3/2} \nu^2 kT \times (\alpha^2 - 1) \langle r^2 \rangle M(\bar{i}, d) - A/12\pi d^2 \quad (24)$$

Thus the main parameters determining the change in free energy on the approach of the two particles are: a, the average number of segments per loop (tail), \bar{i} , or rather the mean square loop size $il^2 = \langle r^2 \rangle_0 \alpha^2$ in which $\langle r^2 \rangle_0$ is proportional to the molecular weight, M , of the loops; b, the number of adsorbed loops (tails) per unit area of surface, ν , here expressed in grams of adsorbed polymer, ω , with $\omega = \nu M/N_a$ (N_a is Avogadro's constant); c, the quality of the solvent, χ , here expressed in the expansion α whereas α and χ are connected by eq 9; d, the mode of attachment of the macromolecules; e, the Hamaker attraction constant.

We will evaluate eq 24 for a number of cases with polystyrene as the adsorbed polymer. We choose M between 10^3 and 10^5 . For long-chain polystyrene Berry³⁴ has found from light-scattering experiments $\langle s^2 \rangle_0/M \cong 7.5 \times 10^{-18} \text{ cm}^2$ where $\langle s^2 \rangle_0^{1/2}$ is the radius of gyration in a θ solvent of a free chain with molecular weight M . With^{17,35,36} $\langle r^2 \rangle_0 = 6\langle s^2 \rangle_0$ we then have adsorbed chains with a root mean square end-to-end distance in solution between 21.2 and 212 Å. We take the amount adsorbed ω between 10^{-10} and 5×10^{-7}

(33) M. J. Vold, *J. Colloid Sci.*, **16**, 1 (1961); B. W. Ninham and V. A. Parsegian, *J. Chem. Phys.*, **52**, 4575 (1970).

(34) G. C. Berry, *ibid.*, **44**, 4550 (1966).

(35) Of course, the use of the factor 6 in the relation between $\langle r^2 \rangle_0$ and $\langle s^2 \rangle_0$ and the extrapolation of Berry's result to such low values of M is not without question because of the deviations³⁶ of short chains from random walk behavior. However, our whole argument is based on random walk behavior, and therefore it is not inconsistent to use this approximation.

(36) H. Sotobayashi and J. Springer, *Advan. Polym. Sci.*, **6**, 473 (1969).

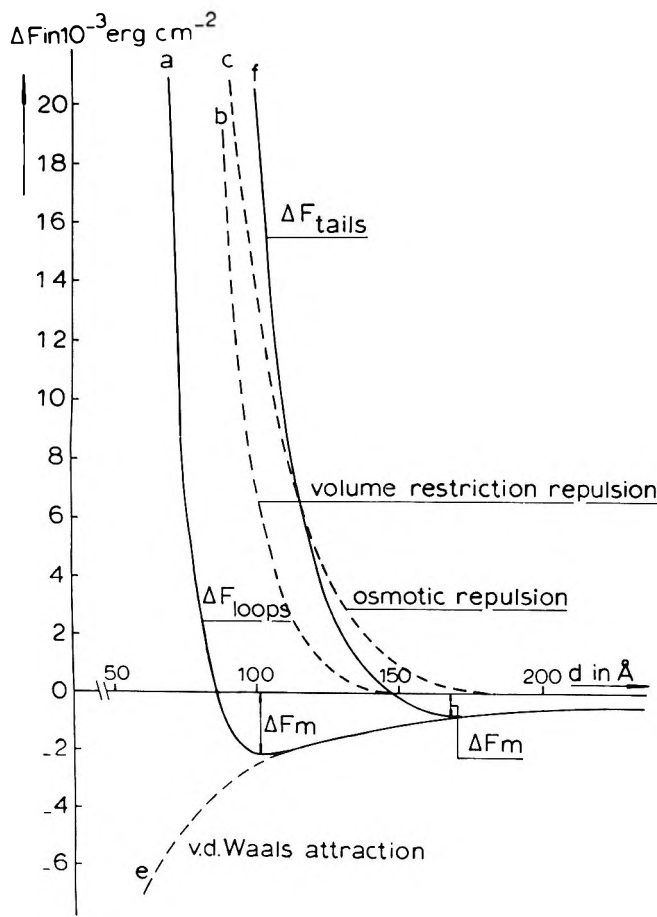


Figure 3. The free energy of interaction *vs.* the distance between particles covered by equal tails (curve *f*) and equal loops (curve *a*). For particles covered by equal tails *b* gives the volume restriction effect and *c* the osmotic repulsion; *f* is the result of the adding up of *b*, *c*, and the van der Waals attraction (*e*). ΔF_m is the depth of the minimum. The curves are calculated for $A = 10^{-13}$ erg, $\alpha = 1.2$, $\omega = 2 \times 10^{-8}$ g cm $^{-2}$, $M = 6000$ (then $\langle r^2 \rangle_0^{1/2} = 52$ Å and the area per chain = 5000 Å 2).

g cm $^{-2}$ and the quality of the solvent 37 between $\alpha = 0.9$ (very poor solvent) and $\alpha = 1.6$ (good solvent). The Hamaker constant is varied between 3×10^{-14} and 3×10^{-12} erg. In the next section we show some of the results mainly for adsorbed tails. The behavior of adsorbed loops and copolymers is then found by comparison having in mind Figures 1 and 2.

Results and Discussion

Figure 3 illustrates the procedure to find the interaction curve for two particles covered by adsorbed macromolecules from the attraction and the two repulsion terms in eq 24. Curve *f* is found by adding the curves *b*, *c*, and *e*; it is the free-energy curve for two flat particles covered by equal tails. Curve *a* is the interaction curve found in an analogous way for particles covered by equal loops. These curves are typical for the stabilization of dispersions by adsorbed macromolecules. At large values of *d* the van der Waals

attraction is predominant, but at shorter distance a very steep repulsion prevents further approach. Unlike the case of electrostatic colloids, 3 we find only one minimum even at very low surface coverage ($\omega = 10^{-10}$ g cm $^{-2}$); the van der Waals attraction may then be predominant over the whole range of *d* up to very short distances. The osmotic repulsion curve *c* starts at higher values of *d* than the curve for the volume restriction. This makes sense because osmotic repulsion starts at the incipient overlap of the polymeric clouds, whereas volume restriction starts when the cloud is hindered by the approaching particle.

The depth ΔF_m of the minimum in the free-energy curve determines the stability of the colloidal state. 38,39 This minimal free energy per cm 2 , ΔF_m , multiplied by the area of interaction h^2 (for flat particles with an edge *h*), is to be compared with the thermal energy of the particles. When $h^2 \Delta F_m < kT$, the particles will not adhere but they will remain single kinetic units, *i.e.*, a stable dispersion. When $h^2 \Delta F_m > kT$, they will have a tendency to adhere and thus to form structures in solution. When this tendency is small, *e.g.*, $kT < h^2 \Delta F_m < 5kT$, simple stirring of the solution may redisperse the particles. Such systems are called thixotropic, and already Freundlich 38 gave an explanation of thixotropy on the basis of free-energy curves of the same general shape as those shown in Figure 3. This thixotropic effect is often found (and essential) in pigment dispersions stabilized by resinlike material. 40 When $h^2 \Delta F_m > 5kT$, the particles will remain together and the system is flocculated. This means that flat, square particles with an edge *h* of 0.1 μ m are stabilized when $\Delta F_m < 5kT/h^2 = 2 \times 10^{-3}$ erg cm $^{-2}$. Thus for the case illustrated in Figure 3 particles covered by tails are stabilized whereas particles covered by loops under otherwise equal conditions are flocculated. For particles with $h = 0.2$ μ m stabilization is found at $\Delta F_m \leq 5 \times 10^{-4}$ erg cm $^{-2}$. Thus in Figure 3 both loops and tails give insufficient stabilization for such particles. Figure 4 shows that a twofold increase in the linear dimension of the particles requires a fourfold increase in the average tail size to ensure stabilization. This influence of particle size on the stability of dispersions stabilized by polymeric layers was already pointed out by Koelmans. 41

For spherical particles with radius *b* large compared to the thickness of the adsorbed layer, the free energy

(37) With Berry's result the relationship between α and χ (eq 9) can be approximated for polystyrene to $\alpha^3(\alpha^2 - 1) = 0.11^{1/2}(\chi - \chi)M^{1/2}$ so that for a good solvent ($\chi = 0.4$) we find $\alpha > 1.2$ for $M > 4000$ (*e.g.*, $\alpha = 1.4$ for $M = 50,000$) whereas for a poor solvent ($\chi = 0.49$) we find $\alpha \leq 1.1$ for $M \leq 10^6$ (*e.g.*, $\alpha = 1.05$ for $M = 10^6$).

(38) H. Freundlich, "Thixotropy," Hermann & Cie., Paris, 1935.

(39) H. C. Hamaker, *Recl. Trav. Chim. Pays-Bas*, **56**, 727 (1937).

(40) F. K. Daniel, VII Fatipecc Congress, 1964, p 280.

(41) H. Koelmans, Dissertation, Utrecht, 1955; H. Koelmans and J. Th. G. Overbeek, *Discuss. Faraday Soc.*, **18**, 52 (1954).

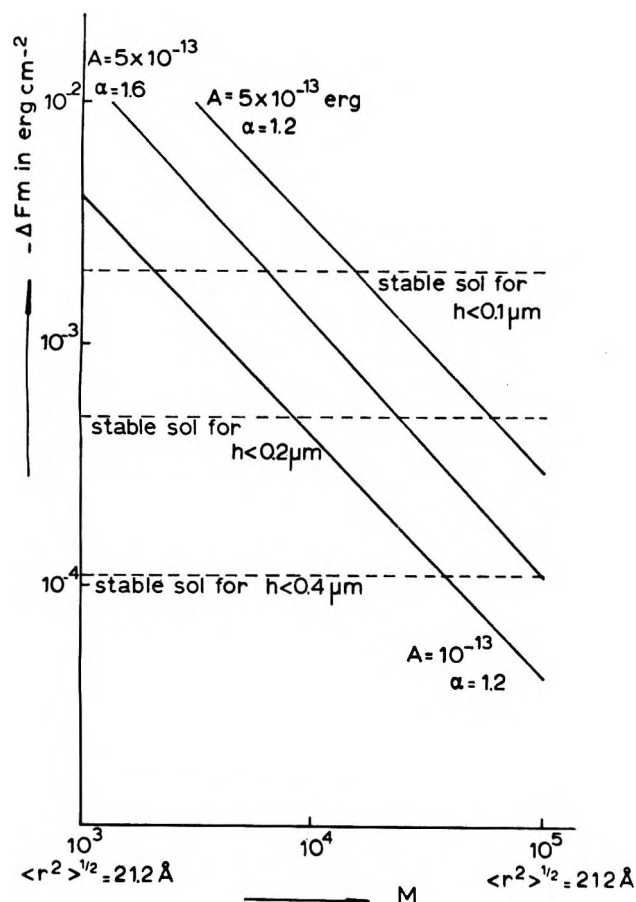


Figure 4. The depth $-\Delta F_m$ in the interaction curve as a function of the molecular weight of the adsorbed tails for $\omega = 2 \times 10^{-8} \text{ g cm}^{-2}$. The stability of the colloidal system is determined by the value of $h^2 \Delta F_m$ compared to kT . For $M = 1000$, $\langle r^2 \rangle^{1/2} = 21.2 \text{ \AA}$ and for $M = 10^5$, $\langle r^2 \rangle^{1/2} = 212 \text{ \AA}$.

of interaction can be calculated using Derjaguin's⁴² procedure to be proportional with b (see Appendix). Thus for spherical particles the influence of particle size will be less dramatic than for flat particles, since for spheres the stability is inversely proportional with b , whereas for flat particles it is inversely proportional with h^2 . Napper's experiments^{43a} on the stability of dispersions in heptane containing particles of polyvinyl acetate (PVAc) and polymethylmethacrylate (PMMA) stabilized by oleophilic chains with some PVAc or PMMA anchor segments and of PVAc^{43b} dispersions in aqueous solution stabilized by polyethylene oxide (PEO) chains indeed show a decrease in stability with increasing particle size, just as Toole, *et al.*,⁴⁴ found for a phthalocyanine blue pigment dispersion stabilized by alkyd resins⁴⁵ in an oil medium.

The two upper curves in Figure 4 show the influence of the solvent on ΔF_m . In Figure 5 the dependence of the stability on the quality of the solvent (α) and on the amount of polymer adsorbed ($\omega \text{ g cm}^{-2}$) is shown. These curves represent cases where $h^2 \Delta F_m \cong 5kT$. To the right of these curves the systems are stable

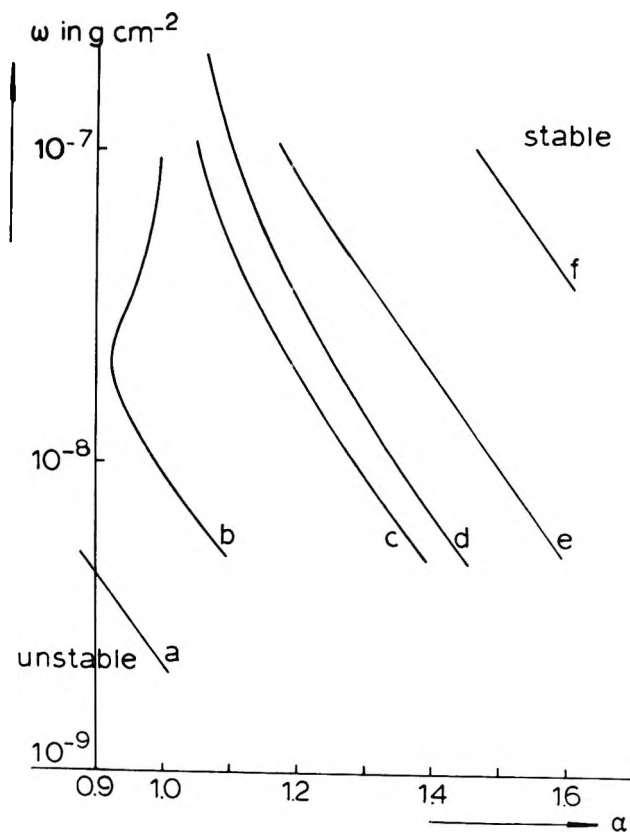


Figure 5. Dependence of the stability on the quality of the solvent and on the amount of polymer adsorbed for some values of the Hamaker constant, of the average molecular weight per tail, and of particle size. To the right of the stability curve the system is stable, to the left it is flocculated. (a), $A = 10^{-13} \text{ erg}$, $M = 10^4$, $h = 0.1 \mu\text{m}$; (b), $A = 5 \times 10^{-13}$, $M = 6 \times 10^4$, $h = 0.1$; (c), $A = 10^{-13}$, $M = 10^4$, $h = 0.2$; (d), $A = 10^{-13}$, $M = 2000$, $h = 0.1$; (e), $A = 5 \times 10^{-13}$, $M = 6 \times 10^4$, $h = 0.2$; (f), $A = 5 \times 10^{-13}$, $M = 10^4$, $h = 0.2$.

($h^2 \Delta F_m < 5kT$), to the left unstable ($h^2 \Delta F_m > 5kT$). Figure 5 shows that with decreasing α the stability decreases. Napper⁴³ found indeed that instability was induced by decreasing the solvent power of the dispersion medium for the stabilizing moieties. Incipient flocculation occurred in media which were either θ solvent ($\alpha = 1$) or which were only of somewhat better solvent power than θ solvents. Heller and Pugh⁴⁶ have found that gold sols in aqueous solution stabilized by adsorbed PEO are flocculated by addition of KCl at a concentration of about 0.5 mol/l. Several^{47,48} authors

(42) B. Derjaguin, *Kolloid Z.*, **69**, 155 (1934).

(43) (a) D. H. Napper, *Trans. Faraday Soc.*, **64**, 1701 (1968); (b) D. H. Napper, *J. Colloid Interface Sci.*, **32**, 106 (1970).

(44) J. Toole, J. S. F. Gill, and R. G. Tainturier, VII Fatigue Congress, 1964, p 289.

(45) W. Black, F. Th. Hesselink, and A. Topham, *Kolloid-Z. Z. Polym.*, **213**, 150 (1966).

(46) W. Heller and T. L. Pugh, *J. Polym. Sci.*, **47**, 203 (1960).

(47) Yu. M. Glazman, *Discuss. Faraday Soc.*, **42**, 255 (1966).

(48) K. G. Mathai and R. H. Ottewill, *Trans. Faraday Soc.*, **62**, 750 (1966).

have described the same phenomenon for other hydrophobic sols (AgI, As₂S₃, latex) stabilized by a nonionic surfactant with a long PEO chain. This is completely in line with Napper's result because water becomes a poor solvent for PEO when the salt concentration comes in this range (salting-out effects). This same phenomenon is also demonstrated by van der Waarde's⁴⁹ finding that the equilibrium thickness of an aqueous film stabilized by a nonionic (PEO) surfactant decreases with increasing NaCl or urea concentration, especially at concentrations above 1 mol/l. Here the decrease of α is directly seen in a decrease of the film thickness.

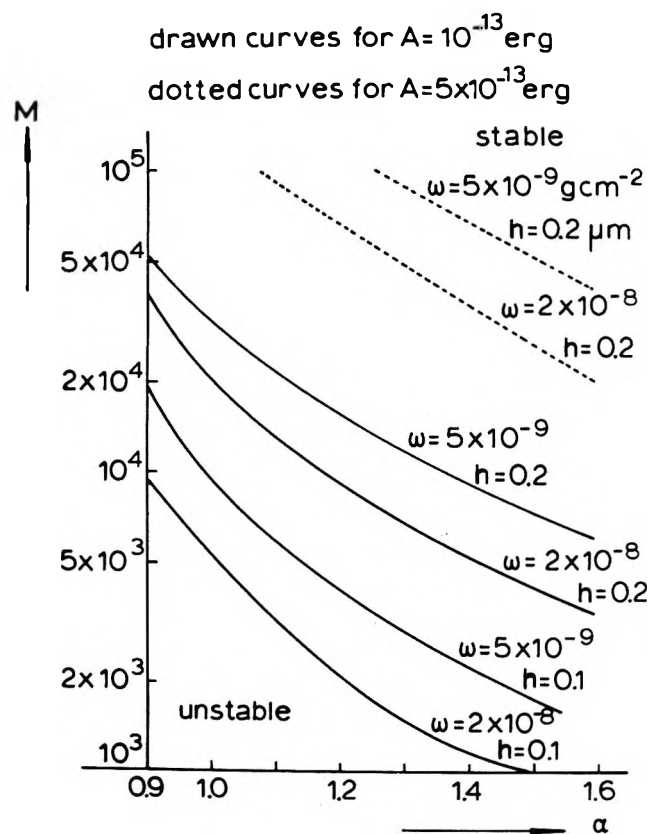


Figure 6. Dependence of the stability on the quality of the solvent (α) and on the average molecular weight per adsorbed tail.

Napper found that the flocculation brought about by decreasing the solvent power of the medium was a reversible process. The system redisperses when the quality of the solvent is restored. The reversibility of flocculation is a general consequence of interaction curves, as shown in Figure 3, which have only one minimum.

Figures 5 and 6 show that also in a good solvent instability can occur when the other stability-determining parameters (ω , M , A , h) are chosen too unfavorably. Curve b in Figure 5 shows an interesting extremum. For an intermediate value of the amount

adsorbed the solvency required for stabilization has a minimum at $\alpha < 1$. The osmotic effect causes an attraction at $\alpha < 1$ ($\Delta F_M < 0$, see eq 10), but at these intermediate values of ω the repulsion due to volume restriction prevails over both van der Waals attraction and osmotic attraction. This is also the reason that in Figure 6 stability is found at $\alpha = 0.9$ at high enough average tail size. At higher ω the stability line b in Figure 5 curves back to $\alpha = 1$, for with increasing ω the osmotic attraction at $\alpha = 0.9$ increases faster than the repulsion due to volume restriction because, as Meier⁵ pointed out, ΔF_M is proportional with ω^2 whereas ΔF_{VR} is proportional with ω .

Figure 6 shows stability lines as a function of average tail size M and solvency of the medium α . The strong influence of M on the stability is understood from the notion that highly extended layers cause repulsion when the particles are far away from each other and the van der Waals attraction is still small. Heller and Pugh find indeed that PEO of $M = 9000$ is more effective than PEO of $M = 6000$ as a stabilizer for gold sols in aqueous solution. Napper,^{43b} however, found that the stability of PVAc dispersions stabilized by PEO was relatively insensitive to the molecular weight of the stabilizing moieties. This difference might in part be due to their different method of measuring the stability (Heller and Pugh increase the salt concentration up to flocculation and Napper the temperature), but also, *e.g.*, to changes in the average tail size due to extra adsorption. For Molau's⁶⁰ polymeric "oil in oil" emulsions—polybutadiene (PB)—polystyrene (PS) in benzene as common solvent stabilized by a two-block PB-PS copolymer with blocks of approximately equal size—the stability is found^{60b} to increase, as we expected, very much with increasing size of the blocks.

In conclusion, we have a theory which gives a satisfactory description of protective action and which is in qualitative agreement with several known aspects of protection. Notable shortcomings of the theory are the *a priori* assumption of the macromolecules being adsorbed on only one particle and the unclear relation between χ and α . Protection by adsorbed homopolymers is not a completely solved problem because of the unreliability of eq 1. Experiments to test the stability of protected sols on systematic variations of the various stability-determining parameters (ω , M , α , A , h) are desirable. Adsorption studies on variations of ω , M , and α (or χ) could give useful additional information.

Acknowledgment. The authors wish to thank Dr. E. M. J. Bertin of the Electronisch Rekencentrum, Utrecht, for his advice in the numerical evaluation of eq 7 and 11.

(49) K. M. van der Waarde, private communication, 1968.

(50) (a) G. E. Molau, *J. Polym. Sci.*, **A3**, 1267, 4235 (1965); (b) G. E. Molau, *Kolloid-Z. Z. Polym.*, **238**, 493 (1970).

Appendix

Derjaguin⁴² considered the repulsive energy between two spheres in a first approximation to be formed by the contributions of infinitesimal small rings parallel to each other at a distance d . The repulsive free energy between two parallel rings covered by adsorbed macromolecules is approximately given by $\Delta F_{VR} + \Delta F_M$. The free energy of repulsion between two spheres of radius b at a minimal distance d_0 (the distance between the centers of the spheres being $2b + d_0$) is then found by integration.⁵¹ The value of the integral does not

$$V_R = 2\pi b \int_{d_0}^{\infty} (\Delta F_{VR} + \Delta F_M) dd$$

depend on b , so that V_R is proportional with b . The van der Waals attraction energy between two spheres is also proportional with b , so that the total free energy of interaction is proportional with b . The stability of the colloidal system is determined by the minimum in the free-energy curve, and of course also this minimal value of the interaction energy is proportional with b .

(51) Reference 3b, Chapter IX, eq 54.

The Adsorption of Fibrinogen. An Electron Microscope Study¹

by R. R. Gorman, G. E. Stoner,* and A. Catlin

Department of Materials Science, University of Virginia, Charlottesville, Virginia 22901 (Received September 25, 1970)

Publication costs assisted by The National Institute of Dental Research

The process of adsorption of fibrinogen onto mica and evaporated carbon has been characterized as completely diffusion controlled by the direct counting of individual molecules through the use of the electron microscope. As applied to adsorption on mica the method produced Hall and Slayter triad molecules, and the deposits were reproducibly and uniformly distributed over the specimens. Under the experimental conditions, the adsorption was strongly dependent on the composition of the substrate, and in the case of mica, it was insensitive to the composition of the suspending buffer.

Introduction

The adsorption of proteins and macromolecules from aqueous suspensions has been investigated by means of several experimental techniques, including streaming potentials,^{2a} isotope and fluorescence labeling,^{2b} depletion of suspension,³ ellipsometry,⁴ and visual observation in the electron microscope.⁵ Fibrinogen adsorption is of special importance because of its unique configuration in the adsorbed stage, its strong tendency to adsorb, and its possible involvement in the initial stages in the interaction of human blood *in vivo* with devices such as artificial heart valves and arteries.^{2b, 6, 7}

The objective of this investigation was to characterize the adsorption of fibrinogen onto muscovite mica and evaporated carbon at short adsorption times from a dilute, unstirred suspension of the protein molecules, and to investigate the effect of the properties of the suspending buffer on the adsorption. An additional objective was to establish a methodology which could be applied to other proteins and solids. The method was the visualization of the adsorbed protein molecules in the electron microscope and the obtaining of kinetic

data by direct counting of the individual adsorbed molecules.

Materials and Equipment

The bovine fibrinogen was the diagnostic product of the General Diagnostics Division of Warner-Chilcott, packaged in vials as 6 mg of clottable protein, 17 mg of sodium chloride.

The human fibrinogen was prepared in this labora-

(1) This work supported by the National Institutes of Health under Grant DE 02111-07.

(2) (a) R. D. Falb, G. A. Grode, M. M. Epstein, B. G. Brand, and R. I. Leininger, June 29, 1965. P. B. 168, 861, U. S. Dept. of Commerce; (b) R. D. Falb, G. A. Grode, M. T. Takshashi, and R. I. Leininger, March 30, 1967. P. B. 175, 668, U. S. Dept. of Commerce.

(3) A. D. McLaren, *J. Phys. Chem.*, **58**, 129 (1954).

(4) L. Vroman, "Blood Clotting Enzymology," W. H. Seegers, Ed., Academic Press, New York, N. Y., 1967, p 279.

(5) D. Lang and P. Coates, *J. Mol. Biol.*, **36**, 137 (1968).

(6) L. Vroman, *J. Biomed. Mater. Res.*, **3**, 669 (1969).

(7) D. J. Lyman, J. L. Brash, and K. G. Klein, Proceedings of the Artificial Heart Conference, R. J. Hegyeli, Ed., Washington, D. C., 1969, pp 113-122.

tory⁸ from fresh citrated human plasma. It was separated from the plasma by a procedure involving adsorption of other components on magnesium sulfate, barium sulfate, and triethylaminoethyl cellulose, and glycine precipitation. The protein component of this preparation was assayed electrophoretically as being 95% fibrinogen. Total fibrinogen assays by absorbance at 280 m μ and clottable protein assays indicated 100% clottability.

Distilled water was used throughout, and the mica was a clear, gray-green Tanganyikan muscovite.

A Micros automatic valving vacuum evaporator, Model VE-10, with an air-cooled diffusion pump was the principal unit used in the evaporation of carbon and platinum. The electron microscope was the JEM 6A with the 6C power supply. The usual accelerating voltage was 50 kV, the usual objective aperture, 50 μ in diameter.

Procedures

Preparation of Solutions. The Warner-Chilcott bovine fibrinogen was obtained in the form of 6-mg freeze-dried batches, each packed in a small vial with 17 mg of NaCl. The fibrinogen was reconstituted by adding 2 ml of distilled water (pH 6–8) to the vial, and then diluted to $1/50$ of its original concentration with the appropriate buffer. A sample of this suspension was assayed for ultraviolet adsorption at 280 nm, and another portion was diluted to $1/100$ of its initial concentration, producing a final fibrinogen concentration of about 0.6×10^{-3} mg/ml.

The human fibrinogen was diluted in the same way, but in some cases was assayed before diluting.

Adsorption and Rinsing. The adsorption was accomplished by immersing 1-in. square pieces of freshly split mica in the unstirred suspensions. For the adsorption on carbon, the mica was coated with an evaporated carbon film after splitting. After the adsorption had proceeded for the desired length of time, the mica specimen was pulled quickly out of the suspension while protein-free buffer was poured over the specimen surface. This pouring was continued for 20 to 300 sec, at a rate of 150 to 300 ml per min. The buffer used for this rinsing was the same as that used to make up the suspension. When the suspending and rinsing buffer was citrate or saline phosphate, a final rinse was made with 50–150 ml of the ammonium acetate buffer at 0.26 M, pH 7, because of its special usefulness in electron microscope preparations. The final step was the blowing off of the remnant film of buffer with room temperature air from a laboratory blower.

An important variation of the standard procedure was the rinsing experiment, in which several specimens were immersed in the fibrinogen suspension for the same length of time and then rinsed for different times, ranging from 40 sec to 5 min.

The other variation was the splitting of the mica

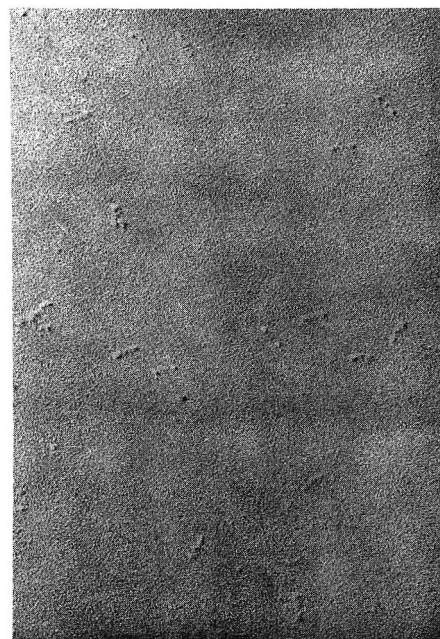


Figure 1. Bovine fibrinogen on mica.

while immersed in the fibrinogen suspension, in order to produce a surface which had never been exposed to the atmosphere, and which had not been drawn through the air-suspension interface.

Platinum Shadowing. The platinum shadowing technique was in essence that applied to the visualization of fibrinogen by Hall and Slayter.⁹ The specimens, with their deposits of adsorbed fibrinogen, were placed in a vacuum evaporator and were shadowed with platinum and then coated, if necessary, with a strengthening film of carbon. The specimens were then removed from the evaporator and the double film or pseudoreplica was stripped off on a water bath and mounted on electron microscope grids.

Results and Discussion

Adsorption on Mica. The technique produced well-defined fibrinogen triads on mica, similar to those found by Hall and Slayter. Typical photomicrographs are shown in Figures 1 and 2.

The adsorbed fibrinogen molecules were found to be distributed uniformly over the mica surface. This was determined by photographing and counting the number of adsorbed molecules in several (five to seven) areas on each of nine different specimens. The average value of the number of fibrinogen molecules per electron image plate and the standard deviation of these count values were calculated for each specimen. It is seen in Table I, below, that with one exception, the range of counts was within two standard deviations from the mean, and the values of the standard deviations were reasonably

(8) W. L. Walker, submitted for publication.

(9) C. E. Hall and H. S. Slayter, *J. Biophysic. Biochem. Cytol.*, **5**, 11 (1959).

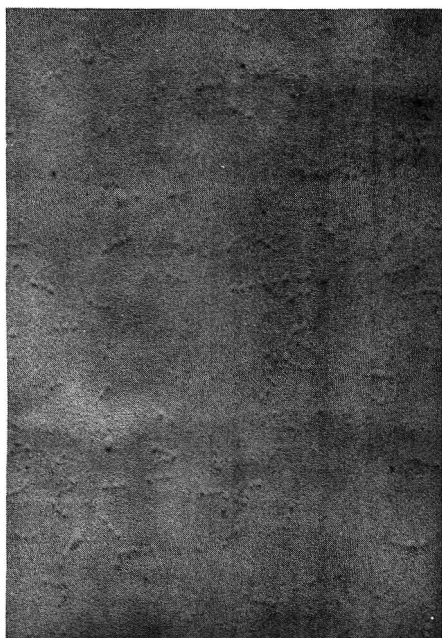


Figure 2. Human fibrinogen on mica; well-defined triads.

close to the square roots of the average counts, a relationship which would be expected of a Poisson distribution of counts per plate.

Table I: Variability of Raw Data

Average count of molecules per E. M. plate	Square root of average count	Observed standard deviation of counts	Range of observed deviations
12	3	2	-1 to +3
15	4	3	-5 to +3
39	6	5	-4 to +9
48	7	11	-14 to +17
59	8	11	-14 to +20
90	9	15	-22 to +20
113	11	14	-18 to +24
185	14	19	-38 to +22
266	16	41	-93 to +63

The data for the time and concentration dependence of the adsorption of bovine fibrinogen on mica are presented graphically in Figure 3. The observed average numbers of molecules, N , divided by C_0 , the bulk fibrinogen concentrations in molecules per milliliter, are plotted against adsorption time in seconds.

The parabolic form of this graph suggests that the adsorption may be a completely diffusion-controlled process, in which there is no significant energy barrier to adsorption nor any significant desorption at the interface. Such a process is described in ref 10

$$\frac{N}{C_0} = 2\left(\frac{D}{\pi}\right)^{1/2} t^{1/2} \quad (1)$$

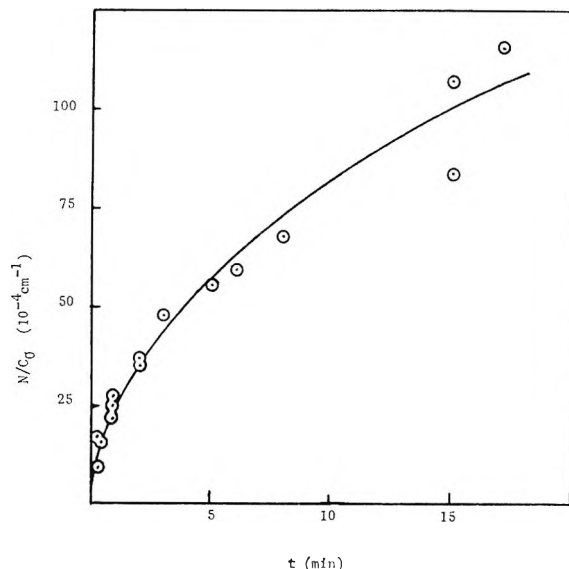


Figure 3. Adsorption kinetic data.

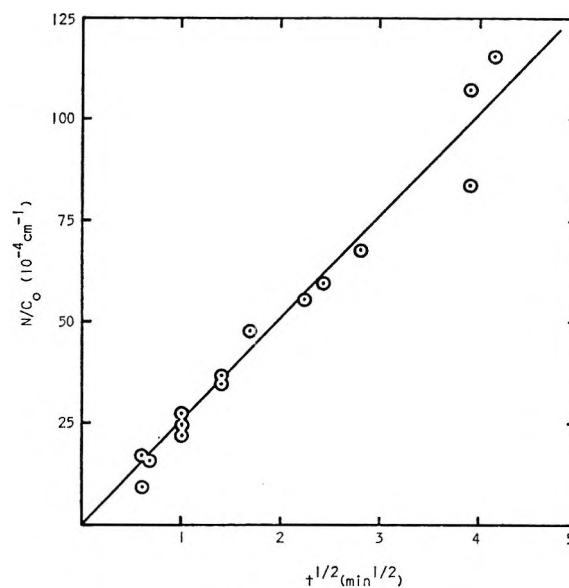


Figure 4. Fit of adsorption data to diffusion curve.

where D is the diffusion coefficient for the molecule. To test this hypothesis, the observed values of N/C_0 were plotted against $t^{1/2}$, and this graph is presented in Figure 4. The value of N for a given experiment was obtained by dividing the average number of molecules per standard electron image plate by the standard plate area, which was $2.02 \times 10^{-8} \text{ cm}^2$. The values for the bulk concentrations of fibrinogen, C_0 in terms of molecules per milliliter, were obtained from the uv adsorption at 280 nm, using for the extinction coefficient 1.6 cm^{-1} , multiplied by the factor 1.1 as an estimate of the effect of the impurity level reported by the supplier, and taking 350,000 for the molecular weight.

A straight line fits the data within the uncertainty

(10) F. C. Goodrich, *J. Chem. Phys.*, **22**, 588 (1954).

Table II: Results of Fibrinogen Adsorption on Mica

Suspending buffer		Fibrinogen			
		Average standard count, molecules/cm ²	Actual concentration, mg/ml	Source	Rinsing time, sec
0.26 M CH ₃ COONH ₄ (ammonium acetate)	pH 6.7	2.8 × 10 ⁹	0.50 × 10 ⁻³	Bovine	30
0.26 M CH ₃ COONH ₄	pH 7.1	2.1 × 10 ⁹	0.55 × 10 ⁻³	Bovine	40
0.26 M CH ₃ COONH ₄	pH 7.6	2.3 × 10 ⁹	0.66 × 10 ⁻³	Bovine	40
0.26 M CH ₃ COONH ₄	pH 7.0	2.6 × 10 ⁹	0.47 × 10 ⁻³	Bovine	40
0.26 M CH ₃ COONH ₄	pH 7.1	2.6 × 10 ⁹	0.98 × 10 ⁻³	Bovine	40
0.40 M NaCl + 0.014 M NaH ₂ PO ₄ + 0.022 M Na ₂ HPO ₄	pH 6.4	2.7 × 10 ⁹	1.16 × 10 ⁻³	Human	60
0.055 M sodium citrate + HCl	pH 8.3	2.7 × 10 ⁹	0.73 × 10 ⁻³	Human	35
0.15 M CH ₃ COONH ₄	pH 7	2.6 × 10 ⁹	0.51 × 10 ⁻³	Bovine	30
0.47 M CH ₃ COONH ₄	pH 7	3.7 × 10 ⁹	0.9 × 10 ⁻³	Human	40
0.47 M CH ₃ COONH ₄	pH 7	3.6 × 10 ⁹	0.9 × 10 ⁻³	Human	120
0.47 M CH ₃ COONH ₄	pH 7	3.5 × 10 ⁹	0.9 × 10 ⁻³	Human	300

established by the spread of the measurements. The diffusion coefficient D is found to be

$$D = 0.91 \times 10^{-7} \text{ cm}^2/\text{sec}$$

This is about half that obtained by Shulman¹¹ from his sedimentation experiments. He suspended fibrinogen in 0.40 *m* NaCl, 0.05 *m* sodium phosphates at pH 6.2, and obtained $D = 2.2 \times 10^{-7} \text{ cm}^2/\text{sec}$.

A reason for this discrepancy may lie in the use of 350,000 for the molecular weight of fibrinogen in eq 1. This value has been reported by several investigators,^{11,12} but others have found 369,000,¹³ 392,000,¹⁴ and even 580,000.¹⁵ Given a pure, monodisperse suspension of fibrinogen and an accurate value for D , this experiment would be an excellent means for measuring the molecular weight. Taking D as $2.2 \times 10^{-7} \text{ cm}^2/\text{sec}$ and taking for N , the average experimental value at 1 min of $26 \times 10^8 \text{ molecules/cm}^2$ one obtains

$$\text{mol wt} = \frac{2C_0}{N} \left(\frac{D}{\pi} \right)^{1/2} t^{1/2} \times 6.02 \times 10^{23} = 570,000$$

The effects of variations in buffer composition and pH and in rinsing time are shown in Table II. The standard 1-min counts of fibrinogen molecules per square centimeter are a convenient way of comparing the results of experiments. They were obtained by converting the counts observed at various adsorption times and concentrations into the values which would be expected at 1 min and a fibrinogen concentration of $0.6 \times 10^{-3} \text{ mg/ml}$, by means of eq 1.

The adsorption counts are seen to have been insensitive to the variations which were made in the buffer composition and in rinsing time.

The results from the experiment in which the mica specimen was split while immersed in the fibrinogen suspension showed no difference when compared with the

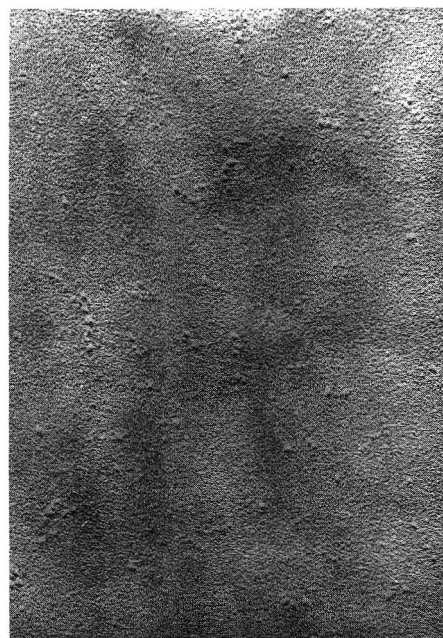


Figure 5. Bovine fibrinogen on carbon.

results obtained by splitting the mica in air and then immersing it.

In no instance was an equilibrium reached in the adsorption onto mica. The maximum coverage observed and counted was roughly $1 \times 10^{10} \text{ molecules/cm}^2$, or $6 \times 10^{-5} \text{ g/m}^2$. At higher coverages it became difficult, because of overlapping, to distinguish and count individual molecules.

(11) S. Shulman, *J. Amer. Chem. Soc.*, **75**, 5846 (1953).

(12) E. A. Kaspary and R. A. Keswick, *Biochem. J.*, **67**, 41 (1957).

(13) B. Blomback and T. C. Laurent, *Ark. Kemi*, **12**, 137 (1957).

(14) E. F. Casassa, *J. Phys. Chem.*, **60**, 926 (1956).

(15) J. L. Oncley, G. Scatchard, and A. Brown, *ibid.*, **51**, 184 (1947)

Adsorption on Carbon. The results from the few experiments which were performed with a vacuum evaporated carbon film as the adsorber were qualitatively and quantitatively different from the mica results. The adsorbed deposit did not (Figure 5), for the most part, have the triad form, and the adsorption apparently reached equilibrium, the counts for 5- and

10-min exposure to the standard fibrinogen concentration (0.6×10^{-3} mg/ml) both being about 2×10^9 molecules/cm².

This is in marked contrast to the adsorption of fibrinogen on mica, where equilibrium was not reached and where the number of molecules adsorbed increased with time in an apparently diffusion-controlled process.

Adsorption Inhibition as a Mechanism for the Antithrombogenic Activity of Some Drugs. I. Competitive Adsorption of Fibrinogen and Heparin on Mica

by G. E. Stoner,* S. Srinivasan, and E. Gileadi

Department of Materials Science, School of Engineering and Applied Science, The University of Virginia, Charlottesville, Virginia, and Electrochemical and Biophysical Laboratory, Department of Surgery and Surgical Research, State University of New York, Downstate Medical Center, Brooklyn, New York 11203 (Received September 23, 1970)

Publication costs assisted by The Center of Advanced Studies, University of Virginia

Heparin has been shown to inhibit the adsorption of fibrinogen on mica surfaces. This effect was observed over several orders of magnitude of heparin concentration and for fibrinogen concentrations ranging from 10^{-4} physiological concentration up to physiological concentration. The inhibition effect of heparin is destroyed when the drug is neutralized with protamine. The results are explained by an electrostatic desorption of fibrinogen by the highly negatively charged drug. This is consistent with adsorption studies of fibrinogen on metals which show desorption on highly negative surfaces. Some insight is given into the mechanism of heparin action in the adsorbed or bound state.

Introduction

Fibrinogen is known to adsorb extensively on most surfaces exposed to blood, plasma, or a buffered solution containing it.¹ The possible importance of this adsorption in the overall processes of formation of thrombi has been discussed out by numerous investigators.²⁻⁵ Recent studies⁶ of adsorption of fibrinogen (from purified buffer solutions) onto freshly cleaved mica surfaces at different pH and concentrations showed nearly complete coverage on the surface even when the concentration in solution was reduced to 0.001 physiological concentration (phys concn). The rate of adsorption was found to be diffusion controlled in the concentration range of 10^{-3} to 10^{-5} phys concn (10^{-8} – 10^{-10} mol/l.). It was also noted in the same study that fibrinogen was held very tenaciously to the surface, and it could not be removed by repeated rinsing, when performed within the normal temperature and pH range.

The mechanism of antithrombogenic activity of drugs such as heparin, when adsorbed on the surface (or bonded in the surface phase by a suitable chemical process) is of major interest. Heparin is a polysaccharide containing a relatively large number of negative

groups (six negative charges per tetrasaccharide unit). A surface covered with a monolayer of this substance will hence appear as a negatively charged surface having a relatively high charge density. Recent work on the adsorption of fibrinogen on mercury as a function of concentration and potential⁷ showed heavy adsorption at positive and at low negative potentials. However, at potential more negative than -1.6 V *vs.* (see) adsorption of fibrinogen did not occur, even at the highest solution concentration studied. This potential was

- (1) L. Vromon, *J. Biomed. Mater. Res.*, **3**, 669 (1969).
- (2) L. Vromon and A. L. Adams, *Thromb. Diath. Haemorrh.*, **18**, 510 (1967).
- (3) D. J. Lyman, J. L. Brash, and K. G. Klein, "Proceedings of the Artificial Heart Conference," R. J. Hegveli, Ed., U. S. Department of Health, Education, and Welfare, Public Health Service, National Institutes of Health, Washington, D. C., 1969, pp 113-122.
- (4) E. Gugler and E. F. Luscher, *Thromb. Diath. Haemorrh.*, **14**, 361 (1965).
- (5) R. E. Baier and R. C. Dutton, *J. Biomed. Mater. Res.*, **3**, 191 (1969).
- (6) R. Gorman, Ph.D. Thesis, University of Virginia, Charlottesville, Va., 1969.
- (7) G. E. Stoner, *J. Biomed. Mater. Res.*, **3**, 645 (1969).

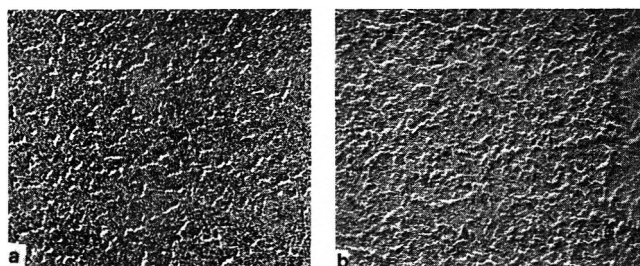


Figure 1. Electron micrographs of fibrinogen adsorbed on mica: (a) 0.001 physiological concentration; (b) physiological concentration.

found to correspond to a surface charge density of $-20 \mu\text{C}/\text{cm}^2$.

The purpose of the present study was to examine the effect of heparin on the adsorption of fibrinogen from human plasma or from purified preparations of fibrinogen in buffer solution on freshly cleaved mica surfaces. The experimental variables were the concentrations of heparin and fibrinogen and the order of exposure of the surface to their solutions. It was also intended to find the effect of protamine, a drug commonly employed clinically to neutralize the effect of heparin, on the ability of heparin to inhibit adsorption of fibrinogen.

Experimental Section

Mica surfaces (Tanganyikan muscovite⁸), freshly cleaved immediately prior to immersion in solution, were used as substrates in all adsorption experiments. Adsorption of fibrinogen was followed by electron microscopy using a Type JEM 6A electron microscope. A shadowing technique, based on a modified Hall and Slayter procedure, was employed.^{9,10}

The supporting electrolyte for all solutions was 0.1 M ammonium acetate, adjusted to pH 7.0. Fibrinogen was prepared from freshly drawn human plasma. Heparin was "Liquamin Sodium"¹¹ 1000 USP units per cc, made up to desired concentrations. Solutions of protamine sulfate were Grade 1 (from Salmon).¹²

Results and Discussion

1. Adsorption of Fibrinogen and Its Inhibition by Heparin. Fibrinogen is adsorbed very extensively on mica surfaces. Figure 1a shows the electron micrograph obtained when mica was dipped in a very dilute (10^{-3} of phys concn) buffered solution of fibrinogen. Figure 1b shows the results obtained for a solution containing fibrinogen at the physiological concentration. A high fractional degree of coverage is obtained in the solution of lower concentration and the individual fibrinogen molecules can be seen clearly on the electron micrograph. At physiological concentration the surface is completely covered with fibrinogen which tends to form clusters and possibly multilayers in certain areas. For this reason a dilute solution of 10^{-3} phys concn (equal to ca. 10^{-8} mol/l.) of fibrinogen was used in all further experiments.

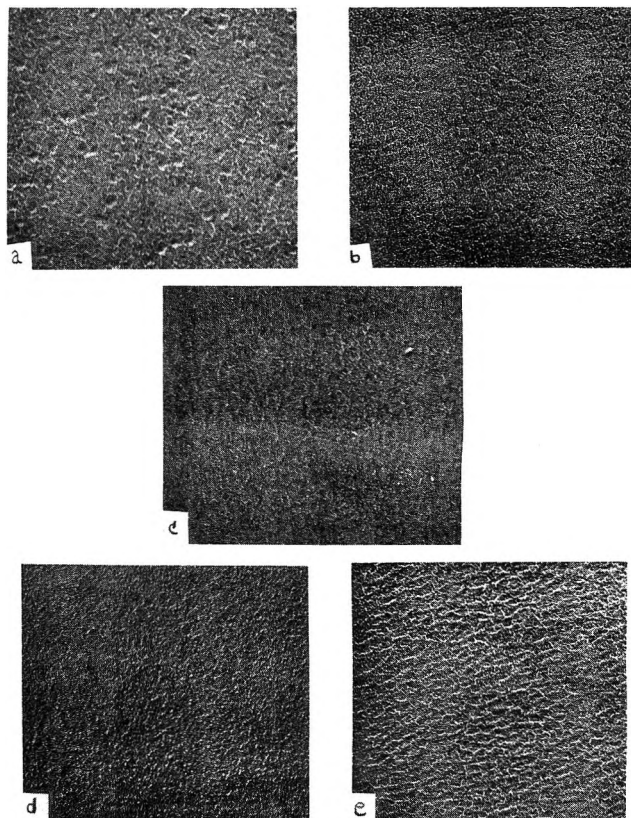


Figure 2. Electron micrographs of: (a) partial inhibition of fibrinogen by prior exposure to 0.0002 units of heparin per ml; (b) and (c) total inhibition by prior exposure to 0.002 and 2 units per ml, respectively; (d) mica surface not exposed to heparin; and (e) mica exposed to 2 units of heparin per ml.

In the experiments shown in Figure 2a, b, and c the mica surface was first exposed to solutions of various concentrations of heparin (in the range of 2×10^{-4} to 2 units per cc = 6×10^{-11} to 6×10^{-7} mol/l.), washed with buffer solution, and then dipped into the fibrinogen solution for 1 min. At the lowest heparin concentration (Figure 2a) only partial inhibition of fibrinogen adsorption occurred, while at a concentration of 6×10^{-10} mol/l. or above, no fibrinogen was adsorbed on the surface (Figure 2b and c). The pattern seen in Figures 2b and c is caused by the adsorption of heparin (although the individual heparin molecules are too small to be seen by this technique). This is verified by comparing the electron micrographs for a bare mica surface (Figure 2d) with that for a mica surface exposed to heparin (Figure 2e).

The structure of the basic tetrasaccharide unit in heparin is shown in Figure 3. This unit has a molecular weight of 936. Thus there are about 20 such units

(8) Asheville-Schoonmaker Mica Co., Newport News, Va.

(9) C. E. Hall and H. S. Slayter, *J. Biophysic. Biochem. Cytol.*, **5**, 11 (1959).

(10) R. R. Gorman, G. E. Stoner, and A. Catlin, *J. Phys. Chem.*, **75**, 2103 (1971).

(11) Organon Inc., West Orange, N. J.

(12) Sigma Chemical Co., St. Louis, Mo.

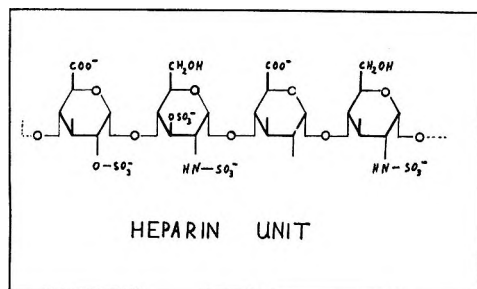


Figure 3. The structure of the tetrasaccharide unit of heparin.

per molecule of heparin (molecular weight $17\text{--}20 \times 10^3$). Assuming that each tetrasaccharide unit adsorbed on the surface occupies an area equal to that of four to five benzene molecules, the maximum surface concentration of heparin is $(3.2\text{--}4) \times 10^{-12}$ mol/cm² (the maximum surface concentration for benzene is 3.2×10^{-10} mol/cm²).¹³

On the basis of this calculation it is easy to see why only partial inhibition could be achieved in the experiment shown in Figure 2a. The total area of the mica used in each experiment was *ca.* 4 cm² and the volume of the solution was 50 cc. Thus, when the concentration of heparin was as low as 6×10^{-11} mol/l., there was not enough heparin in solution to form a monolayer on the surface and total inhibition of fibrinogen adsorption could not be expected. It is rather remarkable that when the concentration of heparin was raised by one order of magnitude, complete inhibition of fibrinogen adsorption *did* occur.

Although the total amount of heparin in this solution was *ca.* 2.5 times the amount required to form a monolayer, it is unlikely that a complete monolayer could indeed be formed in such dilute solutions in the short exposure time of 1 min. This may point to the conclusion that even partial surface coverage by heparin may inhibit entirely the adsorption of fibrinogen, due to the negative charge imparted to the surface, as will be discussed below.

2. *Displacement of Adsorbed Fibrinogen by Heparin.* When a freshly cleaved mica surface was immersed in a solution containing both heparin and fibrinogen, the results were similar to those observed when the surface was first exposed to heparin and then to fibrinogen. Thus at concentrations of heparin of 6×10^{-10} mol/l. or higher (Figures 4a and b) complete inhibition occurred, while at a concentration of 6×10^{-11} mol/l. of heparin the adsorption of fibrinogen was only partially inhibited, as seen in Figure 4c. Comparing the molar concentrations of heparin and fibrinogen it is seen that complete inhibition of adsorption already occurs when the ratio of fibrinogen to heparin molecules is about 16. Thus the possibility that inhibition is due to some reaction between heparin and fibrinogen in the bulk of the solution is excluded. A similar ratio between the number of fibrinogen and heparin molecules

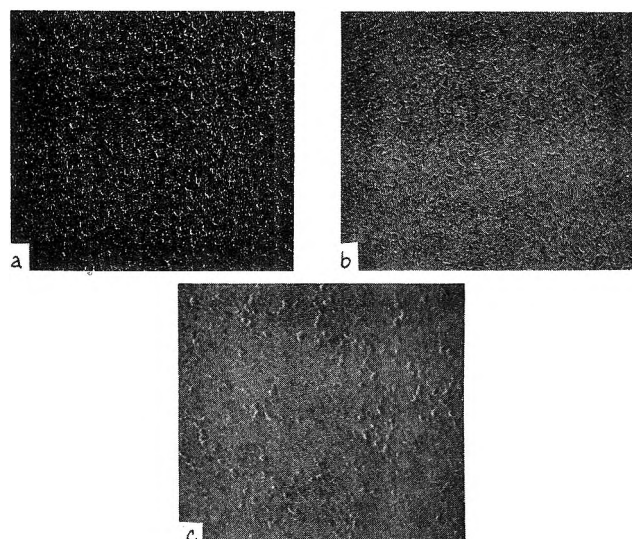


Figure 4. Electron micrographs of competitive adsorption from solutions containing both fibrinogen and heparin: (a) 2 units of heparin/ml; (b) 0.002 units/ml; (c) 0.0002 units/ml. All fibrinogen concentrations are 0.001 physiological.

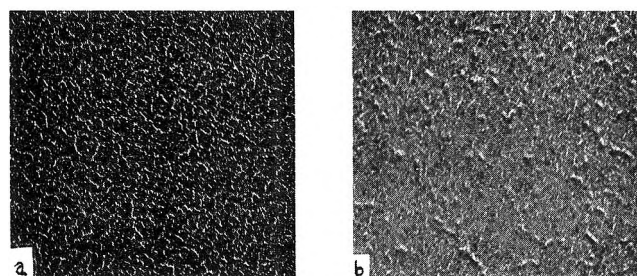


Figure 5. Electron micrographs of mica surfaces first exposed to 0.001 physiological fibrinogen and then: (a) 0.02 units of heparin per ml; and (b) 0.002 units/ml.

also exists in the blood after a usual dosage of heparin has been administered. Thus, inasmuch as the anti-thrombogenic properties of this drug in the adsorbed or bound state may depend on its effect on fibrinogen, there may be an interaction taking place on the surfaces of the blood vessels rather than in the bulk phase. Although the adsorption of fibrinogen is an important step in the formation of thrombi, one cannot conclude, on the basis of the above evidence only, that the physiological effect of heparin is due to the inhibition of this adsorption process. The drug may act in addition (or mainly) by interfering with a crucial enzymatic process leading to thrombus formation, *e.g.*, with the conversion of protrombin into thrombin.

Figures 5a and b show the results of an experiment in which the freshly cleaved mica surface was first exposed to a solution of fibrinogen (10^{-3} of phys concn) and then to solutions of heparin at different concentrations (6×10^{-10} and 6×10^{-9} mol/l., respectively).

(13) This is a lower estimate, based on the assumption that the whole molecule of heparin lies flat on the surface.

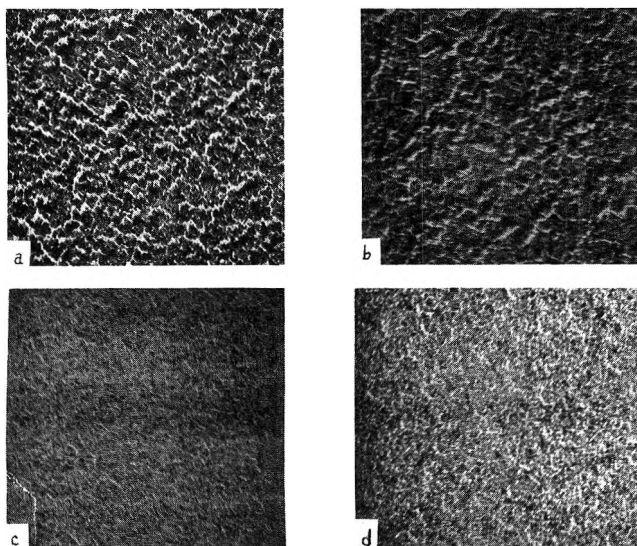


Figure 6. Electron micrographs of mica surfaces exposed to plasma: (a) 0.001 physiological (diluted with buffer); (b) physiological concentration; (c) same as (a) but with prior exposure to 2 units of heparin per ml; (d) same as (b) but with prior exposure to 2 units of heparin per ml.

At the higher concentration of heparin fibrinogen was completely replaced from the surface while at the lower concentration it was only partially replaced.¹⁴ This is a somewhat unexpected result in view of the observation of Gorman, *et al.*,¹⁰ that adsorption of fibrinogen on mica was very irreversible and the adsorbed layer could not be removed by prolonged washing in buffer solution. Two possible mechanisms could be proposed for the replacement process: (i) heparin molecules may interact with adsorbed fibrinogen to form a compound which can be easily desorbed from the surface; (ii) initial adsorption of a few heparin molecules may cause desorption of neighboring fibrinogen molecules due to the negative charge on heparin. This makes place for further adsorption of heparin which then causes further desorption of fibrinogen and so on, until the whole surface layer is replaced.

3. *Adsorption of Blood Proteins from Plasma.* Freshly cleaved mica surfaces exposed to plasma at physiological concentration (Figure 6a) and at 10^{-3} of phys concn (Figure 6b) show extensive adsorption of blood proteins, and primarily of fibrinogen. Preexposure of the surface to heparin solution inhibits the adsorption of all plasma proteins, as seen in Figures 6c and d.

4. *The Effect of Protamine on the Adsorption of Fibrinogen.* Protamine is a drug used clinically to counteract or neutralize the antithrombogenic effect of heparin in the blood. Exposure of a freshly cleaved mica surface to protamine had no appreciable effect on the subsequent adsorption of fibrinogen from a buffer solution on the same surface, as seen in Figure 7a. Moreover, exposure of the surface to a solution containing equivalent amounts of heparin and protamine (both

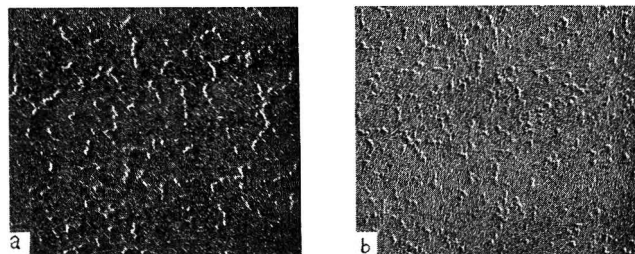


Figure 7. Electron micrographs showing the effect of protamine: (a) adsorption of fibrinogen after exposure to 2 units of protamine/ml; and (b) after exposure to 2 units of heparin per ml neutralized with protamine. All fibrinogen concentrations are 0.001 physiological.

at a concentration which would result in the blood after a regular dosage has been administered) had no inhibiting effect on the adsorption of fibrinogen (Figure 7b). Here again a correlation exists between the thrombogenic and antithrombogenic properties of the drugs tested and their ability to inhibit or enhance the adsorption of fibrinogen on mica.

5. *Adsorption Mechanism for the Activity of Anti-thrombogenic and Thrombogenic Drugs.* From electrokinetic studies on the effects of drugs on the surface charge of the blood vessel wall and of blood cells, it was shown¹⁵ that antithrombogenic drugs increase the magnitude of the negative charge densities of these surfaces while thrombogenic drugs decrease it and often cause a reversal of sign of the surface charge. Of a large number of drugs investigated to date, heparin and protamine have the largest effect. It was proposed¹⁵ that the mechanism of drug action in preventing or accelerating thrombosis is by the adsorption of these compounds on the blood vessel wall and the blood cells. The present work lends further support for this view. On the other hand, many more surfaces and drugs will have to be tested before it can be stated with certainty that the physiological activity of thrombogenic and antithrombogenic drugs is due in part to their effect on the adsorption of fibrinogen on the blood vessel wall.

Considering the structure of heparin (Figure 3) it is seen that six negative charges are associated with each tetrasaccharide unit, or *ca.* 120 unit charges per molecule. Thus, a surface covered with a monolayer of heparin will have an average charge density of $43 \mu\text{C}/\text{cm}^2$ (based on an average value of $3.6 \times 10^{-12} \text{ mol}/\text{cm}^2$ of heparin). In a recent study⁷ of the adsorption of fibrinogen on a mercury electrode, complete desorption occurred when the surface charge density was more negative than $-20 \mu\text{C}/\text{cm}^2$. By correlation it may be estimated about half a monolayer of heparin on the surface should be enough to inhibit completely the

(14) The same concentration of heparin caused complete inhibition of adsorption of fibrinogen when the surface was exposed first to heparin or to a mixture of heparin and fibrinogen.

(15) S. Srinivasan, R. Aaron, P. S. Chopra, T. Lucas, and P. N. Sawyer, *Surgery*, **64**, 827 (1968).

adsorption of fibrinogen. This explains the effectiveness of heparin at very low concentrations, as shown above.

The high charge density on the heparin molecule also supports the second mechanism proposed above for the replacement of fibrinogen by heparin from a mica surface. Thus, since the charge on one heparin molecule is sufficient to replace fibrinogen from an area twice as large as that taken up by the molecule itself, it may cause the desorption of a neighboring fibrinogen molecule, which makes space for the adsorption of several more heparin molecules. The process of replacement of fibrinogen by heparin probably spreads laterally from a relatively small number of points resembling nucleation centers.

Conclusions

Adsorption of fibrinogen is probably an important factor in the adhesion of thrombus deposits on the surface of prosthetic materials in contact with blood. A mica surface was used to study the effect of certain drugs on the adsorption of fibrinogen. Heparin which is a potent antithrombogenic drug was found to inhibit completely the adsorption of fibrinogen on mica. Protamine which is a drug used to neutralize the effect of

heparin in the blood acts similarly with respect to adsorption of fibrinogen. Thus, no inhibition of adsorption was observed when the surface was exposed to a solution containing both heparin and protamine, or to one containing protamine only. The correlation found here between the antithrombogenic activity of a drug and its effect on adsorption of fibrinogen on mica will be tested for other drugs and on other surfaces. The present finding points to the possible importance of adsorption onto either prosthetic materials or the blood vessel wall during the action of antithrombogenic drugs.

Acknowledgments. Financial support from the National Institute of Dental Research, Grant DE-2111-02 (for Glenn Stoner) and from the Artificial Heart Program, National Heart Institute National Institutes of Health, Contract No. PH43-68-75, (for S. Srinivasan) is gratefully acknowledged. S. Srinivasan is the recipient of a Career Scientist Award from the Health Research Council, City of New York, Contract No. I 542. E. Gileadi wishes to thank the Center of Advanced Studies at the University, sponsored by the National Science Foundation, for the award of a University Lecturership.

Spontaneous Dissolution of Metals in Aqueous Electrolytes. I. Kinetic

Isotope Effects in the Reaction of Iron with Hydrochloric Acid

Solutions in Protium and in Deuterium Oxide

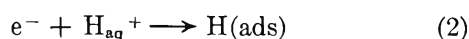
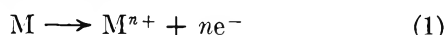
by I. R. Bellobono* and F. Mazza

Istituto di Chimica Fisica dell' Università e Istituto di Elettrochimica e Metallurgia dell' Università, 20133 Milan, Italy
(Received December 2, 1970)

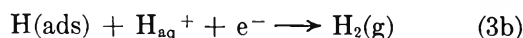
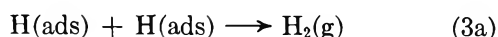
Publication costs borne completely by The Journal of Physical Chemistry

First-order rate coefficients for hydrogen ion disappearance during the dissolution of pure polycrystalline iron at temperatures from 18 to 65° were measured in H₂O and in D₂O solutions containing 10⁻³ to 1 M HCl or DCl, at constant ionic strength (1.0 M). Kinetic coefficients showed an appreciable dependence on pH [(7.1–63) × 10⁻⁶ sec⁻¹ at 25°, for 1 to 10⁻³ M HCl, respectively]. Experimental activation energies resulted: 11.3 kcal/g mol (in H₂O) and 13.1 kcal/g mol (in D₂O). The ratios of rate coefficients (in H₂O and D₂O) varied accordingly from about 3 at 18° to about 2 at 65°. Rates of dissolution in H₂O were employed to evaluate corrosion current densities as a function of hydrogen ion activity in the range 0–3.5 pH. Their values were favorably compared with those predicted using a model which considers the reaction of a hydroxide film, formed at the metal–electrolyte interface, with hydrogen ions, as the rate-determining step for the dissolution process. The good agreement between calculated and experimental isotope effects constitutes another argument in favor of this reaction being responsible for the rate of dissolution.

The reaction by which metals evolve hydrogen from aqueous electrolyte solutions is a multistep process. For acid solutions, there is a general agreement^{1,2} concerning the first steps (discharge of hydrated proton and hydrogen adsorption on the metal surface)

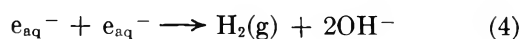


but considerable divergences of opinion exist as to step which leads to the formation of hydrogen molecules



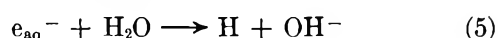
A criterion has been formulated by Bass² for the stability of metals in aqueous solutions, which implies the conservation of energy when an electron tunnels from the metal to a hydrogen ion adjacent to the metal surface, and reaction 2 determines the overall rate of hydrogen evolution.

More recently Pyle and Roberts³ have suggested that hydrogen molecules may be directly formed at a metal–electrolyte interface, by the reaction

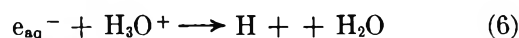


[rate constant $k_4 = (0.45\text{--}0.55) \times 10^{10} M^{-1} \text{sec}^{-1}$ at 20–23° and pH 10.9–13.3^{4,5}], which has been shown⁶ to proceed without the intermediate formation of hydrogen atoms. For metals, which form hydroxides of low solubility, it has been proposed that hydroxyl ions produced by this reaction are adsorbed at the metal surface

and react with formation of a hydroxide film; the dissolution of this latter by hydrogen ions represents the rate-determining step for the whole process. The formation of atomic hydrogen, however, is not entirely prevented. The competition between direct production of molecular hydrogen and the intermediate formation of hydrogen atoms depends, following this scheme, on the concentration of solvated electrons and hydrogen ions, as demanded by reactions 4–6



(rate constant $k_5 = 16 M^{-1} \text{sec}^{-1}$ at pH 8.3–9.0 and 25°)⁷



[rate constant $k_6 = (2.1\text{--}2.3) \times 10^{10} M^{-1} \text{sec}^{-1}$ at 20–23° and pH 2.1–4.7^{6,8}].

Calculations of the rates of spontaneous dissolution of iron in hydrochloric acid made on the basis of the

(1) J. O'M. Bockris, "Modern Aspects of Electrochemistry," J. O'M. Bockris and B. E. Conway, Ed., Vol. I, Butterworths, London, 1954, Chapter IV.

(2) L. Bass, *Proc. Roy. Soc., Ser. A*, **277**, 129 (1964).

(3) T. Pyle and C. Roberts, *J. Electrochem. Soc.*, **115**, 247 (1968).

(4) S. Gordon, E. J. Hart, M. S. Matheson, J. Rabani, and J. K. Thomas, *Discuss. Faraday Soc.*, **36**, 193 (1963).

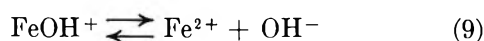
(5) M. S. Matheson and J. Rabani, *J. Phys. Chem.*, **69**, 1324 (1965).

(6) L. M. Dorfman and I. A. Taub, *J. Amer. Chem. Soc.*, **85**, 2370 (1963); cf. J. H. Baxendale, E. M. Fielden, and J. P. Keene, *Proc. Roy. Soc., Ser. A*, **286**, 320 (1965).

(7) E. J. Hart, S. Gordon, and E. M. Fielden, *J. Phys. Chem.*, **70**, 150 (1966).

(8) J. P. Keene, *Radiat. Res.*, **22**, 1 (1964).

above model³ showed good agreement with observed rates. This model substantially parallels that proposed by Bockris, Drazic, and Despic⁹ on the anodic dissolution of iron



with the difference that in the Bockris model reaction 8 is considered to be rate determining.

Conway and MacKinnon¹⁰ have shown many thermodynamic and kinetic difficulties which arise in most cases of metal dissolution, when hydrated electrons are supposed to be the direct precursors of molecular hydrogen evolved. Notwithstanding that the role of solvated electrons at the metal-electrolyte interface may be seriously questioned, the model of the hydroxide film adsorbed on the metal surface, as representing the slow step of the dissolution reaction, deserves adequate testing. In order to investigate further the experimental aspects of this problem and their interpretation, a study has been undertaken of the kinetics of dissolution in acid solution of metals that form hydroxides of low solubility in water. The present paper deals with kinetic isotope effects in the dissolution of pure polycrystalline iron in acid solutions of ionic strength maintained practically constant during each experiment: in these conditions the metal was dissolved at its corrosion potential. Kinetic measurements of this kind had been already effected by Podestà and Arvía¹¹ only in ordinary water. A technique similar to that described by these authors was employed both in protium and in deuterium oxide solutions.

Experimental Section

Materials. Triply distilled water, free from oxygen and carbon dioxide, as well as from any organic contaminant, was used throughout. Deuterium oxide and concentrated [²H] hydrochloric acid in deuterium oxide were supplied by Merck: minimum isotopic purities were 99.7 and 99.5%, respectively (ir and nmr spectra). Solutions, containing 0.001–1 M HCl (or DCl) in protium (or deuterium) oxide were prepared in a nitrogen-filled glove box. The ionic strength of these solutions was corrected (when necessary) by addition of KCl, to the same final value (1.0 M) in all experiments. Iron foil (99.998%) was an Alfa-Inorganics product. It was degreased with boiling chloroform, washed first with ethyl alcohol, then repeatedly with triply distilled water, and finally dipped into a solution having the same composition as that to be used in the kinetic runs.

Glassware and the electrode cell were heated at 220° for several hours, before preparation of D₂O solutions.

p_H Measurements. A Radiometer pH meter, Type TTTIC, was used with glass and saturated calomel electrodes. By means of a scale expander, Type pH A 630

TA, pH values could be read directly to two places of decimals. A jacketed electrode cell of about 120 cm³ was used, kept at a constant temperature of ±0.1° by circulation of thermostated liquid. A polytetrafluoroethylene cover was placed on top, to hold the electrodes. The iron foil, conveniently folded, was completely immersed in the solution, suspended by a glass hook. A tube, with sintered glass at the end, was used to agitate the solution with nitrogen. The inert gas was previously saturated with vapor by bubbling it through a solution of the same composition and temperature as that employed in the kinetic experiment.

The saturated calomel electrode was placed in a glass sleeve ending in a U-shaped capillary tip. In each experiment, the sleeve was filled with the solution used for the kinetic measurements, thus preventing any diffusion of chloride ion from the reference electrode to the bulk of the solution. For measurements in D₂O solutions the reference electrode was filled with a saturated KCl solution in D₂O and the experimentally determined value of ΔpH (*e.g.*, 0.405 at 25°) was added to pH meter readings in order to obtain p_{aD} values (on a molarity scale), following the recommended procedure.^{12,13} The ΔpH values varied slightly with temperature.¹⁴ The glass electrode was conveniently calibrated in the range of pH and temperature at which experiments were run.

Kinetics. All kinetic operations were carried on inside a glove box, with careful air exclusion. The p_{aH} change of solutions during each run was never greater than 0.3 units and the surface of the metal was not appreciably altered.

Experimental results were obtained at temperatures between 18 to 65°. An example of some individual runs in deuterium oxide solutions is shown in Figure 1, where the p_{aD} is plotted as a function of time. Each run was repeated an average of five times. Linear dependence of p_{aH} (or p_{aD}) on time was always observed, within the limits of experimental errors, if the range of p_{aH} (or p_{aD}) variations was sufficiently narrow. Rate coefficients have been calculated on the basis of a first-order rate equation. The ratio (0.10 cm) between the volume of electrolyte (usually 50 ml) and the apparent surface of the iron foil was always the same in all experiments.

Results and Discussion

The rate of dissolution of iron can be calculated either by the kinetic parameters related to the dissolution

(9) J. O'M. Bockris, D. Drazic, and A. R. Despic, *Electrochim. Acta*, **4**, 325 (1961).

(10) B. E. Conway and D. J. MacKinnon, *J. Phys. Chem.*, **74**, 3663 (1970).

(11) J. J. Podestà and A. J. Arvía, *Electrochim. Acta*, **10**, 159 (1965).

(12) R. Gary, R. G. Bates, and R. A. Robinson, *J. Phys. Chem.*, **68**, 3806 (1964).

(13) P. K. Glasoe and F. A. Long, *ibid.*, **64**, 188 (1960).

(14) I. R. Bellobono and P. Beltrame, *J. Chem. Soc. B*, 620 (1969).

Table I: Kinetic Coefficients for the Spontaneous Dissolution of Iron at Various Hydrochloric Acid Concentrations, in Protium and Deuterium Oxide

Temperature, °K	HCl (DCl), ^a M	H ₂ O		D ₂ O		<i>k_H</i> / <i>k_D</i>
		<i>k_H</i> 10 ⁶ , sec ⁻¹	p <i>a_H</i> ^b	<i>k_D</i> 10 ⁶ , sec ⁻¹	p <i>a_D</i> ^b	
291.2	1.00	4.59 ± 0.56	0.35 ± 0.15	1.49 ± 0.25	0.64 ± 0.04	3.08
291.2	0.100	13.2 ± 0.8	1.28 ± 0.10	4.46 ± 0.45	1.73 ± 0.09	2.96
298.2	1.00	7.11 ± 0.65	0.35 ± 0.13	2.55 ± 0.18	0.75 ± 0.15	2.79
298.2	0.100	28.3 ± 1.6	1.25 ± 0.10	9.18 ± 0.76	1.65 ± 0.10	3.08
298.2	0.010	49.6 ± 3.8	2.18 ± 0.08			
298.2	0.001	62.9 ± 5.9	3.10 ± 0.14			
303.2	1.00	10.7 ± 0.6	0.38 ± 0.10	4.11 ± 0.38	0.65 ± 0.15	2.60
313.2	1.00	18.7 ± 1.1	0.31 ± 0.12	6.27 ± 0.54	0.73 ± 0.13	2.98
323.2	1.00	36.5 ± 2.9	0.36 ± 0.15	14.4 ± 0.7	0.80 ± 0.15	2.53
338.2	1.00	67.9 ± 6.1	0.36 ± 0.10	34.0 ± 2.4	0.76 ± 0.15	2.00

^a Initial concentrations. ^b Mean value and maximum range of variation during kinetic runs.

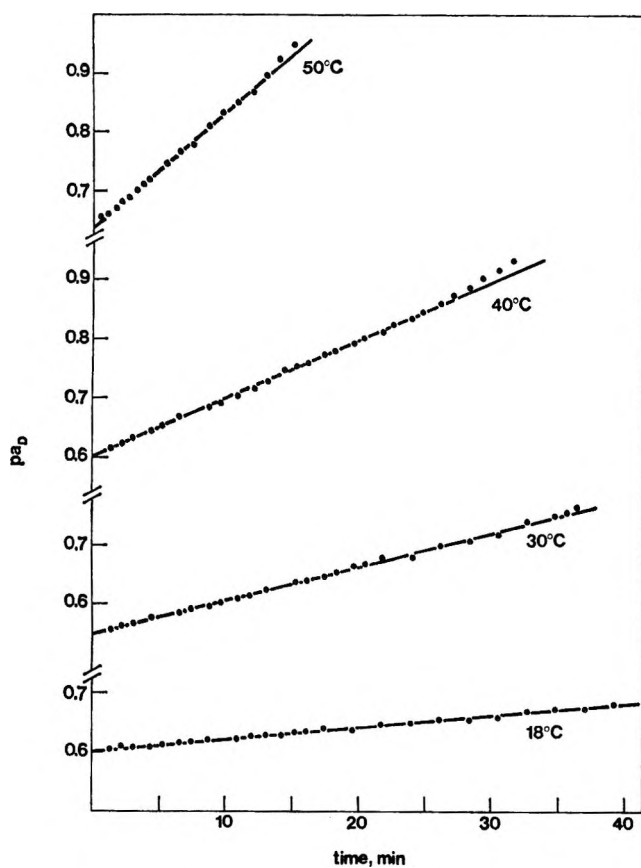


Figure 1. Decreasing rate of hydrogen ion activity in deuterium oxide containing 1.00 M DCl (initial concentration), at various temperatures: plot according to a first-order rate equation (the zero of the time scale does not correspond exactly to the beginning of the run).

reaction, or by the corrosion electrochemical parameters associated with the cathodic and anodic processes. In the present work, it was preferred to evaluate rates of dissolution (*r*) and corrosion current densities (*i*) directly by means of kinetic coefficients for the spontaneous dissolution of the metal. Rates of dissolution of iron (referred to its apparent surface) are related to

kinetic coefficients $k_{H(D)}$ (sec⁻¹) by the equation

$$r(\text{equiv sec}^{-1} \text{ cm}^{-2}) = 10^{-3} k_{H(D)} \frac{v}{s} a_{H(D)} \quad (10)$$

where *v* is the volume of electrolyte solution (cm³), *s* the apparent surface of iron (cm²), and *a_{H(D)}* the activity (equiv/l.) of hydrated proton (or deuteron). In a narrow range of pH variation, *k_{H(D)}* may be considered to be approximately independent of pH, as it was in fact observed, and eq 10 treated as a first-order rate equation. First-order rate coefficients *k_{H(D)}* at temperatures between 18 and 65° were measured in protium or deuterium oxide solutions containing hydrochloric acid (HCl or DCl). Most of the runs were followed in 1.0 M HCl (or DCl) solutions (*cf.* Figure 1); but experiments in a wider pH (or pD) range (p*a_H* 0.3–3; p*a_D* 0.6–1.6; initial value) were also carried out, mainly at 25°. In this latter case, potassium chloride was added in order to obtain the same initial ionic strength (*I* = 1.0 M), which was approximately constant, since the pH (or pD) change during each kinetic run was moderately small.

Mean values of *k_{H(D)}* and their standard deviations, at the various hydrochloric acid concentrations examined, as well as experimental *k_H*/*k_D* ratios, are given in Table I. As the ratio between the volume of solution and the apparent surface of iron was held constant in all experiments, rate coefficients *k_{H(D)}*, simply expressed in second⁻¹ units, were employed to calculate the activation energy, by Arrhenius plots (Figure 2). Experimental activation energies for the corrosion process occurring in protium and in deuterium oxide media resulted: 11.3 ± 0.6 kcal/g mol, in H₂O, and 13.1 ± 0.6 kcal/g mol, in D₂O. As it clearly appears from Table I, kinetic coefficients showed an appreciable dependence on pH (or pD) of solutions, beyond the limit of experimental errors. Rates of dissolution in protium oxide were employed to calculate corrosion current densities at various pH values. The logarithms of corrosion

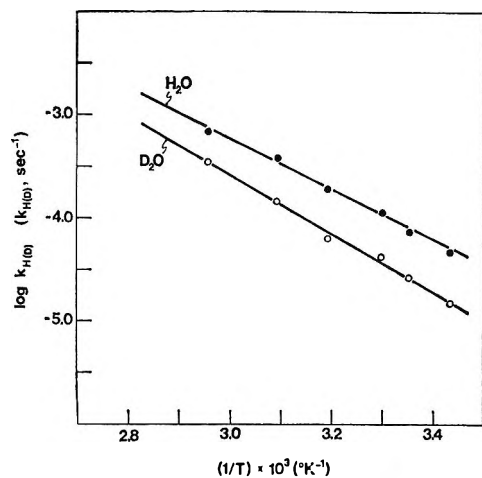


Figure 2. Arrhenius plot of kinetic coefficients k_H (●) and k_D (○) in protium and in deuterium oxide, respectively.

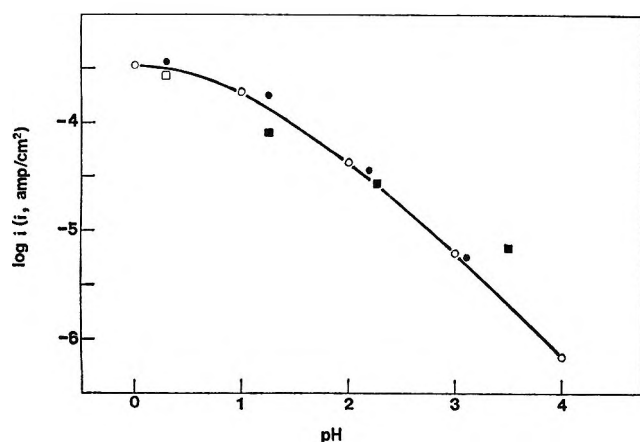


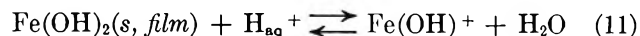
Figure 3. Comparison of calculated³ (○) and experimental rates of dissolution of iron at 300°K: (■), ref 11; (□), ref 15; (●), present work. Dependence of $\log i$ (i = corrosion current density) on pH at 300°K and ionic strength 1.0 M .

current densities, at 300°K, as a function of pH, are reported in Figure 3, together with values calculated by Pyle and Roberts,³ and other experimental values taken from the literature.^{11,15} A slope of about -0.8 is found in the linear range of the plot of $\log i$ vs. pH. However, if experimental values at $\text{pH} < 1$ are also considered, the slope may vary up to about -0.5 . A similar slope was obtained for the corrosion current densities by Bockris, Drazic, and Despic,⁹ who employed sodium sulfate, while a slope of -1 resulted in the case of sodium perchlorate solutions.¹¹ This difference of behavior was attributed to a specific effect of the different anions,^{16,17} a greater adsorption occurring in the presence of chloride ions, as compared with that of perchlorate ions.¹¹ If this is so, the increase in absolute value of the slope, with increasing pH, towards the limiting value (-1) shown by the kinetic equation for hydrogen evolution on iron, would indicate that, when the hydroxyl ion concentration increases, these ions would preferentially cover the metal surface. At low pH, on the contrary,

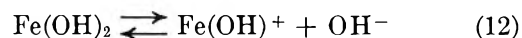
when the amount of adsorbed hydroxyl ion is low, the massive presence of chloride ions exerts an inhibiting effect,¹⁸ consequently the slope of the $\log i$ profile (cf. Figure 3) tends towards a zero value (independence of corrosion current density from hydrogen ion activity). This fact is conveniently accounted for in the Pyle and Robert's model, on one side by the low ratio, exhibited by iron, between the concentration of solvated electrons at the inner Helmholtz plane and the concentration of sites, and on the other by the competition between metal hydroxide and water molecules in the surface film.

The close agreement between absolute rates for the spontaneous dissolution of iron, predicted by the simple model proposed by Pyle and Roberts (when employing the value of 11.4 kcal/g mol for activation energy), and experimental results has been already pointed out, and is favorably confirmed by the present measurements.

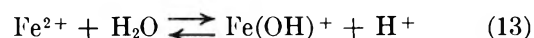
On the basis of this model, it should be the removal of the hydroxide film by the reaction



that determines the rate of dissolution. Consequently the activation energy for forward reaction 11 should be approximatively equal to the activation energy for the iron dissolution process. As activation energy of reaction 11 has not been measured the energy of the dissociation reaction



was used instead of it, by Pyle and Roberts, and the mean value of 11.4 kcal/g mol adopted.³ This value is remarkably close to the experimental ones (11.5 kcal/g mol,¹¹ 11.3 kcal/g mol, present work). However, the choice of 11.4 kcal/g mol as the free energy of reaction 12 may be critically discussed. The equilibrium constant for reaction 12 can be calculated using the values determined by Gayer and Wootner¹⁹ or by Leussing and Kolthoff²⁰ for the equilibrium constant of reaction 13 at 25°



($1.20 \times 10^{-8} M$;¹⁹ $5 \times 10^{-9} M$ ²⁰), and the solubility products of $\text{Fe}(\text{OH})_2$.²⁰ The values of $(9.7 \pm 3.6) \times 10^{-10}$ or $(4 \pm 1.5) \times 10^{-10} M$ are obtained, respectively. Even with a large margin of error, the free energy of reaction 12 may be expected to lie within the range 12.2–13.3 kcal/g mol, which would give rates of

(15) A. P. Bond, Sc.D. Thesis, Department of Metallurgy, Massachusetts Institute of Technology, Cambridge, Mass., 1958.

(16) G. M. Schmid and N. Hackerman, *J. Electrochem. Soc.*, **107**, 647 (1959).

(17) Ja. M. Kolotyrykin, *ibid.*, **108**, 209 (1961).

(18) F. Mazza and N. D. Greene, *Ann. Univ. Ferrara, Sez. 5*, 401 (1966).

(19) K. H. Gayer and L. Wootner, *J. Amer. Chem. Soc.*, **78**, 3944 (1956).

(20) D. L. Leussing and I. M. Kolthoff, *ibid.*, **75**, 2476 (1953).

dissolution differing of one or two orders of magnitude from those calculated with an activation energy of 11.4 kcal/g mol. Greater differences result if the value of $4.6 \times 10^{-4} M$ for the equilibrium constant of reaction 13, as determined by Wells and Salam,²¹ is adopted. (There is a considerable disagreement on the literature values of the equilibrium constant for reaction 13. For a critical discussion, see ref 21.) In the calculation of rates of dissolution of metals following the model of Pyle and Roberts, there is consequently a great uncertainty in the value used for the free energy of reaction 12, which has been chosen arbitrarily as a measure of the activation energy for the dissolution process. A better choice would be to employ activation energy of reaction 11, if available. The use of an experimental value, directly determined for the reaction of metals with acids, would of course completely resolve the problem, because by this way all effects, including the possible anion inhibition,¹⁸ would be taken into account. In fact, the calculated curve of Figure 3 must be considered as the result of a computation employing the experimental value of activation energy for the spontaneous dissolution of iron in hydrochloric acid solutions. Furthermore, a close analogy, oxidation states apart, between reaction 11 and the rate-limiting step during anodic dissolution (reaction 8) may be observed.

Another point, which deserves attention and constitutes another argument in favor of reaction 11 being responsible for the rate of dissolution, is the examination of isotope effects. If reaction 11 represents the rate-determining step, measured kinetic isotope effects should substantially correspond to those of forward reaction 11 and should consequently be related to isotope effect of equilibrium 11. The following equation must hold

$$\log (k_{\text{H}}/k_{\text{D}}) - \log (k_{\text{H}}'/k_{\text{D}}') = -\Delta pK \quad (14)$$

where $k_{\text{H(D)}}$ and $k_{\text{H(D)}}'$ denote rate coefficients for forward and backward reaction 11, respectively, and $\Delta pK \equiv (pK_{\text{D}} - pK_{\text{H}})$ is equal to $\log (K_{\text{H}}/K_{\text{D}})$, K_{H} and K_{D} being the acid dissociation constants of $\text{Fe}(\text{OH})^+$ in protium and in deuterium oxide

$$K_{\text{H(D)}} = a_{\text{H}^+(\text{D})} / a_{\text{Fe}[\text{OH}(\text{D})]^+}$$

The value of ΔpK is not known, but it can be evaluated if the correlation between pK and ΔpK given by Bell²²⁻²⁴ is assumed to be generally valid, at least in a first approximation. The equilibrium constant K_{H} can be calculated from literature data:^{19,20} it = $(1.04 \pm 0.39) \times 10^{-5}$ or $(2.5 \pm 0.9) \times 10^{-5}$ at 25°. The corresponding ΔpK should thus be about 0.50. Calculation of kinetic isotope effect $k_{\text{H}}'/k_{\text{D}}'$ by means of the Eyring-Cagle equation,^{25,26} using for $\text{Fe}(\text{OH})^+$ the O-H stretching vibration of hydrated $\text{Fe}(\text{OH})_3$ (3300 cm^{-1}),²⁷ yields the value of 9.12 at 25°. By eq 14, $k_{\text{H}}/k_{\text{D}} = 2.88$, in excellent agreement with the experimental value at 298.2°K (see Table I).

Acknowledgment. Financial support by Consiglio Nazionale delle Ricerche is gratefully acknowledged.

(21) C. F. Wells and M. A. Salam, *Nature*, **205**, 690 (1965).

(22) R. P. Bell, "The Proton in Chemistry," Cornell University Press, Ithaca, N. Y., 1958, p 188.

(23) R. P. Bell and A. T. Kuhn, *Trans. Faraday Soc.*, **59**, 1789 (1963).

(24) A. O. McDougal and F. A. Long, *J. Phys. Chem.*, **64**, 188 (1960).

(25) H. Eyring and F. W. Cagle, Jr., *ibid.*, **56**, 889 (1952).

(26) Cf. L. Melander, "Isotope Effects on Reaction Rates," Ronald Press, New York, N. Y. 1960, pp 17, 21, 35.

(27) O. Glemser, *Nature*, **183**, 943, 1476 (1959).

The Kinetics of the Reaction between Uranium(III) and $\text{Co}(\text{NH}_3)_4(\text{H}_2\text{O})_2^{3+}$ in Aqueous Perchlorate Solutions¹

by James D. White² and T. W. Newton*

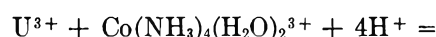
University of California, Los Alamos Scientific Laboratory, Los Alamos, New Mexico 87544 (Received December 7, 1970)

Publication costs assisted by the Los Alamos Scientific Laboratory

The reaction $\text{U}^{3+} + \text{cis-Co}(\text{NH}_3)_4(\text{H}_2\text{O})_2^{3+} + 4\text{H}^+ = \text{U}^{4+} + \text{Co}^{2+} + 4\text{NH}_4^+ + 2\text{H}_2\text{O}$ was studied in acid perchlorate solutions from 0.01 to 1.98 *M* HClO_4 , from 0.8 to 45°, and at ionic strengths from 0.12 to 3.6 *M* (LiClO_4). The predominant term in the rate law is $-\text{d}[\text{U}(\text{III})]/\text{d}t = 1.64 \times 10^3 [\text{U}(\text{III})][\text{Co}(\text{III})][\text{H}^+]^0$ *M* sec^{-1} at 25° and $\mu = 2.0$ *M*. The activation parameters are $\Delta F^* = 13.06$ kcal/mol, $\Delta H^* = 3.67 \pm 0.04$ kcal/mol, and $\Delta S^* = -31.5 \pm 0.3$ cal mol^{-1} deg^{-1} for $\mu = 2.0$ *M*. Chloride ion causes a moderate increase in the rate, first power in $[\text{Cl}^-]$. The ionic strength dependence is in accord with an extended form of the Debye-Hückel equation with the distance of closest approach term equal to 9.3 Å.

Introduction

A study of the kinetics of reaction 1 was undertaken to provide data for comparison with those from anal-



ogous reactions such as the oxidation of U^{3+} by $\text{Co}(\text{NH}_3)_6\text{H}_2\text{O}^{3+}$ and the oxidation of Np^{3+} by $\text{Co}(\text{NH}_3)_4(\text{H}_2\text{O})_2^{3+}$. Wang and Espenson^{3a} have recently made a study of the reduction by U(III) of an extensive series of Co(III) complexes. For $\text{Co}(\text{NH}_3)_4(\text{H}_2\text{O})_2^{3+}$, they report rates at 25° for hydrogen ion concentrations ranging from 0.01 to 0.18 *M*, $\mu = 0.2$ *M* (LiClO_4). In the present paper this work has been extended to include the effects of temperature, ionic strength, chloride ion, and a more thorough study of the hydrogen ion dependence.

The relative rates of reduction of the *cis* and *trans* isomers of various complexes are of interest.⁴ It was planned to make such a study in this work, since it has been reported⁵ that both the *cis* and the *trans* isomers of $\text{Co}(\text{NH}_3)_4(\text{H}_2\text{O})_2^{3+}$ can be prepared. The equilibrium quotient (*trans*)/(*cis*) was found to be 6, and the rates of formation of the *trans* from the *cis* were reported to be 7.2×10^{-3} min^{-1} at 20° and 3.3×10^{-2} min^{-1} at 30°. However, we have been unable to find evidence for the *trans* isomer in any of our preparations and believe that our kinetic results all apply to the *cis* isomer.

Experimental Section

Preparation of Materials. Solutions of U(III) were prepared from twice-crystallized $\text{UO}_2(\text{ClO}_4)_2$ by reduction in 1 *M* HClO_4 on zinc-amalgam.⁶ Further recrystallization of the starting material was found to be without effect on the rates. The same rates were also

found when the $\text{UO}_2(\text{ClO}_4)_2$ was prepared from pure UO_2 . The Zn(II) and possible traces of Cl^- or other impurities from the zinc-amalgam were found to be without effect on the measured rates. Distilled water, LiClO_4 , and HClO_4 solutions were prepared and analyzed as before.⁷ Vacuum redistillation of the HClO_4 and recrystallization of the LiClO_4 were found to be without significant effect on the rates.

The nitrate and perchlorate salts of $\text{Co}(\text{NH}_3)_4\text{CO}_3^+$ were prepared by standard procedures.⁸ The perchlorate was crystallized twice from water and analyzed for Co and NH_3 . Calcd for $\text{Co}(\text{NH}_3)_4\text{CO}_3\text{ClO}_4$: Co, 20.6; NH_3 , 23.7. Found: Co, 20.3; NH_3 , 23.5. The perchlorate salt of $\text{Co}(\text{NH}_3)_4(\text{H}_2\text{O})_2^{3+}$ was prepared from $\text{Co}(\text{NH}_3)_4\text{CO}_3\text{NO}_3$ by acidification and repeated crystallization from dilute HClO_4 . Samples of this were further purified by crystallization from concentrated HClO_4 , by fractional crystallization from dilute HClO_4 , and by ion exchange. The fractionally crystallized material was analyzed. Calcd for $\text{Co}(\text{NH}_3)_4(\text{H}_2\text{O})_2(\text{ClO}_4)_3$: Co, 12.8; NH_3 , 14.7; ClO_4 , 64.7. Found: Co, 12.8; NH_3 , 14.0; ClO_4 , 64.4. Cobalt was determined spectrophotometrically as CoCl_4^{2-} in 12 *M* HCl , the effective absorptivity was determined using a standard made from pure Co metal. Ammonia was determined using a Kjeldahl method, and perchlorate was determined indirectly using Dowex-50 in the acid form.

- (1) Work supported by the U. S. Atomic Energy Commission.
- (2) Los Alamos Scientific Laboratory Postdoctoral Fellow.
- (3) (a) R. T. Wang and J. H. Espenson, *J. Amer. Chem. Soc.*, **93**, 380 (1971); (b) J. H. Espenson, personal communication.
- (4) P. R. Guenther and R. G. Linck, *J. Amer. Chem. Soc.*, **91**, 3769 (1969).
- (5) R. G. Yalman and T. Kuwana, *J. Phys. Chem.*, **59**, 298 (1955).
- (6) T. W. Newton and R. B. Fulton, *ibid.*, **74**, 2797 (1970).
- (7) T. W. Newton and F. B. Baker, *ibid.*, **67**, 1425 (1963).
- (8) G. Schlessinger, *Inorg. Syn.*, **6**, 173 (1960).

The near-ultraviolet absorption spectra of various preparations were determined to establish relative purity and to check for possible isomeric changes. All the solutions showed maxima at 353.5 nm with $\epsilon = 43.0 \pm 0.3 M^{-1} \text{ cm}^{-1}$, in agreement with previous results.^{3b} The wavelength and absorptivity for the adjacent minima were found to depend somewhat on the history of the sample, as shown in Table I. Here the wavelength of minimum absorbance near 300 nm and $A(\text{min})/A(353.5)$ are given. The reported^{3b} value for this ratio is 0.239; the lower values in Table I indicate that our perchlorate salts are probably purer than those previously used.^{3a}

Table I: Spectral Characteristics of Various Samples of $\text{Co}(\text{NH}_3)_4(\text{H}_2\text{O})_2^{3+}$ in HClO_4 at 23°

Description	Wave-length, min, nm	$A(\text{min})/A(353.5)$
1. $\text{Co}(\text{NH}_3)_4\text{CO}_3\text{NO}_3$, crystallized once from H_2O		
(a) Freshly dissolved in 1 M HClO_4	318	0.55
(b) 1a heated at 53° for 2.5 hr	288	0.221
2. $\text{Co}(\text{NH}_3)_4\text{CO}_3\text{NO}_3$, crystallized three times from H_2O		
(a) In 0.1 M HClO_4	284	0.313
(b) 2a heated at 53° for 1 hr	284	0.214
3. Sample 1a adsorbed on a Dowex-50 column, eluted with 2 M HClO_4 , temperature about 4° during ion exchange	293	0.084
4. $\text{Co}(\text{NH}_3)_4(\text{H}_2\text{O})_2(\text{ClO}_4)_3$, from $\text{Co}(\text{NH}_3)_4(\text{H}_2\text{O})_2\text{NO}_3$ by acidification and repeated crystallizations from dilute HClO_4 , finally dissolved in 1 M HClO_4	290	0.141
5. $\text{Co}(\text{NH}_3)_4\text{CO}_3\text{ClO}_4$, crystallized two times from H_2O		
(a) Freshly dissolved in 0.1 M HClO_4	290	0.075
(b) 5a heated at 53° for 1.5 hr	290	0.062
6. <i>trans</i> - $\text{Co}(\text{NH}_3)_4\text{Cl}_2\text{Cl}^a$ treated with $\text{Hg}(\text{II})$, adsorbed on a Dowex-50 column, eluted with 1.5 M HClO_4 , all near 0°	290	0.094

^a Prepared according to C. Brauer, Ed., "Handbook of Preparative Inorganic Chemistry," Vol. 2, 2nd ed, Academic Press, New York, N. Y., 1965, p 1537.

Acidified solutions of $\text{Co}(\text{NH}_3)_4\text{CO}_3\text{NO}_3$ showed absorbance changes near 300 nm at room temperature which were considerably slower than those previously observed.⁵ At higher temperatures linear plots of $\log(A - A_\infty)$ were obtained; apparent first-order rate constants of 0.03 and 0.05 min^{-1} were obtained at 44 and 51°, respectively. We attribute these changes to reactions of impurities, rather than to isomerization, because the absorbance change depends on the number of crystallizations of the nitrate salt (1 and 2 in Table I). Also, solutions of the perchlorate salt showed almost no change with heating. Contrary to the earlier con-

clusions,⁵ these results show that either the trans isomer is not formed by mild heating of solutions of the cis, or that the spectra of the two isomers are essentially the same near 300 nm. In addition, the kinetic results, discussed later, indicate that if the trans isomer is readily formed, its rate of reaction with U(III) is essentially the same as that of the cis.

Some preliminary nmr results are consistent with the suggestion that the trans isomer is not readily formed. Pmr spectra of various preparations of the complex were measured in solutions of $\text{DMSO}-d_6$ acidified with D_2SO_4 . All the solutions showed two peaks of about equal intensity, $\pm 10\%$, which we attribute to the protons on the two kinds of nitrogen atoms on the cis isomer. These peaks were at shifts of δ 3.3 and 4.3 ppm with respect to tetramethylsilane. A peak due to the protons of the coordinated water was identified by adding very small quantities of H_2O to the solutions. Attempts to fractionate equilibrated solutions by crystallization or by ion exchange gave solutions with spectra similar to that described above. These results suggest that no more than 10% of the trans isomer was present in any of the preparations.

Procedure. Reaction rates were determined spectrophotometrically in stirred absorption cells as previously described.⁷ For nearly all runs, absorbance was recorded *vs.* time until the reaction was at least 95% complete. The wavelength was 350 nm, where the extinction coefficients of all species except U(III) are relatively small. U(III) was the first reactant to be added to the cell and its initial concentration was calculated from the initial absorbance using ϵ 1620 $M^{-1} \text{ cm}^{-1}$, as previously determined.⁶ The initial concentration of the Co(III) complex was determined from the volume and concentration of the stock solution used. These were analyzed spectrophotometrically. All of the solutions were thoroughly deaerated with purified argon, and the reaction cells were blanketed with argon during the runs.

Stoichiometry. The stoichiometry of the reaction which occurs when the Co(III) complex is added to U(III) was determined by the use of a spectrophotometric titration. U(III) was put into a stirred 1-cm absorption cell, and its concentration was determined from the absorbance at 350 nm. The solution was then titrated with deaerated 0.01008 M $\text{Co}(\text{NH}_3)_4(\text{H}_2\text{O})_2(\text{ClO}_4)_3$, delivered from a micrometer syringe. The titration curves were straight lines with sharp breaks at the end points. In one determination 0.01403 mmol of U(III) took 0.0145 mmol of Co(III), and in another the corresponding figures were 0.0144 and 0.0148. These results indicate that an average of 1.03 mol of Co(III) are required for each mole of U(III). This is within the experimental error of that required by eq 1.

Kinetic Results. Absorbance *vs.* time data were found to be in good agreement with a second-order rate law of the form given by (2).

$$-d[\text{U(III)}]/dt = k'[\text{U(III)}][\text{Co(III)}] \quad (2)$$

Values for the apparent second-order rate constant, k' , were determined from the data by a least-squares calculation which minimized the quantity

$$\sum(A_{\text{obsd}} - A_{\text{calcd}})^2$$

where the A 's are absorbance values.

Various preparations of the Co(III) complex gave essentially the same values for k' , as shown in Table II.

Table II: Apparent Second-Order Rate Constants^a Obtained Using $\text{Co}(\text{NH}_3)_4(\text{H}_2\text{O})_2^{3+}$ from Various Preparations

Preparation	No. of determinations	k' , $M^{-1} \text{sec}^{-1}$	Mean dev
1. $\text{Co}(\text{NH}_3)_4(\text{H}_2\text{O})_2(\text{ClO}_4)_3$			
(a) Crystallized from concentrated HClO_4	2	466	6
(b) Crystallized from dilute HClO_4	3	483	3
(c) Mother liquor from 1b	3	549	14
2. Solution of $\text{Co}(\text{NH}_3)_4(\text{H}_2\text{O})_2(\text{ClO}_4)_3$			
(a) Eluted from Dowex-50 with 2 M HClO_4	3	497	10
(b) 2a crystallized by removing solvent under reduced pressure	3	480	3
(c) 2b stood in solution 65 hr at 23°	4	493	6
3. $\text{Co}(\text{NH}_3)\text{CO}_3\text{NO}_3$ dissolved in 2 M HClO_4 , adsorbed on Dowex-50, eluted with 2 M HClO_4	3	483	4
4. Twice crystallized $\text{Co}(\text{NH}_3)_4\text{CO}_3\text{ClO}_4$			
(a) Freshly dissolved in 1 M HClO_4	3	471	6
(b) 4a heated to 53° for 2 hr	3	488	6

^a Conditions, 0.8° and 1.00 M HClO_4 .

The products of the reaction, U(IV) , Co(II) , and NH_4^+ were shown to be without effect on the rates. When the initial concentrations of these ions were made 2.2×10^{-4} , 1.7×10^{-4} , and $6.8 \times 10^{-4} M$, respectively, the average value of k' for four runs was within 1% of the value found in the initial absence of these ions. These runs were made at 25.2° in 1.00 M HClO_4 with average initial reactant concentrations of $3 \times 10^{-5} M$ U(III) and $7 \times 10^{-5} M$ Co(III) .

The effect of initial Co(III) concentration was studied at 0.8° in 1.00 M HClO_4 . Runs made in the range from 3.5×10^{-5} to $3.0 \times 10^{-4} M$ Co(III) agreed within 2% and showed no apparent trend with concentration. For these runs the initial U(III) concentration was close to $3 \times 10^{-5} M$. In contrast to these results a small effect of U(III) on k' was observed. Decreasing U(III) to $4 \times 10^{-6} M$ caused about a 5% increase in k' , while increasing it to $3 \times 10^{-4} M$ caused a decrease of about 6%. Although eq 2 describes the rates quite well, possible additional minor terms in the rate law will be considered later.

The hydrogen ion dependence was studied at 25.2°

in LiClO_4 solutions with $\mu = 2.00$ and 0.20 M . No dependence was found for the 2.00 M solutions in the H^+ range from 0.016 to 1.94 M ; the least-squares best straight line through the data is $k' = (1637 \pm 11) + (0.20 \pm 0.49)[\text{H}^+]^{-1} M^{-1} \text{sec}^{-1}$, where the uncertainties are the standard deviations. In contrast, the 0.20 M solutions showed a small but definite dependence: $k' = (210 \pm 2) + (0.47 \pm 0.03)[\text{H}^+]^{-1} M^{-1} \text{sec}^{-1}$. At 0.8°, - 2 M solutions also showed a small dependence: $k' = (864 \pm 6) + (1.3 \pm 0.6)[\text{H}^+]^{-1} M^{-1} \text{sec}^{-1}$. The data are summarized in Table III.

Table III: Hydrogen Ion Dependence (LiClO_4 Solutions)

Temp. °C	Ionic strength M	$[\text{HClO}_4]$, M	No. of determinations	Av k' , $M^{-1} \text{sec}^{-1}$	Mean dev	k' calcd., ^d $M^{-1} \text{sec}^{-1}$
25.2	2.00 ^a	0.0163	2	1646	31	1649
		0.0325	2	1646	21	1642
		0.064	3	1640	20	1639
		0.129	2	1662	58	1637
		0.250	1	1596		1636
	0.20 ^b	0.500	3	1660	55	1636
		1.00	4	1624	34	1635
		1.47	2	1638	8	1635
		1.94	3	1632	15	1635
		0.0103	2	256	5	256
0.8	2.00 ^c	0.0199	2	234	4	234
		0.0389	2	222	1	222
		0.0865	2	218	2	216
		0.1976	2	211	1	212
		0.514	3	889	18	890
	0.20 ^b	0.524	2	887	7	867
		0.988	2	865	2	865
		1.924	3	858	4	865

^a $(1.7-4.7) \times 10^{-5} M$ U(III) and $(4.6-9.2) \times 10^{-5} M$ Co(III) .
^b $(4.3-4.6) \times 10^{-5} M$ U(III) and $3.2 \times 10^{-4} M$ Co(III) .
^c $(1.9-4.3) \times 10^{-5} M$ U(III) and $8.8 \times 10^{-5} M$ Co(III) .
^d Calculated using $k' = a + b[\text{H}^+]$; the values for a and b are given in the text.

The ionic strength dependence was studied in HClO_4 - LiClO_4 solutions. The results are summarized in Table IV. At both 0.8 and 25.2° the data are in good agreement with the extended Debye-Hückel equation in the form $\log k' = \log k^\circ + A\Delta z^2\mu^{1/2}/(1 + B\delta\mu^{1/2}) + C\mu$. Best values for the three adjustable parameters, k° , δ , and C , were found by least squares and are listed in the footnote of Table IV. The average value found for δ , 9.3 Å, is in good agreement with the values found for other reactions of ions with high charges. For example, for $\text{Np(III)} + \text{Fe(III)}$, $\delta = 9.0$ Å at 0.8°⁹ and for $\text{V(II)} + \text{Np(IV)}$ $\delta = 9.9$ Å at 25°.¹⁰

The chloride dependence was studied in a short series of experiments at 25.2° in 1.00 M acid solutions. The

(9) T. W. Newton and N. A. Daugherty, *J. Phys. Chem.*, **71**, 3768 (1967).

(10) M. J. Burkhart and T. W. Newton, *ibid.*, **73**, 1741 (1969).

Table IV: Ionic Strength Dependence (HClO₄-LiClO₄ Solutions)

Ionic strength, <i>M</i>	No. of determinations	Av <i>k'</i> , <i>M</i> ⁻¹ sec ⁻¹	Mean dev	<i>k'</i> _{calcd.} ^a , <i>M</i> ⁻¹ sec ⁻¹
25.2°				
0.12	2	143	3	143
0.60	2	583	6	585
1.00	2	901	1	901
2.00	1	1678		1658
3.20	2	2715	44	2661
3.60	1	2941		3039
0.8°				
0.12	2	84.7	2.3	84.5
0.60	2	325	4	327
1.00	3	492	3	493
2.00	2	890	9	879
3.20	2	1362	20	1371

^a Calculated using the extended Debye-Hückel equation with the following values for the parameters: for 25.2°, $k^\circ = 3.95 \pm 0.15$, $A\Delta z^2 = 9.196$, $B = 0.3286$, $\delta = 9.24 \pm 0.13$, and $C = 0.087 \pm 0.05$; for 0.8°, $k^\circ = 2.69 \pm 0.08$, $A\Delta z^2 = 8.800$, $B = 0.3242$, $\delta = 9.35 \pm 0.11$, and $C = 0.080 \pm 0.005$. The adjustable parameters were determined by least squares and the listed uncertainties are the standard deviations.

Table V: Chloride Ion Dependence^a

[Cl ⁻], <i>M</i>	<i>k'</i> , <i>M</i> ⁻¹ sec ⁻¹	<i>k'</i> _{calcd.} ^b , <i>M</i> ⁻¹ sec ⁻¹
0.00	843, 872	857.5
0.052	1280	1278
0.104	1668, 1664	1659
0.156	2006	2006
0.209	2399, 2256	2329

^a Conditions: 25.2°, 1.00 *M* total acid, 4×10^{-6} *M* Co(III), and $(2.8-3.8) \times 10^{-4}$ *M* U(III). ^b Calculated using $k' = (857.5 + 9369[\text{Cl}^-]) / (1 + [\text{Cl}^-])$.

results are summarized in Table V. In terms of species present in the solution, it is reasonable to assume that the rates in chloride solutions are given by eq 3, or in

$$-d[\text{U(III)}]/dt = [\text{U}^{3+}][\text{Co}(\text{NH}_3)_4(\text{H}_2\text{O})_2^{3+}] \times (k_0 + k_1[\text{Cl}^-] + k_2[\text{Cl}^-]^2 + \dots) \quad (3)$$

terms of *k'* and the stoichiometric concentrations according to eq 4.

$$k' = (k_0 + k_1[\text{Cl}^-] + k_2[\text{Cl}^-]^2 + \dots) / (1 + \beta_{\text{U}}[\text{Cl}^-])(1 + \beta_{\text{Co}}[\text{Cl}^-]) \quad (4)$$

The association quotient, β_{U} , for UCl^{2+} may be estimated to be about unity by comparison with the value reported for PuCl^{2+} .¹¹ The association quotient for the cobalt complex is probably much smaller than unity if it is similar to that for $\text{Co}(\text{NH}_3)_6^{3+}$.¹² The data in Table IV can be reproduced very satisfactorily with the expression $k' = (857.5 + 9369[\text{Cl}^-]) / (1 + [\text{Cl}^-]) M^{-1}$

sec⁻¹. Thus if reasonable values for the association quotients are assumed there is no evidence for a term in the rate law which involves $[\text{Cl}^-]$ to powers greater than 1.

The temperature dependence of *k'* was studied between 0.8 and 45.0° in both 1.00 and 2.00 *M* HClO₄. The results are summarized in Table VI. The data

Table VI: Temperature Dependence

Temp, °C	No. of determinations	Av <i>k'</i> , <i>M</i> ⁻¹ sec ⁻¹	Mean dev ^a	<i>k'</i> _{calcd.} ^b , <i>M</i> ⁻¹ sec ⁻¹
1.00 <i>M</i> HClO ₄				
0.8	3	487	5	480
13.5	2	637	6	651
25.2	3	839	19	845
36.0	2	1052	1	1057
45.0	2	1284	6	1260
2.00 <i>M</i> HClO ₄				
0.8	12	887	23	882 ^c
13.5	8	1239	24	1244
25.2	10	1665	29	1668
36.0	6	2142	38	2146
45.0	7	2634	66	2615

^a Mean deviation from the mean. ^b Calculated using $\Delta S^* = -34.43$ cal mol⁻¹ deg⁻¹ and $\Delta H^* = 3.197$ kcal/mol. ^c Calculated using $\Delta S^* = -31.48$ cal mol⁻¹ deg⁻¹ and $\Delta H^* = 3.674$ kcal/mol.

were fitted to the equation $k' = (k_{\text{B}}T/h) \exp(\Delta S^*/R - \Delta H^*/RT)$, and the best values for the heat and entropy of activation were found by least squares. For the 2.00 *M* HClO₄ solutions ΔS^* was found to be -31.5 ± 0.15 cal mol⁻¹ deg⁻¹ and ΔH^* was 3.67 ± 0.04 kcal/mol; the uncertainties listed here are the standard deviations computed as part of the least-squares treatment. These parameters minimize the sum of squares of the per cent deviations and reproduce the experimental data with a root-mean-square deviation of 2.7% and a maximum deviation of 7.9%. For the 1.00 *M* solutions the corresponding values are $\Delta S^* = -34.4 \pm 0.2$ cal mol⁻¹ deg⁻¹ and $\Delta H^* = 3.20 \pm 0.07$ kcal/mol, rms dev = 2.2% and the maximum dev = 3.2%.

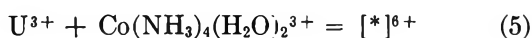
Some rate runs were made in which Np(III) rather than U(III) was used as the reducing agent. These were very much slower and consequently it was difficult to get reliable values for the rate constants. Preliminary results at 25° and $\mu = 2.0$ *M* (LiClO₄) indicate a distinct hydrogen ion dependence of the form $k' = 0.0044 + 0.009[\text{H}^+]^{-1} M^{-1} \text{sec}^{-1}$.

(11) (a) M. Ward and G. A. Welch, *J. Inorg. Nucl. Chem.*, **2**, 395 (1956); (b) J. J. Katz and G. T. Seaborg, "The Chemistry of the Actinide Elements," Methuen and Co., Ltd., London, 1957 (also Wiley, New York, N. Y.), p 305.

(12) E. L. King, J. H. Espenson, and R. E. Visco, *J. Phys. Chem.*, **63**, 755 (1959).

Discussion

The hydrogen ion dependence data in Table III indicate that the most important term in the rate law is hydrogen ion independent and that the predominant net activation process is



The small effect of $[\text{H}^+]$ which leads to a two-term rate law in 0.2 *M* solutions and at 0.8° in 2 *M* solutions is consistent with a parallel path for which the net activation process involves the loss of H^+ prior to the formation of the activated complex. At 25° and an ionic strength of 2 *M* the hydrogen ion dependence is apparently obscured by a compensating medium effect. This is plausible in that when NaClO_4 was substituted for LiClO_4 in 0.064 *M* HClO_4 ($\mu = 2$ *M*) the apparent second-order rate constant dropped from 1640 to about 1200 $\text{M}^{-1} \text{sec}^{-1}$. This medium effect is a little larger than that observed for the V(II)–Np(IV) reaction, where substituting NaClO_4 at $\mu = 2.0$ *M* decreased the rate constant from 2.56 to 1.96 $\text{M}^{-1} \text{sec}^{-1}$.¹⁰

Our value for k' in 0.2 *M* HClO_4 at 25° is $211 \pm 2 \text{M}^{-1} \text{sec}^{-1}$; this is in satisfactory agreement with the previous result which was $223 \pm 10 \text{M}^{-1} \text{sec}^{-1}$.³ However, at lower acid concentrations and the same ionic strength, our values are considerably lower than the previous ones. In 0.01 *M* HClO_4 ($\mu = 0.2$ *M*) 257 is to be compared with 303 $\text{M}^{-1} \text{sec}^{-1}$. For the earlier data, plots of k' vs. $[\text{H}^+]^{-1}$ were not linear, and it was suggested that a simple parallel path mechanism was not satisfactory for the U(III) reduction of $\text{Co}(\text{NH}_3)_5(\text{H}_2\text{O})^{3+}$, $\text{Co}(\text{NH}_3)_4(\text{H}_2\text{O})_2^{3+}$, and *trans*- $\text{Co}(\text{en})_2(\text{NH}_3)\text{H}_2\text{O}^{3+}$.³ Since the data in Table III do give linear plots, and for 0.2 *M* solutions the rate constants are all less than the previously measured corresponding ones,¹³ there is no requirement for a more complicated mechanism for the $\text{Co}(\text{NH}_3)_4(\text{H}_2\text{O})_2^{3+}$ reaction.

Increasing the U(III) concentration by a factor of 75 was found to decrease the rate constant by about 11%. This small effect, if real, suggests the following two rate laws which are indistinguishable on the basis of the available data.

$$-d[\text{U(III)}]/dt = k_0'[\text{Co(III)}][\text{U(III)}] + k''[\text{Co(III)}] \quad (6)$$

and

$$(-d[\text{U(III)}]/dt)^{-1} = (k_0'[\text{Co(III)}][\text{U(III)}])^{-1} + (k'''[\text{Co(III)}])^{-1} \quad (7)$$

Both rate laws suggest the formation of a cobalt-containing intermediate which reacts with U(III) to give products. For eq 6 the intermediate is formed by a path parallel to the principal one and reacts rapidly with U(III), while for eq 7 its formation is reversible and its reaction with U(III) is relatively slow. In either rate law the constant, k_0' , is associated with the most im-

portant net activation process, eq 5. Most of the data were collected using U(III) concentrations near 3×10^{-5} *M*; if eq 6 applies the observed rate constant will be about 5% higher than k_0' , while if eq 7 applies they will be about 5% lower. This uncertainty in interpretation introduces an uncertainty in ΔS^* of about 0.11 cal mol⁻¹ deg⁻¹ in addition to the statistical uncertainty given above.

The relatively small $[\text{Cl}^-]$ dependence is consistent with the idea that Cl does not occupy a bridging position. The rate constant ratio, k_1/k_0 is about 11 M^{-1} , not far from the values found for other reactions which show essentially no hydrogen ion dependence. For the U(III)– $\text{Co}(\text{NH}_3)_6^{3+}$ reaction the corresponding value is about 18 M^{-1} ,³ is about 9 M^{-1} for the Pu(III)–Np(VI) reaction,¹³ and is about 20 M^{-1} for the V(II)–Np(IV) reaction.¹⁰

The activation entropies of a set of related reactions are compared in Table VII. The values are sur-

Table VII: Activation Entropies^a

Reducing agent	Oxidizing agent	$\Delta S^*,^b$ cal mol ⁻¹ deg ⁻¹	Ref
U^{3+}	$\text{Co}(\text{NH}_3)_4(\text{H}_2\text{O})_2^{3+}$	-31.5 ± 0.2	<i>h</i>
Np^{3+}	$\text{V}(\text{H}_2\text{O})_6^{3+}$	-30 ± 2^c	<i>i</i>
Np^{3+}	$\text{Fe}(\text{H}_2\text{O})_6^{3+}$	-36 ± 5^d	<i>j</i>
Pu^{3+}	PuOH^{3+}	-39 ± 5^e	<i>k</i>
Eu^{2+}	$\text{Co}(\text{NH}_3)_5\text{Br}^{2+}$	-32^f	<i>l</i>
U^{3+}	$\text{Co}(\text{NH}_3)_5\text{B}^{2+}$	-33 ± 1^g	<i>m</i>

^a 25° and $\mu = 2.0$ *M*, unless otherwise noted. ^b For the $[\text{H}^+]$ independent term. ^c Calculated from data for the reverse reaction. ^d For the minor term in the rate law. ^e Recalculated from the original data. ^f $\mu = 1.0$ *M*. ^g $\mu = 0.2$ *M*. The value should be 2 ± 1 more positive at $\mu = 2$ *M*. ^h This work. ⁱ See ref 10. ^j See ref 9. ^k T. K. Keenan, *J. Phys. Chem.*, **61**, 1117 (1957). ^l J. P. Candlin, J. Halpern, and D. L. Trimm, *J. Amer. Chem. Soc.*, **86**, 1019 (1964). ^m See ref 3.

prisingly similar in spite of the differences in charge type and in the nature of the coordinated ligands. The value for $\text{Np}^{3+} + \text{V}^{3+}$ was calculated^{14–16} from the data for the reverse reaction, for which the predominant net activation process is $\text{V}^{2+} + \text{Np}^{4+} = [\ast]^{6+}$.

The fact that Np^{3+} reacts much more slowly than U^{3+} is undoubtedly connected with the fact that U^{3+} is a better reducing agent by about 0.79 V or 18.1 kcal. Values for $k_{\text{U}}/k_{\text{Np}}$ are available for some other oxidizing agents as well and are summarized in Table VIII. It is

(13) R. B. Fulton and T. W. Newton, *J. Phys. Chem.*, **74**, 1661 (1970).

(14) For this estimate we have used the published¹⁵ values for the ionic entropies of Np^{3+} and Np^{4+} and have used the equation of Powell and Latimer¹⁶ and the values for Fe^{2+} and Fe^{3+} for ($S^{\circ}_{\text{V}^{2+}} - S^{\circ}_{\text{V}^{3+}}$).

(15) Reference 11b, p 429.

(16) R. E. Powell and W. M. Latimer, *J. Chem. Phys.*, **19**, 1139 (1950).

Table VIII: Relative Rates of Oxidation of U(III) and Np(III)

Oxidizing agent	Potential, ^a V	k_U/k_{Np} , obsd	$\Delta F_{\text{exchange}}^*$, kcal/mol		k_U/k_{Np} , calcd ^b
			Ox. agent	Red. agent	
$\text{Co}(\text{NH}_3)_4(\text{H}_2\text{O})_2^{3+}$	<0.4 ^{c-e}	4×10^6 ^f	24 ^g	16 ^{h,i}	$>1.6 \times 10^6$
CrOH^{2+} ^j	-0.65	5×10^8 ^k	17.4 ^g	12 ^h	8×10^6
UO_2^{2+}	0.063	1.4×10^3 ^l	14 ^m	16 ^h	5×10^6
UO_2^+	<0.58 ^d	3×10^3 ⁿ	20 ^o	16 ^h	$>4 \times 10^4$

^a Reduction potential for the oxidizing agent. ^b Calculated using the Marcus expression in the form: $\Delta F_{12}^* = 0.5(\Delta F_{11}^* + \Delta F_{22}^* + \Delta F_{12}^0) + (\Delta F_{12}^0)^2/[8(\Delta F_{11}^* + \Delta F_{22}^* - w_{11} - w_{22} - 4.9)]$. ^c Estimate based on W. M. Latimer, "Oxidation Potentials," 2nd ed, Prentice-Hall, Englewood Cliffs, N. J., 1952, p 214; and R. G. Yalman, *Inorg. Chem.*, **1**, 16 (1962). ^d The pertinent potential will be less if the immediate product of electron exchange is in an excited state. ^e Decreasing the potential by 0.134 V will increase the calculated rate ratio by a factor of 2. ^f This work. ^g Assumed the same as that for Cr(II)-(III) exchange, A. Anderson and N. A. Bonner, *J. Amer. Chem. Soc.*, **76**, 3826 (1954). ^h Assumed the same as for the Pu(III)-(IV) exchange, see footnote *k*, Table VII. ⁱ Increasing either $\Delta F_{\text{exchange}}^*$ value by 9 kcal/mol will increase the calculated rate ratio by a factor of 2. ^j Reaction assumed to be $\text{M}^{3+} + \text{CrOH}^{2+} = \text{MOH}^{3+} + \text{Cr}^{2+}$, see ref 9. ^k $k_U = 6 \times 10^{-3} \text{ sec}^{-1}$ [R. T. Wang and J. H. Espenson, *J. Amer. Chem. Soc.*, **93**, 1629 (1971)], $k_{Np} = 4.2/(3.8 \times 10^9)$ from rate constant [R. C. Thompson and J. C. Sullivan, *ibid.*, **89**, 1096 (1967)], and the equilibrium quotient. ^l $k_U = 5.5 \times 10^4 \text{ M}^{-1} \text{ sec}^{-1}$, ref 5, $k_{Np} = 39 \text{ M}^{-1} \text{ sec}^{-1}$, T. W. Newton, *J. Phys. Chem.*, **74**, 1655 (1970). ^m Taken equal to that for the Np(V)-(VI) exchange, D. Cohen, J. C. Sullivan, and J. C. Hindman, *J. Amer. Chem. Soc.*, **78**, 1543 (1956). ⁿ $k_U = 1.1 \times 10^6 \text{ M}^{-1} \text{ sec}^{-1}$, ref 5, $k_{Np} = 38 \text{ M}^{-1} \text{ sec}^{-1}$ (see footnote *l*). ^o Estimated.

seen that the rate ratios for the "-yl" ions are distinctly lower than the others. Rate ratios can sometimes be correlated using the Marcus cross relation¹⁷ even though the mechanisms are probably not innersphere.^{9,18,19} The calculated ratios depend primarily on the U(III)-Np(III) potential difference but depend to a lesser extent on the values assumed for the potentials of the oxidizing agents and for the pertinent exchange rate constants. Values for the k_U/k_{Np} ratio estimated in this way are given in Table VIII. It is seen that for $\text{Co}(\text{NH}_3)_4(\text{H}_2\text{O})_2^{3+}$ and $\text{Cr}(\text{H}_2\text{O})_6^{3+}$, reasonable estimates for E^0 and $\Delta F_{\text{exchange}}^*$ lead to rate ratios in satisfactory agreement with the observations. However, other factors are apparently involved in the UO_2^{2+} and UO_2^+ reactions.

Acknowledgments. We thank Professor Henry Taube for many helpful comments on the original manuscript and also Professor J. H. Espenson for his interest and for making the manuscripts for ref 3 and footnote *k* Table VIII (R. T. Wang) available before publication. We are grateful to Dr. A. E. Florin for help in obtaining and interpreting the nmr spectra. We also acknowledge many helpful discussions with Dr. C. E. Holley, Jr., under whose general direction this work was done.

- (17) R. A. Marcus, *J. Phys. Chem.*, **67**, 853 (1963).
 (18) R. C. Patel and J. F. Endicott, *J. Amer. Chem. Soc.*, **90**, 6364 (1968).
 (19) N. Sutin, "Exchange Reactions," International Atomic Energy Agency, Vienna, 1965.

Proton Exchange in Aqueous Urea Solutions

by Donald L. Hunston and Irving M. Klotz*

Department of Chemistry,¹ Northwestern University, Evanston, Illinois 60201 (Received February 8, 1971)

Publication costs assisted by the National Institutes of Health

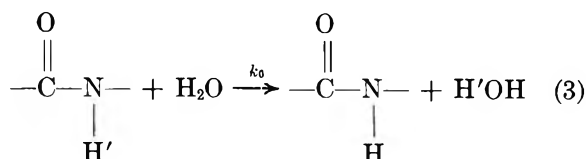
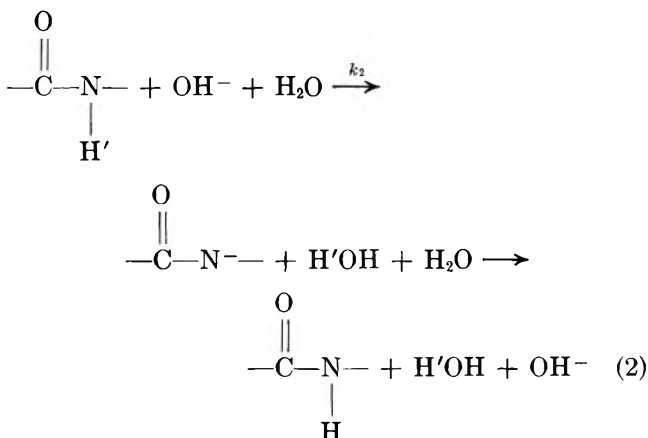
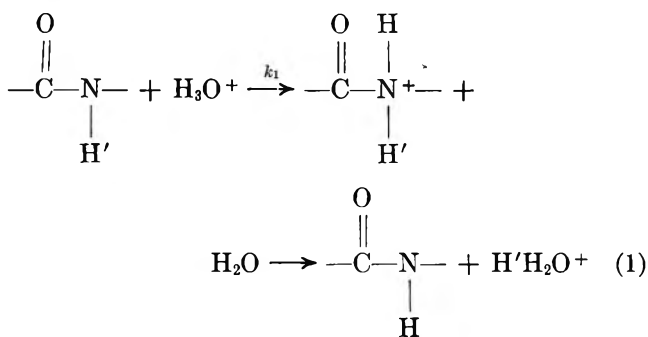
Proton exchange in aqueous urea solutions is acid- and base-catalyzed, as it is in standard amides. The acid-catalyzed rate is much faster, however, and the rate-pH profile is therefore shifted toward higher pH values. This difference can be understood in terms of the stronger basicity of urea.

Introduction

Proton exchange rates between amides and water have been studied very extensively^{2a,b,3} particularly because these systems provide a basis for understanding isotopic hydrogen exchange in proteins. Many of the constitutive and environmental factors that influence these kinetics have now been revealed.³ Urea is a unique type of amide and in addition is of interest because of its perturbing effects on the behavior of proteins in aqueous solution. It has seemed appropriate, therefore, to examine also the kinetics of proton exchange for urea in aqueous solutions.

Analysis of Kinetics of Exchange

For proton exchange in aqueous solutions of amides, the mechanism proposed by Berger, Loewenstein, and Meiboom^{2a} is the generally accepted one. It is comprised of three pathways: acid catalysis, base catalysis, and spontaneous reaction with the solvent



Protonation and proton abstraction are the rate-determining steps in acid and base catalysis, respectively. On the other hand, the exact mechanism and the rate expression for the direct reaction with solvent are uncertain, because the rate of the spontaneous reaction is very slow compared with acid and base catalysis. It is generally assumed that the solvent itself acts as an acid or base with mechanisms similar to those shown in eq 1 and 2.

The "specific" exchange rate, R , can then be written as

$$R = \frac{1}{(\text{N-H})} \frac{d(\text{N-H})}{dt} = \frac{1}{k_1(\text{H}_3\text{O}^+) + k_2(\text{OH}^-) + k_0(\text{H}_2\text{O})} \quad (4)$$

or

$$R = k_1(\text{H}_3\text{O}^+) + k_2K_w/(\text{H}_3\text{O}^+) + k_0(\text{H}_2\text{O}) \quad (5)$$

where K_w is the self-ionization constant of water in the solution. For amides a graph of R vs. pH gives the "U" shaped curve characteristic of acid-base catalysis.^{2b,3}

An alternate graphical display can be obtained by plotting $\log R'$ vs. pH where

$$R' = R - k_0(\text{H}_2\text{O}) \quad (6)$$

Two straight lines are obtained at the extremes of pH. In the region in which acid catalysis is predominant

$$\log R' = \log k_1 - \text{pH} \quad (7)$$

(1) This investigation was supported in part by a grant (GM-09280) from the National Institute of General Medical Sciences, U. S. Public Health Service. It was also assisted by support made available by a U. S. Public Health Service Training Grant (5T1-GM-626) from the National Institute of General Medical Sciences.

(2) (a) A. Berger, A. Loewenstein, and S. Meiboom, *J. Amer. Chem. Soc.*, **81**, 62 (1959); (b) B. H. Leichtling and I. M. Klotz, *Biochemistry*, **5**, 4026 (1966).

(3) I. M. Klotz, *J. Colloid Interface Sci.*, **27**, 804 (1968), and references therein.

and in the range in which base catalysis is predominant

$$\log R' = \log k_2 K_w + \text{pH} \quad (8)$$

A convenient alternative expression to replace eq 5 can be obtained as follows. This equation for R can be rearranged to give

$$R - k_0(\text{H}_2\text{O}) = R' = (k_1 k_2 K_w)^{1/2} \times \left[\left(\frac{k_1}{k_2 K_w} \right)^{1/2} (\text{H}_3\text{O}^+) + \left(\frac{k_2 K_w}{k_1} \right)^{1/2} \frac{1}{(\text{H}_3\text{O}^+)} \right] \quad (9)$$

Defining σ as

$$\sigma = -\log \left(\frac{k_1}{k_2 K_w} \right)^{1/2} - \log (\text{H}_3\text{O}^+) = -\log \left(\frac{k_1}{k_2 K_w} \right)^{1/2} + \text{pH} \quad (10)$$

we can convert eq 9 to

$$R' = 2(k_1 k_2 K_w)^{1/2} (1/2) (e^{2.303\sigma} + e^{-2.303\sigma}) \quad (11)$$

or

$$R' = 2(k_1 k_2 K_w)^{1/2} \cosh (2.303\sigma) \quad (12)$$

This expression represents a U-shaped curve (catenary) that has a minimum value of

$$R'_{\min} = 2(k_1 k_2 K_w)^{1/2} \quad (13)$$

at

$$\sigma = 0 \quad (14)$$

or at

$$\text{pH}_{\min} = -(1/2) \log \left(\frac{k_2 K_w}{k_1} \right) \quad (15)$$

The results of eq 13 and 15, derived previously² in an alternative way, can be combined with eq 6 and 12 to give

$$R = R'_{\min} \cosh (2.303[\text{pH} - \text{pH}_{\min}]) + k_0(\text{H}_2\text{O}) \quad (16)$$

It is clear from this equation that the contribution of the spontaneous reaction is to shift the R vs. pH curve vertically without changing its shape. Its horizontal location is determined by pH_{\min} while the shape of the curve is completely established by R'_{\min} .

These characteristics can also be described in terms of absolute reaction rate theory.⁴ First the rate constant is expressed as

$$k_i = \frac{\kappa_i k T}{h} e^{-\Delta F_i^\ddagger / \mathcal{R} T} \quad (17)$$

where κ is the transmission coefficient, ΔF_i^\ddagger is the free energy of activation, k is the Boltzmann constant, h is Planck's constant, and \mathcal{R} is the gas law constant. This expression can be substituted into eq 13 and 15 to give the equations

$$R'_{\min} = 2 \frac{k T}{h} (\kappa_1 \kappa_2)^{1/2} \times \exp(-[\Delta F_1^\ddagger + \Delta F_2^\ddagger + \Delta F_w^0] / 2 \mathcal{R} T) \quad (18)$$

and

$$\text{pH}_{\min} = -(1/2) \log (\kappa_2 / \kappa_1) + \frac{1}{2.303(2) \mathcal{R} T} (\Delta F_2^\ddagger + \Delta F_w^0 - \Delta F_1^\ddagger) \quad (19)$$

If the transmission coefficients are assumed to be constant, the shape of the curve and the minimum rate (neglecting the spontaneous reaction with solvent) are determined by the sum of the free energies of activation. In contrast pH_{\min} is determined by a difference in activation free energies. It is possible, therefore, in comparing R vs. pH curves for different substances to interpret the results in terms of the relative free energies of the reactants and of the transition states.⁵

Experimental Section

Urea (Mann "ultra pure") was used as received. The low level of metal ion contamination in this urea is essential if accurate (H_3O^+) measurements are to be obtained.⁶ Solutions were prepared by dissolving a fixed weight of urea in a fixed volume of distilled, deionized water, the pH of which had been adjusted with HCl or NaOH. The molar concentrations of water and urea were obtained from the weight of the solution and its density. The pH of the solution was measured with a Radiometer Model 4 pH meter using a combination glass electrode. The H_3O^+ and OH^- ion concentrations were calculated from the measured pH by a procedure that will be discussed later.

The pH in urea solutions tends to drift slowly because of CO_2 absorption and decomposition of the urea. All solutions were used within 4 hr of preparation and unnecessary contact with air was avoided. In weakly buffered solutions the pH drift was less than ± 0.02 unit during this period. Tests with both weakly buffered and unbuffered solutions indicated that the presence of buffer did not affect the measured exchange rate.

The nmr spectrum of each sample was recorded at $22 \pm 1^\circ$ with a Varian A-60 spectrometer equipped with a Varian V-6040 variable temperature controller. As noted by previous investigators,⁷ the spectrum in a neutral solution consists of a sharp water peak and an N-H peak broadened by interaction of the proton magnetic dipole with the rapidly relaxing nitrogen magnetic dipole. (The rapid relaxation of the nitrogen magnetic

(4) A. A. Frost and R. G. Pearson, "Kinetics and Mechanism," Wiley, New York, N. Y., 1961, pp 97-99.

(5) I. M. Klotz and D. D. Mueller, *Biochemistry*, **8**, 12 (1969).

(6) H. B. Bull, K. Breese, G. L. Ferguson, and C. A. Swenson, *Arch. Biochem. Biophys.*, **104**, 297 (1964).

(7) O. Jardetzky and C. D. Jardetzky, *J. Biol. Chem.*, **233**, 383 (1958).

dipole is due, in turn, to coupling of the nitrogen quadrupole to the tumbling motion of the urea molecule.) With increasing or decreasing pH the two peaks broaden, coalesce to a single broad peak, and then narrow to a single sharp peak. To avoid the complications caused by the quadrupole moment of nitrogen,⁸ we made measurements only when two peaks were present. This restriction limits the pH range in which observations can be made; however, the high solubility of urea enables one to examine a number of concentrations and thereby to investigate a large pH range.

For each solution the two peaks were recorded separately a minimum of three times on an expanded scale at a slow sweep rate. An average value for the full width at half-height was obtained for the water peak of each sample and when possible for the N-H peak. For each urea concentration used, several measurements were made in a neutral solution to obtain the line width when there was no measurable exchange. From the amount of broadening, $\delta\nu$, in cycles/sec, the "specific" rate of proton exchange can be calculated.

It is very difficult to measure the exchange rate of the urea protons directly because of the quadrupole broadening of the N-H peak and the intensity of the nearby water peak. On the other hand, the "specific" exchange rate of the reverse reaction, that is exchange of the water protons, can be calculated from broadening of the water line⁹

$$R_r = \frac{1}{(\text{H}_2\text{O})} \frac{d(\text{H}_2\text{O})}{dt} = \pi\delta\nu_{\text{H}_2\text{O}} \quad (20)$$

If the measured exchange is between the water protons and the N-H protons of urea, the "specific" rate for the forward reaction can be calculated from

$$R = R_r \frac{(\text{H}_2\text{O})}{2(\text{urea})} \quad (21)$$

where the factor of 2 accounts for the fact that a urea molecule has twice as many protons as a water molecule. This procedure has been shown to be valid for both *N*-methylacetamide¹ and thiourea.⁸

Vold and Correa⁸ have demonstrated that the validity of eq 21 can be tested by showing that for slow exchange the ratio of exchange broadening of the N-H and water peaks is equal to the ratio of proton concentrations

$$\frac{\delta\nu_{\text{urea}}}{\delta\nu_{\text{H}_2\text{O}}} = \frac{2(\text{H}_2\text{O})}{4(\text{urea})} \quad (22)$$

This ratio was calculated for urea in the slow exchange region for a series of ten samples with a concentration ratio of 4.2. Although the difficulty in measuring the N-H peak broadening led to considerable scatter, the average value of 4.4 was in good agreement with the concentration ratio.

To compare proton exchange in urea solutions with that in amide solutions, it is necessary to know the

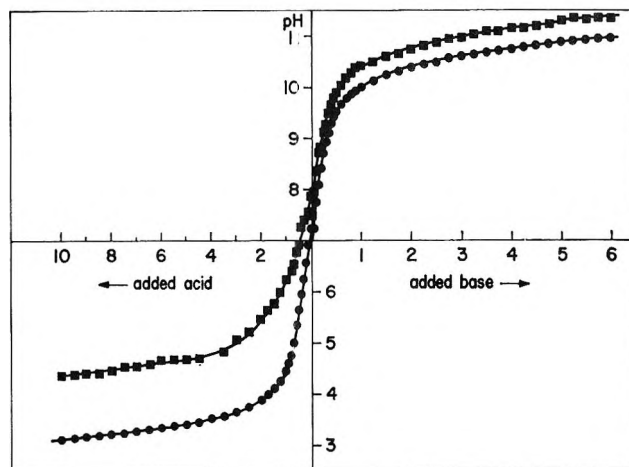
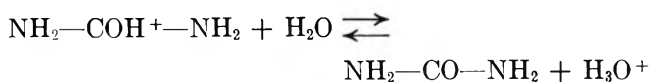


Figure 1. Measured pH in water (●) and in a 5.14 *M* urea solution (■) shown as a function of added acid and base.

hydrogen and hydroxide ion concentrations (eq 4). It has long been realized that the pH measured in solutions containing urea is somewhat higher than when urea is not present.^{6,10} Typical titration curves are shown in Figure 1. The upward shift in the acid range could be attributed to the weak basicity of urea. However, the fact that an upward shift is manifested even in basic solutions indicates that other effects are also present.^{6,10}

In the light of the success of Berger, Loewenstein, and Meiboom's^{2a} procedure with *N*-methylacetamide, a method similar to theirs was followed for obtaining the hydrogen and hydroxyl ion concentrations in aqueous urea solutions. First the amount of acid or base added to the solution was estimated from the titration curves. Then a correction was made for the weak basicity of urea using values of pK_a (0.20 to 0.30) obtained by titrating solutions with strong acid. The reaction corresponding to pK_a is



Thereafter the change in K_w was estimated using the water activities interpolated from the results of Scatchard, *et al.*¹¹

Results and Discussion

A plot of $\log R'$ vs. hydrogen ion or hydroxide ion concentration is shown in Figure 2. Lines are drawn to represent the best fit of the data with eq 6-8. The rate

(8) R. L. Vold and A. Correa, *J. Phys. Chem.*, **74**, 2674 (1970).

(9) J. A. Pople, W. G. Schneider, and H. J. Bernstein, "High-Resolution Nuclear Magnetic Resonance," McGraw-Hill, New York, N. Y., 1959, p 221.

(10) M. Levy, *Compt. Rend. Trav. Lab. Carlsberg, Ser. Chim.*, **30**, 291 (1958).

(11) G. Scatchard, W. J. Hamer, and S. E. Wood, *J. Amer. Chem. Soc.*, **60**, 3061 (1938).

Table I: Rate Constants for Proton Exchange

Compd	Temp, °C	Acid catalysis, k_1 , l. mol ⁻¹ sec ⁻¹	Base catalysis, k_2 , l. mol ⁻¹ sec ⁻¹	Solvent reaction, k_0 , l. mol ⁻¹ sec ⁻¹
Urea ^a	22	$7.0 \pm 2.0 \times 10^6$	$4.8 \pm 1.6 \times 10^6$	$< 8 \times 10^{-2}$
<i>N</i> -Methyl- acetamide ^b	22	$3.8 \pm 0.4 \times 10^2$	$5.2 \pm 1.0 \times 10^6$	$< 5 \times 10^{-6}$
Ethanol ^c	22	2.8×10^6	2.8×10^6	0.8
Thiourea ^{a,d}	35	$5 \pm 1 \times 10^4$		

^a For urea and thiourea the rates are expressed per mole of nitrogen. ^b Reference 2a. ^c Z. Luz, D. Gill, and S. Meiboom, *J. Chem. Phys.*, **30**, 1540 (1959). ^d Reference 8.

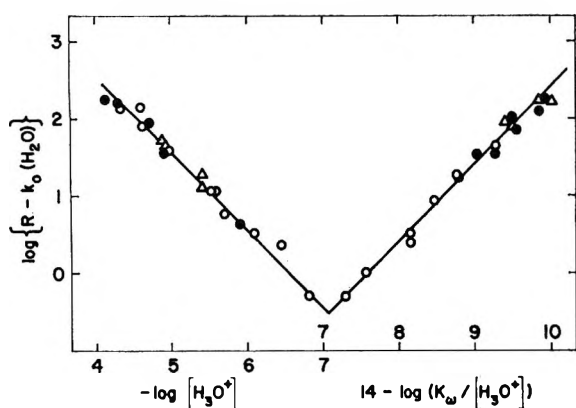


Figure 2. Logarithm of the specific exchange rate, R (in sec^{-1}), less the spontaneous reaction contribution, $k_0(\text{H}_2\text{O})$, as a function of the negative logarithm of the hydrogen ion and hydroxide ion concentrations. Urea concentrations (molar): \bullet , 1.56; Δ , 2.97; \circ , 5.14.

constants obtained are

$$k_1 = 3.5 \pm 1.0 \times 10^6 \text{ l. mol}^{-1} \text{ sec}^{-1}$$

$$k_2 = 2.4 \pm 0.8 \times 10^6 \text{ l. mol}^{-1} \text{ sec}^{-1}$$

$$k_0 = 2 \pm 2 \times 10^{-2} \text{ l. mol}^{-1} \text{ sec}^{-1}$$

when expressed in terms of the molar concentration of urea protons.

The precision of k_1 and k_2 is limited by the uncertainty in hydrogen and hydroxide ion concentrations. The spontaneous reaction is too slow to be measured directly, so the specific rate must be less than 2 sec^{-1} . The best fit of the data is obtained with a value of $k_0 = 2 \times 10^{-2} \text{ l. mol}^{-1} \text{ sec}^{-1}$; however, because of the small contribution made by the spontaneous reaction and the difficulty of working at neutral pH, the uncertainty is very large.

From Figure 2 it is evident that proton exchange in urea solutions follows a pattern similar to that observed for amides.^{2,3} A comparison of rate constants for several different compounds is made in Table I. For this comparison urea and thiourea are considered diamides and the rates are expressed in terms of the molar concentration of amide nitrogen. This is somewhat oversimplified since the two nitrogens are not indepen-

dent; that is, the addition of a proton to the molecule affects the basicity of the unprotonated nitrogen. Nevertheless, since only a small fraction of the molecules are protonated, the concentration of available nitrogen in a urea solution is about twice as large as in an equivalent *N*-methylacetamide solution.

As is evident from Table I, the acid-catalysis constant k_1 is 10^4 times as large for urea as for *N*-methylacetamide. A small part of this may be due to statistical factors: *N*-methylacetamide has one proton on the amide nitrogen, urea has two. After protonation of *N*-methylacetamide, there is a 50% chance that exchange will occur, *i.e.*, that the departing proton in subsequent dissociation will be that originally on the amide nitrogen. In contrast with urea after protonation there is a 67% chance that the departing proton will be one of the two originally on each amide nitrogen.

The major reason for the much larger k_1 for urea presumably lies in the substantially greater basicity of the amide nitrogen in this molecule as compared with *N*-methylacetamide. Protonation of these molecules measured by direct experiments gives $\text{p}K_{\text{a},\text{O}}$, the acid dissociation constant of the O-protonated species. What we need to know, however, is $\text{p}K_{\text{a},\text{N}}$, the $\text{p}K_{\text{a}}$ of the N-protonated species, since it is this protonation that leads to exchange.^{2a} An estimate of $\text{p}K_{\text{a},\text{N}}$ can be obtained by the following considerations. Amines have $\text{p}K_{\text{a}}$ values¹² of about 10. When the nitrogen of an amide is protonated, 21 kcal mol⁻¹ of resonance energy¹³ must also be compensated for. Thus $\text{p}K_{\text{a},\text{N}}$ for an amide should drop to about -5.4 (Pauling suggests a value of -6 for acetamide).¹⁴ For urea, on the other hand, there are three resonance structures (Figure 3) and its resonance energy¹³ is 37 kcal mol⁻¹. Protonation of one of its amide nitrogens results in a loss of only one resonance form (see Figure 3). The protonated species has resonance structures similar to the amide resonance forms; hence a resonance energy of about 21 kcal mol⁻¹ should be retained. The protonation of one

(12) J. D. Roberts and M. C. Caserio, "Basic Principles of Organic Chemistry," W. A. Benjamin, New York, N. Y., 1964, p 650.

(13) L. Pauling, "The Nature of the Chemical Bond," 3rd ed, Cornell University Press, Ithaca, N. Y., 1960, p 197.

(14) Reference 13, p 281.

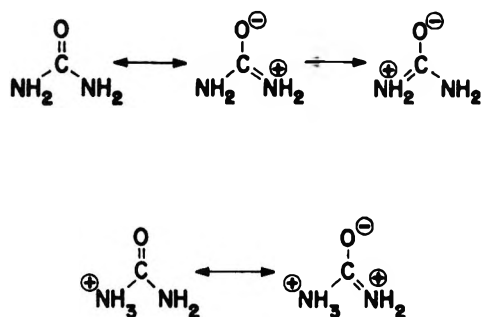
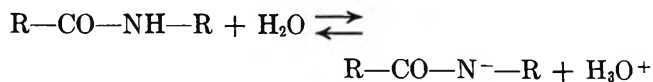


Figure 3. Resonance structures for protonated and unprotonated forms of urea.

amide nitrogen in urea should therefore be accompanied by a loss of 16 kcal mol⁻¹ of resonance energy. This would shift the $pK_{a,N}$ down to -1.7. This decrease in acidity of the protonated species, or increase in basicity of the ground state, unprotonated nitrogen, should change the activation ΔF_1^\ddagger for acid catalysis by about 5 kcal and the corresponding rate constant by about 10^4 .

It is interesting to note that the exchange rate constant k_1 for thiourea is smaller than that for urea; the measured basicity¹⁵ is also less than that for urea.

Turning to base catalysis, we note that Sheinblatt¹⁶ has shown a relationship between the acidity of the exchanging site and the base catalysis rate. The acidity constant, pK_{a2} , corresponds to the reaction



For *N*-methylacetamide and ethanol, the closeness of the values of pK_{a2} , 15.1 and 15.5, respectively,³ corresponds very well with the very similar values of k_2 , 5.2×10^6 and 2.8×10^6 (Table I). A corresponding comparison for urea cannot be made precisely since, to our knowledge, pK_{a2} for this substance has not been measured despite several attempts to do so.^{10,17} Nevertheless, it seems likely from the structure of urea (Figure 3) that acid strength of the neutral species should be near that of an amide. Consequently a base-catalysis constant near that of *N*-methylacetamide seems reasonable.

Thus proton exchange in aqueous urea solutions is similar in pH profile with that of simple amides. In other words, it is acid and base catalyzed. The large differences in position of the catenary rate constant-pH curve—the shift horizontally by several pH units and vertically by several orders of magnitude—is merely a manifestation of the much increased acid catalysis constant, which in turn arises from the stronger basicity of urea.

(15) D. D. Perrin, "Dissociation Constants of Organic Bases in Aqueous Solution," Butterworths, London, p 449.

(16) M. Sheinblatt, *J. Amer. Chem. Soc.*, **92**, 2505 (1970).

(17) J. Bell, W. A. Gillespie, and D. B. Taylor, *Trans. Faraday Soc.*, **39**, 137 (1943).

Complex Formation between Some Acetylenic Compounds and Benzene

by David M. Coleman, Y. Aviva Sataty, and J. Tyrrell

Department of Chemistry, Southern Illinois University, Carbondale, Illinois 62901 (Received November 23, 1970)

Publication costs borne completely by The Journal of Physical Chemistry

The proton resonance signals of the methylene hydrogens in 1,4-dichlorobut-2-yne and of the methylene and acetylenic hydrogens in propargyl chloride and propargyl bromide shift upfield in going from cyclohexane to benzene as a solvent. The data are examined from the standpoint of the existence of only 1:1 complexes, only 1:2 complexes involving two molecules of benzene, or a combination of both. A detailed statistical analysis of the data clearly indicates the existence of only 1:1 complexes in propargyl halide-benzene solutions. In the case of 1,4-dichlorobut-2-yne, analysis indicates either 1:1 complexes or a combination of 1:1 and 1:2 complexes. The need for a statistical analysis in cases where more than one model is feasible is emphasized. The possible structure and nature of the complexes are discussed.

Introduction

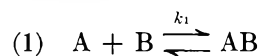
Solute-solvent complex formation in aromatic solvents has been the subject of considerable investigation.¹⁻⁴ In particular, there have been a number of investigations involving complex formation between acetylenes and aromatic solvents where the upfield shift of the proton resonance signal of the acetylenic hydrogen has been used to determine the extent of complexation.⁵ This upfield shift has led to the belief that the complex formation is a result of hydrogen bonding between the acetylenic hydrogen and the π electrons of the aromatic ring. While this may well be true, it has also been observed that similar upfield shifts result for the proton resonance signals of methylene groups attached to acetylenes⁶ and of methyl groups in methyl halides.⁷ It is not generally accepted that the hydrogens of a methylene or a methyl group can hydrogen bond to a donor so that the resonance shifts observed may possibly be a direct or indirect result of complex formation which may involve hydrogen bonding, π - π interactions, or some other mechanism. However, since these observed shifts are concentration dependent, they can be used as a means of studying complex formation.

Propargyl chloride and propargyl bromide possess both an acetylenic hydrogen and methylene hydrogens, and the proton resonance signals of both types of hydrogen shift upfield in going from cyclohexane to benzene as solvent. The 1,4-dichlorobut-2-yne has two sets of equivalent methylene protons with an environment similar to that in propargyl chloride. It was decided to investigate the complex formation of these compounds with benzene using the acetylenic proton shift and/or the methylene proton shift.

The theoretical models for complex formation involving more than one complex have been studied in some detail.⁸ The chemical shift in cycles per second from cyclohexane (used here as the internal reference as well as the inert solvent) of the proton resonance sig-

nal in pure cyclohexane is denoted by δ_A^M and δ_A^E for the methylene and ethynyl protons, respectively. The chemical shift in the mixed benzene-cyclohexane solvent is denoted by δ_1^M and δ_1^E again for the methylene and ethynyl protons, respectively. Then the chemical shift, due to complex formation, for the methylene protons is given by $\delta_M = \delta_A^M - \delta_1^M$ and for the ethynyl proton is given by $\delta_E = \delta_A^E - \delta_1^E$. The mole fraction of benzene in cyclohexane is given by X_B , and δ_{AB^M} , δ_{AB^E} , and δ_{AB_2} are taken to be the chemical shifts if complex formation is complete. These symbols refer, respectively, to the species AB^M (if only methylene protons are involved), to AB^E (if only ethynyl protons are involved), and to AB_2 (if both sets of protons are involved). The symbol A refers to the acetylene and B to the benzene. Equations relating the chemical shifts to the equilibrium parameters are now given. Equations 1a through 6a relate the chemical shifts to the equilibrium parameters for six possible models of complexation between the propargyl halides and benzene. Similarly, eq 1b through 3b correspond to three possible models of complexation between 1,4-dichlorobut-2-yne and benzene.

(a) Propargyl Halides



(1) P. Laszlo and D. H. Williams, *J. Amer. Chem. Soc.*, **88**, 2799 (1966).

(2) M. D. Johnston, F. P. Gasparro, and I. D. Kuntz, *ibid.*, **91**, 5715 (1969).

(3) P. Laszlo in "Progress in NMR Spectroscopy," Vol. III, J. W. Emsley, J. Feeney, and L. H. Sutcliffe, Ed., Pergamon Press, London, 1967, Chapter 6.

(4) R. G. Wilson and D. H. Williams, *Tetrahedron*, **25**, 155 (1969).

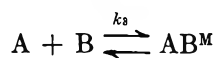
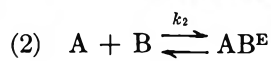
(5) J. C. D. Brand, G. Eglinton, and J. Tyrrell, *J. Chem. Soc.*, 5914 (1965).

(6) J. V. Hatton and R. E. Richards, *Trans. Faraday Soc.*, **57**, 28 (1961).

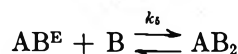
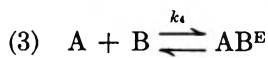
(7) R. J. Abrahams, *Mol. Phys.*, **4**, 369 (1961).

(8) I. D. Kuntz and M. D. Johnston, *J. Amer. Chem. Soc.*, **89**, 6008 (1967).

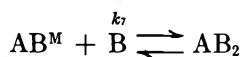
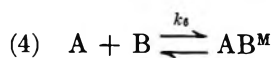
$$\delta_M - \delta_E = \frac{K_1 X_B (\delta_{AB}^M - \delta_{AB}^E)}{1 + K_1 X_B} \quad (1a)$$



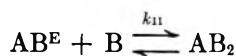
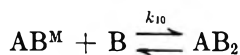
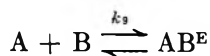
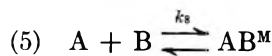
$$\delta_M - \delta_E = \frac{X_B (K_3 \delta_{AB}^M - K_2 \delta_{AB}^E)}{1 + X_B (K_2 + K_3)} \quad (2a)$$



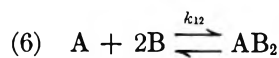
$$\delta_M - \delta_E = \frac{K_4 K_5 (\delta_{AB}^M - \delta_{AB}^E) X_B^2 - K_4 \delta_{AB}^E X_B}{1 + K_4 X_B + K_4 K_5 X_B^2} \quad (3a)$$



$$\delta_M - \delta_E = \frac{K_6 K_7 (\delta_{AB}^M - \delta_{AB}^E) X_B^2 + K_6 \delta_{AB}^M X_B}{1 + K_6 X_B + K_6 K_7 X_B^2} \quad (4a)$$



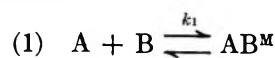
$$\delta_M - \delta_E = \frac{(K_8 \delta_{AB}^M - K_9 \delta_{AB}^E) X_B + K_8 K_{10} (\delta_{AB}^M - \delta_{AB}^E) X_B^2}{1 + (K_8 + K_9) X_B + K_8 K_{10} X_B^2} \quad (5a)$$



$$\delta_M - \delta_E = \frac{K_{12} (\delta_{AB}^M - \delta_{AB}^E) X_B^2}{1 + K_{12} X_B^2} \quad (6a)$$

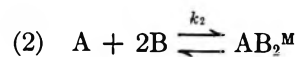
An important point which should be noted at this time is that of the six models considered it can be shown that for models 1, 2, and 6 the ratio δ_M/δ_E is a constant, being equal to $\delta_{AB}^M/\delta_{AB}^E$ for models 1 and 6 and to $K_3 \delta_{AB}^M/K_2 \delta_{AB}^E$ for model 2. This is not the case for the other three models. It should also be noted that models 1 and 2 are mathematically indistinguishable and only one of these (model 1) will be further considered. It is of course possible to postulate complex species of the form AB_3 and A_2B_2 for the propargyl halides. However, the former could only be produced by a mechanism similar to model 5, and we have already shown this model to be inappropriate. The latter species could result from a combination of the simpler complex AB with itself, but this is very unlikely because of the low concentration of the species AB .

(b) 1,4-Dichlorobut-2-yne



For the above equilibrium the following equation results.

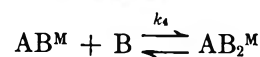
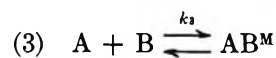
$$\delta = \frac{K_1 X_B \delta_{AB}^M}{1 + K_1 X_B} \quad (1b)$$



This gives the equation

$$\delta = \frac{K_2 X_B^2 \delta_{AB_2}^M}{1 + K_2 X_B^2} \quad (2b)$$

and finally



gives the equation

$$\delta = \frac{K_3 \delta_{AB_2}^M X_B (0.5 + K_4 X_B^2)}{1 + K_3 X_B + K_3 K_4 X_B^2} \quad (3b)$$

This equation contains the assumption that $\delta_{AB}^M = \delta_{AB_2}^M/2$, suggesting that the two methylene groups are essentially independent. This point will be referred to later in the discussion.

The equations above are derived using a method devised by Landauer and McConnell⁹ and contain the assumption that the amount of benzene in the complex is insignificant compared to the uncomplexed benzene.

Experimental Section

The acetylenes were obtained commercially and fractionally distilled before use. The benzene and cyclohexane were of spectroscopic grade and were used without further purification. The investigations were carried out at a concentration of 0.1 *M* of 1,4-dichlorobut-2-yne and of 0.19 *M* of the propargyl halides, these concentrations being low enough to eliminate possible self-association. The solvent ranged from pure cyclohexane through various mole fractions of benzene in cyclohexane. The cyclohexane was used as an internal reference.

A Varian 56/60 nmr spectrometer was used, all measurements being taken at 30° using the 60-Mc probe. Calibration was obtained from side bands of cyclohexane generated by a Hewlett-Packard Model 200CD wide range audio oscillator and measured using a Hewlett-Packard 5532A electronic counter. The side bands were chosen so as to bracket the proton resonance signal being studied. A total of ten observations, alternately running upfield and downfield, were taken for each sample.

(9) J. Landauer and H. McConnell, *J. Amer. Chem. Soc.*, **84**, 1221 (1952).

Results

The data obtained for the propargyl halides are listed in Tables I and II and the data for the 1,4-dichlorobut-2-yne are listed in Table III. For the purposes of convenience the values listed are the average of the data points obtained for each mole fraction sample studied. Also listed in these tables are the theoretical values of the chemical shifts based on the various models described earlier. It should be noted in the case of the propargyl halides that only models 1 and 6 are applied. This is because it was observed that the ratio of δ_M/δ_E was a constant both for propargyl chloride and for propargyl bromide, being 1.807 and 1.842, respectively, thus eliminating models 3, 4, and 5 from consideration.

Table I: Propargyl Chloride in Benzene-Cyclohexane (Shifts Measured Relative to Cyclohexane)^a

X_B , mole fraction	δ_M^b Hz	δ_E^b Hz	$\delta_M - \delta_E$ Hz	$\delta_M - \delta_E^c$ Hz	$\delta_M - \delta_E^{c'}$ Hz
0.0	0.0	0.0	0.0	0.0	0.0
0.1	5.7	3.1	2.6	2.5	1.2
0.2	10.5	5.8	4.7	4.6	3.8
0.3	14.6	8.2	6.4	6.4	6.5
0.4	18.1	10.1	8.0	8.0	8.5
0.5	21.2	11.9	9.3	9.3	10.0
0.6	23.8	13.4	10.4	10.6	11.0
0.7	26.1	14.4	11.7	11.6	11.8
0.8	28.0	15.4	12.6	12.6	12.3
0.9	29.6	16.0	13.6	13.4	12.7

^a The uncertainty in each of the averaged experimental values listed is less than ± 0.3 Hz. ^b $\delta_A^M = 148.7$ Hz, $\delta_A^E = 47.0$ Hz. ^c Calculated shifts using models 1 and 6, respectively.

Table II: Propargyl Bromide in Benzene-Cyclohexane (Shifts Measured Relative to Cyclohexane)^a

X_B , mole fraction	δ_M^b Hz	δ_E^b Hz	$\delta_M - \delta_E$ Hz	$\delta_M - \delta_E^c$ Hz	$\delta_M - \delta_E^{c'}$ Hz
0.0	0.0	0.0	0.0	0.0	0.0
0.1	5.9	3.1	2.8	2.6	1.2
0.2	10.7	5.9	4.8	4.8	3.9
0.3	15.0	8.2	6.8	6.7	6.7
0.4	18.6	10.3	8.3	8.3	8.9
0.5	21.7	12.0	9.7	9.8	10.5
0.6	24.4	13.4	11.0	11.1	11.6
0.7	26.7	14.6	12.1	12.2	12.4
0.8	28.7	15.4	13.3	13.3	13.0
0.9	30.4	16.0	14.4	14.2	13.4

^a The uncertainty in each of the averaged experimental values listed is less than ± 0.3 Hz. ^b $\delta_A^M = 134.3$ Hz, $\delta_A^E = 47.1$ Hz. ^c Calculated shifts using models 1 and 6, respectively.

The data were fitted to the various models using a nonlinear least-squares program developed by Marquardt and available through Share. A number of

Table III: 1,4-Dichlorobut-2-yne in Benzene-Cyclohexane (Shifts Measured Relative to Cyclohexane)^a

X_B , mole fraction	δ_M^b Hz	δ_M Hz	δ_M^b Hz	δ_M^b Hz	δ_M^c Hz
0.0	153.7 ^c	0.0	0.0	0.0	0.0
0.1	147.1	6.6	7.1	3.7	6.5
0.2	141.1	12.6	12.8	11.2	12.5
0.3	136.5	17.2	17.4	18.2	17.5
0.4	131.9	21.8	21.3	23.2	21.7
0.6	125.6	28.1	27.5	28.8	27.8
0.7	123.7	30.0	30.0	30.4	30.1
0.8	121.6	32.1	32.1	31.5	32.0
0.9	120.1	33.6	34.0	32.3	33.6

^a The uncertainty in each of the averaged experimental values listed is less than ± 0.3 Hz. ^b Calculated shifts using models 1, 2, and 3, respectively. ^c δ_A^M .

different sets of postulated parameters each converged to the same final set of parameters for each system. These final parameters and a variety of statistical terms are given for each model considered for the propargyl halides in Table IV and for 1,4-dichlorobut-2-yne in Table V.

Discussion

The interpretation of the observed proton resonance shifts as being due to complex formation is based on a theoretical study of the factors contributing to chemical shifts by Buckingham, *et al.*¹⁰ The use of the cyclohexane as inert solvent and internal reference essentially eliminates the contributions from van der Waals forces, the reaction field, and the bulk diamagnetic susceptibility. The remaining contributions result from the solvent magnetic anisotropy and complex formation. Schneider¹¹ has shown that the former, for aromatic solvents, is usually large and positive while the latter is usually negative. One can therefore attribute the upfield shift of the proton resonance signals of the methylene and ethynyl protons to complex formation in which the relatively small effect on the chemical shift due to complex formation is enhanced by the resultant magnetic anisotropic effect of the benzene. The latter effect occurs because complex formation places the protons in the appropriate part of the magnetic field of the benzene.

A detailed study of the application of least-squares techniques to a 1:1 complex system has been carried out by Wentworth, *et al.*¹² We are here applying the same techniques to systems containing one or possibly more complexes. The hope is that the application of statistical techniques will enable a clear differentiation

(10) A. D. Buckingham, T. P. Schaefer, and W. G. Schneider, *J. Chem. Phys.*, **32**, 1227 (1960).

(11) W. G. Schneider, *J. Phys. Chem.*, **66**, 2653 (1962).

(12) W. E. Wentworth, W. Hirsch, and E. Chen, *ibid.*, **71**, 218 (1967).

Table IV: The Equilibrium and Statistical Parameters for the Propargyl Halide-Benzene Systems

	Model 1	Model 6
	(a) Propargyl Chloride	
Equilibrium constants ^a	$K_1 = 0.924 \pm 0.005$	$K_{12} = 9.05 \pm 0.02$
Chemical shifts, Hz	$(\delta_{AB}^M - \delta_{AB}^E) = 29.6 \pm 0.1$	$(\delta_{AB}^M - \delta_{AB}^E) = 14.42 \pm 0.08$
Σr_i^2	13.567	486.1
Variance	0.015	0.541
	(b) Propargyl Bromide	
Equilibrium constants ^a	$K_1 = 0.869 \pm 0.005$	$K_{12} = 8.66 \pm 0.17$
Chemical shifts, Hz	$(\delta_{AB}^M - \delta_{AB}^E) = 32.4 \pm 0.1$	$(\delta_{AB}^M - \delta_{AB}^E) = 15.32 \pm 0.08$
Σr_i^2	13.713	559.2
Variance	0.015	0.623

^a Units of K_1 are (mole fraction)⁻¹ and of K_{12} are (mole fraction)⁻².

Table V: The Equilibrium and Statistical Parameters for the 1,4-Dichlorobut-2-yne-Benzene System

	Model 1	Model 2	Model 3
Equilibrium constants ^a	$K_1 = 1.23 \pm 0.03$	$K_2 = 11.40 \pm 0.53$	$K_3 = 2.56 \pm 0.04$ $K_4 = 1.55 \pm 0.10$
Chemical shifts, Hz	$\delta_{AB}^M = 64.7 \pm 1.7$	$\delta_{AB_2}^M = 35.9 \pm 2.1$	$\delta_{AB}^M = 25.1 \pm 0.4$ $\delta_{AB_2}^M = 50.2 \pm 0.8$
Σr_i^2	15.192	161.09	6.467
Variance	0.195	2.065	0.084

^a Units of K_1 , K_3 , and K_4 are (mole fraction)⁻¹ and of K_2 are (mole fraction)⁻².

of the various models with regard to the degree to which they fit the data. Two important statistical parameters used in comparing various models are the sum of the squares of the residuals, Σr_i^2 , and the variance which is expressed as

$$\text{variance} = \frac{\Sigma r_i^2}{N - M}$$

where N is the number of data points and M is the number of degrees of freedom.

If we first consider the complex formation between the propargyl halides and benzene, it can be quickly shown that models 3, 4, and 5 do not apply to our situation, since for them the ratio δ_M/δ_E is concentration dependent while it is found experimentally to be constant. Since models 1 and 2 are mathematically indistinguishable, it is impossible to determine whether there is only one 1:1 complex or two 1:1 complexes. We therefore limit our consideration to models 1 and 6. The values of the Σr_i^2 and the variance for the two models both for propargyl chloride and for propargyl bromide as indicated in Table IV would indicate that model 1 gives a much better fit to the data than does model 6. It should be noted that these results are based on a total of 900 data points for each system, since all possible combinations of $\delta_M - \delta_E$ for each mole fraction are considered. A further more rigorous comparison of the two models can be made using the "F-distribution" test. In this test the ratio of the var-

iances for any two models is compared with sets of values tabulated for the number of degrees of freedom of each model at a number of confidence limits.¹³ When this test is applied to the propargyl chloride results a value of 35.82 is obtained, indicating a statistically significant difference between the two models in fitting the data at a confidence level of at least 95% clearly favoring the 1:1 complex over the 1:2 complex. Similarly, with the propargyl bromide results a ratio of the variances of 40.79 is obtained, indicating the superiority of the 1:1 complex over the 1:2 complex at a confidence level of at least 97.5%. It would seem therefore that, for the propargyl halide-benzene systems, the data unequivocally indicate that only 1:1 complexes are present.

When the same statistical techniques are applied to the 1,4-dichlorobut-2-yne-benzene system, it can be seen from the values of Σr_i^2 and the variance listed in Table V that model 3 gives the best fit to the data followed by model 1 with model 2 a poor third. When the F-distribution test is applied we get a ratio of 10.61 for models 1 and 2, 24.58 for models 2 and 3, and 2.32 for models 1 and 3. These results indicate that both models 1 and 3 give a statistically superior fit to the data than does model 2 to the extent of at least 90% confidence for model 1 and at least 97.5% confidence

(13) "Handbook of Mathematical Functions," M. Abramowitz and I. A. Stegun, Ed., National Bureau of Standards, Washington, D. C., 1964, pp 986-989.

for model 3. The ratio for models 1 and 3, however, indicates a statistical differentiation at a confidence level considerably less than 75%. This indicates that the data do not permit a clear distinction to be made between models 1 and 3. It is therefore proposed that until data become available which would indicate a definite need for the more complex interpretation of model 3, the simpler 1:1 complex would appear to be adequate. The fact that only 1:1 complexes are present in the propargyl halide-benzene systems, which should be analogous to the 1,4-dichlorobut-2-yne-benzene system, tends to support this choice.

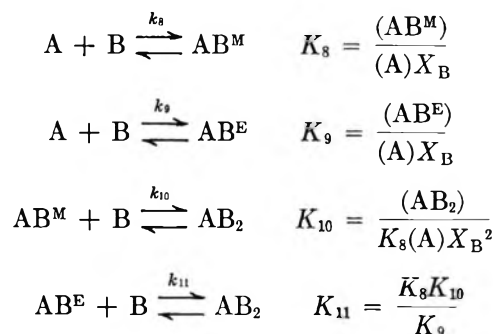
While the results for both the propargyl halides and 1,4-dichlorobut-2-yne indicate the existence of only 1:1 complexes with benzene, they do not indicate how many 1:1 complexes are present or their nature. It is not clear whether we are dealing with π - π complexes as occur between tetracyanoethylene and benzene, with complexes resulting from hydrogen bonding, or a mixture of both. Any model which is postulated for these complexes must explain a number of experimental observations. These observations include the broadening and shift to lower frequency of the acetylenic C-H stretching mode in going from cyclohexane to benzene as solvent, an observation normally associated with hydrogen bonding. Also to be explained is the very large upfield shift observed for the methylene proton signal, almost twice that observed for the acetylenic proton in the propargyl halides. The average values of $\delta_M/\delta_E = \delta_{AB^M}/\delta_{AB^E}$ are 1.807 for propargyl chloride and 1.842 for propargyl bromide. Combining these data with the respective values of $\delta_{AB^M} - \delta_{AB^E}$ in Table IV, we obtain values of δ_{AB^M} and δ_{AB^E} . For propargyl chloride we obtain $\delta_{AB^M} = 66.3$ Hz and $\delta_{AB^E} = 36.7$ Hz and for propargyl bromide $\delta_{AB^M} = 70.9$ Hz and $\delta_{AB^E} = 38.5$ Hz. The values of δ_{AB^M} obtained for the propargyl halides compare well with $\delta_{AB^M} = 64.7$ Hz in 1,4-dichlorobut-2-yne, suggesting the same degree and possibly type of association.

If the association is the result of π - π interaction between the π orbitals of benzene and the triple bond, we would expect only a single 1:1 complex in all three cases. If, with 1,4-dichlorobut-2-yne, the benzene were symmetrically placed over the triple bond, then both sets of methylene protons would lie outside that sphere of influence of the benzene which causes an upfield shift. It would be necessary to postulate a benzene placed very asymmetrically with regard to the triple bond to bring the methylene protons into the appropriate region of the benzene molecule's magnetic field. The resultant molecular complex would appear to be almost indistinguishable from one in which bonding was between the methylene protons and the benzene. Incidentally, similar upfield shifts have been observed for the methylene protons of methylene chloride in aromatic solvents² where a definite interaction between the protons and the π orbitals of the aromatic ring must occur. One

can construct a model for the propargyl halides and benzene in which the methylene protons are closer to the plane of the benzene ring and therefore more under the influence of the π system than the ethynyl proton. In this model the triple bond is above and at an angle to the plane of the benzene ring. An alternative model would involve individual 1:1 complexes involving interaction between either the methylene protons or the acetylenic proton and a benzene, this being ascribed in the latter case at least to hydrogen bonding. The assumption in model 3 for the 1,4-dichlorobut-2-yne-benzene complex that $\delta_{AB^M} = \delta_{AB_2^M}/2$ supplies indirect evidence that the methylene groups interact independently with the benzene. It was found to be impossible to carry out a least-squares analysis using model 3 without reducing the number of independent parameters to three, and this involves assuming a relationship between δ_{AB^M} and $\delta_{AB_2^M}$. The best fit of the data to the model was obtained for $\delta_{AB^M} = \delta_{AB_2^M}/2$ and this corresponds to independent methylene groups. However, while some evidence does suggest independent complexes of the benzene with the acetylenic and methylene protons, this evidence is by no means conclusive and π - π interaction cannot be ruled out.

Appendix

The derivation of eq 5a follows.



() = mol/l.; X_B = mole fraction of B. If $(A)_0$ = total concentration of A in all forms

$$\begin{aligned} (A)_0 &= (A) + (AB^M) + (AB^E) + (AB_2) \\ (A)_0 &= (A) + K_8(A)X_B + K_9(A)X_B + K_8K_{10}(A)X_B^2 \\ (A)_0\delta_M &= K_8(A)X_B\delta_{AB^M} + K_8K_{10}(A)X_B^2\delta_{AB^M} \\ (A)_0\delta_E &= K_9(A)X_B\delta_{AB^E} + K_8K_{10}(A)X_B^2\delta_{AB^E} \\ \delta_M - \delta_E &= \frac{(A)_0(\delta_M - \delta_E)}{(A)_0} = \\ &= \frac{(K_8\delta_{AB^M} - K_9\delta_{AB^E})X_B + K_8K_{10}(\delta_{AB^M} - \delta_{AB^E})X_B^2}{1 + (K_8 + K_9)X_B + K_8K_{10}X_B^2} \end{aligned}$$

also

$$\frac{\delta_M}{\delta_E} = \frac{1 + K_{10}X_B}{K_9\delta_{AB^E}} + \frac{K_{10}\delta_{AB^E}}{\delta_{AB^M}} X_B$$

A Dielectric Constant Study of Molecular Association in Polar-Polar Mixtures. *o*-Dichlorobenzene-Butyl Alcohol¹

by L. L. Combs,*

Departments of Chemistry and Physics, Mississippi State University, State College, Mississippi 39762

William H. McMahan, Jr., and Stephen H. Farish

Department of Chemistry, Mississippi State University, State College, Mississippi 39762
(Received February 25, 1971)

Publication costs assisted by Mississippi State University

The dielectric constants of mixtures of *o*-dichlorobenzene and four butyl alcohol isomers have been measured. Calculated values of the dielectric constant based on the significant-structure model demonstrate substantial deviations from the experimental values. This is apparently due to the formation of a complex between the components of the system which affects the random mixing term of the equation. Apparent molar polarization calculations further support this observation. The method of continuous variations (Job's method) is applied to the molar polarization curves for an interpretation of the stoichiometry of the complex. Equilibrium constants for the complex formation are then estimated from the molar polarization curves.

Introduction

One often requires at least a qualitative understanding of the liquid structure of some mixed solvent systems, and various experimental techniques are available for their study.^{2,3} However, it would be extremely advantageous if data available from other research techniques could be applied to a solvent system structure analysis. The presentation of such a method is the primary purpose of this communication.

The solvent system *o*-dichlorobenzene-butanol (OD-CB-BuOH) has been studied in this laboratory as a possible solvent for electrochemical research. As part of this study the dielectric constant as a function of mole fraction alcohol had been measured using all the butanol isomers. We then wished to extend this study by using the dielectric constant data in a series of calculations to obtain some knowledge of the liquid structure of the system.

Some determination of the amount of complex formation between molecules can be ascertained by studying apparent molar polarizations of alcohol isomers. This can be performed by the method outlined by Earp and Glasstone⁴ and has been useful in determining the nature of molecular interaction for other systems.⁵

The method of continuous variations⁶ has been used quite often for determining the stoichiometry factors of a complex when the concentration of the complex is known as a function of one component. We decided to investigate the application of this method when the concentration of the complex is indirectly measured. If the stoichiometry factor could thus be obtained then the equilibrium constants could be estimated from the available data.

It is always desirable to have a model available for a

structure elucidation problem. The model chosen for this study was that of Eyring and coworkers,⁷ which describes a liquid as being composed of solid-like and gas-like molecules. The model has been applied to water,⁷ pure alcohols,⁸ and mixed polar solvents⁹ with adequate success regarding dielectric constant correlation. This investigation is apparently the first application to a polar-polar mixture involving a liquid without hydrogen bonds and one with extensive hydrogen bonding.

Experimental Section

The *n*-, *i*-, and *sec*-BuOH were obtained with a reported purity of 99+ mol % (Eastman). All were further purified by fractional distillation using a 60-cm insulated column, packed with glass helices. The middle fraction coming over at the reported boiling point¹⁰ (*n*-, 108.0; *sec*-, 99.5°) was taken for use. The *tert*-BuOH was received with a reported purity of 99+ mol % (J. T. Baker). It was further purified by stirring with sodium metal in a container protected from the atmosphere, and it was then fractionally distilled.

(1) This work was supported in part by the Physical and Biological Science Institute of Mississippi State University.

(2) A. K. Chandra and A. B. Sannigrahi, *J. Phys. Chem.*, **69**, 2494 (1965).

(3) L. W. Lewis and W. G. Sneider, *Can. J. Chem.*, **35**, 251 (1957).

(4) D. P. Earp and S. Glasstone, *J. Chem. Soc.*, 1709 (1935).

(5) R. P. Rastogi and J. Nath, *Indian J. Chem.*, **5**, 249 (1967).

(6) P. Job, *C. R. Acad. Sci. Paris*, **180**, 928 (1925).

(7) M. S. Hobbs, M. S. Jhon, and H. Eyring, *Proc. Nat. Acad. Sci. U. S.*, **56**, 31 (1966).

(8) M. S. Jhon, E. R. VanArtsdalen, J. Grosh, and H. Eyring, *J. Chem. Phys.*, **47**, 2231 (1967).

(9) M. S. Jhon and H. Eyring, *J. Amer. Chem. Soc.*, **90**, 3071 (1968).

(10) J. Timmermans, "Physico-Chemical Constants of Pure Organic Compounds," Elsevier, New York, N. Y., 1950, pp 318-326.

The middle fraction boiling at $+82.5^\circ$ was taken for use.¹⁰

To establish an upper limit of purity, gas chromatograms were made of the alcohols using an Aerograph Autoprep. A column (20 ft \times $\frac{3}{8}$ in.) packed with SE 30 on firebrick was used. It was found that 0.1% water could be detected. The chromatograms of the unpurified alcohols had peaks corresponding to both water and isomers. These peaks were absent in the chromatograms of the purified alcohols.

The ODCB was obtained with a reported purity of 99+ mol % (Aldrich and Eastman). It was further purified by passage through a column (33 cm \times 2 cm) of neutral activated alumina, sealed from the atmosphere. The refractive index of the ODCB agreed very well with the literature¹⁰ after one passage through the column. All solutions were made up by mass.

Dielectric constants were determined using a dipolemeter employing the heterodyne beat method (Model DM, Kahl Scientific Corp.). Cell MFL 2 was used, with a range in dielectric constant from 7 to 21. The cell held approximately 50 ml of solution, and the measurements were made at 2 MHz. The temperature of the cell was controlled to $\pm 0.05^\circ$ by circulating water from a constant-temperature bath.

Refractive indices were measured using an Abbe refractometer (Bausch and Lomb, Model I3), thermostated to $\pm 0.05^\circ$. The refractometer was calibrated with benzene.

Densities were measured with a Springer-Ostwald pycnometer having a volume of about 12 ml. Temperature control was $\pm 0.01^\circ$. Density values were corrected to vacuum.¹¹

Some of the refractive indices and densities were interpolated from large-scale graphs (110 cm \times 52 cm) of the measured values against mole fraction of alcohol. Densities at the freezing point were found by extrapolation to the freezing point¹² and adding a 10% contraction correction for the phase change.⁷

Results and Discussion

The experimental dielectric constants and molar polarizations are presented in Figures 1, 2, and 3, respectively. A pronounced minimum is observed in the dielectric constant curve which is not a common observation in most solvent systems. Another observed anomaly is that the molar polarization for the *n*-BuOH system approaches a value higher than the pure ODCB value as $X_{alc} \rightarrow 0$.

The equation relating the dielectric constant to the dipole moment for a binary system as obtained from the significant-structure model is⁷

$$\epsilon_M = n_M^2/2 + n_M^4/(2\epsilon_M) + \frac{3}{2}(4\pi) \frac{N}{V_M} [V_M^{-1}(V_{sA}X_A + V_{sB}X_B) \times (X_A^2\mu_A^2G_A/kT + X_B^2\mu_B^2G_B/kT +$$

$$2X_AX_B\mu_A\mu_B\sqrt{G_AG_B}/(kT)) + V_M^{-1}(V_M - V_{sA}X_A - V_{sB}X_B) \times (\mu_A^2X_A/(3kT) + \mu_B^2X_B/(3kT))] \times [(n_M^2 + 2)/3]^2 \quad (1)$$

The subscripts A, B, and M refer to liquid A, liquid B, and the mixture, respectively. The molar volume of

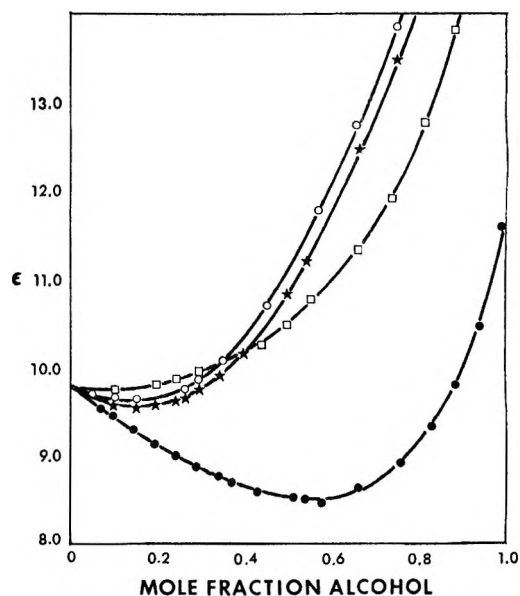


Figure 1. The variation of dielectric constants with mole fraction of alcohol for the four BuOH-ODCB systems at 30.0° : O, *n*-BuOH; \star , *i*-BuOH; \square , *sec*-BuOH; \bullet , *tert*-BuOH.

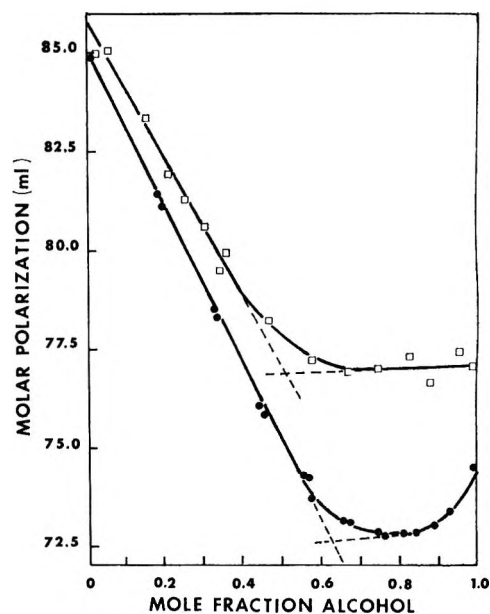


Figure 2. The variation of molar polarization with mole fraction of alcohol for two BuOH-ODCB systems at 30.0° : \square , *sec*-BuOH; \bullet , *tert*-BuOH.

(11) N. Bauer and S. Z. Lewin, *Tech. Org. Chem.*, 158 (1959).

(12) N. A. Lange, "Handbook of Chemistry," 7th ed, Handbook Publishers, Inc., Sandusky, Ohio, 1949, p 404.

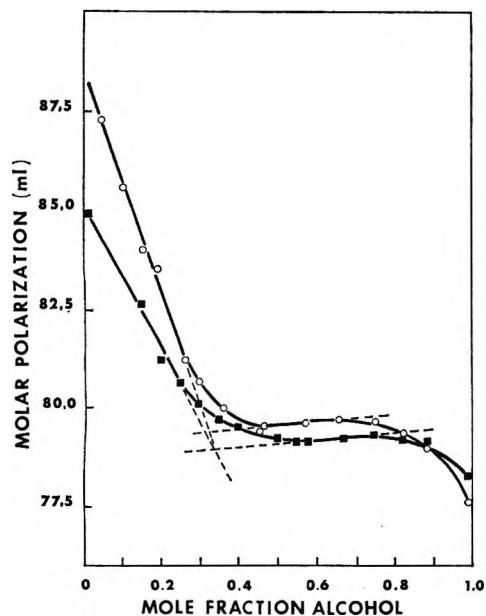


Figure 3. The variation of molar polarization with mole fraction of alcohol for two BuOH-ODCB systems at 30.0°: O, *n*-BuOH; ■, *i*-BuOH.

the mixture is V , V_s is the molar volume of the pure liquid at the freezing point, ϵ is the dielectric constant, and n is the refractive index. The G term is a structure parameter of the theory and is evaluated for each pure component from experimental values by reducing eq 1 to one component. Relevant data and subsequent G values are presented in Table I. The other symbols in

Table I: Parameters for the Evaluation of G at 30.0°

Liquid	V_s	V	ϵ^a	n	μ^b	G_{calcd}
ODCB	113.591	117.376	9.875	1.5473	2.74	0.222
<i>n</i> -BuOH	76.104	92.417	16.82	1.3953	1.69	1.245
<i>i</i> -BuOH	94.945	93.312	16.82	1.3916	1.70	1.273
<i>sec</i> -BuOH	74.363	92.777	15.77	1.3934	1.65	1.250
<i>tert</i> -BuOH	94.921	95.521	11.62	1.3855	1.66	0.794

^a W. Dannhauser and L. W. Bahe, *J. Chem. Phys.*, **40**, 3058 (1964). ^b C. P. Smyth, "Dielectric Behavior and Structure," McGraw-Hill, New York, N. Y., 1955.

eq 1 have their usual meanings.

A comparison of experimental and calculated dielectric constants using eq 1 for the ODCB-*n*-BuOH system is presented in Figure 4. The agreement is seen to be quite bad with similar comparisons observed for the other systems. Aside from the general theory, one would ascertain the major source of error to be the interaction term

$$I = 2X_A X_B \mu_A \mu_B G_A G_B / (kT) \quad (2)$$

This arises from assuming random mixing and does not allow for the possibility of formation of a complex.

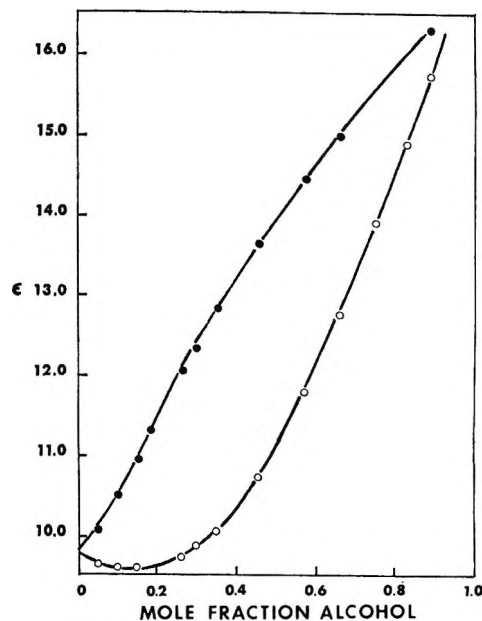


Figure 4. Comparison of experimental and calculated (from the significant structure model) dielectric constants against mole fraction of alcohol for the *n*-BuOH-ODCB system: O, experimental; ●, calculated.

Since neither assumption may be valid, we decided to simply treat this term as a variable parameter. The results for the ODCB-*n*-BuOH system are listed in Table II; they are excellent but perhaps physically

Table II: Dielectric Constants for the *n*-BuOH System at 30°

Mole fraction alcohol	ϵ_{obsd}	ϵ_{calcd}	% error	$I \times 10^{28}$
0.0500	9.6590	9.6582	0.0083	0.07049
0.1010	9.6150	9.6141	0.0094	0.12518
0.1510	9.6000	0.5994	0.0063	0.16833
0.1850	9.7950	9.7940	0.0102	0.20968
0.2620	9.7450	9.7443	0.0072	0.23523
0.2980	9.8750	9.8740	0.0101	0.25673
0.3500	10.0670	10.0663	0.0070	0.27088
0.3630	10.2820	10.2814	0.0058	0.29083
0.4550	10.7180	10.7170	0.0093	0.29883
0.4630	10.8920	10.8911	0.0083	0.31043
0.5730	11.7950	11.7943	0.0059	0.31098
0.6610	12.7560	12.7553	0.0055	0.29883
0.7520	13.8810	13.8801	0.0065	0.26853
0.2870	14.8720	14.8714	0.0040	0.22488
0.8890	15.7320	15.7314	0.0038	0.17548

meaningless. This interaction term in the Eyring equation is the subject of further investigation and will be presented in another communication. At this time, the variable treatment appears to be physically meaningful (note the maximum of I in Table II) and the derivation of another interaction term is being conducted to avoid further parameterization.

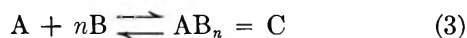
However, our immediate goal is a structure elucidation

tion rather than a model study so the apparent molar polarizations of the butyl alcohols were calculated. The results are presented in Figures 5 and 6 and clearly indicate the formation of a complex. The more pronounced the flat portion of the apparent molar polarization curves, the more stable is the complex. This would indicate that the order of stability of the complexes in terms of the alcohols is *tert*-butyl > isobutyl > *n*-butyl. The apparent molar polarizations of the *n*-BuOH system are seen to rise sharply as $X_{alc} \rightarrow 0$. This apparently reflects the instability of the complex and a resultant statistically significant amount of dipole association occurring which increases the dipole moment and thus the molar polarization. The molar polarization would then approach a higher value than that of pure ODCB as was previously noted in Figure 3.

We now consider that three separate and mutually supporting arguments have been presented to support the claim that in all of these systems a molecular complex is being formed: the minimum in the dielectric constant curves; the inadequacy of the significant-structure model due to the contact term; and the behavior of the apparent molar polarization curves. The latter phenomena are unusual in that one "normally" sees a maximum apparent polarization at zero mole fraction and then the curve approaches the pure value with no minimum. Our results appear to indicate two separate behavior patterns intersecting. At low concentrations of alcohol, self-polymerization would be inconsequential and a complex with ODCB could be formed which would have a lower dipole moment than the pure alcohol. At high concentrations of alcohol, self-polymerization becomes the dominating factor and the formation of a complex with ODCB becomes less probable with a resulting increase in the dipole moment of the system. In between these limits somewhere the maximum mole per cent of complex should be formed as is also indicated by the molar polarization curves.

We then conclude that a maximum mole per cent complex is formed between the X_{alc} extremes for all systems and that the molar polarization curves can be treated as two separate regions: one of low X_{alc} and one of high X_{alc} .

The presence of a maximum mole per cent complex is reminiscent of Job's method⁶ for determining the stoichiometry factors of a complex by spectrophotometrically determining the amount of the complex concentration. We are not directly determining the amount of the complex formation, but the amount of complex present is responsible for the shape of our polarization curves and the minimum in the curves is caused by the presence of a complex (or complexes). We can assume a single complex is formed in the complexation reaction



where A represents ODCB, B represents the butyl alcohol, and C represents the complex.

Imposing the extremum condition $d[C]/dx = 0$ then leads to the relationship

$$n = X/(1 - X) \quad (4)$$

where X is the mole fraction of B at the extremum. The presence of a sharp maximum or minimum in plots of $[C]$ vs. X indicates a single very stable complex is the preponderant species. A single species of moderate stability is usually indicated by a broadened peak of smaller magnitude. If other complexes are present in significant proportions the position of the peak is shifted so an integer is not obtained for n . The molar polarization curves indicate the formation of a moderately stable complex in the ordinary interpretation by Job's method. It has been demonstrated that the determination of the stoichiometry of a single complex by Job's method is valid even if many other types of equilibria are present¹³ as is undoubtedly true in this case. It then appears quite reasonable to assume that we can apply this technique for an interpretation of complex formation in these systems. We can interpret Figures 2 and 3 as representing two regions (high and low alcohol concentrations) as previously discussed. The intersection of the straight lines representing these separate regions can be interpreted as ideally representing the point of maximum concentration of complex. The value of X_{alc} at this point can then be used in eq 4 to determine n .

We thus obtain for the *n*-BuOH and *i*-BuOH systems an intersection at about 0.33 X_{alc} which corresponds to a 1:2 complex in ODCB. This type of complex formation has been postulated for other π -electron-proton donating systems.³ The proton is shared by the chloro groups on two ODCB molecules.¹⁴ The intersection for the *sec*-BuOH system occurs at 0.55 X_{alc} which corresponds to a 1:1 complex. This type of adduct has been postulated for many systems^{2,15} and reflects the lower acidic character of *sec*-BuOH or *i*-BuOH.² The intersection for the *tert*-BuOH system occurs at about 0.66 X_{alc} which would correspond to an adduct of 2:1 stoichiometry in *tert*-BuOH. This reflects the further reduction of acidic character by branching of the alkyl chain.² The high X_{alc} region is not well defined for the *tert*-BuOH system and can be attributed to a more stable complex as indicated by the apparent molar polarization curves. This stable complex would also explain the larger deviation from the normal illustrated by the dielectric constants of this system.

Since the stoichiometry factor has been determined we may now estimate the equilibrium constants. Again we assume the establishment of only one equilibrium, *i.e.*, eq 3. The mole fraction of free ODCB at

(13) M. M. Jones, *J. Amer. Chem. Soc.*, **81**, 4485 (1959).

(14) D. Cleveron, G. B. Collins, and J. W. Smith, *J. Chem. Soc.*, 4499 (1956).

(15) K. Szczepaniak and A. Tramer, *J. Phys. Chem.*, **71**, 3034 (1967).

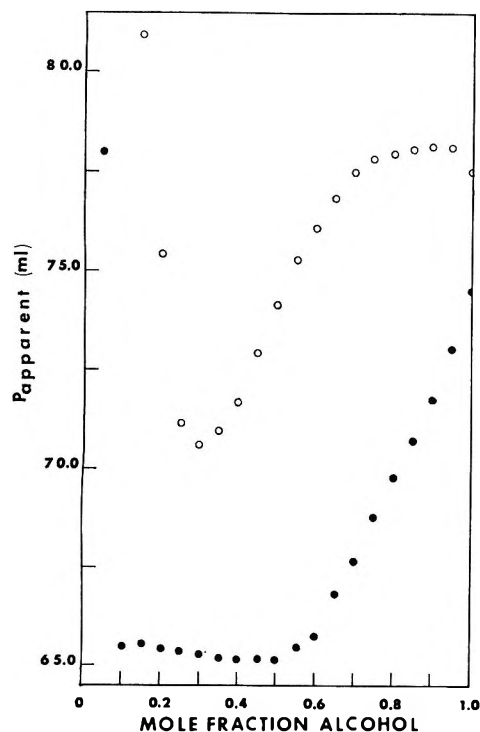


Figure 5. The variation of apparent molar polarizations with mole fraction of alcohol for two BuOH-ODCB systems at 30°: ○, *n*-BuOH; ●, *tert*-BuOH.

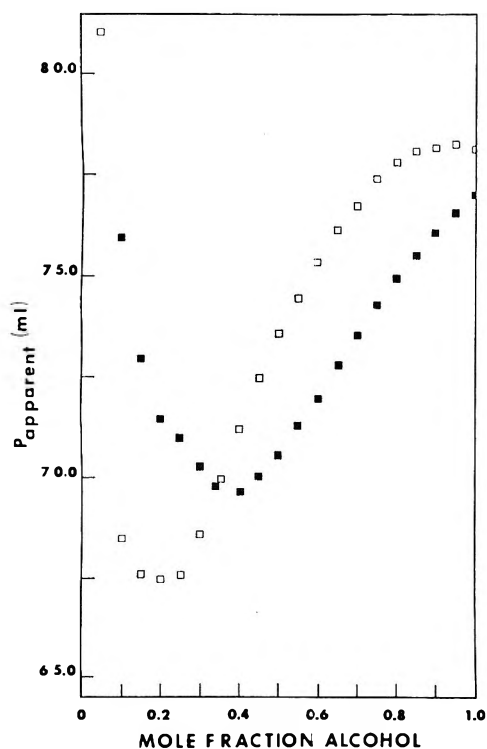


Figure 6. The variation of apparent molar polarizations with mole fraction of alcohol for two BuOH-ODCB systems at 30.0°: ■, *i*-BuOH; □, *sec*-BuOH.

any time is then given by the expression

$$X_{\text{ODCB}} = X_{\text{ODCB}}^T - X_C \quad (5)$$

and for free butyl alcohol we obtain

$$X_{\text{alc}} = X_{\text{alc}}^T - nX_C \quad (6)$$

The superscript T designates total mole fraction. We may now substitute these expressions into the equation for molar polarization

$$P = X_{\text{ODCB}}P_{\text{ODCB}} + X_{\text{alc}}P_{\text{alc}} + X_C P_C \quad (7)$$

to obtain

$$X_C = \frac{(P - X_{\text{ODCB}}^T P_{\text{ODCB}} - X_{\text{alc}}^T P_{\text{alc}})}{(P_C - P_{\text{ODCB}} - nP_{\text{alc}})} \quad (8)$$

If we can thus obtain X_C then the equilibrium constant may be determined from

$$K = X_C / (X_{\text{ODCB}} X_{\text{alc}}^n) \quad (9)$$

Since the straight line intersections were used to obtain the stoichiometry factors we will use the value of P at this juncture in eq 8. The use of factors obtained at the region of maximum concentration of complex should minimize errors introduced by assuming the formation of only one complex. The only remaining unknown is P_C . In the region of high alcohol concentration we can make the following assumptions. (a) All ODCB is involved in complex formation so $X_{\text{ODCB}} \sim 0$ and $X_C \sim X_{\text{ODCB}}^T$. (b) The amount of alcohol involved in complex formation is negligible compared to the total amount of alcohol so $X_{\text{alc}} \sim X_{\text{alc}}^T$. Employing these assumptions, eq 7 becomes

$$P = P_C + (P_{\text{alc}} - P_C) X_{\text{alc}}^T \quad (10)$$

The intersection of this straight line will then determine P_C so we can now calculate X_C using eq 8 and then calculate K from eq 9. The results of these calculations are presented in Table III.

Table III: Equilibrium Constants for Complex Formation with ODCB

Alcohol	P_{complex}	X_{complex}	K
<i>n</i> -Butyl	79.0	0.019	0.15
Isobutyl	78.6	0.021	0.17
<i>sec</i> -Butyl	76.7	0.052	0.26
<i>tert</i> -Butyl	72.0	0.154	0.59

A number of reasonable assumptions have been made so the absolute values of the equilibrium constants may be unimportant. However, the trend should be valid especially since all of our treatments are self-supporting in this respect. The equilibrium constants follow the same trend among the isomers as well as the same order-of-magnitude differences that have been observed in other systems by Chandra and Sannigrahi.² The trend evidenced in Table III corresponds to the alcohols behaving as proton acceptors in the work of Chandra and Sannigrahi. Since no such protons are available in our system, we make a logic transfer to the Lewis acid-base concept and say that the trend represents the

ability of the alcohols to donate electrons. If we accept the arguments of Chandra and Sannigrahi then we could say that the complex formation is primarily due to

electron sharing with the order of electron donating power of the alcohols being tertiary > secondary > primary.

Biionic Potentials of a Liquid-Membrane Electrode Selective toward Calcium

by J. Bagg, O. Nicholson, and R. Vinen

Department of Industrial Science, University of Melbourne, Parkville, Victoria 3052, Australia
(Received September 21, 1970)

Publication costs borne completely by The Journal of Physical Chemistry

The biionic potentials of a liquid-membrane electrode (calcium salt of didecylphosphoric acid) immersed in mixed solutions of $\text{CaCl}_2\text{-MX}$ where MX are the chlorides or nitrates of Li, Na, K, Rb, Cs, or ammonium have been measured at total ionic strengths from 0.03 to 3.0 and mole ratios MX:CaCl₂ from 0.5 to 100. The interference potential, defined as the difference between the observed biionic potential and the potential calculated assuming no interference, was found to fit the following equation: $E_M = -RT/F \ln \{1 + K_{MAM^+}/(a_{\text{Ca}^{2+}})^{1/2}\}$. Within the range of total ionic strength 0.03–0.3, the selectivity parameters were $K_{\text{Li}} = 0.33$, K_{Na} , K_{K} , K_{Rb} , $K_{\text{Cs}} \leq 0.006$ and, within the mole ratio limits 0.5–5.0, $K_{\text{NH}_4} \leq 0.006$. A simple theoretical treatment which accounts for the form of the above equation predicts that K_M should be governed primarily by the equilibrium at the membrane–solution boundary. Equilibrium data for the partition of alkali metal ions between an aqueous phase and an organic phase containing a dialkylphosphoric acid confirmed this prediction.

Introduction

The interference potentials of liquid-membrane electrodes selective toward calcium ions immersed in mixed solutions containing both Ca and Na, K, or H ions have been measured by Ross^{1,2} and were found to obey the following empirical equation

$$E_M = \frac{RT}{2F} \ln \{1 + S_M(a_{M^+})^2/a_{\text{Ca}^{2+}}\} \quad (1)$$

with selectivity parameters, $S_{\text{Na}} = 0.0016$ and $S_{\text{H}} = 10^7$.²

Fleet and Rechnitz made similar measurements in a flow system and reported the following dynamic parameters: $S_{\text{Li}} = 0.156$, $S_{\text{Na}} = 0.01$, and $S_{\text{K}} = 0.006$.³

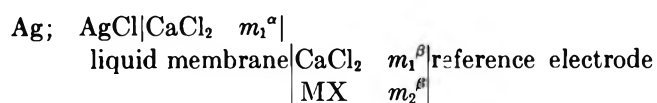
Selectivity parameters appear to be constant only over a limited range of ionic strengths; for example, S_{Na} is greatly increased in a solution of 6 *m* compared with solutions of 0.1 *m* or less, and at the high molality varies with solution composition.⁴ Theoretical treatments of multiionic potentials which can account for the form of eq 1 have been carried out both for solid^{5,6} and liquid-membrane electrodes⁷ in 1:1 electrolytes but only for solid-membrane electrodes in 2:1 electrolytes.⁸

In this paper further measurements of interference potentials in a very wide range of solutions are reported and these results are used to elucidate some of the fac-

tors governing selectivity and to provide operating limits for analytical applications.

Experimental Section

The following solution chain was used



where m_1^α is the molal concentration of CaCl₂ in the interior compartment and m_1^β and m_2^β are the molal concentrations of CaCl₂ and MX, respectively, in the exterior solution. The liquid-membrane electrode was an Orion Research Inc., Type 92-20 [0.1 *m* calcium salt of didecylphosphoric acid (DDP) in dioctylphenylphosphonate]. The exterior reference electrode was a Beckman Ag–AgCl or an E.I.L., Type RJ-23 (satd. KCl, Hg₂Cl₂; Hg). The Ag–AgCl reference was chosen

- (1) J. W. Ross, *Science*, **156**, 3780 (1967).
- (2) J. W. Ross, *Nat. Bur. Stand. (U. S.), Spec. Publ.*, **314**, 57 (1969).
- (3) B. Fleet and G. Rechnitz, *Anal. Chem.*, **42**, 690 (1970).
- (4) R. Huston and J. N. Butler, *ibid.*, **41**, 200 (1969).
- (5) F. Helfferich, "Ion Exchange," McGraw-Hill, New York, N. Y., 1963, p 339.
- (6) R. Schlögl, *Z. Phys. Chem. (Frankfurt am Main)*, **1**, 305 (1954).
- (7) J. Sandblom, G. Eisenmann, and J. L. Walker, Jr., *J. Phys. Chem.*, **71**, 3862 (1967).
- (8) J. Bagg and H. P. Gregor, *J. Amer. Chem. Soc.*, **86**, 3626 (1964).

in order to determine selectivity parameters without making extrathermodynamic assumptions and the calomel because of its widespread analytical applications. A comparison of data from both reference electrodes was made to test some assumptions about single-ion activity coefficients and liquid-junction potentials.

All solutions were prepared from distilled water and analytical grade chemicals. The mole ratio $MX/CaCl_2$ was varied from 0.5 to 100 and the total ionic strength, μ_T , from 0.03 to 3.0. MX were the chlorides of Li, Na, K, Rb, Cs, and NH_4 except at $\mu_T = 3.0$ when the nitrates of Li, Na, K, or NH_4 were used. The electrodes and solution were contained in a glass cell, electrically shielded and maintained at $25 \pm 0.1^\circ$; the electrodes were immersed to a depth of 1.5 cm. The emf of the cell was measured with a Keithly 610C electrometer and a recorder.

The resistance of the membrane electrode immediately after filling the interior compartment and then immersing in the exterior solution was greater than 10^{10} ohms. After standing for approximately 1 hr the resistance fell to $\sim 10^7$ ohms and remained at this level for the working life of the electrode. This decrease of resistance seems to be associated with the entry of water into the organic phase. Ir spectra taken of the liquid-ion exchanger before and after contact with 0.1 *m* $CaCl_2$ showed an additional absorption in the region 3200–3600 cm^{-1} attributable to water. The liquid-ion exchanger was held on a thin porous membrane, 0.1 mm thickness, and no obvious visible change was observed after contact with 0.1 *m* $CaCl_2$. Upon contact of a few milliliters of the ion exchanger with 0.1 *m* $CaCl_2$, however, a milky layer was clearly visible at the interface. A possible explanation for this effect is the formation of a second phase upon the entry of water into the ion exchanger in the same manner as reported for some other organophosphorous exchangers.⁹

After the initial conditioning period stable values of emf were attained within 1–2 min upon immersion in fresh solutions and were then reproducible to within ± 1 mV over a period of several weeks. Response was rapid even upon changing from solutions containing the most strongly interfering ion, Li, back to pure $CaCl_2$. For example, in the sequence calibration in 0.1 *m* $CaCl_2$, immersion in a solution $\mu_T = 0.6$, $LiCl/CaCl_2 = 100$, reimmersion in 0.1 *m* $CaCl_2$, stable emf values were reached within 1–2 min after each change and the final emf was equal to the original calibration.

Results

The emf of the cell with calomel reference, E_{cal} , was measured with solutions in which the mole ratio R varied but μ_T was maintained constant. The emf, E_{ref} , was then measured with pure $CaCl_2$ at the same value of μ_T . The difference in emf given by

$$E_R = E_{cal} - E_{ref}$$

may be compared with E_{ideal} which was calculated assuming no interference and that the single-ion activity coefficient, $\gamma_{Ca^{2+}}$, depended only upon μ_T but not upon composition.

$$E_{ideal} = \frac{RT}{2F} \ln \left\{ \frac{\mu_T}{3m_1^\beta} \right\}$$

In the absence of any interference E_R and E_{ideal} may still differ because of residual liquid-junction potential differences. The liquid-junction potential measurements made by Bates and Alfenaar¹⁰ in $CaCl_2$, $NaCl$, and $NaCl-KCl$ solutions showed that the junction potential depended primarily upon ionic strength and not upon composition. The residual junction potential is likely to be small, probably less than 1 mV. The interference potential, E_M , is finally given by

$$E_M = E_R - E_{ideal}$$

and may be attributed almost entirely to the effect of alkali metal ions.

The emf of the cell with $Ag/AgCl$ reference, assuming no interference, is

$$E_{rev} = \frac{RT}{2F} \ln \left\{ \frac{4(m_1^\alpha \gamma_{13}^\alpha)^3}{m_1^\beta (2m_1^\beta + m_2^\beta)^2 (\gamma_{13}^\beta)^3} \right\}$$

where γ_{13}^α and γ_{13}^β are the mean molal activity coefficients of $CaCl_2$ assumed to be only dependent upon μ_T . Isopiestic measurements of γ_{13}^β in $CaCl_2-NaCl$ or $CaCl_2-KCl$ solutions are the basis for this assumption.^{11,12} For MnO_3-CaCl_2 solutions, $m_2^\beta = 0$, and γ_{13}^β was set equal to the mean molal activity coefficient of $CaCl_2$ in a $CaCl_2-Ca(NO_3)_2$ solution with the same ratio $Cl-NO_3$ and μ_T as the test solution. E_M is given by

$$E_M = E_{Ag/AgCl} - E_{rev}$$

The values of E_{Li} at $\mu_T = 0.3$ obtained with either $Ag-AgCl$ or calomel showed good agreement with a maximum difference of only 2 mV. The assumptions made above concerning single-ion activities and liquid-junction potentials appear, therefore, to be reasonable and this method of calibration for calomel electrodes is to be recommended for analytical practice.¹⁰ Even at $R = 100$ and $\mu_T = 0.3$ no significant interference was observed in solutions containing Na, K, Rb, or Cs ions. At $\mu_T = 0.6$ interference by Na at all $R > 5$ and by K at $R = 100$ was significant but interference by Rb or Cs was still not significant. Strong interference was observed with Li over the range 0.03–3.0 in ionic strength.

(9) A. S. Kertter, "Solvent Extraction Chemistry of Metals," Proceedings from the International Conference sponsored by the United Kingdom Atomic Energy Authority, 1965, p 377.

(10) R. G. Bates and M. Alfenaar, *Nat. Bur. Stand. (U. S.), Spec. Publ.*, **314**, 191 (1969).

(11) R. A. Robinson and V. E. Bower, *J. Res. Nat. Bur. Stand., Sect. A*, **70**, 313 (1966).

(12) R. A. Robinson and A. K. Covington, *ibid.*, **72**, 239 (1968).

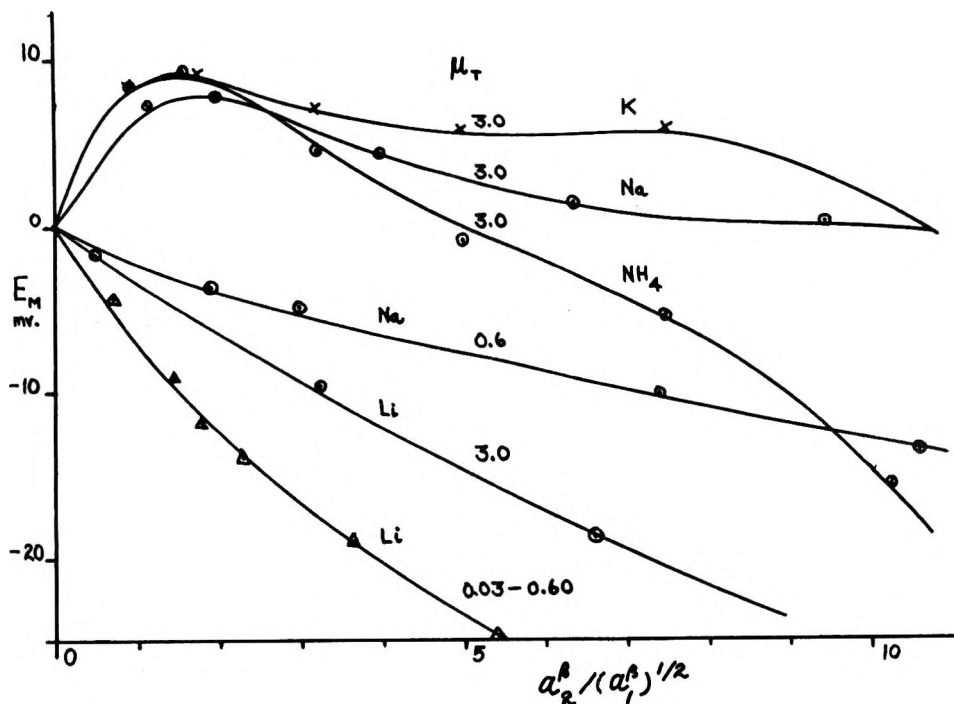


Figure 1. Interference potential, mV, vs. $a_2^\beta / (a_1^\beta)^{1/2}$ for mixed CaCl_2 -MX solutions. At $\mu_T = 3.0$, MX were LiNO_3 , NaNO_3 , KNO_3 , and NH_4NO_3 . At $\mu_T = 0.6$ -0.03, MX were LiCl and NaCl .

Interpretation of the results with ammonium salts is complicated by appreciable H ion concentration at large values of R . No significant interference was found for $\mu_T \leq 0.3$, $R \leq 5$; interference at larger values of R is almost certainly due to H-ion interference (Ross gives $S_H = 10^7$ compared with $S_{\text{Na}} = 0.0016^2$). The results are summarized in Figure 1, which shows the interference potential vs. $a_2^\beta / (a_1^\beta)^{1/2}$ for a number of mixed solutions and ionic strengths.

E_{Li} is independent of ionic strength for Li in the range 0.03-0.6 but is lower for any given $a_2^\beta / (a_1^\beta)^{1/2}$ at $\mu_T = 3.0$. A very marked difference in behavior was observed for solutions containing Na, K, or NH_4 ions at $\mu_T = 3.0$; the interference potential was of the opposite sign to that observed at lower ionic strengths.

Discussion

The results of Figure 1 could not be fitted satisfactorily to eq 1 but selectivity parameters for Li, $\mu_T = 0.03$ -0.6, and Na, $\mu_T = 0.6$ could be obtained by fitting to the equation

$$E_M = -\frac{RT}{F} \ln \{1 + K_M a_2^\beta / (a_1^\beta)^{1/2}\} \quad (2)$$

In Figures 2 and 3 the graphs of $\exp(-E_M F/RT)$ vs. $a_2^\beta / (a_1^\beta)^{1/2}$ are shown and for both Li and Na straight lines passing through (0,1) were obtained. K_K was estimated from the potential of the solution $\mu_T = 0.6$, $R = 100$. Upper limits to K_{Na} , K_K , and K_{NH_4} in the range $\mu_T = 0.03$ -0.3 and K_{Rb} , K_{Cs} in the range $\mu_T =$

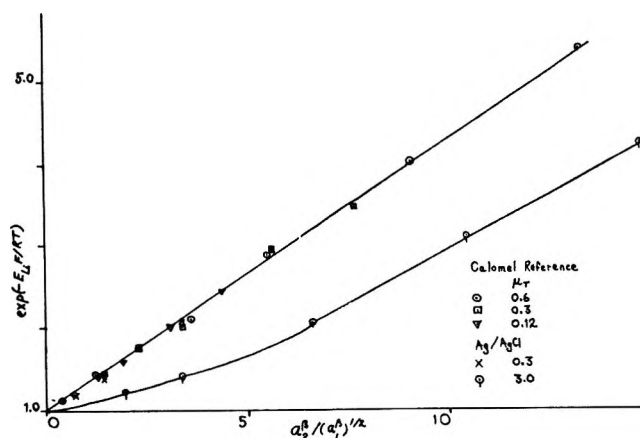


Figure 2. $\exp(-E_{\text{Li}} F/RT)$ vs. $a_2^\beta / (a_1^\beta)^{1/2}$ for CaCl_2 -LiX solutions.

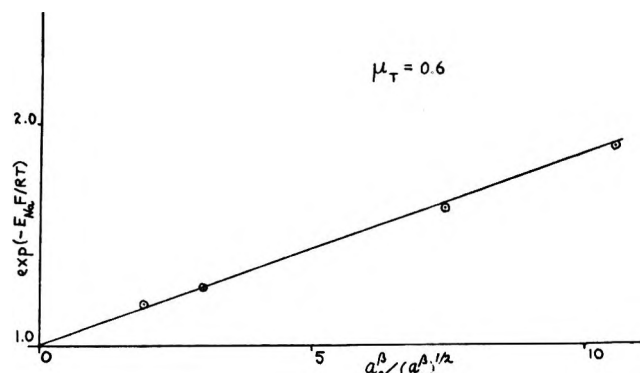


Figure 3. $\exp(-E_{\text{Na}} F/RT)$ vs. $a_2^\beta / (a_1^\beta)^{1/2}$ for CaCl_2 -NaCl solutions.

0.03–0.6 were made by setting the uncertainty in the potential measurement (95% confidence limits ± 1.5 mV) equal to the interference potential and substituting into eq 2 with the maximum of R . All these values are summarized in Table I. The very marked interference

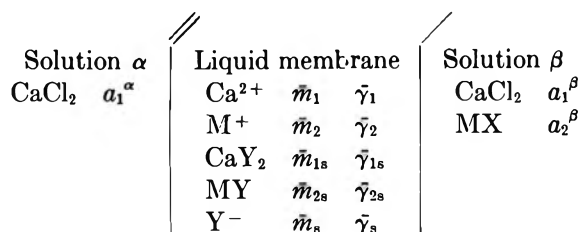
Table I: Selectivity Parameters K_M (95% Confidence Limits Shown)

	$\mu_T =$ 0.03–0.30	$\mu_T =$ 0.6
Li	0.33 ± 0.03	0.33 ± 0.03
Na	≤ 0.006	0.07 ± 0.01
K	≤ 0.006	0.02 ± 0.01
Rb	≤ 0.006	≤ 0.006
Cs	≤ 0.006	≤ 0.006
NH ₄ ($R = 5$)	≤ 0.006	

by Li compared with the other alkali metal ions is very apparent. The selectivity parameters of Na and K are ionic-strength dependent and, at $\mu_T = 0.6$, $K_{Na} > K_K$ confirming the previous qualitative finding of this difference.¹³ The overall sequence of alkali metals in order of decreasing interference is, therefore, $Li > Na > K > Rb, Cs$.

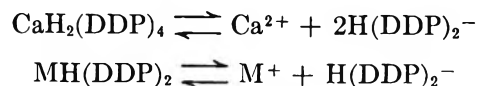
An upper limit for S_{Na} was found by substituting into eq 1 for $\mu_T = 0.3$ in the manner described above. This substitution yielded $S_{Na} \leq 0.0012$ in reasonable agreement with Ross's value of 0.0016.² The order of selectivity of Li, Na, and K agrees with that found in the dynamic experiments³ but the magnitude of the selectivity parameters differs.

An analytical expression for the multiionic potential of a liquid membrane immersed in a mixed solution containing monovalent cations has been derived from theoretical considerations by Sandblom, Eisenman, and Walker.⁷ A similar derivation for mixed solutions containing both mono- and divalent ions does not seem possible without employing numerical methods. The necessary data for such an attempt, dissociation constants and mobilities, are not available at present. Because of these difficulties only a very approximate treatment, based upon the model of Sandblom, Eisenman, and Walker, is carried out in this paper. Although not rigorous, this treatment does lead to some reasonable conclusions about the properties of this electrode. The cell may be shown diagrammatically as follows



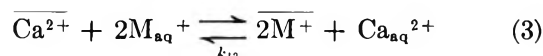
where \bar{m} and $\bar{\gamma}$ with the appropriate subscripts refer to the molal concentrations and activity coefficients of the various species within the membrane.

There is good evidence that dialkylphosphoric acids exist as dimers in organic solvents^{14,15} and that before complete neutralization by alkali or alkaline earth hydroxide the equilibria in the organic phase should be written



In the case of sodium even higher complexes with bis(2-ethylhexyl)orthophosphoric acid have been proposed.¹⁶ The liquid membrane was prepared from completely neutralized HDDP and only came into contact with solutions in which the $(Ca + M)/H$ ratio was very high so that the formation of the complexes shown above should not be appreciable.

The presence of water in the membrane implies that the cations carry some of their hydration shell into the organic phase.¹⁶ There is also a strong possibility that the dialkylphosphate is complexed with the solvent, dioctylphenylphosphonate (DOP). Baes has observed a synergistic effect in the extraction of cations by neutral organophosphates and dialkylphosphoric acids which was attributed to such complex formation.¹⁷ The phosphonates are more basic than the phosphates and should form complexes more readily.¹⁸ The formation of complexes and the degree of hydration may influence the equilibrium constant but will not be expected to alter the simple stoichiometry of the exchange. The equilibrium of exchange at the membrane-solution interface will, therefore, be written simply as



The membrane is assumed immiscible with water with only cations (probably hydrated) crossing the membrane-solution interface.

The fluxes of CaY₂, MY, and Y⁻ at any point inside the membrane are given, respectively, by

$$J_{1s} = -\bar{u}_{1s} \left(RT \frac{d\bar{m}_{1s}}{dx} + RT \bar{m}_{1s} \frac{d \ln \bar{\gamma}_{1s}}{dx} \right) \quad (4)$$

$$J_{2s} = -\bar{u}_{2s} \left(RT \frac{d\bar{m}_{2s}}{dx} + RT \bar{m}_{2s} \frac{d \ln \bar{\gamma}_{2s}}{dx} \right) \quad (5)$$

$$J_s = -\bar{u}_s \left(RT \frac{d\bar{m}_s}{dx} + RT \bar{m}_s \frac{d \ln \bar{\gamma}_s}{dx} - \bar{m}_s F \frac{d\psi}{dx} \right) \quad (6)$$

(13) "Instruction Manual," Calcium Electrode, Model 92-20, Orion Research, Inc., 1966, p 10.

(14) K. Kimura, *Bull. Chem. Soc. Jap.*, **34**, 63 (1961).

(15) Z. Kolarik, J. Hejna, and H. Pankova, *J. Inorg. Nucl. Chem.*, **30**, 253 (1968).

(16) W. J. McDowell and C. F. Coleman, *ibid.*, **27**, 1117 (1965).

(17) C. F. Baes, Jr., *ibid.*, **24**, 707 (1962).

(18) F. Krasovec and C. Klafutor, *ibid.*, **30**, 1640 (1968).

where \bar{u}_{1s} , \bar{u}_{2s} , and \bar{u}_s are the mobilities of the respective species and ψ is the potential. The variation of $\bar{\gamma}$ with compositional gradient is unknown and terms containing $d \ln \bar{\gamma}/dx$ are neglected. In the steady state

$$2J_{1s} + J_{2s} + J_s = 0 \quad (7)$$

Combining eq 4-7 and integrating between the two membrane boundaries leads to the following expression for the diffusion potential.

$$\Delta\psi = \frac{RT}{F} \ln \left[\frac{\bar{m}_s'''}{\bar{m}_s'} \right] + \frac{RT}{F} \int' \frac{2\bar{u}_{1s}d\bar{m}_{1s} + \bar{u}_{2s}d\bar{m}_{2s}}{\bar{u}_s\bar{m}_s} \quad (8)$$

The total membrane potential, V_T , is the sum of the diffusion potential and the phase boundary potentials

$$V_T = \frac{RT}{2F} \ln \left[\frac{a_1^\alpha}{a_1^\beta} \right] + \frac{RT}{2F} \ln \left[\frac{\bar{m}_1'\bar{\gamma}_1'}{\bar{m}_1''\bar{\gamma}_1''} \right] + \frac{RT}{F} \ln \left[\frac{\bar{m}_s'''}{\bar{m}_s'} \right] + \frac{RT}{F} \int' \frac{2\bar{u}_{1s}d\bar{m}_{1s} + \bar{u}_{2s}d\bar{m}_{2s}}{\bar{u}_s\bar{m}_s} \quad (9)$$

The interference potential is given by

$$E_M = V_T - \frac{RT}{2F} \ln \left[\frac{a_1^\alpha}{a_1^\beta} \right] \quad (10)$$

In the steady state, electroneutrality is a good approximation¹⁹

$$\bar{m}_s' = 2\bar{m}_1' + \bar{m}_2'; \quad \bar{m}_s''' = 2\bar{m}_1''' \quad (11)$$

By combining eq 9-11 and rearranging, an expression for E_M can be obtained.

$$E_M = -\frac{RT}{F} \ln \left\{ \left[\frac{\bar{m}_1'\bar{\gamma}_1'''}{\bar{m}_1''\bar{\gamma}_1'} \right]^{1/2} + \frac{\bar{m}_2'}{2(\bar{m}_1')^{1/2}} \left[\frac{\bar{\gamma}_1'''}{\bar{m}_1''\bar{\gamma}_1'} \right]^{1/2} \right\} + \frac{RT}{F} \int' \frac{2\bar{u}_{1s}d\bar{m}_{1s} + \bar{u}_{2s}d\bar{m}_{2s}}{\bar{u}_s\bar{m}_s} \quad (12)$$

Equation 12 may be further simplified by considering the equilibrium constant at the exterior membrane-solution interface, shown in eq 3.

$$\frac{a_2^\beta(\bar{m}_1'\bar{\gamma}_1')^{1/2}}{(a_1^\beta)^{1/2}(\bar{m}_2'\bar{\gamma}_2')} = K_{12}^{-1/2} \quad (13)$$

Substituting from (13) into (12) leads to

$$E_M = -\frac{RT}{F} \ln \left\{ \left[\frac{\bar{m}_1'\bar{\gamma}_1'''}{\bar{m}_1''\bar{\gamma}_1'} \right]^{1/2} + \left[\frac{K_{12}\bar{\gamma}_1'''}{\bar{m}_1''(\bar{\gamma}_2')^2} \right]^{1/2} \frac{a_2^\beta}{2(a_1^\beta)^{1/2}} \right\} + \frac{RT}{F} \int' \frac{2\bar{u}_{1s}d\bar{m}_{1s} + \bar{u}_{2s}d\bar{m}_{2s}}{\bar{u}_s\bar{m}_s} \quad (14)$$

The total concentration, \bar{m}_Y , of species containing DDP at any point within the membrane is given by

$$\bar{m}_Y = 2\bar{m}_{1s} + \bar{m}_{2s} + \bar{m}_s$$

and as the total number of these species within the membrane is constant

$$1/d \int' \bar{m}_Y dx = \text{constant} = C$$

where d is the membrane thickness. At the low current densities used in this work ($\sim 10^{-6}$ A/cm²) the concentration gradient of \bar{m}_Y has been shown to be very small²⁰ so that $\bar{m}_Y \approx C$ throughout the membrane.

The dielectric constant of organophosphorous compounds is usually low; for example, $D = 7.8$ for tributylphosphate.²¹ The presence of small amounts of water in the membrane will increase the dielectric constant but it is reasonable to assume that the degree of dissociation of the DDP salts will still be very small, *i.e.*, $\bar{m}_s \ll 2\bar{m}_{1s} + \bar{m}_{2s}$. The size and shape of CaY₂ and MY will be governed primarily by the bulky didecyl phosphate groups and be almost independent of the cation so the assumption is made that the mobilities of the species are almost equal. The consequence of these assumptions is

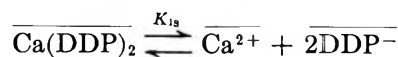
$$2\bar{u}_{1s}d\bar{m}_{1s} + \bar{u}_{2s}d\bar{m}_{2s} \approx 0 \quad (15)$$

From the known strong selectivity of Ca over alkali metal ions in extraction studies with dialkylphosphoric acids²² and the rapid response of the electrode upon changing solutions it appears that, with the exception of lithium, the concentration of alkali metal in the membrane is very low, *i.e.*, $\bar{m}_{2s} \ll \bar{m}_{1s}$, and for this reason the approximation

$$\left[\frac{\bar{m}_1'\bar{\gamma}_1'''}{\bar{m}_1''\bar{\gamma}_1'} \right]^{1/2} \approx 1 \quad (16)$$

is made. An estimation (to be published later) of the calcium concentration in the membrane after immersion in mixed calcium-lithium chloride solutions showed that, up to $R = 20$ and $\mu_T = 0.3$, the ratio $\bar{m}_{1s}'/\bar{m}_{1s}'' \geq 0.8$. From the similarity in their inorganic phosphates it might be concluded that the degrees of dissociation of the organophosphates of calcium and lithium are similar, so that the approximation shown in eq 16 is also likely to apply to Ca-Li solutions in the range mentioned above. At greater values of R and μ_T the approximation will break down.

From consideration of dissociation within the membrane



it follows that

$$\bar{m}_1''' \approx (K_{1s}C/8)^{1/3} \quad (17)$$

(19) H. J. Hickman, *Chem. Eng. Sci.*, **25**, 381 (1970).

(20) J. Sandblom, G. Eisenman, and J. L. Walker, Jr., *J. Phys. Chem.*, **71**, 3871 (1967).

(21) J. H. Miles, *J. Inorg. Nucl. Chem.*, **26**, 2308 (1964).

(22) K. Kimura, *Bull. Chem. Soc. Jap.*, **33**, 1038 (1960).

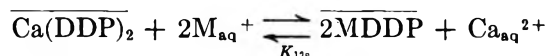
and substitution of eq 15-17 into eq 14 gives an approximation for E_M

$$E_M = -\frac{RT}{F} \ln \left\{ 1 + \frac{K_M a_2^\beta}{(a_1^\beta)^{1/2}} \right\}$$

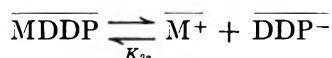
with

$$K_M = \left[\frac{K_{12} \bar{\gamma}_1''}{2(\bar{\gamma}_2')^2 (K_{1s} C)^{1/3}} \right]^{1/2}$$

This treatment thus leads to an equation of the same form as the observed eq 2. Data are not available for K_{12} and it is more convenient to express K_M in terms of the equilibrium constant for the undissociated species rather than the ionic equilibrium shown in eq 3



and, in conjunction with the dissociation of MDDP within the membrane



leads to an alternative expression for K_M

$$\bar{K}_M = \left[\frac{K_{12s} K_{2s}^2 \bar{\gamma}_1''}{2K_{1s}^{1/3} (\bar{\gamma}_2')^2 C^{1/3}} \right]^{1/2}$$

Equilibrium data are not available for didecylphosphoric acid but equilibrium parameters, K_p , are available for alkali metals and bis(2-ethylhexyl)phosphoric acid (HDEHP). The equilibrium parameter is given by

$$K_p = \frac{a_1(\bar{m}_2 + \bar{m}_{2s})^2}{a_2^2(\bar{m}_1 + \bar{m}_{1s})}$$

Because the degree of dissociation in the membrane phase is very small, K_p may be taken as a reasonable approximation to K_{12s} . In extraction studies of alkali metal ions from aqueous solution by HDEHP dis-

solved in organic solvents^{22,23} the order of equilibrium parameters was $\text{Li} > \text{Na} > \text{K} > \text{Rb} > \text{Cs}$, in good agreement with the order of selectivity parameters, K_M . This result implies that the variation between the dissociation constants of the alkali organophosphates in the organic phase is small compared with the variation between the values of K_{12s} . At high ionic strengths the selectivity parameters become dependent upon ionic strength and composition. This effect is least for Li, K_{Li} being independent of ionic strength and composition for $\mu_T \leq 0.6$. The results at $\mu_T = 3.0$ (lower graph in Figure 2) show an apparent decrease in K_{Li} from 0.33 to 0.1 for $a_2^\beta / (a_1^\beta)^{1/2} \leq 5$ and to 0.28 for 5-15. One reason for the deviation may be that the assumption of constant activity coefficients in mixed solutions necessary to calculate $a_2^\beta / (a_1^\beta)^{1/2}$ will almost certainly break down at high ionic strengths. Furthermore, substantial amounts of lithium will enter the membrane at the highest values of R so that the assumption of eq 16 will no longer be true.

Very marked changes in the selectivity parameters of Na, K, and NH_4 were observed at $\mu_T = 3.0$. The reversal of sign of the interference potential seems too large an effect to be accounted for by uncertainty in activity coefficients. It is possible that at these high concentrations the membrane no longer completely excludes anions. The formation of complexes between dialkylphosphates, water, and anions within the organic phase has been reported in the extraction of ferric ions from aqueous solutions.¹⁷ At low values of R , a diffusion potential governed by anion concentration gradient might be set up leading to a reversal of sign. At higher values of R cation exchange may nullify this effect and the sign again becomes negative.

(23) W. E. Keder, E. C. Martin, and L. A. Bray, "Solvent Extraction Chemistry of Metals," Proceedings from the International Conference sponsored by U.K.A.E.A., 1965, p 343.

The Mean Molal Activity Coefficient of Polymethacrylic Acid at Various Degrees of Neutralization

by G. Torrence, S. Amdur, and J. A. Marinsky*¹

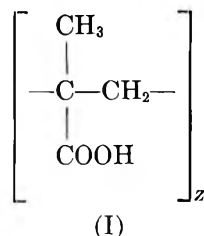
Department of Chemistry, State University of New York at Buffalo, Buffalo, New York 14214 (Received June 29, 1970)

Publication costs borne completely by The Journal of Physical Chemistry

The osmotic and potentiometric properties of polymethacrylic acid, neutralized with standard sodium hydroxide to provide several fixed degrees of neutralization, α , have been measured over a moderate concentration range at each selected α value. The osmotic data have been employed in the Gibbs–Duhem equation to compute the ratio of mean molal activity coefficients of a reference solution and a sample solution. This has been compared with the change in the corresponding deviation from ideality that is identified by the difference, ΔpK , between $\text{pH} - \log \alpha/(1 - \alpha)$ and $\text{p}K$, the negative logarithm of the intrinsic dissociation constant of its repeating monomer unit. The deviation term computed from the osmotic data and the deviation term obtained from the potentiometric data are in reasonable agreement in almost every experimental situation tested.

Introduction

Much effort has been expended in an attempt to interpret potentiometric titration^{2–8} and osmotic data^{7,9} that have been obtained for polymethacrylic acid, PMA (I). A most informative examination of this



problem is provided in the approach used by Arnold,³ where potentiometric titration data are plotted as $\text{pH} - \log \alpha/(1 - \alpha)$ (or $\text{p}K$) vs. α . Ideally $\text{pH} - \log \alpha/(1 - \alpha) = \text{p}K_0$ and any distortion from a straight line of zero slope is believed to provide a quantitative estimate of the deviation from ideal behavior of the system as the polyion is progressively dissociated. Representative plots intercept the ordinate at a value of 4.85.³ Since there is no ionization of the polymer at $\alpha = 0$, this number should correspond to the negative logarithm of the intrinsic dissociation constant of the repeating acidic group of PMA. This intercept value, indeed, is in reasonable accord with the dissociation constant of the basic monomer unit, isobutyric acid, which is reported as 4.84 at 25°.³ As α is raised the $\text{p}K$ value for the polyelectrolyte deviates increasingly from that of the monomeric acid unit. This discrepancy (ΔpK) is attributed to the change in electrostatic free energy of the molecule accompanying the ionization process at the polyion surface due to group–group interactions³ and has been expressed as $0.434 [\epsilon\psi(a)]/(kT)$

where ϵ is the charge of the proton and $\psi(a)$ is the electrostatic potential at the surface of the polyion.¹⁰

In this model the solution of polyelectrolyte is assumed to exhibit ideal behavior in the absence of macroion–counterion forces, the partial free energy of a mole of polyelectrolyte, \bar{G}_p , being expressed as

$$\bar{G}_p = \bar{G}_p(\text{ideal}) + \Delta\bar{G}_p(\text{el}) \quad (1)$$

or

$$\bar{G}_p^\circ + RT \ln \gamma_{\pm p} + RT \ln m_p = \bar{G}_p^\circ + RT \ln m_p + \Delta\bar{G}_p(\text{el}) \quad (2)$$

m_p being the molality of the polyelectrolyte, $\gamma_{\pm p}$, its mean molal activity coefficient, and \bar{G}_p° referring to its hypothetical standard state. At any α value the deviation from ideality should then correspond to the mean molal activity coefficient of the polyelectrolyte according to eq 3.

$$\ln \gamma_{\pm p} = \frac{\Delta\bar{G}_p(\text{el})}{RT} = -\frac{\epsilon\psi(a)}{RT} = 2.3(\Delta pK) \quad (3)$$

(1) Department of Chemistry, McGill University, Montreal, Quebec, Canada.

(2) (a) A. Katchalsky and P. Spitnik, *J. Polym. Sci.*, **2**, 432 (1947); (b) A. Katchalsky and J. Gillis, *Recl. Trav. Chim. Pays-Bas*, **68**, 879 (1949).

(3) R. Arnold and J. Th. G. Overbeek, *ibid.*, **69**, 192 (1950).

(4) A. Oth and P. Doty, *J. Phys. Chem.*, **56**, 43 (1952).

(5) H. Gregor and M. Frederick, *J. Polym. Sci.*, **23**, 451 (1957).

(6) E. E. Kern and D. K. Anderson, *ibid.*, Part A-1, **6**, 2765 (1968).

(7) Z. Alexandrowicz and A. Katchalsky, *ibid.*, Part A, **1**, 3231 (1963).

(8) H. P. Gregor, M. J. Hamilton, J. Becher, and F. Bernstein, *J. Phys. Chem.*, **59**, 874 (1955).

(9) Z. Alexandrowicz, *J. Polym. Sci.*, **40**, 98 (1959).

(10) J. A. Marinsky, "Ion Exchange," Vol. 1, Marcel Dekker, New York, N. Y., 1966, Chapter 9.

This concept can and should be tested by employing the Gibbs–Duhem relation. For electrolyte solutions¹¹

$$-\ln \gamma_{\pm m} = \int_0^m (1 - \phi) \frac{dm}{m} + 1 - \phi \quad (4)$$

Here $\gamma_{\pm m}$ is the mean molal activity coefficient of the electrolyte at its molal concentration m and ϕ is the osmotic coefficient for the system. The value of $\gamma_{\pm m}$ is obtained directly from graphical integration of the integral of eq 4, values of ϕ in the dilute concentration range inaccessible to experiment ($<0.03 m$) being estimated with reasonable assurance by linear extrapolation of a ϕ vs. $m^{1/2}$ plot. With polyelectrolytes, however, nonideal behavior is enhanced with decreasing concentration, the potential, $\psi(a)$, increasing because of less effective screening by counterions and the osmotic properties in the experimentally inaccessible dilute concentration range are not predictable. An eventual approach to ideal behavior is not expected since infinite dilution cannot be approached from conceptual reasons. It is therefore only possible to use the Gibbs–Duhem equation to determine mean molal activity coefficients relative to a reference state whose osmotic properties are known.

Such a relationship, presented by Ise,¹² for polyelectrolytes, is given below

$$\ln \frac{\gamma_r}{\gamma_{m_i}} = \phi_r - \phi_{m_i} + 2 \int_{m_i}^{m_r} \frac{(\phi_{m_i} - 1)}{\sqrt{m_i}} d\sqrt{m_i} \quad (5)$$

where γ_r/γ_{m_i} is the ratio of the mean molal activity coefficient of the reference solution and the sample being studied, $\phi_r - \phi_{m_i}$ is the difference in osmotic coefficients of the reference and sample solutions, respectively, and m_r and m_i are the molal concentrations on a monomer basis of the reference and sample. It can be used to test the concept proposed above by comparing the ratio $\ln \gamma_r/\gamma_{m_i}$ with the experimentally determined value of $\Delta pK_r - \Delta pK_{m_i}$, $\Delta(\Delta pK)$.

It was the objective of this research program to examine the above concept by comparing $\log \gamma_r/\gamma_{m_i}$ values obtained from analysis of PMA osmotic data with $\Delta pK_r - \Delta pK_{m_i}$ values obtained potentiometrically for the identical systems. Although all deviation from ideality is assigned exclusively to electrostatic interactions in the model outlined above, the validity of this oversimplification is not important to the research program objective. It was of interest only to show that the ΔpK term is or is not a true measure of nonideality in the polyelectrolyte system.

Experimental Section

Two separate sources of PMA, batch numbers LW-1523 and BC-920, were obtained from the Rohm and Haas Co. A molecular weight of 5000 corresponding to an average of 58 monomer units per polymer ($Z_{av} = 58$) was specified by the distributor for each material. Prior to their use the PMA samples were dialyzed for

24 to 36 hr. After dialysis, the PMA was passed through a mixed-bed ion exchanger to reduce further the concentration of cation and anion impurity. All product solutions were shown to be free of Na^+ and Cl^- ion by the standard sensitive tests for these ions.

These solutions were concentrated by slow evaporation in a current of air at the ambient temperature and weighed aliquots were potentiometrically titrated with standard CO_2 -free NaOH for a differential end point concentration determination. These standard solutions were then passed through Millipore microporous filters to assure the absence of bacterial growth in each of the samples employed in the measurement program.

In the preparation of samples at specified α values and concentrations weighed aliquot portions of the standard PMA were neutralized with precisely measured portions of standard 1 m NaOH . More dilute samples at the fixed α values were prepared by appropriate dilution of the initial mixtures with water initially distilled prior to percolation through mixed-bed ion-exchange columns (Illco-Way Research Model).

Potentiometric examination of each sample was made with a Model 12 Corning Expandomatic pH meter or a Model 4 Radiometer pH meter which were calibrated before and after a series of measurements by either the method of Eger, Anspach, and Marinsky¹³ or by the use of three standard reference buffers covering the pH range from 4.008 to 9.180. Throughout, a measurement scrubbed nitrogen was passed over the magnetically stirred sample to avoid the presence of CO_2 . The temperature of samples during measurement was maintained at $25 \pm 0.1^\circ$ with a Precision Scientific water bath. The measurements are estimated to have a precision range of 0.015 pH unit.

The osmotic data were obtained with samples prepared from the second PMA source at the various fixed degrees of neutralization, (0.2, 0.3, 0.5, and 0.8) by using the Mechrolab vapor pressure osmometer according to the procedure outlined by Amdur.¹⁴ Calibration of the osmometer was performed with reagent grade (Fisher Scientific) potassium chloride solutions of known molal concentration and known osmotic coefficient.¹⁵ The osmotic coefficients are reliable to ± 0.01 .¹⁶

Results and Discussion

The pH_I and pH_{II} values that are reported in Table I for samples from the two different PMA sources that

(11) E. A. Guggenheim, "Thermodynamics, an Advanced Treatment for Chemists and Physicists," North-Holland Publishing Co., Amsterdam, 1959, Chapter 8.

(12) N. Ise and T. Okubo, *J. Phys. Chem.*, **71**, 1287 (1967).

(13) C. Eger, W. M. Anspach, and J. A. Marinsky, *J. Inorg. Nucl. Chem.*, **30**, 1899 (1968).

(14) S. Amdur, *J. Phys. Chem.*, **73**, 1163 (1969).

(15) N. Ise and T. Okubo, *ibid.*, **70**, 1930 (1966).

(16) M. Reddy, A. Sarkar, and J. A. Marinsky, *ibid.*, **74**, 3891 (1970).

Table I: Comparison of $-\log \gamma_r/\gamma_{m_i}$ and $\Delta(\Delta pK)$

m_i	pH _I	pH _{II}	$\Delta(\Delta pK)_I^b$	$\Delta(\Delta pK)_{II}^b$	$\log \frac{\gamma_r^c}{\gamma_{m_i}}$
$\alpha = 0.8$					
0.557	6.590	6.692	0.225	0.227	0.182
0.429	6.679	6.804	0.136	0.115	0.107
0.349	6.742	6.875	0.068	0.044	0.041
0.293	6.815	6.919		Reference	
0.679		6.590		0.345	0.214
0.566		6.705		0.240	0.171
0.400		6.831		0.114	0.090
0.275		6.945		Reference	
$\alpha = 0.5$					
0.669	5.635	5.701	0.210	0.200	0.176
0.492	5.701	5.811	0.144	0.090	0.095
0.389	5.770	5.857	0.075	0.044	0.044
0.322	5.840	5.901		Reference	
0.893		5.602		0.387	0.271
0.700		5.687		0.302	0.232
0.531		5.771		0.218	0.186
0.216		5.989		Reference	
$\alpha = 0.3$					
0.773	5.269	5.260	0.165	0.173	0.191
0.544	5.326	5.339	0.099	0.094	0.098
0.419	5.380	5.395	0.045	0.038	0.041
0.341	5.425	5.433		Reference	
1.040		5.188		0.209, 0.184 ^a	0.161
0.746		5.270		0.127, 0.111	0.103
0.600		5.324		0.073, 0.065	0.062
0.425		5.397		Reference	
$\alpha = 0.2$					
0.837	5.016	4.958	0.199	0.166	0.133
0.575	5.103	5.036	0.112	0.088	0.077
0.438	5.175	5.087	0.040	0.037	0.033
0.354	5.215	5.124		Reference	
1.304		4.876		0.211	0.168
1.005		4.924		0.163	0.130
0.723		4.986		0.101	0.079
0.442		5.087		Reference	

^a Separate measurements with separately prepared samples; the second set is interpolated to the concentration of the first set. ^b Estimated precision range is ± 0.015 pH unit. ^c Estimated precision range is ± 0.010 to ± 0.015 unit.

were used in the experimental program have been reduced to the same concentration base at each of the four different α values selected for investigation to permit an estimate of reproducibility of the materials employed. The pH_I values were interpolated from the titration curves obtained in the first series of experiments with one PMA source to define each PMA concentration. The pH_{II} values corresponding to these PMA concentrations were interpolated from a smooth curve drawn through the pH values obtained at different molalities for each specified α value in the second series of experiments with the other PMA source. The pH data that were obtained directly for the samples

prepared from the second PMA source are also listed in Table I.

The variation of pH as a function of PMA concentration, when α is held constant, is a direct measure of $\Delta(\Delta pK)$ and the difference in pH between the most dilute solution (reference) and the others at a given α value yields the $\Delta(\Delta pK)$ values that are presented in Table I for the two series of experiments. In the last column of the table the values of $\log \gamma_r/\gamma_{m_i}$, computed with eq 5 by using the osmotic data obtained with corresponding samples from the second PMA source, are given for comparison with the experimental $\Delta(\Delta pK)$ term.

There is only fair agreement between the pH_I and pH_{II} values, pH_I being consistently smaller than pH_{II} at $\alpha = 0.8$ (~ 0.1 pH unit) and $\alpha = 0.5$ (~ 0.08 pH unit); they are almost equal at $\alpha = 0.3$ and at $\alpha = 0.2$ pH_I becomes larger than pH_{II} (~ 0.07 pH unit). There is, however, much better agreement between $\Delta(\Delta pK)_I$ and $\Delta(\Delta pK)_{II}$ with only the largest discrepancy of 0.054 pH units significantly exceeding the estimated precision limits of ± 0.015 pH unit expected in potentiometric studies of this kind. (See Figure 1.)

The differences that are observed between pH_I and pH_{II} exceed the possible experimental error range significantly and the discrepancy must be attributable to some other factor. Since the PMA sources were different it is quite conceivable that even though the average molecular weights of the two PMA sources were essentially the same the molecular weight distribution of polymer units in these low-molecular weight materials was sufficiently different after dialysis to affect the observed potentiometric characteristics but with only minor disturbance of the $\Delta(\Delta pK)$ term.

There is a sizeable difference as well between the osmotic coefficients measured in this research and the lower values reported by Alexandrowicz⁹ for high-molecular weight ($Z \approx 1000$) PMA. Discrepancy could arise from the presence of a small fraction of really low ($Z < 58$) molecular weight fragments considered likely to be present in our samples. Our attempt to minimize this possibility by the dialysis treatment described earlier was probably too inefficient. Exhaustive dialysis resulted in too low a yield of PMA product forcing us to compromise this preparative step. It should be noted as well that in a recent study of the osmotic properties of sodium and hydrogen polystyrenesulfonate¹⁶ it was shown that a membrane osmometry method of measurement similar to that used by Alexandrowicz in his PMA studies⁹ yielded consistently lower osmotic coefficients than isopiestic and vapor pressure osmometer measurements which gave identical results.

The agreement between $\log \gamma_r/\gamma_{m_i}$ and $\Delta(\Delta pK)$ is, on the whole, acceptable, discrepancies between the two terms falling within or just outside the precision range estimated for the potentiometric and osmotic measurements in all but 7 of the 27 trials. The lack of agree-

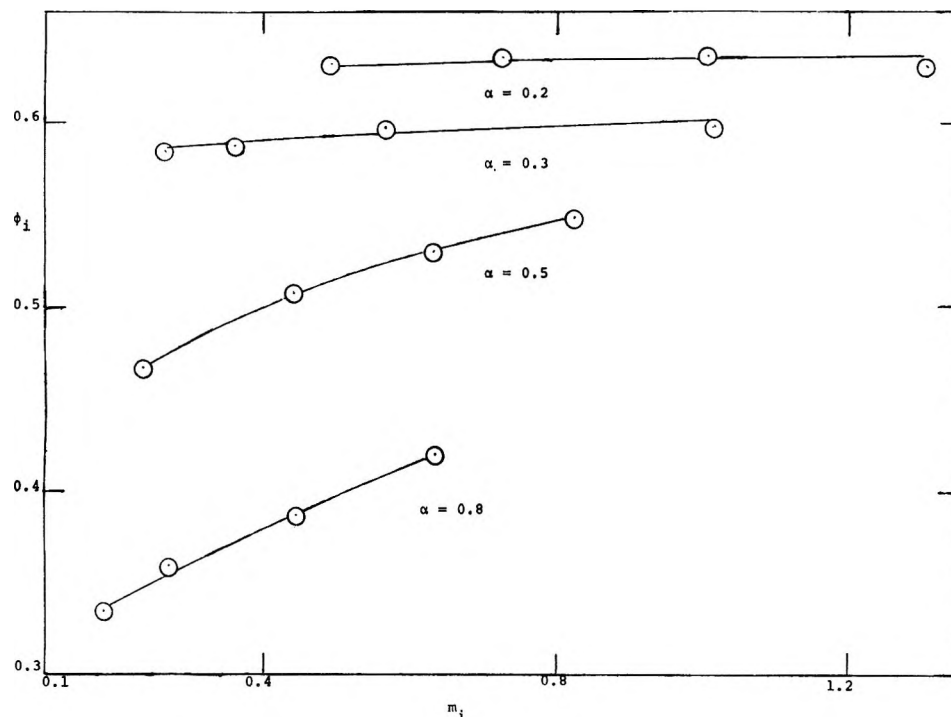


Figure 1. Osmotic coefficient variation with molality at several different degrees of neutralization.

ment between the two terms in these instances (highest PMA concentrations at $\alpha = 0.2$ to 0.8) is probably a consequence of experimental bias. The assumption that the liquid-junction potential between KCl solution of the calomel electrode and the sample does not vary with the concentration of PMA at a fixed degree of neutralization is probably incorrect, its failure becoming most noticeable at the higher concentrations of the most dissociated PMA solutions. The research objective of this program is believed to have been obtained. It can be concluded with reasonable assurance that the ΔpK term is indeed a true measure of nonideality in the polyelectrolyte system.

This demonstration of the correlation between potentiometric and osmotic data also suggests an important potential application of potentiometric measurements of weakly acidic polyelectrolytes. Their osmotic properties, experimentally inaccessible in the dilute concentration region, can apparently be computed with reasonable accuracy by potentiometric examination at

these low polyelectrolyte concentrations. This substantiates the earlier related studies of Shatkay and Michaeli.¹⁷

Finally, we suggest that (1) since the ΔpK term is indeed a measure of ideality and (2) since it can be referred to the standard state of the repeating monomer unit (in this case isobutyric acid) at infinite dilution it can indeed be used to evaluate directly meaningful mean molal activity coefficients of polyelectrolytes over a large concentration and neutralization range.

Acknowledgment. The authors wish to express their appreciation to the United States Atomic Energy Commission for financial support through Contract No. AT(30-1)-2269. They are grateful to R. L. Gustafson of Rohm and Haas for kindly supplying the two PMA samples.

(17) A. Shatkay and I. Michaeli, *J. Polym. Sci., Part A-2*, **5**, 1061 (1967).

Free Energy Changes on Mixing Solutions of Alkali Halides and Symmetrical Tetraalkylammonium Halides

by Wen-Yang Wen,* Koichiro Miyajima, and Akinobu Otsuka

Jeppson Laboratory, Chemistry Department, Clark University, Worcester, Massachusetts 01610 (Received October 15, 1970)

Publication costs assisted by the National Science Foundation and the Public Health Service

The excess free energy changes on mixing solutions of alkali halides and tetraalkylammonium halides having common anions were determined at 25° by the isopiestic method. The systems studied include KBr-R₄NBr (where R = Me, Et, Pr, and Bu), Pr₄NBr-MBr (where M = Li, Na, K, Cs, Me, and Et), Me₄NBr-R₄NBr (where R = Et, Pr, and Bu), and KCl-Bu₄NCl at $y = 0.5$ and $I = 0.1$ to 4.0, where I is the total molal ionic strength and y is the fraction of ionic strength due to an electrolyte in a mixture of two electrolytes. For the KBr-Pr₄NBr system, y was varied from 0.1 to 0.9. The experimental osmotic coefficients were treated by the formalisms of Scatchard and of Friedman to yield the excess free energy, ΔG^{ex} , and the free energy interaction parameter, g_0 . Values of g_0 obtained were discussed in terms of the ionic solution theory of Friedman to gain insights into the nature of the cation-cation interaction. The results have been interpreted to indicate that, in dilute solution ($I = 0.5$), the free energies of interaction between two large tetraalkylammonium cations are small, probably much smaller than those between two alkali metal ions. The relative mutual attraction between two tetraalkylammonium ions may be an instance of hydrophobic interaction.

Introduction

The osmotic and activity coefficients for aqueous mixtures of two electrolytes having a common ion were first reported by Owen and Cooke¹ in 1937 for LiCl-KCl system at 25°. Since 1952 Robinson and his co-workers² have investigated for many years mixtures containing alkali metal ions and alkaline earth metal ions. Recently, Rush and his coworkers in the Oak Ridge National Laboratory³ have determined osmotic coefficients for various three-component systems (two electrolytes and water) and treated their experimental results with equations suggested by Scatchard.⁴ Using these equations Rush⁵ has recalculated the parameters of osmotic and activity coefficients for 31 aqueous mixtures of two electrolytes at 25°. A more elegant approach in dealing with the free energies of mixed electrolyte solutions has been proposed by Friedman,⁶ who has pointed out the existence of a limiting slope for the interaction parameters at infinite dilution. This approach has been taken up by others, particularly by Wood and his coworkers.⁷

The studies mentioned above have dealt with systems containing only inorganic electrolytes. There seems to be no investigation of excess free energy of mixing involving organic electrolytes. On the other hand, various workers have investigated aqueous solutions of tetraalkylammonium halides and uncovered many interesting properties.⁸ One of the physical properties of these salts which is of particular interest to us is the nature of cation-cation interaction between the large tetraalkylammonium ions. Studies on volume changes on mixing⁹ and enthalpy changes on mixing¹⁰ seem to suggest the importance of the cation-cation pair inter-

action and cation-anion-cation triplet interaction. This and other related questions on hydrophobic interaction¹¹ have led us to investigate the excess free energy of mixing solutions of tetraalkylammonium halides and alkali halides having common anions. The thermodynamic parameters were derived from osmotic coefficients obtained by the isopiestic method at 25°.

(1) B. B. Owen and T. F. Cooke, *J. Amer. Chem. Soc.*, **59**, 2273 (1937).

(2) (a) R. A. Robinson, *ibid.*, **74**, 6035 (1952); (b) R. A. Robinson and C. K. Lim, *Trans. Faraday Soc.*, **49**, 1144 (1953); (c) R. A. Robinson, *ibid.*, **49**, 1147 (1953); (d) R. A. Robinson, *J. Phys. Chem.*, **65**, 662 (1961); (e) R. A. Robinson and V. E. Bower, *J. Res. Nat. Bur. Stand. Sect. A*, **69**, 19, 439 (1965); *ibid.*, **70**, 313 (1966); (f) R. A. Robinson and A. K. Covington, *ibid.*, **72**, 239 (1968).

(3) (a) R. M. Rush and R. A. Robinson, *J. Tenn. Acad. Sci.*, **43**, 22 (1968); (b) R. M. Rush and J. S. Johnson, *J. Phys. Chem.*, **72**, 767 (1968); (c) Y. C. Wu, R. M. Rush, and G. Scatchard, *ibid.*, **72**, 4048 (1968); **73**, 2047 (1969).

(4) G. Scatchard, *J. Amer. Chem. Soc.*, **83**, 2636 (1961).

(5) R. M. Rush, "Parameters for the Calculation of Osmotic and Activity Coefficients and Tables of These Coefficients for 22 Aqueous Mixtures of Two Electrolytes at 25°C," Oak Ridge National Laboratory, ORNL-4402, 1969.

(6) (a) H. L. Friedman, *J. Chem. Phys.*, **32**, 1134, 1351 (1960); (b) H. L. Friedman, "Ionic Solution Theory," Interscience, New York, N. Y., 1962; (c) J. C. Rasaiah and H. L. Friedman, *J. Chem. Phys.*, **48**, 2742 (1968).

(7) P. J. Reilly and R. H. Wood, *J. Phys. Chem.*, **73**, 4292 (1969), and references cited therein.

(8) See, e.g., references cited in W.-Y. Wen and J. H. Hung, *ibid.*, **74**, 170 (1970).

(9) (a) W.-Y. Wen and K. Nara, *ibid.*, **71**, 3907 (1967); (b) W.-Y. Wen and K. Nara, *ibid.*, **72**, 1137 (1968); (c) W.-Y. Wen, K. Nara, and R. H. Wood, *ibid.*, **72**, 3048 (1968).

(10) R. H. Wood and H. L. Anderson, *ibid.*, **71**, 1871 (1967).

(11) (a) W. Kauzmann, *Advan. Protein Chem.*, **14**, 1 (1959); (b) G. Nemethy and H. A. Scheraga, *J. Phys. Chem.*, **66**, 1773 (1962); **67**, 2888 (1963); (c) H. Nemethy, *Angew. Chem.*, **6**, 195 (1967).

Procedure

A. *Formalism According to Friedman.* Friedman has extended Mayer's ionic solution theory¹² to mixed electrolyte solutions and derived the excess free energy of mixing

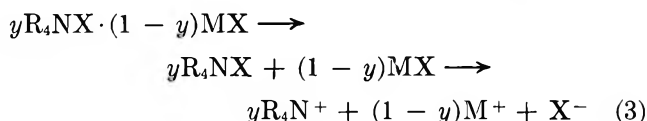
$$\Delta G^{\text{ex}}(y, I) = I^2 RT y(1 - y) \times [g_0 + g_1(1 - 2y) + g_2(1 - 2y)^2 + \dots] \quad (1)$$

where R and T have their usual meaning, I is the molal ionic strength, y is the fraction of ionic strength due to an electrolyte in a mixture of two electrolytes AX and BX, and the g 's are interaction parameters. The excess free energy of the mixed solution is defined as

$$\Delta G^{\text{ex}}(y, I) = G^{\text{ex}}(y, I) - yG^{\text{ex}}(1, I) - (1 - y)G^{\text{ex}}(0, I) \quad (2)$$

where $G^{\text{ex}}(1, I)$ applies to a solution of pure AX and $G^{\text{ex}}(0, I)$ applies to a solution of pure BX. The quantity ΔG^{ex} is clearly the increase in excess free energy on forming the mixture from the component solutions at the same I , T , and pressure, and is a measure of the change in molecular interaction in the process.

The changes of excess free energies on mixing solutions of R_4NX and MX at constant total ionic strength can be determined by use of the concept of a pseudo-binary solution. The pseudo-binary salt $yR_4NX \cdot (1 - y)MX$ dissociates in water according to



The mean activity coefficient of the pseudo-salt may be defined as

$$\gamma_{\pm} = \gamma_{\pm}^{y(R_4NX)} \gamma_{\pm}^{(1-y)(MX)} = (\gamma_{R_4N^+}^y \cdot \gamma_{M^+}^{1-y} \cdot \gamma_{X^-})^{1/2} \quad (4)$$

The change in excess free energies is given by eq 2 where I is the total molality in this case and y is the mole fraction of R_4NX in the mixture. To obtain G^{ex} we start from the Bjerrum form of the Gibbs-Duhem equation, namely

$$m d \ln \gamma_{\pm} = -d[m(1 - \phi)] \quad (5)$$

where γ_{\pm} is the "mixed" coefficient as defined in eq 4 and ϕ is the osmotic coefficient of the pseudo-binary solution to be determined by the isopiestic experiments. Thus, by measuring ϕ at any constant y it would be possible to get the pseudo-binary γ_{\pm} for that y as a function of total ionic strength. It turns out, however, that it is not necessary to evaluate the values of γ_{\pm} to obtain the values of G^{ex} .

An expression for the excess free energy of a simple salt is

$$G^{\text{ex}} = 2RTI [\ln \gamma_{\pm} + (1 - \phi)] \quad (6)$$

From eq 5 we obtain

$$\ln \gamma_{\pm} = -(1 - \phi) - \int_0^I \frac{1 - \phi}{I} dI \quad (7)$$

and substitution of eq 7 into eq 6 yields

$$\begin{aligned} G^{\text{ex}}(y, I) &= -2RTI \int_0^I \frac{1 - \phi}{I} dI = \\ &= -4RTI \int_0^I \frac{1 - \phi}{\sqrt{I}} d\sqrt{I} \quad (8) \end{aligned}$$

Since the osmotic and activity coefficients of R_4NX solution (subscript A) and MX solution (subscript B) are available in literature, one can obtain the values of ΔG^{ex} by use of eq 2, 8-10.

$$G^{\text{ex}}(1, I) = 2RTI [\ln \gamma_{\pm(A)} + (1 - \phi_A)] \quad (9)$$

$$G^{\text{ex}}(0, I) = 2RTI [\ln \gamma_{\pm(B)} + (1 - \phi_B)] \quad (10)$$

The integral in eq 8 for the mixed electrolyte solutions was evaluated by two methods. The first method is the graphical method in which the values of $(1 - \phi)/\sqrt{I}$ are plotted against \sqrt{I} and the area under the curve is evaluated. In this plot $(1 - \phi)/\sqrt{I}$ approaches a value of 0.3908 as I approaches zero according to the Debye-Hückel limiting law for 1-1 electrolytes at 25°. The second method concerns with the least-squares evaluation of the coefficients (A_2 through A_7) in the following empirical equation.

$$1 - \phi = \sum_{i=1}^7 A_i I^{i/2}; \quad (A_1 = 0.3908) \quad (11)$$

Once these coefficients are determined by a computer program, it can be easily shown that

$$\begin{aligned} G^{\text{ex}}(y, I) &= -4RT \sum_{i=1}^7 (A_i/i) I^{(i+2)/2}; \\ & \quad (A_1 = 0.3908) \quad (12) \end{aligned}$$

B. *Formalism According to Scatchard.* Equations employed in this formalism are derived from those of Scatchard.^{4,13} The b parameters were derived from the observed osmotic coefficients (ϕ) at ionic strength I and ionic strength fraction y_B . These same parameters can then be used to calculate the activity coefficients γ_{\pm} of either component. The other relationships used are

$$\alpha_J = 2m_J(\phi_J - 1)/I_J$$

$$(A_J + \alpha_J) = (2m_J/I_J) \ln \gamma_{\pm J(J)}$$

where ϕ_J is the osmotic coefficient of pure J and $\gamma_{\pm J(J)}$ is the activity coefficient of component J in pure J both taken at the ionic strength of the mixture in question. It is thus possible to calculate the contributions of the

(12) J. E. Mayer, *J. Chem. Phys.*, **18**, 1426 (1950).

(13) Notations of this formalism are conveniently summarized in Table I, p 8 of ref 5.

Table I: Osmotic and Activity Coefficients of CsBr, Pr₄NBr, and Bu₄NBr in Water at 25°

Molality, <i>m</i>	CsBr		Pr ₄ NBr		Bu ₄ NBr	
	ϕ	γ_{\pm}	ϕ	γ_{\pm}	ϕ	γ_{\pm}
0.1	0.912	0.742	0.884	0.701	0.879	0.693
0.2	0.893	0.681	0.841	0.610	0.833	0.599
0.3	0.882	0.642	0.813	0.554	0.802	0.538
0.4	0.872	0.614	0.792	0.512	0.780	0.496
0.5	0.865	0.592	0.776	0.480	0.761	0.463
0.6	0.860	0.575	0.765	0.455	0.747	0.437
0.7	0.855	0.560	0.757	0.435	0.737	0.415
0.8	0.851	0.547	0.753	0.420	0.729	0.398
0.9	0.849	0.537	0.751	0.407	0.721	0.381
1.0	0.846	0.526	0.751	0.396	0.713	0.367
1.2	0.842	0.509	0.754	0.380	0.698	0.344
1.4	0.839	0.495	0.762	0.369	0.682	0.323
1.6	0.837	0.483	0.773	0.361	0.666	0.304
1.8	0.835	0.473	0.787	0.357	0.651	0.287
2.0	0.834	0.465	0.802	0.355	0.635	0.272
2.5	0.834	0.448	0.842	0.355	0.602	0.240
3.0	0.836	0.436	0.885	0.361	0.572	0.215
3.5	0.839	0.426	0.926	0.371	0.545	0.198
4.0	0.841	0.418	0.958	0.380	0.520	0.181

pure components to ϕ and $\ln \gamma_{\pm}$ using either the analytical expressions for α and $(A + \alpha)$ or the above equations and tabular data on the pure components such as those given by Robinson and Stokes.¹⁴

In terms of the Scatchard's formalism the excess free energy and interaction parameters are given by

$$\Delta G^{\text{ex}} = RTI[B_{AB}^{(0)}y_Ay_B + B_{AB}^{(1)}y_Ay_B(y_A - y_B)] \quad (13)$$

$$g_0 = B_{AB}^{(0)}/I = b_{AB}^{(0,1)} + (1/2)b_{AB}^{(0,2)}I + (1/3)b_{AB}^{(0,3)}I^2 \quad (14)$$

$$g_1 = B_{BA}^{(1)}/I = (1/2)b_{AB}^{(1,2)}I + (1/3)b_{AB}^{(1,3)}I^2 \quad (15)$$

Experimental Section

Materials. Fisher¹⁵ certified potassium chloride and bromide and sodium bromide were recrystallized twice from water and dried before use. These halides were analyzed gravimetrically and found to be in 99.9% or better agreement with the calculated value. Cesium bromide and lithium bromide were purchased from Chemicals Procurement Laboratories, Inc. and Matheson Coleman and Bell Co., respectively; they were dried and used without further purification. Cesium bromide was carefully analyzed gravimetrically using silver bromide for the bromide ion analysis and cesium tetraphenylboride for the cesium ion analysis: both results indicated the purity of the salt to be at least 99.9%. Five tetraalkylammonium salts (Me₄NBr, Et₄NBr, Pr₄NBr, Bu₄NBr, and Bu₄NCl) were obtained from Eastman Kodak Co. and each salt was recrystallized twice or more from the suitable solvents¹⁶ and dried at proper temperatures¹⁷ before use.

Apparatus and Procedure. The osmotic coefficients were determined by the gravimetric isopiestic comparison method with an apparatus which has been described previously.¹⁸ Several sets of four dishes (made of gold or gold-plated silver) with dimensions of 4 × 4 × 1.75 cm³ were used on a 3.5-cm thick copper block having a diameter of 15 cm. All contact surfaces of the dishes and the copper block have been carefully polished to render good heat conduction. To initiate a measurement, appropriate amounts of mixed electrolyte solutions and a pair of NaCl reference solutions were accurately weighed into separate dishes. Four dishes of a set were tightly clamped onto the copper block and placed in a desiccator which was then immersed in a large constant-temperature bath held at 25 ± 0.01°. To increase the speed of distillation, the pressure in each of the five desiccators used was carefully reduced in steps to 25 Torr by means of a water aspirator. Solutions were made in pair to check the attainment of equilibrium. After shaking the desiccators in the water bath for 3 days to 2 weeks depending on the concentration of the solutions under investigation, the dishes were reweighed and the equilibrium concentrations of the reference solutions as well as the mixed electrolyte solutions were calculated. The solutions in duplicate dishes were considered to be in equilibrium when they arrived at the same molality to within 0.05%. Our osmotic and activity coefficient data are precise to within 0.1 and 0.5%, respectively.

Results

I. Data on Single Electrolyte Solutions. Osmotic and activity coefficients of single electrolytes in water at 25° are taken from the following sources: LiBr, NaBr, and KBr from Robinson and Stokes,¹⁴ Me₄NBr from Levien,¹⁹ and Et₄NBr and Bu₄NCl from Lindenbaum and Boyd.²⁰ The osmotic and activity coefficients of CsBr, Pr₄NBr, and Bu₄NBr were redetermined in our laboratory. Our experimentally obtained values for Pr₄NBr and Bu₄NBr are slightly better than those reported by Lindenbaum and Boyd,²⁰ since their isopiestic concentrations did not go below 0.5 *m*. Our data for CsBr at concentrations below 1 *m* are in fair agreement with those of Robinson, but our data at concentrations above 1 *m* are in serious disagreement with those of Robinson.²¹ The values of ϕ and γ_{\pm} for these salts are given in Table I.

(14) R. A. Robinson and R. H. Stokes, "Electrolyte Solutions," 2nd ed, Butterworth, London, 1959.

(15) Fisher Scientific Co., Pittsburgh, Pa.

(16) R. E. Verrall, Ph.D. Thesis, University of Ottawa, 1966.

(17) A. K. R. Unni, Ph.D. Thesis, McGill University, Montreal, 1958.

(18) (a) W.-Y. Wen and C. L. Chen, *J. Phys. Chem.*, **73**, 2895 (1969); (b) W.-Y. Wen and S. Saito, *ibid.*, **69**, 3569 (1965); (c) W.-Y. Wen, S. Saito, and S. M. Lee, *ibid.*, **70**, 1244 (1966).

(19) B. J. Levien, *Austr. J. Chem.*, **18**, 1161 (1965).

(20) S. Lindenbaum and G. E. Boyd, *J. Phys. Chem.*, **68**, 911 (1964).

(21) R. A. Robinson, *J. Amer. Chem. Soc.*, **57**, 1161 (1935); R. A. Robinson, *ibid.*, **59**, 84 (1937).

Table II: Osmotic Coefficients of Pr₄NBr-KBr Mixed Solutions at 25°

$y = 0.1$		$y = 0.2$		$y = 0.3$		$y = 0.4$		$y = 0.5$	
I	ϕ	I	ϕ	I	ϕ	I	ϕ	I	ϕ
0.0693	0.9320	0.0925	0.9252	0.0903	0.9218	0.0905	0.9194	0.0909	0.9152
0.0938	0.9297	0.1466	0.9144	0.1477	0.9080	0.1065	0.9163	0.1354	0.9010
0.1459	0.9190	0.4015	0.8957	0.4053	0.8871	0.1485	0.9029	0.1872	0.8936
0.2500	0.9127	0.5338	0.8926	0.4964	0.8831	0.4053	0.8874	0.2835	0.8759
0.2651	0.9082	0.8041	0.8933	0.5396	0.8830	0.5026	0.8722	0.3921	0.8663
0.3986	0.9023	0.9921	0.8972	0.6722	0.8817	0.5469	0.8712	0.3950	0.8653
0.4982	0.9027	1.0528	0.8990	0.7381	0.8839	0.7709	0.8780	0.5106	0.8586
0.5999	0.8999	1.1644	0.9000	0.8136	0.8829	0.8263	0.8693	0.5185	0.8586
0.7971	0.9012	1.2665	0.9021	1.0036	0.8869	1.0491	0.8718	0.5642	0.8559
0.9839	0.9047	1.3920	0.9055	1.0329	0.8854	1.1460	0.8741	0.6933	0.8549
1.0441	0.9065	1.9496	0.9256	1.0749	0.8882	1.2285	0.8878	0.7625	0.8555
1.0600	0.9054	1.9905	0.9268	1.1777	0.8899	1.3946	0.8804	0.7737	0.8533
1.1550	0.9074	2.6569	0.9523	1.4117	0.8929	1.6552	0.8892	0.8722	0.8529
1.3577	0.9126	3.2983	0.9810	1.9531	0.9020	1.9792	0.9012	1.0684	0.8560
1.3792	0.9139	3.8406	1.0053	1.9713	0.9155	2.0139	0.9039	1.2089	0.8580
1.8922	0.9296	4.1850	1.0192	2.0113	0.9172	2.1037	0.9055	1.4143	0.8643
1.9797	0.9328			2.5862	0.9415	2.3269	0.9037	1.4236	0.8626
2.6517	0.9546			3.3136	0.9765	2.6152	0.9310	1.6876	0.8992
3.2878	0.9841			3.8822	1.0010	3.0827	0.9300	2.0095	0.8907
3.8515	1.0025			4.1956	1.0166	3.8020	0.9889	2.0040	0.8909
4.1730	1.0221					3.9075	0.9946	2.1348	0.8923
								2.3269	0.9037
								2.7509	0.9342
								3.0543	0.9386
								3.8342	0.9806

$y = 0.6$		$y = 0.7$		$y = 0.8$		$y = 0.9$	
I	ϕ	I	ϕ	I	ϕ	I	ϕ
0.0899	0.9092	0.1047	0.9018	0.1056	0.8941	0.1063	0.8883
0.1153	0.8994	0.4051	0.8384	0.1092	0.8951	0.2129	0.8497
0.1885	0.8859	0.5386	0.8265	0.4091	0.8241	0.3168	0.8226
0.2868	0.8658	0.6452	0.8214	0.5445	0.8102	0.4184	0.8059
0.4392	0.8529	0.8081	0.8192	0.6613	0.8014	0.5691	0.7903
0.5279	0.8433	1.0193	0.8177	0.8343	0.7966	0.6789	0.7906
0.6313	0.8395	1.0682	0.8179	1.0464	0.7965	0.8571	0.7755
0.7896	0.8360	1.1966	0.8213	1.0963	0.7969	1.0761	0.7746
0.9961	0.8367	1.4847	0.8289	1.2269	0.8010	1.1254	0.7763
1.0437	0.8373	1.6826	0.8267	1.5186	0.8104	1.2599	0.7801
1.1700	0.8400	1.7349	0.8449	1.6950	0.8207	1.5539	0.7920
1.4538	0.8465	2.3131	0.8725	1.9290	0.8363	1.7335	0.8025
2.0416	0.8736	2.3926	0.8789	2.0387	0.8422	1.9570	0.8243
2.6781	0.9092	2.7750	0.9020	2.1319	0.8497	2.0728	0.8284
3.0216	0.9488	4.1632	0.9825	2.6909	0.8884	2.1674	0.8358
3.9667	0.9797	4.4660	0.9992	2.8217	0.8953	2.5926	0.8706
				3.2324	0.9259	2.7181	0.8795
				3.9362	0.9679	2.8502	0.8863
				4.2013	0.9823	3.2638	0.9165
						3.9525	0.9679
						4.2232	0.9772

II. Mixed Electrolyte Solutions. A. Pr₄NBr-KBr System. The osmotic coefficients of Pr₄NBr-KBr mixed solutions at 25° determined by the isopiestic method are given in Table II where y , the ionic strength fraction of Pr₄NBr, is varied from 0.1 to 0.9 in increments of 0.1. Using the method outlined in the previous section, the values of $\Delta G^{ex}(y, I)$ for Pr₄NBr-KBr system have been calculated. The integral of eq 8 was evaluated by the graphical method and also by the method of least squares. Results obtained by these two methods

are in reasonable agreement. The values of ΔG^{ex} obtained were plotted against y at various ionic strengths I in Figure 1. (For numerical values of ΔG^{ex} , see ref 22.)

(22) Listings of the numerical values of excess free energy of mixing and activity coefficients in mixed electrolyte solutions will appear immediately following this article in the microfilm edition of this volume of the journal. Single copies may be obtained from the Reprint Department, ACS Publications, 1155 Sixteenth Street, N.W., Washington, D. C. 20036. Remit \$3.00 for photocopy or \$2.00 for microfilm.

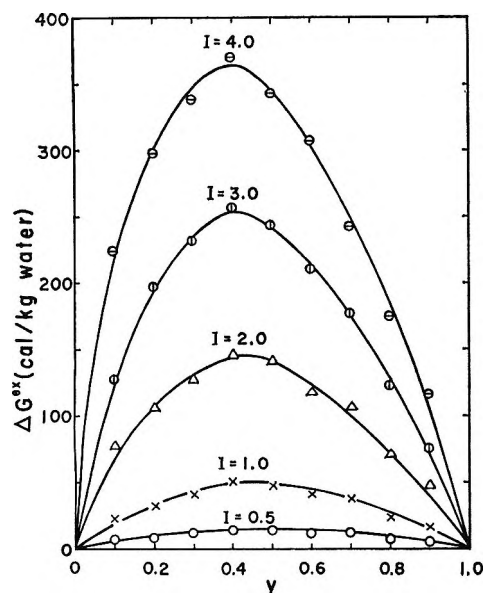


Figure 1. Excess free energy of mixing (ΔG^{ex}) aqueous Pr_4NBr and KBr solutions at constant ionic strength (I) plotted against y , the mole fraction of Pr_4NBr in the mixed electrolyte at 25° .

When y is equal to 0.5, eq 1 reduces to

$$\Delta G^{\text{ex}}(0.5, I) = 0.25I^2RTg_0 \quad (16)$$

from which the values of g_0 can be obtained as a function of I . Osmotic coefficient data given in Table II have also been treated according to the Scatchard's formalism by Dr. Rush of Oak Ridge National Laboratory and yielded the following set of parameters

$$\begin{aligned} b_{\text{AB}}^{(0,1)} &= 0.39807, & b_{\text{AB}}^{(0,2)} &= -0.20009, \\ b_{\text{AB}}^{(0,3)} &= 0.027573, & b_{\text{AB}}^{(1,2)} &= 0.021725, \\ & & b_{\text{AB}}^{(1,3)} &= 0.0 \end{aligned} \quad (17)$$

From these b parameters the values of g_0 have been calculated by use of eq 14. g_0 values obtained by the two different formalisms are given in Table III for comparison. Activity coefficients of Pr_4NBr and KBr in the mixed electrolyte solutions have been computed by Dr. Rush. The results obtained are plotted in Figure 2. (For numerical values of activity coefficients, see ref 22.)

B. $\text{Me}_4\text{NBr-KBr}$, $\text{Et}_4\text{NBr-KBr}$, $\text{Bu}_4\text{NBr-KBr}$, and $\text{Bu}_4\text{NCl-KCl}$ Systems at $y = 0.5$. The osmotic coefficients of these mixed solutions at a single y value of 0.5 were determined at 25° and the values of ϕ obtained are given in Table IV. As stated in the previous section, the values of ΔG^{ex} were obtained by two methods. (For numerical values, see ref 22.) The values of g_0 obtained by eq 16 are listed in Table V for comparison. b parameters of the Scatchard formalism are given in Table VI.

C. $\text{Pr}_4\text{NBr-LiBr}$, $\text{Pr}_4\text{NBr-NaBr}$, $\text{Pr}_4\text{NBr-CsBr}$, $\text{Pr}_4\text{NBr-Me}_4\text{NBr}$, and $\text{Pr}_4\text{NBr-Et}_4\text{NBr}$ Systems at $y =$

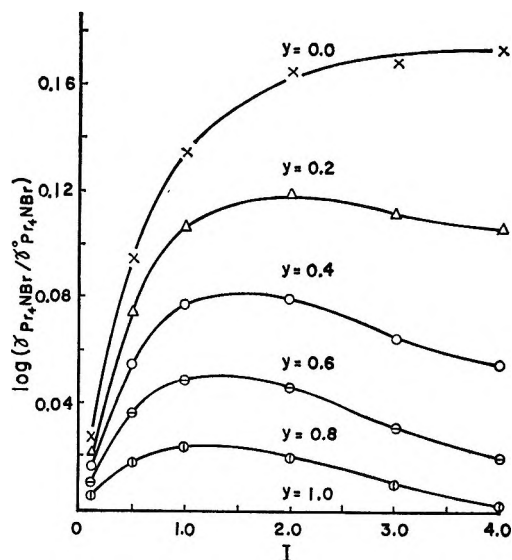


Figure 2. Plot of $\log(\gamma_A/\gamma_A^0)$ vs. I at constant y for aqueous solution at 25° . γ_A is the activity coefficient of Pr_4NBr in the aqueous mixture of Pr_4NBr and KBr , and γ_A^0 is the activity coefficient of Pr_4NBr in water.

Table III: Interaction Parameter g_0 for $\text{Pr}_4\text{NBr-KBr}$ System at 25°

I	g_0, mcl^{-1}	
	a^a	b^b
0.1	0.283	0.388
0.2	0.419	0.378
0.4	0.383	0.360
0.5	0.370	0.350
1.0	0.314	0.307
2.0	0.238	0.235
3.0	0.182	0.181
4.0	0.145	0.145

^a Values obtained by use of the Friedman formalism.

^b Values obtained by use of the Scatchard formalism.

0.5. Thermodynamic parameters for these systems are similarly calculated and the results are given in the following tables: ϕ in Table VII, g_0 in Table VIII, and b parameters in Table VI. (For numerical values of ΔG^{ex} , see ref 22.)

D. $\text{Me}_4\text{NBr-Et}_4\text{NBr}$ and $\text{Me}_4\text{NBr-Bu}_4\text{NBr}$ Systems at $y = 0.5$. Results for these systems are given in the following tables: ϕ in Table IX, g_0 in Table X, and b parameters in Table VI. (For numerical values of ΔG^{ex} , see ref 22.)

Discussion

As shown in Figure 1, ΔG^{ex} plotted against y for the $\text{Pr}_4\text{NBr-KBr}$ system at constant I give usual parabolic forms. The maximum height of the curve increases with I as expected but the curves at large I values are definitely skewed toward the left with their maximum points located at y values less than 0.5. In the study of the excess volume of mixing for $\text{Pr}_4\text{NBr-KBr}$ system,

Table IV: Osmotic Coefficients of R₄NX–KX Mixed Solutions at 25°

Me ₄ NBr–KBr		Et ₄ NBr–KBr		Bu ₄ NBr–KBr		Bu ₄ NCl–KCl		Bu ₄ NF–KF	
<i>I</i>	ϕ	<i>I</i>	ϕ	<i>I</i>	ϕ	<i>I</i>	ϕ	<i>I</i>	ϕ
0.1099	0.9116	0.1003	0.9152	0.1014	0.9050	0.0995	0.9300	0.0957	0.9671
0.1129	0.9116	0.1630	0.9023	0.1976	0.8900	0.1649	0.9256	0.0996	0.9681
0.1977	0.8954	0.2099	0.8877	0.2917	0.8777	0.2042	0.9184	0.1558	0.9801
0.2562	0.8880	0.2582	0.8810	0.5204	0.8652	0.2884	0.9223	0.1896	0.9900
0.3891	0.8747	0.3481	0.8721	0.7022	0.8546	0.4046	0.9211	0.2650	1.0119
0.5185	0.8682	0.4148	0.8681	1.0800	0.8532	0.4888	0.9272	0.3607	1.0332
0.6919	0.8629	0.5865	0.8572	1.2185	0.8547	0.5419	0.9278	0.4342	1.0557
1.0372	0.8600	0.5204	0.8597	1.6733	0.8559	0.8908	0.9563	0.4711	1.0671
1.3350	0.8609	1.1312	0.8476	2.1405	0.8528	1.1120	0.9717	0.7389	1.1530
1.4367	0.8602	1.8030	0.8631	2.7822	0.8470	1.7659	1.0257	0.9057	1.2016
2.0628	0.8751	2.7624	0.8851	2.7388	0.8486	2.3711	1.0523	1.3488	1.3428
2.1307	0.8730	4.4188	0.9800	4.9956	0.8252	3.4019	1.0816	1.7266	1.4453
2.1705	0.8797							1.7669	1.4768
2.8473	0.8952							2.3090	1.5935
3.3966	0.9161							2.9949	1.7313
4.4861	0.9554								

Table V: Interaction Parameter g_0 for R₄NX–KX Systems at 25°

<i>I</i>	g_0, m^{-1}							
	Me ₄ NBr–KBr		Et ₄ NBr–KBr		Bu ₄ NBr–KBr		Bu ₄ NCl–KCl	
	<i>a</i> ^a	<i>b</i> ^b	<i>a</i> ^a	<i>b</i> ^b	<i>a</i> ^a	<i>b</i> ^b	<i>a</i> ^a	<i>b</i> ^b
0.5	0.088	0.054	0.235	0.219	0.485	0.414	0.476	0.402
1.0	0.075	0.054	0.191	0.197	0.448	0.409	0.436	0.395
2.0	0.069	0.064	0.175	0.160	0.385	0.371	0.390	0.379
3.0	0.072	0.064	0.120	0.132	0.331	0.333	0.373	0.364
4.0	0.064	0.064	0.104	0.114	0.302	0.287	0.360	0.349

^a Values obtained by use of the Friedman formalism. ^b Values obtained by use of the Scatchard formalism.

Table VI: Values of *b* Parameters for R₄NX–MX Systems at 25°^{a,b}

	$b_{AB(0,1)}$	$b_{A3(0,2)}$	$b_{AB(0,3)}$	σ^a
Me ₄ NBr–KBr	0.0637	0	0	0.0015
Et ₄ NBr–KBr	0.243	-0.101	0.0136	0.0029
Bu ₄ NBr–KBr	0.425	-0.039	-0.0113	0.0038
Bu ₄ NCl–KCl	0.410	-0.0306	0	0.0028
Pr ₄ NBr–LiBr	0.047	-0.247	0.0304	0.0050
Pr ₄ NBr–NaBr	0.360	-0.207	0.0242	0.0029
Pr ₄ NBr–CsBr	0.338	-0.199	0.305	0.0022
Pr ₄ NBr–Me ₄ NBr	-0.036	-0.072	0.0116	0.0039
Pr ₄ NBr–Et ₄ NBr	-0.0583	0.0211	0	0.0020
Bu ₄ NBr–Me ₄ NBr	-0.135	0.172	-0.0229	0.0037

^a $\sigma = [\sum d^2 / (n - k)]^{1/2}$, where $d = \phi_{obsd} - \phi_{calcd}$, $n =$ no. of observations, and $k =$ no. of variable parameters. ^b See ref 22.

similar skewness was observed in ΔV^{ex} vs. y curves.^{9a} The skewness is due to the nonzero value of g_1 which may indicate the presence of ion triplets and higher multiplets in solution. In Figure 2 the values of $\log(\gamma_A/\tau_A^0)$ are plotted against I for Pr₄NBr (where A stands for Pr₄NBr) in the Pr₄NBr–KBr system at constant y . At $y = 0.0$, $\log(\gamma_A/\tau_A^0)$ is positive and increases with I indicating either the salting-out effect of

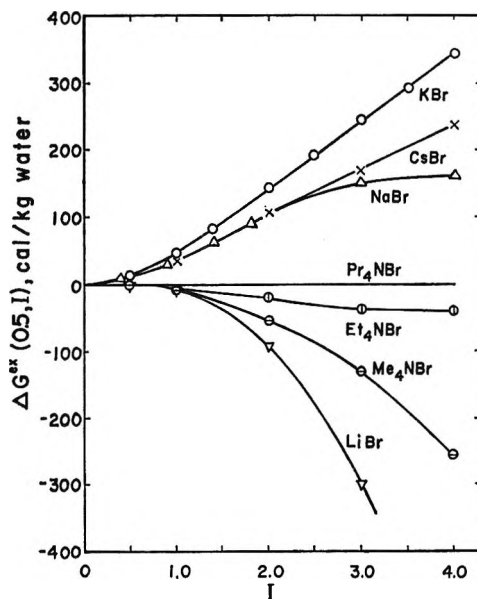


Figure 3. Plot of ΔG^{ex} vs. I for mixed solution of Pr₄NBr and MBr at $y = 0.5$ and 25°, where M denotes Li, Na, K, Cs, Me₄N, and Et₄N.

K⁺ toward Pr₄N⁺ or, more likely, the removal of the self-salting-in effect of Pr₄N⁺ by the increasing concen-

Table VII: Osmotic Coefficients of Pr₄NBr-MBr Mixed Solutions at 25°

PrNBr-LiBr		PrNBr-NaBr		PrNBr-CsBr		PrNBr-Me ₄ NBr		PrNBr-Et ₄ NBr	
<i>I</i>	ϕ	<i>I</i>	ϕ	<i>I</i>	ϕ	<i>I</i>	ϕ	<i>I</i>	ϕ
0.1033	0.9118	0.0676	0.9208	0.0664	0.9149	0.1044	0.8894	0.1274	0.8718
0.2144	0.8922	0.1198	0.9071	0.1192	0.8946	0.1061	0.8876	0.2914	0.8229
0.2466	0.8916	0.2780	0.8872	0.1218	0.8931	0.2598	0.8463	0.2918	0.8227
0.4716	0.8775	0.5470	0.8735	0.1262	0.8919	0.3212	0.8282	0.5888	0.7722
0.5401	0.8707	0.6966	0.8706	0.2852	0.8620	0.5167	0.8009	0.7390	0.7589
0.7480	0.8689	1.0184	0.8768	0.4116	0.8451	0.5756	0.7871	1.0716	0.7461
1.0137	0.8725	1.0204	0.8771	0.5498	0.8363	0.5981	0.7863	1.1106	0.7454
1.1450	0.8649	1.3473	0.8879	0.5620	0.8331	0.8305	0.7691	1.5004	0.7497
1.7285	0.9028	1.9724	0.9204	0.8532	0.8218	1.1702	0.7601	2.1946	0.7826
2.0056	0.9174	2.8189	0.9713	1.1560	0.8189	1.3160	0.7525	2.8975	0.8322
2.5865	0.9512	3.1230	0.9896	1.2392	0.8189	1.7350	0.7520	3.4349	0.8778
4.0531	1.0452	4.1419	1.0491	1.6604	0.8233	2.0523	0.7603	4.1464	0.9360
				2.1231	0.8369	2.3855	0.7713		
				2.3772	0.8455	2.3960	0.7699		
				2.5728	0.8532	3.0803	0.7989		
				3.1329	0.8750	4.7993	0.8827		
				3.7918	0.9026				

Table VIII: Interaction Parameter g_0 for Pr₄NBr-MBr Systems at 25°

<i>I</i>	PrNBr-LiBr		PrNBr-NaBr		PrNBr-CsBr		PrNBr-Me ₄ NBr		PrNBr-Et ₄ NBr	
	a^a	b^b	a^a	b^b	a^a	b^b	a^a	b^b	a^a	b^b
0.5	-0.015	-0.012	0.316	0.310	0.304	0.291	-0.046	-0.053	-0.020	-0.053
1.0	-0.054	-0.066	0.265	0.265	0.258	0.249	-0.053	-0.068	-0.032	-0.048
2.0	-0.156	-0.160	0.174	0.185	0.177	0.180	-0.090	-0.093	-0.035	-0.037
3.0	-0.226	-0.232	0.113	0.122	0.127	0.131	-0.099	-0.109	-0.030	-0.027
4.0	-0.275	-0.285	0.068	0.075	0.100	0.103	-0.109	-0.118	-0.017	-0.016

^a Values obtained by use of the Friedman formalism. ^b Values obtained by use of the Scatchard formalism.

Table IX: Osmotic Coefficients of Me₄NBr-Et₄NBr and Me₄NBr-Bu₄NBr Mixed Solutions at 25°

Me ₄ NBr-Et ₄ NBr		Me ₄ NBr-Bu ₄ NBr	
<i>I</i>	ϕ	<i>I</i>	ϕ
0.1270	0.8791	0.1276	0.8726
0.2848	0.8441	0.1284	0.8715
0.5777	0.8024	0.2964	0.8291
0.7118	0.7913	0.5884	0.7822
1.0298	0.7720	0.7126	0.7692
1.0499	0.7748	1.0513	0.7523
1.5885	0.7603	1.3823	0.7439
2.0870	0.7624	2.0446	0.7426
2.8328	0.7766	2.6220	0.7469
4.1898	0.8221	3.8856	0.7617

Table X: Interaction Parameter g_0 for Me₄NBr-Et₄NBr and Me₄NBr-Bu₄NBr Systems at 25°

<i>I</i>	Me ₄ NBr-Et ₄ NBr		Me ₄ NBr-Bu ₄ NBr	
	a^a	b^b	a^a	b^b
0.5	-0.039	-0.108	-0.094	-0.094
1.0	-0.023	-0.061	-0.057	-0.057
2.0	-0.025	0.003	0.007	0.007
3.0	-0.025	0.057	0.055	0.055
4.0	-0.031	0.083	0.087	0.087

^a Values obtained by use of the Friedman formalism. ^b Values obtained by use of the Scatchard formalism.

tration of K⁺. With the increase of y , the effect of K⁺ is seen to decrease at constant I as expected. The values of $\log(\gamma_A/\gamma_A^0)$, however, go through broad maxima in the range of I values between 1.0 and 2.0 suggesting a relatively strong self-salting-in effect of Pr₄N⁺ at high ionic strengths.

The values of ΔG^{ex} at $y = 0.5$ are plotted against I for Pr₄NBr-MBr systems (where M denotes here Li, Na, K, Cs, and Me₄N) in Figure 3. ΔG^{ex} values are

positive for systems with M = Na, K, and Cs but negative for systems with M = Li, Me₄N, and Et₄N. For these systems g_0 values calculated from eq 14 and 16 are plotted against I in Figure 4. The values of g_0 obtained by use of the Friedman formalism and the Scatchard formalism are in good agreement when I values are greater than 0.5. However, when the values of I are less than 0.5, g_0 values obtained by the two formalisms may deviate from each other considerably.

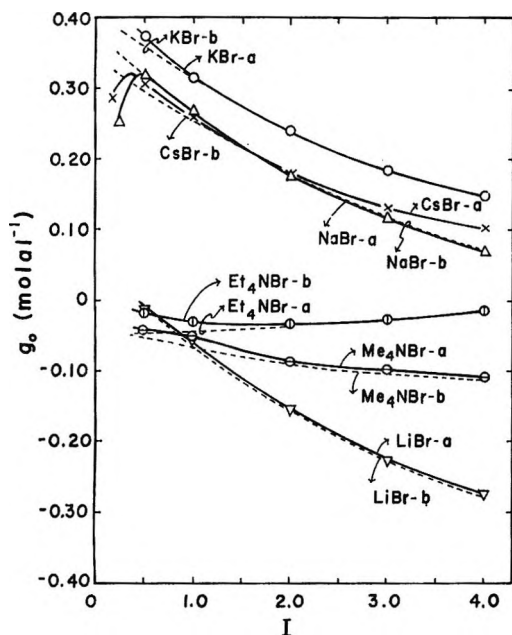


Figure 4. Plot of the free-energy interaction parameter, g_0 , vs. I for mixed solution of Pr_4NBr and MBr at 25° , where M denotes Li , Na , K , Cs , Me_4N , and Et_4N : a, calculated according to the Friedman formalism; b, calculated according to the Scatchard formalism.

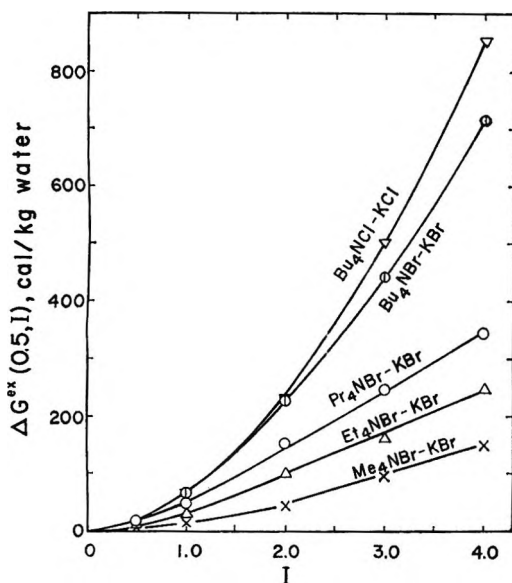


Figure 5. Plot of ΔG^{ex} vs. I for mixed solution of KBr and R_4NBr at $y = 0.5$ and 25° , where R denotes Me , Et , Pr , and Bu .

The deviation is probably due to the fact that the Scatchard formalism does not take into account the existence of the limiting law between $\log g_0$ and \sqrt{I} . According to Friedman^{6b} the limiting slope for two 1-1 electrolytes in water at 25° is given by

$$(1/g_0)dg_0/d\sqrt{I} = 2.353 \text{ as } I \rightarrow 0$$

Similarly, the values of ΔG^{ex} at $y = 0.5$ are plotted against I for $\text{KCl}-\text{Bu}_4\text{NCl}$ and $\text{KBr}-\text{R}_4\text{NBr}$ systems

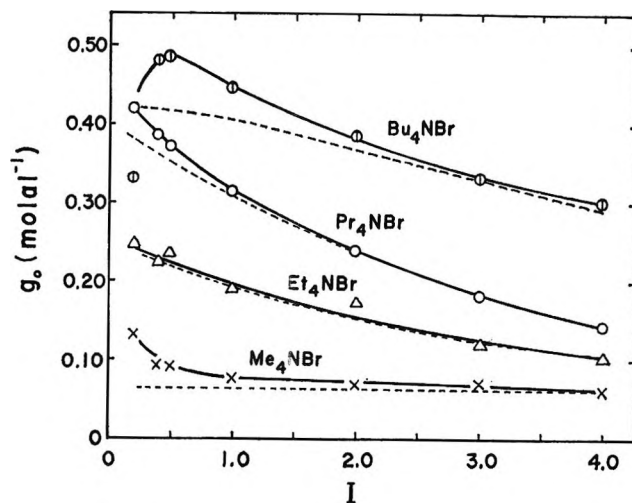


Figure 6. Plot of g_0 vs. I for mixed solution of KBr and R_4NBr at 25° , where R denotes Me , Et , Pr , and Bu : a, calculated according to the Friedman formalism; b, calculated according to the Scatchard formalism.

(where R denotes here Me , Et , Pr , and Bu) in Figure 5. ΔG^{ex} values are all positive for these systems and increase both with I and ion size of R_4N^+ . Corresponding g_0 values are plotted against I in Figure 6. Similar comments as above can be made concerning g_0 values at low ionic strengths obtained by the two formalisms.

The values of g_0 at $I = 0.5$ for various systems are summarized in Table XI. Values of h_0 , the enthalpy

Table XI: Values of g_0 and h_0 at $I = 0.5$ for Various Systems at 25°

System	g_0 , m^{-1}	System	h_0 , m^{-1} ^a
$\text{KBr}-\text{Me}_4\text{NBr}$	0.088	$\text{KCl}-\text{Me}_4\text{NCl}$	0.201
$\text{KBr}-\text{Et}_4\text{NBr}$	0.235	$\text{KCl}-\text{Et}_4\text{NCl}$	0.198
$\text{KBr}-\text{Pr}_4\text{NBr}$	0.350	$\text{KCl}-\text{Pr}_4\text{NCl}$	-0.588
$\text{KBr}-\text{Bu}_4\text{NBr}$	0.485		
$\text{KCl}-\text{Bu}_4\text{NCl}$	0.476	$\text{Pr}_4\text{NCl}-\text{LiCl}$	-1.171
$\text{Pr}_4\text{NBr}-\text{LiBr}$	-0.015	$\text{Pr}_4\text{NCl}-\text{CsCl}$	-0.741
$\text{Pr}_4\text{NBr}-\text{NaBr}$	0.316	$\text{Pr}_4\text{NCl}-\text{Me}_4\text{NCl}$	-1.036
$\text{Pr}_4\text{NBr}-\text{CsBr}$	0.304	$\text{Pr}_4\text{NCl}-\text{Et}_4\text{NCl}$	-0.521
$\text{Pr}_4\text{NBr}-\text{Me}_4\text{NBr}$	-0.046	$\text{Me}_4\text{NCl}-\text{Et}_4\text{NCl}$	-0.084
$\text{Pr}_4\text{NBr}-\text{Et}_4\text{NBr}$	-0.020		
$\text{Me}_4\text{NBr}-\text{Et}_4\text{NBr}$	-0.059		
$\text{Me}_4\text{NBr}-\text{Bu}_4\text{NBr}$	-0.108		

^a Data taken from ref 10.

interaction parameter, for similar systems reported by Wood and Anderson¹⁰ are also tabulated for comparison. As shown in the table, the values of g_0 and h_0 are quite different when Pr_4N^+ ions are involved and, in general, the absolute values of g_0 are considerably smaller than those of h_0 . In the study of the excess volume of mixing, the volume interaction parameters v_0 have been found to be particularly large when Pr_4N^+ and Bu_4N^+

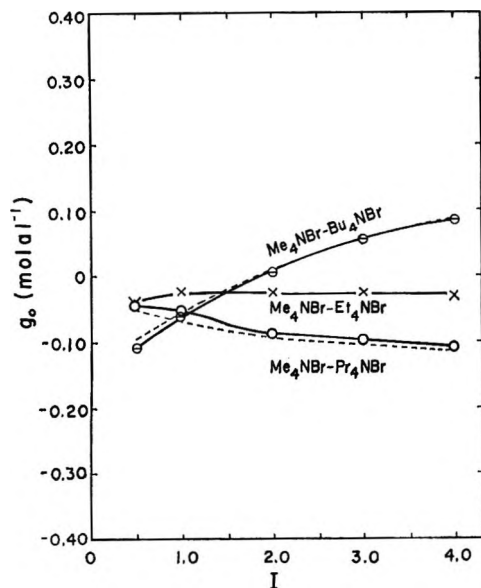


Figure 7. Plot of g_0 vs. I for mixed solution of Me_4NBr and R_4NBr at $y = 0.5$ and 25° , where R denotes Et , Pr , and Bu .

ions are involved.⁹ A positive g_0 on mixing AX and BX solutions implies that replacing A-A and B-B interactions by A-B interactions produces an increase in the free energy of the system. This means that such replacements will take place less frequently than would be expected on a purely chance basis. A negative g_0 means, on the other hand, that the formation of A-B pairs is more favored than would be expected from statistical encounters of A and B . In this context, A-B pairs such as $\text{Li}^+-\text{Pr}_4\text{N}^+$, $\text{Me}_4\text{N}^+-\text{Et}_4\text{N}^+$, $\text{Me}_4\text{N}^+-\text{Pr}_4\text{N}^+$, $\text{Me}_4\text{N}^+-\text{Bu}_4\text{N}^+$, and $\text{Et}_4\text{N}^+-\text{Pr}_4\text{N}^+$ are favored but $\text{K}^+-\text{R}_4\text{N}^+$, $\text{Na}^+-\text{Pr}_4\text{N}^+$, and $\text{Cs}^+-\text{Pr}_4\text{N}^+$ pairs are disfavored when they are compared with the corresponding A-A and B-B pairs. If g_0 changes sign with the change of ionic strength, the situation would be more complicated. The case in point is $\text{Me}_4\text{NBr}-\text{Bu}_4\text{NBr}$ system shown in Figure 7. For this mixed electrolyte solution g_0 is negative when I is less than 2.0 but it becomes positive when I is greater than 2.0. At high ionic strengths A-A and B-B pairs are favored over A-B pairs presumably due to the strong attraction between Bu_4N^+ ions. The relative mutual attraction between two large tetraalkylammonium ions may be an instance of "hydrophobic bonding"¹¹ arising from the large entropy change of water which accompanies the formation of pairs and higher multiplets.

In this connection it is important to recognize the difference which exists between g_0 on one hand and h_0 or v_0 on the other. Two factors influence the numerical value of g_0 : the first is the relative probabilities that A-B pairs will form compared with A-A and B-B pairs; the second is the effect on ΔG^{ex} when A-B pairs do form. The values of h_0 and v_0 are similarly influenced by the first factor but not by the second, because the probability of formation of pairs is not directly affected by

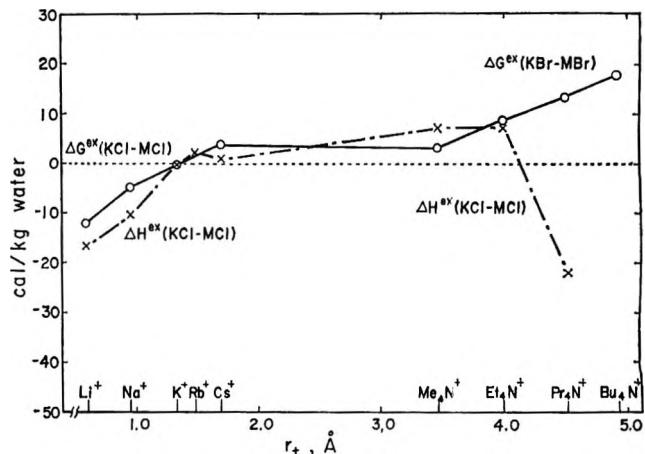


Figure 8. ΔG^{ex} and ΔH^{ex} for aqueous KX-MX mixtures at $I = 0.5$ and 25° plotted against the crystallographic radii of M^+ . ΔG^{ex} values for KCl-LiCl , KCl-NaCl , and KCl-CsCl are taken from ref 1, 2d and 3a, and ref 2c, respectively. ΔH^{ex} values for KCl-MCl are taken from ref 10, and Y. C. Wu, M. B. Smith, and T. F. Young, *J. Phys. Chem.*, **69**, 1868 (1965).

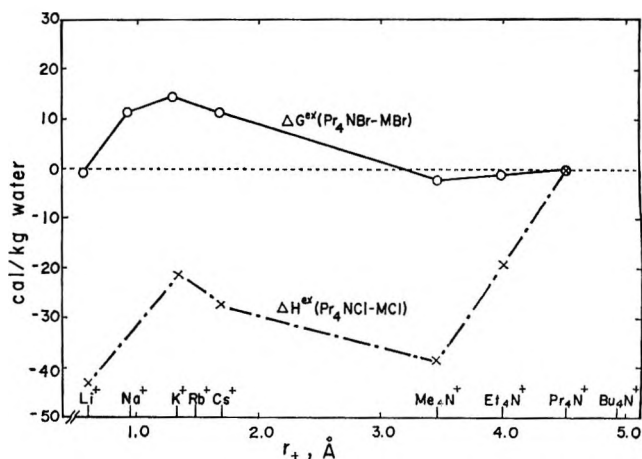


Figure 9. ΔG^{ex} and ΔH^{ex} for aqueous $\text{Pr}_4\text{NX-MX}$ mixtures at $I = 0.5$ and 25° plotted against the crystallographic radii of M^+ . ΔH^{ex} values are taken from ref 10.

the extent of pair formation. In other words, if the formation of a pair makes a positive contribution and fewer or more A-B pairs form than expected, then this fact disrupts or promotes the pair formation and the value of g_0 itself is affected by this "feedback." In contrast this "feedback" is not present for h_0 or v_0 .

In symmetrical mixtures of AX and BX solutions, g_0 consists mainly of free energies of the pairwise interaction and triplet interaction⁷

$$g_0 = g_{\text{pairs}}^* + I g_{\text{triplets}}^*$$

$$g_0 = 2g_{\text{AB}}^* - g_{\text{AA}}^* - g_{\text{BB}}^* + I(2g_{\text{ABX}}^* - g_{\text{AAX}}^* - g_{\text{BBX}}^*) + \text{triplets formed from three ions of the same charge} \quad (27)$$

where g_{ij}^* is the free energy of interaction of ions i and j , and g_{ijk}^* is the free energy of interaction of three ions i, j , and k . Though it will be of great interest to find the values of g_{ij}^* and g_{ijk}^* , it is clearly impossible with our experimental approach at this stage. Qualitatively, however, our results seem to be consistent with the postulate of hydrophobic interaction in which the values of $g_{R_iN^+ - R_jN^+}^*$ are small, probably much smaller than those of g_{ij}^* , where i and j are both alkali metal ions. Theoretical calculations of these interaction free energies using the method of Friedman and Ramanathan²³ may be a useful next step and we are working toward this direction.

In Figure 8, values of ΔG^{ex} and ΔH^{ex} for KCl-MCl and KBr-MBr systems are plotted against the crystallographic radii of M^+ ions. In the mixing processes involving the same pair of cations the change of common anion from chloride to bromide should not have any great effect on the excess thermodynamic quantities when I is 0.5.²⁴ On this basis we can obtain $T\Delta S^{\text{ex}}$ by subtracting ΔG^{ex} from ΔH^{ex} . As shown in Figure 8, the values of ΔG^{ex} and ΔH^{ex} are not greatly different for $K^+ - M^+$ where M^+ stands for alkali metal ions, Me_4N^+ , or Et_4N^+ . For $K^+ - \text{Pr}_4\text{N}^+$, however, the difference between ΔG^{ex} and ΔH^{ex} is very large, indicating

large negative ΔS^{ex} . This result is expected from the water-structure promoting effect of Pr_4N^+ . In Figure 9 similar plots are shown for $\text{Pr}_4\text{NCl} - \text{MCl}$ and $\text{Pr}_4\text{NBr} - \text{MBr}$ systems. Here ΔG^{ex} vs. r_+ plot is widely separated from and nearly parallel to ΔH^{ex} vs. r_+ plot indicating that ΔS^{ex} is large negative and approximately constant regardless of the type of M^+ ions. It shows clearly that the entropy effect of Pr_4N^+ is large and dominating over the corresponding effect of M^+ . A similar conclusion on the large structural effect of Pr_4N^+ ions in aqueous solution has been reached by Wood and Anderson.¹⁰

Acknowledgments. We wish to express our sincere gratitude to Dr. Richard M. Rush for his generous assistance on the computer calculation carried out at the Oak Ridge National Laboratory. We are indebted for valuable suggestions and comments of Professors Henry S. Frank and Harold L. Friedman. This research has been supported by the National Science Foundation (GP-8870) and the Public Health Service.

(23) H. L. Friedman and P. S. Ramanathan, *J. Phys. Chem.*, **74**, 3756 (1970).

(24) We found this to be true for KCl-Bu₄NCl and KBr-Bu₄NBr systems. At infinite dilution the difference due to the use of different common anion should vanish.

Formation of Diamond. IV. The Behavior of the Diamond-Forming Reaction^{1a,b} with Respect to Catalyst Composition

by P. Cannon* and E. T. Conlin, II

General Electric Research and Development Center, Schenectady, New York (Received June 29, 1970)

Publication costs assisted by the General Electric Co.

Changes in the chemical composition of the catalysts used in the diamond-forming reaction lead to wide variations in the formation, growth, and properties of diamond crystals. Catalysts containing more than one metallic component were studied: examples were Ni-Cu, Cu-Mn, and Mn-Ni systems. The information gained concerns the numbers of crystals formed, their size, and their rates of growth. Catalyst systems in which only one component is a known catalyst yield different results from those in which more than one component is an effective catalyst. For the former, growth processes are not particularly dependent on catalyst composition. However, the latter give spectacular composition-dependent effects which are shown to be the consequence of a number of simultaneous and possibly unrelated reactions such as diamond formation, carbon dissolution, and the formation of interstitial carbides. Attention is also drawn to the ability of some catalyst components to absorb air gases and hydrogen.

Introduction

The transition metal catalyzed graphite-diamond¹ reaction is subject to strong chemical effects from impurities.^{2,3} In this work, we study the involvement of the transition metal in the reaction by making gross changes in the chemical composition of the catalyst.

Ni-Cu, Cu-Mn, and Ni-Mn catalyst alloys were used under conditions such that the diamonds formed were monocrystals. Quantitative nucleation and growth responses could thus be measured. Nickel was studied because it is a powerful catalyst for the transformation, and copper was included because of the existence of a continuous range of solid solutions with Ni (and Mn) of simple melting behavior. The inclusion of manganese permitted the study of metals from each of groups VII, VIII, and I.

Diamond formation was studied at a variety of catalyst compositions and pressure-temperature conditions. Carbon solubilities were measured in the Ni-Mn system, where the rate of diamond formation was found to be highly composition dependent.

Experimental Section

(i) *General.* The statistical experimental designs of Box⁴ were used to separate the effects of pressure, temperature, metal-carbon ratio, and catalyst composition.

The high-pressure synthesis technique has been described before.^{1b} We used indirectly heated cells of about 2-cc internal volume, and specimens were loaded into the sample holders by extrusion at 500 psi. The elapsed time at pressure-temperature conditions was usually 20 min.

Graphite was of spectroscopic quality, with Na, Mg, and Si present in the 1-3-ppm range; the copper was

Mackay electrolytic powder, % oxygen was 1.0; the nickel was Inco grade C (spectroscopic), which contains a slight trace of Fe but no B, Co, or Si; the manganese was Fisher Certified Reagent, assay 99.94%.

The measured responses included the weight and number of crystals formed in each run plus the weight of growth on a seed (usually a rotation twin).

(ii) *Ni-Cu System.* In preliminary work, the composition Ni:Cu equal to 2:1:8 (atomic) gave, at 1450° and 55 kbars, small yields of high-quality green diamonds, and good, even growth was observed on the (111) faces of natural twin seed crystals. The effects of the copper were then studied at the conditions at which nucleation occurred in nickel alone; this was the technique used earlier² to study poisons.

Even though many of the *P-T* levels used were well within the graphite-diamond phase boundary, some etching of the seeds was still seen. New growth on seeds is shown in Table I.

These results show an almost negligible effect on growth of increases in the copper content of the alloy, from 33 to 66%. Spontaneous nucleation of new diamond was seen only at the higher temperatures and pressures. The system is apparently insensitive to the depression in melting point which might be expected for the change in composition from 33 Cu to 66% Cu,⁵

(1) (a) F. P. Bundy, *et al.*, *Nature*, **176**, 51 (1955); (b) H. P. Bovenkerk, *et al.*, *ibid.*, **184**, 1094 (1959).

(2) P. Cannon and E. T. Conlin, *Int. Symp. Reactiv. Solids [Proc.]*, **5th**, 1964, 362 (1965).

(3) P. Cannon, *J. Amer. Chem. Soc.*, **84**, 4255 (1962).

(4) G. E. P. Box, *Biometrics*, **10**, 16 (1954).

(5) See, for example, "The Constitution of Binary Alloys," 2nd ed., M. Hanson, Ed., McGraw-Hill, New York, N. Y., 1958, p 602. The melting point shift at 1 atm shown there for the cited composition change is approximately 130°.

Table I: Seed Growth Response (in mg) in the Diamond Forming System Ni-Cu-C

Temp. °C	Pressure, kbars	Metal:carbon ratio (atomic)			
		1:3		3:1	
		Cu:Ni (atomic)			
		1:2	2:1	1:2	2:1
1260	48	+0.05	+0.08	-0.11	+0.17
	56	+0.17 ^a		+0.03 ^a	+0.36
1450	48	-0.16	-0.21	-0.27	-0.92
	56	... ^a	-0.16	+0.78 ^a	+1.21

^a Result is statistically significant.

assuming the general characteristics of the Ni-Cu room pressure phase diagram are retained.

(iii) *Cu-Mn System.* The lack of Cu-Mn alloy tube for use as cell liners was an experimental difficulty. Exploration was done using Ti, Ta, Zr, Nb, Ni, and Ni-Cu-Mn liner tubes. It was found that diamond could be grown in such arrangements provided the temperature was in excess of 1250°, even though the catalyst could be melted well below this value. Nucleation occurred especially when the metal sleeve had the ability to absorb gases. Systematic experiments were then done in Ti sleeves at conditions within the following ranges: temperature, 1000–1300°; pressure; 40–50 kbars; Cu:Mn atomic ratio, 2:1–1:2, and metal:carbon atomic ratio, 1:3–3:1. Large variances were observed in the quantitative results, obscuring any general conclusions, though conditions involving higher pressures and temperatures usually caused measurable nucleation and growth of diamond.

A peculiar distribution of fluorescence characteristics was observed in this set of seeds after exposure to high-pressure, high-temperature conditions, depending only on the particular Cu-Mn composition involved, as outlined in Table II.

Table II: Fluorescence Characteristics of Seed from Copper-Manganese Catalysts

Cu:Mn ^a		
1:3	1:1	3:1
Yellow (w)	Yellow (v-w)	Yellow-blue (m)
Blue (m)	Yellow-blue (m)	Yellow (m)
Yellow (s)	Yellow (w)	Blue (m)
Yellow (w)	Yellow-blue (m)	Blue (m)
Yellow (w)	Blue (m)	Blue (m)
Yellow (v-w)	Blue (m)	
Yellow (w)		

^a The results come from runs made at various *p*, *T* conditions for each catalyst composition.

(iv) *Ni-Mn System.* *Yield and Particle Count Data.* This system forms large numbers of small crystals. Mass yields are shown in Table III. The crystals

varied in color from a strong green at the high nickel concentrations to a beautiful, almost imperceptible lime green at Mn concentrations higher than 60%. As the Mn concentration in the reaction mix was increased, the particle size distributions peaked at progressively lower mesh sizes, and there was also a tendency for cubic crystals to be formed. There is a profound effect of metal:carbon ratio on mass yield, statistically significant at better than the 99% confidence level, even in the composition range metal:carbon less than 3:1. Also, when the metal:carbon ratio was 6:1, regardless of pressure-temperature conditions, there was no formation of new diamond and the seeds were badly etched. The formation of a metal carbide phase, M:C > 3:1, may offer effective competition for the carbon which might otherwise form diamond; textural evidence supporting this point of view was also obtained. The other variables having a significant effect on the yield response were pressure, Mn:Ni ratio, and all the binary interactions which involve metal:carbon ratio and the other variables. The complex form of the effect of Mn:Ni ratio on the yield response is summarized in Figure 1.

Table III: Mass Yield of Diamond Crystals in mg (Mn-Ni System)

Response	<i>T</i> , °C	<i>P</i> , kbars	Metal:carbon ratio (Mn:Ni)			
			1:3		3:1	
			1:2	2:1	1:2	2:1
1225	48.0	43.0	47.2	263.3 ^a	Nil ^a	
	57.5	39.0 ^a	93.6	839.0 ^a	Nil	
1440	48.0	Nil	Nil	505.3 ^a	Nil	
	57.5	35.4	57.1	963.8	1002.9	

^a Statistically significant result.

Using the particle count/mass yield quotient as the response rather than mass yield alone, the effect of metal:carbon ratio disappears (Table IV). The effect of pressure now becomes significant at the 99% level, with increases giving larger quotients which are further increased by the positive interaction between pressure and temperature. Such changes also cause concre-

Table IV: Diamond Yield from Mn-Ni System, Particle Number/mg

<i>T</i> , °C	<i>P</i> , kbars	Metal:carbon 1:3 Mn:Ni ratio (atomic)			
		1:3		3:1	
		1:2	2:1	1:2	2:1
1225	48.0	14	24	14	Nil
	57.5	171	219	226	Nil
1410	48.0	Nil	Nil	27	Nil
	57.5	95	100	144	57

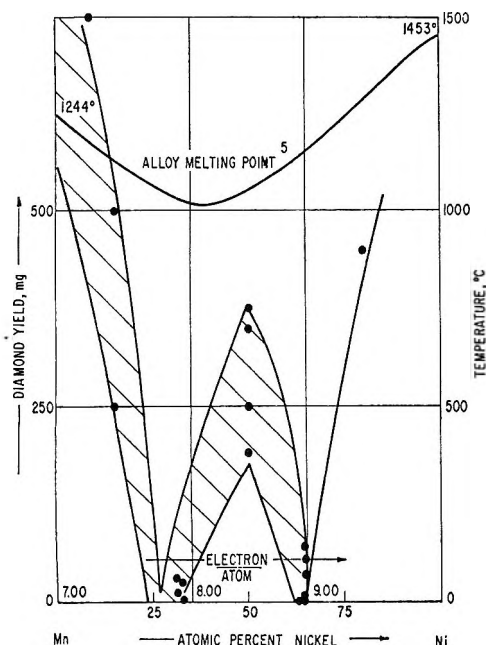


Figure 1. Complex dependence of diamond yield on nickel-manganese catalyst composition.

tionary polycrystalline overgrowth, in contrast with the more nearly coherent overgrowth observed in the Ni-Cu experiments.

(v) *Ni-Mn System, Kinetic Effects.* By varying the synthesis time and by measuring both the yield and particle count/weight, two processes can be distinguished. The experimental data are shown in Figures 2 and 3. There is no increase in the total particle count after about 90 sec, while the mass yield continues to increase over a period that is at least twice as long. A remarkable feature of this system is the reproducibility of the particle count data, each point representing the result from a separate synthesis run; the absolute count is dependent on conditions and sample geometry.

(vi) *Ni-Mn System. Carbon Solubilities in the Alloy at Superpressure Conditions, and Metallographic Data.* Carbon solubility experiments were made by exposing disks of Ni-Mn alloys, encased in an excess of graphite, to superpressure conditions, (41 kbars, 1200°, just below the threshold for diamond formation), for various times. The disks were removed, cleaned, surface ground, and analyzed. Metallographic examination of duplicate samples was made by Mrs. T. Brassard of this laboratory. Samples of graphite which had been adjacent to the disks were analyzed for their nitrogen content. The results are shown in Tables V and VI.

The metallographic examination showed: (a) small flakes and nodules of graphite dispersed in a cracked primary phase (33 Mn-66 Ni) (Figure 4); (b) patterns like those of divergent pearlite, almost complete transformation of the specimen (50 Mn-50 Ni) in Figure 5; (c) a eutectoid pattern, shown in Figure 6 (66 Mn-33 Ni). Some specimens in this composition

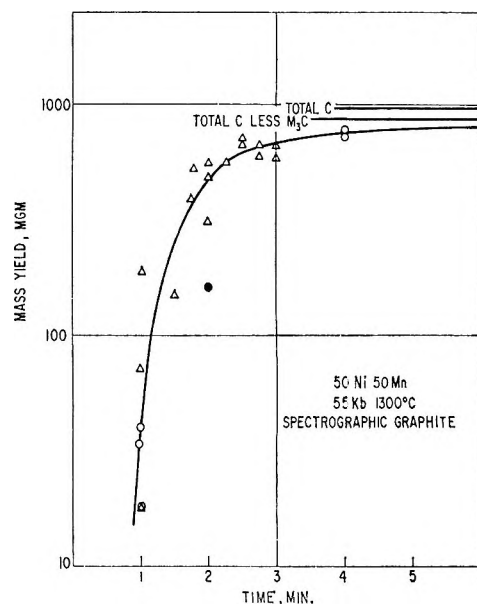


Figure 2. Mass yield of diamond vs. time 50:50 (atomic) nickel-manganese catalyst; 55 kbars, 1300°.

Table V: Carbon Contents (wt %) After 10 min at 41 kbars, 1200° in Ni-Mn Alloys Contained in Graphite Tubes

(A) 66 Mn-34 Ni Al ₂ O ₃ liner	(B) 50 Mn-50 Ni Al ₂ O ₃ liner	(C) 33 Mn-67 Ni Al ₂ O ₃ liner
0.453	3.58	0.562
0.396	3.38	0.644
0.539		
0.381		
Av wt % 0.44	3.48	0.60

Table VI: Kinetic Effects in Solubility of Carbon in 66 Mn-34 Ni at 41 kbars, 1200° (Al₂O₃ Liners Throughout)^a

Time, min	Wt % C ^b
10	0.528, 0.514, 0.449, 0.486
30	0.661, 0.87
60	1.03, 1.13

^a Control, unequilibrated alloy slugs: 0.046, 0.044, 0.045, 0.046. ^b Ten determinations on separate graphite samples from different runs gave nitrogen contents of 0.009% (ranging from 0.007 to 0.012%).

range show less complete eutectoid formation, but the total carbon content values were almost identical; (d) the metallographs could not themselves be used for the determination of carbon solubility; (e) the location of the eutectoid near 66 Mn-33 Ni (consisting of primary phase and carbide crystals), and the monophasic near 33 Mn-66 Ni, indicates that the phase diagram must shift considerably from the room pressure behavior; (f) the growth rate of the carbide phase is sen-

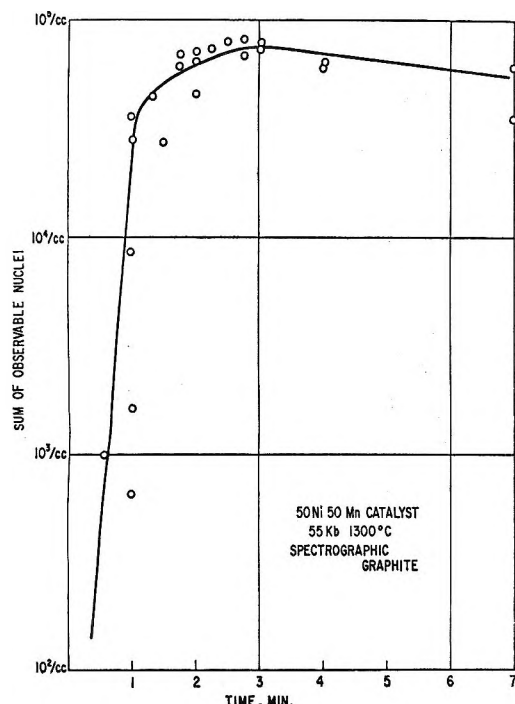


Figure 3. Number of observable diamond crystals per cubic centimeter of reaction volume 50:50 (atomic nickel-manganese catalyst; 55 kbars, 1300°).

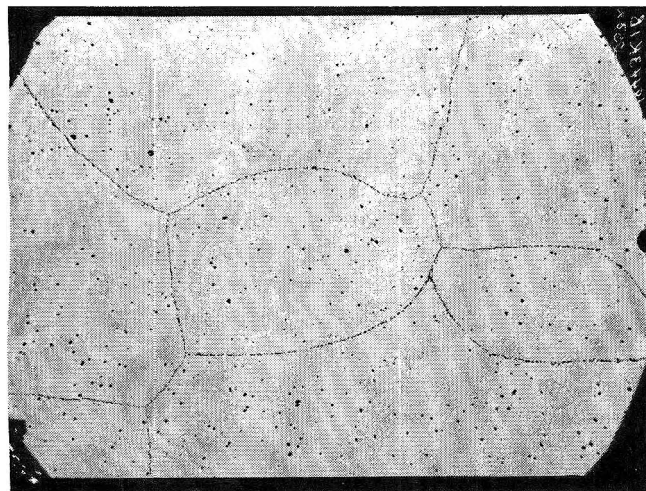


Figure 4. Small flakes and nodules of graphite dispersed in a cracked primary phase (33 Mn-67 Ni), approximately 150 \times .

sitive to the Mn:Ni ratio (from 66 Mn-34 Ni to 75 Mn-25 Ni), for great increases in crystallite size can be obtained by holding such specimens for periods up to 1 hr at superpressure conditions; (g) this carbide phase is involved in the diamond-forming process in an inhibitory way (Figure 7). A mass of diamond was grown at the edge of an Ni-Mn slug, at 50 kbars and 1200°. The slug showed a eutectic field around the diamond mass. The diamond crystals had grown up to and around the carbide particles; the carbide took up space and carbon which would presumably otherwise have been used by the system to form diamond. The interface between

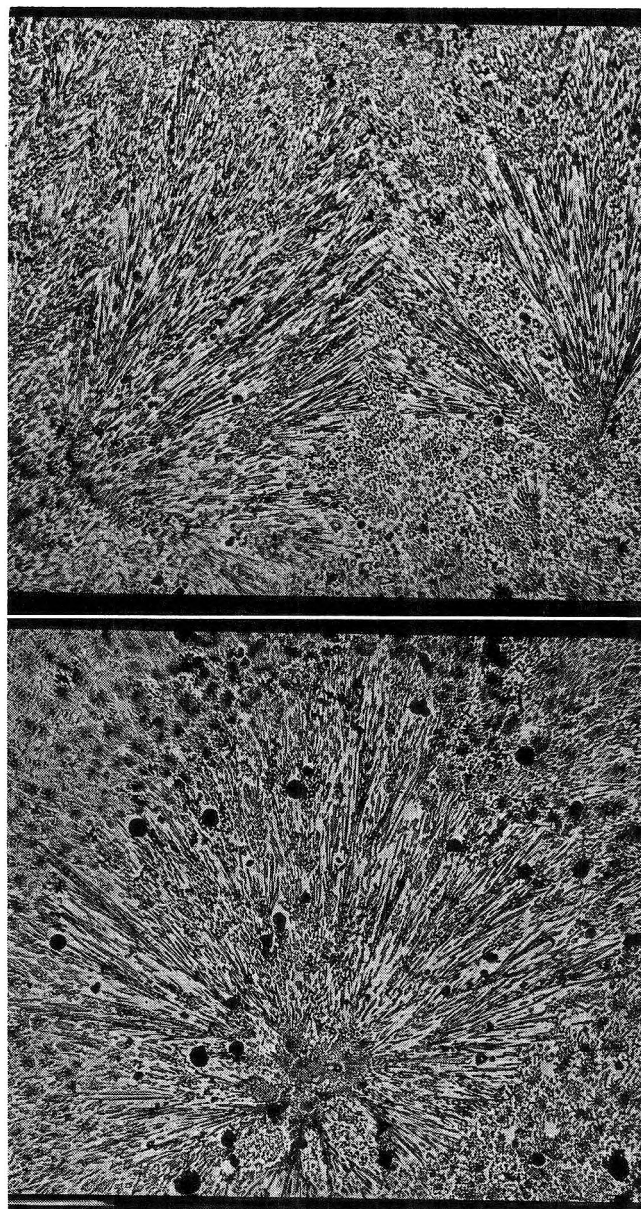


Figure 5. Divergent pearlitic patterns showing almost complete transformation of the specimen with some spheroidal graphite. 50 Mn-50 Ni + approximately 3% carbon; quenched from 45 kbars and 1200°, approximately 150 \times .

carbide and primary phase was curved, indicating that the carbide was decomposing; however, the process of diamond formation itself occurred not at this interface, but many microns away at the interface between primary phase and diamond. (h) Samples which contained pearlite fans were found to be under so much internal stress that they cracked and/or underwent a process of surface relieving within about 14 days. Examination of the specimens after 6 months showed no further changes.

Discussion

(i) *Synopsis of Results.* There are at least two major classes of results of the addition of the second component of a diamond-forming catalyst alloy. In the first of these, the second component appears as a

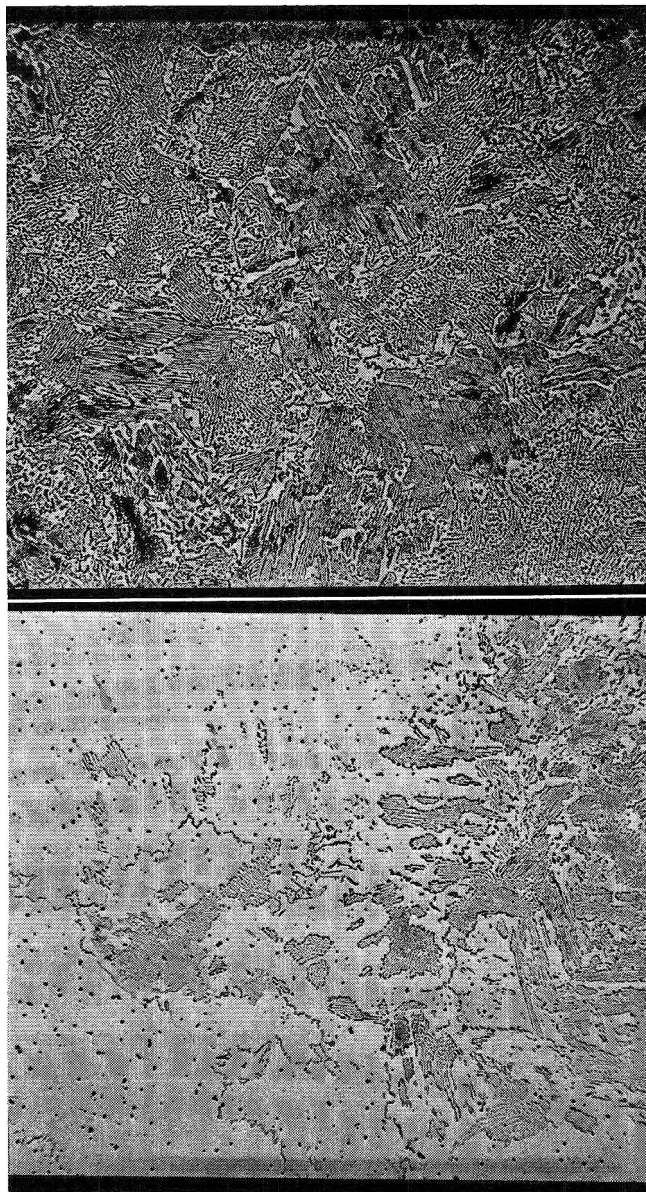


Figure 6. Eutectic field in 66 Mn-34 Ni after exposure to 45 kbars and 1200°, approximately 150 \times .

diluent (as in the case of Cu in Ni-Cu catalysts) since the overall diamond nucleating characteristics of the catalyst alloy are relatively insensitive to changes in its composition. Quite low concentrations of the primary component will continue to cause the nucleation of diamond, and in fact use of the alloy 95% Cu-5% Ni as a catalyst⁶ has been successful. The diluent component does not appear to have any direct effect on the habit of the crystals formed unless it can be incorporated into the growing diamonds (as is the case with silicon⁷).

Two-component diluted catalysts will not necessarily demonstrate their diamond-forming ability at temperatures as low as the alloy melting point. In Ni-Cu, diamond nucleation occurs at temperatures nearer to the melting point of the Ni-C high-pressure eutectic than to the melting point of the Ni-Cu alloy. Again,

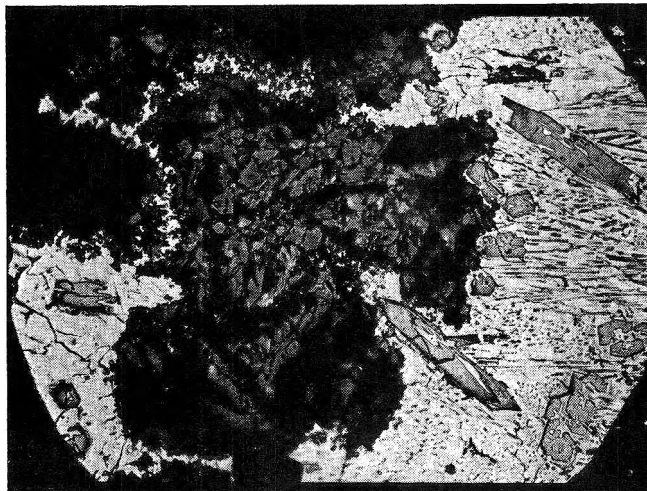


Figure 7. Diamond growth in the presence of Ni-Mn catalyst at 50 kbars and 1200°. The diamond is the dark phase on the left of the micrograph; the carbide particles shown on the right are in the process of decomposition, but this decomposition is not sufficiently fast to prevent the incorporation of large amounts of metal and some carbide particles in the diamond formed, approximately 200 \times .

in Cu-Mn, in spite of the experimental difficulties, the system's diamond-forming abilities were simply not in evidence at the alloy minimum melting point, which is very low (ca. 870° for the eutectoid at 1 atm). The main effect of the presence of the diluent thus appears to involve the rate of growth of diamond crystals rather than the rate of nucleation. This was shown by the ease with which even, coherent seeded growth could be deposited using the Ni-Cu catalyst; in other cases, the rates of diamond growth were so great as to make the deposition of such smooth material rather difficult.

The other major class of results appears when the second component is effective by itself as a catalyst. Here, spectacular and complex composition-dependent effects are seen, especially at conditions near the threshold for the reaction. Thus, in the Ni-Mn case, transformation of graphite to diamond is slowest when the average number of electrons per atom in the catalyst alloy has the integral values 8 and 9, especially at pressure-temperature conditions not far removed from the threshold values for successful nucleation. In addition, the evidence is strong that the formation of a carbide phase (metal:carbon ratio > 3:1) effectively competes for carbon with the diamond forming reaction. Near the composition 70 Mn-30 Ni, an extensive formation of a carbide phase with a pearlite morphology occurs, and this phase is so stable that exposure to high temperature conditions over a period of hours is required to sustain decomposition to metal plus graphite. The rate of diamond formation here is very low. The

(6) H. M. Strong, *J. Chem. Phys.*, **39**, 2057 (1963).

(7) P. Cannon and E. T. Conlin, II, *J. Amer. Chem. Soc.*, **86**, 4540 (1964).

function of the second component of the catalyst, itself a catalyst for the reaction, is then to modify the rate of appearance of microscopically observable crystals as well as their rate of growth. That these two processes are separable is shown by the data on Figures 2 and 3.

A third function of the metallic components involves a sensitivity to air gases, hydrogen and other extraneous impurities of low atomic number. The varying abilities of the catalyst metals to trap these species have profound effects on the reaction, exemplified by the Cu-Mn system. Some iron-based catalyst systems are equally sensitive, but Ni-based systems usually are not so strongly affected. In addition to a direct electronic poisoning effect, some of these phenomena may be caused by the decomposition of a carbide by nitrogen, to yield a stable nitride which would be ineffective as a catalyst and a transport medium. However, a general description of the known behavior of the catalyst systems on the basis of such reaction schemes is not yet possible as more superpressure thermodynamic data on the interstitial compounds are needed.

The solubility data for carbon in Ni-Mn alloy shows variations in the 10-min uptake data which depend on both the rate of dissolution of carbon and upon impurity uptake from the experimental vessel. Thus, when pyrophyllite vessels (which give off sulfur-bearing gases) are used to contain the solubility experiments, the results for carbon content are always lower than when pure alumina liners are employed. The dissolution of carbon in these alloys appears to occupy periods sometimes longer than 1 hr, while diamond formation (at only slightly higher pressures) occurs quite rapidly and is essentially complete in minutes. It is unlikely that there is any direct, causal relation between the rate of solution of carbon and the rate of diamond formation: they proceed on different time bases. Some systems, *e.g.*, 50 Mn-50 Ni, will transform all the available carbon to diamond in less time than they take to reach equilibrium during the dissolution of carbon at only marginally lower pressures. This is a clear indication of the nonequilibrium nature of the diamond-forming reaction.

(ii) *Interpretation.* The overall results depend on the simultaneous operation of three and perhaps four kinds of chemical reaction. These are the uptake and transport of carbon by the molten catalyst metal, the removal of growth and catalyst poisons, for example S or O, by the catalyst itself, the excitation of the carbon

into a diamond-forming state and its subsequent removal as solid diamond from the reaction mix, and the side reaction of carbon and the catalyst to yield a solid carbide. The relative importance of these steps on the overall progress of the reaction is affected by the composition of the catalyst. Equilibrium carbon solubilities do not markedly influence the rate of formation of diamond, though the rates of carbon transport through the molten metals affect the rate of growth on seed diamonds. It has already been demonstrated³ that monoatomic carbon is directly involved in the growth of diamond by the catalyzed reaction; from the present results it would seem likely that single atoms or very small clusters of the catalyst metal are in their turn the active form of the catalyst. The reasons for asserting this to be so are as follows: first, the catalyst metal in all the cases discussed here had to be in the liquid state; secondly, the further the temperature is removed from the alloy melting point the faster the reaction goes.

The catalytic effectiveness of dilute alloys also suggests an interatomic encounter between the catalyst and the carbon. Interpretations involving the formation of extremely carbon-rich carbide phases as an integral part of the reaction pathway⁸ leading to diamond cannot be supported by this work; rather the formation of carbide phases seems to represent a diversion of carbon from the desired route. Variations in observed metallographic textures at the same nominal composition could thus be ascribed to the time and purity dependent effects of growth and decomposition of such carbide phases. Previous evidence for competing carbide-forming reactions was found in systems containing Al² and Si⁷ as catalyst components. That some transition metal carbides may be stable against diamond formation at super pressure conditions has been shown thermodynamically for Fe by Hilliard⁹ and photomicrographically for Cr by Hull.¹⁰

Acknowledgment. We are happy to thank our colleagues H. P. Bovenkerk, F. P. Bundy, the late E. H. Hull, A. J. Nerad, H. M. Strong, and R. H. Wentorf, Jr., for extensive discussions on these and related topics.

(8) A. A. Giardini and J. G. Tydings, *Amer. Mineral.*, **47**, 1393 (1962).

(9) J. A. Hilliard, *Trans. Met. Soc. AIME*, **227**, 429 (1963).

(10) E. H. Hull, private communication, relating to the formation of whiskers of chromium carbide in diamond.

Intramolecular Energy Relaxation.

Nonrandom Decomposition of Hexafluorobicyclopropyl^{1a}

by J. D. Rynbrandt^{1b} and B. S. Rabinovitch*

Department of Chemistry, University of Washington, Seattle, Washington 98105 (Received March 8, 1971)

Publication costs assisted by the National Science Foundation

Nonrandom decomposition of vibrationally excited hexafluorobicyclopropyl-*d*₂ (HBC) has been observed. HBC* was chemically activated at room temperature to ~ 111 kcal mol⁻¹ by the addition of ¹CD₂ or ¹CH₂ to hexafluorovinylcyclopropane (HVC) or HVC-*d*₂, respectively. HBC* decomposes to tetrafluorovinylcyclopropane-*d*₂ (TVC) with a specific rate of 2.3×10^9 sec⁻¹. Mass spectral analysis of TVC products indicates that $\sim 3.5\%$ was formed *via* a nonrandom decomposition of the newly formed ring of HBC*; this nonrandom decomposition is substantially noninterceptible at the highest pressure (4 atm) to which studies were carried. A rate of intramolecular energy relaxation of 1.1×10^{12} sec⁻¹ is obtained for HBC* by consideration of the rate of nonrandom decomposition of the newly formed ring whose initial value is calculated to be $\sim 3.5 \times 10^{11}$ sec⁻¹.

Introduction

The Rice, Ramsperger, Kassel, and Marcus (RRKM) theory^{1,2} of unimolecular decomposition assumes that internal energy relaxation occurs on a shorter time scale than decomposition. Various experimental tests have supported the general validity of this postulate, some of them under conditions more severe than are normally encountered.³ However, theoretical examination indicates that this assumption may not be valid under all experimental conditions, particularly at high pressures.^{4,5}

Chemical activation is a logical technique for testing this postulate. Large amounts of energy enter a localized region of the substrate molecule by a reaction event that occurs in a short period of time. The energy is thus introduced by a particular mechanism and in a nonrandom fashion. In thermal activation it is usually assumed collisional events transfer energy randomly into a molecule. Deviations from random behavior will be more apparent with the chemical activation technique.

In chemical activation systems the high-pressure reaction rate may be enhanced, reduced, or unchanged as pressure is increased, depending upon the position of the region of phase space corresponding to activation relative to the reaction surface.⁶ Two high-pressure systems have been examined. These are the geometric isomerization of cyclopropane-*d*₂ which was studied at pressures up to 40 atm of ethylene bath molecules⁷ and the decomposition of *sec*-butyl radicals which was first studied up to 115 atm of H₂ bath molecules⁶ and later extended to 200 atm.⁸ No anomalous behavior in the reaction rates was observed in either of these systems.

Butler and Kistiakowsky⁹ used competing reactions of methylcyclopropane, chemically activated by two

alternate activation routes, in order to test the randomization postulate at ordinary pressures. They compared product ratios in the two systems and concluded that the mode and level of activation did not alter the relative reaction rates.

In a related but different kind of measurement, *sec*-butyl radicals activated in two different ways were found to decompose at similar rates.¹¹

Recently, Bott and Jacobs¹¹ have concluded from a shock tube study of SF₆ decomposition that not all vibration modes of the molecule are active.

Present System. The decomposition of highly vibrationally excited hexafluorobicyclopropyl (HBC) has several novel features which suit it for intramolecular energy relaxation studies.¹² Addition of methylene-*d*₂

(1) (a) This work was supported by the National Science Foundation; abstracted from the Ph.D. Thesis, University of Washington, 1970, of J. D. Rynbrandt; (b) Standard Oil Predoctoral Fellow.

(2) (a) L. Kassel, "Kinetics of Homogeneous Gas Reactions," Reinhold, New York, N. Y., 1932; (b) R. A. Marcus and O. K. Rice, *J. Phys. Colloid Chem.*, **55**, 894 (1951).

(3) For a review see L. D. Spicer and B. S. Rabinovitch, *Ann. Rev. Phys. Chem.*, **21**, 349 (1970).

(4) (a) F. P. Buff and D. J. Wilson, *J. Chem. Phys.*, **32**, 677 (1960); D. J. Wilson, *J. Phys. Chem.*, **64**, 323 (1960) F. P. Buff and D. J. Wilson, *J. Amer. Chem. Soc.*, **84**, 4063 (1962); (b) R. C. Baetzold and D. J. Wilson, *J. Phys. Chem.*, **68**, 3141 (1964).

(5) D. L. Bunker, *J. Chem. Phys.*, **40**, 1946 (1964).

(6) D. W. Placzek, B. S. Rabinovitch, and E. H. Dorer, *ibid.*, **44**, 279 (1966).

(7) B. S. Rabinovitch, E. Tschuikow-Roux, and E. S. Schlag, *J. Amer. Chem. Soc.*, **81**, 1081 (1959).

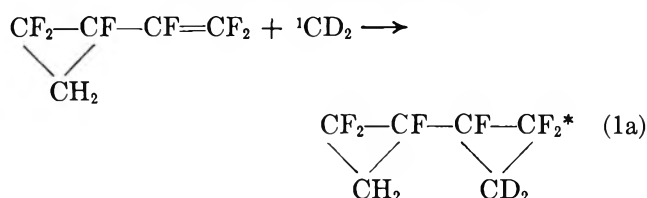
(8) I. Oref, D. Schuetzle, and B. S. Rabinovitch, *J. Chem. Phys.*, **54**, 575 (1971).

(9) J. N. Butler and G. B. Kistiakowsky, *J. Amer. Chem. Soc.*, **82**, 759 (1960).

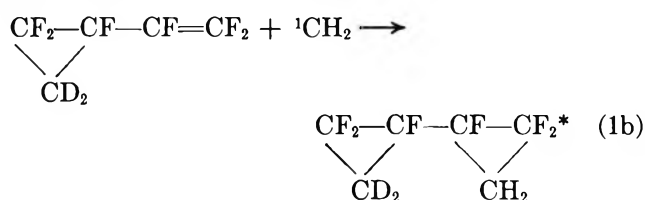
(10) R. E. Harrington, B. S. Rabinovitch, and H. M. Frey, *J. Chem. Phys.*, **33**, 1271 (1960).

(11) J. F. Bott and T. A. Jacobs, *ibid.*, **50**, 3851 (1969).

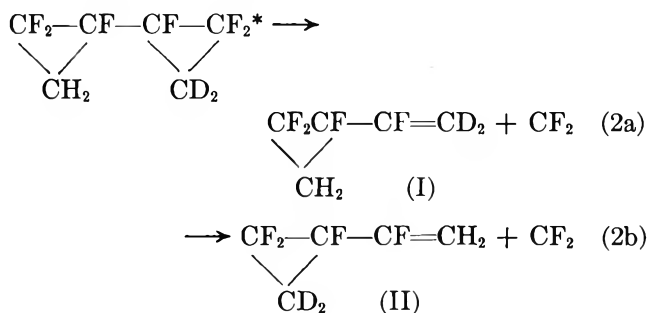
to hexafluorovinylcyclopropane (HVC) produces chemically symmetrical vibrationally excited HBC*



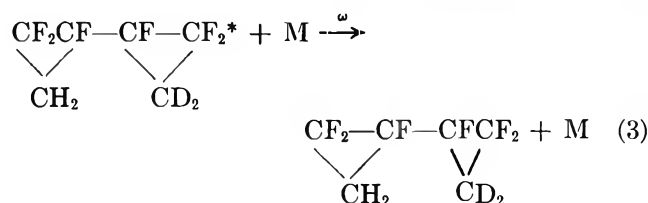
where the asterisk signifies vibrational excitation. D atoms were used as tracers to distinguish the original and product rings, and otherwise differ unimportantly from H atoms. The residual isotope effect was examined by reversing the labeling



HBC* reacts by splitting off CF₂ from either ring¹³ to give tetrafluorovinylcyclopropane (TVF). Equation 2a represents disruption of the product ring which was the original site of activation and eq 2b illustrates rup-



ture of the original ring; reversal of these descriptions applies for HBC formed *via* eq 1b. Variation of the pressure in the system changes the rate, ω , of collisional stabilization of hot HBC* (eq 3) and provides a time



scale against which the rate of internal relaxation can be measured.

CF₂ elimination reactions of this type are fast; the thermal rates have high-frequency factors with activation energies roughly 10–15 kcal below those for hydrogen migration in the hydrocarbon analogs.¹⁴ Rapid reactions are plausibly more sensitive to a nonrandom distribution of energy resulting from chemical activation at relatively low S/D than would be a slower process. Other desirable qualities of the HBC reaction are

apparent from the reaction scheme. The isotopic label does not participate directly in the decomposition reaction. HBC is somewhat compartmentalized in that the two cyclopropyl rings are connected by a single carbon-carbon bond. The product proportions, rather than their measured rates of formation are the indicator of nonrandom behavior; the potential for increased precision due to this last property will be obvious to workers in the field of kinetics.

The work of Doering, Gilbert, and Leermakers¹⁵ with spiro-pentane and bicyclopropyl has come to our attention since the present work was completed. They did not observe any nonrandom effects in spiro-pentane decomposition at a total system pressure of 150 mm; they experienced chemical difficulties in the bicyclopropyl system and could not make a test.

Experimental Section

Materials. Ketene and ketene-*d*₂ were prepared by the pyrolysis of light and deuterated acetic anhydrides and were purified by trap-to-trap distillations between -78 and -196°. The acetic anhydride-*d*₆ (Stohler Isotopic Chemicals) had 99% isotopic purity as verified by mass spectral analysis of the ketene.

HVC and HVC-*d*₂ were prepared by photolyzing a 2:1 mixture of hexafluorobutadiene-1,3 (Peninsular ChemResearch, Inc.) and ketene at 2 atm in a Pyrex vessel at 25° with the nonfiltered light from a GE A-H6 high-pressure mercury lamp. A cold finger of this vessel was kept at 0° to remove the higher boiling photolysis products from the reaction zone. The reaction percentages were about 20% of ketene-*d*₂ and 5% of ketene. HVC was purified by repeated gas chromatographic separations until it was 98% pure; its identity was confirmed from its mass spectrum, which had the correct parent mass and a dominant peak at $M(\text{parent}) - M(\text{CF}_2)$.

Apparatus and Procedure. HBC* was produced by photolyzing 20:0.5–1:0.4–2 mixtures of CO–0.5%O₂, ketene, and HVC with the filtered light from a GE A-H6 high-pressure mercury lamp; ketene decomposition was caused by light centered at 2800 Å.¹⁶ These reactions were carried out at room temperature in 600- or 2000-cc quartz vessels fitted with a Teflon-Viton O-ring stopcock. The fraction of HVC in the reaction mixture was limited by its vapor pressure at room temperature, ~14 cm; the proportion of ketene in the

(12) J. D. Rynbrandt and B. S. Rabinovitch, *J. Phys. Chem.*, **74**, 4175 (1970).

(13) N. C. Craig, T. Hu, and P. H. Martyn, *ibid.*, **72**, 2234 (1968).

(14) (a) F. P. Herbert, J. A. Kerr, and A. F. Trotman-Dickenson, *J. Chem. Soc. London*, 5710 (1965); (b) S. W. Benson and H. E. O'Neal, "Kinetic Data on Gas Phase Unimolecular Reactions," U. S. Department of Commerce, National Bureau of Standards, Washington, D. C., NSRDS-NBS 21, 1970, p 250.

(15) W. Von E. Doering, J. C. Gilbert, and P. A. Leermakers, *Tetrahedron*, **24**, 6863 (1968).

(16) J. D. Rynbrandt and B. S. Rabinovitch, *J. Phys. Chem.*, **74**, 1679 (1970).

mixture was made least at highest reaction pressure in order to inhibit polymerization.

Analysis and Separation. A small portion of the reaction mixture was first analyzed on a 100-ft Perkin-Elmer SCOT low-load squalane column at room temperature. In order to separate compounds of interest, the remainder of the reaction mixture was then injected into a 35-ft \times $3/16$ -in. 5% squalane on 32-45 mesh firebrick column at 45°. This column retained TVC for 15 min so that it followed the HVC starting material by 5 min. The column effluent ($1/25$) was diverted to a flame detector and the rest entered an arrangement of two four-way valves in series.¹⁷ A 10-ft length of $1/16$ -in. Teflon tube was used to ballast the main flow so that each component reached the valves at the same time that it reached the flame detector. The valve arrangement permitted the collection of TVC and of HVC in separate traps, without interruption of the helium flow in any portion of the system. HVC was subsequently purified for reuse.

TVC was then injected into a 30-ft \times $3/16$ -in. 5% Kel-F on 32-45 mesh firebrick column at room temperature for further purification. In high-pressure runs where lower percentage yields of TVC were obtained, this step was repeated. The final purification was performed by using the 100-ft SCOT column cooled to 0°. TVC was collected in a 3-mm Pyrex trap at -196° and the entry arm was then sealed off; the trap was immersed in a 1-propanol slush, the helium carrier gas and some carbon dioxide were pumped out, and the exit arm was sealed. The sample tubes were broken into the gas inlet system of an AEI MS9 mass spectrometer. Repeated mass spectrograms were taken with a 70-eV electron beam at a rapid scan rate with the source and collector slits opened. Rapid scans were necessary because the sample had a residence half-life in the inlet system of 15 min.

The purification reduced the ratio HVC-TVC in the product mixture from ~ 3000 to 0.05 in the most unfavorable case and well below that in others. In any case the HVC correction to TVC mass spectra was easily made. Other reaction products with retention time similar to TVC were clearly separated from it so that no neighboring peaks or shoulders were observed in the final separation.

Results

Identification of Products. The lack of reference samples of various reaction products complicated their identification. In most cases the quantity of each product was too small to permit observation of their spectra. Three methods were used in varying degrees to establish the identity of the products: of these, mass spectroscopy was the most definitive; the second, variation of the relative yields of products with pressure; and third, comparison of the gas chromatographic

retention times of products on several different columns were diagnostic and confirmatory.

HVC was identified as the principal higher boiling product of the "high pressure" photolysis of ketene-hexafluorobutadiene-1,3 mixtures above 1 atm. The parent masses were 176 and 178, from light and heavy ketene reaction mixtures, respectively. The mass spectral peak at mass 126, or 128, corresponding to CF_2 split-off, was the most abundant; all other peaks agreed with the postulated identity. The mass spectra of these compounds are listed in ref 1a.

TVC- d_2 was identified as the main product of the low-pressure addition of CD_2 to HVC and of CH_2 to HVC- d_2 . As expected, it followed HVC on a squalane chromatographic column and moved closer to HVC by a factor of 2 on a fluorocarbon column. Its identity was confirmed by mass spectrometry: the parent mass was 142 and the principal peak corresponded to CF_2 split-off at mass 92. The similar intensities of masses 95 and 97, and 45 and 47, provided further corroboration; they correspond, respectively, to the trifluorocyclopropyl and trifluorocyclopropyl- d_2 and to the fluorovinyl and fluorovinyl- d_2 moieties of the molecule.

HBC- d_2 was identified as the last major stabilization product to exit from the squalane column. This behavior paralleled that of its hydrocarbon analog which was first investigated. This compound had the correct parent ion mass, 192, as well as two principal peaks of similar intensities as masses 126 and 128 (see eq 5a) which result from $C_2D_2F_2$ and $C_2H_2F_2$ elimination and which correspond to positive ions with the same elementary composition as the predominant ions in the mass spectra of HVC and HVC- d_2 .

Two other stabilization peaks were observed in the chromatograms. These also had parent masses of 192; the presence of a common mass 162 peak, corresponding to loss of $C_2H_2D_2$, and their virtually identical mass spectra implied that these two products were geometric isomers of the C-H insertion product.

Mass Spectra Discrimination of TVC Isomers I and II. TVC product was a mixture of isomers I and II. Ideally, decomposition by electron impact would produce cyclopropyl and vinyl ions with resulting mass spectral peaks at masses 47 and 95 from I and 45 and 97 from II. However, the mass spectrum of HVC- d_2 indicates that 13.5% of the cyclopropyl- d_2 ions lose a deuterium and contribute to the mass 95 peak. This correction and the correction for residual starting material were the only ones made to the data of Table I and Figure 1.

A peak at mass 96 was indicative of some H and D scrambling in the mass spectrometer; it was 18% of the total intensity of masses 95, 96, and 97. This implies that from 1 to 9% of the 95 and of the 97 mass peaks each originated from TVC ions having cyclopropyl

(17) J. D. Rynbrandt, D. F. Ring, and B. S. Rabinovitch, *J. Gas Chromatogr.*, **6**, 531 (1968).

Table I: Mass Spectral Product Ratios

<i>P</i> , mm	<i>m</i> (47)/ <i>m</i> (45)	<i>m</i> (95)/ <i>m</i> (97)
HVC + CD ₂		
1922	1.36	1.87
806	1.28	1.61
416	1.24	1.50
311	1.11	1.40
53.5	1.18	1.25
26.3	1.07	1.18
25.1	1.02	1.22
21.6	1.17	1.22
9.23	1.13	1.23
5.09	1.06	1.23
1.00	1.07	1.21
0.98	1.07	1.21
HVC-d ₂ + CH ₂		
3324	0.94	0.64
1462	0.99	0.70
830	1.00	0.80
425	1.03	0.81
235	1.05	0.87
85.0	1.10	0.97
47.6	1.07	1.00
9.13	1.10	1.01
5.90	1.08	1.03
1.34	1.06	1.08
1.15	1.10	1.04
0.42	1.07	1.07

groups with opposite labeling; the percentage depends upon whether scrambling is a consecutive or a statistical process. Correction for this effect was not made because of its minor magnitude even in the worst case and because the low-pressure difference and departure from constancy of the mass 95:97 ratios, and not the magnitude of the ratios themselves, is the key observation.

HVC and HVC-d₂ mass spectra reveal that rupture of the cyclopropyl groups can make a contribution to the fluorovinyl mass peaks at 45 and 47. Consequently, the general trend of the 47:45 mass ratios shown in

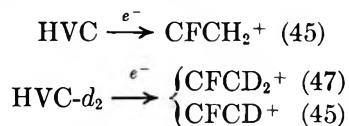


Figure 2 and Table I should be regarded as confirmatory of the primary data, *i.e.*, the 95:97 ratio, rather than as diagnostic.

Triplet Methylene. The effects of ³CH₂ are believed negligible in these experiments. Carbon monoxide in tenfold excess is a rather efficient inhibitor of ³CH₂ products in hydrocarbon systems.¹⁸ Also, the addition of 0.5% O₂ to the CO bath molecules brought the methylene collision rate with O₂ to 1/20 of that with TVC; in the dimethylcyclopropane system,^{19a} this ratio was sufficient to remove most triplet effects. In addition,

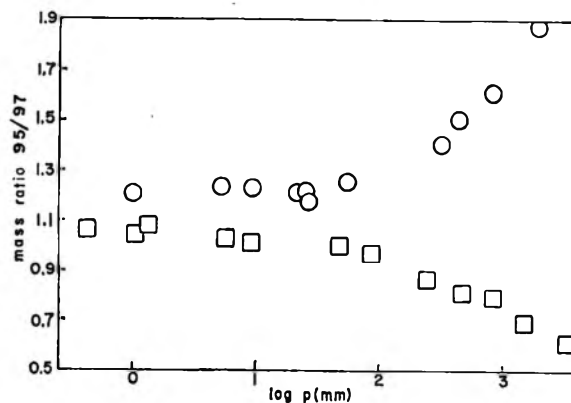


Figure 1. Mass ratios (95:97) for the HVC + CD₂ system: ○, and the HVC-d₂ + CH₂ system; □, corrected as described in the text.

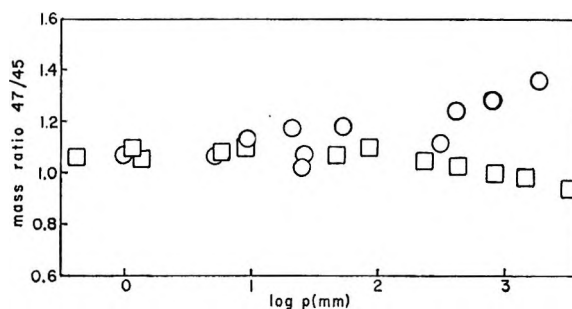


Figure 2. Uncorrected mass 47:45 ratios for the HVC + CD₂ system, ○ and the HVC-d₂ + CH₂ system, □.

fluorinated double bonds were found to be less reactive with methylene²⁰ than their hydrocarbon analog.

Competing Reactions. Although high intensities of ion masses 126 and 128 corresponding to difluoroethylene elimination were found in the mass spectrum of HVC, no evidence for this reaction was observed in the decomposition of the chemically activated molecule. In low-pressure runs, careful comparison of the chromatograms of low-boiling reaction products with those of known compounds failed to reveal the presence of the species in question. The possibility that difluoroethylene arose from difluoromethylene reaction with ketene would make its origin ambiguous so that the search for difluoroethylene was not pressed further.

There is a possibility that complications may arise from direct photolysis of HVC with elimination of CF₂. This would produce 1,1,2,3-tetrafluorobutadiene-1,3 (TB) which could complicate the interpretation of the results by providing an alternate route for the formation of TVC. The TVC formed *via* this mechanism

(18) B. A. DeGraff and G. B. Kistiakowsky, *J. Phys. Chem.*, **71**, 1553 (1967).

(19) (a) J. W. Simons and B. S. Rabinovitch, *ibid.*, **68**, 1322 (1964); (b) D. W. Setser and B. S. Rabinovitch, *J. Amer. Chem. Soc.*, **86**, 564 (1964).

(20) F. Casas, J. A. Kerr, and A. F. Trotman-Dickinson, *J. Chem. Soc.* 1141 (1965).

would be isotopically labeled oppositely from the TVC which results by CF_2 elimination from the activated ring in HBC*. A careful search was made for TB in blank runs with HVC. Reaction products in the appropriate region of the gas chromatograms were isolated and their mass spectra taken, but none corresponded to TB. Even if identification was missed due to overlap, the peaks in question were too small ($< 0.3\%$ of HVC) to be significant: methylene addition to the fluorinated double bond of TB should be similar in rate to that to HVC so that any contribution to TVC from this source would be small. Also, activated TVC* formed *via* such addition would react more rapidly than HBC*; thus, if TB were a complicating factor, its effect would be greatest at high pressures where less HBC* decomposed; it should not affect the determination of the pressure at which nonrandom decomposition first causes alteration of the low-pressure 95:97 ratio.

Total Reaction Rate of HBC*. The gas chromatograms of reaction products in this system were quite complex, especially in the higher pressure runs, and it was difficult to measure the principal stabilization and decomposition product peaks accurately. Consequently, there was considerable scatter in the measured apparent rate constants for decomposition calculated from the expression, $k_a = \omega D/S$, where ω is the collision frequency, D is decomposition, and S is stabilization amount. The rates were estimated from the plot of $\log S/D$ vs. p (Figure 3) by setting k_a equal to the value of ω at the point where $S/D = 1$; this value corresponds to $k_a = 8 \times 10^9 \text{ sec}^{-1}$; k_a varies a little with pressure if the formed molecules are not monoenergetic. This rate is quite high and it is possible that some of the stabilization product was lost to an involatile wall deposit which was removed from the reaction vessel after each higher pressure run. A more accurate and self-consistent method of evaluating k_a from the data is discussed below.

Discussion

Figure 1 shows that some HBC* decomposes before the internal energy completely relaxes to a random distribution: there is a difference in the low-pressure 95:97 mass ratios in the two systems and an increasing separation of these ratios at higher pressures where decomposition of randomized HBC* is inhibited by collisional stabilization.

The amount of nonrandom decomposition may be taken to be the same fraction of the total decomposition in both systems (eq 1a and 1b). Two sources could cause some error in this assumption. First, the deuterated ring should display a slightly lower rate of decomposition, at a given energy, due to a secondary isotope effect;¹⁹ however, the intramolecular relaxation rate might also be reduced in this case and be compensatory; a net error of as much as 10% would affect x

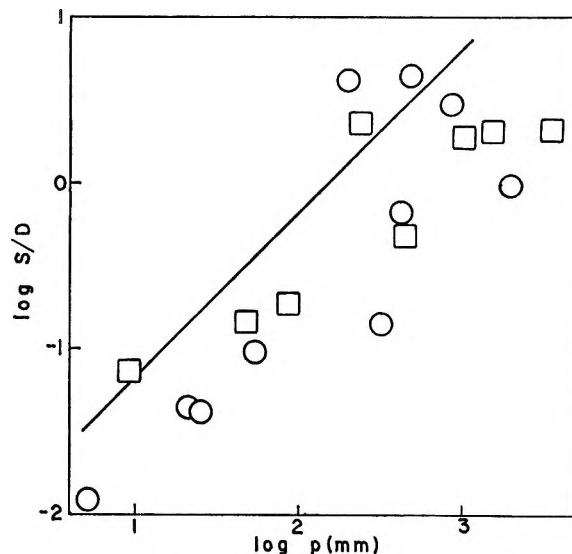


Figure 3. S/D for HVC + CD_2 system, O and for HVC- d_2 + CH_2 , □. The line represents values from the 95:97 mass ratio with $k_a = 2.3 \times 10^9 \text{ sec}^{-1}$.

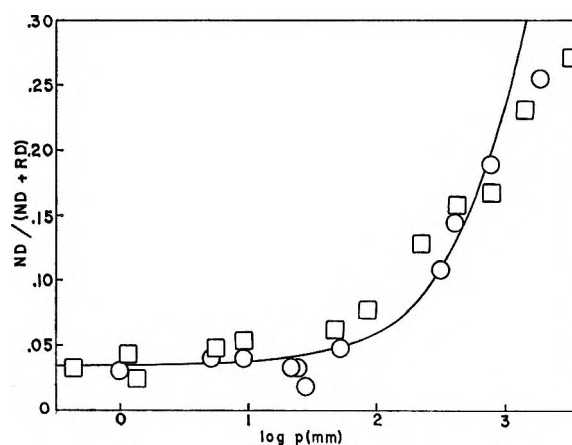


Figure 4. Ratio of (nonrandom decomposition) to (total decomposition) as measured for HVC + CD_2 , O, and for HVC- d_2 + CH_2 , □; and calculated curve, —.

(see below) by only half that amount. Second, $^1\text{CH}_2$ and $^1\text{CD}_2$ may carry different amounts of energy into HBC* in the two systems. In any case, failure of the assumption is not discernible in the data: both systems depart from constancy of the 95:97 mass ratio in the same pressure region (Figure 1) and by the same relative amounts; the latter point is amplified in the discussion which follows and in Figure 4.

The amount of nonrandom decomposition can be calculated by setting the low-pressure 95:97 mass ratios equal in its absence

$$\frac{R_{a0} - (1.0 + R_{a0})x}{1.0} = \frac{R_{b0}}{1.0 - (R_{b0} + 1.0)x}$$

where x , the low-pressure fraction of TVC formed *via* nonrandom HBC* decomposition, is equal to 0.035; and R_{a0} and R_{b0} , the experimentally determined low-

pressure 95:97 mass ratios for reactions 2a and 2b are 1.22 and 1.06, respectively. Neither the overlap correction that was made to the 95 mass peak nor a scrambling correction described in the Results, which was not made, greatly affects the magnitude of the difference of R_{a0} and R_{b0} . The error in the difference, which may be determined from the consistency of the low-pressure ratios, is estimated as $\pm 15\%$. This error applies directly to x . However, even an error of 100% in x would have no importance for the principal conclusions derived from this study.

The 95:97 mass ratio in the absence of nonrandom contributions is 1.14; *i.e.*, 53% of the randomized HBC* decomposition occurs *via* CF_2 elimination from the deuterated ring. This percentage implies a 6.5% variation in the reaction rate per deuterium as a total net isotope effect resulting both from the original decomposition and from electron impact in the analysis.

The amount of nonrandom decomposition is small in absolute amount even at low pressures, which is explicable in terms of a faster rate of internal energy relaxation. In practice then, scarcely any nonrandom decomposition is collisionally interceptible and it may be used as an internal standard to indicate the original amount of HBC* formed, *i.e.*, the total amounts of random decomposition and of stabilization. The reaction rate of randomized HBC* is $k_a = \omega D/S$ and is calculable from the relations

$$D = (RD/ND)_p / (RD/ND)_0$$

and

$$S = 1.0 - D$$

where RD and ND represent the amounts of random and nonrandom decomposition, and subscripts p and 0 refer, respectively, to the ratio observed in a particular run and to the average low-pressure ratio. RD and ND are calculated from the following sets of simultaneous equations: for reaction 1a

$$R_a = \frac{(0.53RD + ND)}{0.47RD}$$

and

$$R_a + 1.0 = RD + ND$$

where R_a is the observed value of the 95:97 mass ratio at the pressure in question; similarly, for reaction 1b

$$R_b = \frac{0.53RD}{(0.47RD + ND)}$$

and

$$R_b + 1.0 = RD + ND$$

The nonrandom fraction of the total decomposition is plotted in Figure 4. The resultant k_a value is roughly a factor of 4 lower than that calculated from the peak

areas in the chromatograms and is more consistent. Because the experimental complications tend to pull the 95:97 mass ratios toward unity, the former rate constant should be an upper value so that the internally consistent constant $k_a = 2.3 \times 10^9 \text{ sec}^{-1}$ based upon mass ratios is the best experimental value.

If the chromatogram-based rates were accurate and consistent, ND could be estimated from the two sets of data separately and the chromatogram-based k_a values. However, this value of k_a gives rise to an inconsistency in the relative magnitudes of the 95:97 mass ratios which would be expected in the absence of nonrandom effects. This result substantiates the finding above that $k_a = 8 \times 10^{19} \text{ sec}^{-1}$ is an overestimate. Taking $k_a = 2.3 \times 10^9 \text{ sec}^{-1}$, ND may be calculated from the pressure dependence of the observed 95:97 ratio, in each given system. Then

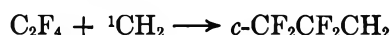
$$x_a = 0.032 \pm 0.001$$

and

$$x_b = 0.034 \pm 0.020$$

where x_a and x_b are the geometric mean values for the systems represented by eq 1a and 1b, respectively. This calculation involves more uncertainties than the first calculation, but the deviation from the preferred earlier value is of negligible importance for the conclusions to be made.

Thermochemistry. The level of activation of HBC* is not exactly known and was estimated from the thermochemistry of the process



The minimum exothermicity of this reaction, 88 kcal mol⁻¹, is given by $\{\Delta H_f^\circ(\text{C}_3\text{H}_2\text{F}_4) = \Delta H_f^\circ(\text{CH}_2) - \Delta H_f^\circ(\text{C}_2\text{F}_4)\}$, where $\Delta H_f^\circ_{298}(\text{C}_3\text{H}_2\text{F}_4)$ has been estimated^{14b} as $-155.0 \text{ kcal mol}^{-1}$, $\Delta H_f^\circ_{298}(\text{CH}_2)$ is²¹ $\geq 92 \text{ kcal mol}^{-1}$, and $\Delta H_f^\circ_{298}(\text{C}_2\text{F}_4)$ is $-155.0 \text{ kcal mol}^{-1}$.^{14b} Excess photolysis energy is carried by methylene from its genesis. This amount is not known exactly here but has been estimated previously to be $\sim 60\%$ of the excess light energy,^{16,22} or $\sim 14 \text{ kcal mol}^{-1}$ for 2800-Å radiation. Finally, the heat capacity and the relative translational energy of the reactants contribute 4.5 kcal to HBC*. In this way the total internal energy of HBC* is estimated as 111 kcal mol⁻¹. It could well be at least several kilocalories per mole higher if the values of Chupka, *et al.*, for $\Delta H_f^\circ(\text{CH}_2)$ refer to the triplet rather than the singlet state, as suggested by those workers.²¹

Relaxation Rate. Rice²³ early pointed out that if all

(21) (a) W. A. Chupka and C. Lifshitz, *J. Chem. Phys.*, **48**, 1109 (1968); (b) W. A. Chupka, J. Berkowitz, and K. M. A. Refaey, *ibid.*, **50**, 1938 (1969).

(22) D. W. Setser and B. S. Rabinovitch, *Can. J. Chem.*, **40**, 1425 (1962).

(23) O. K. Rice, *Z. Phys. Chem. Abt. B*, **7**, 226 (1930).

"parts" of the molecule were not coupled, a reactive molecule would behave effectively as a smaller one. RRKM formulation was used to calculate decomposition rates for two arbitrary, different moieties of HBC* which may be considered initially to contain all of the energy of excitation.

The following procedure was used. An activated complex (Appendix) was chosen based on the Arrhenius parameters for thermal tetrafluorocyclopropane decomposition¹⁴

$$k_{\infty} = 10^{16.27} e^{-48.6/RT}$$

then the critical threshold is $E_0 = 46.5$ kcal mol⁻¹. This complex was used with minor changes to calculate the values of k_E for normal random decomposition of HBC* at energy E . A weak-collider stochastic calculation of k_a for random decomposition was made. CO collisions were represented by a 1600-cm⁻¹ exponential model, as was found to be appropriate previously for CO in the dimethylcyclopropane system at the same level of total and excess energy.¹⁶ A calculated rate, $k_a = 2.3 \times 10^9$ sec⁻¹, is obtained with E equal to 110 kcal mol⁻¹ and with E_0 lowered from 46.5 kcal by 2 kcal.

Selection of the effectively nonrandom initial portion of the nascent HBC* molecule is somewhat arbitrary. The changes made in the molecular frequencies to generate the HBC complex were carried into decomposition complexes for two moieties involving 19 and 21 modes (*i.e.*, in both cases roughly half of the whole molecule) of the trifluorocyclopropyl group. The nonrandom energy of the moiety is ~ 108 kcal mol⁻¹, which accounts for the fact that ~ 4 kcal mol⁻¹ of thermal energy was randomly distributed initially in the substrate ring. The calculated decomposition rates k_{ND}^0 of the two moieties differ by only a factor of 2 and the average value 3.5×10^{11} sec⁻¹ is employed henceforth for the initial rate of nonrandom decomposition.

Bunker⁵ used a set of coupled differential equations in conjunction with a Monte Carlo calculation in order to describe the transfer of energy among s modes of a molecule characterized by frequencies $\nu_1 \dots \nu_s$; where

$$-dE_j/dt = \sum_{k \neq j} k_{jk} E_j - \sum_{k \neq j} k_{kj} E_k, \quad 1 < j < s$$

The solution for any E_j is given as

$$E_j(t) = C_1 - \sum_2^s C_i \exp(-\lambda_i t)$$

where the C_i are constants related to k_{jk} and the initial conditions; the λ_i are the rate constants for intramolecular energy relaxation which control the rates of energy transfer between the various modes.

For the present calculation, the original energy E^0 in the nonrandom moiety is treated as declining exponentially

$$E = E^0 e^{-\Lambda t}$$

where Λ is a composite, effective rate of relaxation. Thus the rate of nonrandom decomposition, $k_{ND}(E)$, evolves in time as

$$k_{ND}(t) = k_{ND}(E^0 e^{-\Lambda t})$$

The energy relaxes internally on a time scale which is short relative to collision times, so that Λ is the only process that competes with k_{ND} and the question of the proper model of collision efficiency does not apply to nonrandom decomposition.

The time dependence of the rate of randomized HBC* decomposition, k_{RD} , has little effect on the conclusions since energy is effectively randomized before any significant component of random decomposition arises. The following expression has the correct qualitative form and was used for the simplicity of calculation that it afforded

$$k_{RD}(t) = k_{RD}^{\infty} (1 - k_{ND}(t)/k_{ND}^0)$$

where the superscripts on k_{ND}^0 and k_{RD}^{∞} refer to limiting (initial and final, respectively) values. k_{ND} and k_{RD} compete with collisional stabilization, ω . Relative probabilities of the three events were found by computer integration

$$S = \int_0^{\infty} N_{HBC^*}(t) \omega dt$$

$$RD = \int_0^{\infty} N_{HBC^*}(t) k_{RD}(t) dt$$

$$ND = \int_0^{\infty} N_{HBC^*}(t) k_{ND}(t) dt$$

where $N_{HBC^*}(t)$ is the concentration of active HBC* which survives to time t .

The low-pressure value of $ND/(S+RD+ND)$ was previously calculated to be only 0.035. It is evident that $k_{ND}(t)$ quickly relaxes to zero as the nonrandomly excited HBC* relaxes to a random energy distribution. The Λ value which combines with k_{ND}^0 and k_{RD}^{∞} to reproduce the experimental results is 1.1×10^{12} sec⁻¹ for $k_{ND}^0 = 3.5 \times 10^{11}$ sec⁻¹. The demonstration of nonrandom effects in HBC* following its formation raises the interesting possibility that the 95:97 ratio of 1.14 which would arise in the absence of nonrandom effects may conceivably arise from the unsymmetrical nature of a molecular energy-coordinate hyperspace, due to unsymmetrical isotope substitution of the molecule, and which is excluded in the RRKM formulation; this would represent a type of nonrandom energy level density isotope effect. This effect should be most pronounced in systems where the average energy of the decomposition species is close to the critical threshold.

Figure 4 reveals an apparent discrepancy at highest pressure between the calculated and observed behavior. This is not surprising in view of the crude models for internal relaxation and nonrandom decomposition that

were used. On the other hand, it would be quite naive not to maintain reservations concerning the reliability of such details of the experimental results, and refinement of the calculations is not worth pursuing at this stage. Other related experiments are under way.

Appendix

Rates of HBC and TC Decomposition. The following parameters and frequencies were used to calculate the k_E for HBC: $E_0 = 15, 556$; $I^+/I = 2.1$

HBC Frequencies. 364, 865, 547, 250, 505, 1300, 590, 367, 1100, 450, 500, 1280, 1275, 367, 3025, 1475, 1028, 3101, 1100, 739, 865, 364, 865, 547, 250, 505, 1300, 590, 367, 125, 450, 300, 1280, 1275, 367, 2211, 1074, 887, 329, 928, 528, 720.

HBC Complex Frequencies. 544, 365, 367, 261, 171,

1500, 100, 200, 1100, 450, 500, 1280, 1275, 367, 3025, 1475, 1028, 3101, 1100, 739, 720, 364, 865, 547, 250, 505, 1300, 590, 367, 125, 450, 300, 1280, 1275, 367, 2211, 1074, 887, 2329, 928, 528.

The following parameters and frequencies were used to calculate the k_E for tetrafluorocyclopropane (TC): $E_0 = 15, 556$; $I^+/I = 2.20$.

TC Molecular Frequencies. 364, 865, 547, 250, 505, 1300, 590, 367, 1000, 450, 202, 1280, 1275, 367, 3025, 1475, 1028, 3101, 1100, 739, 865.

TC Complex Frequencies. 644, 365, 397, 261, 171, 1500, 100, 200, 1000, 450, 202, 1280, 1275, 367, 3025, 1475, 1028, 3101, 1100, 739.

Collision Frequency. For effective collision diameters taken as 3.8 and 7.5 Å for CO and HBC, respectively, $\omega = 1.65 \times 10^7 \text{ sec}^{-1}$ per mm of CO.

Energy Transfer in Thermal Isocyanide Isomerization. *n*-Alkanes and *n*-Alkenes in the Ethyl Isocyanide System¹

by S. P. Pavlou and B. S. Rabinovitch*

Department of Chemistry, University of Washington, Seattle, Washington 98106 (Received February 3, 1971)

Publication costs assisted by the National Science Foundation

The effect of *n*-alkane and *n*-alkene bath molecules on the thermal isomerization of ethyl isocyanide has been studied at 231° in the lower region of falloff. Members of the respective homologous series up to C₆ were investigated. Relative activation-deactivation efficiencies, $\beta_{\omega}'(D)$ and $\beta_{\omega}(D)$, were determined with use of inert molecule cross sections appropriate for this system. The measured incremental collision diameters, Δs_{AM} , were compared with earlier values obtained from energy-transfer studies with the simpler CH₃NC homolog. In the C₂H₅NC system, the critical molecule complexity (C₂ member), beyond which increasing chain length induces no enhancement of intrinsic collisional efficiency, is reduced for both homologous series relative to the methyl system. This effect is discussed in terms of the structural and internal parameter changes of the substrate molecule.

Introduction

The collisional efficiencies of a large number of inert bath gases for the thermal isomerization of CH₃NC in the second-order region has been studied.^{2,3} The behavior of homologous series of *n*-alkanes, 1-alkenes, 1-alkynes, *n*-perfluoroalkanes, and *n*-nitriles was investigated at infinite dilution of substrate.^{4,5} These studies revealed that the relative activation-deactivation efficiencies increase with chain length of the members of a homologous series; however, constant efficiency is achieved at some critical chain length, n_c ; apparent further increase in collisional efficiency for $n > n_c$ is merely a display of the increase in the effective colli-

sional diameter, s_{AM} , for larger bath gases and does not represent an increase in intrinsic efficiency per collision.

(1) (a) This work was supported by the National Science Foundation; (b) From the Ph.D. Thesis of S. P. Pavlou, University of Washington, Seattle, Wash. 1970.

(2) F. J. Fletcher, B. S. Rabinovitch, K. W. Watkins, and D. J. Locker, *J. Phys. Chem.*, **70**, 2823 (1966).

(3) S. C. Chan, B. S. Rabinovitch, J. T. Bryant, L. D. Spicer, T. Fujimoto, Y. N. Lin, and S. P. Pavlou, *ibid.*, **74**, 3160 (1970).

(4) Y. N. Lin, S. C. Chan, and B. S. Rabinovitch, *ibid.*, **72**, 1932 (1968).

(5) S. C. Chan, J. T. Bryant, L. D. Spicer, and B. S. Rabinovitch, *ibid.*, **74**, 2058 (1970).

To investigate this phenomenon further, similar studies have been pursued in the C_2H_5NC system. The advantages of extending the experimental work on bath gas behavior to higher isocyanide homologs have been pointed out.^{2,6}

Experimental Section

Materials. The sources and purification of ethyl isocyanide have been described in I.⁶ Methane, ethylene, propylene, and 1-butene (all research grade from Phillips Petroleum Co.) were used without purification. Ethane, propane, and *n*-butane (Matheson Co., CP grade) were analyzed chromatographically; only 2% hydrocarbon impurities were present. *n*-1-Pentene, 1-hexene, *n*-pentane, and *n*-hexane (Chemical Samples Co., 99.5%) required no purification. Condensable gases were deoxygenated by the freeze-pump method.

Apparatus and Procedure. The experimental setup and procedure were the same as those described in I. Rate determinations were made in a static system. The reaction vessel was a 229-l. Pyrex flask heated in a stirred furnace. The temperature was controlled by a proportional controller and was measured by using eight calibrated chromel-alumel thermocouples placed in good thermal contact with various points of the reaction vessel. During a run the temperature was constant to $\pm 0.3^\circ$ and the agreement between all thermocouple readings was $\pm 0.2^\circ$. Various amounts of inert gases were added to a constant amount of substrate ($\sim 3 \times 10^{-4}$ mm) such that the dilution, D , varied on a collision basis from approximately 20 to 200 throughout the series of runs, depending on the gas. The lower range corresponded to the more efficient (strong) colliders so that dilution was near-infinite in all cases. Isomerization was carried to between 8 and 35% reaction.

Analysis. The analytical technique was similar to that employed in I. All analyses were made by gas chromatography. Two different columns were used to optimize separation of the propionitrile product peak from the inert gas peak: these were a 12-ft column of 5% tricresyl phosphate on acid-washed Chromosorb G, for runs with hydrocarbon bath gases up to C_4 , and a 25-ft column of 1% squalane on Fluoropak-80, for the C_6 and C_8 homologs. Calibrations of the columns were made before and after each series of analyses. In a few cases, rate constants were obtained on both an "absolute" and "internal" standard basis as in I; good reproducibility between internal and absolute values was achieved. Some inert gas interference with the acetonitrile peak occurred, and only absolute values were obtained in most cases.

Results and Discussion

Treatment of the Data. The experimental corrections described in I were applied to the present data. All rate data were brought to a standard temperature of 231° .

Time correction for sample removal averaged 8.5, 3, and 5% for CH_4 , C_2H_6 , and C_2H_4 , respectively. For all other members in both series, pump-out time corrections were usually less than 2%, depending on the total pressure and the reaction time. Rates of isomerization were obtained in a region of falloff, $k/k_\infty \geq 0.03$, where wall effects were small. (The observed rate constants are summarized in the Table VI.)

Collisional Efficiencies. A detailed discussion of the experimental relative collisional efficiency quantities appropriate for these studies and their dependence on reaction order and dilution (D) of substrate has been given in I. Relative efficiencies on a pressure-to-pressure basis, $\bar{\beta}_p'(D)$ and $\bar{\beta}_p(D)$, and on a reduced mass-corrected basis, $\bar{\beta}_\mu'(D)$ and $\bar{\beta}_\mu(D)$, were obtained from the relations described there. For an appropriate narrow range of dilution, and for a narrow range of falloff, the dependence of β quantities on D and reaction order, ϕ , is small. The width of these ranges depends on the efficiency of the bath gas. All members of both homologous series, except CH_4 , exhibit near-strong collider behavior and averaging of the β quantities is appropriate, in principle, for the dilution range ($200 > D > 20$) and falloff range ($0.03 < k/k_\infty < 0.13$) used here. For some gases, a trend in the β values with pressure seems to exist. Its origin, if real, is not known and values were averaged. (All β quantities are gathered in the Table VI.)

Extrapolation of the high dilution $\bar{\beta}_\mu'(\infty)$ and $\bar{\beta}_\mu(\infty)$ quantities to their second-order limit $\beta_{0\mu}(\infty)$ was made for each bath gas in the same manner as described in I; their values are shown in Table I and the simplified designation β_μ will be used in the future.

Incremental Cross Sections. In most work in chemical kinetics, collision diameters have conventionally been selected by fiat or calculated with the use of hard-

Table I: Low-Pressure Mass-Corrected Relative Efficiencies ($D = \infty$)

	$\bar{\beta}_\mu'(\infty)$	$\bar{\beta}_\mu(\infty)$	$\beta_{0\mu}(\infty)$
<i>n</i> -Alkanes			
CH_4	0.38	0.25	0.32
C_2H_6	0.62	0.50	0.56
C_3H_8	0.71	0.62	0.67
C_4H_{10}	0.85	0.78	0.82
C_5H_{12}	0.94	0.90	0.92
C_6H_{14}	1.01	1.02	1.01
<i>n</i> -Alkenes			
C_2H_4	0.62	0.51	0.57
C_3H_6	0.66	0.57	0.62
C_4H_8	0.78	0.73	0.76
C_5H_{10}	0.87	0.82	0.85
C_6H_{12}	0.93	0.92	0.93

(6) S. P. Pavlou and B. S. Rabinovitch, *J. Phys. Chem.*, **75**, 1366 (1971).

Table II: Incremental Collision Diameters in the EtNC System, Å

	<i>n</i> -Alkanes		<i>n</i> -1-Alkenes	
s_{AM_2}	4.81 ^{a,b}	5.28 ^c	4.85 ^{a,b}	5.13 ^c
$\Delta s_{AM}/s_{AM_2}$	0.089 ± 0.01		0.074 ± 0.02	
Δs_{AM}	0.43	0.47	0.36	0.38
	Mean = 0.395			
$\Delta\sigma_M$	0.61			
$\Delta\sigma_M$ (CH ₃ NC system)	0.57			

^a Internally consistent value, based on $\beta_0(\infty) = 1$ for M_2 (see Table III). ^b Preferred values in bold face. ^c Viscosity-derived value, ref 5.

sphere cross sections evaluated from transport data. In earlier work on isocyanide isomerization the desirability of determining a self-consistent set of molecular cross sections appropriate for the energy-transfer system under investigation was pointed out. Values of relative collision diameters for several homologous series, including *n*-alkanes and *n*-alkenes, have been obtained from measurements of incremental collision diameters, Δs_{AM} , in the CH₃NC system.⁴ Determination of these quantities in the C₂H₅NC system is based on the same considerations.

The postulate is made, as was confirmed experimentally^{4,5} for CH₃NC, that at and above some critical chain length, n_c , the relative low-pressure limiting

Table III: Effective Collision Diameters, Å, for Hydrocarbons ($s_{AA} = 6.43$ Å)

<i>n</i>	I ^a		II		III ^c		$\epsilon_{M_n/k}$, °K	$\Omega_{AM_n(2,2)}$ *
	s_{AM_n}	σ_{M_n}	s_{AN_n} ^b	σ_{M_n}	s_{AM_n}	σ_{M_n}		
<i>n</i> -Alkanes								
1	4.31 ^d	2.42			4.74	3.80	144	1.16
2	4.81	3.58			5.28	4.42	230	1.26
3	5.24	4.28			5.69	5.06	254	1.28
4	5.67	4.78	5.95	5.23	5.93	5.20	325	1.35
5	6.10	5.52	6.26	5.77	6.22	5.70	325	1.35
6	6.53	6.26	6.58	6.31	6.52	6.20	325	1.35
<i>n</i> -1-Alkenes								
2	4.85	3.74			5.13	4.23	205	1.23
3	5.21	4.06			5.60	4.67	303	1.33
4	5.57	4.60	5.85	5.09	5.96	5.31	310	1.34
5	5.93	5.22	6.18	5.65			310	1.34
6	6.29	5.84	6.50	6.21			310	1.34

^a Values based on Δs_{AM} (Table II) with s_{AM_2} determined by $\beta_0(\infty) = 1$ for $n_c = 2$. ^b From collision diameters, σ_{M_n} , determined in the CH₃NC system for which $\beta_0(\infty) = 1$ at $n_c \geq 4$. ^c From viscosity values of σ_{M_n} (ref 4 and 5). ^d Value on the basis of the internally consistent s_{AM_2} value in set I relative to its value in set III.

Table IV: $\beta_0(\infty)$ Values of Hydrocarbons for the C₂H₅NC and CH₃NC Systems

	C ₂ H ₅ NC		CH ₃ NC
	I ^a	III ^a	
<i>n</i> -Alkanes			
1	0.70	0.59	0.61
2	1.0	0.83	0.76
3	0.99	0.85	0.79
4	0.95	0.91	1.00
5	0.98	0.96	1.01
6	1.02	1.0	0.99
<i>n</i> -1-Alkenes			
2	1.0	0.87	0.60
3	1.06	0.86	0.80
4	0.99	0.90	1.00
5	1.0	0.92	0.99
6	1.03	0.94	1.01

^a As in Table III.

efficiency on a collision-per-collision basis $\beta_0(\infty)$ reaches a constant value (unity) for higher members in the series. Then for all members of the homologous series for which $n \geq n_c$

$$\beta_{\mu(n+i)}/\beta_{\mu n} = (s_{AM_n} + i\Delta s_{AM})^2/s_{AM_n}^2 \quad (1)$$

where i is the increment in carbon number of the chain and s_{AM_n} is the effective collision diameter of the colliding partners, A-M_{*n*}. Δs_{AM} may be treated as constant with each CH₂ increment, for a small number of increments, i . Thus

$$[\beta_{\mu(n+i)}/\beta_{\mu n}]^{1/2} - 1 = R_{ni} = i\Delta s_{AM}/s_{AM_n} \quad (2)$$

A plot of R_{ni} vs i should display linear behavior. Δs_{AM} can be calculated directly from the slope and the value s_{AM_n} .

From the plots of R_{ni} vs. i (Figure 1) with trial values of $n_c = 1$ and $n_c = 2$ for alkanes and $n_c = 2$ for alkenes, one observes that $n_c = 2$ is the critical value for both

Table V: Summary of Rate Data and Relative Collisional Efficiencies

D^a	$P(\text{Mix}),$ 10^{-2} mm	$k(\text{Mix}),^b$ 10^{-4} sec^{-1}	$\bar{\beta}_p'(D)$	$\bar{\beta}_p(D)$	$\bar{\beta}_\mu'(D)$	$\bar{\beta}_\mu(D)$	$(\mu_{AA}/\mu_{AM})^{1/2}$
CH₄							
26	0.86 ^c	3.23 ± 0.19^d	0.52	0.40	0.40	0.27	1.49
38	1.43	4.78 ± 0.38	0.54	0.42	0.41	0.28	
52	2.09	5.97 ± 0.37	0.51	0.40	0.39	0.27	
75	3.18	7.71 ± 0.64	0.49	0.37	0.37	0.26	
100	4.10	8.65	0.46	0.34	0.35	0.23	
185	6.61	11.0 ± 0.51	0.43	0.30	0.33	0.20	
C₂H₆							
25	1.02	4.80	0.69	0.59	0.62	0.50	1.19
23	1.06	5.03	0.71	0.61	0.63	0.58	
25	1.07	5.11	0.71	0.62	0.64	0.52	
30	1.46	6.47	0.72	0.64	0.65	0.53	
58	2.06	7.93	0.68	0.60	0.63	0.51	
73	2.60	9.19 ± 0.12	0.67	0.58	0.60	0.49	
70	2.79	9.15 ± 0.38	0.64	0.54	0.57	0.46	
105	3.81	11.7 ± 0.02	0.65	0.55	0.59	0.47	
180	6.07	16.9 ± 0.18	0.69	0.57	0.63	0.48	
206	9.96	20.7	0.61	0.47	0.55	0.42	
C₃H₈							
24	0.91	4.89	0.77	0.68	0.74	0.64	1.06
41	1.54	7.91	0.85	0.80	0.82	0.76	
64	2.63	10.6	0.77	0.70	0.74	0.60	
71	2.77	10.7	0.75	0.68	0.72	0.64	
80	3.34	11.2	0.69	0.59	0.66	0.56	
145	5.47	16.2	0.71	0.60	0.68	0.57	
185	6.53	16.9	0.66	0.53	0.64	0.50	
C₄H₁₀							
20	0.86	4.25	0.69	0.59	0.71	0.60	0.98
21	0.78	5.59	0.98	0.98	1.00	1.00	
29	1.15	6.65	0.88	0.83	0.90	0.84	
30	1.27	7.14	0.89	0.85	0.90	0.87	
46	1.80	8.84	0.85	0.79	0.86	0.81	
65	2.58	11.6	0.85	0.80	0.87	0.82	
78	2.81	11.8	0.82	0.76	0.89	0.77	
83	3.44	12.3	0.73	0.65	0.74	0.67	
206	7.36	20.3	0.74	0.62	0.75	0.62	
C₅H₁₂							
28	1.01	6.01	0.88	0.83	0.91	0.88	0.93
39	1.40	8.74	1.00	1.01	0.96	1.07	
48	0.88	6.19	0.99	0.99	1.03	1.05	
80	2.69	10.4	0.91	0.87	0.97	0.92	
98	2.74	12.8	0.74	0.66	0.96	0.70	
109	3.44	14.0	0.83	0.78	0.87	0.82	
140	5.03	18.3	0.85	0.78	0.88	0.83	
C₆H₁₄							
27	0.87	6.19	0.91	0.86	1.02	1.03	0.90
51	1.48	8.00	0.92	0.90	1.06	1.08	
67	1.95	10.3	0.92	0.90	1.00	1.00	
117	3.80	16.6	0.89	0.84	1.00	1.00	
124	4.70	18.8	1.00	1.00	0.97	0.96	
C₂H₄							
12	0.609	4.04	0.83	0.76	0.73	0.63	1.22
19	1.07	5.46	0.74	0.64	0.64	0.53	
32	2.02	8.52	0.72	0.63	0.62	0.52	
41	2.17	8.11	0.65	0.55	0.56	0.45	
60	3.43	10.8	0.62	0.53	0.55	0.43	

Table V. (Continued)

D^a	$P(\text{Mix})$, 10^{-3} mm	$k(\text{Mix})^b$ 10^{-6} sec $^{-1}$	$\bar{\beta}_p'(D)$	$\bar{\beta}_p(D)$	$\bar{\beta}_\mu'(D)$	$\bar{\beta}_\mu(D)$	$(\mu_{AA}/\mu_{AM})^{1/2}$
C_2H_6							
20	0.894	4.76	0.76	0.67	0.72	0.63	1.07
45	1.39	6.11	0.71	0.62	0.67	0.58	
46	2.01	7.55	0.67	0.58	0.63	0.54	
90	3.13	10.8	0.69	0.54	0.61	0.50	
76	3.40	10.5	0.63	0.61	0.66	0.57	
C_2H_4							
16	0.64	4.42	0.89	0.85	0.89	0.85	1.00
20	0.85	4.69	0.71	0.69	0.71	0.69	
32	1.13	5.47	0.74	0.65	0.74	0.65	
55	2.01	8.82	0.78	0.71	0.78	0.71	
C_2H_{10}							
18	0.61	4.91	1.02	1.03	1.09	1.05	0.94
36	1.35	7.00	0.82	0.81	0.86	0.85	
95	1.42	7.57	0.69	0.61	0.72	0.64	
77	2.54	10.4	0.78	0.71	0.82	0.76	
C_2H_{12}							
16	0.504	3.84	0.91	0.87	0.96	0.95	
38	1.09	6.44	0.89	0.84	0.95	0.92	
40	1.30	7.82	0.95	0.93	1.01	1.02	
52	1.69	8.64	0.86	0.82	0.93	0.90	
73	2.55	10.3	0.77	0.70	0.82	0.78	

^a Dilution, D , is on a collision basis where $\omega = \omega(A,D) + \omega(M,D) = 1.59 \times 10^7 P(A,D) + 1.97 \times 10^6 (s_{AM}^2/\mu_{AM}^{1/2}) P(M,D)$; the collision cross sections, $s_{AM,n}$, used are the values given in set I, Table III with $s_{AA} = 6.43 \text{ \AA}$. ^b $k_\infty = 1.56 \times 10^{-3} \text{ sec}^{-1}$. ^c Lower falloff value which was excluded in averaging. ^d Average deviation of absolute and internal standard values from the mean.

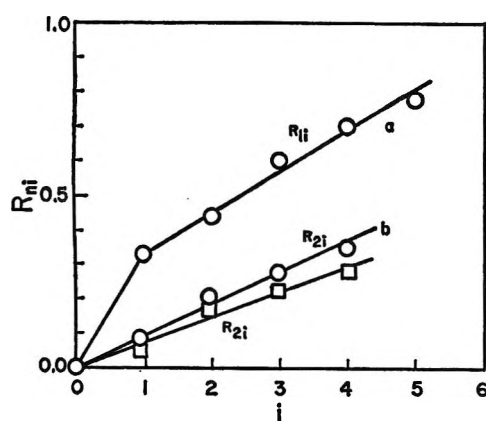


Figure 1. Plots of R_{ni} vs. i for n -alkanes, \circ , with: a, $n_c = 1$; and b, $n_c = 2$; and for n -1-alkenes, \square , with $n_c = 2$.

series (Figure 1, curves a and b). A least-squares treatment of the data for $n_c = 2$ gives values for the slope of the lines, $\Delta s_{AM}/s_{AM,2}$, and $s_{AM,n}$ is then fixed once the value of $s_{AM,2}$ is assigned.

Two different bases may be used to assign $s_{AM,n}$. Conventionally, these quantities have been obtained from other sources, principally viscosity measurements. On this basis,⁶ $\sigma_A = 5.00 \text{ \AA}$, $\delta_{mBx} = 1.12$, $\Omega_{AA}^{(2,2)*} = 1.65$, and $s_{AA} = 6.43 \text{ \AA}$; also $\sigma_{M,1}$ was taken as ³⁻⁶ 4.42 and 4.23 \AA , with $\epsilon_M/k = 230$ and 205 $^\circ\text{K}$, for

C_2H_6 and C_2H_4 , respectively, with values of $\Omega_{AM}^{(2,2)*}$ of 1.26 and 1.23. The standard combining rules are used.

A second, internally consistent set of $s_{AM,n}$ values appropriate to the present phenomenon may be calculated by adopting the value $\beta_0(\infty) = 1$ for the critical member of each series ($n_c = 2$ for both), and using this condition to evaluate $s_{AM,1}$.

All higher $s_{AM,n}$ were obtained from Δs_{AM} , $s_{AM,2}$, and eq 1 or 2. The results are tabulated in Tables II and III. For the n -alkane series, the agreement of these values (set I, Table III) with those based on viscosity data (set III) is also good.

Similar concordance has been previously found in the CH_3NC system.^{4,5}

Values of $\sigma_{M,n}$ have been computed from the relation, $s_{AM,n} = \sigma_{AM,n}[\Omega^{(2,2)*}]^{1/2}$, and the combining rules for $\sigma_{AM,n}$ and $\epsilon_{AM,n}$, and are given in Table III.

Comparison with the CH_3NC System. From energy-transfer results in the CH_3NC system, a mean value of $\Delta s_{AM} = 0.31 \text{ \AA}$ was determined for the present two homologous series and a mean of 0.33 \AA if values for the related n -alkyne series are also included. The latter value corresponds to $\Delta\sigma_M = 0.57 \text{ \AA}$ per CH_2 group in the hydrocarbon chain.⁵ In the present studies, the value $\Delta\sigma_M = 0.64 \text{ \AA}$ is deduced from the mean value of $\Delta s_{AM} = 0.395 \text{ \AA}$ (Table II). All values are encom-

passed by $\Delta\sigma_M = 0.60 \pm 0.04 \text{ \AA}$. Good agreement of these s values with earlier results from CH_3NC is found (cf. I and II, Table III).

The relative collisional efficiencies on a collision-per-collision basis, $\beta_0(\infty)$, calculated from the deduced s_{AM} values are gathered in Table IV; the corresponding quantities determined in the CH_3NC system are also given. Constancy of $\beta_0(\infty)$, near unity for $n \geq 2$ was noted above when the internally consistent s_{AM} values for ethane were used (set I). The viscosity-based values (set III) are less consistent and show an increase.

The enhanced collisional efficiencies of C_2H_6 and C_2H_4 for $\text{C}_2\text{H}_5\text{NC}$, relative to their efficiencies for CH_3NC , can be rationalized in terms of similar arguments presented in I.

A summary of data and collisional efficiencies is given in Table V.

1. *Angular Momentum Conservation.*⁷ These restrictions may be less severe for the $\text{C}_2\text{H}_5\text{NC}$ case since the orbital moment of inertia value for RNC collisions with C_2H_6 or C_2H_4 , I_L , is closer in magnitude to the principal moments, I_B and I_C of $\text{C}_2\text{H}_5\text{NC}$ than of CH_3NC , e.g., $I_L^{\text{C}_2\text{H}_6} \simeq 420$; $I_B^A \simeq 97$, $I_C^A \simeq 110$, amu \AA^2 , for EtNC ; and $I_L^{\text{C}_2\text{H}_4} \simeq 370$, $I_C^A \simeq 50$ amu \AA^2 , for CH_3NC . More effective coupling of these moments *via* the collision complex occurs in the $\text{C}_2\text{H}_5\text{NC}$ case, such

that obedience to conservation of total angular momentum is more favorable, relative to the CH_3NC case, for collision with energy transfer.

On the other hand, the values of the moments of inertia, I_A , I_B , I_C , for C_2H_4 and C_2H_6 (Table VI) which contribute to the total rotational angular momentum are more comparable with the I_C^A values of CH_3NC than with $I_{B,C}^A$ of $\text{C}_2\text{H}_5\text{NC}$, and rotational coupling is, on this basis, expected to be more enhanced, especially for C_2H_4 , in the CH_3NC case.

2. *Effective Number of Transitional Modes of the Collision Complex.* The molecule figure axis rotation may be taken active for intermolecular energy exchange for $\text{C}_2\text{H}_5\text{NC}$, in contrast to its role as an ineffective heat reservoir for transfer of internal energy from CH_3NC .^{7,8} Thus the effective number of transition modes is larger for $\text{C}_2\text{H}_5\text{NC}$ and results in an increase of energy-transfer efficiency.

3. *Substrate Complexity.* The change in complexity of the substrate molecule provides a counterbalancing factor to the observed trend; $\text{C}_2\text{H}_5\text{NC}$ is a larger energy sink than CH_3NC and the removal of energy is expected to be a less efficient process in the former case.

4. *Chemical Similarity.* It was pointed out earlier^{3,7} that for efficient complex deactivators, such as higher members of hydrocarbon series, some of the internal modes are probably active for intermolecular energy exchange. Since the alkyl moiety of the $\text{C}_2\text{H}_5\text{NC}$ molecule resembles the hydrocarbon bath molecule more than that of CH_3NC , some internal modes in this group of the substrate molecule might provide an energy removal path that is not as favored for the CH_3NC homolog with its smaller and tighter methyl alkyl group.

Table VI: Moments of Inertia, amu \AA^2

	C_2H_6^a	C_2H_4^b	CH_3NC^c	$\text{C}_2\text{H}_5\text{NC}^c$
I_A	3.0	6.5	3.2	12.6
I_B	17.0	25.3	50.3	97.8
I_C	20.0	25.3	50.3	110.4

^a Reference 7. ^b B. S. Rabinovitch and D. W. Setser, *Advan. Photochem.*, **3**, 1 (1964). ^c K. M. Maloney and B. S. Rabinovitch, *J. Phys. Chem.*, **73**, 1652 (1969).

- (7) Y. N. Lin and B. S. Rabinovitch, *J. Phys. Chem.*, **74**, 3151 (1970).
 (8) K. M. Maloney and B. J. Rabinovitch, *ibid.*, **73**, 1652 (1969).

Flash Photolysis of Chlorate Ion in Aqueous Solution

by F. Barat, L. Gilles, B. Hickel, and B. Lesigne

Service de Chimie Physique, Cen-Saclay, B.P. No. 2, 91 Gif S/Yvette, France (Received November 23, 1970)

Publication costs assisted by Commissariat a L'Énergie Atomique

The flash photolysis of aqueous deaerated or oxygenated solutions of chlorate ion in its 200-nm absorption band gives rise to OH, ClO⁻, O₃, and ClO₂ species. This latter is partly consumed by reaction with OH radicals; the rate constant $k_{\text{OH}+\text{ClO}_2}$ is found to be $1.3 \pm 0.4 \times 10^9 \text{ M}^{-1} \text{ sec}^{-1}$. The formation of these species may be explained on the basis of four decomposition processes from the excited singlet state of the ClO₃⁻ ion. The ratio between the rate constants of direct recombination of O(³P) atoms and of ozone formation $[k_{\text{O}(\text{3P})+\text{O}(\text{3P})}]/[k_{\text{O}(\text{3P})+\text{O}_2}] = 7.0 \pm 0.5$.

Introduction

The flash photolysis of BrO₃^{-1,2} and IO₃⁻³ ions in aqueous solution has been studied recently, but the publications dealing with the chlorate ion are few: Bridge and Matheson⁴ mention a short-lived transient species (<90 μsec) in the wavelength range below 250 nm.

The chlorate ion absorbs in the far-uv but the molar extinction coefficients are small, this being one of the main experimental difficulties of photolysis. Farkas and Klein⁵ ascribe this spectrum to a charge transfer to the solvent, but more recently certain authors have pointed out that it is more probably due to an allowed electronic transition of the ¹E ← ¹A₁ type^{6a} or ¹A₁ ← ¹A₁ type.^{6b}

The purpose of the present work is to study the nature and kinetics of the transient species generated by excitation of the ClO₃⁻ ion in its 200-nm absorption band.

Experimental Section

The flash photolysis setup was the same as described elsewhere.⁷ The flash lamp was made of high-purity silica (Quartz & Silice Pursil 453; 70% transmission at 200 nm) and its coaxial shielding permitted the cell (Suprasil) to be well illuminated, so that micromolar concentrations of transient species were obtained with a flash energy of 1300 J (4 μsec width at half intensity).

We used 150 UVP or CVP (Radiotechnique) or 1P28 (RCA) photomultipliers for kinetic studies.

Weak absorption signals below 300 nm are perturbed for about 50 μsec by light scattered from the photolytic flash, so in order to make measurements under these conditions, we replaced the usual monitoring light source (xenon arc XBO 450W) by a flash of long duration (1 msec) obtained by discharging eight capacitors (70 μF), connected in parallel with appropriate inductances, through a silica capillary lamp. The shape of this flash varies with the wavelength, but it is possible

to isolate a "plateau" of about 200 μsec, during which the absorption measurements were made.

The solutions, usually $2 \times 10^{-3} \text{ M}$, were prepared by dissolving analytical grade potassium chlorate (Pro-labo, RP) in triply distilled water. They were deaerated by argon bubbling. Under these conditions, the remaining oxygen concentration was held below $5 \times 10^{-7} \text{ M}$ and the pH was 5.8. No buffers were employed because they absorb light in the same wavelength range as ClO₃⁻. For the same reason no useful experiments may be performed in alkaline media above pH 10. In some experiments, the solutions were acidified with perchloric acid (Merck).

Results

1. Spectroscopic Observations. The absorption spectrum of the chlorate ion between 195 and 250 nm obtained with a Cary 14 spectrophotometer was identical with that found by Farkas and Klein.⁵

Figure 1 shows the spectrum of transient species recorded 250 μsec after the flash, which permits the ClO₂ radical to be identified; this radical has already been observed in our laboratory as a primary product of photolysis⁸ with maximum absorption at 360 nm.⁹ The absorption band with a maximum between 290 and 300 nm, which is not observed in acid media (pH 2), is attributed to the ClO⁻ ion.¹⁰ On the basis of its sharp

- (1) O. Amichai and A. Treinin, *Chem. Phys. Lett.*, **3**, 611 (1969).
- (2) O. Amichai, G. Czapski, and A. Treinin, *Israel J. Chem.*, **7**, 351 (1969).
- (3) O. Amichai and A. Treinin, *J. Phys. Chem.*, **74**, 830 (1970).
- (4) N. K. Bridge and M. S. Matheson, *ibid.*, **64**, 1280 (1960).
- (5) L. Farkas and F. S. Klein, *J. Chem. Phys.*, **16**, 886 (1948).
- (6) (a) R. F. W. Bader, *Mol. Phys.*, **3**, 137 (1960); *Can. J. Chem.*, **40**, 1164 (1962); (b) A. Treinin and M. Yaacobi, *J. Phys. Chem.*, **68**, 2487 (1964).
- (7) F. Barat, L. Gilles, B. Hickel, and J. Sutton, *J. Chem. Soc. A*, 1982 (1970).
- (8) F. Barat, L. Gilles, B. Hickel, and J. Sutton, *Chem. Commun.*, 1485 (1969).
- (9) N. Konopik, J. Derkosch, and E. Berger, *Monatsh. Chem.*, **84**, 214 (1963).
- (10) M. Anbar and I. Dostrovsky, *J. Chem. Soc.*, 1105 (1954).

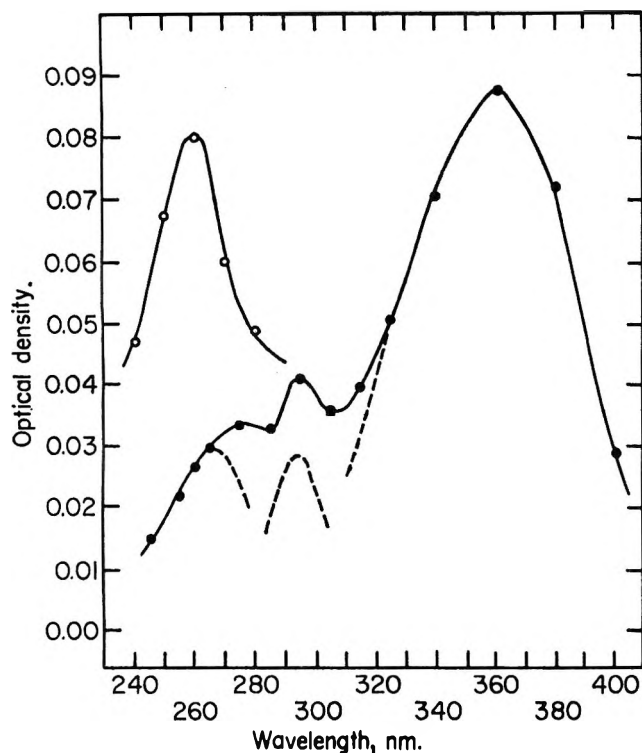


Figure 1. Absorption spectrum of transient species formed in the flash photolysis of $2 \times 10^{-3} M$ ClO_3^- solution recorded 250 μsec after the flash: ●, deaerated solution; ○, aerated solution.

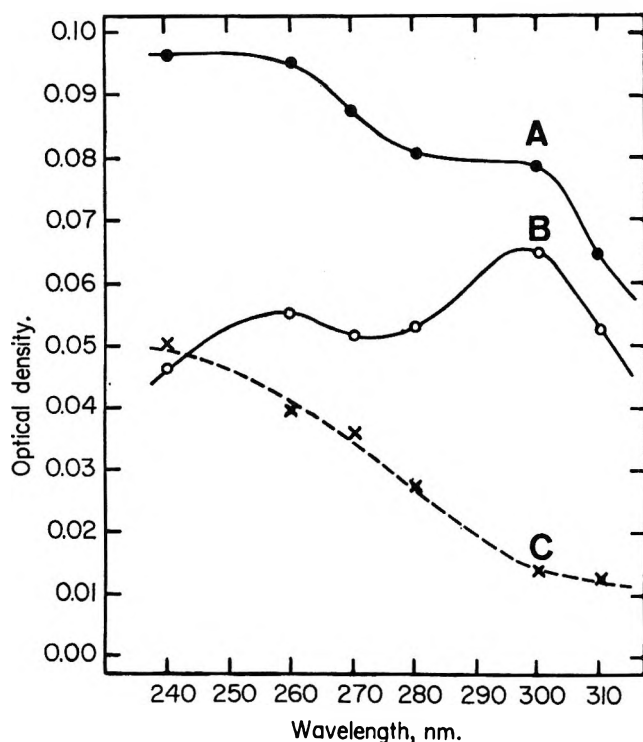


Figure 2. Absorption spectrum of transient species in the flash photolysis of $2 \times 10^{-3} M$ ClO_3^- deaerated solution: (A) ●, recorded 30 μsec after the flash; (B) ○, recorded 500 μsec after the flash; (C) × dashed curve, OH absorption spectrum.

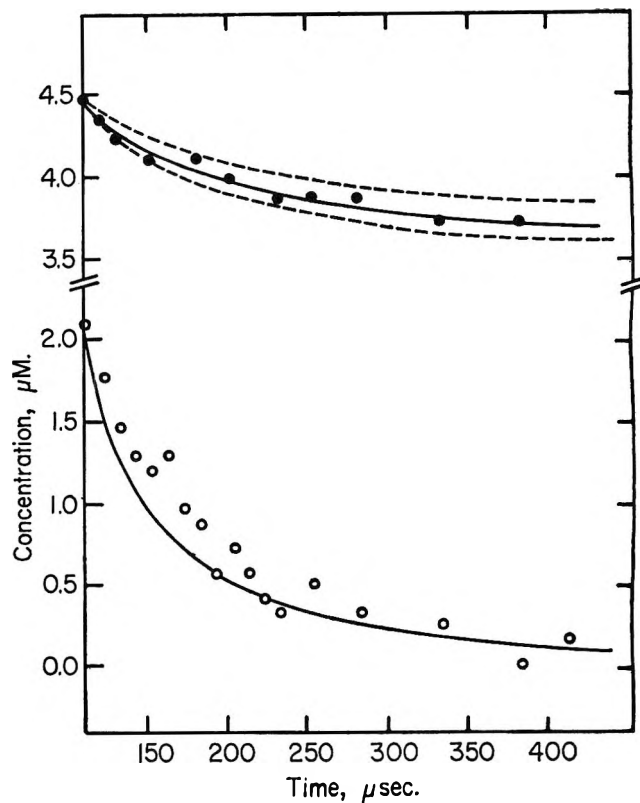


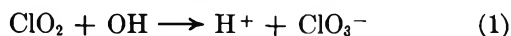
Figure 3. Decay of ClO_2 and OH concentrations vs. time in the flash photolysis of $2 \times 10^{-3} M$ ClO_3^- deaerated solution: ●, ClO_2 experimental results (360 nm); ○, OH experimental results (240 nm); full curve, theoretical decay of ClO_2 and OH ($k_{\text{OH}+\text{OH}} = 5 \times 10^9 M^{-1} \text{sec}^{-1}$; $k_{\text{OH}+\text{ClO}_2} = 1.3 \times 10^9 M^{-1} \text{sec}^{-1}$); dashed curve, theoretical decay of ClO_2 with $k_{\text{OH}+\text{ClO}_2} = 1.0 \times 10^9 M^{-1} \text{sec}^{-1}$ (upper curve) and $k_{\text{OH}+\text{ClO}_2} = 1.6 \times 10^9 M^{-1} \text{sec}^{-1}$ (lower curve).

increase in intensity in aerated media, the absorption band peaking at 260 nm is attributed to ozone.¹¹

The absorption spectrum between 240 and 300 nm of transients present 30 μsec after the photolytic flash (long duration spectroscopic flash) is illustrated in Figure 2, curve A. Curve B shows the same spectrum as observed using this technique, but after a delay of 500 μsec . We again find the results of Figure 1, *i.e.*, the spectra of ClO^- and O_3 . Curve C represents the difference A minus B, and is probably the spectrum of the OH radical.¹²

2. *Decay of ClO_2 and OH .* The study of the variation of ClO_2 concentration with time, as observed at 360 nm, shows that this radical is partly consumed during about 400 μsec after the photolytic flash; this is precisely the time required for complete disappearance of the OH radicals (Figure 3).

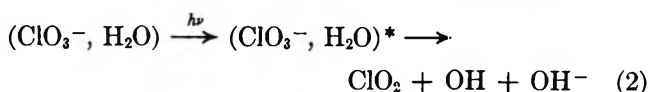
We think that the reaction



(11) M. L. Kalpatrick, C. C. Herrick, and M. Kilpatrick, *J. Amer. Chem. Soc.*, **78**, 1784 (1956).

(12) P. Pagsberg, H. Christensen, J. Rabani, G. Nilsson, J. Fenger, and S. O. Nielsen, *J. Phys. Chem.*, **73**, 1029 (1969).

which is the reverse of the photodissociation process



competes with the recombination of the hydroxyl radicals



and so accounts for the partial decrease of ClO_2 .

The dashed curves in Figure 3 were computed on the assumption that $k_{(\text{OH}+\text{OH})} = 5 \times 10^9 \text{ M}^{-1} \text{ sec}^{-1}$,¹² with $k_{(\text{OH}+\text{ClO}_2)}$ being different values ranging between $1.0 \times 10^9 \text{ M}^{-1} \text{ sec}^{-1}$ and $1.6 \times 10^9 \text{ M}^{-1} \text{ sec}^{-1}$ (ϵ_{ClO_2} at 360 nm and ϵ_{OH} at 240 nm were taken equal to $1240 \text{ M}^{-1} \text{ cm}^{-1}$ ¹³ and $500 \text{ M}^{-1} \text{ cm}^{-1}$,¹² respectively). The value which best fits our experimental data is

$$k_{(\text{OH}+\text{ClO}_2)} = 1.3 \pm 0.4 \times 10^9 \text{ M}^{-1} \text{ sec}^{-1}$$

From the good agreement between experimental and calculated values, we conclude that in the flash photolysis of the chlorate ion, the disappearance of OH radicals is mainly due to the reactions 1 and 3 and that reactions like



are not important under our experimental conditions. Assuming that these reactions do not participate more than 10% in the general scheme, we may derive upper limiting values for k_4 and k_5

$$k_4 \leq 4 \times 10^5 \text{ M}^{-1} \text{ sec}^{-1}$$

$$k_5 \leq 2 \times 10^8 \text{ M}^{-1} \text{ sec}^{-1}$$

This latter seems to be very low compared with the corresponding rate constant of the reaction between hydroxyl radicals and BrO^- .¹⁴

Another method was used to determine k_1 . Figure 4 represents ClO_2 vs. time after the photolysis of a solution of $2 \times 10^{-3} \text{ M}$ chlorate containing an initial concentration of $8.7 \times 10^{-6} \text{ M}$ ClO_2 . Under these conditions, an amount of ClO_2 equal to the concentration of OH radicals produced during the flash disappears, and we conclude that reaction 1 is the main decay process for these radicals. The plot of $\log [\text{OH}]/[\text{ClO}_2]$ vs. time is a straight line (Figure 5), whose slope gives $k_1 = 1.6 \pm 0.4 \times 10^9 \text{ M}^{-1} \text{ sec}^{-1}$, in good agreement with the previous result. In this experiment, possible error may arise from the slight photolytic decomposition of the ClO_2 molecule.

3. *Decay of O_3 .* The disappearance of O_3 formed in an oxygenated chlorate solution is a pseudo-first-order reaction (Figure 6); the experimental rate constant is 5.2 sec^{-1} , a value ten times greater than that found in the flash photolysis of the bromate ion (0.53 sec^{-1}).¹⁵ This rate constant, which does not depend on

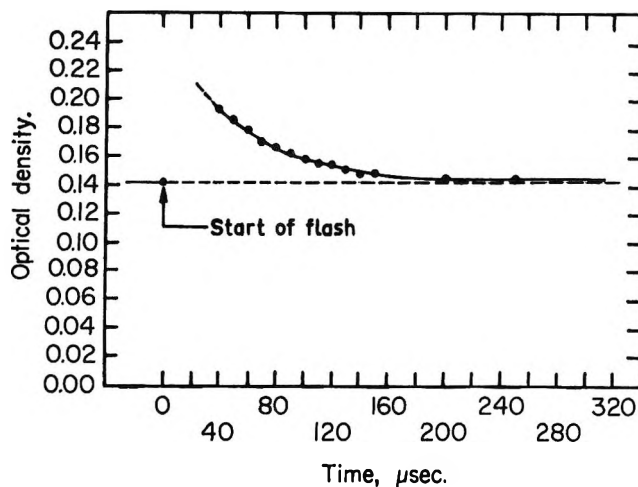


Figure 4. Flash photolysis of ClO_3^- ($2 \times 10^{-3} \text{ M}$) containing ClO_2 ($8.7 \times 10^{-6} \text{ M}$). Decay of ClO_2 vs. time.

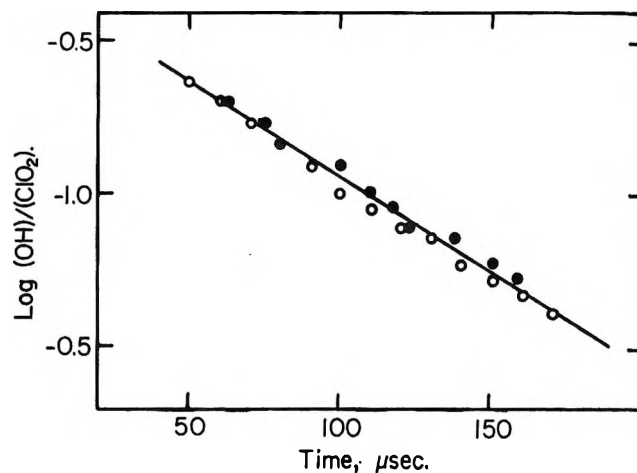


Figure 5. Flash photolysis of ClO_3^- ($2 \times 10^{-3} \text{ M}$) containing ClO_2 ($8.7 \times 10^{-6} \text{ M}$): experimental points for the second-order reaction between OH and ClO_2 : O, first series of experiments; ●, second series of experiments.

chlorate concentration and pH (5.8–2.0), increases after a second photolysis ($k_{\text{obsd}} = 6.8 \text{ sec}^{-1}$) (Figure 6), thus showing that O_3 probably disappears by reaction with long-lived photolysis products, such as ClO^- and ClO_2 in neutral media or HClO and ClO_2 in acid media. The initial concentrations of ClO^- and ClO_2 , three times greater than the O_3 concentration, may explain the pseudo-first order observed.

4. *Decay of ClO^- .* In the photolyzed solutions (initial pH 5.8), the rate of decay of ClO^- at 292 nm is slow; this ion totally disappears after about 2 sec. The pK of HClO is 7.4;¹⁰ ClO^{16} is probably slowly

(13) R. G. Kieffer, Ph.D. Thesis, University of Maryland, 1966.

(14) G. V. Buxton and F. S. Dainton, *Proc. Roy. Soc., Ser. A*, 304, 427 (1968).

(15) F. Barat, L. Gilles, B. Hickel, and B. Lesigne, unpublished work.

(16) P. Pascal, "Nouveau Traité de Chimie Minérale," Vol. XVI, Masson et Cie, Paris, 1960, p 246.

protonated, the hypochlorous acid formed during the reaction having a lower extinction coefficient at 292 nm (ca. $30 M^{-1} \text{cm}^{-1}$)¹⁰ than the ClO^- ion.

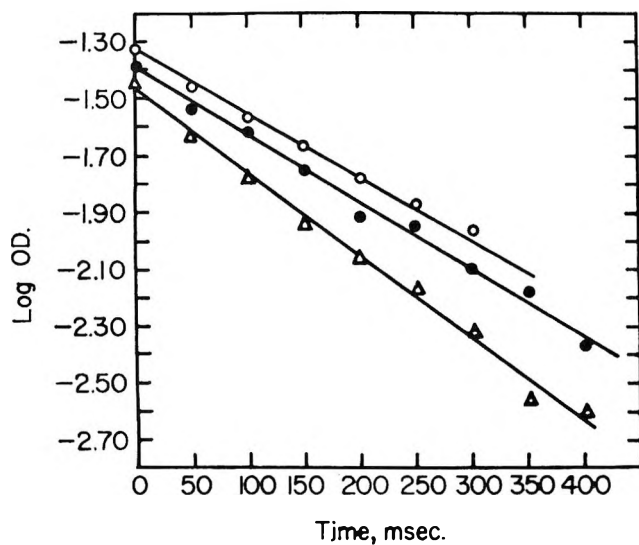
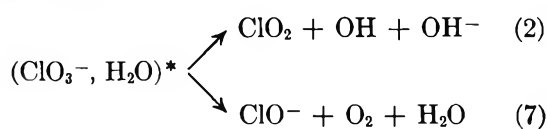
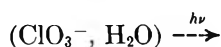


Figure 6. Pseudo-first-order decay of O_3 : ○ and ●, first photolysis (two different experiments); Δ, second photolysis.

Discussion

1. Primary Processes Involved in Photodissociation.

The results of the flash photolysis of the chlorate ion provide evidence that two mechanisms are responsible for primary dissociation of the molecule in the excited single state.



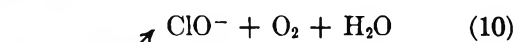
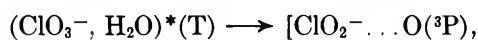
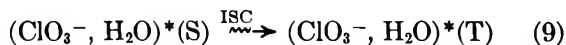
This first mechanism (radical dissociation) is common to all halate ions,^{2,3,8} though in the case of the IO_3^- ion there is a conflicting attribution of the IO_2 spectrum.^{3,8}

The second mechanism, which leads to the formation of XO^- species, has been observed in our laboratory for the BrO_3^- ion; the BrO^- fragment was rapidly oxidized by the hydroxyl radicals

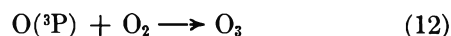


with $k_8 = 4.5 \times 10^9 M^{-1} \text{sec}^{-1}$.¹⁴

However, we may ask whether the ClO^- ion produced by flash photolysis of the ClO_3^- ion is generated in one or more steps. It could be formed indeed by a third process, namely, the dissociation of a triplet state of ClO_3^- , derived from the excited singlet state by intersystem crossing.

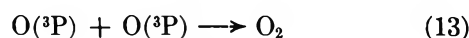
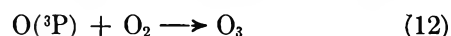
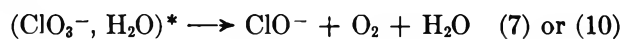


Amichai and Treinin reported¹⁷ that by adding allyl alcohol, which is a good scavenger for O atoms, the formation of molecular oxygen during flash photolysis of bromate ions is suppressed. In our study, the ozone spectrum observed also gives good evidence of $\text{O}(^3\text{P})$ production, since reaction 11 is followed by reaction 12.

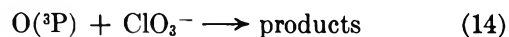


Unfortunately, no experiment can be performed to show the occurrence of reaction 10, since all the $\text{O}(^3\text{P})$ atom scavengers having molar or decimolar concentrations absorb light in the same wavelength range as ClO_3^- .

2. *Reactions with O Atoms. Formation of Molecular Oxygen and Ozone.* The experimental results show that the flash photolysis of the chlorate ion in a deaerated aqueous solution gives rise to ozone production (Figure 1). This production mainly depends on three reactions.



The slowest among these (reaction 12) probably has a rate constant greater than $10^9 M^{-1} \text{sec}^{-1}$ (according to studies made in the gaseous phase).¹⁸ Thus reaction 14



does not intervene, since the rate constant k_{14} is smaller than $10^{-4} \times k_{13}$.¹

In order to obtain a value of the ratio k_{13}/k_{12} (rate constants of direct recombination of $\text{O}(^3\text{P})$ atoms in solution vs. ozone formation), from the growth curve of O_3 , it is necessary to know the initial concentrations of O_2 and $\text{O}(^3\text{P})$ formed in the reactions 7 or 10 and 11. The initial concentration of O_2 ($6 \times 10^{-6} M$) was supposed equal to the initial ClO^- concentration and this latter was estimated (a) from the optical density of ClO^- obtained by Gaussian analysis of the spectrum of Figure 1 taking ϵ_{ClO^-} at 290 nm = $340 M^{-1} \text{cm}^{-1}$,¹⁰ and (b) from the change in optical density at 290 nm in passing from neutral to acid pH ($\epsilon_{\text{HClO}} \ll \epsilon_{\text{ClO}^-}$). Both methods gave the same results.

(17) O. Amichai and A. Treinin, unpublished work.

(18) F. Kaufmann in "Progress in Reaction Kinetics," Vol. 1, G. Porter, Ed., Pergamon Press, London, 1961, p 1.

The initial concentration of $O(^3P)$ atoms ($2.1 \times 10^{-6} M$) was taken equal to the concentration of ozone produced by photolysis of an oxygenated solution assuming that reaction 12 alone is efficient (ϵ_{O_3} at 260 nm is $2900 M^{-1} cm^{-1}$).^{11,19}

This enabled the ratio k_{13}/k_{12} to be determined by computer calculations.

This ratio is equal to 7.0 ± 0.5 , which is in good agreement with the results obtained in the gaseous phase, which give k_{13}/k_{12} for reactions 12 and 13 written in the form of three-body collisions ranging from 4 to 20.¹⁸

(19) J. W. Boyle, J. A. Ghormley, and C. J. Hochanadel, Chemistry Division Annual Progress Report, May 20, 1969, ORNL 4437, p 49.

Reaction of Hexamethyldisilazane with Silica

by W. Hertl and M. L. Hair*¹

Research and Development Laboratories, Corning Glass Works, Corning, New York 14830 (Received November 5, 1969)

Publication costs assisted by Corning Glass Works

Infrared spectroscopy has been used to determine the kinetics of the reaction of hexamethyldisilazane (HMDS) with the OH groups on the surface of silica. The reaction with the freely vibrating OH groups follows second-order kinetics (*i.e.*, two OH are removed when one HMDS molecule reacts) and has an activation energy of 18.5 kcal/mol. The reaction rate is given by: $rate = A \exp(-18,500/RT) [OH]^{2.0} [\theta]^{1.7}$, where A is a constant, $[OH]$ is the fraction of OH present at any time, and $[\theta]$ is the fraction of OH groups covered by physically adsorbed HMDS. Only a small fraction of mutually H-bonded OH groups react with HMDS. Two reaction schemes are considered and the significance of the intermediate physically adsorbed state is discussed.

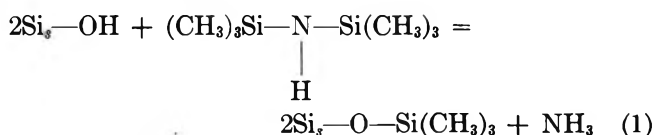
Introduction

Hexamethyldisilazane is widely used for deactivating gas chromatographic support materials.² In view of its importance for this purpose, a kinetic study was undertaken in order to better understand the mechanism of the reaction and to determine the optimum conditions for the reaction with silica.

Previous studies³⁻⁵ with other coupling and deactivating agents such as the chloro- and methoxysilanes have shown that the principal bonding site on silica is the freely vibrating hydroxyl group. These other studies have also helped to better elucidate the nature of the surface hydroxyl groups. The chemical properties of the silica OH groups which are of importance in these surface bonding reactions can be summarized as follows. (i) The freely vibrating hydroxyl groups can occur in a geminal $[Si-(OH)_2]$ or single $[Si-(OH)]$ configuration on the surface. With the silica used in these studies, about 60% of the OH groups are in a geminal and 40% in a single configuration. (ii) The freely vibrating hydroxyl groups are essentially monoenergetic, *i.e.*, the reactivity of all the OH groups is the same. This means that these groups react randomly. No particular preference is shown in the reactivity of the single or geminal groups, and the presence of these groups is shown by the stoichiometry of the reaction rather than by any difference in reactivity.

(iii) Since these OH groups are monoenergetic, physical adsorption results in the same fraction of OH groups being covered for a given pressure and temperature, whether there are many or few OH groups on the surface. (iv) In general, mutually H-bonded OH groups on the surface are essentially nonreactive toward the various bonding agents.

With hexamethyldisilazane (HMDS) the overall reaction taking place with the surface is



By spectroscopically measuring the disappearance of Si_3-OH during the course of the reaction, a reaction curve can be obtained. Since the OH groups react monoenergetically, the kinetic analysis of the reaction is relatively straightforward. This paper describes such an analysis.

(1) Xerox Corporation, Research Laboratories, Rochester, N. Y. 14603.

(2) J. Bohemen, S. H. Langer, R. H. Perrett, and J. H. Purnell, *J. Chem. Soc., London*, 2444 (1960).

(3) W. Hertl, *J. Phys. Chem.*, **72**, 1248 (1968).

(4) W. Hertl, *ibid.*, **72**, 3993 (1968).

(5) M. L. Hair and W. Hertl, *ibid.*, **73**, 2372 (1969).

Experimental Section

The experimental apparatus and procedures used were similar to those described previously for similar studies.³⁻⁵ Briefly, a silica disk, mounted in a furnace connected to a vacuum rack, was placed in an infrared spectrophotometer. The gaseous reagent was admitted to the furnace and allowed to react for a given time; the furnace was then evacuated. A spectrum was taken and the procedure was repeated. Spectra were taken at intervals of a few per cent reaction so that the gas-phase composition was essentially constant during the course of the reaction.

Kinetic Analysis of the Reaction Curves

Measurement of the intensity of the band due to the freely vibrating hydroxyl group (3745 cm^{-1}) at various times during the course of the reaction gives the reaction curve. The points from the reaction curves were plotted using the integrated form of various order rate equations. The order of the integrated rate equation m , which gives a linear plot for the greater part of the reaction ($>75\%$ reaction) gives the order of the reaction with respect to the number of surface sites (the OH groups) removed when one siloxane molecule reacts with the surface. This interpretation is valid since the OH groups are monoenergetic and react randomly. The generalized integrated rate equation has the form

$$kt = \frac{1}{(m-1)} \left[\frac{1}{(a-x)^{m-1}} \right] = \frac{1}{(a)^{m-1}} \quad (2)$$

where k is the experimental rate constant, a is the initial concentration of OH groups, here defined as 1.00, x is the fraction of the OH which reacted at time t , and m is the order of the reaction.

Comparison of the peak intensity of the OH band with the gas present at any time during the reaction with that under vacuum gives the fraction of OH groups not covered by physically adsorbed molecules ($1 - \theta$). The fraction of unreacted OH groups covered by physically adsorbed HMDS (θ), at any given temperature and pressure, remains constant during the course of a reaction. At a given temperature a log-log plot of the rates obtained with various HMDS pressures against the fraction of OH groups covered by physically adsorbed HMDS (θ) at that pressure results in a linear plot; the slope (n) of this plot gives the dependence of the rate as a function of θ (i.e., θ^n). The quantity, n , is interpreted as the number of sites occupied by one physically adsorbed HMDS molecule and is in agreement with data obtained for the physical adsorption of ammonia on surface silanol groups. The specific rate constant, then, is k/θ^n .

By measuring both θ and the reaction rates at various temperatures, an Arrhenius plot of k/θ^n can be obtained, which gives the experimental activation energy of the reaction.

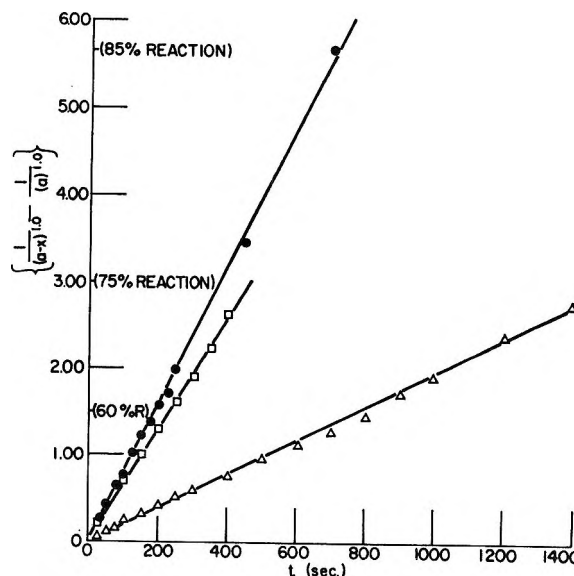


Figure 1. Some typical second-order kinetic plots for reaction of HMDS with silica: Δ , $P = 5$ Torr of HMDS, $T = 31^\circ$; \square , $P = 15$ Torr of HMDS, $T = 31^\circ$; \bullet , $P = 10$ Torr of HMDS, $T = 65^\circ$.

It should be noted that in most studies of this type, the rate dependence on the surface coverage is usually given by a complex function of the pressure, which represents the adsorption isotherm. In this study this is unnecessary, since the surface coverage is measured directly.

Results and Discussion

After following a number of HMDS-SiO₂ reactions, it was found that linear plots were obtained when a second-order rate equation was used. Figure 1 shows some typical second-order kinetic plots.

It should be noted that no consistent initial fast reaction is revealed by these plots, although some do show a small positive intercept. If this intercept is real, it amounts to 8% or less of the total reaction. (In the case of the chlorosilanes, a large initial fast reaction, approximately 15%, was always observed.)

To determine the dependence of the reaction rate on surface coverage, a series of runs were carried out using various pressures of HMDS. Measurements of the surface coverage (θ) were also made at each pressure. As the absolute surface reactivities varied from silica sample to silica sample, the first 40% of each reaction was carried out under standardized conditions (in this case 5 Torr of HMDS) and the remainder of the reaction used the desired pressure. By comparing the slope of the latter part of the kinetic plot with the initial part, a relative rate constant (k/k_{ref}) was obtained. The upper part of Figure 2 gives the values of the relative rate constants measured at various pressures, and the lower part gives the measured surface coverage (θ) at the same pressures. Figure 3 gives log-log plots of the relative rate constants against the surface coverage

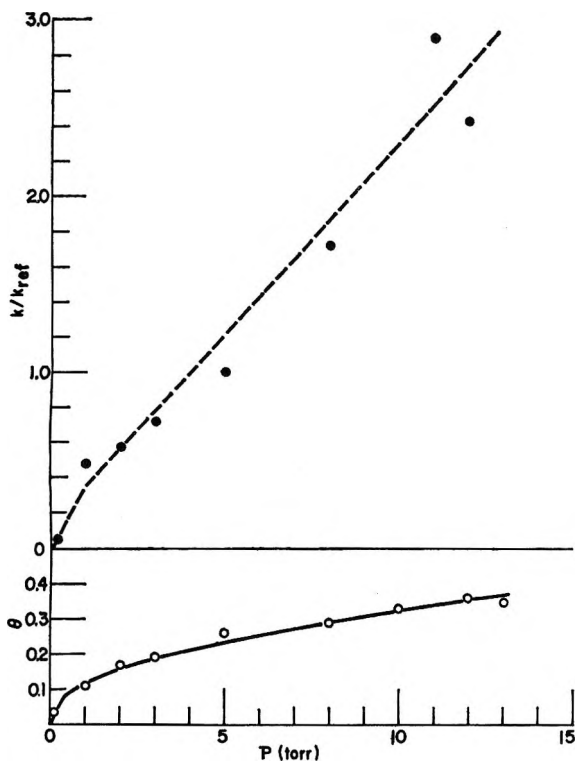


Figure 2. Top, plots of the relative rate constants, k/k_{ref} , for various pressures of HMDS at 65° . k_{ref} is the rate constant with 5 Torr of HMDS. Bottom, surface coverage of the hydroxyl groups (θ) for various pressures of HMDS.

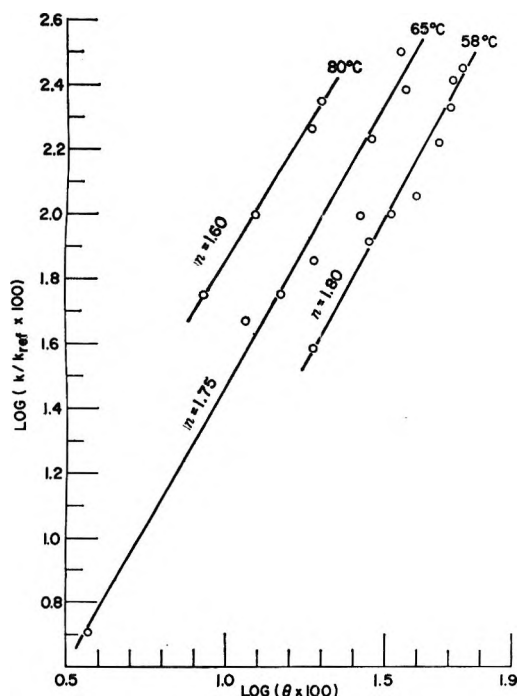


Figure 3. Log-log plots of k/k_{ref} against θ for three different temperatures ($n = \text{slope}$). The data for 65° are taken from Figure 2.

for three different temperatures. The average of the three slopes is 1.72, so that the rate of the reaction varies as $\theta^{1.72}$. The rapidity of the reaction makes it difficult

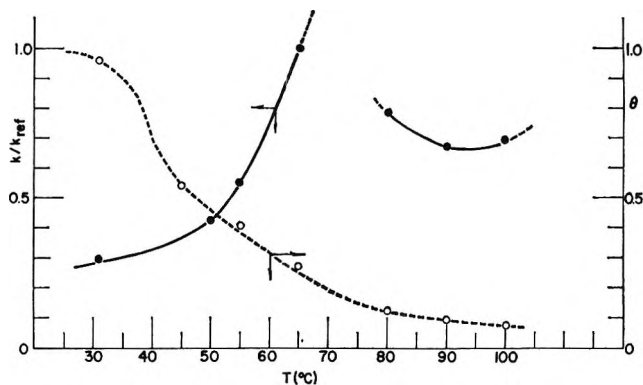


Figure 4. Plots of relative rate constants, k/k_{ref} , (solid line) and fraction of OH groups (θ) covered by physically adsorbed HMDS (dashed line) at various temperatures. All pressures are 5 Torr; k_{ref} measured at 65° .

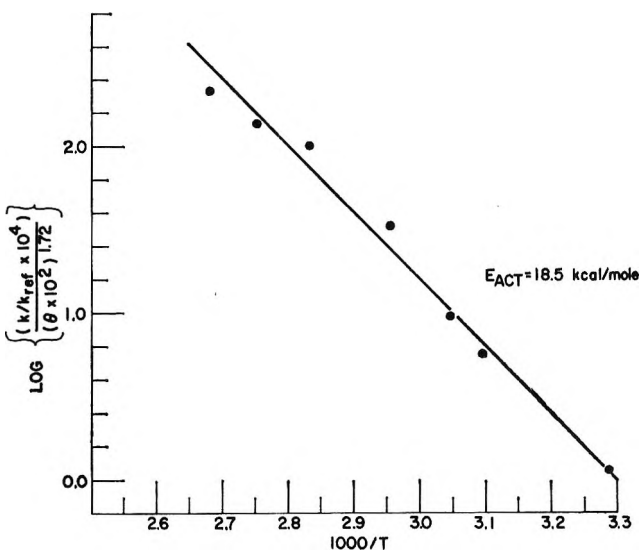


Figure 5. Arrhenius plot of specific rate constants, $(k/k_{ref})/\theta^n$. The data are taken from Figure 4.

to obtain the precise values of the surface coverages at the various temperatures and pressures, resulting in a rather large amount of scatter in the data.

In Figure 4 both the relative rate constants and the surface coverages are plotted as a function of temperature at a constant pressure. It is seen that the reaction rate goes through a maximum due to the fact that the rate of the bonding reaction increases continuously with increasing temperature, but the surface coverage decreases with increasing temperature. In order to obtain the specific rate constant, the calculated values of the relative rate constant must be divided by the surface coverage dependence (*i.e.*, by $\theta^{1.72}$). These are given on the Arrhenius plot in Figure 5. The slope of this plot gives the experimental activation energy of 18.5 kcal/mol.

The experimental reaction rate at 31° is independent of HMDS pressure (from 4 to 15 Torr). Figure 4 shows that with 5 Torr of HMDS the surface coverage is

about 97%. Thus, any increase in pressure could only make the surface coverage approach 100%, the difference between these two values being too small in which to detect a difference in rate.

HMDS is considerably more reactive than any of the other silanes previously studied. The HMDS reaction proceeds at a rapid rate at 30°, compared with 200° for the methoxysilanes and 350° for the chlorosilanes.

Role of H-Bonded OH Groups

With other coupling agents (methoxysilanes, chlorosilanes) it was found that the H-bonded OH groups, if present on the silica surface, reacted only slightly. Experiments with HMDS on a silica surface containing H-bonded OH groups showed that this reagent, also, reacts only slightly with these groups. Even at 200° no further reaction with the H-bonded OH groups is observed. The HMDS reacts only with those H-bonded OH groups which give rise to the high frequency end of the OH band (above 3650 cm⁻¹) and this slight amount of reaction takes place only initially during the reaction. Snyder and Ward⁶ observed a similar effect in the reaction of methylchlorosilanes with silica.

As with the other systems which have been studied, the reactivity of the silica varied from sample to sample (hence the need to measure relative rate constants), but no correlation was found between the reactivity and the presence or absence of H-bonded OH groups. Such a correlation had been found with the methoxysilanes.

Reaction with Adsorbed Water

With polyfunctional coupling agents, it is possible to obtain a polymerization reaction when the surface contains adsorbed water. This reaction can be differentiated from simple interaction with the surface hydroxyl groups by spectroscopically measuring the amount of organic material (the intensity of the C-H stretching bands) which is present on the sample after complete reaction with a number of wet and dry silica samples. Results are given in Table I. These results show that only a slightly larger amount of organic material is present on the wet samples than on the dry samples. This slightly larger amount is probably due to the concurrent presence of the H-bonded OH groups, which have been shown to react slightly, rather than to chemical reaction with the water that is present.

Spectra taken at the end of the reaction show no evidence of perturbed hydroxyl groups, thus indicating that all the freely vibrating OH groups are removed by chemical reaction and that none of them are tied up *via* hydrogen bonding with the other groups which are present on the surface (*i.e.*, with the -Si(CH₃)₃ groups).

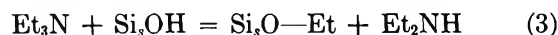
Reaction with Other Amines

Since diethylamine, Et₂NH, has a somewhat similar structure to HMDS, some experiments were carried out to see if this compound reacted with silica. Although it did not react with the silica surface, it did

Table I: Normalized Intensity of C-H Bands at End of Reaction

Silica treatment	Reaction conditions		C-H intensity
800°	31°	5 Torr of HMDS	0.456
800°	31°	10 Torr of HMDS	0.451
800°	31°	5 Torr of HMDS	0.483
800°	100°	5 Torr of HMDS	0.473
800°	65°	5 Torr of HMDS	0.514
800°	65°	5 Torr of HMDS	0.447
800°	65°	5 Torr of HMDS	0.454
Wet	31°	15 Torr of HMDS	0.565
Wet	31°	liquid reagent	0.558

physically adsorb at 400°, to the extent of about $\theta = 0.04$. At 400° this corresponds to $p/p_0 \simeq 10^{-3}$. Triethylamine did react, however, and at 400° about 30% of the hydroxyl groups were removed after 7 hr. None of the observed bands occur when silica reacts with NH₃ at high temperatures (800°) and thus the reaction taking place must be of the type



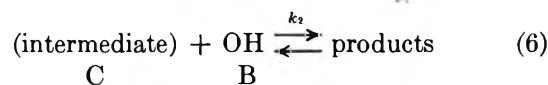
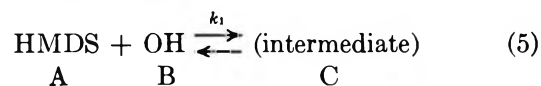
or



Interpretation of Kinetic Parameters

The second-order kinetics observed in these experiments can be accounted for by two reaction schemes. The first scheme is simply that shown in eq 1 where a simple, one-step, three-centered reaction is proposed. This scheme implies that all the hydroxyl groups on the surface are sufficiently close together that they can react in pairs.

Alternatively, the reaction might be considered to consist of the following reactions.



$$-\frac{dB}{dt} = k_1AB + k_2CB \quad (7)$$

The steady-state approximation $dC/dt = 0$ gives $C = k_1/k_2A$ and $-dB/dt = 2k_1AB$, which is first order in B . However, it is experimentally known that, for given conditions, the fraction of B covered by A remains constant, thus $A = k'B$ and $-dB/dt = 2k_1k'B^2$, thus accounting for the second-order kinetics. (Alternatively in these surface reactions it seems reasonable to assume that the intermediate C is adsorbed on B . In

(6) L. R. Snyder and J. W. Ward, *J. Phys. Chem.*, **70**, 3941 (1966).

this case its concentration will vary as the concentration of B and $C = k''B$. Then

$$-\frac{dB}{dt} = k_1k'B^2 + k_2k''B^2 \quad (8)$$

$$= (k_1k' + k_2k'')B^2 \quad (9)$$

and the reaction is second order in B.)

The rate of the surface reaction can be given by an equation of the form

$$\text{rate} = A \exp(-E/RT)[\text{OH}]^m[\theta]^n \quad (10)$$

or, at constant temperature

$$\text{rate} = r = k[\text{OH}]^m[\theta]^n \quad (11)$$

Two possibilities can be envisaged. If $m = n$, then eq 11 can be written

$$\text{rate} = k\{[\text{OH}] \cdot [\theta]\}^m \quad (12)$$

The product $[\text{OH}] \cdot [\theta]$ is just the total number of OH available at any time which are actually covered with an adsorbed reactive molecule. This quantity is the actual "active mass" which can enter into reaction at any given time, and the value of OH which must be considered is not the total number which remain unreacted at any time, but the number which remain unreacted and which are also covered with a physically adsorbed molecule. This implies that the rate-determining step involves a rearrangement of a "(reacting molecule)-(OH group)" complex. In this case m must always be equal to n and is determined by the stoichiometry of the reaction. If $m = n$, this indicates that the rate-determining step is the reaction between the physically adsorbed molecule and the OH group. In this case, m is controlled by the stoichiometry of the reaction and n is controlled by the stoichiometry of the adsorption process.

Experimentally, eq 2 is found to be

$$r = A \exp(-18,500/RT)[\text{OH}]^{2.0}[\theta]^{1.72} \quad (13)$$

The dependence of the reaction rate on the surface coverage is $\theta^{1.72}$ and one interpretation of this is that 1.72 surface sites, on average, are covered by an adsorbed HMDS molecule (since the molecule must be physically adsorbed before it can react). This value of 1.72, on average, corresponds to about 70% of the

molecules adsorbed on two sites and 30% adsorbed on a single site. This is in agreement with previous data for silica surfaces which indicated that about 60% of the surface OH groups are in a geminal configuration and 40% are single.⁷ It appears, then, that the HMDS molecules adsorb randomly on the surface OH groups (which is consistent with their being monoenergetic); those adsorbed on a single OH group, of course, occupy one site, and those adsorbed on geminal OH groups occupy both OH groups.

The value of $\theta^{1.72}$ is proportional to the effective surface concentration of HMDS, [HMDS], and thus eq 4 reduces to

$$r = k[\text{OH}]^{2.0}[\text{HMDS}] \quad (14)$$

This indicates that the rate-determining step is the reaction between the physically adsorbed molecules and the OH groups.

These points have been considered in some detail as in most surface kinetic studies they are either ignored or avoided by adjusting an isotherm equation to fit the data. Previously obtained values for m and n are collected in Table II. It is seen that for the methoxysilane systems, where it is possible to compare the values of m and n , the evidence indicates that $m = n$ and that the first explanation could be correct.

Table II: Rate Parameters for Reactions of Various Silanes with Silica^a

Silane	m	n	E , kcal/mol
Monomethoxy trimethyl	1.6	1.7	22 ± 3
Dimethoxy dimethyl	2.2	2.2	32 ± 1.5
Trimethoxy monomethyl	3.0	3.0	30.6
Monochlorotrimethyl	1.0		22.0
Dichlorodimethyl	1.6		22.6
Trichloromethyl	1.6		21.0
Tetrachloro	1.6		22.0
HMDS	2.0	ca. 1.7	18.5

^a The parameters m , n , and E are defined by eq 5.

Acknowledgment. The authors thank Miss E. R. Herritt for assistance in the experimental work.

(7) M. L. Hair and W. Hertl, *J. Phys. Chem.*, **70**, 4269 (1969).

The Rate and Mechanism of Interaction of Oxygen Atoms and Hydrogen Atoms with Silver and Gold¹

by Bernard J. Wood

*Surface Physics and Chemistry Group, Stanford Research Institute, Menlo Park, California 94025
(Received October 30, 1970)*

Publication costs assisted by the Stanford Research Institute

Rates of adsorption, occlusion, and recombination of oxygen atoms on silver and gold and of hydrogen atoms on gold were determined at 300°K by means of ultrahigh vacuum techniques. Oxygen atoms interact with clean silver primarily by adsorption and occlusion, whereas on gold recombination by way of an Eley-Rideal mechanism is the kinetically predominant process. The same recombination path for hydrogen atoms on gold is also highly favored, but the rate of recombination is limited by a slow adsorption step. Gaseous hydrogen atoms react with oxygen atoms preadsorbed on gold with unit efficiency.

Introduction

Studies of the physical and chemical interaction of gaseous atoms with solid surfaces have been carried out by a number of investigators for many years.² We have recently examined atom-surface interactions on initially clean surfaces at very low partial pressures of gaseous atoms. Our experiments, carried out with ultrahigh vacuum (UHV) apparatus and techniques, enabled us to evaluate the rates and paths of elementary processes involved in the interaction of oxygen atoms with silver and gold and hydrogen atoms with gold.

In general, four elementary processes can be postulated to cover the various modes of atom-surface interaction that result in loss of atoms from the gas phase. These include: a, adsorption (capture); b, occlusion (reaction with solid phase); c, recombination; d, reaction with other adsorbed species. Our objective was to discover and evaluate quantitatively the role of each of these processes in each of the gas-solid systems studied. By a combination of techniques we were able to measure the total rate of atom loss together with direct rate measurements of certain specific processes. The results provide considerable insight into the overall picture of atom surface interaction on the studied surfaces.

Experimental Approach

We measured the total atom-loss rate on a particular metal by observing the diminution in atom flux at the outlet of a reaction vessel in parallel experiments with and without a specimen of the metal in the vessel. (The total gas pressure and the entering flux of atoms in the reactor were held constant.) The experimental apparatus consisted of a cylindrical reaction vessel through which atoms flowed from a source at one end to a high-capacity vacuum pump at the opposite end. A mass spectrometer monitored the flux and composition of gas through the exit. Under the conditions of molecular flow, which apply throughout the pressure

range 10^{-5} to 10^{-9} Torr employed in this apparatus, simple kinetic theory suggests that once an atom enters the reactor it will depart through the exit or entrance aperture after suffering multiple collisions with the reactor wall. Hence, in principle, the probability of interaction (adsorption, recombination, occlusion) of the atom with the surface may be evaluated by measuring the change in transmission probability of the reactor when a portion of the reactor wall is covered with the material of interest. In practice, determination of a quantitative value of an atom-loss probability for the wall requires an analytical model for the system which specifies outlet flux as a function of wall loss coefficient. A number of such models have been developed for straight cylindrical pipes with uniformly reactive walls (*cf.* ref 7). The reactor employed in our experiments was cylindrical, but the ends of the cylinder were capped with closures containing smaller apertures, and the metal specimens did not cover the entire interior wall of the reactor. Consequently, it was necessary to develop an analytical model for the particular geometry employed in our experiments.

In our analysis,³ the interior surface of the reactor is divided into ring elements of finite width, each of which possesses a discrete value of atom-loss coefficient α . Atoms striking the surface of one of these elements are assumed to be removed (adsorbed, recombined, or occluded) with probability α or reflected with a spatial distribution density varying with the cosine law. Based on this assumption, we can state an "influence function" which defines the fraction of atoms emitted from one element of surface incident on a second element, and *vice versa*. For steady state, then, we may write a

(1) This research was sponsored by the National Aeronautics and Space Administration under Contract NASr-49(30).

(2) H. Wise and B. J. Wood, *Advan. At. Mol. Phys.*, **3**, 296 (1967).

(3) B. R. Baker and B. J. Wood, *J. Vac. Sci. Technol.*, in press.

system of integral equations which describes the net flux of atoms at any point on the surface in the reactor as the summation over the surface elements of the product of the emitted atom flux and the appropriate influence functions. An exit aperture of radius r_e is accounted for by setting $\alpha = 1$ for $0 < r < r_e$ in the outlet end of the reactor. The inlet aperture is represented by a cosine-distribution source function with unit flux intensity. The system of equations can be solved by numerical methods to give the average net incident atom flux intensity on any finite element of surface in the reactor. The analysis is thus applicable to reactors in which the atom-loss coefficient varies from point to point on the surface, as is the case in our experiments where the metal specimen occupies only a portion of the surface in the reactor.

The flux value of interest in our experiments is that at the reactor outlet. Hence we carried out a series of computations in which the inlet flux is held constant (at a nominal value of 1.0), the specimen dimensions are fixed, and the total exit flux is calculated for various values of α . These values of exit atom flux are then normalized with respect to the total outlet atom flux for the case for no specimen in the reactor ($\alpha = 0$). Figure 1 shows the predicted mass flow rate of atoms, Q , through the reactor exit when $1/2$ of the reactor wall is covered with a surface with loss coefficient α , relative to Q^* , the mass flow rate from a reactor with nonreactive walls ($\alpha = 0$). This particular specimen geometry was employed in a number of our experiments with the atomic oxygen-silver system. A detailed description of the analytical model is published elsewhere.³

We quantitatively determined the rates of specific elementary processes, such as adsorption, by using flash filament techniques. In these experiments specimens in the form of foil ribbons were mounted in the reactor in such a way that they could be heated by passage of an electric current.

Experimental Apparatus and Procedure

1. *Apparatus.* Our reactor (Figure 2) is a cylinder of Pyrex or quartz situated in an ion-pumped, ultrahigh vacuum system. Flash filament data were obtained with a Pyrex reactor of 2.2 cm inside diameter and 12 cm length; quantitative total atom loss probability on silver was determined in a reactor with length and diameter identically 5.1 cm.

Atoms are generated by thermal dissociation of molecular oxygen or hydrogen or an electrically heated tungsten ribbon in a water-cooled chamber at the lower end of the reactor. The reactor inlet is a 0.25-cm radius hole in a 0.3-cm thick glass plate situated in close proximity to the tungsten ribbon. A radiation shield of tungsten foil between the hot ribbon and the glass plate prevents overheating of the glass parts of the reactor in this vicinity. The conductance of this inlet

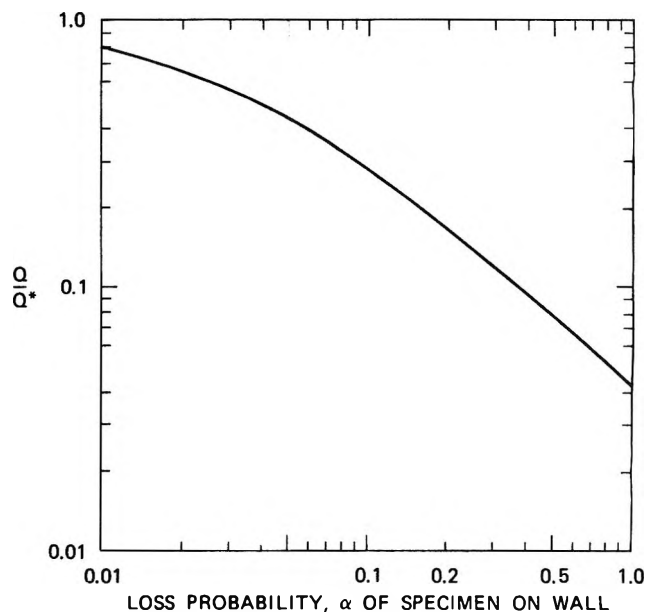


Figure 1. Relative outlet flux [Q , with metal specimen in reactor; Q^* , without specimen], as a function of loss probability α of specimen on wall of reactor, predicted by analytical model. Reactor dimensions (cm): length 5.1, radius 2.55, inlet radius 0.3, exit radius 0.625. Specimen covers one-half of reactor wall nearest exit end.

computed from the formula for free-molecular flow through a short pipe⁴ ($r = 0.25$ cm, $l = 0.3$ cm) is equivalent to a thin-edge aperture with an area of approximately 0.02 cm². Only the atoms originating on a central area of this size on the tungsten ribbon have access by a direct path to the interior of the reactor.

Hence, the total steady-state mass flow rate of atoms into the reactor is assumed to be the integrated flux emitted from this region of the tungsten ribbon at a fixed temperature and gas pressure. At tungsten temperatures greater than 2100°K, it has been shown⁵ that the emitted flux of oxygen atoms is more than an order of magnitude greater than the emitted flux of any volatile tungsten oxide. Consequently, we always conducted our experiments with the central portion of the tungsten ribbon at temperatures in excess of 2100°K as measured by an optical pyrometer. Oxides that formed and evaporated from the cooler end portions of the tungsten ribbon were denied access to the reactor by virtue of the small effective inlet aperture diameter, and thus they were permanently trapped in the source chamber by condensation on the cooled walls.

The reactor outlet is a 0.55-cm radius hole in an 0.3-cm thick glass plate, which leads directly to a large chamber pumped to low pressure by a titanium sublimation pump and an ion getter pump. This chamber contains a quadrupole mass spectrometer⁶ placed so

(4) A. Guthrie and R. K. Wakerling, "Vacuum Equipment and Techniques," McGraw-Hill, New York, N. Y., 1949, p 12 ff.

(5) P. O. Schissel and O. C. Trulson, *J. Chem. Phys.*, **43**, 737 (1965).

(6) Model QUAD 250, Electronic Associates, Inc., Palo Alto, Calif.

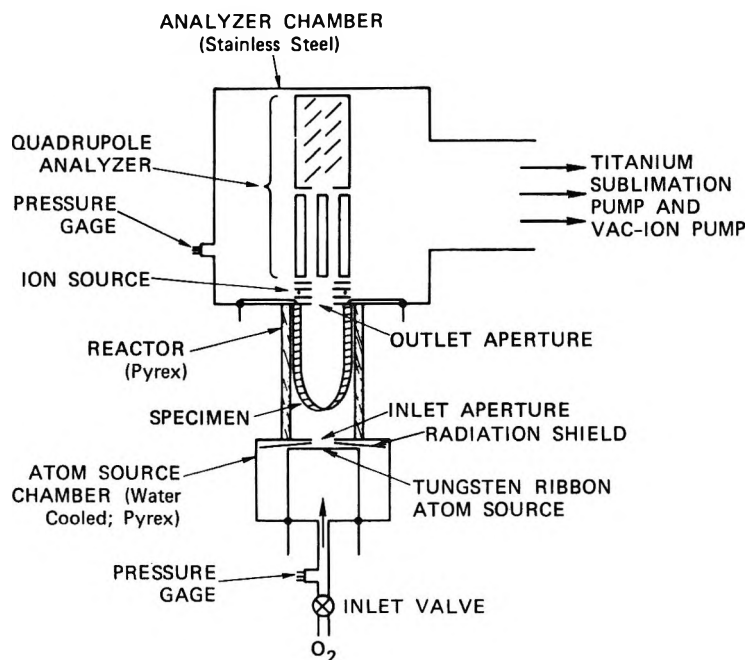


Figure 2. Schematic diagram of apparatus.

that its ion source is immediately adjacent to the reactor exit. The pressure in the system is measured by ion gauges near the oxygen inlet and on the analyzer chamber.

Our specimens for flash filament experiments were foil ribbons with a length of approximately 20 cm and a width of about 0.5 cm. These ribbons were suspended from their ends by spot-welding to electrical feed-throughs at the upper end of the reactor. For cases where reactor and specimen geometry were unchanged, and the oxygen pressure and source temperature were constant, the relative atom-loss characteristics of the two metals could be evaluated by a comparison of the fraction of atoms measured in the reactor effluent for each specimen.

2. *Mass Spectrometer Calibration.* The geometry of the apparatus is such that the mass spectrometer detects the effective flux of species emerging from the exit aperture of the reactor. For calibration, the total mass flow of gas Q through the reactor was computed from measured pressure differences between the inlet and analyzer ion gauges and the calculated overall conductance of the apparatus between these two pressure-measuring points. In the range $10^{-6} < Q < 10^{-3}$ Torr-l./sec, the mass spectrometer signal was found to be proportional to Q . From the observed value of Q we could estimate the steady-state values of pressure in the reactor near the inlet and near the outlet by using the basic Knudsen flow equation

$$Q = F_R(P_1 - P_2) = F_e(P_2 - P_3) \quad (1)$$

where P_1 and P_2 are the pressures at the inlet and outlet ends of the reactor, respectively, P_3 is the pressure out-

side the reactor outlet, F_R is the conductance of the reactor, and F_e that of the exit aperture. Each value of gas pressure and collision frequency reported for the reactor in this paper is an arithmetic mean between P_1 and P_2 . We used similar computations to estimate total gas pressures in other parts of the apparatus, such as the atom source chamber.

The mass spectrometer was calibrated before and after each experiment to allow corrections for variations in electron multiplier sensitivity. Also, cracking patterns for the gases of interest were determined empirically, and the mass spectrometer was operated at a fixed resolution setting for the entire series of experiments.

3. *Experimental Procedure.* a. *Total Atom-Loss Measurement.* The total loss of atoms due to interactions at the surfaces in the reactor is related to the surviving fraction of atoms measured in the reactor effluent. Of course, even in a reactor with completely inert and noncatalytic walls, the steady-state absolute flux of atoms at the outlet is less than that at the inlet by the factor representative of the net transmission probability⁷ of the reactor and its apertures. We computed the net transmission probability of our apparatus from formulas for molecular flow through uniform cylindrical pipes connected in series.^{4,7} We used this figure to predict the atom flow-rate through the outlet of the empty reactor from the kinetic data of Schissel and Trulson⁵ for oxygen dissociation on a hot tungsten surface. A comparison of these flow rates with those actually measured (Table I) indicated that atom loss on glass and quartz is negligibly small. This conclusion was con-

(7) W. Steckelmacher, *Vacuum*, **11**, 561 (1966).

Table I: Survival of Oxygen Atoms in Pyrex and Quartz Reactors (Tungsten Ribbon Source Temperature: $2150 \pm 25^\circ\text{K}$)

Reactor dimensions— Length, cm	Diameter, cm	P_{O_2} (calcd) in source chamber, Torr $\times 10^4$	Atom mass flow rate —at reactor outlet—	
			Measured, Torr-l./sec $\times 10^7$	Predicted from data in ref 5 ^a Torr-l./sec $\times 10^7$
12	2.2	0.50	3.5	3.4
		2.5	11	9.2
5.1	5.1	0.48	15	9.1
		4.3	83	36

^a Corrected for total transmission probability of reactor and apertures assuming no loss of atoms on reactor wall.

firmed in an experiment in which the radius of the exit hole was reduced to a degree such that the average number of wall collisions by atoms in the reactor approximately doubled. This change caused no variation in the fraction of atoms in the effluent within the precision of our measurement. These observations are in agreement with reported² values of the catalytic activity of glass and quartz for oxygen atom recombination ($\gamma \cong 10^{-4}$, i.e., only one out of 10^4 collisions results in atom loss by recombination).

We determined relative atom loss for each metal by making separate measurements of the fractional atom flux $Q_{\text{O}}/Q_{\text{O}_2}$ in the reactor effluent, over a range of source temperatures T_w and source oxygen pressures, with and without metal specimens in the reactor. Typical results for a wall specimen of silver foil are shown in Figure 3.

b. Atom Adsorption Rate Measurements. We determined the mass of atomic species adsorbed or occluded on a metal specimen during a specified exposure time to a constant atom flux by means of flash desorption experiments. The metal specimen in the form of a ribbon was flash heated to an elevated temperature (Ag, 730°K ; Au, 890°K) by passage of an electric current. The flow rate of atomic and molecular oxygen into the reactor was maintained constant during the flash. Consequently, the desorption of gas from the metal surface was manifested as a pressure pulse detected by the mass spectrometer locked on the appropriate atomic mass unit value. In accordance with established flash-filament experimental analysis,⁸ the total mass of gas desorbed from the ribbon during the heating period was evaluated by integration of the pressure rise with respect to time. By observing the total mass of gas desorbed as a function of the time of exposure of the specimen at 300°K to the gaseous atoms, we could measure the rate of adsorption of atoms by the metal. The ratio of rate of adsorption to incident collision rate of atoms is termed the sticking coefficient S . Incident collision rates were computed from kinetic theory using the arithmetic mean value of the steady-state number

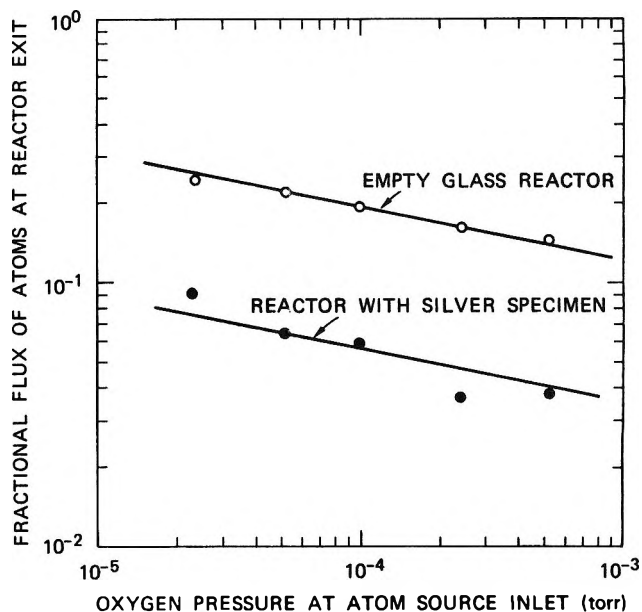


Figure 3. Fractional oxygen-atom flux Q at reactor exit as a function of atom source pressure. Reactor dimensions (cm): length 5.1, radius 2.55, inlet radius 0.3, exit radius 0.625. Silver specimen of area 40 cm^2 covers one-half of reactor wall nearest exit end.

densities of atoms at the inlet and the outlet of the reactor. Values of atom number density at these points were calculated from the measured exit flux using eq 1.

c. Atom Desorption Rate Measurements. Surface sorbed atoms were observed to desorb (as molecules) spontaneously from the metal surfaces at room temperature. This process represented recombination of adatoms by the Langmuir-Hinshelwood mechanism.² We measured the rate of this desorption by the following procedure. The specimen was first exposed to a constant flux of gaseous atoms for a fixed length of time to provide a reproducible characteristic coverage. The atom source was then cooled to a temperature at which thermal dissociation was negligible even though the total pressure in the system was not changed significantly. After a period of time (a "dwell period" in an atmosphere of molecular oxygen) the metal ribbon was flash heated and the quantity of gas desorbed was determined. This procedure was repeated for a number of different dwell periods up to 90 min in duration.

d. The Behavior of Impurity Gases. Carbon monoxide was the major residual impurity in our vacuum system. This gas has been reported⁹ to chemisorb strongly on some metals; hence we felt it important to evaluate the rate of sorption and the degree of coverage exhibited by carbon monoxide under the conditions of our experiments. The rate of coverage and sticking coefficient in the absence of atomic species were deter-

(8) G. Ehrlich, *Advan. Catal.*, **14**, 255 (1963).

(9) B. M. W. Trapnell, *Proc. Roy. Soc., Ser. A*, **218**, 566 (1953).

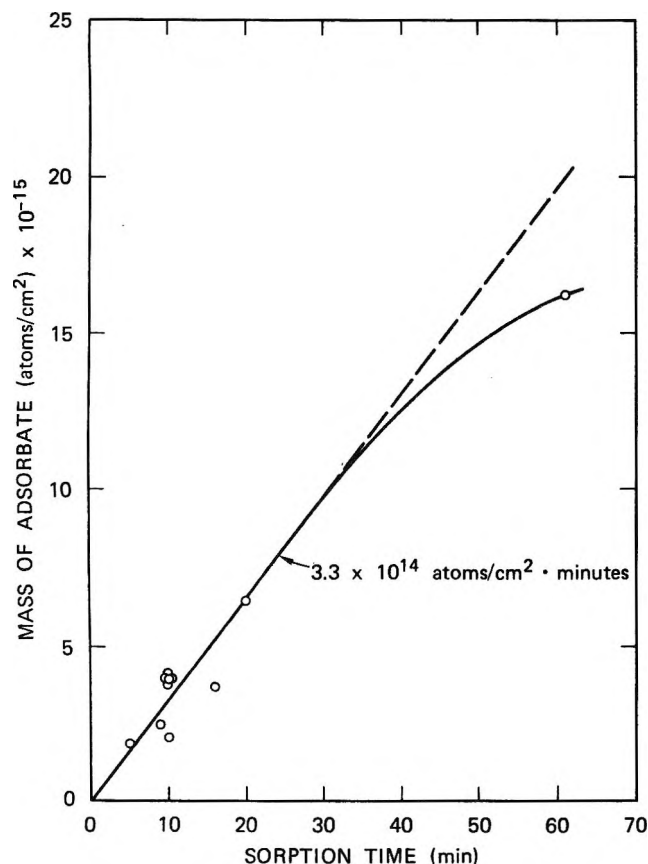


Figure 4. Adsorption/occlusion of oxygen atoms by silver at 300°K. $P_{\text{O}} \cong 1.4 \times 10^{-7}$ Torr.

mined in a manner identical with that employed for atoms.

In experiments with hydrogen atoms we employed the same thermal atom source used to produce atomic oxygen, because hydrogen has been reported to dissociate readily on tungsten¹⁰ at $T > 2000^\circ\text{K}$. In these experiments we observed atomic hydrogen but we also observed a mass flux of water (amu 18) in the reactor effluent as large as or larger than that of molecular hydrogen. The presence of water was undesirable because it contributed substantially to the amu 1 peak due to cracking in the ion source of our mass spectrometer. The cracking pattern of water was determined over a range of pressures and ionizing electron energies, but the contribution of amu 18 to amu 1 could never be reduced below 3%. This amount represented a sizeable correction to apply to observed amu 1 amplitudes in all the experiments carried out in our apparatus.

Results and Discussion

1. *Oxygen Atom Interactions. a. Silver.* An absolute quantitative determination of the total oxygen atom loss probability was made only for silver. We chose silver for this measurement because of its demonstrated¹¹ indifference to CO as a catalytic poison for oxygen surface reactions. Consistent with this reported charac-

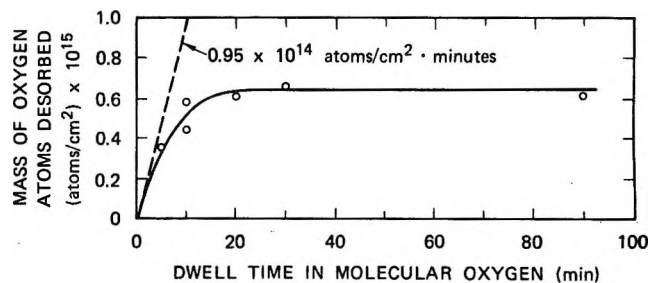


Figure 5. Spontaneous desorption of oxygen from silver at 300°K. At time = 0, silver had been exposed to a constant flux of gaseous oxygen atoms ($P_{\text{O}} \cong 1.4 \times 10^{-7}$ Torr) for 10 min. $P_{\text{O}_2} \cong 2 \times 10^{-5}$ Torr.

teristic, we found no evidence that CO interferes with the uptake of oxygen by silver in an atmosphere containing atomic oxygen. We determined that CO sorbs on silver rather slowly, exhibiting an initial sticking coefficient of 0.003 in CO partial pressures up to 10^{-6} Torr. Therefore, we felt confident that silver would exhibit its characteristic steady-state activity toward atomic oxygen without periodic flash cleaning.

The data from this experiment (Figure 3) demonstrate a constant fractional diminution in the flux of oxygen atoms that survive transit through the reactor with the silver wall, over a range of pressure. The analytical model³ permits interpretation of this fractional loss in terms of a loss coefficient, α . The average observed value of relative exit flux, $Q/Q^* = 0.31$, corresponds to an overall loss coefficient, $\alpha \cong 0.1$ (Figure 1) according to the analytical model.

Flash filament experiments show that at 300°K silver takes up atomic oxygen at a nearly constant rate well beyond monolayer coverage (Figure 4), suggesting occlusion of the atomic species in the metal. Determination of the rate of spontaneous desorption of oxygen from silver at 300°K, however, indicated that a mass equivalent to less than a monolayer of the oxygen associated with the solid is rather weakly bound. These data are shown in Figure 5 as the difference between the amount of oxygen atoms sorbed during an exposure of 10 min duration to atomic oxygen (Figure 4) and the amount recovered during the heating flash after the specified dwell period in molecular oxygen. (Neither silver nor gold adsorbed oxygen from the molecular state of the gas under the conditions of our experiments.)

It is of interest to note that the combined measured rates of occlusion (3.3×10^{14} atoms/cm² min, Figure 4) and Langmuir-Hinshelwood recombination (1×10^{14} atoms/cm² min, Figure 5) represent $1/10$ of the rate of atom impingement calculated from the average partial pressure of atomic oxygen in the reactor. This value

(10) G. C. Moore and F. C. Unterwald, *J. Chem. Phys.*, **40**, 2639 (1964).

(11) A. W. Czanderna, *J. Phys. Chem.*, **68**, 2765 (1964).

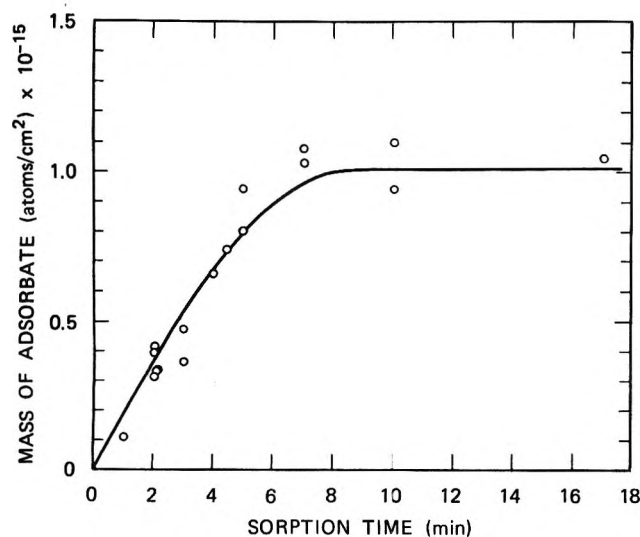


Figure 6. Adsorption of oxygen atoms on gold at 300°K.
 $P_{O_2} \cong 1.4 \times 10^{-7}$ Torr.

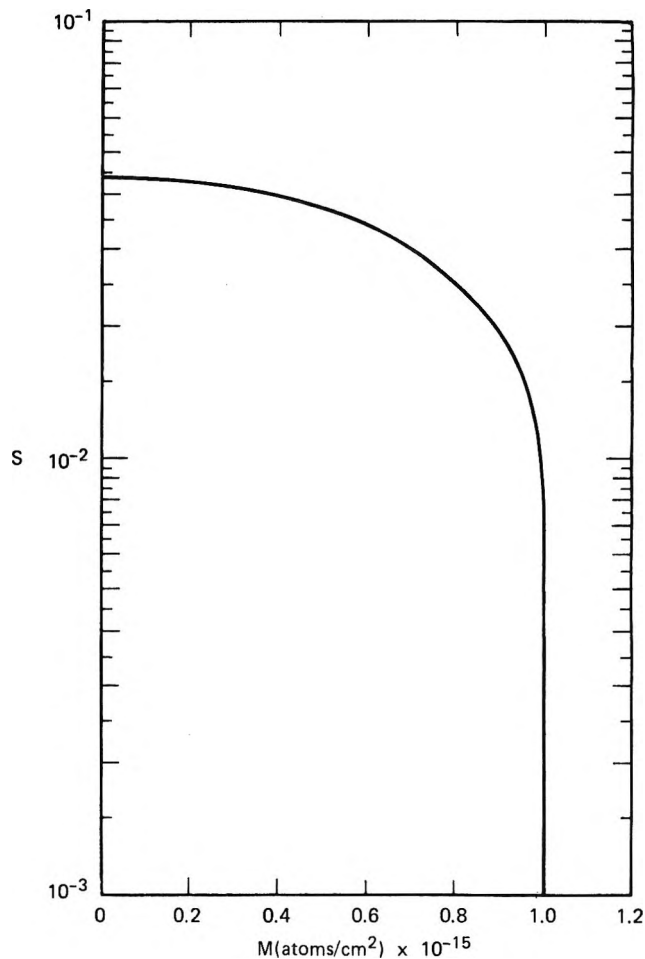


Figure 7. Sticking probability S of oxygen atoms on gold at 300°K as a function of surface coverage M (curve derived from data in Figure 6)

of 0.1 is comparable to the observed total atom loss coefficient for silver, which leads us to conclude that the rate of recombination by way of an Eley-Rideal path is small and that occlusion-chemical reaction is the major mode for gaseous atom loss on silver. It is possible that the high values of recombination efficiency reported by others² may in reality represent a combined reaction efficiency for recombination and occlusion. Direct comparison of the results is hazardous, however, for many of the higher pressure experiments were carried out with well characterized silver oxide surfaces.

The nature of the occluded state cannot be determined from our measurements. The rather prolonged constant rate of uptake of oxygen exhibited by our specimen (Figure 4) suggests that the occlusion process is not hampered by the formation of a discrete phase in the form of a layer of some silver oxide. On the basis of available thermodynamic data,¹² both AgO and Ag₂O would be stable at 300°K in the partial pressure of oxygen atoms attained in our experiments. McBee and Yolken,¹³ using an ellipsometric technique, noted that film growth on a silver surface exposed to an undetermined flux of oxygen atoms was nearly linear with time up to a thickness of over 1000 Å. Therefore, the formation of a surface oxide phase cannot be ruled out as the mechanism of occlusion in our experiments.

b. Gold. In similar experiments with ribbons of identical dimensions in the same reactor, the surviving flux of oxygen atoms with a gold specimen was $\frac{1}{3}$ that observed with a silver specimen. This suggests that gold exhibits an overall loss coefficient $\alpha \cong 0.3$. Flash filament experiments indicate that gold adsorbs up to a maximum of one monolayer of oxygen atoms at 300°K with a rate that diminished with coverage (Figure 6). The sticking probability is shown as a function of coverage in Figure 7. The oxygen-covered gold exhibits a relatively low adatom-adatom (Langmuir-

Hinshelwood) recombination rate at 300°K (Figure 8) which cannot be attributed to displacement of oxygen adatoms by strongly bound CO (dashed curve in Figure 8).

We note here that the sticking coefficient of CO on gold (Figure 9) is nearly an order of magnitude less than that for atomic oxygen (Figure 7). The saturation coverage by CO observed in our experiments is about $\frac{1}{6}$ that of oxygen, but there was some evidence that this coverage exhibits a dependence on CO pressure.

Although gold possesses an oxygen atom overall loss coefficient greater than silver by a factor of 3, the Langmuir-Hinshelwood rate of recombination is nearly a factor of 10 lower for gold (Figure 8) than for silver (Figure 5). In addition, gold exhibits no occlusion of atomic oxygen nor gives any evidence of oxide formation. Consequently, we conclude that atom loss occurs on gold primarily by an Eley-Rideal mechanism at a rate of approximately 1×10^{15} atoms/cm² min,

(12) C. E. Wicks and F. E. Block, *U. S. Bur. Mines Bull.*, No. 605 (1963); JANAF Thermochemical Tables, Dow Chemical Co.

(13) M. J. McBee and H. T. Yolken, *Nat. Bur. Stand. (U. S.) Report*, No. 9802 (1968).

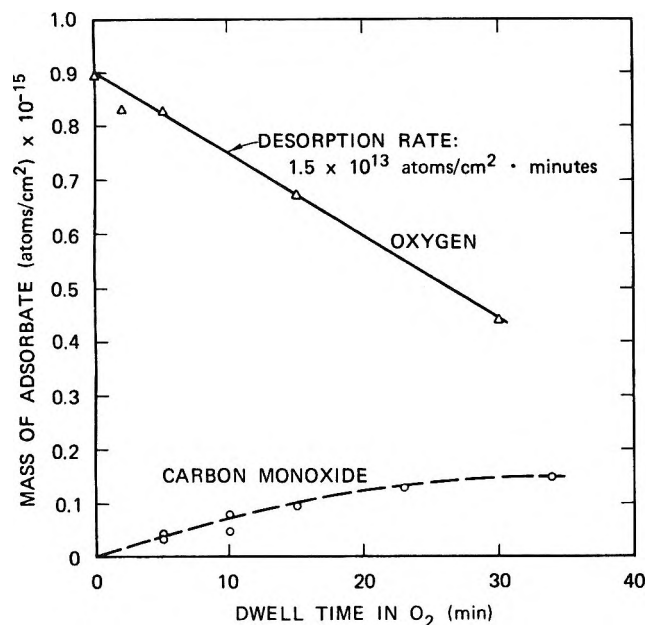


Figure 8. Spontaneous desorption of oxygen from gold at 300°K. At time = 0 gold surface had approximately monolayer oxygen coverage $P_{O_2} \cong 5 \times 10^{-6}$ Torr. Rate of adsorption of CO is shown by dashed curve. $P_{CO} \cong 5 \times 10^{-6}$ Torr.

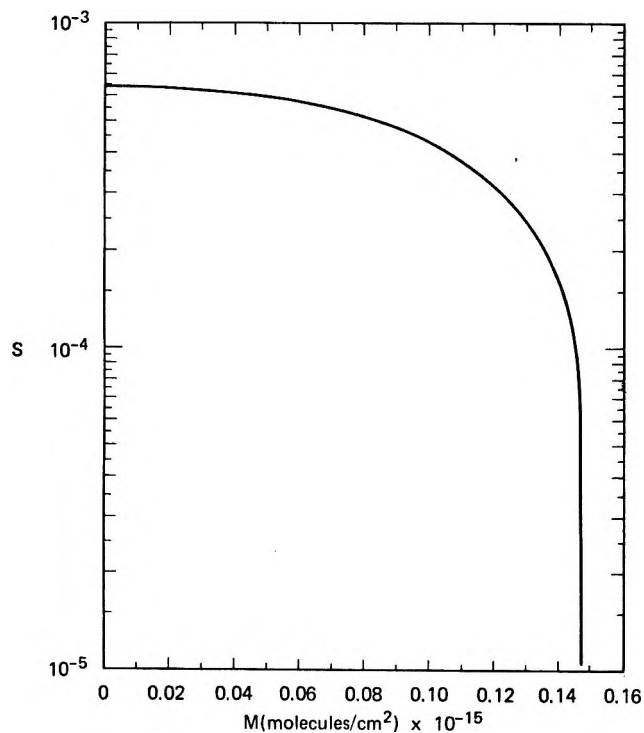


Figure 9. Sticking coefficient of CO on gold at 300°K, $P_{CO} \cong 5 \times 10^{-6}$ Torr.

i.e., three times as fast as the rate of occlusion of oxygen by silver (*cf.* Figure 4). This difference could be attributed to a chemisorbed oxygen state on gold with a greater binding energy than that on silver. The stronger binding energy for gold provides an oxygen ad-

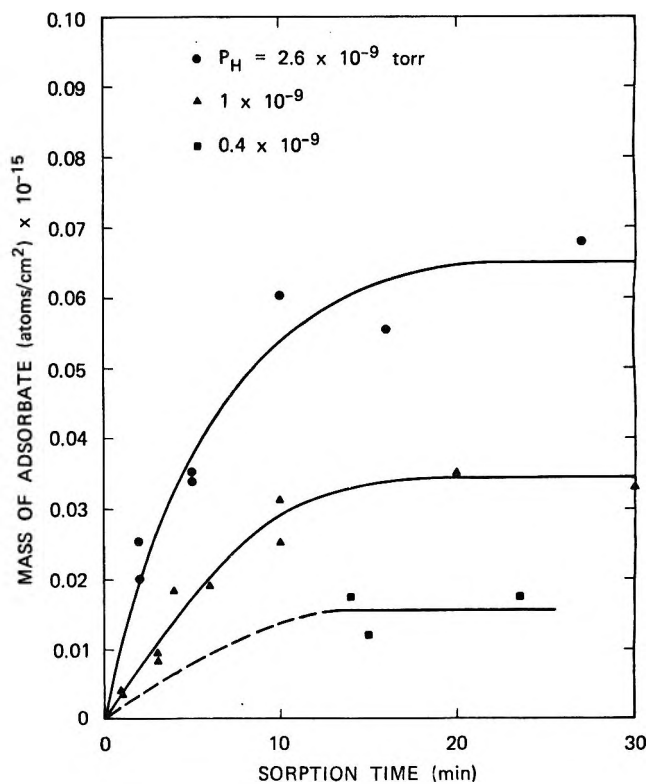


Figure 10. The adsorption of atomic hydrogen on gold at 300°K as a function of pressure of hydrogen atoms.

atom population with relatively low mobility and nearly total coverage, thus ensuring a high probability for gas atom-atom collision. On silver the weakly sorbed atoms are more sparse and highly mobile, residing for very brief periods on any one site so that a very low fraction of the incident atoms encounters adatoms. The silver lattice, which possesses a great affinity and large capacity for occlusion of oxygen, competes favorably with recombination for removal of the weakly bound oxygen adatoms.

2. *Hydrogen Atom Interaction on Gold.* The absolute surviving flux of hydrogen atoms, even with no specimen in the reactor, was quite small, but the insertion of a gold specimen into the reactor reduced the observed flux by a factor of 0.62. This specimen is the identical piece of foil with a geometric surface area of 24.5 cm² employed in our earlier experiments with atomic oxygen. Comparison of the values of the relative exit flux of atoms obtained in these respective sets of experiments indicates that the gold exhibits a total loss probability of 0.1 for hydrogen atoms.

Our first measurement of the rate of adsorption of atomic hydrogen on gold indicated the saturation coverage to be well below 0.1 monolayer. This value seemed insufficient to account for the observed total loss of atoms on the gold surface; hence we performed additional experiments to investigate the dependence of the surface kinetics on atomic hydrogen pressure and coverage.

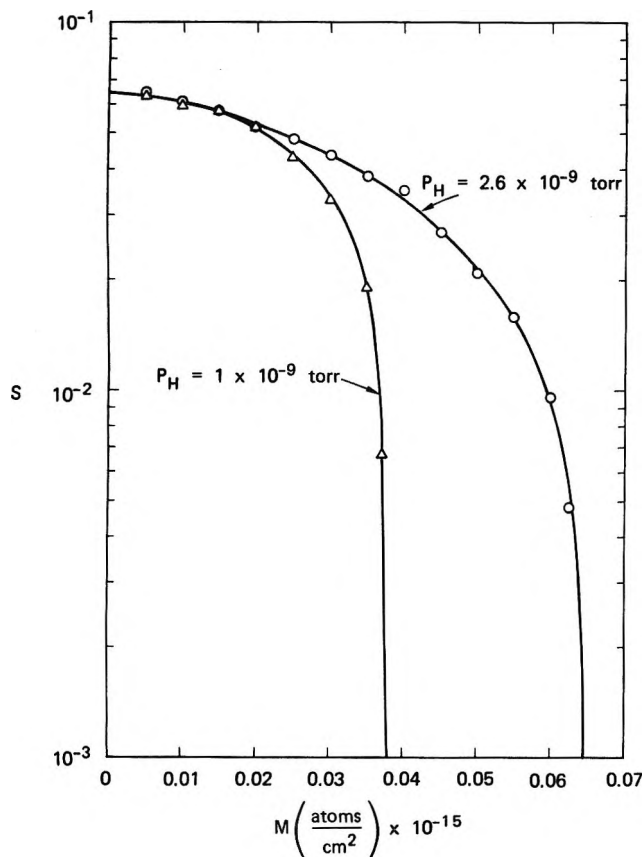


Figure 11. Sticking coefficient S of atomic hydrogen on gold at 300°K as a function of surface coverage of adatoms M . Points are normalized to coincide at $M = 0$ within precision of pressure measurements.

We varied the atom partial pressure by changing the total hydrogen flux through the reactor. This change affects both atomic and molecular hydrogen pressures in the reactor, but the rate of adsorption of molecular hydrogen on gold is negligibly small at the temperature of our experiment (300°K). The results of these experiments (Figure 10) show the steady-state surface coverage increases with the pressure of atomic hydrogen. The initial rate of adsorption on clean gold, however, seems to be first order with respect to atom pressure within the precision of our pressure measurements. Hence, the value of the sticking coefficient, S remains constant with atom pressure at low surface coverages (Figure 11).

We also measured the rate of desorption of hydrogen (as molecules) from gold. The observed rate (Figure 12) from an initial coverage of 0.016×10^{15} atoms/cm² is about a factor of 10 lower than the clean-surface adsorption rate at an atomic hydrogen pressure which gives this steady-state coverage (compare with Figure 10, $P_H = 0.4 \times 10^{-9}$ Torr).

The observed characteristics of the atomic hydrogen-gold system can be interpreted in terms of the kinetics of three elementary processes² occurring at the surface. The following list associates these processes with mathe-

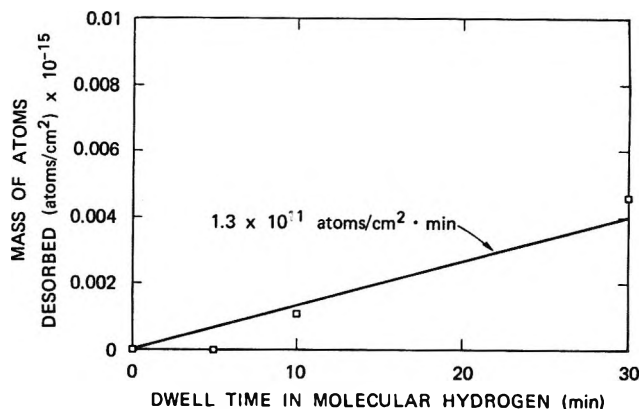
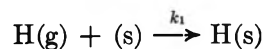


Figure 12. Spontaneous desorption of hydrogen adatoms from gold at 300°K. Initial coverage at time 0 = 0.016×10^{15} atoms/cm².

tical expressions relating the rate of population or depopulation of hydrogen on the surface to the concentration of gaseous atoms n , the surface number density of available adsorption sites N , and the fraction of sites occupied by adatoms θ

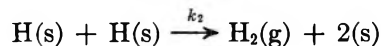
sorption



$$\frac{d[\text{H(s)}]}{dt} = k_1 N(1 - \theta)n \quad (2)$$

recombination

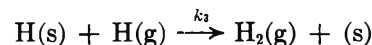
(Langmuir-Hinshelwood)



$$-\frac{d[\text{H(s)}]}{dt} = k_2(N\theta)^2 \quad (3)$$

recombination

(Eley-Rideal)



$$-\frac{d[\text{H(s)}]}{dt} = k_3 N\theta n \quad (4)$$

Based on equilibrium data, the probability of atom desorption from gold is virtually nil, so we need not consider the reverse of reaction 2. In addition, under the conditions of our experiments, we do not observe sorption of hydrogen from the molecular state; hence, the reverse of reactions 3 and 4 is eliminated from our consideration.

Using these elementary steps and assuming a mass balance in a dynamic steady state, we can equate the rate of sorption to the combined rates of recombination

$$k_1 N(1 - \theta)n = k_2(N\theta)^2 + k_3 N\theta n \quad (5)$$

Rearrangement of eq 5 gives a statement of the functional dependence of θ on n

$$n = \frac{k_2 N \theta^2}{k_1(1 - \theta) - k_3 \theta} \quad (6)$$

The reaction rate constants (k_1 , k_2 , k_3) in eq 6 may be evaluated from our experimental rate data: k_1 , computed from data in Figure 10 using eq 2 = 1.25×10^{-10} (atoms/cm³)⁻¹ min⁻¹; k_2 , obtained for the observed coverage from data in Figure 12 using eq 3 = 5.1×10^{-16} (atoms/cm²)⁻¹ min⁻¹; k_3 , obtained from eq 4, first computing the value of $k_3 N \theta n$, for the observed coverage using eq 5 = 7.2×10^{-9} (atoms/cm³)⁻¹ min⁻¹.

The adsorption isotherm (θ vs. n) obtained by solving eq 6 using these values of the rate constants predicts a maximum steady-state surface coverage less than 0.02 monolayer as $n \rightarrow \infty$. This value is considerably smaller than the maximum observed in our experiments (Figure 10). However, based on the observed value of total atom loss probability = 0.1, it is evident that a significant fraction of the incident atoms do not recombine. Consequently, k_3 was adjusted to a lower value [2×10^{-9} (atoms/cm³)⁻¹ min⁻¹] to give an isotherm in reasonable agreement with the data (Figure 13).

The relative values of the rate constants indicate that adsorption is the rate-limiting process in the recombination of hydrogen atoms on gold even though recombination occurs primarily by way of the Eley-Rideal mechanism. This conclusion is supported by the close correspondence between the initial value of the sticking coefficient (Figure 11) and the observed value of total atom loss probability. Further evidence is provided by the similarity in value of the recombination coefficient γ determined previously² at a relatively high pressure ($P_H \cong 10^{-3}$ Torr; $\gamma = 0.072$) and the clean-surface sticking coefficient ($S = 0.065$). We may compute k_3 from this value of γ on the basis of first-order Eley-Rideal kinetics²

$$k_3 = \frac{\gamma \bar{c}}{4N\theta}$$

where \bar{c} is the mean atomic velocity. If we assume the high-pressure limit of $\theta = 0.06$, this computation gives $k_3 = 4 \times 10^{-9}$ (atoms/cm³)⁻¹ min⁻¹ in reasonable agreement with the value derived from our low-pressure rate measurements.

We also investigated the rate of reaction between gaseous hydrogen atoms and oxygen adatoms by means of the flash-filament technique. The gold ribbon specimen, flash cleaned, was exposed to a flux of atomic oxygen for a sufficient time to saturate the surface with a monolayer of adatoms. The oxygen supply to the system was then cut off, and, following a brief period of evacuation, hydrogen at a predetermined constant flux was admitted to the atom source and the reactor for a period of time. The results, corrected for Langmuir-Hinshelwood oxygen atom recombination, are shown in Figure 14. The initial rate, shown by the

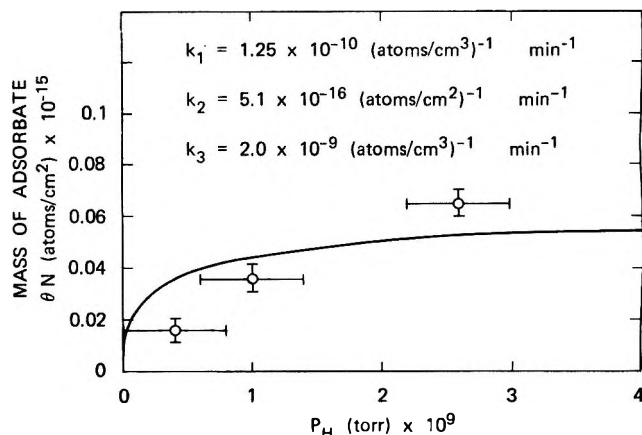


Figure 13. Isotherm for atomic hydrogen adsorption on gold at 300°K. Curve computed from eq 6 using indicated values for rate constants; experimental points from data in Figure 10.

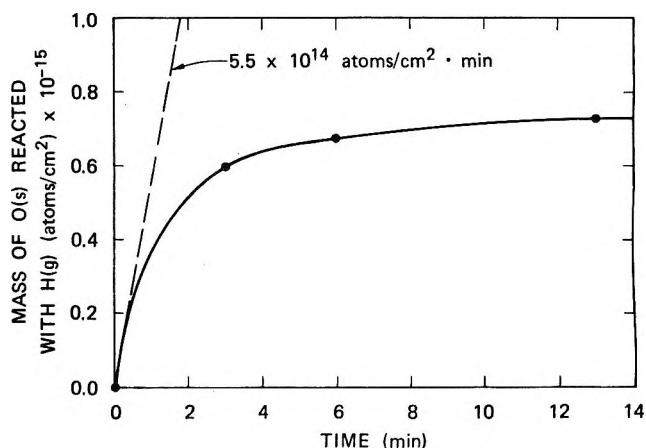


Figure 14. Rate of reaction of gaseous atomic hydrogen with oxygen adatoms on gold at 300°K. $P_H = 3 \times 10^{-9}$ Torr. At time = 0, gold surface coverage with oxygen $\theta N = 1.7 \times 10^{16}$ atoms/cm².

dashed line, is comparable to the calculated incident flux of hydrogen atoms under the conditions of the experiment ($P_H \cong 5 \times 10^{-9}$ Torr), and indicates that the reaction occurs with approximately unit efficiency. The products of the reaction could not be determined. A blank experiment, in which an oxygen-covered gold surface was exposed for 8 min to a flux of molecular hydrogen at $P_{H_2} \cong 10^{-6}$ Torr, indicated that the rate of reaction of gaseous molecular hydrogen with oxygen adatoms on gold is negligibly small. Our results are in qualitative agreement with those reported by Ponc and associates,¹⁴ who noted that only atomic hydrogen will react with preadsorbed oxygen on certain transition metals. They concluded that adsorption of both reactants on the metal surface is a prerequisite to reaction.

3. *Practical Application.* The results of our study are of practical interest in the interpretation of upper atmosphere composition data reported by rocket- and satellite-borne mass spectrometers.¹⁵ At altitudes

(14) V. Ponc, Z. Knor, and S. Cerny, *J. Catal.*, **4**, 485 (1965).

(15) U. von Zahn, *J. Geophys. Res.*, **72**, 5933 (1967) (a critical review).

greater than 100 km, oxygen atoms become a major atmospheric constituent. Silver and gold are two metals which have been employed in the sampling chambers of two major aeronomy satellites, Explorer XXXII and OGO-F, respectively. In principle, our kinetic data may be employed to assess quantitatively the fractional loss of gaseous atoms in these instruments and

make appropriate corrections to the ambient atom number density values reported by the mass spectrometers.

Acknowledgment. I am grateful to Drs. Henry Wise and Bjorn Bergsnov-Hansen for helpful and stimulating discussions during the course of this work, and to Mr. Jan van Gastel for assistance in the design and fabrication of the glass reactor.

Temperature-Dependent Splitting Constants in the Electron Spin Resonance Spectra of Cation Radicals. III.¹ The Hydroxyl Group

by Paul D. Sullivan

Department of Chemistry, Ohio University, Athens, Ohio 45701 (Received January 25, 1971)

Publication costs borne completely by The Journal of Physical Chemistry

The temperature dependence of the hydroxyl proton splitting constant has been studied for a number of compounds. Theories regarding the mechanism of the hydroxyl group hyperfine interaction are discussed and a model for this interaction is proposed. The temperature dependence of the hydroxyl group is then calculated and compared with the experimental values. Estimates for the potential barrier to rotation about the carbon-oxygen bond are obtained for the hydroquinone, duroquinol, 1,4-dihydroxynaphthalene, 2,3-dimethyl-1,4-dihydroxynaphthalene, and 9,10-dihydroxyanthracene cation radicals of 10 ± 2 , 6.6 ± 1.5 , 5.9 ± 1.5 , 4.6 ± 1.3 , and $3.2\text{--}4.0$ kcal/mol, respectively. Additionally the potential barriers for the neutral hydroxymethyl and monoprotonated benzoquinone radicals were estimated to be in the range 3.5–5.0 and 3.2–4.0 kcal/mol. The potential barriers were compared, where possible, with similar barriers obtained from line-width alternation studies.

Introduction

Hyperfine splittings from hydroxyl group protons are well documented. They have been observed in negatively charged radicals, *i.e.*, hydroxy-substituted benzosemiquinones,² naphthosemiquinones,^{3,4} and anthra-semiquinones.^{4,5} Neutral radicals containing hydroxyl group splittings include monoprotonated benzoquinones,^{6–10} hydroxyperinaphthyl,¹¹ hydroxy radicals formed by photolysis of aromatic carbonyl compounds,^{12,13} and radicals formed *via* hydrogen abstraction from alcohols.^{14–19} Positively charged hydroxy radicals are derived from hydroquinone and its derivatives,^{20–26} hydroxy naphthalenes and anthracenes,^{27,28} and dihydroxy biphenyls.²⁹ A relatively large temperature dependence of the hydroxyl proton splitting constant has been noted in several of these examples.^{7,8,12,13,16,18,23,24,28}

The previous paper in this series¹ examined the temperature dependence of methoxyl group protons and a model was developed to explain this temperature dependence. From the model it was then possible to

estimate the potential barrier to rotation about the C-(aryl)-oxygen bond. It is the purpose of this paper to

- (1) Part II: P. D. Sullivan, *J. Phys. Chem.*, **74**, 2563 (1970).
- (2) I. C. P. Smith and A. Carrington, *Mol. Phys.*, **8**, 101 (1964).
- (3) (a) G. P. Rabold, R. T. Ogata, M. Okamura, L. H. Piette, R. E. Moore, and P. J. Scheuer, *J. Chem. Phys.*, **46**, 1161 (1967); (b) L. H. Piette, M. Okamura, G. P. Rabold, R. T. Ogata, R. E. Moore, and P. J. Scheuer, *J. Phys. Chem.*, **71**, 29 (1967).
- (4) (a) J. H. Freed and G. K. Fraenkel, *J. Chem. Phys.*, **38**, 2040 (1963); (b) J. Gendell, W. R. Miller, and G. K. Fraenkel, *J. Amer. Chem. Soc.*, **91**, 4369 (1969).
- (5) A. E. Lutskii, I. S. Romodanov, and Yu A. Kruglyak, *Theor. Exp. Chem. (USSR)*, **2**, 456, 461 (1966).
- (6) T. A. Claxton, T. E. Gough, and M. C. R. Symons, *Trans. Faraday Soc.*, **62**, 279 (1966).
- (7) (a) T. E. Gough, *ibid.*, **62**, 2321 (1966); (b) T. E. Gough, *Can. J. Chem.*, **47**, 331 (1969).
- (8) T. E. Gough and G. A. Taylor, *ibid.*, **47**, 3717 (1969).
- (9) T. A. Claxton, J. Oakes, and M. C. R. Symons, *Trans. Faraday Soc.*, **63**, 2125 (1967).
- (10) I. C. P. Smith and A. Carrington, *Mol. Phys.*, **12**, 439 (1967).
- (11) (a) G. P. Rabold, K. H. Bar-Eli, E. Reid, and K. Weiss, *J. Chem. Phys.*, **42**, 2438 (1965); (b) G. P. Rabold, K. H. Bar-Eli, and K. Weiss, *Chem. Commun.*, 38 (1965).

Table I: Summary of the Experimental Splitting Constants

Compd	Position		Splitting constant	Temperature coefficient, mG/deg	ρ factor
1,4-Dihydroxynaphthalene (-47°) ^b	$a_{\text{CH}^{\text{H}}}$ (2,3)	=	3.085 ± 0.006	-0.35 ± 0.10	
	$a_{\text{CH}^{\text{H}}}$ (5,8)	=	1.635 ± 0.005	0.45 ± 0.10	2.00323 ±
	$a_{\text{CH}^{\text{H}}}$ (6,7)	=	0.818 ± 0.004	+0.09 ± 0.10	0.00002
	$a_{\text{OH}^{\text{H}}}$	=	2.449 ± 0.005	-1.43 ± 0.19	
9,10-Dihydroxyanthracene (-56°)	$a_{\text{CH}^{\text{H}}}$ (1,4,5,8)	=	1.551 ± 0.001	+0.20 ± 0.10	2.00309 ±
	$a_{\text{CH}^{\text{H}}}$ (2,3,6,7)	=	1.037 ± 0.002	+0.15 ± 0.10	0.00002
	$a_{\text{OH}^{\text{H}}}$	=	1.276 ± 0.002	-2.86 ± 0.08	
2,3-Dimethyl-1,4-dihydroxynaphthalene (-67°)	$a_{\text{CH}_3^{\text{H}}}$	=	2.666 ± 0.002	<i>a</i>	2.00318 ±
	$a_{\text{CH}^{\text{H}}}$ (5,8)	=	1.678 ± 0.004	<i>a</i>	0.00002
	$a_{\text{CH}^{\text{H}}}$ (6,7)	=	0.896 ± 0.006	<i>a</i>	
	$a_{\text{OH}^{\text{H}}}$	=	1.956 ± 0.004	-1.93 ± 0.21	
Duroquinol (-90°)	$a_{\text{CH}_3^{\text{H}}}$	=	2.045 ± 0.010	<i>a</i>	2.00330 ±
	$a_{\text{OH}^{\text{H}}}$	=	2.742 ± 0.006	-1.39 ± 0.04	0.00002
Hydroquinone	$a_{\text{CH}^{\text{H}}}$	=	2.25 ± 0.10	<i>a</i>	2.00350 ±
	$a_{\text{OH}^{\text{H}}}$	=	3.303 ± 0.010	-0.83 ± 0.09	0.00002

^a Not measurable. ^b Temperature at which the splitting constants were measured.

develop a similar model for hydroxyl groups. The temperature dependence of the hydroxyl group splitting constant was accurately measured for a series of compounds and additional data were also obtained from the literature. A comparison of the experimentally obtained temperature coefficients with those calculated from our model allow estimates to be made for the potential barriers to rotation. These potential barriers obtained from the temperature dependencies may then be compared, in certain cases, with the values for the same potential barrier obtained from line-width alternation studies.

Experimental Section

Hydroquinone, duroquinol (1,2,4,5-tetramethyl-3,6-dihydroxybenzene), 1,4-dihydroxynaphthalene, and anthraquinone were commercially available samples. 2,3-Dimethyl-1,4-dihydroxynaphthalene was a gift from Dr. J. R. Bolton. The cation radicals were prepared in either the aluminum chloride-nitromethane system³⁰ or in the sulfuric acid-nitromethane system.³¹ (For further details in specific cases, see the Results section.) The esr spectra were measured, as previously described,¹ in a dual cavity using a sample of Wurster's Blue cation radical as a secondary standard. Spectral analysis was also carried out in the previously described manner.¹

Results

Hydroquinone (HQ). The HQ cation radical has been previously studied^{23,26,32} in $\text{AlCl}_3\text{-CH}_3\text{NO}_2$ in great detail and has been shown to exist as cis and trans isomers at temperatures below $\sim -20^\circ$. The temperature dependence of the hydroxyl group splitting constant was obtained from the previously published results³² by a least-squares analysis assuming the temperature

dependence to be linear over the range studied³³ and was found to be -0.83 ± 0.09 mG/deg (Table I).

(12) (a) R. Wilson, *J. Chem. Soc. B*, 84 (1968); (b) R. Wilson, *ibid.*, 1581 (1968).

(13) R. S. Davidson and R. Wilson, *ibid.*, 71 (1970).

(14) (a) W. T. Dixon and R. O. C. Norman, *J. Chem. Soc.*, 3119 (1963); (b) M. McMillan and R. O. C. Norman, *J. Chem. Soc. B*, 590 (1968); (c) R. O. C. Norman and R. J. Pritchett, *J. Chem. Soc. A*, 378 (1967); (d) R. J. Pritchett, *Mol. Phys.*, 12, 481 (1967).

(15) (a) R. Livingston and H. Zeldes, *J. Chem. Phys.*, 44, 1245 (1966); (b) H. Zeldes and R. Livingston, *ibid.*, 45, 1946 (1966); (c) R. Livingston and H. Zeldes, *ibid.*, 47, 1465 (1967); (d) R. Livingston and H. Zeldes, *ibid.*, 53, 1406 (1970).

(16) (a) H. Fischer, *Mol. Phys.*, 9, 149 (1965); (b) H. Fischer, *Z. Naturforsch.*, 20, 488 (1965).

(17) J. Q. Adams, *J. Amer. Chem. Soc.*, 90, 5363 (1968).

(18) (a) A. Hudson, *J. Chem. Soc. A*, 2513 (1968); (b) A. Hudson and K. D. J. Root, *Tetrahedron*, 25, 5311 (1969).

(19) P. Smith, J. T. Pearson, P. B. Wood, and T. C. Smith, *J. Chem. Phys.*, 43, 1535 (1965).

(20) J. R. Bolton and A. Carrington, *Proc. Chem. Soc., London*, 385 (1961).

(21) J. R. Bolton and A. Carrington, *Mol. Phys.*, 5, 161 (1962).

(22) J. R. Bolton, A. Carrington, and J. dos Santos-Veiga, *ibid.*, 5, 465 (1962).

(23) A. B. Barabas, W. F. Forbes, and P. D. Sullivan, *Can. J. Chem.*, 45, 267 (1967).

(24) P. D. Sullivan, *J. Amer. Chem. Soc.*, 89, 4294 (1967).

(25) P. D. Sullivan and J. R. Bolton, *ibid.*, 90, 5366 (1968).

(26) P. D. Sullivan, J. R. Bolton, and W. E. Geiger, *ibid.*, 92, 4176 (1970).

(27) J. R. Bolton, A. Carrington, and P. F. Todd, *Mol. Phys.*, 6, 169 (1963).

(28) P. D. Sullivan, *J. Phys. Chem.*, 73, 2790 (1969).

(29) P. D. Sullivan, unpublished information.

(30) W. F. Forbes and P. D. Sullivan, *J. Amer. Chem. Soc.*, 88, 2862 (1966).

(31) P. D. Sullivan and J. R. Bolton, *J. Magn. Resonance*, 1, 356 (1969).

(32) W. F. Forbes, P. D. Sullivan, and H. M. Wang, *J. Amer. Chem. Soc.*, 89, 2705 (1967).

(33) The temperature dependence of the hydroxyl group splitting constant is found to be approximately linear for all the compounds studied.

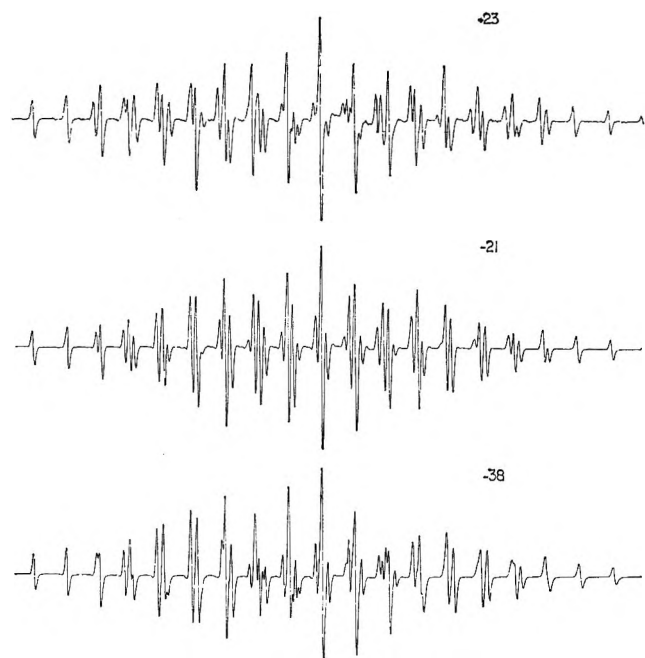


Figure 1. The esr spectrum of the 1,4-dihydroxynaphthalene cation radical in $\text{H}_2\text{SO}_4\text{-CH}_3\text{NO}_2$ at $+23$, -21 , and -38° .

Duroquinol (DQ). The DQ cation radical has also been studied extensively in previous publications.^{24,27} From these studies the temperature dependence of the hydroxyl group splitting constant was found to be -1.39 ± 0.04 mG/deg.

1,4-Dihydroxynaphthalene (DHN). Attempts to produce the cation radical of DHN in $\text{AlCl}_3\text{-CH}_3\text{NO}_2$ were not successful. In the $\text{H}_2\text{SO}_4\text{-CH}_3\text{NO}_2$ system, however, it was possible to obtain good esr spectra from the DHN cation radical over the temperature range $+23^\circ$ to -61° (cf. Figure 1). The spectra are readily interpreted in terms of splittings from four pairs of equivalent protons with values in approximate agreement with those previously reported for DHN in H_2SO_4 at room temperature.²² The change in appearance of the spectrum with temperature (see Figure 1) is caused almost entirely by a change in just one of the splitting constants. That this splitting constant is associated with the hydroxyl protons is easily proven by examining the spectrum in $\text{D}_2\text{SO}_4\text{-CH}_3\text{NO}_2$ where only the hydroxyl protons are exchanged for deuterium.²⁹ The other proton splitting constants were assigned to the appropriate ring positions by means of the molecular orbital calculations (see later) and are in agreement with previous assignments.²²

Since the $\text{H}_2\text{SO}_4\text{-CH}_3\text{NO}_2$ system suffers from the disadvantage that the actual composition of the radical solution is unknown it was decided to test the reproducibility of the absolute magnitudes of the splitting constants and their temperature dependencies by analyzing the results from three independent samples. This analysis showed that the absolute values and temperature coefficients of the three ring proton splitting

constants were reproducible within the standard deviations given (see Table I). The absolute magnitude of the hydroxyl proton splitting constant was less reproducible (within three standard deviations), suggesting that it depends quite sensitively on the solvent composition. The temperature coefficient, however, was in good agreement for all three samples. Representative results for the absolute magnitudes and temperature coefficients are shown in Table I. The hydroxyl group splitting constant shows a temperature coefficient of -1.43 ± 0.19 mG/deg; the ring protons at positions 2 and 3, 5 and 8, 6 and 7 have temperature coefficients of -0.35 ± 0.10 , $+0.45 \pm 0.10$, and $+0.09 \pm 0.10$ mG/deg, respectively.

9,10-Dihydroxyanthracene (DHA). The method of obtaining the cation radical from this compound was somewhat unusual. It was obtained by reacting 9,10-anthraquinone in the $\text{H}_2\text{SO}_4\text{-CH}_3\text{NO}_2$ system. The spectrum obtained was well resolved and analyzed in terms of two groups of four and one group of two equivalent protons (Table I). The values of the splitting constants are in good agreement with those previously reported in H_2SO_4 at room temperature.²² Spectra in $\text{D}_2\text{SO}_4\text{-CH}_3\text{NO}_2$ ²⁹ again verified that the two equivalent protons were the hydroxyl protons and the two sets of four equivalent ring protons were assigned from the molecular orbital calculations. Spectra were obtained over the temperature range -56° to $+23^\circ$ and the hydroxyl group splitting constant was found to be very temperature dependent having a coefficient of -2.86 ± 0.08 mG/deg. The two groups of ring protons were found to have only very small positive temperature coefficients.

2,3-Dimethyl-1,4-dihydroxynaphthalene (DMDHN). Under low resolution conditions in concentrated H_2SO_4 at room temperature the cation radical of DMDHN has an esr spectrum consisting of 29 equally spaced lines.³⁴ In $\text{H}_2\text{SO}_4\text{-CH}_3\text{NO}_2$ it was possible to resolve this accidental degeneracy under higher resolution. The spectrum was analyzed in terms of splittings from a group of six and three groups of two equivalent protons (Table I). The hydroxyl group splitting constant was identified by comparison with the spectrum in $\text{D}_2\text{SO}_4\text{-CH}_3\text{NO}_2$ ²⁹ and from its relatively large temperature coefficient of -1.93 ± 0.21 mG/deg. The splitting constants from the other groups of protons were found to be almost independent of temperature.

Other Hydroxyl-Containing Radicals. Data on the temperature dependence of the hydroxyl group splitting constant in the hydroxymethyl and monoprotonated benzoquinone radicals were obtained from the values reported in the literature.^{15,17}

Calculations

It has been postulated for some time that there are

(34) J. R. Bolton, Thesis, Cambridge University, Cambridge, 1963.

two major mechanisms contributing to the splitting constant of the hydroxyl group proton in a $>C-O-H$ fragment.^{7,13,15,24,35,36} Firstly, there is polarization of the electrons in the $O-H$ bond arising from the unpaired spin density in the oxygen $p-\pi$ orbital. This interaction which is analogous to the well-known interactions in $C-H$ bonds is expected to be of negative sign. It will be at a maximum when the $p-\pi$ overlap between the oxygen and carbon is maximized. This occurs when the hydroxyl group is in the nodal plane of the carbon $p-\pi$ orbital. The interaction is anticipated to be close to zero when the hydroxyl group is twisted 90° out of the nodal plane. Secondly, by analogy to protons in a $>C-C-H$ fragment (β protons), hyperconjugative interactions between the hydroxyl proton and the unpaired spin density in the carbon $p-\pi$ orbital are anticipated. As is expected of β proton interactions, the sign of the interaction should be positive. This mechanism should give a maximum contribution when the hydroxyl group is 90° out of the nodal plane and a minimum contribution when it is in the nodal plane additionally it is expected to follow a $\cos^2 \theta$ relationship for all intermediate angles.

The temperature dependence of the hydroxyl group splitting constant has been attributed to its temperature-dependent torsional oscillations. These oscillations have been variously postulated as leading to a temperature-dependent hyperconjugative interaction plus a temperature-independent spin polarization interaction^{5,15,18} or temperature-dependent hyperconjugative and spin polarization interactions.^{24,28} In either case, the amount of the temperature dependence will depend upon the depth and shape of the potential surface in which the hydroxyl group finds itself constrained. Two obvious factors which are expected to affect the depth of the potential well are the bond order of the carbon-oxygen bond which will tend to constrain the hydroxyl group in the nodal plane and steric interactions which will try to force the group out of the plane. In certain circumstances, provided that the torsional oscillations can be increased sufficiently, one can envisage the possibility of starting with a negative hydroxyl splitting constant which will decrease to zero and then increase as a positive splitting constant. It is perhaps appropriate to review some of the experimental evidence in support of the above hypotheses. The experimental results for the hydroquinone cation radicals²³⁻²⁵ have indicated that in those species the hydroxyl group is very close to the nodal plane of the π system. Thus, cis and trans isomers have been detected for both hydroquinone and duroquinol. The reason for the near coplanarity of the hydroxyl group is thought to be the partial double bond character of the $C-O$ bond. This can be counteracted by steric forces as is shown by the fact that only one species is observed for the 2,5- and 2,3-dimethylhydroquinones. Evidence for the sign of the hydroxyl proton interaction is obtained from

line-width variations which are always high-field broad in these systems³⁷ and from the temperature coefficients which are negative. Both of these facts are consistent with a negative sign for the hyperfine interaction, in agreement with the sign expected from the theory proposed above.

The neutral monoprotinated benzoquinone radical⁸ has a hydroxyl group splitting constant which, from line-width effects and from a negative temperature coefficient, is again consistent with a negative hyperfine interaction. The monoprotinated duroquinone radical,⁸ however, can apparently have either a negative or positive hyperfine interaction depending upon the solvent used. In tetrahydrofuran, the lines from the hydroxyl protons broaden to high field and the splitting constant has a negative temperature coefficient, consistent with a negative hyperfine interaction. In tri-*n*-butyl phosphate, the lines from the hydroxyl protons broaden to low field and the splitting constant has a positive temperature coefficient, consistent with a positive hyperfine interaction. This effect is attributed to the large solvent molecule which reinforces the steric effects of the *o*-methyl groups and thus forces the hydroxyl group further out of the nodal plane.

Further insight into the effect of steric interactions on the hydroxyl group splitting constant can be obtained by comparing the results of hydroxymethyl¹⁸ ($\dot{C}H_2OH$), α -hydroxybenzyl,¹² ($Ph\dot{C}HOH$), and diphenylhydroxymethyl¹² ($Ph_2\dot{C}OH$) radicals. At 25° the hydroxyl group splitting constants for these radicals are 1.15, 0.61, and 2.91 G, respectively. The temperature coefficients are negative, negative, and positive indicating that the absolute values of the splitting constants are -1.15 , -0.61 , and $+2.91$ G. Additionally the hydroxymethyl radical is resolvable into cis and trans isomers at low temperatures. These results may be interpreted by considering that for the $\dot{C}H_2OH$ and $Ph\dot{C}HOH$ radicals the hydroxyl group is constrained reasonably close to the aromatic plane, but that for the $Ph_2\dot{C}OH$ radical the steric effects are strong enough to push the hydroxyl group quite far out of the nodal plane.

From these experimental considerations it is apparent that at least qualitatively the hydroxyl group seems to behave in the manner which has been postulated. An attempt to provide a more quantitative explanation for the hydroxyl group splitting constant is therefore justified.

The simplest expression which has been proposed for the hydroxyl group splitting constant (a_{OH^H}) is of the form of eq 1

$$a_{OH^H} = Q_{OH^H} \rho_{O^\pi} \quad (1)$$

(35) W. Derbyshire, *Mol. Phys.*, **5**, 225 (1962).

(36) D. A. Whiffen, *Cons. Nat. Recher. Sci.*, 167 (1967).

(37) A. Carrington and H. C. Longuet-Higgins, *Mol. Phys.*, **5**, 447 (1962).

Clearly, from all our previous considerations this direct relationship between the splitting constant and the unpaired spin density on the adjacent oxygen atom (Q_{OH}^{H} being a constant) can only apply if the hydroxyl group is rigidly constrained in the nodal plane. The experimental results suggest that this might be so in a small number of examples but eq 1 is by no means a general equation. Another expression which has been proposed and which takes into account out-of-plane movements of the hydroxyl group is of the form of eq 2.³⁸

$$a_{\text{OH}}^{\text{H}} = Q_{\text{OH}}^{\text{H}}\rho_{\text{O}}^{\pi} + Q_{\text{COH}}^{\text{H}}\rho_{\text{C}}^{\pi} \sin^2 \theta \quad (2)$$

Here, the hydroxyl group splitting constant is taken to be the sum of two contributions, a torsionally independent term proportional to the π -spin density on oxygen and a torsionally dependent term proportional to the spin density on the adjacent carbon atom. Obviously, in order to be consistent with the theories previously outlined and to take into account the spin polarization and hyperconjugative mechanisms the signs of the constants Q_{OH}^{H} and $Q_{\text{COH}}^{\text{H}}$ should be negative and positive, respectively. When $\theta = 0^\circ$ eq 2 is equivalent to eq 1. Further consideration of the effect of an out-of-plane movement of the hydroxyl group suggests that perhaps eq 2 should be modified to eq 3.

$$a_{\text{OH}}^{\text{H}} = Q_{\text{OH}}^{\text{H}}\rho_{\text{O}}^{\pi} \cos^2 \theta + Q_{\text{COH}}^{\text{H}}\rho_{\text{C}}^{\pi} \sin^2 \theta \quad (3)$$

The reasoning behind this modification of the first term of eq 2 is that on twisting the hydroxyl group out of the plane by some angle θ the overlap between the carbon and oxygen p - π orbitals will be decreased, thus decreasing the π -spin density on the oxygen atom. To a first approximation we anticipate that this decrease in spin density will be proportional to $\sin^2 \theta$. This is similar to the model used to describe the temperature dependence of the methoxyl group.¹ Again when $\theta = 0^\circ$ eq 3 reduces to eq 1, and in the limit of $\theta = 90^\circ$ eq 3 reduces to eq 4.

$$a_{\text{OH}}^{\text{H}}(\theta = 90^\circ) = Q_{\text{COH}}^{\text{H}}\rho_{\text{C}}^{\pi} \quad (4)$$

Finally, since the hydroxyl group is torsionally oscillating the θ values in eq 3 should be replaced by time-averaged quantities, thus giving eq 5.

$$a_{\text{OH}}^{\text{H}} = Q_{\text{OH}}^{\text{H}}\rho_{\text{O}}^{\pi} \langle \cos^2 \theta \rangle + Q_{\text{COH}}^{\text{H}}\rho_{\text{C}}^{\pi} \langle \sin^2 \theta \rangle \quad (5)$$

In principle, if $\langle \cos^2 \theta \rangle$ can be calculated at various temperatures, if $\langle \cos^2 \theta \rangle + \langle \sin^2 \theta \rangle = 1$ and if the values of Q_{OH}^{H} , $Q_{\text{COH}}^{\text{H}}$, ρ_{O}^{π} , and ρ_{C}^{π} are known it should be possible to calculate the temperature dependence of the hydroxyl group splitting constant. Since $\langle \cos^2 \theta \rangle$ will be a function of the barrier height, by comparing the experimental and calculated temperature coefficients an estimate of the barrier height should be obtained.

In practice the values of $\langle \cos^2 \theta \rangle$ and $\langle \sin^2 \theta \rangle$ can be evaluated using the program³⁹ previously described for the methoxyl group.¹ Thus, it is assumed that the hydroxyl group is oscillating harmonically in a sinu-

soidal twofold potential of maximum barrier height V_0 , with a potential minimum occurring at $\theta = 0^\circ$ (in the nodal plane). The time-averaged value of $\cos^2 \theta$ can then be evaluated assuming a Boltzmann distribution over the energy states. For values of the energy $E_i < V_0$, the limiting harmonic oscillator functions are used while for $E_i > V_0$ the limiting free rotator functions are used.^{40,41} The input parameters required for the program are the maximum barrier height V_0 and the reduced moment of inertia, I_r . The value of I_r for HQ, DQ, DHN, DHA, and DMDHN was calculated to be $0.019 \times 10^{-38} \text{ g cm}^2$. Values of $\langle \cos^2 \theta \rangle$ and $\langle \sin^2 \theta \rangle$ were then calculated for various barrier heights (1–20 kcal) and over a range of temperatures. The procedure for hydroxyl groups now differs appreciably from that used previously for methoxyl groups since we must substitute values for the four constants Q_{OH}^{H} , $Q_{\text{COH}}^{\text{H}}$, ρ_{C}^{π} , and ρ_{O}^{π} before a temperature dependence can be calculated. In order to proceed further with our analysis, let us consider each compound separately.

Hydroquinone (HQ). From studies on the carbon-13 and oxygen-17 hyperfine interactions two possible spin distributions were determined.²⁶ For the $>\text{C}-\text{O}-\text{H}$ fragment $\rho_{\text{C}}^{\pi} = 0.2373$, $\rho_{\text{O}}^{\pi} = 0.0958$ or $\rho_{\text{C}}^{\pi} = 0.2327$, $\rho_{\text{O}}^{\pi} = 0.1010$. These two possibilities were reproduced semiempirically using the McLachlan perturbation correction to the Hückel LCAO-MO method with coulomb and resonance integral parameters for oxygen of $h_{\text{O}} = 2.01$, $k_{\text{OC}} = 1.104$ or $h_{\text{O}} = 1.97$, $k_{\text{OC}} = 1.106$. It is assumed that these spin densities may be substituted directly in eq 5, leaving only Q_{OH}^{H} and $Q_{\text{COH}}^{\text{H}}$ as unknowns. Rather than assuming values for these last two parameters it was decided to use the experimental values of a_{OH}^{H} at a series of temperatures to evaluate Q_{OH}^{H} and $Q_{\text{COH}}^{\text{H}}$. From a least-squares fit of the experimental data, $a_{\text{OH}}^{\text{H}}(210^\circ) = -3.303 \text{ G}$ and $a_{\text{OH}}^{\text{H}}(290^\circ) = -3.236 \text{ G}$. Using the $\langle \cos^2 \theta \rangle$, $\langle \sin^2 \theta \rangle$ values calculated over the temperature range 210° to 290° and combining these with the ρ_{C}^{π} and ρ_{O}^{π} values quoted above it is then possible to solve for the appropriate values of Q_{OH}^{H} and $Q_{\text{COH}}^{\text{H}}$ which give agreement between the calculated and experimental temperature dependences. This procedure is carried out for a range of barrier heights, giving a set of Q_{OH}^{H} and $Q_{\text{COH}}^{\text{H}}$ values for each potential barrier (see Table II). Several points may be noted with regard to these calculations. Firstly, Q_{OH}^{H} is not very sensitive to the barrier height varying between -38 and -45 G for barrier heights of 1 to 20 kcal. Q_{OH}^{H} is dependent on the value of ρ_{O}^{π} , the larger ρ_{O}^{π} , the smaller Q_{OH}^{H} . Secondly, $Q_{\text{COH}}^{\text{H}}$ varies very rapidly with barrier height from -10 to

(38) Note that $\theta = 0^\circ$ when the OH is in the nodal plane and $\theta = 90^\circ$ when the OH group is perpendicular to the nodal plane. This is opposite to the usual convention of defining θ for β protons.

(39) M. K. Carter, Dissertation, University of Washington, 1966.

(40) E. W. Stone and A. H. Maki, *J. Chem. Phys.*, **37**, 1326 (1962).

(41) M. D. Sevilla and G. Vincow, *J. Phys. Chem.*, **72**, 3647 (1968).

Table II: Calculations on Hydroquinone Cation Radical

Potential barrier (V_0), kcal/mol	$Q_{OH^H}^a$	$Q_{COH^H}^a$	$Q_{OH^H}^b$	$Q_{COH^H}^b$
1	-38.1	-9.4	-36.2	-9.6
3	-36.6	-4.8	-34.7	-4.9
5	-37.9	10.3	-36.0	10.5
7	-38.8	24.8	-36.8	25.3
8	-39.2	32.4	-37.2	33.0
9	-39.6	40.9	-37.6	41.7
10	-40.1	50.0	-38.0	50.9
11	-40.6	59.9	-38.5	61.0
12	-41.1	70.5	-39.0	71.9
14	-42.2	94.6	-40.0	96.4
16	-43.5	122.4	-41.2	124.8
18	-44.9	154.5	-42.6	157.7

^a Spin densities $\rho_C^\pi = 0.2373$, $\rho_O^\pi = 0.0958$; splitting constants $a_{OH^H}(210^\circ) = -3.303$ G, $a_{OH^H}(290^\circ) = -3.236$ G.

^b Spin densities $\rho_C^\pi = 0.2327$, $\rho_O^\pi = 0.1010$; splitting constants $a_{OH^H}(210^\circ) = -3.303$ G, $a_{OH^H}(290^\circ) = -3.236$ G.

+172 G for barriers of 1 to 20 kcal. It is not very sensitive to changes in ρ_C^π , showing only a slight increase when ρ_C^π is increased. In order to estimate the barrier height we need to select the correct values of Q_{OH^H} and Q_{COH^H} . From the previous work on the HQ cation radical it was found that if the calculated ρ_O^π values were substituted into eq 1 values of $Q_{OH^H} = -32$ to -34 G were obtained. Since it has been stressed that eq 1 is only valid for coplanar hydroxyl groups and since this cannot be the true situation (if it was no temperature dependence would be expected) it must be assumed that the correct value of Q_{OH^H} should be somewhat larger than the value obtained from eq 1. A value of Q_{OH^H} in the range -32 to -40 G would seem appropriate. The choice of a value for Q_{COH^H} is not as straightforward and is based on the following criteria: (a) β protons in a $>C-C-H$ fragment obey the equation⁴² $a_{\beta H^H} = B \cos^2 \theta$, where B is equal to $+40$ to $+50$ G; (b) suggested value of Whiffen³⁶ for Q_{COH^H} of $+31$ G; and (c) semiempirical molecular orbital calculations in the INDO approximation⁴³ on the hydroxymethyl radical which suggest a value of Q_{COH^H} of $+60$ G when the hydroxyl group is 90° out of plane.

A consideration of these factors leads us to propose that $Q_{COH^H} = 50 \pm 10$ G. Since Q_{COH^H} varies rapidly with barrier height this then becomes our major criterion for estimating the barriers. Using this criterion we obtain for the two possible spin distributions of hydroquinone that $V_0 = 10 \pm 1$ kcal with $Q_{OH^H} = -40$ G, $Q_{COH^H} = 50 \pm 10$ when $\rho_C^\pi = 0.2373$ and $\rho_O^\pi = 0.0958$ or $V_0 = 9.9 \pm 1$ kcal with $Q_{OH^H} = -38$ G, $Q_{COH^H} = 50 \pm 10$ G when $\rho_C^\pi = 0.2327$ and $\rho_O^\pi = 0.1010$. Since our experimental temperature coefficient has uncertainties involved in its determination, further calculations of the barrier height were made to take these deviations into account. The overall result

for the hydroquinone cation radical is that taking the temperature coefficient to be -0.83 ± 0.09 mG/deg and $Q_{COH^H} = 50 \pm 10$ G then $V_0 = 10 \pm 2$ kcal/mol when $Q_{OH^H} = -38.0 \pm 1.2$ G. This result is very encouraging when compared with the value of V_0 of 10 ± 3 kcal/mol found from the analysis of the line-width alternation effects.²³

Duroquinol (DQ). The first difficulty with DQ is that the spin density distribution is not known with any certainty since only the methyl and hydroxyl proton splitting constants have been measured. As a working hypothesis we have chosen to assume that the spin distribution is the same as that of HQ, with one additional modification that suggests we should correct the spin densities using the calculated $\langle \cos^2 \theta \rangle$ values to give $\rho_C^\pi = 0.2281$ and $\rho_O^\pi = 0.1046$ for a coplanar hydroxyl group. Combining these spin densities with the experimental splitting constants of -2.707 and -2.595 G at 210 and 290°K, respectively, values of Q_{OH^H} and Q_{COH^H} can be calculated for various barrier heights (Table III). The overall result, when due re-

Table III: Summary of Calculations for Duroquinol and 1,4-Dihydroxynaphthalene

—Duroquinol ^a —			—1,4-Dihydroxynaphthalene ^b —		
Potential barrier (V_0), kcal/mol	Q_{OH^H}	Q_{COH^H}	Potential barrier (V_0), kcal/mol	Q_{OH^H}	Q_{COH^H}
1	-31.5	-4.0	5.0	-33.3	42.6
2	-30.0	2.5	5.2	-33.3	43.9
3	-29.0	4.0	5.4	-33.9	50.7
4	-30.7	20.4	5.6	-34.0	53.6
5	-31.1	30.1	5.8	-34.2	56.5
5.5	-31.6	37.5	6.0	-34.0	59.5
6	-31.9	43.2	6.2	-34.4	62.5
6.5	-32.2	49.1			
7	-32.5	55.3			
8	-33.1	68.6			
9	-33.7	83.2			

^a Spin densities, $\rho_C^\pi = 0.2281$, $\rho_O^\pi = 0.1046$, splitting constants $a_{OH^H}(210^\circ) = -2.707$ G, $a_{OH^H}(290^\circ) = -2.5953$ G.

^b Spin densities, $\rho_C^\pi = 0.2006$, $\rho_O^\pi = 0.09306$, splitting constants, $a_{OH^H}(230^\circ) = -2.441$ G, $a_{OH^H}(270^\circ) = -2.3763$ G.

gard is taken of the standard deviations of a_{OH^H} and the uncertainty of Q_{COH^H} , is that $V_0 = 6.6 \pm 1.5$ kcal/mol with $Q_{OH^H} = -32.2 \pm 1.2$ G. This result is to be compared with a value of 4.2 ± 0.6 kcal obtained from line-width alternation studies.²⁴ It is disappointing that better agreement between the two methods are not obtained in this case and reasons for the discrepancy are discussed later.

(42) C. Heller and H. M. McConnell, *J. Chem. Phys.*, **32**, 1535 (1960).

(43) J. A. Pople, D. L. Beveridge, and P. A. Dobosh, *J. Amer. Chem. Soc.*, **90**, 4201 (1968).

1,4-Dihydroxynaphthalene (DHN). In order to proceed with this compound it was necessary to estimate a spin-density distribution using a semiempirical molecular orbital calculation. Assuming that $Q_{\text{CH}^{\text{H}}} = 27$ G in McConnell's equation three spin densities can be calculated from the experimental ring proton splitting constants. Rough calculations with parameters similar to those employed for the HQ cation radical enables one to assign the largest ring proton splitting (3.085 G) to the 2,3 positions, the next largest (1.634 G) to the 5,8 positions, and the smallest (0.818 G) to the 6,7 positions. More precise calculations show that agreement between the calculated and experimental spin densities at all three positions cannot be obtained by merely varying the coulomb (h_0) and resonance integral (k_{OC}) parameters of the oxygen atom and oxygen-carbon bond. As was the case for 1,4-dimethoxynaphthalene, it was necessary to take into account the electrostatic effect of the δ^+ charge of the OH protons on the coulomb integrals of the carbon atoms at the 2 and 3 positions. This presumes that the primary configuration is one in which the OH groups are cis to one another. Careful calculations then gave precise agreement between the experimental and calculated spin densities when $h_0 = 1.814$, $k_{\text{OC}} = 1.134$, $h_{\text{C}(2)} = h_{\text{C}(3)} = 0.038$. (See Table IV.) The appropriate values for our calculations are

Table IV: Summary of Molecular Orbital Calculations for DHN and DMDHN

Compd	Position	$\rho_i(\text{calcd})$	$a_i(\text{calcd})^a$	$a_i(\text{exptl})$
1,4-Dihydroxynaphthalene ^b	1	0.2055		
	2	0.1143	3.085	3.085
	5	0.06052	1.634	1.635
	6	0.03030	0.818	0.818
	9	0.00122		
	11(0)	0.08821		
1,2-Dimethyl-1,4-dihydroxynaphthalene ^c	1	0.2200		
	2	0.1078		2.66 (CH ₃)
	5	0.06213	1.677	1.678
	6	0.03315	0.895	0.896
	9	0.0048		
	11(0)	0.06554		

^a Calculated from $a_{\text{CH}^{\text{H}}} = Q_{\text{CH}^{\text{H}}}\rho_{\text{C}^{\text{T}}}$, where $Q_{\text{CH}^{\text{H}}} = |27|$ G.
^b Parameters used were $h_0 = 1.814$, $k_{\text{OC}} = 1.134$, $h_{\text{C}(2)} = h_{\text{C}(3)} = 0.038$.
^c Parameters used were $h_0 = 2.31$, $k_{\text{OH}} = 1.305$.

thus $\rho_{\text{C}^{\text{T}}} = 0.2055$ and $\rho_{\text{O}^{\text{T}}} = 0.08821$. The experimental hydroxyl splitting constants at 230 and 270° are -2.441 and -2.376 G. Substitution of these numbers then allows us to calculate $Q_{\text{OH}^{\text{H}}}$ and $Q_{\text{COH}^{\text{H}}}$ values for various barrier heights (Table III). From these calculations, taking into account the deviations in $a_{\text{OH}^{\text{H}}}$ and $Q_{\text{OH}^{\text{H}}}$, the potential barrier to rotation is estimated to be 5.9 ± 1.5 kcal/mol and $Q_{\text{OH}^{\text{H}}} = -33.2 \pm 1.5$ kcal. No other estimate of the potential barrier is available for this compound.

2,3-Dimethyl-1,4-dihydroxynaphthalene (DMDHN). The appropriate spin densities for the calculations on this compound are difficult to estimate. They can either be assumed equal to the spin densities as calculated for DHN or they can be recalculated until agreement is obtained with the experimental spin densities calculated from the two sets of ring-proton splitting constants. In the latter case, no auxiliary parameters were used and good agreement was obtained when $h_0 = 2.31$ and $k_{\text{OC}} = 1.305$ (see Table IV). The hydroxyl proton splitting constant varies linearly from -1.933 G at 210°K to -1.778 G at 290°K. Together with the spin densities assumed equal to those of DHN ($\rho_{\text{C}^{\text{T}}} = 0.2006$, $\rho_{\text{O}^{\text{T}}} = 0.0931$) the calculations were consistent with $V_0 = 4.6 \pm 1.3$ kcal/mol, $Q_{\text{OH}^{\text{H}}} = -28.6 \pm 1.5$ G, allowing for the deviations in $a_{\text{OH}^{\text{H}}}$ and $Q_{\text{COH}^{\text{H}}}$. If the recalculated spin densities are used ($\rho_{\text{C}^{\text{T}}} = 0.2200$, $\rho_{\text{O}^{\text{T}}} = 0.0655$), the results are $V_0 = 4.8 \pm 1.3$ kcal/mol, $Q_{\text{OH}^{\text{H}}} = -40.6 \pm 2.0$. (See Table V.) Thus the major

Table V: Summary of Calculations for 2,3-Dimethyl-1,4-dihydroxynaphthalene

Potential barrier, V_0 , kcal/mol	$Q_{\text{OH}^{\text{H}}}^a$	$Q_{\text{COH}^{\text{H}}}^a$	$Q_{\text{OH}^{\text{H}}}^b$	$Q_{\text{COH}^{\text{H}}}^b$
3.2	-29.0	38.0	-41.1	34.6
3.6	-28.0	35.7	-39.7	32.5
4.0	-28.2	41.1	-40.0	37.5
4.4	-28.5	46.9	-40.4	42.8
5.0	-28.9	56.4	-41.1	48.5
5.4	-29.6	66.3	-42.1	52.8
5.8	-29.9	73.3	-42.5	63.6

^a Spin densities, $\rho_{\text{C}^{\text{T}}} = 0.20064$, $\rho_{\text{O}^{\text{T}}} = 0.09306$, splitting constants $a_{\text{OH}^{\text{H}}}(210^\circ) = -1.9329$, $a_{\text{OH}^{\text{H}}}(290^\circ) = -1.7785$ G.
^b Spin densities, $\rho_{\text{C}^{\text{T}}} = 0.22005$, $\rho_{\text{O}^{\text{T}}} = 0.06554$, splitting constants $a_{\text{OH}^{\text{H}}}(210^\circ) = -1.9329$, $a_{\text{OH}^{\text{H}}}(290^\circ) = -1.7785$ G.

effect of the change in the spin densities is in the value of $Q_{\text{OH}^{\text{H}}}$, the value of V_0 being only slightly changed.

9,10-Dihydroxyanthracene (DHA). Molecular orbital calculations were carried out to estimate the spin-density distributions. The two-ring proton splitting constants define the spin densities at the 1 and 2 positions of the anthracene ring. Calculations in which only the coulomb and resonance integral parameters h_0 and k_{OC} are varied show that the calculated spin density at position 2 increases asymptotically with h_0 to a value less than that determined from the experimental splitting constant. This result is similar to that obtained with 9,10-dimethoxyanthracene¹ and may be resolved in the same way. That is, $Q_{\text{CH}^{\text{H}}}$ is allowed to increase so that agreement for both ρ_1 and ρ_2 is obtained. The value of $Q_{\text{CH}^{\text{H}}}$ is, however, uncertain and a range of possible values exists. If $Q_{\text{CH}^{\text{H}}} = 28.5$, agreement for the ring proton splitting constants is obtained when $h_0 = 2.20$, $k_{\text{OC}} = 1.08$ and the $\rho_{\text{C}^{\text{T}}}$ and $\rho_{\text{O}^{\text{T}}}$ of interest

are 0.2351 and 0.0492. When $Q_{\text{CH}^{\text{H}}} = 31.8$, $h_{\text{O}} = 1.30$, $k_{\text{OC}} = 0.86$, and $\rho_{\text{C}^{\pi}} = 0.2128$, and $\rho_{\text{O}^{\pi}} = 0.0932$. Calculations of the temperature dependence of $a_{\text{OH}^{\text{H}}}$ were carried out for both of the above spin density distributions. The calculations of $A_{\text{OH}^{\text{H}}}$ are obtained as before and one observes that for both spin density distributions if $Q_{\text{COH}^{\text{H}}}$ is the major criterion of agreement that the estimated barrier height is in the range 3.2 to 4.0 kcal/mol. (See Table VI.) The major difference

Table VI: Summary of Calculations for 9,10-Dihydroxyanthracene

Potential barrier, V_0 , kcal/mol	$Q_{\text{OH}^{\text{H}}}$ ^a	$Q_{\text{COH}^{\text{H}}}$ ^a	$Q_{\text{OH}^{\text{H}}}$ ^b	$Q_{\text{COH}^{\text{H}}}$ ^b
2.0	-22.3	25.2	-42.2	22.9
2.4	-21.4	23.6	-40.5	21.4
2.8	-21.1	26.6	-39.9	24.0
3.0	-21.0	28.3	-39.8	25.6
3.2	-26.0	60.3	-49.2	54.6
3.4	-26.0	63.7	-49.2	57.6
3.6	-24.4	56.4	-46.2	51.1
3.8	-24.5	60.0	-46.4	54.3
4.0	-24.7	63.7	-46.7	57.6
4.4	-25.0	71.4	-47.4	64.7
4.8			-48.1	72.2
5.2			-48.3	88.9

^a Spin densities, $\rho_{\text{C}^{\pi}} = 0.2128$, $\rho_{\text{O}^{\pi}} = 0.0932$; splitting constants $a_{\text{OH}^{\text{H}}}(220^\circ) = -1.2633$ G, $a_{\text{OH}^{\text{H}}}(300^\circ) = -1.0338$ G.

^b Spin densities, $\rho_{\text{C}^{\pi}} = 0.2351$, $\rho_{\text{O}^{\pi}} = 0.0492$; splitting constants $a_{\text{OH}^{\text{H}}}(220^\circ) = -1.2633$ G, $a_{\text{OH}^{\text{H}}}(300^\circ) = -1.0338$ G.

between the two possible spin distributions is that $Q_{\text{OH}^{\text{H}}}$ is predicted to be quite high for the first case (-46 G) and low for the second case (-24 G). A perusal of the values of $Q_{\text{OH}^{\text{H}}}$ and $Q_{\text{COH}^{\text{H}}}$ for these low barrier heights brings to light an unfortunate problem with the calculations. One observes that at these low barrier heights there are often large discontinuities in the derived values of $Q_{\text{COH}^{\text{H}}}$ and $Q_{\text{OH}^{\text{H}}}$. (For example, note the values of these parameters at 3.0 and 3.2 kcal/mol and at 3.4 and 3.6 kcal/mol in Table VI.) The reason for these discontinuities is the small reduced moment of inertia of the compounds which results in the prediction that only a small number of vibrational states are occupied. Also, the lowest rotational level occupied is quite small. Changes in the number of these vibrational and rotational levels due to changes in the barrier height results in these large changes in $Q_{\text{CH}^{\text{H}}}$ and $Q_{\text{COH}^{\text{H}}}$ at small barrier heights. Thus, at 3.0 kcal the final vibrational level is 4 and the first rotational level is 6, but at 3.2 kcal the final vibrational level is 4 and the first rotational level is 8. These discrepancies in the calculations thus make it difficult to draw firm conclusions regarding the barrier height. The best we can say is that the model is consistent with an estimated barrier height in the region of 3.2 to 4.0 kcal/mol.

Hydroxymethyl Radical. This radical has been studied previously by several workers. From the data of Livingston and Zeldes¹⁵ the temperature dependence of the hydroxyl group splitting constant was obtained. Thus $a_{\text{OH}^{\text{H}}} = -1.00$ G at 314°K and -1.75 G at -223°K . The appropriate values of $\rho_{\text{C}^{\pi}}$ and $\rho_{\text{O}^{\pi}}$ were suggested from a molecular orbital calculation in the INDO approximation to be 0.850 and 0.150, respectively. Carrying out the usual calculation at various barrier heights the values of $Q_{\text{OH}^{\text{H}}}$ and $Q_{\text{COH}^{\text{H}}}$ were those obtained as shown in Table VII. These results are con-

Table VII: Summary of Calculations for the Hydroxymethyl and Monoprotonated Benzoquinone Radicals

Hydroxymethyl ^a			Monoprotonated benzoquinone ^b		
Potential barrier, V_0 , kcal/mol	$Q_{\text{OH}^{\text{H}}}$	$Q_{\text{COH}^{\text{H}}}$	Potential barrier, V_0 , kcal/mol	$Q_{\text{OH}^{\text{H}}}$	$Q_{\text{COH}^{\text{H}}}$
1.0	-34.9	10.0	2.0	-39.4	22.0
1.5	-28.0	17.1	2.4	-38.2	20.2
2.0	-26.1	18.7	2.8	-37.9	23.4
2.5	-24.5	18.0	3.0	-37.9	25.3
3.0	-24.0	20.7	3.2	-44.2	57.0
3.5	-29.5	38.3	3.4	-44.3	60.5
4.0	-30.1	44.2	3.6	-42.3	53.9
4.5	-30.8	50.8	3.8	-42.5	57.6
5.0	-31.7	57.8	4.0	-42.7	61.5
5.5	-33.7	68.8	4.4	-43.2	69.6
6.0	-34.6	76.8	4.8	-43.8	78.3

^a Spin densities, $\rho_{\text{C}^{\pi}} = 0.850$, $\rho_{\text{O}^{\pi}} = 0.150$; splitting constants $a_{\text{OH}^{\text{H}}}(220^\circ) = -1.76$ G, $a_{\text{OH}^{\text{H}}}(300^\circ) = -1.15$ G. ^b Spin densities, $\rho_{\text{C}^{\pi}} = 0.220$, $\rho_{\text{O}^{\pi}} = 0.074$; splitting constants $a_{\text{OH}^{\text{H}}}(210^\circ) = -2.101$ G, $a_{\text{OH}^{\text{H}}}(290^\circ) = -1.864$ G.

sistent with a potential barrier in the range of 3.5-5 kcal/mol with $Q_{\text{OH}^{\text{H}}} \approx -31 \pm 1$ G. This barrier compares favorably with the barrier calculated from the INDO calculations (using standard bond lengths and angles) of 3.8 kcal/mol. However, from line-width alternation studies, Hudson¹⁸ has obtained a value of 2.3 ± 0.4 kcal/mol.

Monoprotonated Benzoquinone. Gough and Taylor⁸ have measured the temperature dependence of the monoprotonated benzoquinone radical in a variety of solvents. A least-squares analysis of their published data shows that in ethanol the hydroxyl group-splitting constant has a temperature coefficient of -2.96 ± 0.01 mG/deg with similar values for the other solvents. For our calculations estimates of the spin density at the oxygen and carbon atoms adjacent to the hydroxyl proton are required. Semiempirical molecular orbital calculations led us to estimate the spin densities between $\rho_{\text{C}^{\pi}} = 0.2200$, $\rho_{\text{O}^{\pi}} = 0.0740$ and $\rho_{\text{C}^{\pi}} = 0.2142$, $\rho_{\text{O}^{\pi}} = 0.0540$. Calculations of $Q_{\text{OH}^{\text{H}}}$ and $Q_{\text{COH}^{\text{H}}}$ for the former case are shown in Table VII. Again, difficulties due to discontinuities are experienced with these calculations

and thus the only conclusion to be drawn from them is that they are consistent with a potential barrier in the range 3.2 to 4.0 kcal/mol. This value may be compared to that of 7.4–9.6 kcal/mol estimated by Gough⁷ from line-width alternation studies.

Discussion

The calculated potential barriers are summarized in Table VIII and are compared with the experimental

Table VIII: Summary of Potential Barriers and Temperature Coefficients

Compd	Potential barrier from temperature dependence, kcal/mol	Potential barrier from line-width alternation, kcal/mol	Temperature coefficient
Hydroquinone	10 ± 2	10 ± 3 ^a	-0.83 ± 0.09
Duroquinol	6.6 ± 1.5	4.2 ± 0.6 ^b	-1.39 ± 0.04
1,4-Dihydroxy-naphthalene	5.9 ± 1.5		-1.43 ± 0.20
2,3-Dimethyl-1,4-dihydroxy-naphthalene	4.6 ± 1.3		-1.93 ± 0.21
9,10-Dihydroxy-anthracene	3.2–4.0		-2.86 ± 0.08
Hydroxymethyl	3.5–5.0	2.3 ± 0.4 ^c	-8.24 ^d
Monoprotonated benzoquinone	3.2–4.0	7.4–9.6 ^e	-2.96 ± 0.10 ^e

^a Reference 23. ^b Reference 24. ^c Reference 18. ^d Reference 15. ^e Reference 7.

temperature coefficients of the hydroxyl group. Qualitatively, at least, the potential barriers are in the order one would have anticipated, *i.e.*, HQ > DQ ≅ DHN > DMDHN > DHA. The results also suggest (with the exception of the hydroxymethyl radical) that there is an approximate correlation between the temperature coefficients and the estimated barrier heights. This seems reasonable when one considers that the ρ_C^π and ρ_O^π values for all the compounds except hydroxymethyl fall in a very narrow range and as we have already noted small changes in the ρ_C^π and ρ_O^π values change the estimated potential barriers only very slightly.

A comparison of the barrier heights estimated from line-width alternation studies with those obtained in this study show excellent agreement for the hydroquinone cation, somewhat poorer agreement for duroquinol and hydroxymethyl, and very poor agreement for monoprotonated benzoquinone. That the best agreement is found for the hydroquinone cation is not unexpected since this compound seems the one most likely to fit our model for the hydroxyl-group interaction. That is, the equilibrium configuration is one in which the hydroxyl group is coplanar with the aromatic ring and that the hydroxyl group is constrained within a twofold sinusoidal potential barrier. In the case of duroquinol

we might anticipate that instead of having a potential minimum in the nodal plane, the hydroxyl group would be constrained in a potential well having a double potential minimum at $\pm\theta^\circ$ out of the nodal plane. Indeed, calculations which assume an equilibrium configuration of 10 or 20° out of the plane (although still maintaining a sinusoidal twofold potential) do in fact result in a lower estimate for the potential barrier. The lowering is not sufficient to give exact agreement with the value obtained from the line-width alternation studies but does support our reason for the discrepancy.

The agreement for the hydroxymethyl radical is not good, although the value obtained from the temperature coefficient (3.5–5.0 kcal) is similar to that obtained from molecular orbital calculations in the INDO approximation (3.8 kcal/mol). The value obtained from line-width alternation studies is significantly lower (2.3 ± 0.4). A possible source of error in the calculation of the temperature dependence is the estimate of the spin-density distribution. In addition, as has already been pointed out, difficulties arise in the calculations at these low barrier heights which may also contribute to the disagreement.

In the case of the monoprotonated benzoquinone the disagreement between the two methods of estimating the barrier height is rather large. It is also significant that, whereas for duroquinol and hydroxymethyl the barrier estimated from the temperature coefficient was greater than that obtained from line-width alternations, for monoprotonated benzoquinone the reverse trend is noted. The barrier obtained from line-width alternation⁷ is rather high (7.4–9.6 kcal/mol) and is of the same order as that obtained for the hydroquinone cation (10 ± 3 kcal). This result seems rather surprising since one would anticipate that a major contribution to the barrier arises from the partial double-bond character of the C–O bond. In the case of hydroquinone this contribution should be quite large, based on the number of valence-bond structures that can be written containing a double bond between the carbon and oxygen atoms. Similar structures cannot be written for the monoprotonated benzoquinone, which might, therefore, be better thought of as a hydroxy-substituted phenoxy radical, in which case the hydroxyl group should be similar to a phenolic hydroxyl group. The barrier to rotation in phenol⁴⁴ has been obtained from the microwave spectrum of several monodeuteriophenols as 3.36 ± 0.06 kcal. This value is very similar to our estimate of 3.2–4.0 kcal obtained from the temperature coefficient of the hydroxyl-splitting constant.

Conclusion

Our results indicate that an equation of the form of eq 6 adequately describes the hyperfine interaction of an hydroxyl-group proton.

(44) T. Pederson, N. W. Larsen, and L. Nygaard, *J. Mol. Struct.*, **4**, 59 (1969).

$$a_{\text{OH}}^{\text{H}} = -35 \pm 5\rho_{\text{O}}^{\tau}(\cos^2 \theta) + 50 \pm 10\rho_{\text{C}}^{\tau}(\sin^2 \theta) \quad (6)$$

Calculations of the temperature dependence of the hydroxyl-group interaction based on this equation enable estimates to be made of the potential barriers to rotation about the carbon-oxygen bond. These barriers compare favorably with the same potential barriers estimated from previous line-width alternation studies. Difficulties in the calculations arose when the barrier height was less than 3 kcal/mol, under these conditions the method is less than satisfactory and a different approach⁴⁵ may be justified for these low-barrier heights.

Acknowledgments. Acknowledgment is made to the donors of the Petroleum Research Fund, administered by the American Chemical Society, for support of this research. The author is also indebted to Dr. J. R. Bolton for much helpful advice and to Dr. T. E. Gough for copies of his manuscripts prior to publication.

(45) N. L. Bauld, J. D. McDermed, C. E. Hudson, Y. S. Rim, J. Zoeller, R. D. Gordon, and J. S. Hyde, *J. Amer. Chem. Soc.*, **91**, 6666 (1969).

The Spectrum of Matrix-Isolated Carbon Disulfide

by L. Bajema, M. Gouterman, and B. Meyer*

Department of Chemistry, University of Washington, Seattle, Washington 98105 (Received January 18, 1971)

Publication costs borne completely by The Journal of Physical Chemistry

We have studied the absorption and emission spectrum of CS₂ in argon, nitrogen, and methane matrices at 20°K and in an isopentane-cyclohexane glass at 77°K in the spectral region between 2400 and 6000 Å. In all samples, one strong absorption system originating around 30,000 cm⁻¹ is observed. We assign this to the transition ¹B₂ ← ¹Σ_g⁺. The well-resolved bands are formed by a vibrational progression of ν₁' = 580 ± 30 cm⁻¹. The fine structure suggests a Renner-Teller effect and the presence of aggregates. Weaker bands in a thick layer of CS₂ in an organic glass observed at shorter wavelength might be due to ¹A₂ ← ¹Σ_g⁺. A broad emission, which decays nonexponentially with a long time decay life-time of ~2 msec, is assigned to emission from the lowest triplet state.

Introduction

Although the band spectrum of gaseous CS₂ in the region 2900–4300 Å has been subjected to a number of investigations,^{1–10} the nature of these transitions remains unresolved. The assignment of the region 3300–4300 Å to ³Δ_u(³A₂) and the region 2900–3300 Å to ¹Δ_u(¹B₂) is incomplete, and the assignments have been debated.^{11–13} The spacing of the vapor absorption bands in the region 2900–3300 Å is uneven, and the gas phase emission excited in the 2900–3300-Å region has an unexpectedly long lifetime.¹⁰

The purpose of the present work is to investigate the absorption region 2400–4300 Å and to undertake emission studies of CS₂ in inert gas matrices at 20°K, and in glasses at 77°K. No such studies have been reported. However, Rodloff,¹⁴ in a study which has been overlooked by recent workers, reported bands belonging to at least two different transitions in the 3500-Å area in pure CS₂ at 20 and 77°K.

Experimental Section

CS₂ (25 μmol) was deposited on a sapphire window as a 1/125 mole fraction in Ar, N₂, or CH₄. A 1-μmol quan-

- (1) E. D. Wilson, *Astrophys. J.*, **69**, 34 (1929).
- (2) F. A. Jenkins, *ibid.*, **70**, 191 (1929).
- (3) W. W. Watson and A. E. Parker, *Phys. Rev.*, **37**, 1013, 1484 (1931).
- (4) L. N. Liebermann, *ibid.*, **58**, 183 (1940); **59**, 106 (1941); **60**, 496 (1941).
- (5) P. Kusch and F. W. Loomis, *ibid.*, **55**, 850 (1939).
- (6) C. Ramasastry, *Proc. Nat. Inst. Sci. India, Part A*, **18**, 621 (1952).
- (7) B. Klemm, *Can. J. Phys.*, **41**, 2034 (1963).
- (8) J. Heicklen, *J. Amer. Chem. Soc.*, **85**, 3562 (1963).
- (9) A. E. Douglas and E. R. V. Milton, *J. Chem. Phys.*, **41**, 357 (1964).
- (10) A. E. Douglas, *ibid.*, **45**, 1007 (1966).
- (11) A. D. Walsh, *J. Chem. Soc. London*, **2**, 2266 (1953).
- (12) R. S. Mulliken, *Can. J. Chem.*, **36**, 10 (1958).
- (13) J. T. Hougen, *J. Chem. Phys.*, **41**, 363 (1964).
- (14) C. Rodloff, *Z. Phys.*, **91**, 527 (1934).

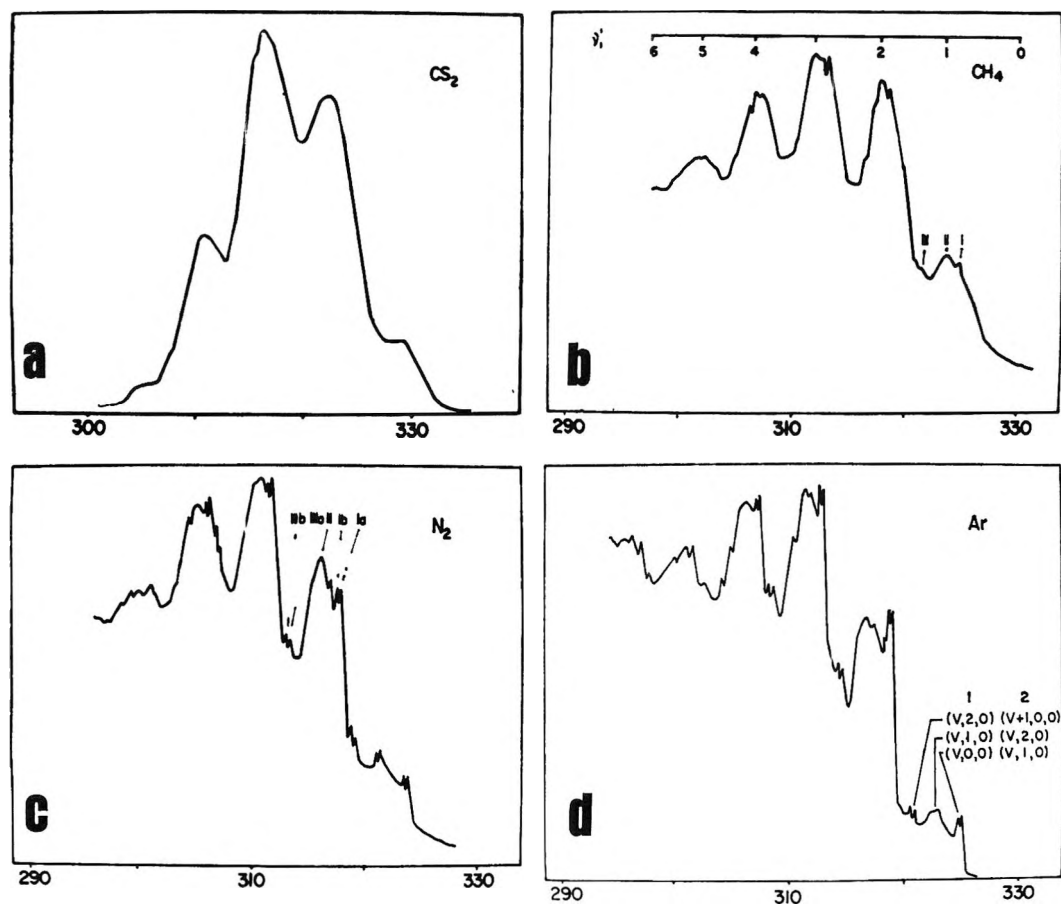


Figure 1. Densitometer traces of the absorption spectrum of CS₂ at 20°K: (a) pure CS₂; (b) CS₂ in methane matrix; (c) CS₂ in nitrogen matrix; (d) CS₂ in argon matrix.

tity of CS₂ was adequate for study of the pure CS₂ absorption and 10 μ mol for its emission studies. The CS₂ was reagent ACS, B and A quality from the Baker and Adamson Co., Morristown, N. J. The inert gases were Matheson high-purity products.

A Cryo-Tip refrigerator AC-2L (Air Products and Chemicals, Allentown, Pa.) was used to cool the sapphire target, and a copper *vs.* gold-cobalt thermocouple was used to measure the target temperature.

We found that the best glass for CS₂ studies was a 1:2 mixture of isopentane-cyclohexane (iPC). The absorption cell was 25 mm long and 15 mm in diameter. The cell windows were part of the inner wall of a specially built, partly silvered dewar flask which fitted into a Cary 14 spectrophotometer.

Absorption spectra were photographed on a Jarrell-Ash *f*/6.3 Czerny-Turner instrument equipped with a grating blazed for 5000 \AA giving a dispersion of 10 $\text{\AA}/\text{mm}$. Polaroid film and Kodak spectroscopic plates Type 103a-F were used. Emission was scanned with a McPherson Model 218 spectrograph equipped with a 1200 lines/mm grating blazed for 5000 \AA , and an E.M.I. 9502S photomultiplier. Emission was excited with a AH-4 medium pressure mercury arc. An *f*/3 monochromator and filters were used to isolate 2600- \AA light.

For lifetime measurements, flash excitation came

from a General Radio Strobotac Type 1531-AB electronic stroboscope,¹⁵ whose light passed through a Corning filter No. CS5-74. The flash duration was 2.7 μ sec when the flashing rate was 4000 flashes/min. Luminescence decays were displayed on a Tektronix type 545B oscilloscope. A waveform eductor (Princeton Applied Research Model TDH-9) was used to improve the signal to noise ratio, and the educted signal traced on a recorder.

The gaseous CS₂ spectrum was recorded on a Cary 14 spectrophotometer. Several drops of CS₂ at the bottom of a 1-cm Cary cell gave sufficient vapor pressure so the spectrum in the region 2800–3400 \AA could be recorded at room temperature. More experimental details are given in ref 16.

Results

1. *Absorption.* Figure 1 contains densitometer tracings of the absorption of solid CS₂ and of CS₂ in CH₄, N₂, and Ar matrices at 20°K. Figure 2b shows the absorption spectrum of CS₂ in a 1:2 isopentane-cyclohexane glass at 77°K. Each spectrum consists of five or six well-resolved bands. Both the solid CS₂ and the CS₂ in glass show unstructured spectra with

(15) S. J. Ladner and R. S. Becker, *J. Chem. Phys.*, **43**, 3344 (1965).

(16) L. Bajema, Ph.D. Thesis, University of Washington, 1970.

Table I: Absorption Peaks of CS₂ in Various Low-Temperature Solids at 20°K

Tentative assignment		Feature	Glass		CH ₄		Ar		N ₂		CS ₂		CS ₂ (77°K)
1	2		E ^a	I ^b	E ^a	I ^b	E ^a	I ^b	E ^a	I ^b	E ^a	I ^c	I ^c
0,0,0	0,1,0	Ia b			30,807		30,781 30,804		30,832 30,848				
0,1,0	0,2,0	II	30,855	(5)	30,892	(4)	30,984	(4)	31,083	(3)	30,381	(2)	(7)
0,2,0	1,0,0	IIIa b			31,170		31,168 31,207		31,290 31,337				
1,0,0	1,1,0	Ia b			31,383		31,358 31,381		31,419 31,435				
1,1,0	1,2,0	II	31,437	(9)	31,430	(9)	31,556	(9)	31,592	(8)	30,968	(8)	(10)
1,2,0	2,0,0	IIIa b			31,764		31,775 31,812		31,865 31,904				
2,0,0	2,1,0	Ia b			31,909		31,948 31,973		32,009 32,025				
2,1,0	2,2,0	II	31,965	(10)	32,020	(10)	32,099	(10)	32,150	(10)	31,552	(10)	(8)
2,2,0	3,0,0	IIIa b			32,358		32,415 32,455		32,505 32,555				
3,0,0	3,1,0	Ia b			32,450		32,517 32,544		32,602 32,619				
3,1,0	3,2,0	II	32,458	(7)	32,570	(7)	32,650	(7)	32,694	(6)	32,152	(5)	(4)
3,2,0	4,0,0	IIIa b					33,013		33,107				
4,0,0	4,1,0	Ia b			33,012		33,128		33,151				
4,1,0	4,2,0	II	33,048	(5)	33,124	(3)	33,213	(4)	33,273	(3)	32,775	(1)	(2)
4,2,0	5,0,0	IIIa b					33,570						
5,0,0	5,1,0	Ia b					33,658						
5,1,0	5,2,0	II	33,717	(3)			33,785	(2)			33,360		(1)
5,2,0	6,0,0	IIIa b											

^a Transition energy in cm⁻¹. ^b Qualitative estimate of relative intensity, with 10 chosen for strongest band in each sample. ^c In this table, bands are placed according to intensity. A better frequency match is obtained if all bands in this column are moved up by one place.

half-widths of 300 cm⁻¹. The spectrum of the solid CS₂ shows a strong temperature dependence of the intensity distribution, as shown in Table I. The general similarity of the spectra of solid CS₂ and CS₂ in glass (10⁻³ M solvent to solute ratio 1500:1) suggests weak intermolecular interaction in the solid.

The matrix spectra show fine structure. The spectrum in CH₄ is the simplest, generally showing two features in each band, labeled I and II in Figure 1b, and another feature labeled III between the bands. The features I and III show a doublet structure in Ar and N₂ (Figure 1c and 1d). The subcomponents are labeled a and b and are separated by 50 cm⁻¹ or less. The absorption maxima are listed in Table I. Feature II tends to be broad and the maxima do not always correspond to the center of the half-width.

The matrix absorption maxima are blue shifted in the order glass < CH₄ < Ar < N₂. The first observed band in solid CS₂ is considerably to the red of these. However, the first band of solid CS₂ may be the (0,0,0) band that is missing in the solution spectra, according

to our assignment.¹⁶ If this assignment is correct, then the maxima in solid CS₂ are quite close to those in an Ar matrix.

Finally, we note that Figure 2a gives the room temperature vapor spectrum which is considerably different from the solution spectra. Elsewhere¹⁶ we have tabulated various combination and difference frequencies for vapor, solid, and solution spectra. We do not report them here as they are rather erratic.

2. *Emission.* Pure CS₂ and CS₂ in CH₄, N₂, and Ar at 20°K, excited at 2600 Å and with X-rays, emit blue light. The spectrum consists of a broad continuum peaking around 4400 Å and extending from 3500 to 5500 Å. The luminescence decay is nonexponential. At 20°K the long time decay gives lifetimes of 1.9, 2.6, and 1.8 msec for solid CS₂, CS₂ in Ar, and CS₂ in N₂, respectively. The time decay curves appeared to be independent of emission frequency.

Discussion

1. *Vibrational and Fine Structure.* The most striking

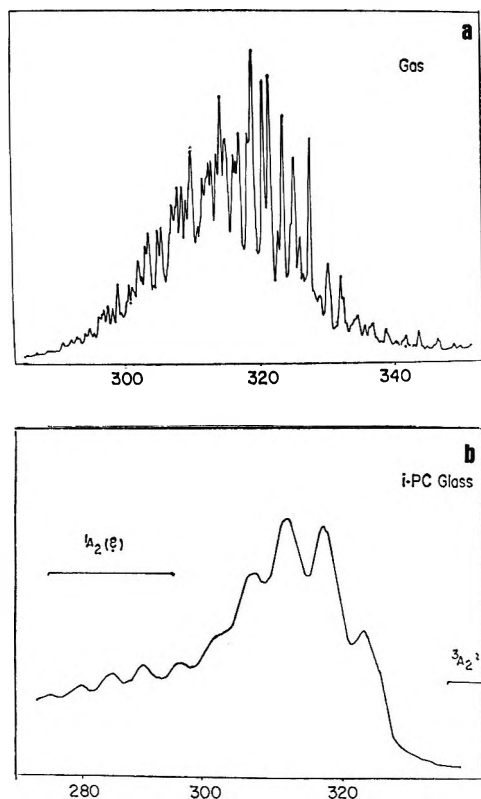


Figure 2. Optical density of: (a) CS₂ gas phase spectrum; (b) CS₂ in isopentane-cyclohexane (iPC) glass at 77°K.

ing feature of these spectra is that the very complex structure shown by the spectrum of vapor CS₂ in Figure 2a is absent in the spectrum of solid CS₂ and CS₂ in matrices. Both solid CS₂ (Figure 1a) and CS₂ in isopentane-cyclohexane glass (Figure 2b) show a very simple unstructured progression of broad bands. In matrices of CH₄, N₂, and Ar, the CS₂ spectrum is similar except for the appearance of fine structure. The average separation of the bands of the main apparent progression is 580 cm⁻¹. This value fits the symmetric stretching mode ν_1 observed in the gas phase⁶ and correlates with a ground-state value of 657 cm⁻¹ observed in the vapor.¹⁷

Two different vibrational assignments of the spectrum seem possible. In assignment 1 (see Figure 1d), progression I arises from the transition $(\nu_1, 0, 0)' \leftarrow (0, 0, 0)''$; II from the transition $(\nu_1, 1, 0)' \leftarrow (0, 0, 0)''$; and III from a $(\nu_1, 2, 0)' \leftarrow (0, 0, 0)''$ transition. This gives an average symmetric stretching frequency of about 580 cm⁻¹, which varies by ± 30 cm⁻¹ for the various matrices, but it leads to a somewhat erratic bending mode frequency. In assignment 2, progression I comes from a $(\nu_1, 1, 0)' \leftarrow (0, 0, 0)''$ transition, II from $(\nu_1, 2, 0)' \leftarrow (0, 0, 0)''$, and III from $(\nu_1 + 1, 0, 0)' \leftarrow (0, 0, 0)''$. The stretching frequency would be the same as in assignment 1, *i.e.*, 580 cm⁻¹. The lack of a (0,0,0) band in this assignment is consistent with the assignment of the vapor phase, where this band is also

weak. It is not possible, at this time, to decide whether assignment one or two is correct.

The complexity of the vapor spectrum is perhaps attributable to the Renner-Teller effect, which can lead to erratic vibrational structure due to strong coupling between vibrational and electronic angular momenta. The very different spectrum in the matrix may arise because angular momentum is quenched in the solid.¹⁵ The matrix spectra may also have peaks due to dimer and aggregate formation. One notes that feature II, which is more intense and broader than I and III, very closely matches a broad band of pure CS₂. It is possible that due to the small M/R ratio and diffusion during condensation aggregates form. Thus, aggregates might account for part of the intensity and line width of progression II.

2. Electronic Assignment. The progression of bands in Table I is assigned to the transition ${}^1B_2 \leftarrow {}^1\Sigma_g^+$ on the basis of intensity considerations. From theoretical calculations, the order of the states available¹² according to their expected relative intensities is ${}^1\Sigma_u^+({}^1B_2) \gg {}^1\Delta_u({}^1B_2) > {}^1\Delta_u({}^1A_2) \sim {}^1\Sigma_u^-({}^1A_2) > {}^3\Sigma_u^+({}^3B_2) > {}^3\Delta_u-({}^3A_2, {}^3B_2) \geq {}^3\Sigma_u^-({}^3A_2)$. The order of energies is shown in Figure 3.

The strongly allowed ${}^1\Sigma_u^+({}^1B_2)$ corresponds to the strong absorption in the region from 1800 to 2300 Å. The region from 3300 to 4300 Å can be assigned to a ${}^3\Delta_u({}^3A_2) \leftarrow {}^1\Sigma_g^+$ transition because of the Zeeman effect observed by Douglas in this region.^{9,13} This assignment is supported by our emission studies discussed below. The choice between the 3A_2 and 3B_2 state is in favor of 3A_2 because of the rotational structure which is compatible with a 1B_2 state. Only the 3A_2 state has a B_2 component. We prefer ${}^3\Delta_u({}^3A_2)$ to ${}^3\Sigma_u^-({}^3A_2)$ on the basis of the transition energy.¹²

This leaves the 2900 to 3300 Å region, which is 10 to 100 times as strong as the 3300 to 4300-Å region, for assignment to either a 1B_2 or 1A_2 state. Previous work⁶ assigned this region to the 1A_2 state. We chose ${}^1\Delta_u-({}^1B_2)$ because transitions to the 1A_2 state are strictly forbidden by group theory. However, transitions to 1A_2 are more allowed than to the 3A_2 state. Thus, ${}^1A_2 \leftarrow {}^1\Sigma_g^+$ might correspond to the weak unassigned bands at higher energy observed in the spectrum of CS₂ in a glass (Figure 2b). In a thick film of pure CS₂ and in a 5-cm layer of 10⁻¹ M CS₂, two weak peaks are observed toward the red at 28,700 and 29,220 cm⁻¹. These peaks match peaks already reported by Rodloff.¹⁴ At 20°K they split into a triplet.¹⁴ They may be ${}^1\Sigma_u^-({}^1A_2) \leftarrow {}^1\Sigma_g^+$ or perhaps a Franck-Condon maximum belonging to the system observed in emission.

3. Emission. Absorption in the 2900 to 3300-Å system and X-ray excitation yield blue emission. The lifetime and transition energy of the origin indicate

(17) D. Agar, E. K. Plyler, and E. D. Tidwell, *J. Res. Nat. Bur. Stand. Sect. A*, **66**, 259 (1962).

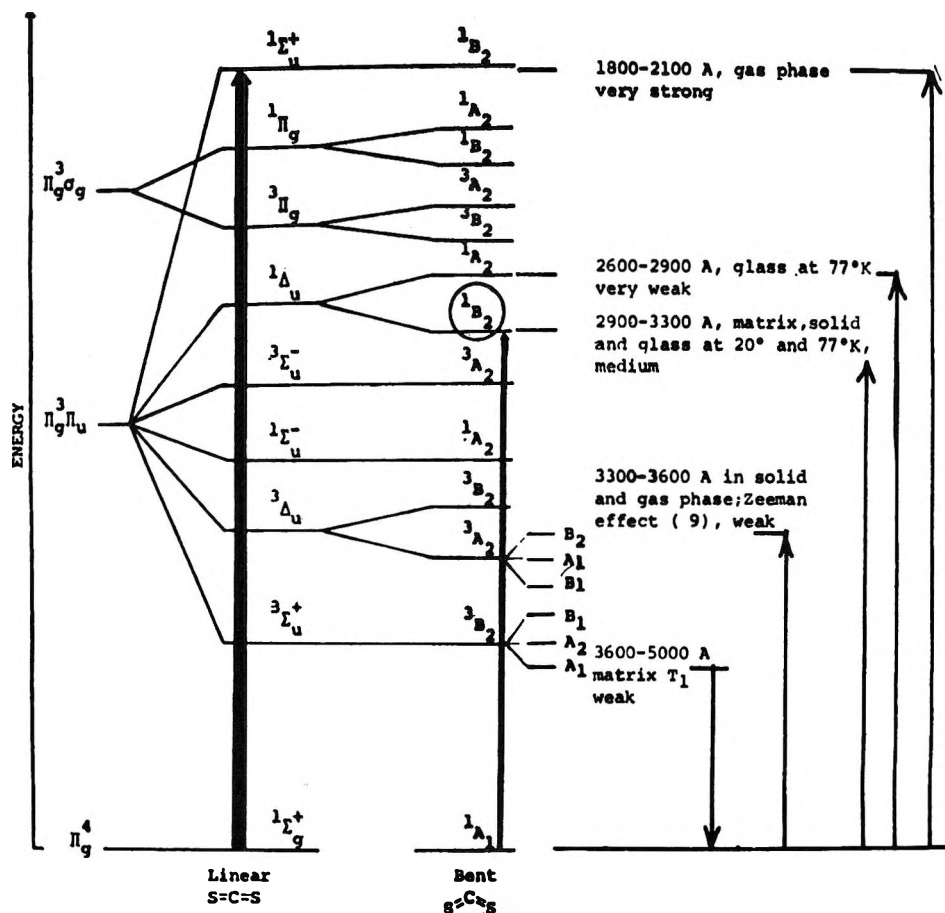


Figure 3. Relative positions of electronic states of CS₂.¹²

that the emission is phosphorescence rather than fluorescence. This corresponds to observations in most low-temperature solids.¹⁸ Phosphorescence is due to solvent-induced intersystem crossing from higher excited states to a lower triplet. Presumably the emission is from either $^3\Delta_u(^3B_2)$ or $^3\Delta_u(^3A_2)$ discussed above. The emission is broad and structureless and is similar in all solvents and in solid CS₂. This is puzzling in view of the sharp absorption lines observed in this region. Conceivably, the spectrum is due to emission from CS₂ aggregates, which are likely because of the high CS₂ concentration in the matrix. In any case, the emission confirms the existence of a triplet at lower energies than the first absorption, in agreement with Douglas' observation of a Zeeman effect and our spectral assignments given above.

Conclusion

This work shows that the near-uv absorption spectrum of CS₂ consists of a progression of strong bands which can be assigned to $^1B_2 \leftarrow ^1\Sigma_g^+$. The vibrational progressions and the difference between vapor and matrix spectra are consistent with a Renner-Teller effect. However, a detailed interpretation remains to be worked out. The emission work confirms the existence of a low-energy triplet.

Acknowledgments. This work was supported by the National Science Foundation. We wish to thank Miss B. Gotthardt, who performed experiments involving organic glasses.

(18) B. Meyer, *Science*, **168**, 783 (1970).

On the Interpretation of Electrode Admittance in the Case of Specific Reactant Adsorption. Application to the Bis(ethylenediamine)cobalt(III-II) System

by M. Sluyters-Rehbach and J. H. Sluyters*

Laboratory of Analytical Chemistry, State University, Utrecht, The Netherlands (Received December 4, 1970)

Publication costs borne completely by The Journal of Physical Chemistry

The results of a recent study by Sherwood and Laitinen of the bis(ethylenediamine)cobalt(III-II) electrode reaction are reconsidered. It turns out that the impedance data can be well explained on the assumption of an infinitely fast charge transfer with reactant adsorption. The literature on the mathematical formulation of this problem is briefly commented upon.

Introduction

Recently, Sherwood and Laitinen¹ have presented in this journal a study of the admittance of the bis(ethylenediamine)cobalt(III)-bis(ethylenediamine)cobalt(II) system, which evidently belongs to the class of systems that exhibit specific reactant adsorption. Their interpretation of experimental results, which is inspired by our work in this field, gives us the idea that there is still confusion in literature about the problem how to handle these systems. Therefore it was thought worthwhile to make some comments, mainly meant as a short review of the equations describing the electrode admittance in the case of reactant adsorption and the possibility of using simplified expressions. As a consequence of these considerations it appeared possible to reinterpret Sherwood and Laitinen's data, the results of which will be presented in this paper.

Theory

In general the equivalent admittance of an electrode-solution interface has to account for the electrode process which is occurring and for the charging of the electrical double layer. If there is no reactant adsorption, both processes can be treated separately and the double layer contribution has only to do with the charge density q

$$i_c = \frac{dq}{dt} = \frac{dq}{dE} \frac{dE}{dt} \quad (1)$$

where i_c is the charging current.

If there is reactant adsorption, the charging process and the faradaic process can no longer be separated,² because in the first place q will also be a function of the concentrations of the redox components

$$\frac{dq}{dt} = \left(\frac{\partial q}{\partial c_0} \right)_{c_R, E} \frac{dc_0}{dt} + \left(\frac{\partial q}{\partial c_R} \right)_{c_0, E} \frac{dc_R}{dt} + \left(\frac{\partial q}{\partial E} \right)_{c_0, c_R} \frac{dE}{dt} \quad (2)$$

Further, one deals with the surface excesses Γ_0 and Γ_R of the redox components, which are functions of c_0 , c_R , and E

$$\frac{d\Gamma_i}{dt} = \left(\frac{\partial \Gamma_i}{\partial c_0} \right)_{c_R, E} \frac{dc_0}{dt} + \left(\frac{\partial \Gamma_i}{\partial c_R} \right)_{c_0, E} \frac{dc_R}{dt} + \left(\frac{\partial \Gamma_i}{\partial E} \right)_{c_0, c_R} \frac{dE}{dt} \quad (3)$$

where i stands for either O or R.

In the early stage, after Delahay had pointed out the above mentioned inseparability,² he derived expressions for the interfacial admittance,³ $y' + iy''$, however in fact using the expression

$$\frac{d\Gamma_i}{dt} = \frac{d\Gamma_i}{dE} \frac{dE}{dt} \quad (4)$$

instead of eq 3, and eq 1 instead of eq 2. We showed⁴ that his results could be written in the simple form

$$y' = \frac{\omega^{1/2}}{\sigma} \frac{p+1}{p^2+2p+2} + \omega K \frac{p}{p^2+2p+2} \quad (5a)$$

$$y'' = \frac{\omega^{1/2}}{\sigma} \frac{1}{p^2+2p+2} + \omega K \frac{p+2}{p^2+2p+2} + \omega C_d \quad (5b)$$

(1) P. J. Sherwood and H. A. Laitinen, *J. Phys. Chem.*, **74**, 1757 (1970).

(2) P. Delahay, *ibid.*, **70**, 2373 (1966).

(3) P. Delahay and G. G. Susbielles, *ibid.*, **70**, 3150 (1966).

(4) M. Sluyters-Rehbach, B. Timmer, and J. H. Sluyters, *J. Electroanal. Chem.*, **15**, 151 (1967).

where

$$p = p'\omega^{1/2} = \theta/\sigma\omega^{-1/2} \quad (6)$$

$$K = \frac{\sigma_0}{\sigma} nF \frac{d\Gamma_0}{dE} + \frac{\sigma_R}{\sigma} nF \frac{d\Gamma_R}{dE} \quad (7)$$

$$\sigma = \sigma_0 + \sigma_R \quad (8)$$

θ being the transfer resistance, σ_0 and σ_R the Warburg coefficients, and C_d the double-layer capacity. We analyzed the system $\text{Pb}^{2+}/\text{Pb}(\text{Hg})$ in 1 M KCl successfully with eq 5.

The incorrectness of using eq 1 and 4 was soon recognized both by Timmer⁵ and Delahay⁶ and a new derivation has been given by Delahay and coworkers,⁷ now using the proper eq 2 and 3. However, the resulting expressions for the interfacial admittance are very complicated and contain too many parameters to allow an unambiguous analysis of experimental data. It is therefore certainly worthwhile to examine whether in some special case eq 5, or possibly another simplification, may be valid as a good approximation.

In their paper, Sherwood and Laitinen follow a proposal by Timmer⁸ to assume that the rate constant is so large that the overvoltage is governed by the Nernst equation. This makes one of the three variables c_0 , C_R , and E dependent of the others, so that one derivative can be left out in eq 2 and 3, e.g.

$$\frac{d\Gamma_i}{dt} = \left(\frac{\partial\Gamma_i}{\partial c_0}\right)_E \frac{dc_0}{dt} + \left(\frac{\partial\Gamma_i}{\partial E}\right)_{c_0} \frac{dE}{dt} = \left(\frac{\partial\Gamma_i}{\partial c_R}\right)_E \frac{dc_R}{dt} + \left(\frac{\partial\Gamma_i}{\partial E}\right)_{c_R} \frac{dE}{dt} \quad (9)$$

Further, they assume that either O or R is only weakly adsorbed. However, we cannot agree with the conclusions they draw from this assumption. If, for example, R is not or weakly adsorbed, eq 9 for the reduction component becomes

$$\frac{d\Gamma_R}{dt} = 0 \quad (10)$$

but for the oxidation component one has still

$$\frac{d\Gamma_0}{dt} = \left(\frac{\partial\Gamma_0}{\partial c_0}\right)_E \frac{dc_0}{dt} + \left(\frac{\partial\Gamma_0}{\partial E}\right)_{c_0} \frac{dE}{dt} = \left(\frac{\partial\Gamma_0}{\partial c_R}\right)_E \frac{dc_R}{dt} + \left(\frac{\partial\Gamma_0}{\partial E}\right)_{c_R} \frac{dE}{dt} \quad (11)$$

and not eq 4, as was stated by Sherwood and Laitinen.¹ Note that $(\partial\Gamma_0/\partial c_R)_E$ is certainly not zero, because its physical meaning is the change in Γ_0 , when c_R changes at constant E , i.e., with a simultaneous change in c_0 . There is also no reason why eq 2, reduced by the Nernst equation to a similar form as eq 9, should reduce further when $\Gamma_R \approx 0$ or $\Gamma_0 \approx 0$.

In our opinion not only eq 9, but even eq 3 could reduce to eq 4 only if Γ_i depends much less on the concen-

trations c_0 and c_R than on the potential E . This occurs if the adsorption has reached saturation coverage, a case also mentioned by Sherwood and Laitinen. It is, however, not likely that saturation coverage will be reached at the rather low concentrations, required for admittance measurements (note that, when saturation coverage occurs, K should be found independent of concentration). It is rather more likely that the adsorption isotherm can be represented by

$$\Gamma_i = k_i c_i \quad (12)$$

Then the above-mentioned condition requires that

$$\frac{1}{c_i} \frac{dc_i}{dE} \ll \frac{1}{k_i} \frac{dk_i}{dE} \quad (13)$$

in other words, k_i must be strongly potential dependent. Even if this is the case, it is still not allowed to simplify eq 2. This can be inferred from the Gibbs equation, which we, for the sake of simplicity, write down for O being the only adsorbed species.⁹

$$-d\gamma = qdE + \Gamma_0 d\mu_0 \quad (14)$$

From eq 14 it follows that

$$\left(\frac{\partial\Gamma_0}{\partial E}\right)_{c_0} = \left(\frac{\partial q}{\partial \mu_0}\right)_E = \frac{c_0}{RT} \left(\frac{\partial q}{\partial c_0}\right)_E \quad (15)$$

Therefore, if $(\partial\Gamma_0/\partial E)_{c_0} = c_0(\partial k_i/\partial E)_{c_0}$ has a substantial value, $(\partial q/\partial c_0)_E$ is most probably not negligible.

The arguments given above lead to the conclusion that on theoretical grounds eq 5 is not suitable to analyze admittance data. Consequently the analysis performed by Sherwood and Laitinen must be rejected, as well as the conclusions they draw from the evaluated parameters. If one wishes to account for both reactant adsorption and charge-transfer control, one should use the rigorous equations given by Delahay.⁷

If a simpler expression is required, in order to reduce the number of parameters, the only possibility is to assume the validity of the Nernst equation, as was proposed by Timmer.⁸ One should be well aware that it is not sufficient to assume that the system is reversible in the dc sense, but that the Nernst equation should hold for the ac perturbations, so that it would be inconsequent to incorporate any contribution of charge transfer in the admittance equations.

The equations for Nernstian behavior are⁹

$$y' = \frac{\omega^{1/2}}{2\sigma} + \omega(C_{LF} - C_{HF}) \frac{u}{u^2 + 2u + 2} \quad (15a)$$

(5) B. Timmer, M. Sluyters-Rehbach, and J. H. Sluyters, *J. Electroanal. Chem.*, **15**, 343 (1967).

(6) P. Delahay, K. Holub, G. Susbielles, and G. Tessari, *J. Phys. Chem.*, **71**, 779 (1967).

(7) K. Holub, C. Tessari, and P. Delahay, *ibid.*, **71**, 2612 (1967).

(8) B. Timmer, M. Sluyters-Rehbach, and J. H. Sluyters, *J. Electroanal. Chem.*, **18**, 93 (1968).

(9) M. Sluyters-Rehbach and J. H. Sluyters in "Electroanalytical Chemistry," Vol. 4, A. J. Bard, Ed., Marcel Dekker, New York, N. Y., 1970.

Table I

Co(III), mM	Co(II), mM	-E, mV	$u' \times 10^4$, sec ^{1/2}	C_{LF} , $\mu\text{F}/\text{cm}^2$	C_{HF} , $\mu\text{F}/\text{cm}^2$	σ , ohm cm ² sec ^{-1/2}
0.5	0	425	5 ± 1	36 ± 0.3	23 ± 2	666.9
0.5	0	430	5 ± 1	36.0 ± 0.3	22 ± 1	656.4
0.5	0	435	6.5 ± 1.5	36.0 ± 0.3	23.5 ± 1.5	659.0
0.5	0	440	6 ± 1	35.5 ± 0.1	23.0 ± 1	676.0
0.5	0	445	8 ± 1	35.3 ± 0.2	25.0 ± 1	704.2
1.061	0	446	24 ± 2	66 ± 1	27 ± 1	361.7
1.061	0	446	20 ± 3	59 ± 1	26.5 ± 1	335.0
1.283	2.467	448	~28 ± 5	97 ± 4	36 ± 2	96.68
3.701	0	435	~20 ± 5	99 ± 5	38 ± 5	89.02
3.765	0	440	14 ± 1	92.5 ± 1.5	10 ± 2	89.81

$$y'' = \frac{\omega^{1/2}}{2\sigma} + \omega(C_{LF} - C_{HF}) \frac{u + 2}{u^2 + 2u + 2} + \omega C_{HF} \quad (15b)$$

with

$$C_{LF} = \left(\frac{\partial q}{\partial E} \right)_{\psi} + \frac{\sigma_0}{\sigma} nF \left(\frac{\partial \Gamma_0}{\partial E} \right)_{\psi} - \frac{\sigma_R}{\sigma} nF \left(\frac{\partial \Gamma_R}{\partial E} \right)_{\psi} \quad (16)$$

$$C_{HF} = \left(\frac{\partial q}{\partial E} \right)_{\Gamma_0 + \Gamma_R} + nF \left(\frac{\partial \Gamma_0}{\partial E} \right)_{\Gamma_0 + \Gamma_R} \quad (17)$$

$$u = u' \omega^{1/2} = 2\omega^{1/2} \left(\frac{\partial [\Gamma_0 + \Gamma_R]}{\partial \psi} \right)_E \quad (18)$$

$$\psi = c_0 D_0^{1/2} + c_R D_R^{1/2} \quad (19)$$

Also with these equations the Pb^{2+} - $\text{Pb}(\text{Hg})$ system in KCl could be described very well. This is not surprising in view of the similarity in frequency dependence of eq 5 and 15, although the meaning of the parameters is quite different.

Reinterpretation of the Bis(ethylenediamine)cobalt Data

Sherwood and Laitinen presented in their Table II a set of data (0.5 mM Co(III) at -440 mV), which we tried to fit to eq 15. When this appeared to be successful, Dr. Sherwood and Professor Laitinen kindly supplied also the data pertaining to the measurements indicated in their Table I. Using the σ values, listed in that table, we could establish a good fit to eq 15, except for the cases 1.283 mM Co(III) + 2.467 mM Co(II) at -448 mV and 3.701 mM Co(III) at -435 mV. It should be noted that the data for these cases showed a considerable scatter. Based on these results, which are tabulated in Table I, the following remarks can be made.

1. The experimental data of Sherwood and Laitinen indicate that the bis(diethylenediamine)Co(III-II) system belongs to the class of electrode reactions which can be described by the most simple model of infinitely

rapid charge transfer combined with reactant adsorption. This means that it is pointless to invoke Delahay's more rigorous equations, since extension of the number of parameters can never lead to unambiguous solutions.

2. It is remarkable that C_{HF} is found to be lower than the double layer capacitance C_d in the pure supporting electrolyte: cf. $C_{HF} = 23$ - $26 \mu\text{F cm}^{-2}$ for 0.5 and 1.061 mM Co(III), $C_{HF} = 10 \mu\text{F cm}^{-2}$ for 3.765 mM Co(III) (a very good fit was obtained here, opposed to the other high concentration cases) and $C_d = 32$ - $30 \mu\text{F cm}^{-2}$. This phenomenon has not been observed before, as in the metal ion-amalgam systems, investigated by us, $C_{HF} \approx C_d$ was always found. The question arises which of the two terms in eq 17 is responsible for this. It seems reasonable that the second term, which mainly represents the conversion of Red into Ox at constant Γ , will have a positive sign, or is equal to zero if $\Gamma_R = 0$. Therefore one is apt to conclude that the first term, representing the change in q with E at constant amount of reactant adsorption, is smaller than the original double-layer capacity, which represents the change in q with E in the absence of adsorption of the Co complex.

3. Sherwood and Laitinen observed a depression in the double-layer capacitance, which is comparable to our observation of a difference between C_d and C_{HF} . They conclude further that this depression indicates a stronger adsorption of the Co(III) complex. The exact meaning of C_{HF} in our interpretation makes such a conclusion rather impossible. It seems to us that difference in adsorption of the ox- and red-component can be better investigated by considering the double-layer capacitances outside, or in any case at the extreme ends, of the faradaic region. The present data do not allow this. Besides, one would intuitively assume that both species are adsorbed in comparative amounts, since the complexing agent is responsible for the adsorption.

4. Equation 10 in Sherwood and Laitinen's paper, derived by Timmer,⁵ is still based on the erroneous concept connected to eq 5 to 8 of our present communica-

tion. The model, pertaining to eq 16-19, leads to a better version, *viz.*⁹

$$-\left(\frac{\partial^2 \gamma}{\partial E^2}\right) = C_{LF} - \frac{n^2 F^2}{RT} \frac{\sigma_0 \sigma_R}{\sigma^2} (\Gamma_0 + \Gamma_R) \quad (20)$$

This equation implies that the interfacial tension γ is measured at varying E with constant $C_0 \sqrt{D_0} + C_R \sqrt{D_R}$, *i.e.*, under normal polarographic conditions.

The value $(\partial^2 \gamma / \partial E^2) = -13.87 \mu\text{F}/\text{cm}^2$ reported by Sherwood and Laitinen for 1.061 mM Co(III) at -446 mV leads, combined with $C_{LF} \approx 60 \mu\text{F}/\text{cm}^2$ (see Table I), to a new value for $\Gamma_0 + \Gamma_R$, namely $0.54 \times 10^{-10} \text{ mol}/\text{cm}^2$.

Acknowledgment. We wish to express our gratitude to Professor H. A. Laitinen and Dr. P. Sherwood for supplying the impedance data used for the calculations of the data in Table I.

NOTES

An Investigation of Aqueous Mixtures of Nonionic Surfactants by Membrane Osmometry

by D. Attwood,* P. H. Elworthy, and S. B. Kayne

School of Pharmaceutical Sciences, University of Strathclyde, Glasgow, C.I. United Kingdom (Received July 13, 1970)

Publication costs borne completely by The Journal of Physical Chemistry

Recently, Coll^{1,2} and Attwood, Elworthy, and Kayne^{3,4} have reported the use of membrane osmometry in the examination of aqueous micellar systems of single micelle-forming components. This present investigation reports on the application of this technique to the study of micellization in a mixture of two nonionic surfactants.

Most of the published work on mixed micellar systems has been concerned with mixtures consisting of an ionic and a nonionic component and has been reviewed previously.⁵ Evidence for the existence of a mixed micelle in such systems was first provided by the electrophoretic studies of Nakagawa and Inoue,⁶ and this has been substantiated by subsequent investigations of these systems. Similarly, electrophoretic measurements⁷ on mixtures of ionic surfactants have indicated mixed micelle formation, and the composition of the mixed micelles formed in mixtures of sodium decyl and dodecyl sulfates and ω -phenylpentyl- and ω -phenyloctyltrimethylammonium bromides have been deduced from conductivity⁸ and nmr⁹ studies, respectively. Most of the reported work on mixtures of nonionic surfactants has been restricted to the determination of the critical micelle concentration (cmc)¹⁰ and assumes rather than establishes that the nonionic components interact completely to form mixed micelles. The small-system thermodynamics of Hill¹¹ has been

applied to mixed micellar systems of nonionic surfactants^{12,13} and an equation has been derived enabling the prediction of the aggregation number of a perfect mixed micellar system.

In this paper the number-average micellar weights, M_n , of mixed solutions of n -hexadecyl nonaoxyethylene monoether ($C_{16}n_9$) and n -dodecyl hexaoxyethylene monoether ($C_{12}n_6$) are determined as a function of the composition of the system. The M_n values are compared with values calculated assuming the two components to exist independently in solution and with values predicted by small-system thermodynamics.

Experimental Section

Materials. The samples of n -hexadecyl nonaoxyethylene monoether and n -dodecyl hexaoxyethylene monoether prepared previously⁴ were used in this investigation.

Membrane Osmometry. Measurements were made on a Hewlett-Packard 503 high-speed osmometer using

- (1) H. Coll, *J. Amer. Oil Chem. Soc.*, **46**, 593 (1969).
- (2) H. Coll, *J. Phys. Chem.*, **74**, 520 (1970).
- (3) D. Attwood, P. H. Elworthy, and S. B. Kayne, *J. Pharm. Pharmacol.*, **21**, 619 (1969).
- (4) D. Attwood, P. H. Elworthy, and S. B. Kayne, *J. Phys. Chem.*, **74**, 3529 (1970).
- (5) P. Becher in "Nonionic Surfactants," M. J. Schick, Ed., Marcel Dekker, New York, N. Y., 1967, p 508.
- (6) T. Nakagawa and H. Inoue, *J. Chem. Soc. Jap.*, **78**, 636 (1957).
- (7) H. W. Hoyer and A. Marmo, *J. Phys. Chem.*, **65**, 1807 (1961).
- (8) K. J. Mysels and R. J. Otter, *J. Colloid Sci.*, **16**, 462 (1961).
- (9) H. Inoue and T. Nakagawa, *J. Phys. Chem.*, **70**, 1108 (1966).
- (10) K. Shinoda, T. Nakagawa, B. Tamamushi, and T. Isemura, "Colloidal Surfactants: Some Physicochemical Properties," Academic Press, New York, N. Y., 1963, p 68.
- (11) T. L. Hill, "Thermodynamics of Small Systems," Vol. 1 and 2, W. A. Benjamin, New York, N. Y., 1964.
- (12) D. G. Hall and B. A. Pethica in "Nonionic Surfactants," M. J. Schick, Ed., Marcel Dekker, New York, N. Y., 1967, p 516.
- (13) D. G. Hall, *Trans. Faraday Soc.*, **66**, 1351, 1359 (1970).

B.19 cellulose acetate membranes (Schleicher and Schuell). Solutions with concentrations, c' , in excess of the cmc's of the mixtures were placed in the solvent compartment of the osmometer. In this way, contributions to the measured osmotic pressure, π , from the monomeric species were reduced to a minimum, since the sample solution and the "solvent" contain approximately the same concentration of monomers. It should be noted that in the mixed micellar systems investigated here the concentration of monomers present in solution is low and errors arising from this effect will not be excessive. A series of mixtures with varying molar ratios of $C_{12}n_6$ and $C_{16}n_9$ were examined. For each ratio, a stock solution was prepared and its osmotic pressure recorded over several hours in order to ascertain the permeability of the osmometer membrane to the micelles. Subsequent measurements were made on dilutions of this solution in which the same molar ratio was maintained. All measurements were made at $36 \pm 0.1^\circ$, since previous investigations⁴ had established membrane impermeability to the micelles of both surfactants at this temperature.

Results and Discussion

Micellar weights were calculated from²

$$\pi = sRT(c - c')/M_n + sRTB[(c - c')^2 + 2(c - c')(c' - \text{cmc})] \quad (1)$$

where c is the total concentration of surfactant in g/l., B is the second virial coefficient, and RT has the usual meaning. The Staverman coefficient, s , is related to the permeability characteristics of the membrane to the micellar species. Figure 1 shows the variation of osmotic pressure with time for the mixtures studied. In all cases the osmotic pressure quickly reached an equilibrium value which remained constant for at least 1 hr. The attainment of an equilibrium pressure in this way has previously been shown³ to indicate membrane impermeability to the micellar species, and hence $s = 1$ for these systems. Graphs of $\pi/(c - c')$ vs. $(c - c')$ were extrapolated to $c = c'$ (see Figure 2) and M_n values calculated from the intercept, which is given by

$$(\pi/c - c')_{c=c'} = RT/M_n + 2RTB(c' - \text{cmc}) \quad (2)$$

The cmc's of the mixed systems were estimated from the mole compositions of the mixtures¹⁰ using the cmc of 7.2×10^{-5} mol/l. quoted¹⁴ for $C_{12}n_6$ at 35° and a value of 2.1×10^{-6} mol/l. for the cmc of $C_{16}n_9$. The latter value is that reported¹⁵ for 25° ; however, the correction term $2RTB(c' - \text{cmc})$ had no significant effect on the values of M_n and hence accurate values for the cmc's were not required. The values obtained for M_n and B are summarized in Table I. The second virial coefficient for $C_{12}n_6$ alone is in agreement with a theoretical value of 0.06×10^{-4} ml mol g⁻² calculated on the basis of its excluded volume. Since M_n is decreased by the addition of $C_{16}n_9$, a corresponding increase in

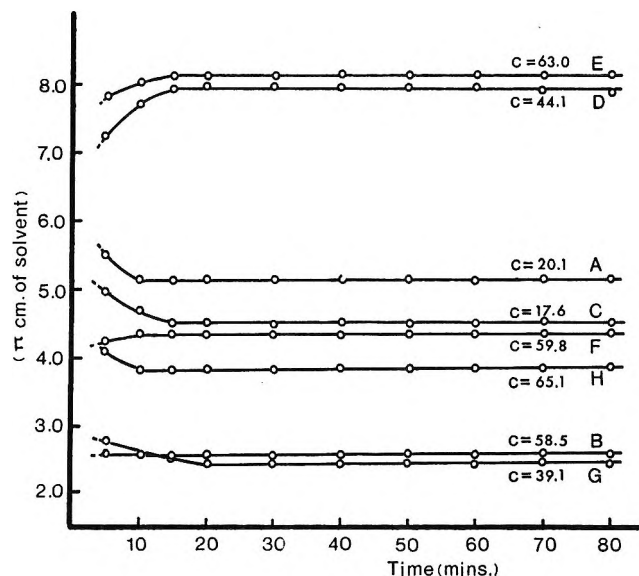


Figure 1. Change of osmotic pressure with time for aqueous solutions of A, $C_{16}n_9$ and B, $C_{12}n_6$ and mixtures with $C_{16}n_9:C_{12}n_6$ molar ratios of C, 2.9:1; D, 2:1; E, 1:1; F, 1:2.6; G, 1:4; H, 1:7.1 at various concentrations c g/l.

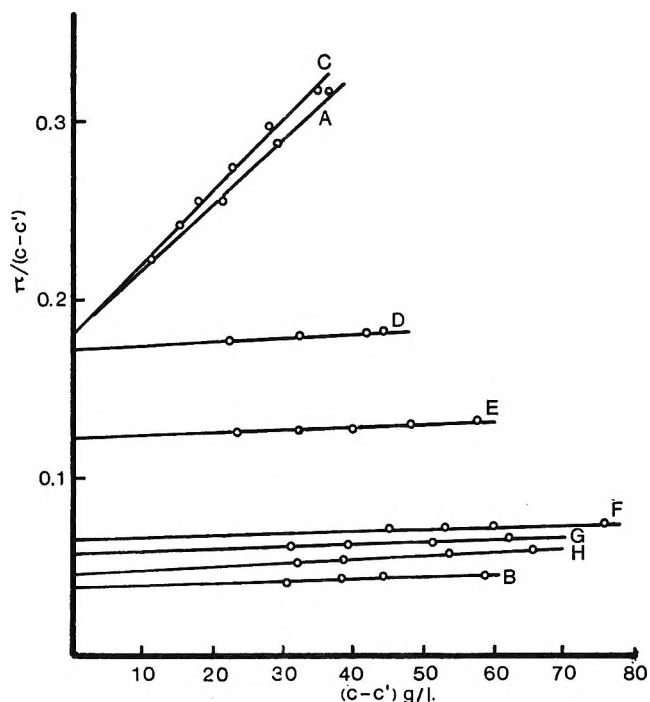


Figure 2. Variation of reduced osmotic pressure with concentration for solutions of A, $C_{16}n_9$ and B, $C_{12}n_6$ and mixtures with $C_{16}n_9:C_{12}n_6$ molar ratios of C, 2.9:1; D, 2:1; E, 1:1; F, 1:2.6; G, 1:4; H, 1:7.1.

the value of B might be expected. However, the values for $C_{16}n_9$ alone and in the presence of small amounts of $C_{12}n_6$ are appreciably higher than the

(14) J. M. Corkill, J. F. Goodman, and R. H. Ottewill, *Trans. Faraday Soc.*, **57** 1627 (1961).

(15) P. H. Elworthy and C. B. Macfarlane, *J. Pharm. Pharmacol.*, **14**, 100T (1962).

theoretical value of 0.49×10^{-4} ml mol g^{-2} for the hydrated micelle of $C_{16}n_9$, the discrepancy being too large to be explained in terms of experimental error. A similar lack of agreement between theoretical and experimental values of B for $C_{16}n_9$ was noted from light-scattering measurements,¹⁶ which indicated values of the same order as those observed here (3.28×10^{-4} and 1.95×10^{-4} ml mol g^{-2} at 25 and 45°, respectively). These discrepancies are not fully understood, although possible explanations have been suggested.¹⁶

Table I: Number-Average Micellar Weights and Second Virial Coefficients for Mixed Micellar Systems of $C_{12}n_6$ and $C_{16}n_9$ at 36°

Mole fraction $C_{12}n_6$	$M_n \times 10^{-5}$	$B \times 10^4$, ml mol g^{-2}
$C_{16}n_9$ alone	1.41	1.25
0.260	1.42	1.53
0.339	1.53	0.08
0.500	2.19	0.07
0.726	3.98	0.04
0.800	4.60	0.05
0.875	5.66	0.08
$C_{12}n_6$ alone	6.65	0.04

This treatment assumes a constancy of micellar composition over the concentration range used in the osmotic pressure measurements. The results of Mysels and Otter⁸ imply that a change in micellar composition occurred in the region of the cmc for mixtures of sodium decyl and dodecyl sulfates, which was apparent even when the cmc had been exceeded severalfold. In this investigation, solutions with a minimum concentration of approximately 500 cmc were used and it is likely that changes in micellar composition will occur at these high concentrations. The linearity of the reduced osmotic pressure *vs.* concentration plots supports this assumption.

For a mixed micellar system of c components in which the surfactants do not interact to form mixed micelles but remain as independent micellar entities, M_n is given by

$$M_n = \frac{\sum_{i=1}^c m_i M_i}{\sum_{i=1}^c m_i} \quad (3)$$

where m_i is the number of moles of micelles of the i th component and M_i is the micellar weight of pure i . The M_n values calculated from eq 3 are compared with the experimental values in Figure 3. The discrepancy between calculated and experimental values, which is particularly pronounced in mixtures containing a high content of $C_{12}n_6$, is outside the limits of error of the osmometric technique ($\pm 3\%$) and indicates significant interaction between the components of the mixture.

Hall and Pethica¹² have applied small-system thermo-

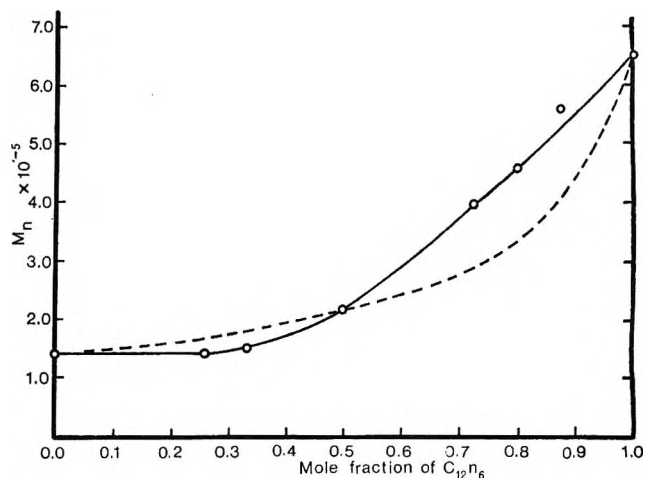


Figure 3. Variation of the micellar weight of $C_{16}n_9$: $C_{12}n_6$ mixtures with the mole composition of the mixture. Continuous line represents experimental values; dashed line represents values calculated assuming noninteraction of the surfactants.

dynamics to mixed micellar solutions of nonionic surfactants and have defined a perfect mixed system as one in which the chemical potential, μ_i , of the i th component of the mixture is given by

$$\mu_i = \mu_i^0(T, p, \epsilon) + kT \ln x_i \quad (4)$$

where x_i is the mole fraction of the component i and μ_i is the chemical potential of pure i at the same temperature T , pressure p , and subdivision potential ϵ as the mixed system. For perfect small systems defined in this way the aggregation number, \bar{N} , of the mixed micellar species is given by

$$1 = \bar{N} \sum_{i=1}^c x_i / \bar{N}_i^0 \quad (5)$$

where \bar{N}_i^0 is the aggregation number of micelles of pure i . Assuming that the ratio of the components in the mixed micelle is identical with that of the mixture, the aggregation number, \bar{N}_i , of component i in the mixed micelle can be calculated from

$$\bar{N} = \sum_{i=1}^c \bar{N}_i \quad (6)$$

The variation of \bar{N}_i with the composition of the mixture, as calculated from eq 5 and 6, is compared in Figure 4 with that calculated from the experimental M_n values. It is seen that the aggregation numbers of the two micellar components for systems in which the mole fraction of $C_{12}n_6$ is less than 0.5 approximate closely those predicted assuming perfect mixing. However, for systems containing greater proportions of $C_{12}n_6$ the aggregation numbers of both components are in excess of the predicted values; *i.e.*, these systems deviate from perfect behavior.

(16) P. H. Elworthy and C. McDonald, *Kolloid-Z. Z. Polym.*, **195**, 16 (1964).

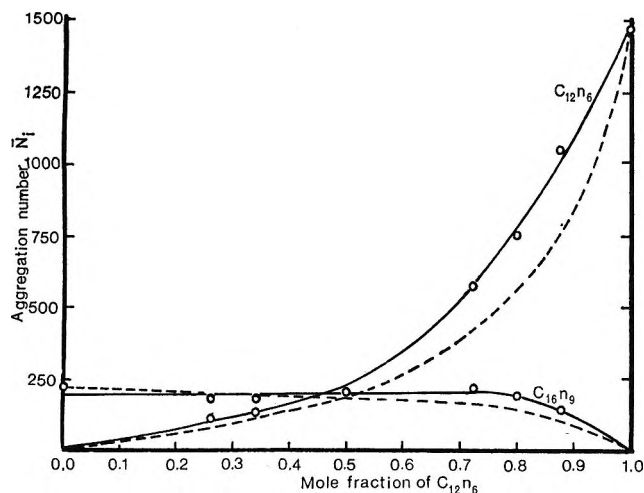


Figure 4. The composition of the mixed micelles as a function of the mole composition of the mixture. Continuous line represents experimental values; dashed line represents values predicted by small-system thermodynamics assuming perfect mixing of micellar components.

There are differences in the lengths of both the hydrophilic and hydrophobic groups of the two surfactants and it is probably this dissimilarity of chemical composition which is the cause of the observed deviations from ideality. A closer approximation to perfect behavior might be expected with surfactants more closely resembling each other, and an investigation of such systems is proposed.

Acknowledgment. The authors wish to thank the Science Research Council for the award of a Research Studentship to S. B. K.

On the Use of "Concentration-Time" Integrals in the Solutions of Complex Kinetic Equations

by B. Saville¹

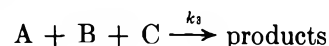
*The Natural Rubber Producers' Research Association,
Welwyn, Garden City, Hertfordshire, England
(Received December 24, 1970)*

Publication costs assisted by The Natural Rubber Producers' Research Association

We wish to record methods of solving complex kinetic equations of composite second and higher orders through use of experimentally (graphically) determinable concentration-time integrals, as opposed to simple time, as a plotted variable. The concentration-time integral used and understood here is merely the area (in mol sec l.⁻¹) under a graph of a species concentration against time and is thus directly available from conventional concentration-time data. Thus for a

reactant B, the concentration-time integral, designated B_t , is

The use of such an integral appears first to have been used by French,² but its general utility in kinetics was not emphasized. Essentially, the effective kinetic order of a reaction can be reduced by one through use of such integrals. Consider the case of a third-order equation with all three reactants different. Then, classically, for



we have

$$\frac{-d[A]}{dt} = k_3[A][B][C]$$

thus

$$\frac{-d[A]}{[A][B]} = k_3[C] dt$$

so that with

$$[B] = [B_0] - [A_0] + [A]$$

$$-\int \frac{d[A]}{[A]([B_0] - [A_0] + [A])} = k_3 \int_0^t [C] dt$$

or

$$\frac{1}{[B_0] - [A_c]} \ln \frac{[A_0][B]}{[B_0][A]} = k_3 C_t$$

(Note that this is the same as the integrated form of a second-order kinetic equation with concentration-time integral, C_t , replacing time, t .) Thus a plot of $\log [B]/[A]$ vs. the experimental integrals, C_t , immediately gives a straight line of slope $k_3([B_0] - [A_0])/2.303$. Operationally, this may be compared with the extraction of k_3 from the usual equation, which is

$$k_3 t = \{ ([A_0] - [B_0])([B_0] - [C_0])([C_0] - [A_0]) \}^{-1} \times$$

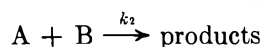
$$\ln \left[\left(\frac{[A]}{[A_0]} \right)^{[B_0] - [C_0]} \left(\frac{[B]}{[B_0]} \right)^{[C_0] - [A_0]} \left(\frac{[C]}{[C_0]} \right)^{[A_0] - [B_0]} \right]$$

Application of the concentration-time integral concept to the following case is even more interesting because it is not normally at all capable of solution.

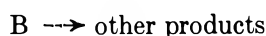
(1) Principal Scientist, Research Division.

(2) D. French, *J. Amer. Chem. Soc.*, **72**, 4806 (1950).

Suppose one has a bimolecular reaction, so that



but that we additionally have B disappearing through other unspecified reactions which do not consume A, *i.e.*



Then since

$$\frac{-d[A]}{dt} = k_2[A][B]$$

it is always true that

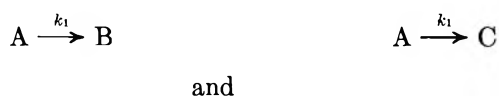
$$-\int \frac{d[A]}{[A]} = k_2 \int_0^t [B] dt$$

Therefore

$$\ln \frac{[A_0]}{[A]} = k_2 B_t$$

(Note that this is the same as the integrated form of a first-order kinetic equation with concentration-time integral, B_t , replacing time, t .) A simple plot of $\log [A]$ against the concentration-time integrals, B_t , for various extents of reaction gives a straight line of slope $-k_2/2.303$, *no matter what other decomposition paths B may take*. (This procedure has recently been applied by Knight and Nunn of the authors¹ group in determining second-order rate constants for the reactions of alkenes ($\equiv A$) with nitrosoarenes ($\equiv B$) in which the latter disappears superstoichiometrically through reactions with initially formed products.)

The consecutive, and parallel, first- and second-order reactions schematized as



both give the following decay law for reactant A

$$\frac{-d[A]}{dt} = k_1[A] + k_2[A][B]$$

With the present working this becomes

$$-\int \frac{d[A]}{[A]} = \int k_1 dt + \int k_2[B] dt$$

so that

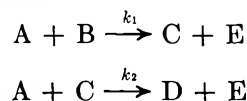
$$\ln \frac{[A_0]}{[A]} = k_1 t + k_2 B_t$$

Since, for selected values of time, t and B_t are measurable the above equation serves as the basis for a pair of simultaneous equations from which k_1 and k_2 are easily calculable, *i.e.*

$$\left. \begin{aligned} \ln \frac{[A_0]}{[A_{t_1}]} &= k_1 t_1 + k_2 B_{t_1} \\ \ln \frac{[A_0]}{[A_{t_2}]} &= k_1 t_2 + k_2 B_{t_2} \end{aligned} \right\}$$

The usual integrated form of the parallel first- and second-order reaction equation is not immediately capable of giving the individual rate constants,³ whereas for the case of consecutive first- and second-order reactions the usual analyses⁴ take one into the realms of higher mathematics where complete solutions may be impossible without approximations.⁵ On the other hand, our approach employing concentration-time integrals will hold good even if B disappears by other concurrent alternative pathways.

The difficult analysis of competitive consecutive second-order reactions, studied by Ingold,⁶ Westheimer,⁷ and others,^{2,8} and only partly resolved in terms of approximate equations and difficultly extractable kinetic constants, is again very easily rationalized using the experimental concentration-time integral approach. Thus, we have for



that

$$\frac{-d[A]}{dt} = k_1[A][B] + k_2[A][C]$$

when

$$-f d \ln [A] = k_1 f[B] dt + k_2 f[C] dt$$

so that

$$\ln \frac{[A_0]}{[A]} = k_1 B_t + k_2 C_t$$

As in the former case, the values of the integrals and B_t and C_t to any desired times are experimentally determinable from the $[B]$ vs. t and $[C]$ vs. t plots, so that a pair of simultaneous equations

$$\left. \begin{aligned} \ln \frac{[A_0]}{[A_{t_1}]} &= k_1 B_{t_1} + k_2 C_{t_1} \\ \ln \frac{[A_0]}{[A_{t_2}]} &= k_1 B_{t_2} + k_2 C_{t_2} \end{aligned} \right\}$$

(3) A. A. Frost and R. G. Pearson, "Kinetics and Mechanism," Wiley, New York, N. Y., 1961, pp 177-178.

(4) J. Chien, *J. Amer. Chem. Soc.*, **70**, 2256 (1948).

(5) Reference 3, p 178.

(6) C. K. Ingold, *J. Chem. Soc.*, 2170 (1931).

(7) F. W. Westheimer, W. A. Jones, and R. A. Lord, *J. Chem. Phys.*, **10**, 478 (1942).

(8) D. French and R. L. McIntire, *J. Amer. Chem. Soc.*, **72**, 5148 (1950); M. Ritchie, *J. Chem. Soc.*, 3112 (1931); A. A. Frost and W. C. Schwemer, *J. Amer. Chem. Soc.*, **74**, 1268 (1952).

immediately permits calculations of the required kinetic constants k_1 and k_2 . Such data, however, as kindly indicated by a referee, might be more completely handled by standard regression analysis, particularly if a computer were available.

No doubt there will be many other cases where "concentration-time" integrals, as new experimentally determinable variables, can be applied with advantage in chemical kinetics, since it is now often possible with present-day modes of chemical analysis to obtain decay data for *all* reactants, and it is also a relatively easy matter with desk calculators to compute areas under experimental curves.

Acknowledgment. Mr. G. T. Knight is thanked for supplying data used successfully to check some of these methods. This work was sponsored by the Board of The Natural Rubber Producers' Research Association.

The Radiolysis of Liquid

1,1,2-Trichlorotrifluoroethane¹

by A. R. Kazanjian* and D. R. Horrell

The Dow Chemical Company, Rocky Flats Division, Golden, Colorado 80401 (Received January 4, 1971)

Publication costs assisted by The Dow Chemical Company

The radiation chemistry of chlorofluorocarbons presents an interesting study because of the three possible types of bond rupture. These are the carbon-carbon, carbon-fluorine, and carbon-chlorine bonds. The relative proportion of each type of bond scission will determine the final radiolysis products. This problem has been investigated using 1,1,2-trichloro-1,2,2-trifluoroethane. The compound was γ -irradiated and the products were analyzed. A mechanism was deduced from a knowledge of the final products.

There are no previous reports on the radiolysis of chlorofluorocarbons and very little work has been done on fluorocarbons. One previous investigation² has shown that radiolytic scission of the C-C bond is of the same order as the C-F bond break in the γ radiolysis of liquid hexafluoroethane. This occurred in a compound in which the C-F bond energy (106 kcal/mol) is 20 kcal/mol greater than the C-C bond energy (86 kcal/mol). Other reports of predominant C-F bond rupture have been made by Fallgatter and Hanrahan³ and MacKenzie, *et al.*,⁴ in their work on cyclic and aromatic perfluorocarbons. These conclusions are not in accord with the results obtained in an esr study of irradiated liquid C₂F₆.⁵ There was no evidence in the

esr work of the production of other than the CF₂ radical, indicating little or no C-F bond scission. Trichlorotrifluoroethane contains, in addition, C-Cl bonds with an energy of 72-80 kcal/mol. On the basis of bond energy, this latter cleavage appears to be the most likely.

Experimental Section

The 1,1,2-trichloro-1,2,2-trifluoroethane was obtained in a very pure state (99.996%) from Allied Chemical Co. under the trade name of Genesolv-D and used without further treatment. Liquid samples were γ -irradiated in a Gammacell-220, a source containing about 3200 Ci of ⁶⁰Co. The dose rate in a Fricke solution was approximately 2.5×10^{17} eV/ml min. Energy absorption in the irradiated trichlorotrifluoroethane was calculated on the basis of electron density, and exact dose rates were determined for each container and position within the irradiation chamber. Conversion of the parent was usually less than 1%.

Samples were irradiated in Pyrex, quartz, stainless steel, Teflon, platinum, and Monel tubes. Results were essentially the same in all the tubes. Sample temperature was 30°. Samples were deaerated, either by He sweeping or by evacuating.

Product analyses was made by temperature programmed gas chromatography; see Figure 1. Qualitative analysis was made by comparison of the retention times of the unknown peaks with those of known compounds on two columns. The specific isomers were identified by mass spectrometric (CEC21-110B) analysis of the compounds isolated by gas chromatography. Quantitative measurements were made by comparison of chromatographic peak areas. Standard solutions of CFCl₃ and C₃F₄Cl₄ in trichlorotrifluoroethane were made up and shown to have a relative detector sensitivity of 1 on a weight basis. The other products were also assumed to have the same sensitivity because they are all the same type of compound.

Results and Discussion

The final radiolysis products and their yields are listed in Table I. The variation in *G* values may be as much as 25%. There was no difference in yields over the fourfold increase in applied dose. The material balance, C:F:Cl, obtained for these products was 2:3:3.2. This discrepancy was not resolved. The only other products observed were smaller amounts of Cl₂ and F₂, spot tested with *o*-tolidine and starch iodide. Other oxidizing agents interfere in these tests. There

(1) This work performed under the auspices of the Atomic Energy Commission Contract AT(29-1)-1106.

(2) A. Sokolowska and L. Kevan, *J. Phys. Chem.*, **71**, 2220 (1967).

(3) M. B. Fallgatter and R. J. Hanrahan, *ibid.*, **69**, 2059 (1965).

(4) D. R. MacKenzie, F. W. Block, and R. H. Wisall, Jr., *ibid.*, **69**, 2526 (1965).

(5) R. W. Fessenden and R. H. Schuler, *J. Chem. Phys.*, **43**, 2704 (1965).

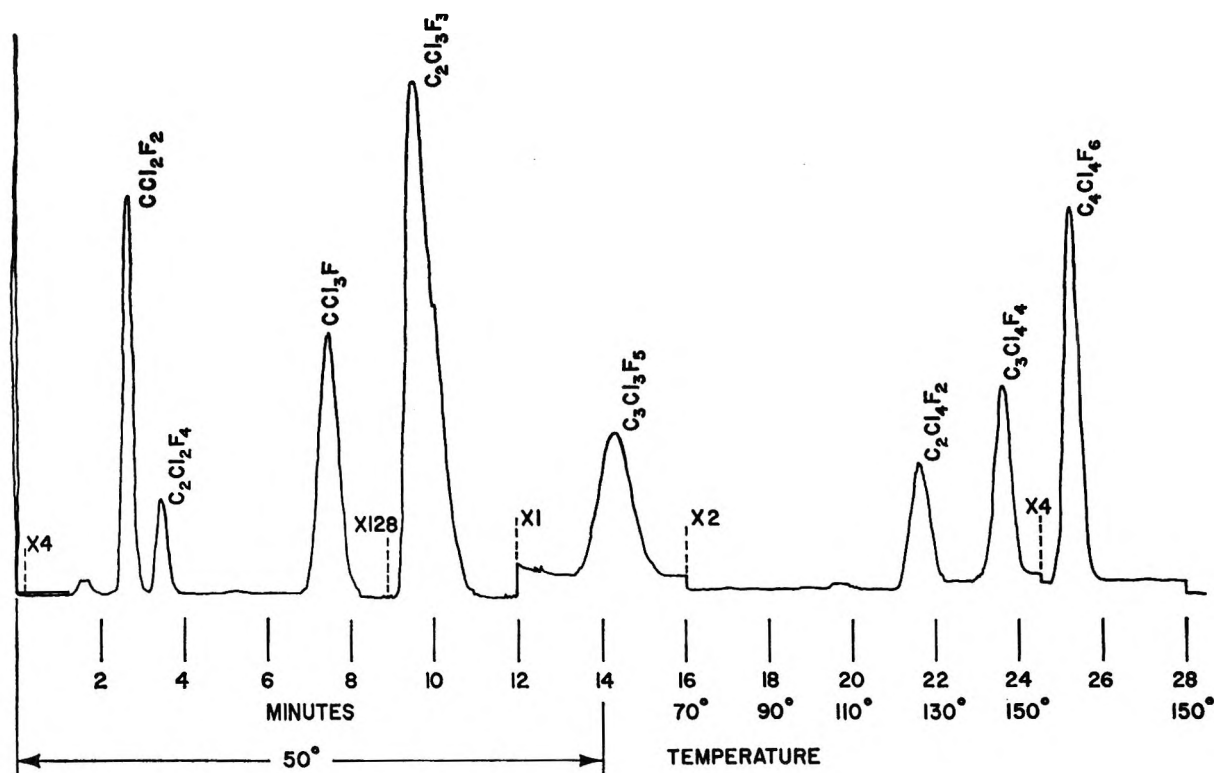


Figure 1. Chromatogram of the radiolysis products from trichlorotrifluoroethane.

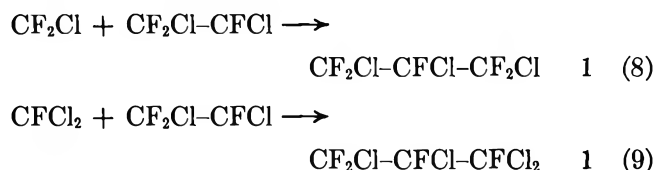
Table I: Radiolysis Products from $C_2F_3Cl_3$

Product	G value	Relative ratio
CF_2Cl_2	1.4	
$C_2F_4Cl_2$ (1,2-dichloro-)	0.20	
$CFCl_3$	1.4	
$C_3F_3Cl_3$ (1,2,3-trichloro-)	0.20	
$C_2F_2Cl_4$ (1,1,2,2-tetrachloro-)	0.20	
$C_3F_4Cl_4$ (1,1,2,3- and 1,2,2,3-tetrachloro-)	0.20	
$C_4F_6Cl_4$ (1,2,3,4-tetrachloro-)	0.70	

$CF_2Cl-CFCl_2 \xrightarrow{\gamma} CF_2Cl-CFCl + Cl$	14 (1)
$CF_2Cl-CFCl_2 \xrightarrow{\gamma} CF_2Cl + CFCl_2$	10 (2)
$Cl + CF_2Cl \rightarrow CF_2Cl_2$	7 (3)
$Cl + CFCl_2 \rightarrow CFCl_3$	7 (4)
$2CF_2Cl-CFCl \rightarrow$	
$CF_2Cl-CFCl-CFCl-CF_2Cl$	3.5 (5)
$2CF_2Cl \rightarrow CF_2Cl-CF_2Cl$	1 (6)
$2CFCl_2 \rightarrow CFCl_2-CFCl_2$	1 (7)
$CF_2Cl + CF_2Cl-CFCl \rightarrow$	
$CF_2Cl-CFCl-CF_2Cl$	1 (8)
$CFCl_2 + CF_2Cl-CFCl \rightarrow$	
$CF_2Cl-CFCl-CFCl_2$	1 (9)

was no evidence for polymer formation in any of the chromatographic or mass spectrometric work.

Considering the products, it appears that only C-Cl and C-C bonds have been broken. The fact that the C-F bond was not broken is not surprising considering its high bond dissociation energy compared with those of the C-Cl and C-C bonds. The following radical mechanism was selected as being most readily accountable for the radiolysis products. The simple combination of the initial free radicals produces exactly those isomers that have been identified. The one exception is the 1,2,2,3-tetrachlorotetrafluoropropane that is formed along with the 1,1,2,3-tetrachloro isomer. The fraction of each isomer is unknown. The reverse reactions of (1) and (2) and the steps that may precede (1) and (2) (such as ion formation) are not included.



The other C-Cl bond could also be broken in reaction 1, even though it was less likely. Apparently this occurrence was very small, as the only four-carbon isomer formed was the one shown in reaction 5. Although it is possible for CF_2Cl radicals to undergo a disproportionation reaction (10), it was neglected because the disproportionation:combination ratio was found to be 0.17.⁶

(6) G. O. Pritchard and M. J. Perona, *J. Phys. Chem.*, **73**, 2944 (1969).



Another possible reaction is the combination of chlorine atoms to form Cl_2 (11), which in turn could scavenge free radicals to form the two predominant products according to (12) and (13).



No attempt has been made to distinguish the above reactions (11–13) from those originally listed (3–9), because they lead to the same products and the same product ratios.

The mechanism can also be used to account for the relative yields. Using whole numbers for simplicity, it can be seen that if reactions 1 and 2 occur in a ratio of 14 to 10, the four radicals formed can subsequently combine to produce the relative yields that were obtained. The yield of the four-carbon compound formed in reaction 5 is somewhat anomalous. According to this scheme, six parts of this compound should have been formed, whereas only 3.5 parts were actually formed. A possible explanation may be that the chromatographic sensitivity is actually less for this compound. This cannot be verified until a standard is obtained. The above mechanism, in which four radicals combine on a 1 to 1 basis to generate the observed products, very conveniently accounts for the products.

Acknowledgment. We wish to thank K. J. Grossaint for his support in doing the mass spectrometric analysis.

Solvent and Temperature Effects on the Hydrogen Bond

by E. A. Robinson, H. D. Schreiber,
and J. N. Spencer*

Lebanon Valley College, Annville, Pennsylvania 17003
(Received January 29, 1971)

Publication costs assisted by Lebanon Valley College

The temperature dependence of the molar absorptivity of the fundamental hydroxyl stretch of various phenols has been determined in the solvents tetrahydrofuran, benzene, and chlorobenzene in which the hydrogen bonding capability of the solvent is well established, in carbon tetrachloride in which hydrogen bonding to the solvent seems likely, and in perfluoromethylcyclohexane.

All spectra were recorded on the Beckman DK-2A spectrophotometer equipped with the Beckman tem-

perature regulated cell holder controlled to $\pm 1^\circ$. Teflon stoppered cells (1-cm) were used for all spectra. The reference cell contained the pure solvent for each system. The cells had previously been shown to be adequately sealed against loss of the solute or solvent by evaporation.¹ The solute concentrations were about 0.002 *M* for phenol, catechol, guaiacol, and *sym*-trichlorophenol, 0.001 *M* for resorcinol, and 0.008 *M* for *o*-nitrophenol for all solutions studied. The molar absorptivities reported are the average molar absorptivities of at least three separate solutions at each temperature. The samples were prepared by adding weighed amounts of each solute to the solvent. All reagents were stored in a dry nitrogen atmosphere and transfers were done quickly in order to avoid water contamination. Standard purification techniques were used for all reagents.

The molar absorptivity of the fundamental hydroxyl stretching frequency of various phenols as a function of temperature is given in Table I. The frequency shifts relative to the gas phase hydroxyl frequency of phenol, 3654 cm^{-1} ,² and the negative fractional change of the molar absorptivity with temperature, $(-1/\epsilon_0)(d\epsilon/dt)$, are also given in Table I. The fractional change of molar absorptivity with temperature is reported because for some solutes the absorption is due to two hydroxyl groups and for other solutes only one hydroxyl group is responsible for the absorption. Thus a common basis is used for comparison. Selected spectra are given in Figures 1, 2, and 3.

The spectra of catechol and guaiacol in benzene, chlorobenzene, and tetrahydrofuran bear a resemblance to the spectra of phenol in these solvents. This similarity of spectra is interpreted as being due to disruption of the intramolecular hydrogen bond in catechol and guaiacol by these solvents. It is seen that the molar absorptivity of catechol in tetrahydrofuran and chlorobenzene is about twice that of guaiacol as would be expected if disruption of the intrabond occurred. However, if the intramolecular bond in catechol should be disrupted by association with the solvent the molar absorptivity would be expected to show nearly the same relation to phenol as does the molar absorptivity of resorcinol in these solvents. Likewise, the molar absorptivity of guaiacol should be nearly that of phenol should the intrabond be disrupted by the solvent. It is seen that in all cases for which data are reported the molar absorptivity of resorcinol is nearly twice that of phenol. The data of Table I show that the molar absorptivity of catechol is less than that of resorcinol and the molar absorptivity of guaiacol is less than that of phenol in benzene, chlorobenzene, and tetrahydrofuran. The fractional change of molar ab-

(1) G. P. Hoover, E. A. Robinson, R. S. McQuate, H. D. Schreiber, and J. N. Spencer, *J. Phys. Chem.*, **73**, 4027 (1969).

(2) L. J. Bellamy, R. L. Williams, and H. E. Hallam, *Trans. Faraday Soc.*, **54**, 1120 (1958).

Table I

Solute	Solvent	ϵ (l. mol ⁻¹ cm ⁻¹), t°C					$\Delta\nu$ (cm ⁻¹) ^a	ϵ_0^b	$-\frac{1}{\epsilon_0} \frac{d\epsilon}{dt} \times 10^3 \text{ deg}^{-1c}$
		20°	30°	40°	50°	60°			
Phenol	Benzene	181	172	164	151	147	99	199	4.47 ± 0.34
Resorcinol		388	371	350	327		95	430	4.74 ± 0.22
Guaiacol		124	122	121	120		108	126	1.03 ± 0.14
Catechol		341	324	312	303	296	105	360	3.08 ± 0.32
<i>sym</i> -Trichloro-phenol		135	131	127	124		135	142	2.61 ± 0.12
Phenol	CCl ₄	210	206	200	191	187	44	223	2.73 ± 0.21
Resorcinol		420	409	398	387	376	52	442	2.49 ± 0.00
Guaiacol		(202)	(200)	(198)	(196)	(194)	(49)	(206)	(0.971 ± 0.266)
Catechol		203	199	191	186	180	42	215	2.74 ± 0.14
Catechol		(203)	(203)	(201)	(200)	(198)	(42)	(206)	(0.631 ± 0.093)
<i>o</i> -Nitrophenol		(67.0)	(65.9)	(64.8)	(63.5)	(62.2)	(365)	(69.5)	(1.73 ± 0.04)
<i>sym</i> -Trichloro-phenol		(238)	(236)	(234)	(233)	(228)	(75)	(243)	(0.947 ± 0.148)
Phenol	THF	132	130	131	135		328	129	-0.775 ± 0.735
Resorcinol		267	271	273	272		315	265	-0.642 ± 0.300
Guaiacol		101	98.2	95.0	92.8		312	107	2.60 ± 0.13
Catechol		197	195	190	187		318	205	1.70 ± 0.19
<i>o</i> -Nitrophenol		34.9	34.7	34.0	33.8		339	35.8	1.12 ± 0.20
<i>sym</i> -Trichloro-phenol		70.4	68.0	68.6	74.0		328	66.3	-1.73 ± 1.87
Phenol	Chlorobenzene	157	154	150	146	139	79	167	2.63 ± 0.25
Resorcinol		314	311	304	292	286	77	331	2.27 ± 0.25
Guaiacol		138	136	132	130	129	120	143	1.67 ± 0.20
Catechol		272	269	262	258	252	93	283	1.80 ± 0.11
<i>sym</i> -Trichloro-phenol		143	140	137	136		140	147	1.63 ± 0.24
Phenol	Perfluoromethyl-cyclohexane	137	137	137	136	135	11	138	0.327 ± 0.110
Guaiacol		(148)	(145)	(143)	(143)	(142)	(63)	(150)	(0.935 ± 0.218)
<i>o</i> -Nitrophenol		(83.2)	(81.3)	(79.7)	(78.2)	(77.9)	(395)	(85.5)	(1.60 ± 0.20)

^a $\Delta\nu$ is the frequency difference between the fundamental OH stretching vibration in the particular solvent and the gaseous phenol absorption, 3654 cm⁻¹.² The frequency shifts given in parentheses refer to the difference between the intrabonded frequency and that of the non-intrabonded frequency in the same solvent. The absorption frequency at 20° was used in all cases. ^b ϵ_0 is the molar absorptivity at 0°, obtained by extrapolation of a plot of ϵ vs. $t^\circ\text{C}$ to 0°. The quantities in parentheses refer to intrabonded interactions. Corrections for changes in concentration for temperature have been made for all molar absorptivities. The absorbance of the maximum peak was used in all cases for the calculation of the molar absorptivity. ^c The fractional change of the molar absorptivity is referred to 0°. The molar absorptivity as a function of temperature is given by: $\epsilon(t^\circ\text{C}) = \epsilon_0[(1/\epsilon_0)(d\epsilon/dt)]t + \epsilon_0$, for all systems given above. The errors given are obtained from the error of the least-squares slope of ϵ vs. t . The quantities in parentheses refer to the intrabonded interactions.

sorptivity with temperature for guaiacol and catechol in these solvents is also seen to be different from that of phenol and resorcinol. Thus it appears that the proximity of the hydroxyl and the hydroxyl methoxy groups in catechol and guaiacol strongly influence the interactions with the solvent. The spectra shown in Figures 1 and 3 show pronounced asymmetry. Mecke³ has attributed the asymmetry of the spectra of phenol in benzene to different orientations of the molecule relative to the phenol hydroxyl group while Szczepaniak and Falk⁴ ascribe the asymmetry of phenol in benzene to OH...CH and OH... π interactions. If the latter interpretation is correct the shoulder on the spectra of Figure 1 would be attributed to OH...CH interaction and the peak to OH... π interaction. The shoulder apparent in the spectra in tetrahydrofuran would be

attributed to OH...CH₂ interaction and the peak to OH...O interaction. A similar explanation would apply to the spectra in chlorobenzene with the peak resulting most probably from OH...Cl interaction. In all spectra the shoulder absorbance increases with temperature. It should also be pointed out that due to the low per cent transmittance of these solvents at this wavelength the shoulder may be an artifact resulting from the rapid opening of the slit on the low wavelength side of the spectra. That the shoulder may be an artifact cannot be ruled out; however, the temperature dependence of the absorbance of the artifact is difficult to reconcile.

(3) R. Mecke, *Discuss. Faraday Soc.*, **9**, 161 (1950).

(4) K. Szczepaniak and M. Falk, *Spectrochim. Acta*, **26**, 883 (1970).

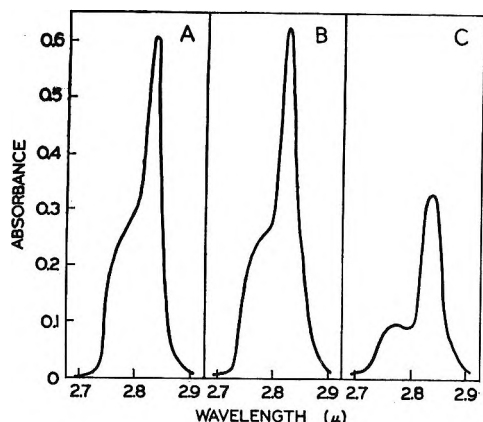


Figure 1. Spectra of the fundamental hydroxyl stretching vibration for various phenols in benzene. All spectra were recorded at 20° with the concentrations given corrected to this temperature: A, 0.00293 *M* phenol in benzene; B, 0.00185 *M* catechol in benzene; C, 0.00273 *M* guaiacol in benzene. The spectra obtained in chlorobenzene solvent are similar in shape to the spectra in benzene solvent.

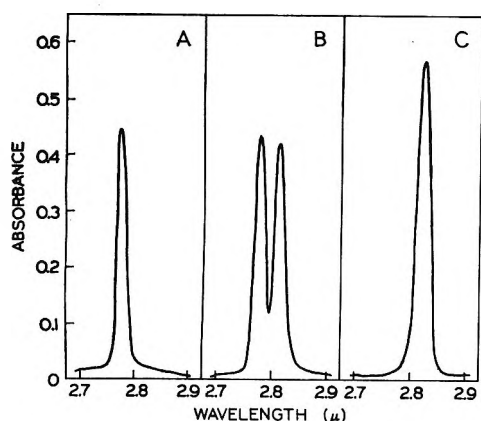


Figure 2. Spectra of the fundamental hydroxyl stretching vibration for various phenols in carbon tetrachloride. All spectra were recorded at 20° with the concentrations given corrected to this temperature: A, 0.00208 *M* phenol in carbon tetrachloride; B, 0.00192 *M* catechol in carbon tetrachloride; C, 0.00276 *M* guaiacol in carbon tetrachloride. Similar spectral shapes are observed in perfluoromethylcyclohexane.

If interactions with different parts of the solvent molecule may occur, an apparent temperature dependence of the molar absorptivity of the peak would result partially from a shift in equilibrium to the temperature favored interaction. That this would only be partially responsible for the temperature dependence of the molar absorptivity is seen by reference to the data and spectra for carbon tetrachloride solvent. Here no shoulder attributable to different interactions appears. Further, the area under the absorption spectra for phenol, resorcinol, and catechol in benzene shows a decrease of 11.5, 11.4, and 5.9%, respectively, over the temperature range given in Table I. In all systems the area under the absorption curve changes with temperature in a fashion similar to the molar absorptivity of the peak.

Discussion

Finch and Lippincott⁵ have attributed the temperature dependence of the molar absorptivity to a Boltzmann distribution of hydrogen bond lengths among the energy levels of the respective X-H...Y potential wells, the higher energy levels having the greater X...Y distances. The physical interpretation of the relative magnitude of the temperature dependence of the molar absorptivity for phenol in carbon tetrachloride and in tetrahydrofuran, in which the molar absorptivity is nearly constant within experimental error, would then

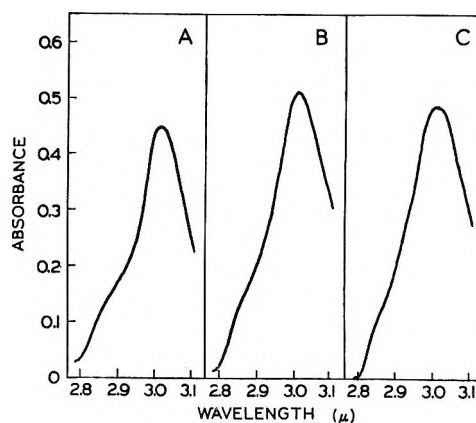


Figure 3. Spectra of the fundamental hydroxyl stretching vibration for various phenols in tetrahydrofuran. All spectra were recorded at 20° with the concentrations given corrected to this temperature: A, 0.00327 *M* phenol in tetrahydrofuran; B, 0.00266 *M* catechol in tetrahydrofuran; C, 0.00472 *M* guaiacol in tetrahydrofuran.

be that the average hydrogen bond length increases more with temperature for OH...Cl bonds than for O-H...O bonds assuming the phenol to associate with the solvent in both cases. This could possibly result from more closely spaced energy levels for the O-H...Cl system. An estimate of the relative spacings of the energy levels for these systems may be found from the potential functions of Schroeder and Lippincott.^{6,7}

An RCA Spectra 70/46 computer was used to calculate the potential wells, force constants, frequency shifts, hydrogen bond energies, and hydrogen bond lengths for OH...O and OH...Cl systems using the parameters given by Schroeder and Lippincott.⁷ A plot of frequency shift vs. force constant for the X...Y potential well was made and using the experimental frequency shifts for phenol in carbon tetrachloride and tetrahydrofuran, the O...O and O...Cl force constants for these systems were found to be 9×10^3 and 5×10^3

(5) J. N. Finch and E. R. Lippincott, *J. Phys. Chem.*, **61**, 894 (1957).

(6) E. R. Lippincott and R. Schroeder, *J. Chem. Phys.*, **23**, 1099 (1955).

(7) R. Schroeder and E. R. Lippincott, *J. Phys. Chem.*, **61**, 921 (1957).

dyn cm⁻¹, respectively. Assuming that the reduced mass for the vibrator may be found from consideration of the X-H...Y motion, the system with the smaller force constant should have the more closely spaced energy levels. As shown by Schroeder and Lippincott,⁶ the effective charge on the oxygen atoms for an O-H...O hydrogen bond increases rapidly with decreasing O...O distance. The same is assumed to be true of O-H...Cl systems. Because the transition probability increases as the square of the dipole moment and the average bond length increases with temperature, the intensity will decrease with temperature to an amount dependent on the spacings of the energy levels in X-H...Y potential wells. Thus since the energy levels are more closely spaced for the phenol-carbon tetrachloride system than for the phenol-tetrahydrofuran system the intensity is a stronger function of temperature for the O-H...Cl bond.

Because the temperature dependence of the molar absorptivity of phenol, resorcinol, and *sym*-trichlorophenol is essentially zero within experimental error in tetrahydrofuran, the temperature range must be insufficient to cause a redistribution of hydrogen bond lengths or if the hypothesis of Szczepaniak and Falk is correct, insufficient to cause an equilibrium shift. The steric effort for guaiacol and catechol in the solvent must be such that more closely spaced energy levels are allowed than for phenol or resorcinol. In systems such as those of this study the temperature dependence of the molar absorptivity or integrated intensity would be dependent upon changes in hydrogen bond lengths as well as equilibrium shifts and any attempt to calculate thermodynamic properties from such spectral data must consider both effects.

Assumptions that the molar absorptivities do not change with temperature must be considered in light of the relatively large temperature changes reported in this work.

The temperature dependence of the molar absorptivity on the intrahydrogen bond, given in Table I as the numbers in parenthesis, is seen to be roughly the same for guaiacol and *o*-nitrophenol in carbon tetrachloride and perfluoromethylcyclohexane, while the temperature dependence of the molar absorptivity of phenol in these two solvents differs considerably. The small frequency shift for phenol in perfluoromethylcyclohexane and small temperature dependence of the molar absorptivity in this solvent is taken to indicate that the perfluorocarbon solvent is relatively inert toward association with the phenol. The larger dependence on temperature of the molar absorptivity of phenol in carbon tetrachloride is thus taken to result from phenol-carbon tetrachloride hydrogen bonding.

Acknowledgment. The authors would like to thank Mr. Donald Bloser and Mr. Joseph Murphy for recording several of the spectra of this work.

An Infrared Spectral Study of Hydrogen Bonding in Solutions Containing Hydrogen Fluoride¹

by Hidekazu Touhara, Haruyuki Shimoda, Koichiro Nakanishi,* and Nobuatsu Watanabe

Department of Industrial Chemistry, Kyoto University, Kyoto, Japan (Received February 8, 1971)

Publication costs borne completely by The Journal of Physical Chemistry

The Lewis acid-base equilibria in systems containing hydrogen fluoride (HF) and various organic compounds involve the formation of hydrogen bond complex^{2,3} or even an ionized complex due to proton transfer.⁴ This kind of specific interaction in hydrogen bonded systems reflects on the frequency shift of absorption peaks due to the stretching vibration of bonds involving the hydrogen atom.⁵ In view of powerful proton donating ability of HF, a large hydrogen bond shift (denoted hereafter as $\Delta\nu_{\text{HF}}$) would be expected. Although HF has been used in the fluorination reactions of various organic compounds, no calorimetric data are available for the HF complex which must be formed as an intermediate state of the reaction. Since such calorimetric measurements will meet with many experimental difficulties, spectroscopic studies should be useful to establish enthalpy data.

The purpose of this note is to show that the hydrogen-bond shift of HF is, as expected, larger than those of any other proton donors. The data for $\Delta\nu_{\text{HF}}$ with sixteen organic compounds are presented and discussed in terms of the base strength, bond dissociation energy of charge-transfer complex, and other hydrogen bond shifts.

Experimental Section

Purification of HF. Hydrogen fluoride used in this study was purified by the distillation method which is similar to that described by Runner, *et al.*⁶ Our distillation system was made entirely of polychlorotrifluoroethylene (Kel-F) and polytetrafluoroethylene (Teflon).⁷ The number of theoretical plates of the column was at least larger than 11, as confirmed by a distillation test with methanol + ethanol solutions. The distilled HF

(1) Studies on Associated Solutions. III. Previous papers: *Bull. Chem. Soc. Jap.*, **43**, 1643, 2671 (1970).

(2) H. Hyman and J. J. Katz, "Non-Aqueous Solvent Systems," T. C. Waddington, Ed., Academic Press, New York, N. Y., 1965, Chapter 2.

(3) M. Kilpatrick and J. G. Jones, "Chemistry of Non-Aqueous Solvents," Vol. II, J. J. Lagowski, Ed., Academic Press, New York, N. Y., 1967.

(4) R. M. Adams and J. J. Katz, *J. Mol. Spectrosc.*, **1**, 306 (1957).

(5) G. C. Pimentel and A. L. McClellan, "Hydrogen Bond," W. H. Freeman, San Francisco, Calif., 1960.

(6) M. E. Runner, G. Balog, and M. Kilpatrick, *J. Amer. Chem. Soc.*, **78**, 5183 (1956).

(7) H. Touhara, H. Shimoda, K. Nakanishi, and N. Watanabe, unpublished work.

was introduced directly into the infrared cell by a single-step distillation without opening the system to the atmosphere. It was important for obtaining highly purified HF to remove moisture from the sample liquids. The water content was checked by electrical conductivity measurements.⁷ It was found that the conductivity decreased from $2.6 \times 10^{-2} \text{ ohm}^{-1} \text{ cm}^{-1}$ for undistilled liquid to $1.5 \times 10^{-5} \text{ ohm}^{-1} \text{ cm}^{-1}$ for distilled HF at -78° . This value is comparable with those of Fredenhagen and Cadenbach⁸ and of Kilpatrick and Luborsky,⁹ but being one order higher than that of Runner, *et al.*⁶ However, conductivity of $2 \times 10^{-4} \text{ ohm}^{-1} \text{ cm}^{-1}$ would correspond to the water content of less than 0.0005 mol/l., provided that water is the only impurity present.⁹ Consequently, our distilled HF was of sufficient purity for infrared spectral study.

Infrared Spectral Measurement. The infrared measurements were made on a Nihon Bunko Model DS-402G grating spectrophotometer. A pair of cells for double-path operations was made of Teflon with calcium fluoride windows as an optical path. These materials were found to be satisfactorily resistant for dilute HF solutions used in the present study. The optical path length of the cells was 150 mm and the diameter and thickness of the windows were 30 mm and 3 mm, respectively. All the sample liquids used were of Merck Spectrograde. The experimental procedure was as follows. Sample solutions (30 ml) containing 0.015 mol/l. of acceptor molecule in carbon tetrachloride were charged in a Teflon mixing vessel and frozen in a methanol-Dry Ice bath. After the vessel was evacuated, a small amount of freshly distilled HF was introduced into the vessel through a Kel-F tubing connected to the still receiver. The sample solution was allowed to warm slowly, while being occasionally agitated and warmed to room temperature, when the content of the cell was thoroughly mixed. The solution was then poured into one of the infrared cells through a flexible Kel-F tubing. The final concentration of HF, usually near 0.015 mol/l., was determined by the thorium nitrate method. The wave number range from 2400 to 4000 cm^{-1} was recorded with expanded scales and with a scanning rate of 10 $\text{cm}^{-1}/\text{min}$. The spectral slit width was 3 cm^{-1} at 3600 cm^{-1} . The wave number of absorptions calibrated with polystyrene film was reproducible within $\pm 1.5 \text{ cm}^{-1}$. The temperature of the sample solutions was $20 \pm 0.5^\circ$ during the measurements.

Results and Discussion

Infrared Spectral Data. The results for the infrared spectral measurements are given in Table I. Spectra for H-F frequency of hydrogen fluoride from the literature^{2,10,11} are also included in the table. The positions of absorption bands due to the HF-organic acceptor complex vary from 2700 to 3860 cm^{-1} depending upon the proton accepting ability of organic molecule used.

They show extraordinary large shifts from unperturbed state. As shown in Table I, we defined the hydrogen bond shift $\Delta\nu_{\text{HF}}$ as the shift from the absorption frequency of monomeric HF in vapor phase.² This choice of reference state is different from a conventional one, where the frequency shift is measured from that in dilute CCl_4 solution. We will discuss this point later.

Table I: Infrared Spectral Data for HF + Proton Acceptor Systems at 20°

Environment	ν_{HF} , cm^{-1}	$\Delta\nu_{\text{HF}}$, cm^{-1}	$\Delta\nu_r$
Vapor (HF monomer)	3961 ^a	0	
Liquid (HF polymer)	3450 ^b		
Solvents			
<i>n</i> -Hexane	3858	103	2.60
Chloroform	3857	104	2.63
Carbon tetrachloride	3856	105	2.65
	3850 ^c		
Benzene	3855	106	2.68
Nitromethane	3855	106	2.68
Nitrobenzene	3849	112	2.83
Acetonitrile	3475	486	12.3
Methanol	3343	618	15.6
Acetone	3313	648	16.4
	3327 ^d		
<i>p</i> -Dioxane	3301	661	16.7
Diethyl ether	3221	740	18.7
Tetrahydrofuran	3210	751	19.0
Diisopropyl ether	3209	752	19.0
<i>N,N</i> -Dimethylformamide	3148	813	20.5
Pyridine	2713	1248	31.5

^a Reference 2. ^b Reference 10. ^c Reference 11a. ^d Reference 11b.

Numerous studies have been made for the hydrogen-bond shifts of various proton donors such as phenols, alcohols, deuteriomethanol, pyrrole, thio alcohols, hydrogen halides, etc.^{5,12} Perhaps the largest shift that has ever been observed is that with HCl.⁵ The present results indicate that the $\Delta\nu_{\text{HF}}$ values are about twice those of $\Delta\nu_{\text{HCl}}$.

As a test of the applicability of the BHW correlation,¹³ Figure 1 gives a plot of the present $\Delta\nu_{\text{HF}}$ values against the methanolic $\Delta\nu_{\text{OH}}$ obtained by one of us.¹⁴

(8) K. Fredenhagen and G. Cadenbach, *Z. Anorg. Allg. Chem.*, **8**, 289 (1929).

(9) M. Kilpatrick and F. E. Luborsky, *J. Amer. Chem. Soc.*, **75**, 577 (1953).

(10) R. H. Maybury, S. Gordon, and J. J. Katz, *J. Chem. Phys.*, **23**, 1277 (1955).

(11) (a) D. N. Schepkin, *Opt. Spectrosk.*, **19**, 709 (1965); (b) *Teor. Eksp. Khim.*, **2**, 276 (1966).

(12) No attempt was made to include all the references in this brief note.

(13) L. J. Bellamy, H. E. Hallam, and R. L. Williams, *Trans. Faraday Soc.*, **54**, 1120 (1958).

(14) K. Nakanishi, S. Ichinose, and H. Shirai, *Ind. Eng. Chem., Fundam.*, **7**, 381 (1968).

Table II: Interactions and Molecular Complex in HF + Proton Acceptor Systems

Type	Acceptor	pK_a^a	$\Delta\nu_r$	Type of interactions	Enthalpy of complex formation, kcal/mol
1	Carbon tetrachloride Benzene		2 ~ 3	Very weak H-bond $\pi \cdots HF$ $Cl \cdots HF$	1.5 ^b
2	Nitromethane Nitrobenzene Acetonitrile	-11.9 -11.3 -11.1	2 ~ 13	Weak H-bond	2 ~ 6 ^c
3	Ketones Ethers Alcohols	-6 ~ -7 -2 ~ -3 -2 ~ -4	15 ~ 20	Strong H-bond and/or Ionized complex ^d	8.4 ^b 8 ~ 10 ^c
4	Pyridine Amines	-2	>30	Formation of salt	$\lesssim 15^c$

^a Reference 15. ^b Estimated for CCl_4 and acetone by Schepkin (ref 11). ^c Estimated from the present infrared shift. ^d See reference 4.

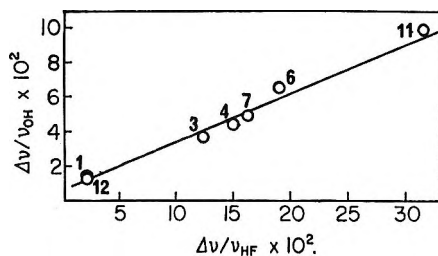


Figure 1. BHW plot of ν_{OH} against the ν_{OH} for methanol. The number of points is the same as that in Figure 2.

It is evident from the figure that the BHW plot is linear between these two kinds of shifts. Since the methanolic OH shift has been proved to correlate well with other shifts, we may conclude that the $\Delta\nu_{HF}$ is essentially of the same nature as those involved in other shifts.

As seen in Table I, the largest $\Delta\nu_{HF}$ was observed with pyridine. Still larger $\Delta\nu_{HF}$ may be expected to occur with aliphatic amines. In this case, however, the frequency of the absorption peak due to HF-amine complex (or possibly salt) was very broad and partly overlapped with the characteristic absorption of N-H vibrational frequency of amines. Although we could not establish reliable $\Delta\nu_{HF}$ values, a roughly estimated value for *n*-butylamine was as large as 1450 cm^{-1} (the center of the band at about 2500 cm^{-1}).

Comparison with pK_a and E_d . The hydrogen-bond interaction between HF and proton acceptors may be regarded as a Lewis acid-base equilibrium. Quantitative correlation has been known between the proton accepting ability and the base strength, pK_a .^{5,15} Moreover, since the hydrogen-bond complex is of charge-transfer type, the $\Delta\nu_{HF}$ value may be related to the bond dissociation energy, E_d , of the charge-transfer complex formed between the electron donor and an acceptor molecule, say, iodine.¹⁶ As shown in Figure 2, the E_d values

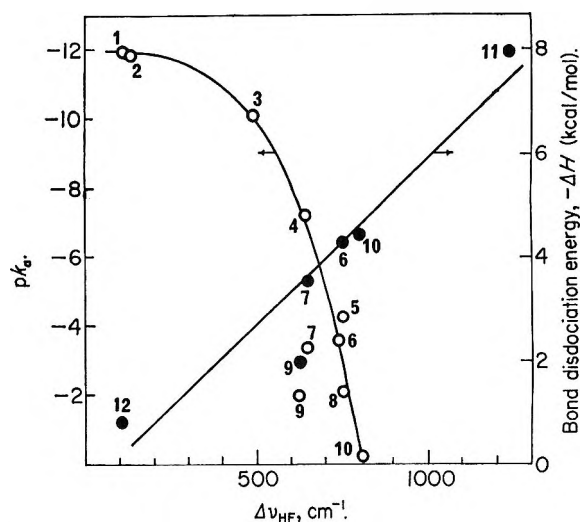


Figure 2. Plots of base strength and bond dissociation energy against $\Delta\nu_{HF}$: 1, nitromethane; 2, nitrobenzene; 3, acetonitrile; 4, acetone; 5, diisopropyl ether; 6, diethyl ether; 7, *p*-dioxane; 8, tetrahydrofuran; 9, methanol; 10, *N,N*-dimethylformamide; 11, pyridine; 12, benzene.

are in better linear correlation with the $\Delta\nu_{HF}$ values than that with the pK_a values.

Interactions with HF. From the magnitude of the relative hydrogen-bond shift $\Delta\nu_r = \Delta\nu_{HF}/\nu_{HF} \times 10^2$ shown in Table I, the interaction between HF and organic acceptors may be classified into four groups given in Table II. It also summarizes the interactions, relative shift, and estimated enthalpy value with an HF complex.

It should be noted that although both hydrocarbons and CCl_4 belong to the first group, their $\Delta\nu_r$ values are very close to each other. On the other hand, there is a

(15) E. M. Arnett, *Progr. Phys. Org. Chem.*, **1**, 223 (1963).

(16) (a) P. A. de Maine, *J. Chem. Phys.*, **26**, 1192 (1957); (b) R. S. Mulliken, *J. Amer. Chem. Soc.*, **76**, 3869 (1954).

significant difference in the shifts of phenolic or alcoholic $\Delta\nu_{\text{OH}}$ with CCl_4 from those with aromatic hydrocarbons, say, benzene. This might be ascribed to the fact that HF interacts with CCl_4 to form an addition complex, though its enthalpy of formation is fairly small.

As usual, such oxygen-containing molecules as alcohols, ethers, or ketones are stronger acceptors than nitrile or nitro compounds. It was reported that molecules of this group (the group 3) form a hydrogen-bonded molecular complex or an ionized protonated complex.⁴ However, the absorption due to the HF_2^- ion which appeared at 2500 to 2600 cm^{-1} ¹⁰ has not been observed in the present measurement. The dielectric constant of the medium will probably be insufficient to produce ionization of the complex in the present dilute HF solutions.

It is interesting to evaluate the enthalpies of complex formation in HF solutions, as they are extremely difficult to measure calorimetrically. Assuming the linear enthalpy-spectral shift correlation¹⁷ and the enthalpy values given for $\text{HF} + \text{CCl}_4$ ^{11a} and +acetone by Schepkin,^{11b} enthalpy of complex formation is estimated for each group as in the last column of Table II. According to this evaluation, the value for pyridine is 16.4 kcal/mol. While such a large value would not be in serious error, it is desirable to ascertain this by direct measurement. We are currently engaged in such a study.

(17) (a) E. R. Lippincott and R. Schroeder, *J. Chem. Phys.*, **23**, 1099 (1955); (b) A. D. Sherry and K. F. Purcell, *J. Amer. Chem. Soc.*, **74**, 3535 (1970).

Pressure Dependence of the Cross-Combination Ratio for CF_3 and CH_3 Radicals

by P. C. Kobrinsky, G. O. Pritchard,* and S. Toby

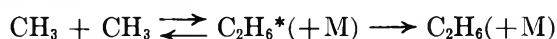
Department of Chemistry, University of California, Santa Barbara, California 93106 (Received March 8, 1971)

Publication costs borne completely by The Journal of Physical Chemistry

CF_3 and CH_3 radicals may be generated by the photolysis of 1,1,1-trifluoroacetone¹ (TFA) or the cophotolysis of acetone (Ac) and hexafluoroacetone (HFA),^{1,2} and the cross-combination ratio for the two radicals in these systems is given by^{1,2}

$$\psi = (R_{\text{CF}_3\text{CH}_3} + R_{\text{CF}_3=\text{CH}_2}) / (R_{\text{C}_2\text{F}_6} \cdot R_{\text{C}_2\text{H}_6})^{1/2}$$

where R denotes rate of formation of the various products. At reduced pressures the falloff in the recombination of CH_3 radicals will occur



before falloff for the heavier radical pairs,³ so that a study of the pressure dependence of ψ affords a simple method for determining the half quenching pressure, $P_{1/2}$, when the rate of collisional stabilization of C_2H_6^* is equal to its decomposition rate. Similar studies have recently been carried out for the radical pairs methyl and ethyl and methyl and isopropyl,^{4,5} and methyl and acetyl.⁶ Below 150° Grotewold, Lissi, *et al.*,^{4,5} find rapidly decreasing values of $P_{1/2}$, and at room temperature they report a value which is two orders of magnitude less than the RRKM calculated value, assuming a "loose" activated complex.⁷

We have examined ψ as a function of pressure at 120°, 150°, and room temperature, using either TFA or mixtures of Ac + HFA as radical sources. Experimental details are given elsewhere.¹ Low-pressure experiments, down to 0.07 mm, were carried out in a 1321- cm^3 cylindrical reaction vessel (5.8 cm in diameter which was fully illuminated) in an Hg-free system.⁸ The surface to volume ratio was 0.73 cm^{-1} . When TFA was photolyzed at 120° and 0.07 mm, $\text{CF}_2=\text{CH}_2$ was the major product (reaction times employed produced between 10^{-6} and 10^{-7} mol of product). Typical relative yields of $\text{CF}_2=\text{CH}_2$, C_2F_6 , CF_3H , C_2H_6 , and CF_3CH_3 were 100, 50, 10, 5, trace, respectively. At higher pressures, C_2H_6 , CF_3H , and CF_3CH_3 formation increased. At room temperature the C_2H_6 yields became extremely small⁹ so that Ac + HFA mixtures were used. The Ac-HFA ratio was varied between approximately 3:1 and 6:1. A plot of ψ^{-2} vs. the logarithm of pressure is shown in Figure 1.

Collision theory predicts a value of $\psi = 2.3$ for CF_3 and CH_3 radicals,¹⁰ and our high-pressure experimental values range from 2.5 to 2.9. These values were obtained in both the present and previous work,^{1,2} so that it is doubtful that the discrepancy between the experimental values and the simple collision theory calcula-

- (1) G. O. Pritchard and M. J. Perona, *Int. J. Chem. Kinet.*, **2**, 281 (1970).
- (2) R. D. Giles and E. Whittle, *Trans. Faraday Soc.*, **61**, 1425 (1965).
- (3) S. W. Benson and G. Haugen, *J. Phys. Chem.*, **69**, 3898 (1965).
- (4) J. Grotewold, E. A. Lissi, and M. G. Neumann, *J. Chem. Soc. A*, 375 (1968).
- (5) F. Casas, C. Previtali, J. Grotewold, and E. A. Lissi, *ibid.*, 1001 (1970).
- (6) F. R. Cala and S. Toby, *J. Phys. Chem.*, **75**, 837 (1971).
- (7) B. S. Rabinovitch and D. W. Setser, *Advan. Photochem.*, **3**, 1 (1964).
- (8) G. O. Pritchard and J. T. Bryant, *J. Phys. Chem.*, **72**, 1603 (1968).
- (9) This corroborates that the primary split at 3130 Å is $\text{TFA} + h\nu \rightarrow \text{CF}_3 + \text{CH}_2\text{CO}$, see E. A. Dawidowicz and C. R. Patrick, *J. Chem. Soc. London*, 4250 (1964).
- (10) It is often mistakenly assumed that cross-combination ratios should be exactly equal to 2 in radical-radical reactions, as calculated from collision theory, see J. A. Kerr and A. F. Trotman-Dickenson, *Progr. React. Kinet.*, **1**, 105 (1961). The value of 2.3 in the present case simply arises from the differences in the reduced masses of the three molecules involved. For CH_3 and C_2F_7 the value is 2.7.

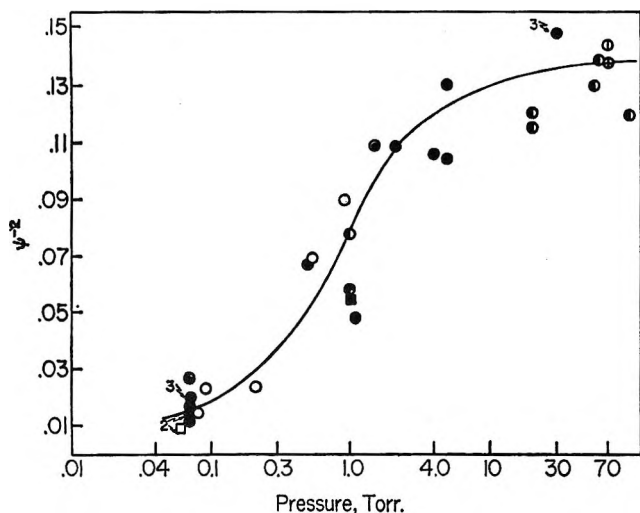


Figure 1. Semilog plot of ψ^{-2} vs. pressure. In the case of mixed bath gases the pressures are taken as additive. Although deactivating efficiencies may vary, as long as some of the excess vibrational energy of $C_2H_6^*$ is transferred on the initial collision, it will not redissociate. Ac + HFA mixtures: \circ , room temperature. All data at 70 mm, work of Giles and Whittle;² \odot , 157°; \oplus , overlapping points from runs at 23, 63, and 103°. TFA: \bullet , $\sim 120^\circ$, numbers refer to overlapping points. Point at 30 mm overlapping points of runs at 90, 130, and 150°; \ominus , reduced light beam: \bullet , $\sim 150^\circ$; \odot , wall reactor; \ominus , 0.07 mm TFA + 1 mm $c-C_6F_{12}$. \square , two points at 220°; \blacksquare , 330°.

tion is due solely to analytical errors, and thus the difference is real, at least below 150°.

A few experiments were carried out at higher temperatures but the possibility of increasing olefin loss due to radical addition reactions^{1,2} cannot be discounted. ψ is found experimentally¹ to be 2 at 300° and 30 mm, presumably, in part at least, due to this cause. Also propane becomes an increasing minor product,¹ which renders the mechanism less clear-cut. A trend toward larger values of $P_{1/2}$ is apparent, in agreement with experiment and theory.^{6,7,11}

Some experiments were also carried out with an incident light beam reduced in diameter to 1.9 cm, so that only the central portion of the reactor was illuminated, and it was found that ψ was unaffected. In addition, a reaction vessel was constructed with three quartz tubes of different diameters mounted axially and running nearly the length of the reactor; the volume was 892 cm³, with a surface to volume ratio of 3.1 cm⁻¹. With this vessel the value of ψ obtained at 0.07 mm agreed reasonably well with the other values, as seen in Figure 1. However, between 1 and 1.5 mm, ψ values of ~ 2.2 were obtained at 120°; some unassessed heterogeneous effect may be involved.¹² The homogeneous pressure-independent value of ψ is clearly > 2.5 in Figure 1. Interestingly enough, the value of the function $R_{CF_3H}/R_{C_2F_6}^{1/2}$ at 120° was independent of the reactor employed and the diameter of the incident light beam at both 0.07 and 1.0 mm.

Approximate values were 2.0×10^{-8} and 8.5×10^{-8} mol^{1/2} cc^{-1/2} sec^{-1/2} at the respective pressures. This strongly suggests that an adsorbed phase reaction between CF_3 radicals and TFA to produce CF_3H does not occur. The reaction $CH_3 + (CH_3COCH_3)_{ads} \rightarrow CH_4 + (CH_3COCH_2)_{ads}$ has recently been established.^{13,14} The reader is referred to Konstantatos and Quinn's paper¹³ for a detailed discussion of the variation in the comparable function $R_{CH_4}/R_{C_2H_6}^{1/2}$ with varying surface to volume ratios.

We see from Figure 1 that $P_{1/2}$ is close to 1 mm ($\sim 0.8 \pm 0.2$ mm) at room temperature and 120°. This value correlates well with published data obtained by other methods¹¹ and is close to the RRKM calculated values in the temperature range, based on a "loose" activated complex.⁷ In their studies below 150°, Grotewold, Lissi, *et al.*,^{4,5} find an increasing discrepancy with Rabinovitch and Setser's calculation,⁷ and at 15° report that $P_{1/2} = 10^{-2}$ mm from their cross-combination study.⁴ The data are interpreted in terms of a more "rigid" activated complex, where the free rotations of the methyl groups are replaced by a low-frequency bending.

Our data would seem to dispose of misgivings concerning the validity of the "loose" complex model for CH_3 recombination, a conclusion arrived at by Hole and Mulcahy.¹¹

Acknowledgments. G. O. Pritchard thanks The National Science Foundation for support and S. Toby thanks Rutgers University for a Faculty Fellowship.

(11) K. J. Hole and M. F. R. Mulcahy, *J. Phys. Chem.*, **73**, 177 (1969).

(12) K. M. Maloney, *ibid.*, **74**, 4177 (1970).

(13) J. Konstantatos and C. P. Quinn, *Trans. Faraday Soc.*, **65**, 2693 (1969).

(14) H. Shaw and S. Toby, *J. Phys. Chem.*, **72**, 2337 (1968).

The Gas-Phase Acidities of Alcohols¹

by Mary Jane McAdams and Larry I. Bone*

Department of Chemistry, East Texas State University, Commerce, Texas 75428 (Received January 15, 1971)

Publication costs assisted by the Robert A. Welch Foundation

Brauman and Blair^{2,3} have reported a scale of the relative acidities of alcohols in the gas phase. Using ion cyclotron resonance techniques, they were able to show that as the size of the alkyl group increases on an

(1) This work is supported by a Faculty Research Grant, East Texas State University, and the Robert A. Welch Foundation.

(2) J. I. Brauman and L. K. Blair, *J. Amer. Chem. Soc.*, **92**, 5987 (1970).

(3) J. I. Brauman and L. K. Blair, *ibid.*, **90**, 6561 (1968).

alcohol, so does the acidity. Tiernan and Hughes⁴ more recently reported the same scale of relative gas-phase acidities using a tandem mass spectrometer. These results indicate gas-phase acidities are opposite those known for the liquid phase. This phenomenon is of interest as it suggests that relative acidities are changed by removing the molecule to the gas phase.

For several years Kebarle⁵ and coworkers have studied ion-solvent interactions in the gas phase. These studies are particularly informative in that they investigate ions surrounded by a cluster of solvent molecules without interference of the bulk of a solvent. In a study of competitive solvation of hydrogen ion by water and methanol, Kebarle⁵ showed that the proton is not associated with any particular solvating molecule and that for small clusters, methanol is taken up preferentially to water. This preference for methanol is because methanol is more polarizable than water and thus provides enhanced charge stabilization. In larger clusters water is favored because of its larger dipole moment.

We have developed a novel technique, which to our knowledge has not been tried before, for studying ion-solvent interactions and how they relate to gas-phase acidities of alcohols. Equimolar mixtures of two alcohols were irradiated with 50-keV X-rays from a Siemens unit operated at 26 mA. During irradiation an electric field of 500 to 1000 V/cm was applied between two 1-in. diameter copper electrodes. At a pressure from 50 to 100 Torr these field strengths were insufficient to contribute substantially to the kinetic energy of the ions but, as ion current measurements indicate, were sufficient to collect 80–100% of the ions produced. Alkoxy ions formed by dissociative electron capture migrate to an anode covered with a mossy silver deposit which binds the surviving ion. Since the ion collides many times in transient to the plate, equilibrium should be well established. After irradiation, the vessel was thoroughly evacuated and the anode was placed in a measured amount of distilled water, where the alkoxy ions were hydrolyzed. This mixture was analyzed on a Hewlett-Packard Model 5750 flame ionization gas chromatograph using a 12-ft 10% Carbowax 20M on Chromosorb W column. The chromatograph was calibrated such that the yield of each alkoxy ion could be determined.

Two sets of control experiments were performed. In both sets the vessel was filled in an identical manner. One set was not irradiated although the electric field was applied while the other set was irradiated without applying the electric field. Analysis showed no alcohol present in the hydrolyzed sample of either set.

If we had been able to carry out these experiments at very low pressures (below a few microns) the following equilibrium would be established.

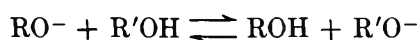


Table I: Equilibrium Constants for Alkoxy-Alcohol Proton Transfer Reactions⁴

Reaction	K_{eq}
$\text{OH}^- + \text{CH}_3\text{OH} \rightleftharpoons \text{CH}_3\text{O}^- + \text{H}_2\text{O}$	80.0
$\text{CH}_3\text{O}^- + \text{C}_2\text{H}_5\text{OH} \rightleftharpoons \text{C}_2\text{H}_5\text{O}^- + \text{CH}_3\text{OH}$	10.9
$\text{C}_2\text{H}_5\text{O}^- + n\text{-C}_3\text{H}_7\text{OH} \rightleftharpoons \text{C}_3\text{H}_7\text{O}^- + \text{C}_2\text{H}_5\text{OH}$	2.6
$\text{C}_3\text{H}_7\text{O}^- + n\text{-C}_4\text{H}_9\text{OH} \rightleftharpoons \text{C}_4\text{H}_9\text{O}^- + \text{C}_3\text{H}_7\text{OH}$	1.4
$\text{C}_4\text{H}_9\text{O}^- + n\text{-C}_5\text{H}_{11}\text{OH} \rightleftharpoons \text{C}_5\text{H}_{11}\text{O}^- + \text{C}_4\text{H}_9\text{OH}$	1.4
$\text{C}_5\text{H}_{11}\text{O}^- + n\text{-C}_6\text{H}_{13}\text{OH} \rightleftharpoons \text{C}_6\text{H}_{13}\text{O}^- + \text{C}_5\text{H}_{11}\text{OH}$	1.7

The equilibrium constant for this reaction is a measure of the acidity of the alcohol since the most abundant alkoxy ion is the conjugate base of the most acidic acid. We were unable to do experiments in this pressure range since even experiments at 50 Torr required some 20 hr radiation time to obtain reliable quantities of product.

Tiernan and Hughes⁴ have reported equilibrium constants for this process for a series of alcohols and water. Their equilibrium constants which are determined mass spectrometrically are calculated from the rate constant for the forward and reverse reactions. Table I reproduces their data. As can be seen from Table I the trends observed by Tiernan and Hughes agree with those reported by Brauman and Blair.^{2,3} As the polarizability of the alcohol increases so does the acidity.

Since our experiments were at pressures between 50 and 100 Torr, the equilibrium studied involves solvated ions. Thus the actual process taking place is more complicated than a simple proton-transfer equilibrium between alkoxy ions. The ion-molecule collisions taking place actually establish the equilibrium concentration of methanol and ethanol in the ion clusters reaching the anode. By comparing ion current measurements with product collected at the anode, we find that there are 4 ± 2 alcohol molecules in the hydrolyzed sample per charge collected. The uncertainty reported is a standard deviation. Assuming this is representative of a gas-phase cluster, we estimate that the cluster size in our experiments averages 4 including what is normally considered the central ion.

Kebarle has pointed out that for small clusters incorporation of the most polarizable molecule is favored. In our experiments where the cluster size is small, ethanol should be more abundant in the cluster than methanol. Furthermore, since by analogy with Kebarle's results the charge is not associated with any particular molecule, the most polarizable molecule should be favored for cluster sizes of one, *i.e.*, single ions. For methanol-ethanol mixtures at low pressure where the ions are unsolvated, $\text{C}_2\text{H}_5\text{O}^-$ should be favored over CH_3O^- . This is consistent with the results reported on gas-phase

(4) T. O. Tiernan and B. M. Hughes, Seventeenth Annual Conference on Mass Spectrometry and Allied Topics, 18-23, Dallas, Tex., May 1969.

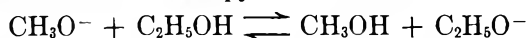
(5) (a) P. Kebarle, R. N. Haynes, and J. G. Collins, *J. Amer. Chem. Soc.*, **89**, 5753 (1967); (b) P. Kebarle, *Advan. Chem. Ser.*, **No. 72** (1967).

acidity. As the number of molecules in the cluster increases the probability of the most polarizable molecule being in the cluster should decrease.

From a series of 14 experiments with methanol and ethanol, the equilibrium constant which can probably best be thought of as the equilibrium for the replacement of a methanol with an ethanol in the solvation sphere was found to be 4.3 ± 1.4 . The reported uncertainty is a standard deviation.

Since our cluster size averages 4, the preference for ethanol in the cluster should result in an equilibrium constant lower than the value of 10.9 observed by Tiernan and Hughes for isolated ions. In fact, as the cluster size continues to increase, one would expect that methanol would appear to be more acidic than ethanol. This is exactly the case at complete solvation or the liquid state.

Using values of heats of formation of positive and negative ions reported by Krimler and Buttrill,⁶ we calculate that the enthalpy for the reaction



assuming unsolvated species is -4.8 ± 6 kcal. Since only a small change in entropy is expected for the reaction,⁵ the free-energy change should be close to the enthalpy change.

From our value of the equilibrium constant, the enthalpy is -830 ± 200 cal. Even though this is within experimental error of the literature value, the comparison is probably not valid because our determination includes solvation enthalpies. Although the data are not sufficiently accurate to warrant such a calculation, the difference in our values and the literature values represents the difference in solvation enthalpies between methanol and ethanol. As Kebarle and Yamdagni⁷ have shown, this value is a function of cluster size.

We have also obtained qualitative results for ethanol-isopropyl alcohol mixtures. However, the large uncertainty in the methanol-ethanol results were compounded by the lower vapor pressure of the higher homologs. For this reason, the project has been at least temporarily discontinued.

(6) P. Krimler and S. E. Buttrill, Jr., *J. Amer. Chem. Soc.*, **92**, 1142 (1970).

(7) R. Yamdagni and P. Kebarle, private communication.

Electron Spin Resonance Spectra of Copper Acetate in Acetic Acid Solutions

by Graeme Nyberg

Physical Chemistry Division, La Trobe University,¹ Bundoora, Victoria, Australia, 3083 (Received January 29, 1971)

Publication costs assisted by La Trobe University

The properties of copper acetate monohydrate in the crystal are well studied. Structurally² there are two

adjacent copper ions bridged by four acetate groups, with the water molecules coordinating in the axial positions of the dimer. The magnetic behavior³ above 20°K is that of a triplet, thermally excited from the singlet ground state. In water solution, on the other hand, the spectrum resembles that of any other simple hydrated (monomer doublet) cupric ion. The question then arises as to the nature of the spectra in acetic acid solvents and the complex ions present. That such solutions do exhibit interesting electron resonance spectra has previously been mentioned,⁴ but without any elaboration.

Results and Discussion

In pure glacial acetic acid there is no observable spectrum. As soon as water is added a signal begins to appear, and by 2% (by volume) its shape is unambiguously established. Continued dilution increases the signal intensity with little effect on the shape until the solvent is about 25% water, after which the intensity remains constant but the shape steadily approaches that of a pure water solution. Spectra for the two quoted dilutions are displayed in Figure 1, along with computed reconstructions.

From the glacial acetic acid result we can immediately conclude that the copper species is a dimer, whose triplet resonance is so broad (in solution) that it is undetectable. While the addition of water must generate the monomer, dissociation of the dimer cannot be complete until about 25% dilution. Since the appearance of the absorption is rather unusual (more like a triplet half-field line than a solution doublet) this raises the possibility that the line shape might be determined by the chemical exchange between dimer triplet and monomer doublet species which are in equilibrium.

Before pursuing this further, however, it was considered advisable to attempt a reconstruction with lorentzian components whose widths are given by the formula

$$W(M_{1,\tau_2}) = (A + BM_1 + CM_1^2)\tau_2 + E/\tau_2$$

This method, which has been previously described,⁵ is easiest to apply when there is a sequence of spectra (over a range of temperatures) which encompasses one with minimum line widths, as this immediately determines $\tau_2 = \tau_0 = \sqrt{E/A}$. Here there is no such minimum, so the fitting process is substantially more difficult. The results displayed in Figure 1 are, however,

(1) Work carried out at the Department of Theoretical Chemistry, University of Cambridge, Cambridge, England.

(2) J. N. Van Niekerk and F. R. L. Schoening, *Acta Crystallogr.*, **6**, 227 (1953).

(3) B. Bleaney and K. D. Bowers, *Proc. Roy. Soc. Ser. A*, **214**, 451 (1952).

(4) G. Nyberg, *Mol. Phys.*, **12**, 69 (1967).

(5) G. Nyberg, *ibid.*, **17**, 87 (1969).

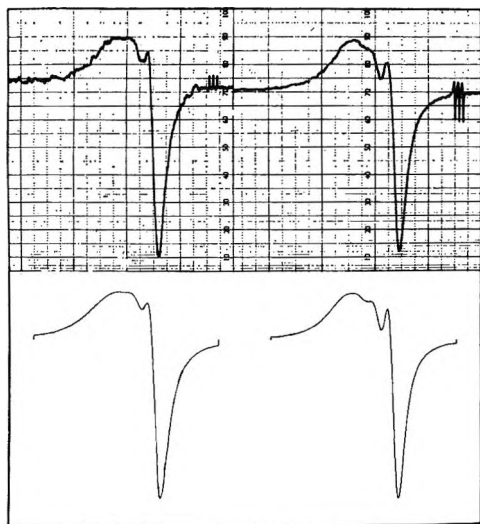


Figure 1. ESR spectra (upper) of copper acetate in acetic acid solutions, 2% and 25% by volume water, compared with fitted curves of superposed Lorentzians. The three small peaks are peroxyamine disulfonate marker (external). High field is to the right. The spectra were taken on a Varian V-4500-10A spectrometer.

so obtained. The parameters for the computed spectra⁵ are

$$W(M_1, \tau_2) = 33 \times 10^7 \{ [1 + (B/A)M_1 + (C/A)M_1^2](\tau_2/\tau_0) + (\tau_0/\tau_2) \} \text{ sec}^{-1}$$

Solution	g	a/G	τ_2/τ_0	B/A	C/A
2% H ₂ O	2.17	45	3.33	0.38	0.033
25% H ₂ O	2.185	45	2.50	0.37	0.033

The agreement in shape would indicate that the spectra can indeed be accounted for by conventional relaxation mechanisms, and that in fact even the spin-rotational contribution (E) is of minor significance.

The variation in g value and the earlier observations are consistent with the following sequence of reactions. Addition of water to the glacial acetic acid converts the (triplet) dimer to doublet monomer



This complex with relatively low g value would presumably be quasitetragonal. It in turn takes on more water in the competing reaction



with the acetates now singly coordinating in the axial positions. The basis for postulating this as the final entity is that even in pure water the spectrum does show hyperfine shoulders, the peak-to-peak separation is slightly greater than that of the hexaaquo ion, and the g value is lower (2.185 vs. 2.20). As for the dimer-monomer exchange reaction, identification of the nuclear hyperfine splitting in the initial doublet shows that the lower limit on the monomer lifetime is 10^{-8} sec.

Acknowledgment. I would like to thank Dr. A. Carington for suggesting this investigation, and the Shell Co. of Australia under the tenure of whose Postgraduate Scholarship the research was carried out

Enthalpy of Transfer of Sodium Chloride from Water to Aqueous Hydrogen Peroxide at 25°

by J. H. Stern* and W. R. Bottenberg, Jr.

California State College at Long Beach,
Long Beach, California 90801 (Received February 2, 1971)

Publication costs assisted by the National Science Foundation

A previous paper¹ reported on the calorimetric enthalpy of transfer $\overline{\Delta H}_2$ of NaCl from pure water to aqueous urea, at five mixed solvent (ms) compositions ranging from dilute urea to urea mole fraction 0.18. The present contribution describes an analogous study of $\overline{\Delta H}_2$ of NaCl from water to aqueous H₂O₂ (up to H₂O₂ mole fraction $X_3 = 0.225$). In contrast to organic nonelectrolytes (ne) (for example, urea,¹ acetic acid, and ethylene glycol²), little is known about the physicochemical effects of this very important inorganic ne on water and its structure. It may be noted that aqueous H₂O₂ has an unusual broad maximum in dielectric constant (ϵ) vs. X_3 isotherms between -40 and 30°.³ At 25° and over the composition range of the present study the transfer occurs under nearly iso- ϵ conditions. This at least minimizes bulk coulombic Born effects⁴ compared with other aqueous organic ms, where large changes often in ϵ occur.

Experimental Section

The enthalpies of transfer were obtained from the difference of the enthalpies of solution of crystalline NaCl in the ms and pure water, ΔH_2 , and ΔH_2° , respectively; $\overline{\Delta H}_2 = \Delta H_2 - \Delta H_2^\circ$. The calorimeter and general calorimetric procedures were described elsewhere.^{1,5} Sodium chloride was AR grade. Hydrogen peroxide solutions were freshly prepared from 30 or 50% stock solutions (Mallinckrodt and Fisher, respectively) and distilled, deionized water. Both were AR grade stabilized with trace phosphates (ca. 0.003–0.03%), and the ms were analyzed by adding excess KI and titrating the released I₃⁻ with thiosulfate.⁶

(1) J. H. Stern and J. D. Kulluk, *J. Phys. Chem.*, **73**, 2725 (1969).

(2) J. H. Stern and J. M. Nobilione, *ibid.*, **72**, 1064, 3937 (1968).

(3) P. M. Gross, Jr., and R. C. Taylor, *J. Amer. Chem. Soc.*, **72**, 2075 (1950).

(4) R. G. Bates in "Hydrogen-Bonded Solvent Systems," A. K. Covington and P. Jones, Ed., Taylor and Francis, London, 1968, p 49.

(5) J. H. Stern and C. W. Anderson, *J. Phys. Chem.*, **68**, 2528 (1964).

(6) I. M. Kolthoff and E. B. Sandell, "Textbook of Quantitative Inorganic Analysis," 3rd ed, Macmillan, New York, N. Y., 1952, p 592.

Table I: Enthalpies of Solution and Transfer of NaCl

X_3	NaCl, g	Solvent, g	ΔH_2 and ΔH_2° , cal/mol	$\overline{\Delta H}_2$, cal/mol
0.000(ΔH_2°)	0.1674	408	997	
	0.4274	417	998	
	0.3328	409	1006	
	0.3164	416	973	
	0.3158	412	1002	
		Mean 990 \pm 15 (975 \pm 5) ^a		
0.0244	0.3204	417	799	
	0.3084	413	770	
	0.3142	423	783	
		Mean 785 \pm 25		-205 \pm 30 ^b
0.0639	0.3112	413	507	
	0.3108	413	513	
	0.3110	427	526	
	0.3150	414	498	
		Mean 510 \pm 15		-480 \pm 20
0.113	0.3048	416	306	
	0.2990	413	286	
	0.3181	415	271	
		Mean 290 \pm 30		-700 \pm 35
0.143	0.3191	419	102	
	0.3041	414	127	
	0.3101	416	121	
		Mean 115 \pm 20		-875 \pm 25
0.225	0.2993	416	-187	
	0.2951	415	-160	
	0.3167	415	-177	
		Mean -175 \pm 25		-1165 \pm 30

^a Calculated from data tabulated by V. B. Parker in "Thermal Properties of Aqueous Uni-univalent Electrolytes," NSRDS-NBS2, National Bureau of Standards, U. S. Government Printing Office, Washington, D. C., 1965. ^b Over-all uncertainty of $\overline{\Delta H}_2$ is $[(e_{\Delta H_2^\circ})^2 + (e_{\Delta H_2})^2]^{1/2}$ where $e_{\Delta H_2^\circ}$ and $e_{\Delta H_2}$ are tabulated uncertainties of ΔH_2° and ΔH_2 , respectively.

Results and Discussion

All enthalpies of solution of NaCl are shown in Table I together with values of ΔH_2 at all experimental compositions. The final NaCl concentration m_2 in the majority of runs was *ca.* 0.01 *m*. The data are reported within 90% confidence limits. It is assumed that ΔH_2 values are approximately equal to those at infinite dilution of NaCl.¹

The negative enthalpies of transfer are lower in magnitude than those in the urea system. For example, at the mole fraction $X_3 = 0.113$ the values of $\overline{\Delta H}_2$ differ by *ca.* 200 cal/mol in the two systems. In the absence of data leading to the free energies of transfer, it may be assumed that $\overline{\Delta H}_2$ is approximately equal to $T\overline{\Delta S}_2$, where $\overline{\Delta S}_2$ is the entropy of transfer. This may be justified on the basis of the well established compensatory effect of the enthalpy and entropy in minimizing the free energy of transfer in a variety of aqueous systems, including urea. This assumption is also supported by the low values of the specific interaction coefficient of H₂O₂ in aqueous NaCl.⁷⁻⁹ As with urea, the negative enthalpy or entropy of transfer indicates that the nonplanar hydrogen peroxide has a strong specific effect on water, resulting in net water structure-breaking.

Acknowledgment. The authors are grateful for financial support by the National Science Foundation.

(7) M. H. Gorin, *J. Amer. Chem. Soc.*, **57**, 1975 (1935).

(8) R. Livingston, *ibid.*, **50**, 3204 (1928).

(9) J. H. Stern, J. Lazartic, and D. Fost, *J. Phys. Chem.*, **72**, 3053 (1968).

Keep pace with the new...

through these basic research journals of the American Chemical Society

The Journal of the American Chemical Society

The premier American chemistry journal publishing original research papers in every field. Biweekly.

*ACS members: U.S. \$22.00 Canada, PUAS \$26.50 Other nations \$27.50
Nonmembers: U.S. \$44.00 Canada, PUAS \$48.50 Other nations \$49.50

The Journal of Organic Chemistry

Embraces the field, from synthesis to structure to behavior. Biweekly publication.

*ACS members: U.S. \$20.00 Canada, PUAS \$24.50 Other nations \$25.50
Nonmembers: U.S. \$40.00 Canada, PUAS \$44.50 Other nations \$45.50

The Journal of Physical Chemistry

Maintains a balance between classical areas of chemistry and modern structural quantum oriented areas. Biweekly.

*ACS members: U.S. \$20.00 Canada, PUAS \$24.00 Other nations \$25.00
Nonmembers: U.S. \$40.00 Canada, PUAS \$44.00 Other nations \$45.00

Biochemistry

Covers enzymes, proteins, carbohydrates, lipids, nucleic acids and their metabolism, genetics, biosynthesis. Biweekly.

*ACS members: U.S. \$20.00 Canada, PUAS \$23.00 Other nations \$23.50
Nonmembers: U.S. \$40.00 Canada, PUAS \$43.00 Other nations \$43.50

The Journal of Agricultural and Food Chemistry

Places special emphasis on the chemical aspects of agricultural and food chemistry. Bimonthly.

*ACS members: U.S. \$10.00 Canada, PUAS \$13.00 Other nations \$13.50
Nonmembers: U.S. \$20.00 Canada, PUAS \$23.00 Other nations \$23.50

The Journal of Medicinal Chemistry

Emphasis is on synthesis, mode of action and pharmacology of medicinal agents. Monthly.

*ACS members: U.S. \$15.00 Canada, PUAS \$18.00 Other nations \$18.50
Nonmembers: U.S. \$30.00 Canada, PUAS \$33.00 Other nations \$33.50

The Journal of Chemical and Engineering Data

Quarterly journal presenting data on properties and behavior of both new and known chemical systems.

*ACS members: U.S. \$15.00 Canada, PUAS \$18.00 Other nations \$18.50
Nonmembers: U.S. \$30.00 Canada, PUAS \$33.00 Other nations \$33.50

Inorganic Chemistry

Publishes original research, both experimental and theoretical, in all phases of inorganic chemistry.

*ACS members: U.S. \$18.00 Canada, PUAS \$21.00 Other nations \$21.50
Nonmembers: U.S. \$36.00 Canada, PUAS \$39.00 Other nations \$39.50

Macromolecules

Presents original research on all fundamental aspects of polymer chemistry. Bimonthly publication.

*ACS members: U.S. \$12.00 Canada, PUAS \$15.00 Other nations \$15.50
Nonmembers: U.S. \$24.00 Canada, PUAS \$27.00 Other nations \$27.50

American Chemical Society / 1155 Sixteenth Street, N.W., Washington, D.C. 20036

Please enter a one year subscription for the following journals:

1	2	3
4	5	6
7	8	9
name	position	
address		
city	state/country	zip
your company	nature of company's business	

I am an ACS member I am not an ACS member Bill me for \$ _____

Payment enclosed (payable to American Chemical Society) in the amount of \$ _____. Payment must be made in U.S. currency, by international money order, UNESCO coupons, or U.S. bank draft; or order through your book dealer.

* NOTE: Subscriptions at ACS member rates are for personal use only.

72A

Platinum Group Metals and Compounds

ADVANCES IN CHEMISTRY SERIES
NO. 98



Eleven papers from a symposium by the Division of Inorganic Chemistry of the American Chemical Society chaired by U. V. Rao.

What new complexes of the platinum group metals have been synthesized? Here is a collection of papers presenting data on chalcogenides, oxides, nitrido and hydrido complexes, as well as the catalytic properties of these metals and their alloys. Information is included on

- synthesis
- structure
- magnetic susceptibility
- double bond migration

The platinum group metals are considered from the viewpoints of both industry and research. Their magnetic and thermodynamic properties are explored, as well as recent chemistry of σ - and π -bonded complexes. Crystal structure is discussed by several authors, with data presented in the form of

- x-ray scattering data
- absorption spectra
- crystal spectra
- infrared spectra
- Mossbauer spectra
- vibrational spectra

165 pages with index. Cloth bound (1971) \$9.00 Postpaid in U.S. and Canada; plus 35 cents elsewhere.

Set of L. C. cards with library orders upon request.

Other books in the ADVANCES IN CHEMISTRY SERIES of interest to inorganic chemists include:

No. 89 Isotope Effects in Chemical Processes
278 pages Cloth bound (1969) \$13.00

No. 82 Radiation Chemistry — II
558 pages Cloth bound (1968) \$16.00

No. 81 Radiation Chemistry — I
616 pages Cloth bound (1968) \$16.00

No. 81 and No. 82 ordered together \$30.00

No. 78 Literature of Chemical Technology
732 pages Cloth bound (1968) \$17.50

No. 73 Trace Inorganics in Water
396 pages Cloth bound (1968) \$12.50

No. 72 Mass Spectrometry in Inorganic Chemistry
329 pages Cloth bound (1968) \$12.00

Order from:
Special Issues Sales
American Chemical Society
1155 16th St., N. W.
Washington, D. C. 20036